B7612

(1)

LBL-12100
UC-13

Dr 3094

MASTER

LBL--12100

DE82 000804

Annual Report 1980

Earth Sciences Division

JULY 1981

LAWRENCE BERKELEY LABORATORY
UNIVERSITY OF CALIFORNIA
BERKELEY, CALIFORNIA 94720

DISTRIBUTION OF THIS DOCUMENT IS UNLIMITED

Prepared for the U.S. Department of Energy under Contract W-7405-ENG-48

DISCLAIMER

This report was prepared as an account of work sponsored by an agency of the United States Government. Neither the United States Government nor any agency Thereof, nor any of their employees, makes any warranty, express or implied, or assumes any legal liability or responsibility for the accuracy, completeness, or usefulness of any information, apparatus, product, or process disclosed, or represents that its use would not infringe privately owned rights. Reference herein to any specific commercial product, process, or service by trade name, trademark, manufacturer, or otherwise does not necessarily constitute or imply its endorsement, recommendation, or favoring by the United States Government or any agency thereof. The views and opinions of authors expressed herein do not necessarily state or reflect those of the United States Government or any agency thereof.

DISCLAIMER

Portions of this document may be illegible in electronic image products. Images are produced from the best available original document.

LEGAL NOTICE

This book was prepared as an account of work sponsored by an agency of the United States Government. Neither the United States Government nor any agency thereof, nor any of their employees, makes any warranty, express or implied, or assumes any legal liability or responsibility for the accuracy, completeness, or usefulness of any information, apparatus, product, or process disclosed, or represents that its use would not infringe privately owned rights. Reference herein to any specific commercial product, process, or service by trade name, trademark, manufacturer, or otherwise, does not necessarily constitute or imply its endorsement, recommendation, or favoring by the United States Government or any agency thereof. The views and opinions of authors expressed herein do not necessarily state or reflect those of the United States Government or any agency thereof.

Printed in the United States of America
Available from
National Technical Information Service
U.S. Department of Commerce
5285 Port Royal Road
Springfield, VA 22161
Price Code: A12

Lawrence Berkeley Laboratory is an equal opportunity employer.

LBL-12100

EARTH SCIENCES DIVISION ANNUAL REPORT 1980

DISCLAIMER

This book was prepared as an account of work sponsored by an agency of the United States Government. Neither the United States Government nor any agency thereof, nor any of their employees, makes any warranty, express or implied, or assumes any legal liability or responsibility for the accuracy, completeness, or usefulness of any information, apparatus, product, or process disclosed, or represents that its use would not infringe privately owned rights. Reference herein to any specific commercial product, process, or service by trade name, trademark, manufacturer, or otherwise, does not necessarily constitute or imply its endorsement, recommendation, or favoring by the United States Government or any agency thereof. The views and opinions of authors expressed herein do not necessarily state or reflect those of the United States Government or any agency thereof.

LAWRENCE BERKELEY LABORATORY
UNIVERSITY OF CALIFORNIA
BERKELEY, CALIFORNIA 94720

Prepared for the U.S. Department of Energy under Contract No. W-7405-ENG-48

DISTRIBUTION OF THIS DOCUMENT IS UNLIMITED

CONTENTS

Introduction 1

GEOSCIENCES 3

BASIC SCIENCES 5

A FEASIBILITY STUDY OF TWO-WELL STORAGE SYSTEMS FOR COMBINED HEATING AND AIR-CONDITIONING BY GROUNDWATER HEAT PUMPS IN SHALLOW AQUIFERS 5
W. Pelka and C. F. Tsang

STATE-OF-THE-ART MODELS FOR GEOTHERMAL RECOVERY PROCESSES 8
C. F. Tsang and J. S. Y. Wang

BUOYANCY FLOWS IN FRACTURES INTERSECTING A NUCLEAR WASTE REPOSITORY 13
J. S. Y. Wang and C. F. Tsang

PROBABILISTIC SIMULATION OF TRANSIENT GROUNDWATER FLOW: AN ALTERNATIVE TO THE MONTE CARLO SCHEME? 19
T. N. Narasimhan, T. E. Buscheck, and P. A. Witherspoon

NUMERICAL SIMULATION OF FRACTURED POROUS MEDIA AS MULTIPLE INTERACTING CONTINUA 25
T. N. Narasimhan

THERMODYNAMICS OF HIGH-TEMPERATURE BRINES 31
K. S. Pitzer, P. Z. Rogers, G. C. Flowers, and J. C. Peiper

THE BEHAVIOR OF ROCK-FLUID SYSTEMS AT ELEVATED TEMPERATURES AND PRESSURES 34
W. H. Somerton

RESULTS OF ALBITE SOLUBILITY MEASUREMENTS AS A FUNCTION OF TEMPERATURE (125–350°C) 41
J. M. Neil and J. A. Apps

THERMODYNAMIC PROPERTIES OF SILICATE LIQUIDS 44
I. S. E. Carmichael, M. S. Ghiorso, L. K. Moret, M. Rivers, and J. Stebbins

CHEMICAL TRANSPORT IN NATURAL SYSTEMS 46
C. L. Carnahan

VISCOSITY OF NaCl, KCl, and $CaCl_2$ SOLUTIONS UP TO 350°C AND 50 MPa 48
S. L. Phillips, H. Ozbek, A. Igbene, and G. Litton

A DATABASE OF CHEMICAL PROPERTIES OF NUCLEAR WASTE ELEMENTS IN AQUEOUS SOLUTIONS 52
S. L. Phillips and A. Igbene

GEOCHEMICAL ASSESSMENT OF FIVE POTENTIAL SITES FOR HYDROTHERMAL MAGMA SYSTEMS 54
A. F. White

DEEP ELECTROMAGNETIC CRUSTAL SOUNDING IN NORTHERN NEVADA 57
M. J. Wilt, N. E. Goldstein, H. F. Morrison, and J. R. Haught

FEASIBILITY OF SHEAR WAVE VIBRATORS FOR DEEP CRUSTAL STUDIES 60
S. Coen

APPLIED RESEARCH STUDIES 61

ENHANCED RECOVERY WITH MOBILITY AND REACTIVE TENSION AGENTS 61
C. J. Radke and W. H. Somerton

AN EVALUATION OF NUCLEAR QUADRUPOLE RESONANCE (NQR) TECHNIQUES FOR THE IN-SITU MEASUREMENT OF STRESS/STRAIN IN SALT 62
E. Schempp, S. M. Klainer, and T. Hirschfeld

THE USE OF FLUORIMETRIC TECHNIQUES IN TRACE ANALYSIS 67
S. M. Klainer, D. L. Perry, H. R. Bowman, and T. Hirschfeld

THE DEVELOPMENT OF ADVANCED MASS SPECTROMETRIC TECHNIQUES 68
M. Michel and W. R. Keyes

SORPTIVE DIFFUSION IN CLAY GELS 70
C. J. Radke

ADVANCES IN FOSSIL ENERGY: COAL MINE VENTILATION SYSTEMS 71
M. McPherson and M. Hood

AQUIFER THERMAL ENERGY STORAGE STUDIES AT LBL IN 1980 75
C. F. Tsang, T. A. Buscheck, and C. Doughty

IRIDIUM IN SPRING WATERS AND SUMMIT CRATER LAKE OF MT. HOOD, OREGON 79
H. Bowman, H. Wollenberg, F. Asaro, and R. G. Bowen

GEOTHERMAL ENERGY DEVELOPMENT 83

EXPLORATION TECHNOLOGY 85

ADVANCES IN ELECTRICAL AND ELECTROMAGNETIC EXPLORATION TECHNIQUES 85

Overview 85
H. F. Morrison

Controlled-source electromagnetic interpretation based on a tilted dipole source 85
J. R. Haught

Transient field responses 86
G. M. Hoversten

Approximation of magnetotelluric topographic effects by the solution of Laplace's equation 87
E. C. Mozley

The utilization of magnetotelluric polar diagrams in a volcanic environment 88
E. C. Mozley

ELECTROMAGNETIC INDUCTION SOUNDING AT GEOTHERMAL PROSPECTS IN NEVADA 89
M. J. Wilt, M. Stark, N. E. Goldstein, and J. R. Haught

AUTOMATED SEISMIC PROCESSOR 93
T. V. McEvilly, E. L. Majer, J. Bartschi, J. Heinsen, and R. O'Connell

ADVANCES IN MAGNETOTELLURIC SURVEY TECHNIQUES AND DATA INTERPRETATION 96
W. M. Goubau, J. Clarke, and R. F. Miracky

RESERVOIR ENGINEERING 99

ADVANCES IN RESERVOIR MODELING 99

Overview 99
K. Pruess

Performance matching and prediction for the Serrazzano geothermal reservoir by means of numerical simulation 100
K. Pruess, O. Weres, and R. Schroeder

Heat and mass transfer in a fault-controlled geothermal reservoir charged at constant pressure 102
K. P. Goyal and T. N. Narasimhan

Thermodynamic models for geothermal and geopressured fluids 105
E. R. Iglesias

ADVANCES IN TRANSIENT WELL-TEST ANALYSIS TECHNIQUES 109

Overview 109
C. W. Miller

An analysis of two-phase production and injection tests 109
M. J. O'Sullivan and K. Pruess

Modeling of wellbore dynamics 113
C. W. Miller

ANALYZE 116
S. M. Benson

ADVANCES IN THE DEVELOPMENT OF TRANSIENT WELL-TESTING EQUIPMENT 120

Overview 120
S. M. Benson

The LBL combined PTQ tool 121
S. M. Benson, C. Goranson, R. Solbau, and A. Biocca

A downhole pressure/temperature probe for low-temperature geothermal applications 124
S. M. Benson, R. Solbau, C. Goranson, and B. Galbraith

INJECTION INTO A FRACTURED GEOTHERMAL RESERVOIR 126
G. S. Bodvarsson and C. F. Tsang

LBL STUDY OF THE VALLES CALDERA GEOTHERMAL RESERVOIR 131

Overview 131
C. F. Tsang

Development of a geological and geophysical model of the Valles Caldera geothermal reservoir 131
S. Vonder Haar and M. J. Wilt

Longevity of the Baca geothermal reservoir—A sensitivity study 137
G. S. Bodvarsson and C. F. Tsang

RESERVOIR EVALUATION OF KLAMATH FALLS, OREGON 140
M. T. O'Brien and S. M. Benson

SUBSURFACE HYDROGEOLOGY OF THE SUSANVILLE, CALIFORNIA, GEOTHERMAL RESOURCE 148
S. M. Benson and M. Bodvarsson

ENERGY UTILIZATION TECHNOLOGY 157

GEOTHERMAL ENERGY UTILIZATION TECHNOLOGY 157
R. L. Fulton

ANALYSIS OF DIRECT-CONTACT HEAT EXCHANGER PERFORMANCE 158
P. M. Rapier

BINARY GEOTHERMAL POWER PLANT INVESTIGATION AT LBL 161
W. L. Pope and P. A. Doyle

BINARY FLUID EXPERIMENT IN 1980 165
B. W. Tleimat, A. D. K. Laird, G. V. Dizon, S. Zhao, H. Rie, and T. Vermeulen

MEXICAN-AMERICAN COOPERATIVE PROGRAM 168

OVERVIEW OF THE MEXICAN-AMERICAN COOPERATIVE PROGRAM **168**
M. J. Lippmann and N. E. Goldstein

GEOLOGY OF THE CERRO PRIETO FIELD **175**
S. Vonder Haar and J. H. Howard

ANALYSIS OF CERRO PRIETO PRODUCTION DATA **179**
K. P. Goyal, C. W. Miller, and M. J. Lippmann

NUCLEAR WASTE ISOLATION 183

TOPICAL INVESTIGATIONS 185

A REVIEW OF THE STATE OF THE ART OF THERMOMECHANICAL-HYDROCHEMICAL MODELING OF A HARD-ROCK WASTE REPOSITORY **185**
C. F. Tsang

MONITORING ACOUSTIC EMISSIONS AT THE CLIMAX STOCK REPOSITORY **191**
E. L. Majer, T. V. McEvilly, and D. Hopkins

MULTICOMPONENT THERMOCHEMICAL TRANSPORT MODEL **193**
P. C. Lichtner and L. V. Benson

SORPTION MODELING STUDIES AND MEASUREMENTS AT LBL IN 1980 FOR THE PACIFIC NORTHWEST LABORATORIES WRIT PROGRAM **194**
R. J. Silva, A. F. White, and A. W. Yee

MASS SPECTROMETRIC DETERMINATION OF $^{234}U/^{238}U$ DISEQUILIBRIUM **199**
M. Michel

PRELIMINARY CHARACTERIZATION AND ASSESSMENT OF THE WELDON SPRING LOW-LEVEL WASTE DISPOSAL SITE **201**
B. Y. Kanehiro, V. Guvanasen, A. Smith, and R. Sterrett

SWEDISH AMERICAN COOPERATIVE PROGRAM 204

STRIPA HEATER TESTS **204**
T. Chan

FRACTURE HYDROLOGY STUDIES AT STRIPA—FY 1980 **208**
J. Gale, P. Fritz, J. Barker, C. Forster, K. Raven, P. A. Witherspoon, and C. R. Wilson

STRIPA MACROPERMEABILITY EXPERIMENT 213
C. R. Wilson

APPLICATION OF GEOPHYSICAL METHODS AT STRIPA 217
P. H. Nelson

HYDRAULIC FRACTURING AND OVERCORING IN-SITU STRESS MEASUREMENTS IN A DEEP BOREHOLE AT THE STRIPA TEST SITE 221
T. Doe

MARINE SCIENCES 227

APPENDIXES

APPENDIX A: PUBLICATIONS 243

APPENDIX B: EARTH SCIENCES DIVISION STAFF 253

APPENDIX C: PRINCIPAL MEETINGS OF 1980 255

INTRODUCTION

The programs of the Earth Sciences Division are organized under four headings: Geosciences, Geothermal Energy Development, Nuclear Waste Isolation, and Marine Sciences. Utilizing both basic and applied research in a wide spectrum of topics, these programs are providing results that will be of value in helping to secure the nation's energy future. More specifically, the division's researchers are applying themselves to the many problems which have surfaced as energy issues have extended man's activities and interests deeper into the earth. The lack of credible knowledge and reliable technology is slowing the exploitation of energy and mineral resources and preventing a full comprehension of important environmental issues such as storage of nuclear wastes.

The Geosciences investigations are designed to provide an improved understanding of the behavior of rock-fluid systems in the earth's crust. The research is concerned with the physics and chemistry of such systems and with the development of much needed data on material properties so that appropriate mathematical models can be constructed. Measurements on earth materials are conducted both in the laboratory and in the field with the aim of interpreting conditions far below the surface. Other work in geosciences is involved with improvements in instrumentation that are needed to address specialized problems.

The Geothermal investigations include studies on exploration technology, reservoir engineering, and energy utilization. The exploration work is a continuation of a program started some years ago to apply various surface geophysical techniques to the problem of locating geothermal systems. Some important advances in electrical, electro-magnetic, and seismic geophysical methods are reported. The reservoir engineering work summarizes recent developments in mathematical modeling and some new techniques in well-test analysis that are now possible using improved field equipment. Results of studies on several different geothermal reservoirs are also presented, including a Mexican-American cooperative program of investigations on the Cerro Prieto geothermal field in Mexico. The energy utilization work has been concentrating on the development of a direct-contact heat exchanger and the use of binary fluids in energy conversion. Results of the past year's efforts are summarized.

The Nuclear Waste Isolation studies are concerned with the complex problem of developing a better understanding of the many diverse factors that are involved in geologic storage of radionuclides. The key problem is that of chemical transport; the results of several investigations are included. Since nuclear waste can generate heat, there is the additional complication of working with rock-fluid systems in which there is an important coupling of thermal, mechanical, and hydraulic effects. About three years ago a major field program of investigations was initiated in an abandoned iron-ore mine at Stripa, Sweden. The current effort in this Swedish-American cooperative program is to analyze and report the results of investigations on thermomechanical effects and

fracture hydrology. The fracture hydrology program involves a new method of measuring the permeability of a very large mass of fractured rock. An important factor at Stripa is the initial state of stress in the rocks; reported here are results of two independent methods of field measurement: hydraulic fracturing and overcoring.

The Marine Sciences program is continuing research activity on the baseline environment for and the possible environmental effects of the overall program of ocean thermal energy conversion. Other activities include compiling marine geologic and other oceanographic data for the west coast of the United States and investigations on the potential for petroleum accumulations in the deep sea beds off the coast of California.

P. A. Witherspoon
Head, Earth Sciences Division

GEOSCIENCES

The summary papers in this section describe fundamental and applied studies addressing a variety of earth science problems in support of the U. S. Department of Energy's missions. They have applications in such diverse areas as energy conversion, geothermal energy, oil and gas recovery, and radioactive waste isolation. Most of the studies are conducted under ongoing projects. For descriptions of earlier work, the reader is referred to the 1977, 1978, and 1979 annual reports of the Earth Sciences Division (LBL-7028, LBL-8648, and LBL-10686) and the 1975 and 1976 annual reports of the Energy and Environment Division of Lawrence Berkeley Laboratory (LBL-5299 and LBL-5982).

The first fifteen papers summarize work performed under the U. S. Department of Energy, Office of Basic Energy Sciences (OBES). Of these, five by T. N. Narasimhan, C. F. Tsang, and their co-workers address various problems relating to the flow of groundwater through porous and fractured rocks. Seven other papers, those by I. S. E. Carmichael, C. L. Carnahan, J. M. Neil and J. A. Apps, S. L. Phillips and co-workers, K. S. Pitzer, and A. F. White address chemical aspects relating to natural systems. The physical properties of rock-fluid systems at elevated pressures and temperatures are being studied by W. H. Somerton, who describes the measurement of a wide range of physical properties--as many as possible, made simultaneously--on sedimentary rocks at elevated temperatures and pressures. Two papers, one by M. J. Wilt and one by S. Coen, describe recent developments in geophysical exploration methods.

Eight papers discuss problems having direct application to various technologies. These include two papers relating to oil recovery by C. L. Radke and W. H. Somerton; three papers concerned with instrument development by S. M. Klainer and co-workers and by M. C. Michel; one C. F. Tsang and his co-workers on aquifer energy storage; one by H. R. Bowman and his co-workers describing the occurrence of iridium in the spring waters of Mt. Hood; and one on coal mine ventilation by M. Hood.

This work was supported by (1) the Office of Energy Research, Office of Basic Energy Sciences, Division of Engineering, Mathematics, and Geosciences; (2) the Assistant Secretary for Conservation and Renewable Energy, Office of Renewable Technology, Division of Geothermal and Hydropower Technologies; (3) the Assistant Secretary for Conservation and Solar Energy, Office of Advanced Conservation Technology, Division of Thermal and Mechanical Storage Systems; and (4) the Assistant Secretary for Fossil Energy, Office of Coal Technology, Division of Coal Mining; and (5) the Assistant Secretary for Fossil Energy, Office of Oil, Gas, and Shale Technology, Division of Oil of the U. S. Department of Energy under Contract No. W-7405-ENG-48.

BASIC SCIENCES

A FEASIBILITY STUDY OF TWO-WELL STORAGE SYSTEMS FOR COMBINED HEATING AND AIR-CONDITIONING BY GROUNDWATER HEAT PUMPS IN SHALLOW AQUIFERS

W. Pelka* and C. F. Tsang

In warmer climates, air-source heat pumps have gained wide acceptance for air conditioning because of their commercial availability, reliability, and moderate capital costs. However, the application of air-source heat pumps in colder climates has several disadvantages. Obviously the air temperature is extremely low in times of great heating demand and very high when space cooling is necessary. This together with the low heat capacity of air implies high air throughput and low efficiency.

The same is true for the direct use of solar energy, especially in northern climates, since during the heating season the solar radiation is at its minimum. Figure 1 shows qualitatively the heating and cooling demand compared with the air temperature and the daily available energy from solar radiation in northern climates.

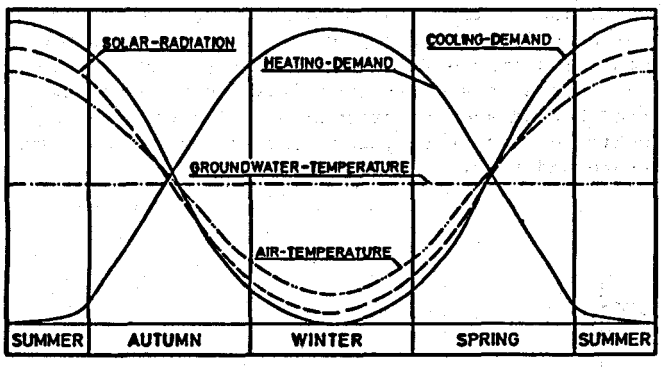

Figure 1. Heating and cooling demand compared with air temperature and solar radiation (qualitative). [XBL 808-11151]

Water-source heat pumps have several advantages over air-source heat pumps. For example, the performance coefficient is about 4 for today's commercially available water-source equipment, whereas that for air-source equipment is much less. The source for this kind of heat pump can be either surface water or groundwater.

A short study has been completed showing that the two-well storage system with groundwater heat pumps may be a feasible method of providing energy for heating and/or cooling offices and homes.

APPROACH

The basic idea of a two-well storage system consisting of a cold water well and a warm-water well is as follows: In winter, when space heating is required, water is pumped from the warm-water well. The heat is extracted from the warm water by the heat pump, after which the cooled water is reinjected into the aquifer through the cold-water (recharge) well. The extracted energy is then used for heating purposes.

In summer, colder water, which was injected during winter is withdrawn from the cold-water well. This water is at a temperature below the average aquifer temperature and absorbs heat from the air conditioning system. It is then injected into the warm-water well at a temperature equal to or higher than the average aquifer temperature.

Any use of an aquifer for space heating or air conditioning, of course, implies changes in the thermal field of the aquifer. These changes could lead to problems that should be considered before exploitation of an aquifer. One potential problem is the effect that the rise and fall of groundwater temperature might have on the biological environment and chemical equilibrium in the aquifer.

In order to avoid or minimize negative effects and to optimize the economic benefits, it is necessary to know how the thermal anomaly will spread in the aquifer. That is, what will be the size of the affected area, and will the anomaly affect other heat pumps in the surrounding area?

In our feasibility study, a numerical model was constructed for the calculation of changes in the flow and temperature field of the aquifer. It is used to evaluate the influences of the planned system on the environment and to optimize the recharge and discharge process.

The transport of heat and mass in an aquifer is a diffusion-convection problem, governed by a system of nonlinear partial differential equations, which is solved by applying Galerkins's approach--i.e., using quadrilateral finite elements for the discretization of the solution area. A weighted finite-difference scheme is used for the integration with respect to time. Heat transfer in both the saturated and the unsaturated zone is considered.

RESULTS

The application of the numerical model to the problem of two-well storage systems is made for a number of hypothetical examples based on realistic aquifer parameters and climatic data. The transient flow field and temperature field around the warm-water and cold-water wells, extraction temperatures, recovery factors, and energy fluxes are calculated for a period of three years.

Consider, for example, a simple cold-water storage system. An aquifer with a 6-m unsaturated zone and a 25-m saturated zone is used as an energy source for space heating and air conditioning by means of a two-well storage system. In winter, groundwater is extracted from the warm-water well. Water at the natural groundwater temperature is led to the water-source heat pump, where part of its energy content is transferred to the heating system. The water is cooled by about 6°C and reinjected into the aquifer via the cold-water well. In summer, when air conditioning is required, water is pumped from the cold-water well to the heat pump. This water is colder than the natural groundwater and can remove more heat from the cooling system. This process heats the water to the natural groundwater temperature, whereupon it is pumped back into the aquifer via the warm-water well.

Figure 2 shows the heating/cooling demand of 750 families, living in multifamily apartment houses under the climatic conditions shown qualitatively in Figure 1. The dependence of the energy demand of each apartment on its position in the house, its area, etc. has been included in our consideration.

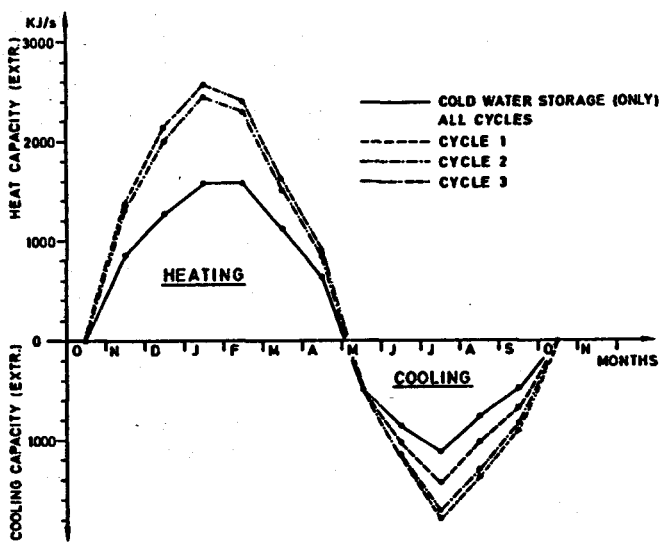

Figure 2. Heating and cooling demand for 750 families. [XBL 808-11171]

Since the water pumped back into the aquifer at the warm-water well is at the natural groundwater temperature of the aquifer, there will be no changes in the temperature field around this well, so that only the temperature field around the cold-water well need be monitored.

The flow field is described by an impermeable lower boundary of the aquifer and by a constant-pressure boundary condition on the circumference.

During the injection period, the temperature and the mass flux of the injected water are known, so that at the injection well the temperature field can be described by a time-dependent Dirichlet condition and the flow rate by a time-dependent Neumann condition.

For the extraction period, only the cooling demand and the desired reinjection temperature are known. The temperature at which the water can be extracted is unknown and depends on the extraction history. The extraction mass flux must be adjusted to satisfy the respective cooling demand, and is described as an iteratively determined time-dependent Neumann condition. Starting with an estimated mass flux for the time interval under consideration, the cooling capacity is calculated by means of this flux and the resulting available temperature. Comparison with the actual cooling demand yields a correction of the mass flux and a new calculation of the timestep. This iterative process is carried out until a satisfactory agreement between cooling demand and cooling capacity is reached for the timestep. The upper Dirichlet condition of the thermal field at the ground surface changes its temperature with the air temperature (see Fig. 1). The lower boundary of the aquifer, on the other hand, is assumed to be isothermal.

Three injection/extraction cycles were calculated for a three-year period. Surface temperature changes, natural groundwater temperature distribution, and cooling/heating demand are assumed to be the same in all three years. Figure 3 shows the mass flux in the well for the first year, including the iteratively determined fluxes during the extraction period and the assumed mass fluxes based on an estimated linear relation between extraction temperature and time.

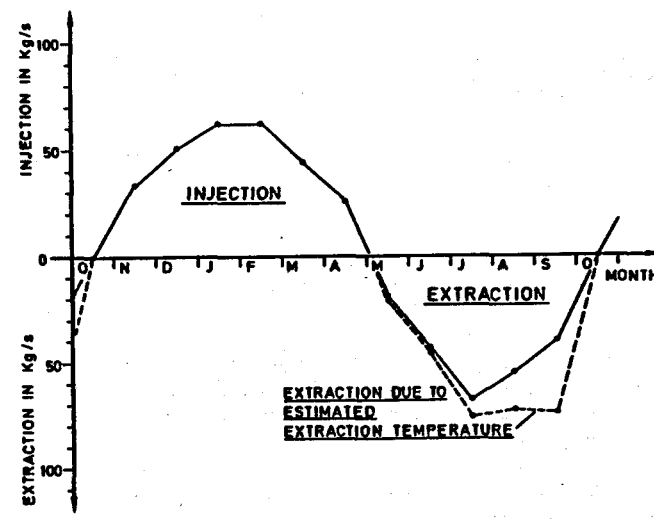

Figure 3. Calculated and estimated mass flow (first cycle). [XBL 808-11166]

In our calculations, 715.4 Gg water with a total cooling capacity of 18.03 TJ was injected during the period October 15 to April 30 and 566.3 Gg was extracted during the rest of the year to satisfy a total cooling demand of 9.06 TJ.

The horizontal extent of the vertically averaged temperature anomaly can be seen in Figure 4, in which the temperatures of the saturated zone are plotted against the radius from the storage well for several characteristic times. It is obvious that

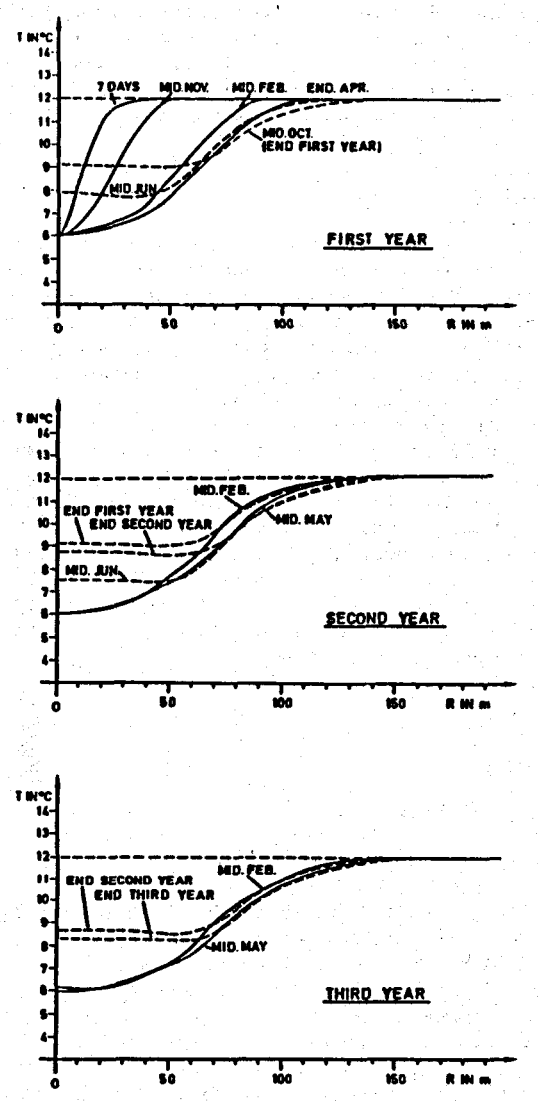

Figure 4. Average temperature of the aquifer versus radius. [XBL 808-11169]

the radius of the influenced area changes insignificantly after two or three injection/extraction cycles. Our results also indicate that, in spite of the low heat conductivity in the unsaturated zone, the temperature changes above the free surface are significant. The temperature gradients change both in magnitude and direction. The heat fluxes between the surface and deeper layers are interrupted, resulting in an overall decrease in the temperatures of the aquifer. Since the average temperature of the aquifer at the cold-water well differs little from that of the injected water, and since the temperature difference at the warm-water well is zero, it is expected that the two-well storage system described here would have minimal environmental effects.

Improving the system poses several problems. The cooling capacity is limited by the air temperatures and by the freezing point of the injected water, and can be increased only by injecting larger volumes of water. Another possibility is to optimize the cooling capacity input and output by adjusting the injection and extraction fluxes.

Improvements on the warm-water side are not so difficult, since there is sufficient distance to the boiling point. Rather than optimizing the cooling capacity, it would be simpler to raise the temperature of the injected water. The restriction of the available air temperature could be overcome by replacing the secondary heat exchanger with a solar collector. This, however, would produce significant changes in the natural groundwater temperatures in the saturated and unsaturated zones, and the environmental effects would have to be assessed.

Numerical models are invaluable tools for the calculating changes in the flow and temperature fields in the aquifer. They enable the designing engineer to evaluate the influences of the planned system on the environment. Numerical methods are also powerful tools for optimizing the recharge and discharge process. This optimization must take environmental requirements adequately into consideration.

The main uncertainties in the present study are found to be the heat transport in the unsaturated zone, effects of meteorological changes, and exact determination of the boundary conditions. A more detailed study of these problems is left for further investigation.

---

* Institut fur Wasserbau und Wasserwirtschaft, Rheinisch-Westfalische Technische Hochschule Aachen, Mies-van-der-Rohe-Str. 1, D-5100 Aachen, Federal Republic of Germany

STATE-OF-THE-ART MODELS FOR GEOTHERMAL RECOVERY PROCESSES

C. F. Tsang and J. S. Y. Wang

Geothermal reservoirs are sometimes classified into two categories on the basis of their fluid composition. The first category includes those that primarily produce steam. Examples are The Geysers in California, Larderello in Italy, and Matsukawa in Japan. Though such reservoirs have been used to produce steam and generate electricity for many years, they are relatively rare. The majority of geothermal reservoirs are in the second category--those whose fluid is predominantly water in the liquid phase. Hot-water reservoirs are known in New Zealand, Mexico, Iceland, El Salvador, and other countries. A few have been exploited for power production and several for space heating or industrial processing. Recently the U. S. Department of Energy (DOE) began a demonstration experiment in cooperation with industry at the Baca site in New Mexico, and a second DOE demonstration experiment has been under negotiation for the reservoir at Heber, California. Both these systems are considered to be liquid-dominated reservoirs. In many cases, as a hot-water reservoir is being produced and fluid pressure is reduced, the reservoir will turn two-phase. For example, this is believed to be the case in Wairakei, New Zealand.

With such interest and activities in geothermal energy development over the years, analytic and numerical models to simulate the system are quite well advanced. Much work has been done in this area, and many models were developed. However, there still remain key areas that require further understanding and study. Recent review papers include Wang, Sterbentz, and Tsang (1980), Pinder (1979), and Sudol, Harrison, and Ramey (1979). The last two papers include the results of work performed under the DOE Geothermal Engineering Management Program managed by the Lawrence Berkeley Laboratory (LBL).

KEY PROCESSES

The flows of fluid and energy are the key processes involved in geothermal reservoir engineering. Subsidence effects associated with depletion of reservoir fluid may also be important in some cases. Rock-fluid interaction and chemical transport and dispersion will be of significance, especially in reservoirs where water is or will be reinjected.

Fluid Flow

In geothermal reservoir engineering, Darcy's law is usually assumed, implying a laminar flow. This is reasonable for fluid flow in a porous medium or in tight fractures. The assumption will not hold for many wellbore fluid-flow problems. With the presence of heat, many parameters associated with fluid flow will be affected. Viscosity depends strongly on temperatures varying by a factor of 3 over a 200°C temperature difference for the liquid phase, and density varies by approximately 20%. These parameters will vary even more drastically when the two-phase condition sets in. Thus much of a reservoir's behavior will be outside the range of experience in isothermal hydrology or petroleum engineering. In the laboratory, the permeability of a rock sample has been shown to depend on temperature. Under reservoir conditions, however, the significance of this relation is not clearly understood, and in nearly all the geothermal models it has not been taken into account.

Energy Flow

The flow of heat takes place mainly by conduction and convection. Except for numerical problems, both transfer mechanisms are well understood in single-phase problems. For two-phase problems considerable work has also been done. However, much care has to be exercised in the modeling of boiling and natural convection, especially in the sensitivity of these phenomena on mesh choice (nonphysical) and on local geological inhomogeneity (physical). The geological inhomogeneity also induces thermal dispersion. This has been noticed in some experiments, but has not been properly understood and modeled. Another area requiring further study is the problem of fluid and heat flow in fractured rock masses. Though several authors have addressed the problem of isothermal fracture flow, a basic formulation of two-phase, two- or three-dimensional fracture-porous flow is still lacking.

Subsidence

With depletion of reservoir fluid, the pressure in the reservoir will decrease and the formation may deform under the overburden pressure. Land subsidence may thus occur. This has been observed in hydrology and petroleum production cases as well as at the Wairakei geothermal field. Much less work has been done in the modeling of this phenomenon. One liquid-phase model CCC assumes one-dimensional reservoir compaction based on the Terzaghi theory coupled with a deformable overburden model. It has been applied to simulate subsidence of systems similar to that at Wairakei. We are not aware of any two-phase models that calculate deformation simultaneously. Together with the lack of modeling, there is also a lack of understanding of the associated basic parameters, such as the elasticity-plasticity property and the effective-stress formulation.

Chemical Transport and Dispersion

A number of models have included simple solute transport and dispersion. The usual assumptions are that the solute moves with the fluid and that dispersive effects may be represented by a simple dispersive coefficient that is a linear function of velocity. Source and sink terms are also included in the models.

Chemical Reactions and Rock-Fluid Interactions

Scaling and corrosion are major problems in development and use of geothermal energy. Many experiments were made to study the chemical reactions of geothermal fluid with the well casing, fluid pipelines, and power generation systems. Empirical understanding and remedial procedures have been developed, but it may be difficult to model these phenomena in detail as a function of temperature, pressure, and time. Rock-fluid interaction may be important when cooled water, or water with a chemical composition different from the native water, is injected. Much work has been done in modeling chemical reactions. However, the modeling of coupled fluid flow and chemical reactions is still in a primitive state.

COMPARATIVE REVIEW OF MODELS

As discussed in the previous section, most of the models have been developed for fluid and energy flows. Some have included solute transport and dispersion. In this section we shall select a few key models for a comparative review to illustrate the present state of the art. This selection is not intended to be complete, but includes the models with which we have some familiarity. Analytic and zero-dimensional lumped models are not considered here.

Table 1 lists the models reviewed. The emphasis is on two-phase models, including those of Coats; Faust and Mercer; Pritchett and Garg; Pruess; Thomas and Pierson; Voss and Pinder; and Toronyi and Ali. There are many more single-phase models, but we have chosen only one for illustration. This is the model developed by Lippmann, which is one of the most well-validated and well-used single-phase nonisothermal models currently available. For fractured systems, the modeling of heat and fluid flow is still in an unsatisfactory state. One approach is the double-porosity model, in which two porosities simultaneously exist and interact with each other, one corresponding to the porosity of the unfractured rock mass and the other to the porosity of fractures. For this approach we have selected the one developed initially by O'Neill.

The main features of these selected models are summarized in Table 1, which indicates that many of them are three-dimensional models; the numerical approaches used include finite-difference, finite-element and integrated-finite-difference methods. Some characteristics of the governing equations of these models are compared in Table 2. The combinations of thermodynamic variables employed are pressure-temperature, pressure-enthalpy, or density-internal energy. Toronyi and Ali's model assumes as its variables pressure and vapor saturation, and is thus limited to the study of two-phase systems. In most of the two-phase models, similar approaches are used in the formulation of the governing equations, and they all assume the same relative permeability functions--Corey's formula. The relative permeability function of steam-water flow in porous media has not been well established. Most of the recent measurements were made at Stanford, and more work needed not only to obtain more measurements but also to improve our understanding of the physics of the phenomenon and its proper inclusion in numerical models.

Table 1. Summary of some of the models.

Model	Current development	Main characteristics
CCC	M. Lippmann, LBL	Flow-heat-consolidation, 3D, IFD, geothermal aquifer storage, waste isolation
O'Neill	K. O'Neill, CRRE A. Shapiro, Princeton	Flow-heat, double-porosity, 3D, FE, geothermal
Coats	K. Coats, Intercomp	Flow-heat, two-phase, 3D, FD, geothermal, petroleum
Faust-Mercer	C. Faust, J. Mercer, Geotrans	Flow-heat, two-phase, 3D, FD, geothermal
MUSHRM	J. Pritchett, S. Garg, S^3	Flow-heat-solute, two-phase, 3D, FD, geothermal, geopressure
SHAFT79	K. Pruess, LBL	Flow-heat, two-phase, 3D, IFD, geothermal, waste isolation
Thomas-Pierson	L. Thomas, R. Pierson, Phillips	Flow-heat, two-phase, 3D, FD, geothermal
Voss-Pinder	C. Voss, G. Pinder, Princeton	Flow-heat, two-phase, 3D, FD, geothermal
Toronyi-Ali	R. Toronyi, Chevron S. Farouq Ali, Alberta	Flow-heat, two-phase, 2D, FD, geothermal

Table 2. Governing equations.

Model	Variables	Fluid	Formation properties
CCC	P, T	Formula and tables	$\phi(\sigma - P)$ $k(\phi)$
O'Neill	P, T^f, T^m	Formula	ϕ^f, ϕ^m, k^f, k^m
Coats	P, T, or P, S	Formula and steam tables	$k_r = k_{rr}\bar{S}^n$
Faust-Mercer	P, H	Formula	Corey's k_r
MUSHRM	ρ, U	Formula	Corey's k_r
SHAFT79	ρ, U	Steam tables	Corey's k_r
Thomas-Pierson	P, T	Formula and steam tables	Corey's k_r
Voss-Pinder	P, H	Formula, or package	Corey's or Arihara's k_r
Toronyi-Ali	P, S	Formula	Corey's k_r

Table 3. Numerical methods.

Model	Upstream weighting	Implicit factor	Nonlinear coefficients	Matrix solver
CCC	$0.5 < a < 1$	$\lambda = 0, 0.5, 1$ (0.57 - 1.)		Direct (Duff)
O'Neill		$\lambda = 0.5, 1$		Direct (Eisenstat and Sherman)
Coats	$a = 1$	$\lambda = 1$	Newton-Raphson	Direct (Price and Coats)
Faust-Mercer	$a = 1$	$\lambda = 1$	Newton-Raphson	Direct (Price and Coats)
MUSHRM	$a = 1$	$\lambda = 1$	Newton-Raphson	Alternating direction implicit
SHAFT79	$0.5 < a < 1$	$\lambda = 1$	Newton-Raphson	Direct (Duff)
Thomas-Pierson	$a = 1$	$\lambda = 1$	Implicit pressure-explicit saturation	Direct (Price and Coats)
Voss-Pinder	Asymmetric weighting function	$0.5 < \lambda < 1$	Total increment method (semi-implicit)	Block interactive (BIFEPS)
Toronyi-Aji	$a = 1$	$\lambda = 1$	Newton-Raphson	Direct (Varga)

Table 3 compares the numerical methods used in the models. A major numerical problem encountered is the very nonlinear coefficients in the governing equations, especially in cases of phase transition. Most of the models use the Newton-Raphson method to overcome this problem. Table 4 summarizes the status of the computer codes and some key references.

A good model that can be used with some confidence requires proper validations against field data. Unfortunately not too many long-term case histories in geothermal energy development are available. In the United States, the major case history should be that of The Geysers geothermal reservoir. However, it is not in the public domain. So far the best available data are those from the Wairakei field in New Zealand. Data from Cerro Prieto, Mexico, and the Italian geothermal fields are also being compiled and organized and will be of considerable use in the validation of numerical models. Table 5 summarizes the field validation and applications of the major model selected for various applications. Obviously, more validations are needed, and further generic studies will be useful.

NEED FOR FURTHER STUDIES

As mentioned earlier, one of the major needs for further work is the validation of currently available models. Not only should they be validated against special cases where analytic solutions are available, but they should also be validated against field data. Another validation that should be done is to verify the models against each other. The Department of Energy (SAN office) has published a Request for Proposal (DOE, 1980) in which six problems are formulated and suggested for proposers to solve with their numerical models. The DOE hopes to make 6-12 awards for this work. Thus 6-12 models could be compared for consistency. No development work is expected under the guidelines of this request for proposal.

However, development and study are necessary for the further understanding and better simulation of geothermal reservoirs. Specific problems that merit further study are listed below under two categories: (a) conceptual models and physical formulation and (b) problems in constitutive equations and numerical solutions.

Problems in Conceptual Models and Physical Formulation

1. The conceptual models for most geothermal fields now being studied are generally well constructed. However, in many cases the fluid recharge and heat source are not well known. In general, boundary conditions are hard to determine. Sensitivity studies will be needed.

2. Many geothermal reservoirs, such as The Geysers and the Baca field, New Mexico, are fracture systems. However, basic formulation of heat and fluid flow in two- or three-dimensional fracture systems are still lacking. The relationships between the porosity of interconnected pore spaces and the porosity of fractures are not clear. Two approaches may be taken. The first considers discrete fractures and models the system in detail. This is possible only for systems that have a few major fractures. Otherwise the computational time becomes formidable. Furthermore, it is probably impossible to obtain such detailed fracture mapping in the field. A second approach is to "smear o[illegible] all the fractures into a secondary porosity in [illegible]tion to the porosity due to pore space. This double-porosity model has been formulated and constructed. Such averaging may not be valid, however, especially

Table 4. Computer codes.

Model	Code listing	Users manual	Computer systems	References
CCC	Yes	Yes	CDC, IBM	Lippman et al., 1977 Mangold et al., 1979 Bodvarsson et al., 1979
O'Neill	Yes	Yes	IBM	O'Neill, 1978
Coats	Intercomp			Coats, 1977 Coats et al., 1977
Faust-Mercer	USGS			Faust & Mercer, 1979a, b Mercer & Faust, 1979
MUSHRM	S^3			Pritchett et al., 1975 Garg et al., 1977, 1980
SHAFT79	Yes	Yes	CDC	Pruess et al., 1979a, b Pruess & Schroeder, 1979
Thomas-Pierson	Phillips			Thomas & Pierson, 1978
Voss-Pinder	Yes	Yes	IBM	Voss, 1978 Voss & Pinder, 1977
Toronyi-Aji	Penn State			Toronyi, 1974 Toronyi & Ali, 1977

near any point of observation which is strongly affected by nearby discrete fractures. A hybrid of the two may be the proper approach.

3. Tracer dispersivity has been much studied. However, thermal dispersion requires further study. The effect of molecular dispersion or fluid-path tortuosity dispersion is probably unimportant. The major part would probably be due to geological inhomogeneity. A proper formulation has to be made, and one should question the validity of the simple linear dependence of dispersivity coefficient on velocity.

4. The dependence of permeability on temperature also needs to be studied and understood.

Problems in Constitutive Equations and Numerical Solutions

1. Relative permeability curves for steam and water need to be better determined.

Table 5. Model field validation and applications.

Model	Field validations	Applications
CCC	Auburn, aquifer storage	Cerro Prieto, reinjection; generic studies: aquifer storage, geothermal, repository; well testing
O'Neill		Hot-water injection
Coats		Two-phase flow in fractures; convection
Faust-Mercer	Wairakei, geothermal	Steam near canister
MUSHRM	Wairakei, geothermal	Gulf Coast, geopressure; Salton Sea, precipitation
SHAFT79	Serrazzano, geothermal	Krafla, geothermal; reservoir depletion; Sandia, repository
Thomas-Pierson		Stanford depletion experiment; production studies
Voss-Pinder		Stanford depletion experiment; production studies
Toronyi-Aji		Production studies

2. Capillary effects and steam-water interface thermodynamics in two-phase systems should be understood.

3. Modeling of phase change, we believe, is still in an early stage of development.

4. Elasticity-plasticity behavior of the fractured-porous systems requires further investigation.

5. Modeling of coupled fluid flow and chemical reactions is still primitive.

6. Development of modeling methods for parameter uncertainties is needed to provide confidence limits for all the modeling results, even if the model is assumed to be mathematically correct.

Many other problems could be listed whose solutions will improve our modeling capability in geothermal reservoir engineering.

REFERENCES CITED

Bodvarsson, G. S., Lippmann, M. J., and Narasimhan, T. N., 1979. Recent modifications of the numerical code "CCC," in Earth Sciences Division Annual Report 1979. Berkeley, Lawrence Berkeley Laboratory, LBL-10686.

Coats, K. H., 1977. Geothermal reservoir modeling. Presented at the 52nd Annual Fall Technical Conference and Exhibition of the Society of Petroleum Engineers of AIME, Denver, Colorado, October 1977. SPE-6892.

Coats, K. H., Ramesh, A. B., and Winestock, A. G., 1977. Numerical modeling of thermal reservoir behavior. Oil Sands, p. 399-410.

Department of Energy, 1980. Request for Proposal No. DE-RP03-80SF10844 for "Geothermal reservoir engineering computer code comparison and validation," June 1980.

Faust, C. R., and Mercer, J. W., 1979a. Geothermal reservoir simulation: 1. Mathematical models for liquid- and vapor-dominated hydrothermal systems. Water Resources Research, v. 15, no. 1, p. 23-30.

____, 1979. Geothermal reservoir simulation: 2. Numerical solution techniques for liquid- and vapor-dominated hydrothermal systems. Water Resources Research, v. 15, no. 1, p.31-46.

Garg, S. K., Pritchett, J. W., Rice, M. H., and Riney, T. D., 1977. U.S. Gulf Coast geopressured geothermal reservoir simulation. La Jolla, California, Systems, Science and Software, SSS-R-77-3147.

Lippmann, M. J., Tsang, C. F., and Witherspoon, P. A., 1977. Analysis of the response of geothermal reservoirs under injection and production procedures. Presented at the 47th Annual California Regional Meeting SPE-AIME, Bakersfield, California, April 1977. SPE-6537.

Mangold, D. C., Tsang, C. F., Lippmann, M. J., and Witherspoon, P. A., 1979. A study of thermal effects in well test analysis. Presented at the 54th Annual Fall Technical Conference SPE-AIME, Las Vegas, Nevada, September 1979. SPE-8232.

Mercer, J. W., and Faust, C. R., 1979. Geothermal reservoir simulation: 3. Application of liquid- and vapor-dominated hydrothermal modeling techniques to Wairakei, New Zealand. Water Resources Research, v. 15, no. 3, p. 653-671.

O'Neill, K., 1978. The transient three-dimensional transport of liquid and heat in fractured porous media (Ph.D. thesis). Princeton, New Jersey, Princeton University, Dept. of Civil Engineering.

Pinder, G. F., 1979. State-of-the-art review of geothermal reservoir modeling. Berkeley, Lawrence Berkeley Laboratory, LBL-9093 (GSRMP 5).

Pritchett, J. W., Garg, S. K., Brownell, D. H., Jr., and Levine, H. B., 1975. Geohydrological environmental effects of geothermal power production, phase I. La Jolla, California, Systems, Science and Software, SSS-R-75-2733.

Pritchett, J. W., Rice, L. F., and Garg, S. K., 1980. Reservoir simulation studies: Wairakei geothermal field, New Zealand. La Jolla, California, Systems, Science and Software, SSS-R-80-4313.

Pruess, K., and Schroeder, R. C., 1979. Geothermal reservoir simulation with SHAFT79. Presented at the 5th Geothermal Reservoir Engineering Workshop, Stanford, California, 1979. Berkeley, Lawrence Berkeley Laboratory, LBL-10066.

Pruess, K., Schroeder, R. C., Witherspoon, P. A., and Zerzan, J. M., 1979a. SHAFT78, a two-phase multidimensional computer program for geothermal reservoir simulation. Berkeley, Lawrence Berkeley Laboratory, LBL-8264.

Pruess, K., Zerzan, J. M., Schroeder, R. C., and Witherspoon, P. A., 1979b. Description of the three-dimensional two-phase simulator SHAFT78 for use in geothermal reservoir studies. Presented at the Fifth Symposium on Reservoir Simulation, Denver, Colorado, 1979. SPE-7699.

Sudol, G. A., Harrison, R. F., and Ramey, H. J., Jr., 1979. Annotated research bibliography for geothermal reservoir engineering. Berkeley, Lawrence Berkeley Laboratory, LBL-8664 (GREMP-1).

Thomas, L. K., and Pierson, R. G., 1978. Three-dimensional geothermal reservoir simulation. Soc. Pet. Eng. J., April, p. 151-161.

Toronyi, R. M., 1974. Two-phase, two-dimensional simulation of a geothermal reservoir and the wellbore system (Ph.D. thesis). University Park, Pennsylvania, Pennsylvania State University. Petroleum and Natural Gas Engineering, Department of Mineral Engineering.

Toronyi, R. M., and Farouq Ali, S. M., 1977. Two-phase, two-dimensional simulation of a geothermal reservoir. Soc. Pet. Eng. J., June, p. 171-183.

Voss, C. I., 1978. Finite element simulation of multiphase geothermal reservoirs (Ph.D. thesis). Princeton, New Jersey, Princeton University, Department of Civil Engineering.

Voss, C. I., and Pinder, G. F., 1977. A block iterative-preprocessed technique for efficient finite element simulation of large non-linear problems. IMACS (AICA), p. 170-177.

Wang, J. S. Y., Sterbentz, R. A., and Tsang, C. F., 1980. The state-of-the-art of numerical modeling of thermohydrologic flow in fractured rock masses. Berkeley, Lawrence Berkeley Laboratory, LBL-10524.

BUOYANCY FLOWS IN FRACTURES INTERSECTING A NUCLEAR WASTE REPOSITORY

J. S. Y. Wang and C. F. Tsang

Heat released from a nuclear waste repository in a geological formation significantly increases the temperature of surrounding rock masses as well as the groundwater in the formations, inducing buoyancy fluid flow. An understanding of the resulting perturbation of the original regional hydrological pattern may be crucial in determining the performance of repositories in which nuclear waste materials are to be isolated from the biosphere.

In low-permeability crystalline rocks, such as granite, groundwater flow is mainly through fractures. In simulating regional flow, several authors have approximated the rock formation with models of porous media representing multiple fractures (Dames and Moore, 1978; Bourke and Hodgkinson, 1979; Burgess et al., 1979). In our study, we adopted a different approach. We assumed that several major fractures may be important and should be simulated in detail. This would be the case if there are natural faults near the repository or if sectionally connected fractures were present. Further, this kind of study may also be used to give a worst-scenario order-of-magnitude result which will provide guidance in our understanding of the problem.

Because of the slow decay of actinides in the nuclear waste and the low thermal conductivity of rocks, the thermohydrological impact of the repository is expected to persist for thousands of years after the emplacement of the wastes. Our simulations are carried out to 10,000 years.

MODEL IDEALIZATION

In our study, the nuclear waste repository is idealized to be a flat, circular disk with a given time-varying power density dependent on the particular form of nuclear waste stored. The repository is assumed to be 1500 m in radius and 500 m below the land surface. Only spent fuel waste is considered, and a surface cooling period of 10 years is arbitrarily taken from the time of discharge from a pressurized water reactor to burial in the repository. Nuclear waste density is adjusted so that the initial areal power density is 10 W/m^2. In Figure 1, a power decay curve for such a case is compared with a corresponding curve for reprocessed high-level waste.

Two types of fracture geometry are assumed. In the first, a single major fracture intersects the repository vertically so that the axis of the repository lies in the plane of the fracture. Recharge and discharge zones are assumed to be situated 5 km on either side of the repository. Studies were made of the thermally induced buoyancy flow in the fracture plane and of its interaction with the natural regional hydrostatic gradient from the recharge to the discharge zones. Three values of hydrostatic gradient were used: 0, i, and 4i, where i is a typical value given by

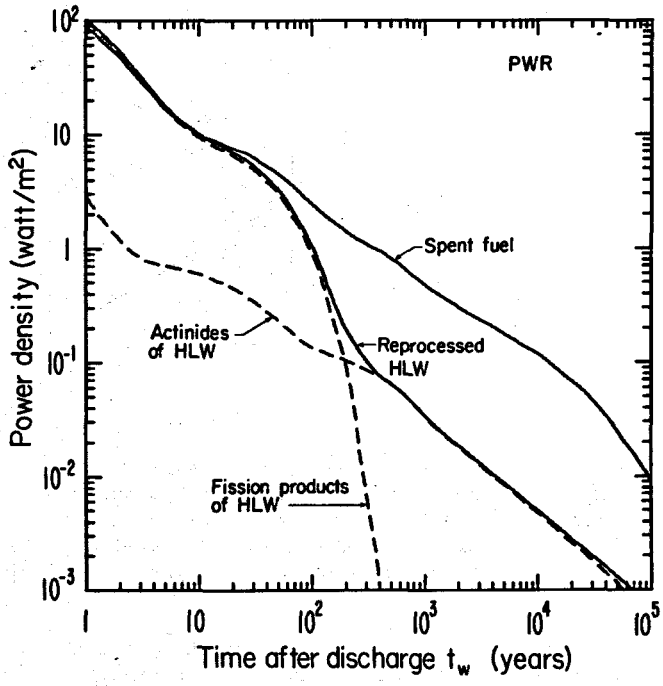

Figure 1. Areal power density of heat generated by the nuclear wastes stored in a repository.
[XBL 7810-11962]

$$i = 0.001 \text{ m/m}; \tag{1}$$

i.e., the water level in the recharge zone is 10 m higher than that in the discharge zone. For a fracture with aperture b = 1 μm and a corresponding "parallel-plate" permeability of

$$k = \frac{b^2}{12} = 8.33 \times 10^{-14} \text{ m}^2, \tag{2}$$

the initial horizontal flow velocity near the land surface (at 20°C) is found to be

$$v_o = \frac{k\rho g}{\mu} i = 8.11 \times 10^{-10} \text{ m/s} = 2.6 \times 10^{-5} \text{ km/yr}, \tag{3}$$

where ρ, μ, and g are, respectively, density, viscosity, and the gravitational constant. Results of flow velocities will be presented in units of v_o.

The second type of geometry studied consists of a two-fracture system. In addition to the fracture described for the first type, a second vertical fracture intersects the original fracture normally, either at the repository axis or at some distance from it. Figure 2 shows examples of intersection along the axis of the repository as well as intersection away from the axis. Studies were made on these models to understand the interaction, or interference, between two intersecting fracture

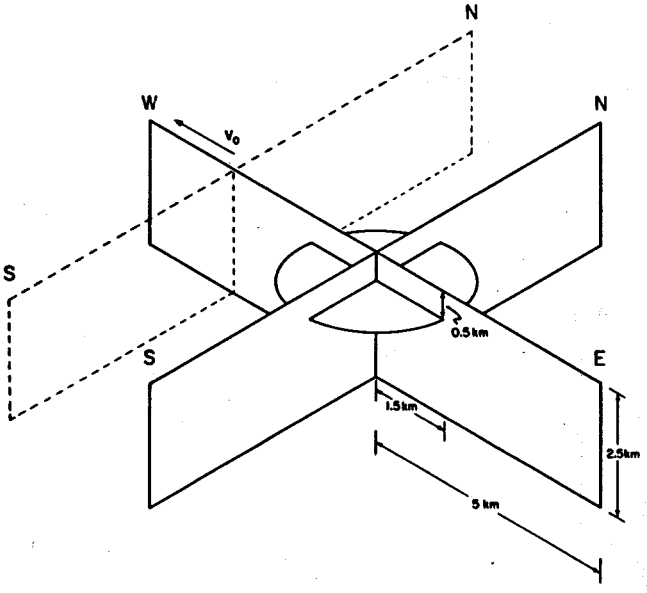

Figure 2. Geometry of two-fracture systems with the E-W fracture (along the regional hydraulic gradient) intersected normally by the N-S fracture at the repository axis (solid N-S fracture) or away from it (broken N-S fracture). [XBL 805-7061]

planes as a function of the intersection locations (one in the E-W direction and the other in the N-S direction).

In both sets of calculations, the upper boundary is maintained at a fixed temperature of 20°C. An ambient geothermal gradient of 30°C/km is assumed. The side boundaries (i.e., recharge or discharge boundary) of each fracture is maintained at hydrostatic pressure and ambient temperature. The lower boundary, at 2 km below the repository and 2.5 km below the land surface, is a no-flow (closed) boundary.

MATHEMATICAL APPROACH

The numerical model CCC, developed at Lawrence Berkeley Laboratory (Lippmann et al., 1977), was used to study the thermohydrological flow in the fractures. The program CCC (named for conduction, convection, and consolidation) uses an integrated-finite-difference scheme to compute single-phase mass and heat flow in a three-dimensional system in which effects of gravity- and temperature-dependent density and viscosity are included. The one-dimensional theory of Terzaghi is used in this program to calculate land subsidence or swelling. It has been well validated, having been verified against nine analytic or semianalytic solutions and one field experiment.

Because of the small volume of water present in the fractures (fracture aperture being only about a micron), the convective contribution to the thermal field is minimal and conduction is the main heat transfer mechanism. Thus the calculation may be carried out in two steps. Conduction calculations were made either by CCC or equivalently by a semianalytical program (Wang et al., 1979) to obtain the temperature field as a function of time. Then, using these results, convection in the fractures was calculated by CCC to obtain fluid velocities as a function of various key parameters. Fluid velocity is of course what is of particular interest in a waste isolation problem. Values of thermal conductivity for granite of 2.5 W/m/°C and thermal diffusivity of 1.15×10^{-6} m^2/s were chosen as inputs to our calculations.

Figure 3 displays the mesh design corresponding to one-half the fracture plane. It is structured to describe the best possible heat and flow gradients and to keep the elements to within a reasonable number to optimize computer cost.

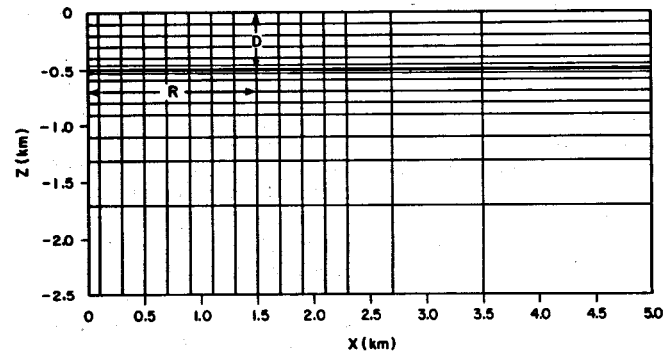

Figure 3. Mesh design corresponding to one-half of the fracture plane. [XBL 805-7062]

INTERACTION OF BUOYANCY FLOW AND REGIONAL FLOW

First let us discuss the temperature field as a function of time after waste emplacement in the repository. Figure 4 displays the temperature versus depth profile along the axis of the repository for different times after waste burial, the repository being assumed to be fully occupied by waste at t = 0. Before waste burial, the profile is a straight line representing a normal original geothermal gradient. The temperature rise is at first localized near the repository depth. After 1000 years, however, heat from the repository has reached the land surface and begun to leak out, and a linear temperature profile again prevails from the land surface to the repository. The vertical temperature gradients, both above and below the repository, drive the bouyancy flow. Radially, the temperature is fairly uniform within the boundary of the repository, beyond which the temperature decreases sharply.

To study the interaction of buoyancy flow and regional flow, a single major fracture through the axis of the repository is assumed. The thermally induced flow patterns within the fracture plane after 1000 years are shown in Figure 5 for a regional hydraulic gradient of zero. In this case, two symmetrical convection cells are developed around the edges of the repository. Heated water flows up from the central area of the repository, and water is drawn in both from the recharge zones, which are situated about 5 km from the repository center on

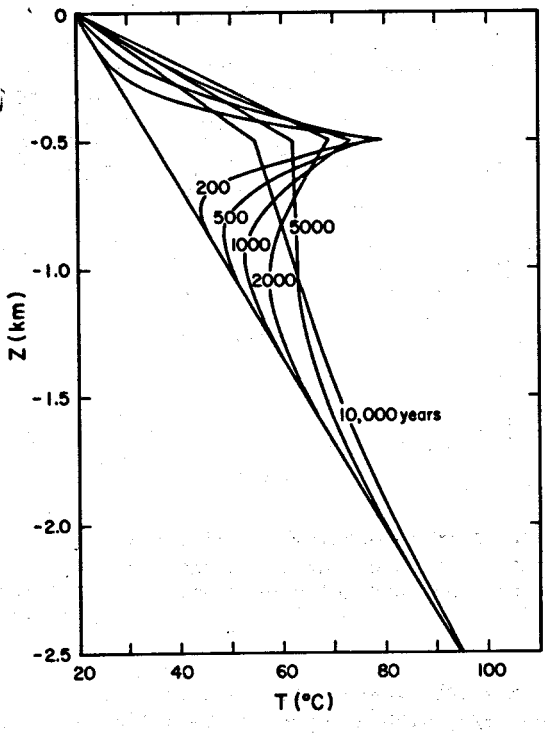

Figure 4. Temperature vs. depth profile along the axis of the repository for different times after waste burial. [XBL 805-7064]

opposite sides of the fracture, and from the ground surface far away from the center of the repository. It is to be noted that large convection cells (i.e., with diameters about equal to the repository depth) are induced during the life of the repository. This cannot be ignored in considering thermohydrological behavior around a repository.

Figure 6 shows the flow velocities at different times as a function of position on the land surface along the length of the fracture. Thus the relative magnitude of the vertical flow velocities

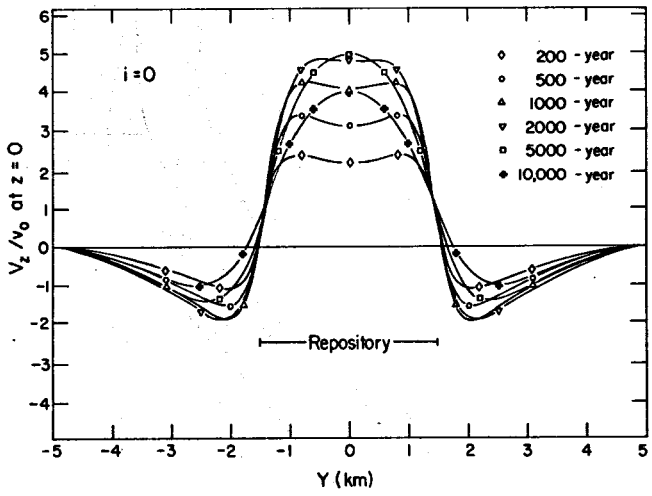

Figure 6. Surface outflow velocities along the length of the fracture at different times for the case of zero regional hydraulic gradient. [XBL 805-939]

near the land surface can be studied. It is seen that these outflow velocities at early times maximize at two symmetric off-center locations, a result of the convective fluid movements. At later times, however, the heat leakage at the surface interferes with the convective flow, and a central maximum develops. The vertical velocities for different times along the axis of the repository are shown in Figure 7. After the initial transient period, the vertical velocities above the repository are approximately independent of depth because of the surface constant-temperature constant-pressure boundary. The zero velocity at depth -2.5 km is due to the imposed no-flow boundary at that depth.

With the presence of a regional hydraulic gradient of i = 0.001 m/m, the flow patterns are distorted from the symmetric zero-regional-gradient results (Fig. 8). On the recharge side (i.e., the

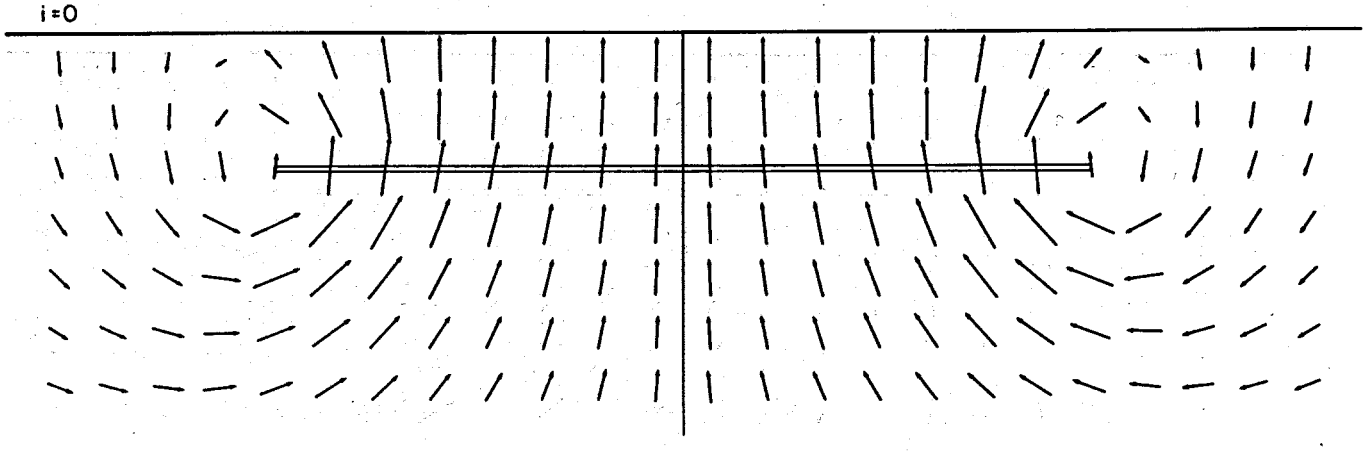

Figure 5. Thermally induced flow patterns within the fracture plane 1000 years after waste burial for the case of zero regional hydraulic gradient. [XBL 806-10034]

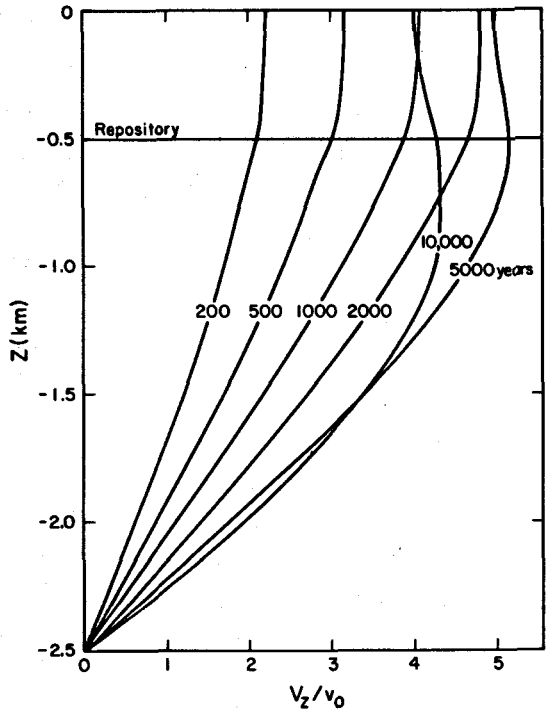

Figure 7. Vertical velocities along the axis of the repository at different times for the case of zero regional hydraulic gradient. [XBL 805-7063]

side with higher hydraulic head), the regional flow counteracts the horizontal convective movement above the repository. On the discharge side (with lower hydraulic head), the opposite effects occur. The influence of the regional flow on vertical outflow velocities along the length of the fracture is shown in Figure 9. Only a slight suppression of the vertical velocity on the recharge side and a slight increase on the discharge side are observed, indicating a weak coupling of buoyancy and natural regional flows. Results are also obtained for regional gradients of i = 0, 0.001, and 0.004 m/m

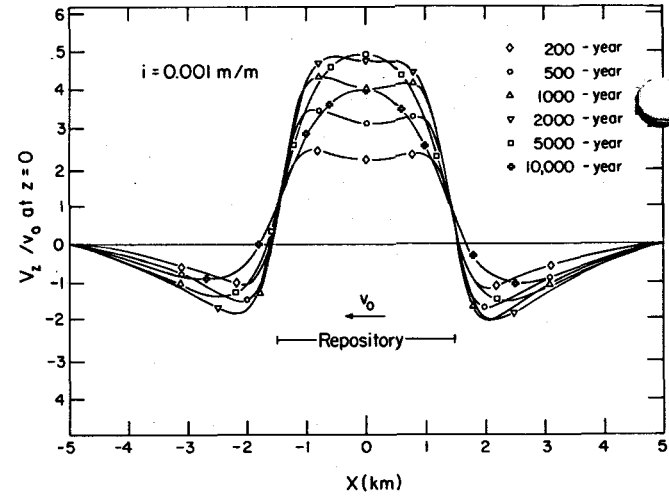

Figure 9. Surface outflow velocities along the length of the fracture at different times for the case of regional hydraulic gradient i = 0.001 m/m. [XBL 805-940]

at time t = 1000 years. The last case for i = 0.004 m/m, with a near-surface velocity of $4v_0$, is approximately equal in magnitude to the vertical outflow velocity at the repository epicenter.

EFFECTS OF FRACTURE-FRACTURE INTERACTION

To investigate the interaction of the buoyancy flows in two intersecting vertical fractures, the basic geometry is the same as that shown in Figure 2. A plane fracture in the E-W direction passes through the axis of the circular-disk repository with or without a regional hydraulic gradient along it. A second plane fracture in the N-S direction intersects the first fracture normally at the axis of the repository or at different distances away from it. This geometry is used to study the influence of the N-S intersecting fracture on the flow velocities in the first E-W fracture.

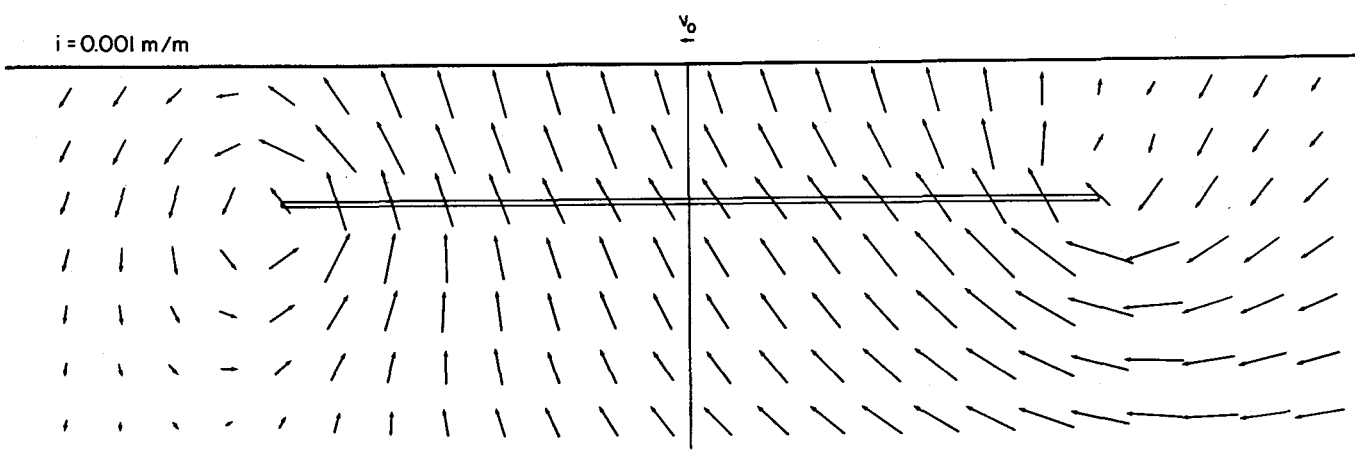

Figure 8. Thermally induced flow patterns within the fracture plane 1000 years after waste burial for the case of regional hydraulic gradient i = 001 m/m. [XBL 806-10035]

The first case considered is the intersection of the two vertical fractures at the axis of the repository (see Fig. 2). A regional hydraulic gradient of i = 0.001 m/m is imposed on the E-W fracture, with the recharge and discharge zones assumed to be at equal distance (5 km) on either side of the repository. The N-S fracture has zero regional gradient. With such a symmetrical geometry, but different regional flows in the two fractures, the interference is found to be negligible. Flow behavior in each fracture is the same as that in a single fracture. Thus the vertical outflow velocities along the E-W fracture and the N-S fracture are exactly the same as those shown in Figure 9 and Figure 6, respectively. Furthermore, the net recharges drawn from all four sides are equivalent.

However, if the E-W fracture is fixed (i.e., passes through the repository axis), significant interaction is noticed when the N-S fracture intersects the E-W fracture at locations away from the repository axis. Calculations were made for intersections at x = -800, -1500, and -2000 m from the repository axis, corresponding to locations within, at, and outside the repository radius. A regional hydraulic gradient is still maintained in the E-W fracture.

The case of x = -800 yields the results shown in Figure 10. The curves labeled E-W fracture (i.e., x-axis). The location at which the N-S fracture intersects it is indicated by the black dot. Thus the intersection point is off center on the x-axis in the E-W direction. The curves labeled N-S give the vertical velocities along the N-S fracture (i.e., y-axis). The black dot on these curves indicates the location at which it is intersected by the E-W fracture (x-axis). It is always at the point of symmetry in the y direction. In the xy-plane, the two black dots represent the same point and thus should have the same value for vertical velocity.

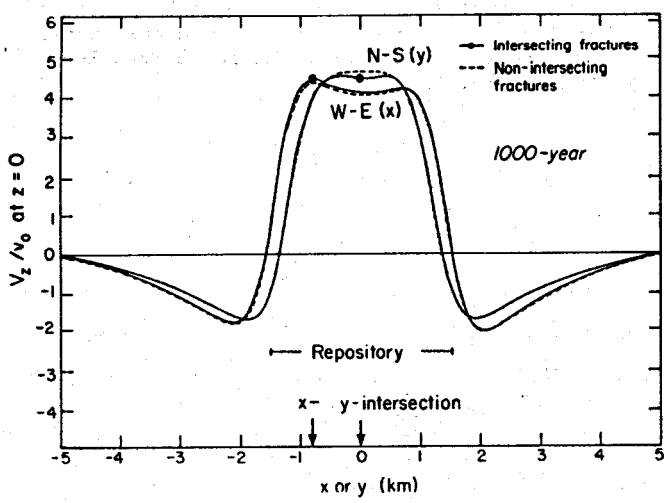

Figure 10. Surface outflow velocities at 1000 years along the length x of the E-W fracture and the length y of the N-S fracture. The fracture-fracture intersection is located at x = -800 m and y = 0 within the repository radius. [XBL 805-945]

The results for each fracture without the presence of the other are shown as broken lines. For the case of x = -800 m (i.e., intersection point within the repository radius), only minor interaction is noticed.

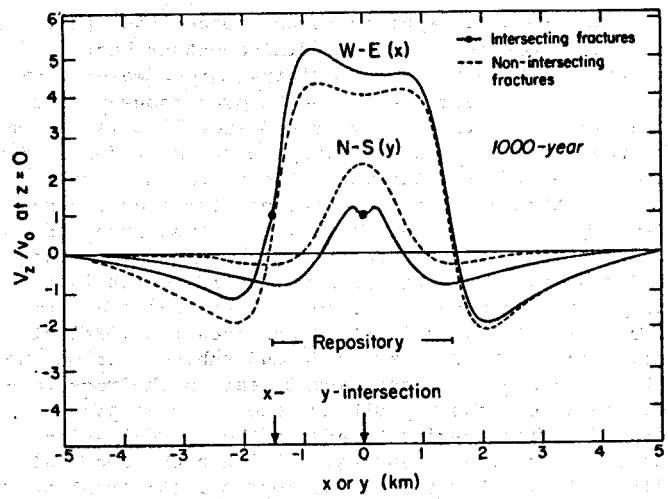

Figure 11. Surface outflow velocities at 1000 years along the length x of the E-W fracture and the length y of the N-S fracture. The fracture-fracture intersection is located at x = -1500 m and y = 0 through the rim of the repository. [XBL 805-944]

For the cases of x = -1500 m and -2000 m, corresponding respectively to intersection locations at the rim of the repository and outside the repository, there is much stronger interaction between the fracture flows. Results for the case of x = -1500 m are shown in Figure 11. This can easily be understood as follows. For the case of x = 0, the vertical flow velocities at the intersection point in either fracture in the absence of the other are equal, since, as shown in the previous section, effects of regional gradient on vertical velocities are negligible. Thus, when the intersection is made, no adjustments in flow velocity are necessary in the common location and the system behaves as independent fractures. On the other hand, for other values of x, the velocities at the interaction point in these fractures in the absence of each other would be quite different, since the temperature fields they experience are quite different. In general, the E-W fracture through the repository axis experiences a much higher temperature rise than the off-axis N-S fracture. Thus when intersection is imposed, fluid flow velocities make strong adjustments. Essentially, the N-S fracture acts as an additional recharge to the stronger flow velocities in the E-W fracture. This influences the convection pattern not only locally but globally over large distances.

DISCUSSION

The magnitude of the groundwater flow depends on the fracture system of the rock formation and the driving forces on the groundwater present.

The proper characterization of a fractured rock mass is site-specific and an outstanding problem of research. In our study we made considerable idealization so that we could focus on two important physical processes: (1) interaction between buoyancy flow and regional hydraulic gradient and (2) fracture-fracture interference.

The results reported in this paper show that the repository represents a finite-extent heat source which perturbs the original groundwater flow and induces convective movements over thousands of years. The nonisothermal groundwater flow is driven by the hydraulic gradient and the buoyancy force of the heated water relative to the surrounding colder water. Although the gravitational force acts vertically along the z-direction, the development of convective cells around the edges of the repository induces changes in the pressure field, which in turn couple to the natural horizontal regional gradient. The regional flow slightly suppresses the vertical movement on the recharge side and enhances it on the discharge side. As the wastes heat up the rock formation around the repository, the presence of the ground surface begins to affect the thermally induced convective movements. Although the regional flow only weakly affects the vertical component of the flow velocity, the addition of the regional horizontal component allows the water particles and radionuclei to flow through possibly longer paths. This, of course, may have important implications in the consideration of radionuclei-rock interactions, such as adsorption and dissolution.

The buoyancy flow depends strongly on the available recharge. Intersecting fractures may act as additional recharge paths from one to another with strong influence on fluid flow patterns. This demonstrates the need for careful considerations when studying single-fracture results.

Although the intersecting fracture model used in our analysis is very simple, it exhibits some of the same physical behavior shown by more complex fracture systems. This mode, complemented with porous-medium and other types of models, should provide insight into the dynamics of the thermohydrological flow in fractured rock masses.

ACKNOWLEDGEMENT

Discussions with P. A. Witherspoon, N. G. W. Cook and other colleagues at Lawrence Berkeley Laboratory and the University of California, Berkeley, are much appreciated.

REFERENCES CITED

Bourke, P. J., and Hodgkinson, D. P., 1979. Assessment of effects of thermally induced water movement on leakage from a radioactive waste depository. Workshop on Low-Flow, Low-Permeability Measurements in Largely Impermeable Rocks, OECD Nuclear Energy Agency, 1979, Paris, France.

Burgess, A. S., Charlwood, R. G., Skiba, E. L., Ratigan, J. L. , Gnirk, P. F., Stille, H., and Lindblom, V. E., 1979. Analysis of groundwater flow around a high-level waste repository in crystalline rock. Workshop on Low-Flow, Low-Permeability Measurements in Largely Impermeable Rocks, OECD Nuclear Energy Agency, 1979, Paris, France.

Dames and Moore, 1978. Technical support for GEIS radioactive waste isolation in geologic formations: Groundwater movement and nuclide transport. Oak Ridge, Tennessee, Office of Waste Isolation, Y/OWI/TM-36/21.

Lippmann, M. J., Tsang, C. F., and Witherspoon, P. A., 1977. Analysis of the response of geothermal reservoirs under injection and production procedures. Presented at 47th Annual California Regional Meeting of the Society of Petroleum Engineers of AIME, Bakersfield, California. SPE-6537.

Wang, J. S. Y., Tsang, C. F., Cook, N. G. W., and Witherspoon, P. A., 1979. A study of regional temperature and thermohydrological effects on an underground repository for nuclear wastes in hard rock. Berkeley, Lawrence Berkeley Laboratory, LBL-8271.

PROBABILISTIC SIMULATION OF TRANSIENT GROUNDWATER FLOW: AN ALTERNATIVE TO THE MONTE CARLO SCHEME?

T. N. Narasimhan, T. E. Buscheck, and P. A. Witherspoon

The use of predictive models for effective management of hydrogeologic systems is now widely recognized. Among these models, numerical methods have become especially well established because of their generality and power. The Reservoir Engineering Group of the Earth Sciences Division has developed several numerical computer codes for mass and energy transport in geologic systems. These include TERZAGI (isothermal, saturated flow with subsidence); TRUST (isothermal, saturated-unsaturated flow with subsidence); CCC (nonisothermal, single-phase flow with subsidence), and SHAFT79 (nonisothermal, two-phase flow). Powerful though they are, these models are of a deterministic nature. That is, they accept as inputs, parameters that are assumed to be known with certainty. The outputs from these models also possess the same certainty as the inputs. Despite the fact that these models are internally self-consistent, they are, in reality, subject to a limitation that transcends their logic. This limitation relates to the fact that the model inputs, which seek to characterize natural field systems, are seldom known with certainty. The uncertainty of field parameters stems from a variety of causes, including inadequacy of sampling, spatial variability of geologic features, and last, but not least, the scale of observation.

The problem of uncertainty has come into ever-increasing focus within the past five years or so, and there is a serious desire to input model parameters as probabilistic quantities and obtain outputs in the form of mean values with associated estimates of variances from the mean. Presumably such an output will greatly help in optimal decision making. The desire to incorporate uncertainty into models is particularly strong in approaching the problem of long-term disposal of radioactive wastes in geologic repositories.

The most widely followed method for incorporating uncertainty into deterministic subsurface fluid flow models is the so-called Monte Carlo method. This is a brute-force method in which each parameter is repeatedly sampled from its probabilistic structure to make large numbers of deterministic runs with the sampled quantities. The model outputs so obtained should give the probabilistic structure of the output. Obviously, the greater the number of sample runs, the better is the probabilistic structure of the output. Moreover, it should also be expected that if one is interested in the probabilistic structure about the mean value, the Monte Carlo simulation will require fewer sample experiments than if one were interested in extreme events governed by the "tails" of the input distributions. In the latter case, the Monte Carlo scheme could become extremely laborious.

Hence it appears desirable to look for a method that provides an alternative to the Monte Carlo scheme. Preliminary work on such a method was initiated during fiscal 1979 (Narasimhan and Buscheck, 1979), when the theoretical basis of the method was carefully examined. Basically, the method consists in replacing arithmetic operations on numbers with arithmetic operations on probability distributions. The logic for such operations is derived directly from the axiomatic foundations of probability theory.

Accomplishments During 1980

On the basis of favorable indications of the preliminary work, the necessary computer subroutines for handling probability arithmetic were generated and incorporated into an explicit version for program TERZAGI, which is an integral finite-difference method (IFDM) (Narasimhan and Witherspoon, 1976). This program solves the transient groundwater flow equation (based on principles identical to those of the heat conduction equation) in one, two, or three dimensions. During fiscal 1980, the modified TERZAGI called PROGRES (acronym for PRObabilistic GRoundwater EquationS) was developed and verified against results from Monte Carlo simulations available from the literature. In addition, a new two-dimensional problem was studied, the results of which were filed as a dissertation in partial fulfillment of the degree of Master of Science at the University of California, Berkeley (Buscheck, 1980).

The Logic

Consider two discrete probabilistic quantities A and B, each described by a histogram with a given number of bars, $i = 1, 2, 3, \ldots, I$. With each bar in the histogram is associated a magnitude $M(A_i)$ and its associated probability $P(A_i)$, $i = 1,2,3,\ldots, I$. Similarly, we shall have $M(B_i)$ and Pb_i. Obviously,

$$\sum_{i=1}^{I} P(A_i) = \sum_{i=1}^{I} P(B_i) = 1. \qquad (1)$$

The problem now is to find the discrete probabilistic structure (histograms) of the output C when A and B are added, subtracted, multiplied, or divided. We shall use the symbol $\bullet$ to denote, in general, any one of the four arithmetic operations.

Note that because of their probabilistic nature, any one of the magnitudes of A can occur simultaneously with any one of the magnitudes of B. Since there are I possibilities of each, the resulting quantity will have I^2 possibilities. Let this quantity be temporarily denoted C':

$$M(C'_{ij}) = M(A_i) * M(B_j), \quad i = 1, 2, 3, \ldots, I \quad j = 1, 2, 3, \ldots, I. \qquad (2)$$

It can be seen from (2) that the probability that event $M(C_{ij})$ will be realized depends on the simultaneous occurrence of the events $M(A_i)$ and $M(B_j)$. Axiomatically, this is the product of the probabilities associated with $M(A_i)$ and $M(B_j)$. Hence

$$P(C'_{ij}) = P(A_i) \times P(B_j). \tag{3}$$

Since each A_i can occur in conjunction with each B_j, there will be I^2 events of C, so that

$$\sum_{i=1}^{I} \sum_{j=1}^{I} P(C'_{ij}) = 1.0. \tag{4}$$

In so far as our input quantities are characterized by I discrete values, we shall need the final output C to be characterized also by I discrete values, whereas the temporary output C'_{ij} has I^2 discrete values. We therefore need to collapse C'_{ij} into C_i. In order to achieve this, we divide the interval between $M(C'_{ij})_{min}$ and $M(C'_{ij})_{max}$ into I equal subintervals. The mean magnitude $M(C_i)$ associated with the ith interval can be defined either as the midpoint of the interval, as has been done here, or as an average of all the events falling within the interval, weighted according to their probabilities. Thus

$$M(C_i) = \frac{\left[\sum_{j=i}^{I} P(C'_{ij})\, M(C'_{ij})\right]}{\sum_{i=j}^{I} P(C'_{ij})}. \tag{5}$$

Once again, we conclude from the axioms that $P(C_i)$ is equal to the sum of the probabilities of all the events occurring in the ith interval. Thus

$$P(C_i) = \sum_{j=i}^{I} P(C'_{ij}). \tag{6}$$

In order to implement the algebra of distributions into any numerical model such as TERZAGI--in which one has to operate on several probability quantities such as hydraulic conductivity, specific storage or fluid potential, taken two at a time--one first has to generate the array

$$C'(ij, ij) = (C'(M(C'_{ij}), P(C'_{ij})) \tag{7}$$

using equations (2) and (3). Next the C' array has to be collapsed into the C array by

$$C(i, i) = C(M(C_i), P(C_i)) \tag{8}$$

using equations (5) and (6). In the program PROGRES, (7) is implemented in subroutine PRODIST while (8) is implemented in subroutine COLAPSE. Thus, whenever one has to operate on distributions A and B, each with I discrete values, one simply enters PRODIST with the arrays A, B, and I, and the output is the array C'. One then calls subroutine COLAPSE, which takes in array C' and generates array C.

Now consider the explicit form of the transient groundwater equation (Narasimhan and Witherspoon, 1976),

$$\Delta\phi_\ell = \frac{\Delta t}{V_\ell S_s} \sum_{\ell m=1}^{M} U_{\ell m} \left(\phi_m^o - \phi_\ell^o\right), \tag{9}$$

where $\Delta\phi_\ell$ is the average change in potential over volume element ℓ; Δt is the size of the explicit time step subject to appropriate restrictions; V_ℓ is the volume of element ℓ; $S_{s\ell}$ is the specific storage of the material in ℓ; $U_{\ell m}$ is the conductance of the interface between elements ℓ and m, defined by

$$U_{\ell m} = \frac{K_{\ell m} \Delta\Gamma_{\ell m}}{D_{\ell m}}, \tag{10}$$

where $K_{\ell m}$ is the mean hydraulic conductivity at the interface, $\Delta\Gamma_{\ell m}$ is the area of the interface; and $D_{\ell m}$ is the distance between the nodal points ℓ and m; ϕ_ℓ^o and ϕ_m^o are the fluid potentials at P and m during the commencement of time step Δt; and m = 1, 2, ..., M denotes the volume elements communicating with element ℓ.

We now wish to compute $\Delta\phi_\ell$ in a probabilistic fashion, given the probabilistic distributions of $U_{\ell m}$, d_m^o, d_ℓ^o, and $S_{s\ell}$ and assuming that the geometric quantities V_ℓ, $\Delta\Gamma_{\ell m}$, and $D_{\ell m}$ are known exactly. In order to do this, we proceed in the following order, going through subroutines PRODIST and COLAPSE at each stage (M and P denote magnitudes and probabilities, respectively):

1. $\phi_m^o(M, P) - \phi_\ell^o(M, P) = \Delta\phi_{\ell m}(M, P)$,

2. $U_{\ell m}(M, P) \times \Delta\phi_{\ell m}(M, P) = F_{\ell m}(M, P)$,

3. $(((F_{\ell 1} + F_{\ell 2}) + F_{\ell 3}) + F_{\ell 4} + \ldots) = H_\ell(M, P)$,

4. $\dfrac{H_\ell(M, P)}{S_{s_\ell}(M, P)} = G_\ell(M, P)$,

5. $\dfrac{Wt}{V_\ell} G_\ell(M, P) = \Delta\phi_\ell(M, P)$.

In the above, $F_{\ell m}$, H_ℓ, and G_ℓ are intermediate arrays.

In developing PRODIST and COLAPSE, the algebra of distributions was first investigated carefully for distributive, associative, and commutative laws of operation. The details are given in Buscheck (1980). One of the basic aims in developing the aforesaid subroutines was to have them in a modular form so that they could be incorporated easily into any deterministic model.

RESULTS

The obvious first task after constructing PROGRES is to verify its practicality. Because of their very nature, however, probabilistic models do not have unique solutions. The output generated is, in a sense, an estimation of chance, and this estimate can vary somewhat between the logics involved in handling discrete quantities in the input as well as the output data. Hence the best that one can do in verifying the model is first to make sure that the computations are internally consistent and second to solve problems already solved by the Monte Carlo technique. We have done both.

In our work, we chose to verify the one-dimensional transient groundwater flow problem already studied by Freeze (1975). Our investigations have shown that there is reasonable agreement with Freeze's Monte Carlo results at early times but that there were some disagreements at late times as well as for steady state. It is not immediately clear whether the discrepancy is inherent in the different logics of the algorithms or whether we did not carry the computations for a sufficient number of cycles. It should be noted here that TERZAGI solves the steady-state problem by letting the transient problem go to a steady state over a large number of cycles, whereas the Monte Carlo method solves the steady-state problem via a one-step matrix solution. Another interesting observation deserving mention is that even after a large number of cycles, we could not get true steady state in our calculations. Instead, we obtained oscillations about an approximate mean value. Is it possible that in a truly probabilistic model of diffusion there cannot be a unique steady state?

For purposes of illustration, we give the following sample results.

One-dimensional Steady-state Flow

Consider a 100-cm column divided into 10 volume elements, each 10 cm wide. At one end of this column, ϕ is maintained at a value of 100 cm; at the other, ϕ is 0. Using PROGRES we solve the problem as a transient one, eventually attaining steady state. We start with the inital condition that everywhere within the column ϕ is about 5 cm more than the deterministic steady-state solution. Two cases were considered. In both cases, the mean value of hydraulic conductivity was 1.0, and the specific storage was arbitrarily held constant since the steady solution is independent of specific storage. But the standard deviation, K_{STD}, was 0.5 and 0.25 in the two cases.

The variation of the potentials at the end of 780 explicit time steps is given in Figure 1, along with an error bar indicating one standard deviation. A similar solution for $K_{STD} = 0.25$ is given in Figure 2. Figure 3 shows the probabilistic distribution of ϕ at two points in the column, one 5 cm from the zero-boundary-condition end and the other 55 cm from the same end after 780 time cycles. The pattern scan in this figure is qualitatively very similar to that obtained by Freeze (1975).

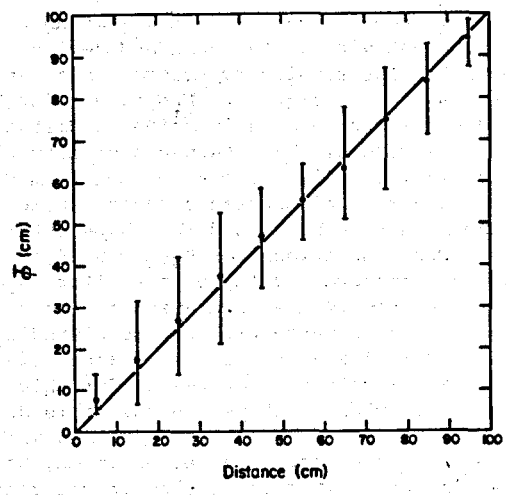

Figure 1. One-dimensional steady-state problem, $K_{STD} = 0.5$. Profile of ϕ with standard deviation. [XBL 805-809]

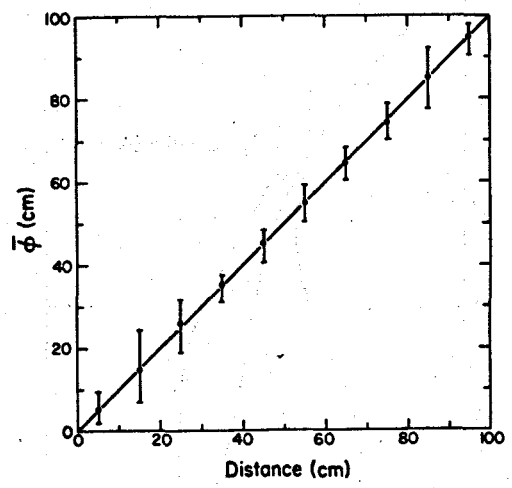

Figure 2. One-dimensional steady-state problem, $K_{STD} = 0.25$. Profile of ϕ with standard deviation. [XBL 805-817]

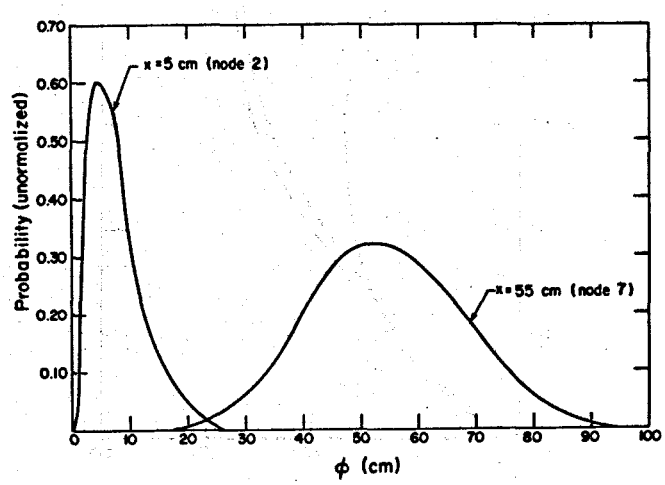

Figure 3. One-dimensional steady-state problem, $K_{STD} = 0.5$. Probability distribution of ϕ at two points in the column. [XBL 805-812]

The influence of the standard deviation of hydraulic conductivity on the standard deviation of the output ϕ was studied by Freeze for several values of K_{STD} (σ_y in Fig. 4). His values for the standard deviation of ϕ as a function of distance are given in Figure 4. We obtained a similar plot for $K_{STD} = 0.5$ (Fig. 5). As can be seen from Figure 5, as the number of transient cycles is increased the results tend toward the shape obtained by Freeze. Our simulations for $K_{STD} = 0.25$ (Fig. 6) show that the standard deviation is smaller toward the center than toward the boundaries of the column. This result is at variance with Freeze's findings that the standard deviation of ϕ increases toward the center of the column. The reason for this disagreement is not clear. It may be that this difference is intrinsic to the present algorithms as opposed to the Monte Carlo scheme, or it may be that in a time-probabilistic simulation the concept of steady state is not well defined. Further study seems warranted.

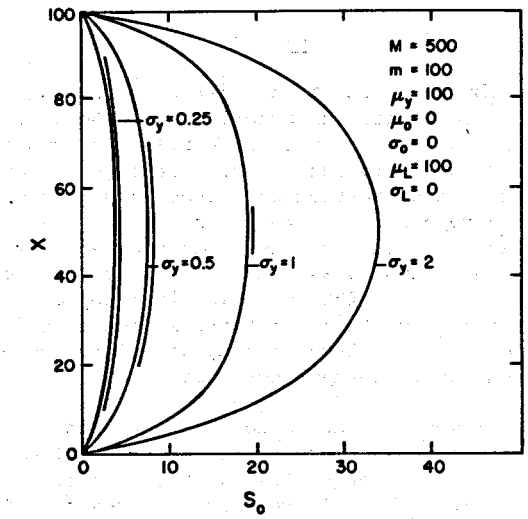

Figure 4. One-dimensional steady-state problem. Standard deviation of ϕ as a function of distance for various values of standard deviation of hydraulic conductivity (σ_y) (after Freeze, 1975). [XBL 805-825]

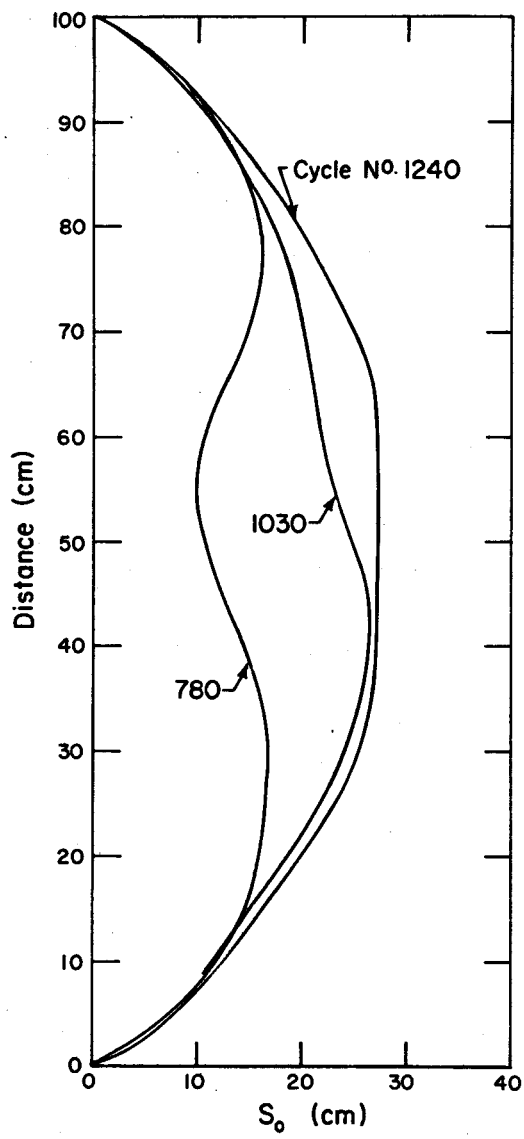

Figure 5. One-dimensional steady-state problem. Standard deviation of ϕ versus distance for $K_{STD} = 0.5$ at various time cycles. [XBL 805-804]

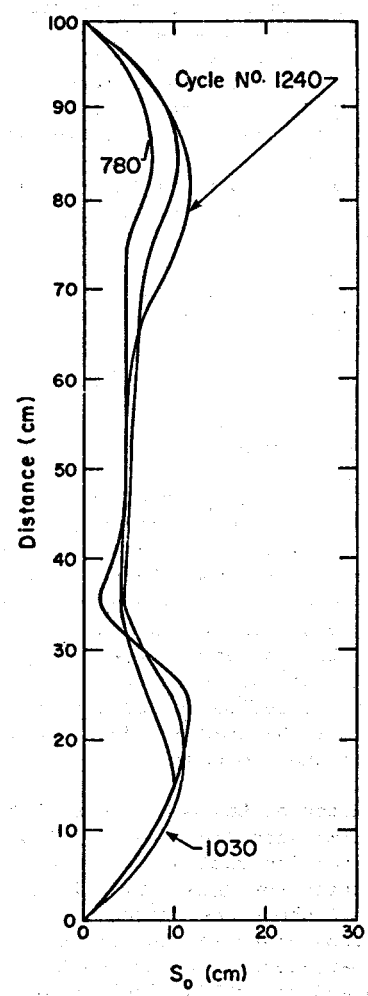

Figure 6. One-dimensional steady-state problem. Standard deviation of ϕ versus distance for $K_{STD} = 0.25$ at various time cycles. [XBL 805-805]

One-dimensional Transient Flow

Freeze (1975) also studied the transient problem of a darkly draining 100-cm column with an initial ϕ = 100 cm everywhere in the column draining at a constant ϕ = 0 at the ends. His results for $K_{STD} = \sigma_y = 0.5$ and 0.25 are given in Figure 7. We solved a similar problem for a 200-cm column, but actually considered only one-half the column symmetry considerations. For $K_{STD} = 0.5$, the variation of $\bar{\phi}$ as a function of distance is given in Figure 8. This result is very similar to Freeze's result and indicates the general pattern that the mean potential in a probabilistic simulation will lag behind the corresponding deterministic solution in time. However, we found a rather marked departure from Freeze's observation in regard to the spatial variation of the standard deviation of ϕ. Note from the upper right plot of Figure 7 that at early times the standard deviation is higher toward the boundaries. As time progresses, the standard deviation at the center exceeds that toward the boundary. The spatial dependence of standard deviation for $K_{STD} = 0.5$ as obtained in our study is given in Figure 9. This plot will qualitatively correspond to the lower half of the upper right-hand plot in Figure 7. By comparing Figures 7 and 9, it can be seen that in our case the standard deviation at the center of the column (toward X = 100 cm) never exceeds that toward the margin. Whether more simulations at more than 1000 cycles will give agreement with Freeze's findings is not clear. On the other hand, we may also recognize one important difference between our algorithms and the Monte Carlo algorithm. In the Monte Carlo algorithms, it is possible to sample the parameters and run through

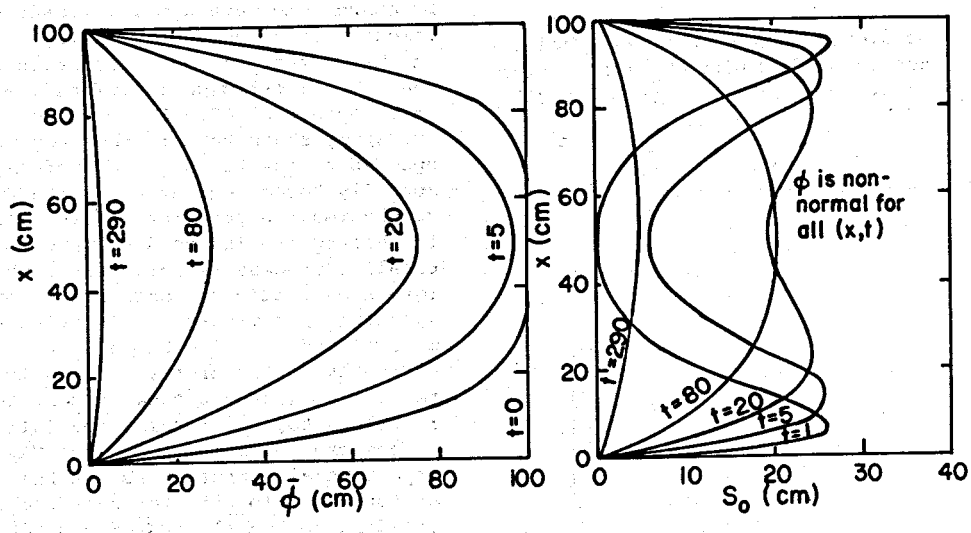

Output plots of $\phi(x,t)$ and $S_o(x,t)$ for $\sigma_y = 0.50$.

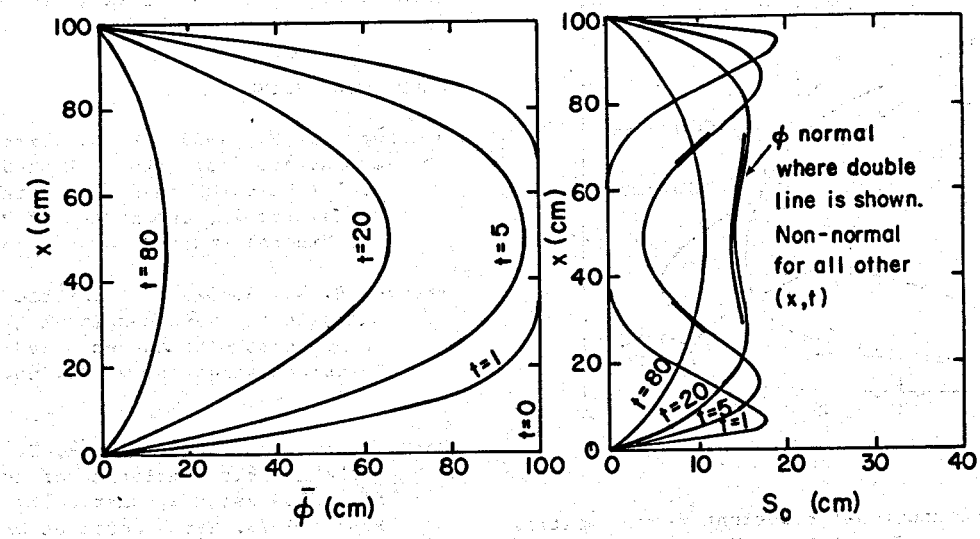

Output plots of $\phi(x,t)$ and $S_o(x,t)$ for $\sigma_y = 0.25$.

Figure 7. One-dimensional transient flow. Variations of $\bar{\phi}$ and standard deviation versus distance for $K_{STD} = 0.5$ and $K_{STD} = 0.25$ (after Freeze, 1975).
[XBL 805-828]

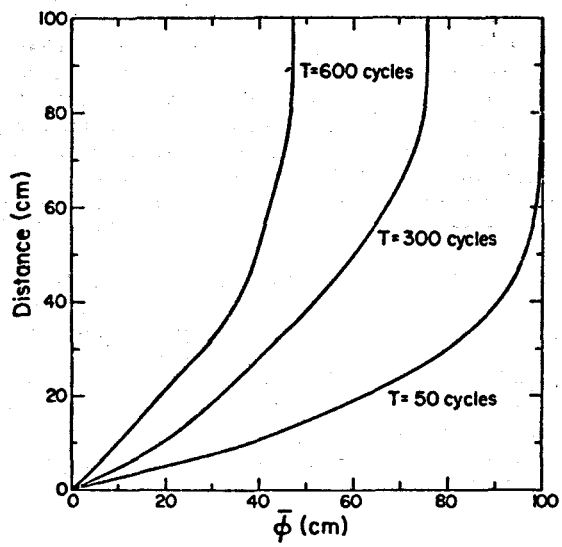

Figure 8. One-dimensional transient flow. Variation of $\bar{\phi}$ as a function of distance at various time cycles for K_{STD} = 0.5. [XBL 805-815]

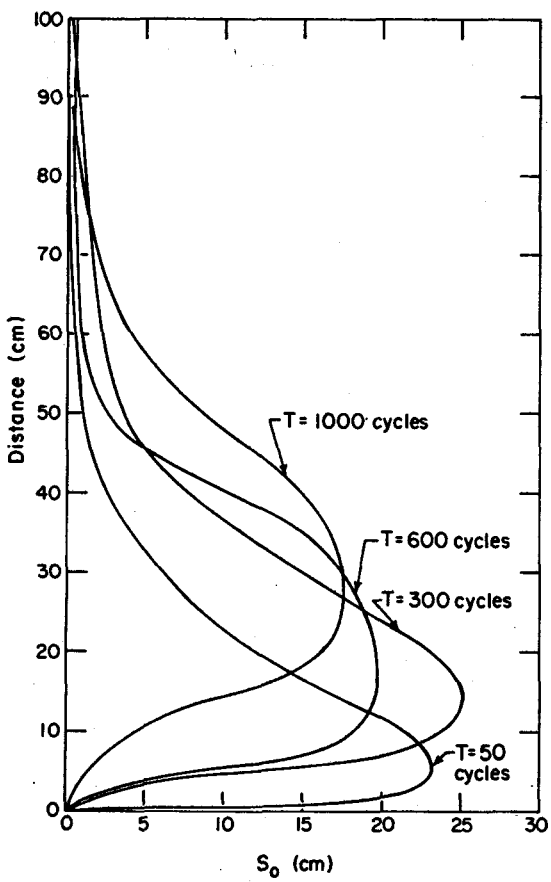

Figure 9. One-dimensional transient flow. Spatial variation of standard deviation of ϕ at various times for K_{STD} = 0.5. [XBL 805-810]

the whole transient process with the chosen samples. Or, one may carry out the sampling for every time step. Obviously the second procedure will require substantial computational effort. We are not sure exactly how Freeze made his calculations, but the algorithms presented in this work are tantamount to considering the probabilities of every transient time-step calculation. All that can be said at present is that further studies are required to understand the process better.

In addition to the above, we also studied certain new problems not already considered in the literature. These included one-dimensional steady and nonsteady flow in a heterogeneous medium and two-dimensional nonsteady flow in a heterogeneous medium. For want of space, we shall not consider them here. Instead, the reader is referred to Buscheck's thesis.

FURTHER WORK

A serious limitation of the algorithms we used is that a simple arithmetic operation is replaced by cumbersome matrix multiplication as well as operations involving the collapsing of matrices. Done in the conventional mode of sequential computation, the probabilistic calculations are very tedious even on the powerful CDC 7600 machine. Nevertheless, our study shows that if the computations can be speeded by one to two orders of magnitude, it may actually become competitive with the Monte Carlo simulation. A most interesting recent development in this regard is the development of the so-called parallel processors which can simultaneously perform a multitude of noncoupled operations, thereby speeding up computations in certain kinds of mathematical models. The Earth Sciences Division is currently in the process of acquiring a VAX computer for dedicated usage. A computer manufacturer in Palo Alto, California, specializes in parallel processors compatible with the VAX machine. Experimental computations are being carried out at LBL and Palo Alto to check the feasibility of speeding up the algebra of distributions using parallel processors. During fiscal 1981, the feasibility of using parallel processors will be further investigated.

REFERENCES CITED

Buscheck, T. E., 1980. Probabilistic simulation of subsurface fluid flow: A study using a numerical scheme (MS thesis). Berkeley, University of California, Department of Materials Science and Mineral Engineering.

Freeze, R. A., 1975. A stochastic-conceptual analysis of one-dimensional groundwater flow in nonuniform homogeneous media. Water Resources Research, v. 11, no. 5, p. 725-741.

Narasimhan, T. N. and Buscheck, T. E., 1979. Probabilistic simulation of transient subsurface flow using a numerical scheme. Annual Report 1979, Earth Sciences Division, Berkeley, California, Lawrence Berkeley Laboratory, LBL-10686.

Narasimhan, T. N. and Witherspoon, P. A., 1976. An integrated finite difference method for fluid flow in porous media. Water Resources Research, v. 12, no. 1, p. 57-64.

NUMERICAL SIMULATION OF FRACTURED POROUS MEDIA AS MULTIPLE INTERACTING CONTINUA

T. N. Narasimhan

Interest in studying the hydrogeology of fractured rock systems has increased considerably within the past few years in connection with the geological disposal of radioactive wastes. From a predictive point of view, the mathematical modeling of fractured rock systems can be approached from three different perspectives, depending on the scale of modeling. The first of these is the discrete fracture approach in which fractures and discontinuities, and intervening rock blocks are all modeled individually. This approach, which is generally considered to be essential for the near-repository region, is limited by its excessive data requirement and computational detail. The second approach is to treat the fractured system as an equivalent porous medium. A limitation of this approach is that no satisfactory technique is as yet available to evaluate large-scale equivalent permeabilities of low-permeability fractured rocks. Yet this is generally taken to be the most realistic way of handling regions far away from the repository. The third approach takes an intermediate position. Originally proposed by Barenblatt et al. (1960) in the Soviet Union, this approach consists of lumping all the fractures into one equivalent continuum, all the porous blocks into another continuum, and letting the two continua interact hydraulically. The fractured continuum is characterized by high permeability and low storage, and the rock continuum is characterized by low permeability and high storage. Hence, in a transient situation the fractured continuum controls early-time response of the system while the late-time behavior is controlled by the matrix continuum, through a process of "delayed drainage." This approach is mathematically analogous to the idealized behavior of unconfined aquifers proposed earlier by Boulton (1954). The interacting continuum approach has found considerable attention in the petroleum engineering literature, in which it is occasionally known as the "double-porosity" concept.

The double-porosity concept has been extensively used to derive analytic solutions (e.g., Streltsova, 1976) and numerical simulations (e.g., Warren and Root, 1963; Duguid and Lee, 1977). Recent examination of the partial differential equations governing the interacting continuum approach has indicated that this approach is indeed contained as a subset within the Integrated Finite-Difference Models (IFDM) (Narasimhan and Witherspoon, 1976) currently used extensively in the Earth Sciences Division for isothermal and nonisothermal multiphase flows. Indeed, it appears that restating the interacting continua approach in terms of integrals rather than in the classical differential equation format not only leads to a much cleaner, simpler statement of the problem but also suggests the possibility of extending the idea to numerically viable multiple interacting continua.

These ideas were presented in a recent workshop conducted at LBL for the Office of Nuclear Waste Isolation and are included in two forthcoming publications (Narasimhan, 1980a, b). This report briefly summarizes the basic concepts involved and a few new results obtained with computer program TERZAGI.

THEORY

Conceptual Framework

The basic law of mass conservation is applicable to any elemental volume ℓ of the flow region, whether that elemental volume constitutes a portion of a fracture, a portion of the rock matrix, or even a combination of both. According to the law of mass conservation, the algebraic sum of the fluxes crossing the surface-enclosing volume element and the arbitrary withdrawal of fluids from ℓ (the sources) equals the rate of change of fluid mass in ℓ. Thus

$$\rho_\ell G_\ell + \int_{\Gamma_\ell} \rho K \vec{\nabla}\phi \cdot \vec{n} d\Gamma = \frac{\partial M_{w,\ell}}{\partial t}, \tag{1}$$

where ρ_ℓ is average fluid density within ℓ; G_ℓ is the volumetric rate of fluid generation from ℓ; ρ is the fluid density at $d\Gamma$; K is the hydraulic conductivity at $d\Gamma$; $\phi = z + \psi$ is the fluid potential, where z is elevation and ψ is pressure head; $\vec{n}$ is the unit outernormal to $d\Gamma$; $M_{w,\ell}$ is the mass of water contained in ℓ; and Γ_ℓ is the closed surface bounding the volume element ℓ. Should the system be fully saturated with water, and should the fluid potential vary smoothly over the volume element, then $M_{w,\ell}$ can be related to the average pressure head $\bar{\psi}_\ell$ at an interior nodal point in the system by the relations

$$M_{w,\ell} = M^{\circ}_{w,\ell} + (dM_{w,\ell}/d\psi_\ell)\bar{\psi}_\ell \tag{2}$$

and

$$dM_{w,\ell}/d\psi_\ell = V_\ell \rho_\ell S_{s,\ell}, \tag{3}$$

where $M^{\circ}_{w,\ell}$ is the mass content of ℓ at $\bar{\psi}_\ell = 0$, V_ℓ is the volume of ℓ, and $S_{s,\ell}$ is the specific storage of the material in P, given by

$$S_{s,\ell} = \rho_\ell g(n\beta + m_{v,\ell}), \tag{4}$$

where g is the acceleration due to gravity, n is the porosity, β is the compressibility of water, and $m_{v,\ell}$ is the coefficient of volume change (rate of change of bulk volume with external pressure) of

the material in element ℓ. Additionally, if we neglect time-dependent changes in elevation of the nodal points due to very small deformations, then, $\Delta\bar{\psi}_\ell = \delta\bar{\phi}_\ell$. Moreover, Γ_ℓ may either be completely interior to the flow region ($\Gamma_{\ell,i}$) or portions of it may coincide with the external bounding surface of the system ($\Gamma_{\ell,b}$). Hence we may rewrite (1) as

$$\rho_\ell g_\ell + \int_{\Gamma_{\ell,i}} \rho K \vec{\nabla}\phi \Gamma \cdot n d\Gamma + \int_{\Gamma_{\ell,b}} \rho K \vec{\nabla}\phi \cdot n d\Gamma = M_{c,\ell} \frac{\partial \phi_\ell}{\partial t} , \qquad (5)$$

where $M_{c,\ell} = dM_w/d\psi$ is the fluid mass capacity of the volume element ℓ, defined as the change in mass of water in ℓ due to a unit change in head under conditions of drainage. In heat-flow problems, the analogous quantity is the heat capacity of an arbitrary mass of material. Note that in (5) the second integral on the right-hand side incorporates the known boundary conditions either in the form of known ϕ (prescribed potential condition) or in the form of known $k\nabla\phi\vec{n}$ (prescribed flux condition). That is, (5) embeds the boundary condition into the conservation statement.

For purposes of numerical computations, one may use the following discretized form of (5),

$$\rho_\ell G_\ell + \int_m \rho_{\ell m} K_{\ell m} (\vec{\nabla}\phi \cdot \vec{n}) \nabla\Gamma_{\ell m} + \int_b \rho_{\ell b} K_{\ell b} (\vec{\nabla}\phi \cdot \vec{n}) \nabla\Gamma_{\ell b} = M_{c,\ell} \frac{\Delta\phi_\ell}{\Delta t} , \qquad (6)$$

in which m denotes all interior surface segments and b denotes all exterior surface segments. Note that (6) applies to any arbitrary volume element and hence is an invariant statement. As shown in Figure 1, (6) may be applied to a portion of a fracture or a portion of a porous medium. When (6) is applied to a fracture (Fig. 1B), then for the segment of Γ_ℓ that represents the fracture-rock interface ($\Delta\Gamma_{f,r}$ in Fig. 1B) one has to use $K_{f,r}$ in applying (6), where $K_{f,r}$ is the hydraulic conductivity of the rock-fracture interface. It is of interest to note here that in the double-porosity model, the flux across this surface is treated as a source term included in G_ℓ. This source term is the internal boundary condition linking the fissure regime and the porous regime. Thus, in the double-porosity model, the term ($\rho_\ell K_{\ell m} \vec{\nabla}\phi \cdot n d\Gamma$) for the fracture-rock interface is replaced by an equivalent term $\rho_\ell \alpha^* K_m(\phi_m - \phi_\ell)$, where ϕ_m is the average potential in the block, ϕ_ℓ is the potential in the fracture, $K_{\ell m} = K_m$ in the matrix hydraulic conductivity, and a^* is a function of the surface area of the fracture interface and a characteristic length of the block. As we shall see later, the model described here is flexible enough to deal with either of the two methods of handling the rock-fracture interface.

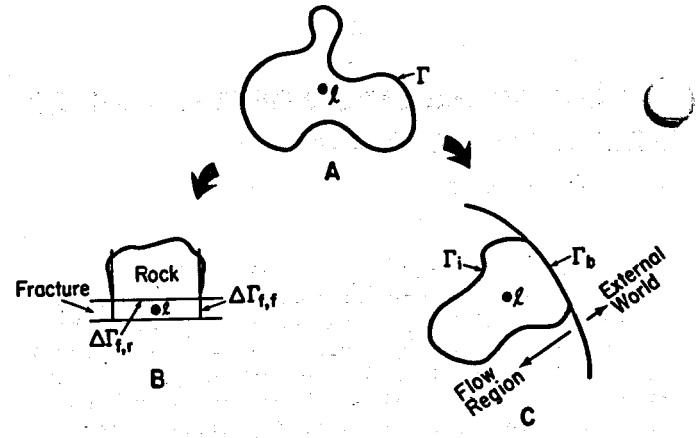

Figure 1. Examples of volume elements, nodal points, and bounding surfaces. [XBL 807-7236]

In the present work, we shall implement the discretized equation (6) by means of the Integral Finite-Difference Method (IFDM). The IFDM algorithm has already been published elsewhere (Edwards, 1972; Narasimhan et al., 1978).

Computer Programs

The basic IFDM model was originally developed by Edwards for heat transport with conduction, convection, and radiation and was incorporated into a program called TRUMP. Subsequently, this model was adapted at the Lawrence Berkeley Laboratory to solve fluid-flow problems in porous media. These programs include: TRUST, for solving saturated-unsaturated flow in deformable media (Narasimhan et al., 1978); TERZAGI, for saturated flow in deformable media; CCC, for heat and water transport in deformable media (Lippmann et al., 1977); and SHAFT79, for two-phase transient flow of heat and mass (Pruess and Schroeder, 1977). The following discussions about simulation of fractures are applicable to all the aforesaid programs subject to suitable modifications. However, the actual applications that follow have been carried out with TERZAGI.

Systems Idealized by Double Porosity

It is perhaps best to discuss the relation of the double-porosity model to a simple idealized system of horizontal fractures as shown in Figure 2. Consider a system of I horizontal fractures with spacing S. The thickness, H, of this system is given by H = (I + 1)S. It is clear that in this system water moves horizontally in the fractures and drains vertically from the intervening blocks to the fractures bounding the matrix. We will now replace this system by two interacting continua, each of thickness H, one representing the flow phenomenon in the fractured milieu; the other, that in the matrix milieu. Obviously, the fracture continuum is characterized only by horizontal flows and the matrix continuum only by vertical flows.

If we assume that flow in the fracture obeys the cubic law, then the total horizontal flux in the horizontal direction in the layer equals I times the flux in each fracture. We may therefore define the

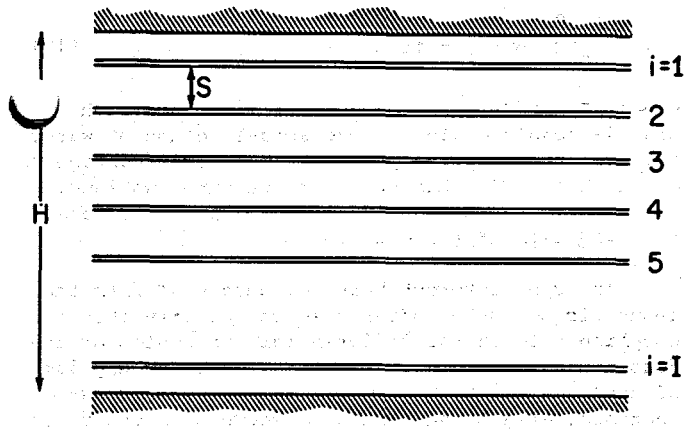

Figure 2. System of horizontal fractures in a permeable medium. [XBL 809-2844]

average hydraulic conductivity, K_f^*, of the fracture continuum by

$$K_f^* = \frac{I(2b)^3 \rho g}{12\mu H} . \tag{7}$$

Similarly, if $S_{s,f}$ is the storativity for one fracture, then $S_{s,f}^*$, the average storativity for the fracture continuum, is

$$S_{s,f}^* = \frac{I[S_{s,f}(2b)]}{H} . \tag{8}$$

Since the fracture aperture is far smaller than the fracture spacing, $K_r^* \approx K$ and $S_{s,r}$, where K_r^* and $S_{s,r}^*$ are the average hydraulic conductivities and storativities of the rock continuum.

Consider an area A_f at the interface between a fracture and an adjoining matrix block. The flux from the block to the fracture is given by

$$Q_{f,r} = \frac{K_r A_f}{0.5S} (\phi_r^* - \phi_f^*) , \tag{9}$$

and the total flux from blocks to fractures is given by $IQ_{f,r} = (IK_r A_f/0.5S)$. In (9), ϕ_r^* and ϕ_f^* are average potentials in the element of each continuum.

If we consider two volume elements at a given location, one in the fracture continuum and one in the porous continuum, each element having an area of cross section A_f and height H, then $V_f^* = V_m^* = A_f H$. For each of these volume elements we may now write conservation equations for the fracture continuum element,

$$\int_\Gamma (\rho K_f^* \nabla \phi_f^* \cdot \vec{n} d\Gamma) + \frac{\rho I K_r A_f}{0.5S} \cdot (\phi_r^* - \phi_f^*)$$

$$= \rho_f V_f^* S_{s_f}^* \frac{\partial \phi_f^*}{\partial t} , \tag{10}$$

and for the rock continuum element,

$$-\frac{\rho I K_r}{0.5S} A_f (\phi_r^* - \phi_f^*) = \rho_m V_r^* S_{s_r} \frac{\partial \phi_r^*}{\partial t_r} . \tag{11}$$

Noting that $V_r^* = V_f^* = A_f H$ and dividing through by V_f^* in (10) and V_r^* in (11) and letting the elements tend to zero in the limit, we now obtain the differential equation

$$-\text{div}\ \rho K_f^* \nabla \phi_f^* + \alpha K_m^* (\phi_m^* - \phi_f^*)$$

$$= S_{s,f}^* \frac{\partial \phi_f^*}{\partial t} - \rho \alpha K_r^* (\phi_r^* - \phi_f^*) \tag{12}$$

$$= S_{s,r}^* \frac{\partial \phi_r^*}{\partial t} , \tag{13}$$

where

$$\alpha = \frac{I}{0.5SH} = \frac{2}{S^2} .$$

Since H = IS, we see that α is obviously a factor controlled by the spacing and the specific surface of the rock blocks. Note also that in the fracture continuum water flows within the continuum as well as across an imaginary interface to the matrix continuum. Hence (12) has a source term as well as a divergence term on the left-hand side. However, it is assumed that, because of the strong permeability contrast between the fracture and the blocks, flow of water within the blocks is restricted to lines normal to fracture-block interfaces. Hence in (13) the divergence term is absent.

In view of (10) and (11), we may now proceed to apply (6) to a double-porosity system. First, we discretize the flow region into subdomains $\ell = 1, 2, 3, \ldots, L$ to represent the elements of the fracture continuum, with K_f^* and $S_{s,f}^*$ defined as in (7) and (8). For each of these subdomains we shall provide all required input data, such as G_ℓ, interior connection data, exterior connection data, and bulk volumes so that one equation such as (6) can be developed for each of the L elements. Simultaneously, we assume that at the location of each $\ell = 1, 2, 3, \ldots, L$ fracture-continuum element there exists a matrix-continuum element $j = 1, 2, 3, \ldots, L$ such that $V_\ell = V_i$ for $\ell = j$. In order to couple the two continua, we will now connect, for each $\ell = j$, the fracture-continuum element ℓ with the matrix-continuum element j in such a fashion that the conductance $U_{\ell,j}$ is given by

$$U_{\ell,j} = \frac{I\rho K_r^* \Delta\Gamma_{\ell,j}}{d_{j,i}} = \frac{I\rho K_r^* A_f}{0.5S} = \rho V_r \alpha K_r^* = \rho V_r \alpha K_r^* . \tag{14}$$

We thus obtain conservation equations for 2L volume elements in all, with one equation for each fracture-continuum and matrix-continuum element. Note that the time constant for the respective elements are given by

$$\Delta t_{stab,\ell} = \frac{V_f S^*_{s,f}}{\int_m U_{\ell,m} + \int_j U_{\ell,j}} \tag{15}$$

where ℓ, m are fracture continuum elements, j is a matrix continuum element, and $j = \ell$; and by

$$\Delta t_{stab,j} = \frac{V_m S^*_{s,m}}{U_{\ell,j}}, \tag{16}$$

where j is a fracture-continuum element, ℓ is a matrix-continuum element, and $j = \ell$.

Since the IFDM is so structured that the geometric quantities ($\Delta\Gamma_{\ell,m}$ and $D_{\ell,m}$) needed for computing the conductances are directly provided as input data, the handling of $V_r\alpha$ needed as input for computing $U_{\ell,j}$ in (16) poses no special problem. Moreover, since the 2L simultaneous equations are formulated, they can be solved by the mixed explicit-implicit method. Indeed, since the double-porosity model gives rise to a stiff matrix (because of the marked differences in the time constants between the fracture-continuum elements and the matrix-continuum elements), the mixed explicit-implicit method is particularly desirable for solution.

A DOUBLE-POROSITY PROBLEM

The illustrative problem is concerned with a fractured system idealized as an equivalent system of two interacting continua. To provide a physical feel for the illustration, we shall consider a system of 10 horizontal fractures, each with a uniform aperture of 10^{-4} m and separated by matrix slabs 1 m in thickness. The aggregate thickness of the rock and fracture is 10 m. If the cubic law is assumed, each fracture has an absolute permeability of $k_f = 8.333 \times 10^{-10}$ m^2. But if we assume that the combined effect of the fractures can be replaced by a fracture continuum 10 m thick, then the equivalent permeability of the fissured continuum amounts to $k^*_f = 8.333 \times 10^{-14}$ m^2. Similarly, if the fracture compressibility is assumed negligible, the specific storage of the fracture continuum is approximately $S^*_{s,f} = 1 \times 10^{-9}$/m of water. It is reasonable to assume that the permeability of the matrix may be smaller than k^*_f by one to three orders of magnitude or more, and a value of 10^{-5}/m is reasonable for the specific storage of the rock, $S_{s,r}$.

Let us now consider the mechanics of fluid transfer between the fissures and the matrix continua. Obviously, in the actual problem, water will drain vertically from the matrix slab upward and downward into adjoining fractures, with the centerline of the slab forming a line of symmetry. If we consider a thin prism of a matrix slab with cross-sectional area A, then the amount of water draining from a slab to one adjoining fracture is given by

$$Q_{f,r} = \frac{k_r \rho g}{\mu} \cdot A \cdot \frac{\psi_r - \psi_f}{D_{f,r}} \tag{17}$$

$$= \frac{k_r \rho g}{\mu} \alpha^* (\psi_r - \psi_f), \tag{18}$$

where $\alpha^* = A/D_{f,r}$ and $D_{f,r} = 0.5$ m. Since each slab is doubly draining, the actual volume of water transfer from a given prism of the matrix continuum of thickness H to the prism of fracture continuum at the same location is 20 times $Q_{f,r}$ and is equal to $(k_m \rho g/\mu)(20\alpha^*)(\psi_r - \psi_f)$.

It is of interest here to compare α^* with the geometric parameter often used to quantify the coupling term in the differential expression of the double-porosity model. For this, consider a prism of each medium at the same location, with cross-sectional area A and height H, where H is the thickness of the media. Then, if we normalize α^* with reference to bulk volume, we get a volume-normalized parameter related to α. That is, α has a dimension of reciprocal area and in the present case α is related by 1/(S)(H).

In order to solve this interacting-continua problem using TERZAGI, a problem that has been studied by Barenblatt et al. (1960), Warren and Root (1963), Odeh (1965), and many others, was chosen. The problem involves a well piercing the fractured-continuum that is areally infinite. The well is produced at a constant rate Q. As has been done by Warren and Root (1963), this problem can be analyzed in terms of four dimensionless groups,

$$T^*_{D_f} = \frac{k^*_f \rho g t}{S^*_{s,f} \mu r_w^2}, \tag{19}$$

$$P^*_{D_f} = \frac{2Tk^*_f \rho g \Delta\psi}{Q\mu}, \tag{20}$$

$$\lambda = \alpha r_w^2 \frac{k_r}{k^*_f}, \tag{21}$$

and

$$\omega = \frac{S^*_{s,f}}{S^*_{s,f} + S_{s,r}}. \tag{22}$$

Using TERZAGI, a number of runs were made to study the effect of varying λ, ω, and the magnitude of wellbore storage capacity. In addition, one run was made with a spatially varying k^*_f to consider the "skin effect" near the wellbore as well as increased fracture intensity beyond about 110 m from the well axis. The results are summarized in three double-logarithmic plots (Figs. 3-5).

In Figure 3 the double-porosity results are compared with the Theis solution for three values of λ. Increasing λ implies increasing matrix permeability. In the numerical model, a well of 0.[illegible] radius was assumed. In one case, in order to approximate the line-source solution, the well was assumed to be packed-off, and hence deriving stora-

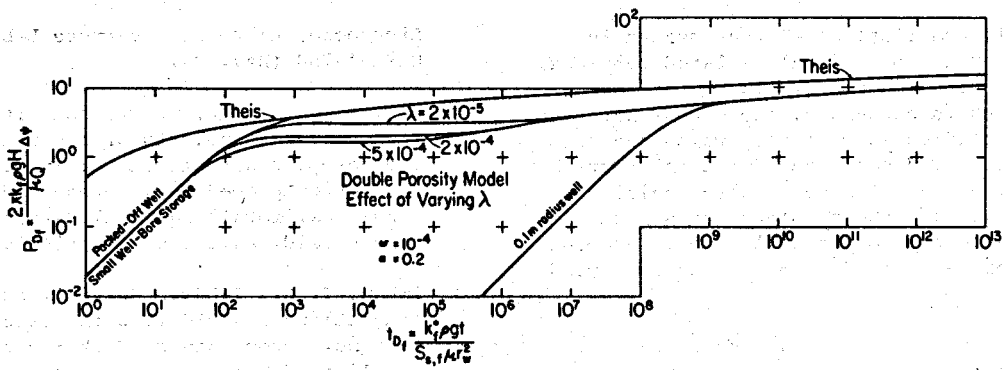

Figure 3. Simulation of a double-porosity medium. Effect of varying λ. [XBL 8010-2849]

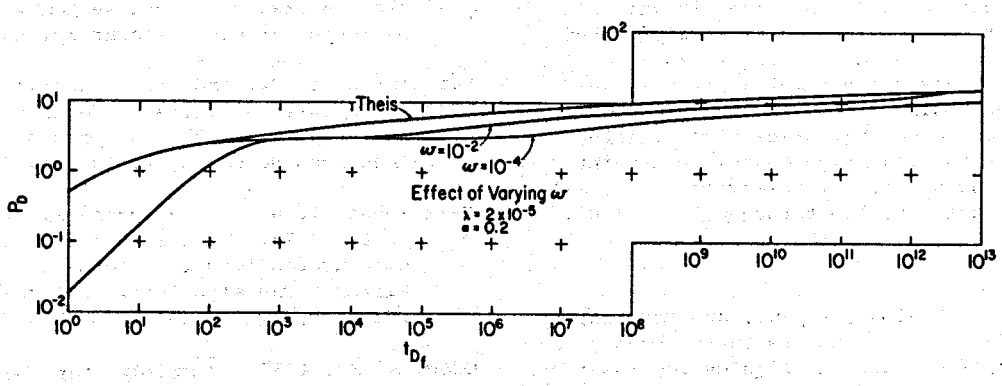

Figure 4. Simulation of flow in a double-porosity medium. Effect of varying ω. [XBL 8010-2848]

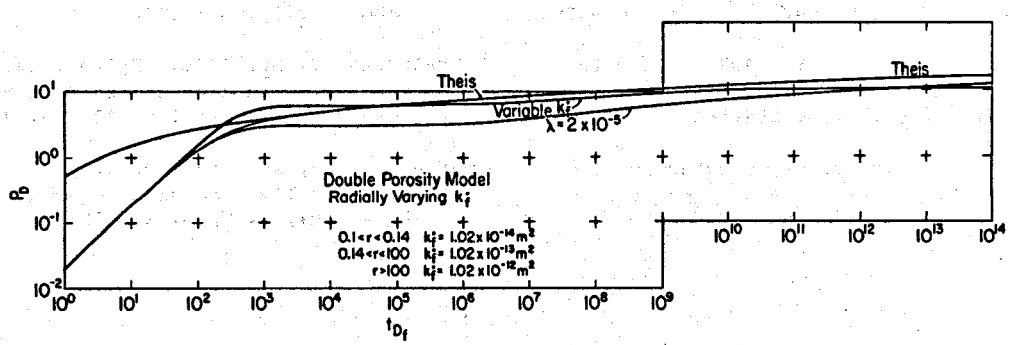

Figure 5. Simulation of a double-porosity medium. Effect of varying permeability. [XBL 8010-2847]

tivity only from the compressibility of water. In another case, the well was assumed to have a fluctuating free surface. In the former case, the capacity of the wellbore was assumed to be 10^{-6} m^3 of water per meter of head charge and in the latter it was $(0.1)^2\pi$. As can be seen from Figure 3, the different cases clearly show effects of delayed drainage from the blocks in the range $10^1 < t_{D_f} < 10^6$ when the wellbore storage is small. It is interesting to note, however, that a realistic wellbore radius of 0.1 m with free fluid surface in the well gives a solution which totally masks all the effects that one could hope to see due to variable λ or, equivalently, variable matrix permeability.

Study of the double-porosity system by many workers has showed that the late-time behavior of the system is dominated by the combined storativities of the matrix and the fractured media but that the intermediate-time behavior is influenced by ω, the ratio of the fissure storativity to matrix storativity. In Figure 4 two cases are compared, $\omega = 10^{-4}$ and $\omega = 10^{-2}$. As should be expected, the late-time solutions for these two cases are distinct from each other.

The final case shown in Figure 5 was actually chosen to illustrate the generality of the numerical approach over the analytical approach. In a

general integral, numerical model, the system is described as a complex of several isolated continua, each interacting with the other. In so far as the numerical approach is concerned, the double-porosity problem is a simplified special case which can be handled with ease. The case considered in Figure 5 considers the fissure-continuum to have radially varying k_f^*, to simulate the existence of a low-permeability skin close to the well, and to account for increased permeability due to fracturing beyond about 100 m from the well.

As can be seen from Figure 5, the presence of the low-permeability skin causes much higher drawdowns than the $\lambda = 2 \times 10^{-5}$ case after $t_{D_f} \sim 10^2$.

FURTHER WORK

The fact that the IFDM is eminently suitable for handling not only two but an arbitrary number of interacting continua makes this method a very powerful tool for analyzing complex natural field systems. On the basis of results presented here, Dr. Karsten Pruess and I have recently initiated work to simulate the injection of cold water into a fractured-porous geothermal reservoir. We shall actively pursue this problem through fiscal 1981.

REFERENCES CITED

Barenblatt, G. I., Zhelkov, P. Yu., and Kochina, I. N., 1960. Basic concepts in the theory of seepage of homogeneous liquids in fissured rocks. J. Appl. Math. (USSR), p. 1286-1303.

Boulton, N. S., 1954. The drawdown of the water table under non-steady conditions near a pumped well in an unconfined formation. Proc. Inst. of Civil Engrs., v. 3, p. 564-579.

Duguid, J. O., and Lee, P. C. Y., 1977. Flow in fractured porous media. Water Resources Research, v. 13, no. 3, p. 558-566.

Edwards, A. L., 1972. TRUMP: A Computer program for transient and steady state temperature distributions in multidimensional systems. Livermore, Lawrence Livermore Laboratory, UCRL-14754 (Rev. 3).

Lippmann, M. J., Tsang, C. F., and Witherspoon, P. A., 1977. Analysis of the response of geothermal reservoirs under injection and production procedures. Presented at the 47th Annual California Regional Meeting SPE-AIME, Bakersfield, California, April 1977. SPE 6537.

Narasimhan, T. N., 1980a. Multidimensional simulation of fluid flow in fractured rock systems. Proceedings, Workshop on Numerical Modeling of Thermohydrological Flow in Fractured Rock Masses, March 1980. Berkeley, Lawrence Berkeley Laboratory.

____, 1980b. Multidimensional simulation of fluid flow in fractured rock systems. Berkeley, Lawrence Berkeley Laboratory, LBL-12087.

Narasimhan, T. N., and Witherspoon, P. A., 1976. An integrated finite difference method for analyzing fluid flow in porous media. Water Resources Research, v. 12, no. 1, p. 57-64.

Narasimhan, T. N., Witherspoon, P. A., and Edwards, A. L., 1978. Numerical model for saturated-unsaturated flow in deformable porous media, Part 2. The algorithm. Water Resources Research, v. 14, no. 2, p. 255-261.

Odeh, A. S., 1965. Unsteady-state behavior of naturally fractured reservoirs. Soc. Pet. Eng. J., v. 3, p. 60-64.

Pruess, K., and Schroeder, R. C., 1977. SHAFT79: User's Manual. Berkeley, Lawrence Berkeley Laboratory, LBL 10861.

Streltsova, T. D., 1976. Hydrodynamics of groundwater flow in a fractured formation. Water Resources Research, v. 12, no. 3, p. 405-414.

Warren, J. E., and Root, P. J., 1963. The behavior of naturally fractured reservoirs. J. Soc. Pet. Eng., v. 9, p. 245-255.

THERMODYNAMICS OF HIGH-TEMPERATURE BRINES

K. S. Pitzer, P. Z. Rogers, G. C. Flowers, and J. C. Peiper

Current interest in the utilization of geothermal resources and geopressured brines has focused attention on the need for a model of aqueous solution properties at high temperatures and pressures. The number of different brines encountered in geothermal applications is large, so that detailed measurement of each of them is impractical. Nevertheless, it is desirable to find a model that can predict the properties of complex brines yet be based on a minimum amount of experimental data from a few key systems. Consequently, a program was initiated in 1975 to study the solution thermodynamics of brine systems, including both modeling and experimental work.

Initial modeling work involved testing a system of equations developed by Pitzer and co-workers (Pitzer, 1973; Pitzer and Mayorga, 1973, 1974; Pitzer and Kim, 1974) for its ability to reproduce experimental data for strong electrolytes at room temperature. Existing data were reproduced to within experimental error, up to concentrations of 6 m, in terms of parameters having physical significance. The model has been extended to cover weak electrolytes (Pitzer and Silvester, 1976; Pitzer et al., 1977). The model also has been used at temperatures up to 300°C to reproduce the thermodynamic properties of sodium chloride solutions (Silvester and Pitzer, 1977; Pitzer et al., 1979).

Extension of the model to a complex mixture requires some knowledge of the properties of each of the pure electrolytes which make up the solution. However, few experimental data for electrolytes, other than sodium chloride, are available at high temperatures and pressures. Thus a major part of the effort to build a model for natural brines has been to obtain basic thermodynamic data. Both a calorimeter and a densimeter, designed to obtain data at high temperatures and at pressures along and above the liquid-vapor saturation curve, have been constructed and successfully tested.

The usefulness of a model for aqueous solutions is not limited to geothermal energy systems. Research and engineering design in the fields of desalination, industrial waste treatment, hydrometallurgy, materials corrosion, solution mining, and hydrothermal ore deposition all depend on a knowledge of brine chemistry.

PROGRAM IN 1980

Calculational and experimental programs have been combined during the past year to yield compact models for two major electrolyte systems, sodium chloride and sodium sulfate. In addition, an initial step was taken toward modeling of carbonate systems. Experimental density data for sodium chloride solutions at 20 bar and 25-200°C have been obtained with a high-temperature densimeter. These data have been used to complete a model of the volumetric properties of sodium chloride solutions to 300°C and 1 Kbar. The model reproduces the experimental data from this study and from the literature data quite accurately, to within 60 ppm below 85°C and to within 300 ppm at higher temperatures. Careful attention also has been paid to reproducing expansivity and compressibility behavior. Figure 1 shows the differences between the specific volume of water and that of sodium chloride solutions as a function of temperature.

The computer model has been used to correct existing heat capacity data from saturation pressure to constant pressure values. In addition, the pressure dependences of heat capacity, enthalpy, and activity data have been calculated, and data obtained for these properties from the literature have been adjusted from the saturation pressure to a convenient constant pressure near 200 bar. This adjustment makes it possible to complete a true isobaric model for the thermal and activity properties of sodium chloride solutions. Combination of the isobaric model and the volumetric model will provide a final equation of state for aqueous sodium chloride.

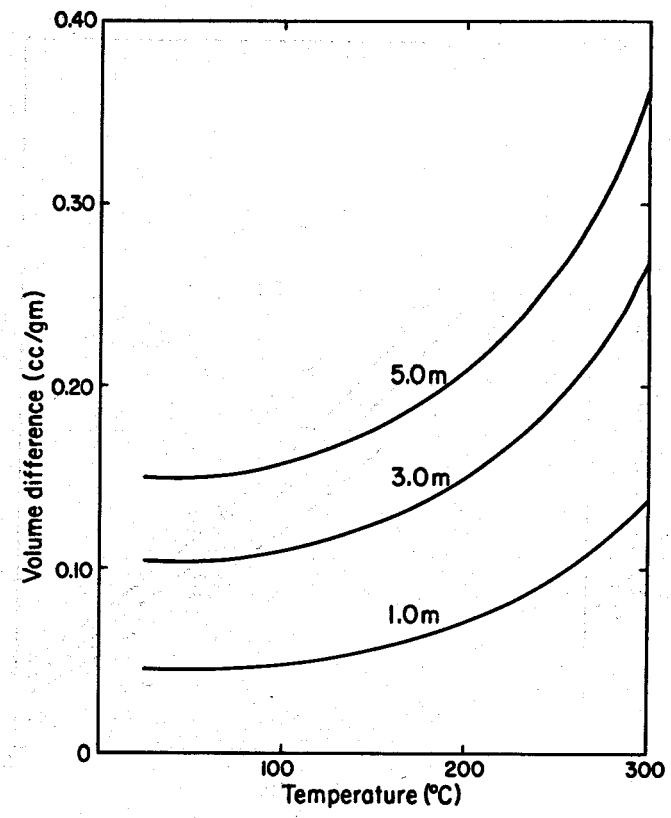

Figure 1. Difference in the specific volumes of water and NaCl solutions at 200 bar pressure as a function of temperature. [XBL 8011-6494]

The main thrust behind the development of an equation of state for sodium chloride, of course, is in the technical utilization of geothermal resources. The equation of state also will be useful in many industrial design problems, where the thermodynamic properties of natural brines or industrial fluids can be estimated using sodium chloride solutions as a model. A specific area of geochemical application will be in the calculation of isochore tables for fluid inclusion research.

A flow microcalorimeter has been used to obtain heat capacity data for Na_2SO_4, another electrolyte important in geochemical and geothermal systems. The data extend from 30°C to 200°C, from saturation pressure to 200 bar, and from 0.05 to 2.5 m. Precision of the data is better than 3×10^{-4} cal/°C-g. The heat capacity data have been fit as a function of molality and temperature using the model system of equations. Figure 2 shows representative heat capacity data and the corresponding calculated curves. These equations have been integrated, using the appropriate thermodynamic relationships and including data from Downes and Pitzer (1976) and Silvester and Pitzer (1978) at 25°C to evaluate the integration constants. The resulting values for the osmotic coefficient are shown as a function of molality for several temperatures in Figure 3, which also shows the few experimental osmotic coefficients that have been measured above room temperature (Liu and Lindsay, 1971; Humphries et al., 1968). Since these osmotic data were not used in the modeling, the agreement is excellent and indicates that this general approach will be useful for other solutes.

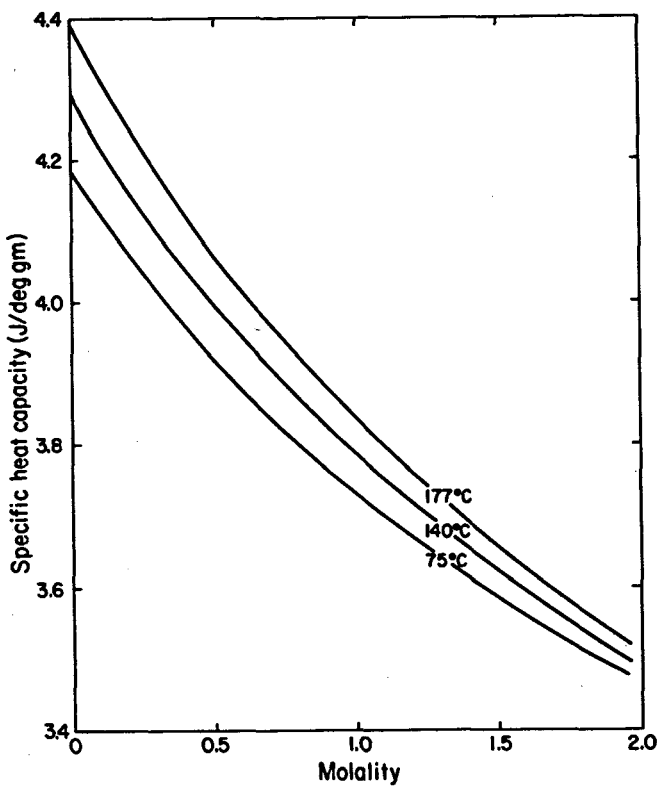

Figure 2. Specific heat capacity of Na_2SO_4 solutions. Solid lines are calculated from the overall fit, are data points. [XBL 8011-6495]

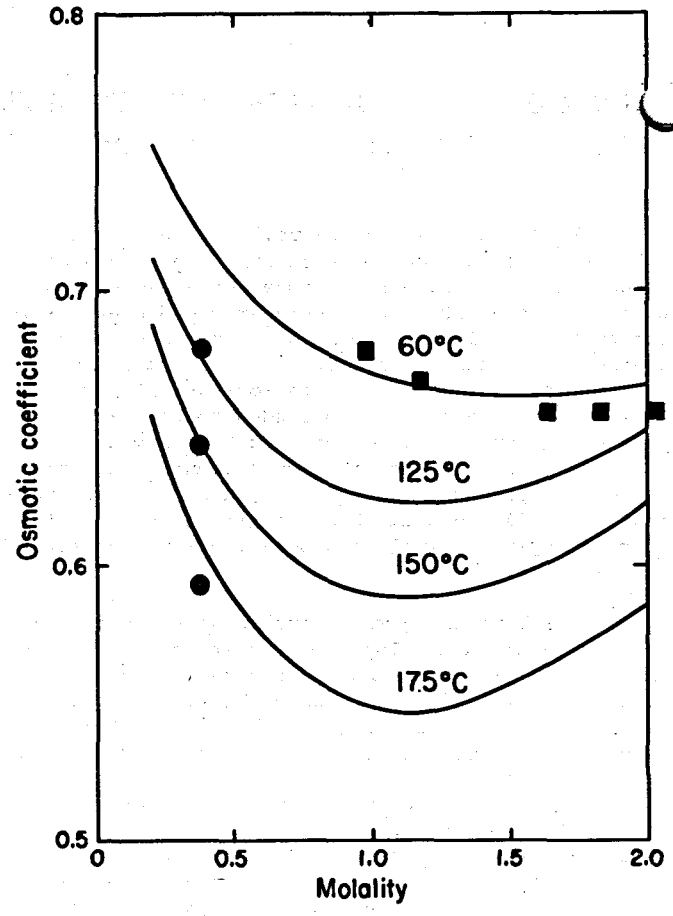

Figure 3. Osmotic coefficients of Na_2SO_4 solutions. Solid lines are calculated from heat capacity data, circles are data of Liu and Lindsay (1971), and squares are data of Humphries et al. (1968). [XBL 8011-6496]

An initial step was taken toward comprehensive modeling for carbonate solutions by a treatment for dilute bicarbonate-chloride mixtures with sodium as the positive ion. The effectiveness of the general equations for other mixed electrolytes provided the justification for applying them to published measurements at temperatures 0-50°C of the electrochemical cell

$$Pt,\ H_2/NaHCO_3(m_1),\ NaCl(m_2),\ CO_2(m_3)/AgCl,\ Ag.$$

These data had been extrapolated to infinite dilution to yield the first ionization constant of carbonic acid. Application of the mixed electrolyte equations together with existing knowledge of the parameters for sodium chloride allowed the determination of parameters for sodium bicarbonate (Pitzer and Peiper, 1980). The generally very useful isopiestic method cannot be used for bicarbonates because of the partial disproportionation and resulting vapor pressure of carbon dioxide. Also there are no electrodes which are reversible to bicarbonate ion. Thus the present results represe[illegible] the first precise determination of the activity [illegible] osmotic coefficients of sodium bicarbonate--either pure or mixed with chloride.

FUTURE WORK

The calorimeter is currently being rebuilt special corrosion-resistant hastelloy, which will permit extension of the measurements on sodium sulfate from 200°C to 300°C. Calorimetric and density measurements will continue for solutes of geochemical interest, including magnesium sulfate. The modeling program will be extended to include (1) the new experimental data for sodium and magnesium sulfates, (2) carbonate-bicarbonate systems more generally, and (3) other systems of geochemical interest as opportunity arises.

REFERENCES CITED

Downes, C. J. and Pitzer, K. S., 1976. Thermodynamics of electrolytes, binary mixtures formed from aqueous NaCl, Na_2SO_4, $CaCl_2$, and $CaSO_4$ at 25°C. J. Soln. Chem. v. 5, p.389.

Humphries, W. T., Kohrt, C. F., and Patterson, C. S., 1968. Osmotic properties of some aqueous electrolytes at 60°. J. Chem. Eng. Data, v. 13, p. 327.

Liu, C. T. and Lindsay, W. T., 1971. Thermodynamic properties of aqueous solutions at high temperatures. OSW Research and Development Progress Report No. 722.

Pitzer, K. S., 1973. Thermodynamics of electrolytes. I. Theoretical basis and general equations. J. Phys. Chem. v. 77, p. 268.

Pitzer, K. S. and Kim, J. J., 1974. Thermodynamics of electrolytes. IV. Activity and osmotic coefficients for mixed electrolytes. J. Am. Chem. Soc., v. 96, p. 5701.

Pitzer, K. S. and Mayorga, G., 1973. Thermodynamics of electrolytes. II. Activity and osmotic coefficients for strong electrolytes with one or both ions univalent. J. Phys. Chem., v. 77, p. 2300.

____, 1974. Thermodynamics of electrolytes. III. Activity and osmotic coefficients for 2-2 electrolytes. J. Soln. Chem. v. 3, p. 539.

Pitzer, K. S. and Peiper, J. C., 1979. The activity coefficient of aqueous $NaHCO_3$. J. Phys. Chem., v. 84, p. 2396.

Pitzer, K. S. and Silvester, L. F., 1976. Thermodynamics of electrolytes. VI. Weak electrolytes including H_3PO_4. J. Soln. Chem., v. 5, p. 269.

Pitzer, K. S., Bradley, D. J., Rogers, P. S. Z., and Peiper, J. C., 1979. Thermodynamics of high-temperature brines. Berkeley, Lawrence Berkeley Laboratory, LBL-8973.

Pitzer, K. S., Roy, R. N., and Silvester, L. F., 1977. Thermodynamics of electrolytes. VII. Sulfuric Acid. J. Am. Chem. Soc., v. 99, p. 4930.

Silvester, L. F. and Pitzer, K. S., 1977. Thermodynamics of electrolytes. VIII. High-temperature properties, including enthalpy and heat capacity, with application to sodium chloride. J. Phys. Chem., v. 81, p. 1822.

____, 1978. Enthalpy and the effect of temperature on the activity coefficient. J. Soln. Chem., v. 7, p. 327.

THE BEHAVIOR OF ROCK-FLUID SYSTEMS AT ELEVATED TEMPERATURES AND PRESSURES

W. H. Somerton

With the increased use of underground processes--some involving heating of rocks and others occurring in natural high-temperature environments--knowledge of the physical properties and behavior of rock-fluid systems under stress and at elevated temperatures has become important in designing, controlling, and analyzing those processes. We have an active research project in progress in which we are studying the following properties: deformation properties, including pore and bulk compressibilities and thermal expansions; P- and S-wave velocities; absolute permeability; electrical resistivity factor; and thermal properties, including conductivity, diffusivity, and specific heats. In addition to this ongoing research, we are also developing a new apparatus which will increase the range of temperature and pressure under which we can operate and will allow us to measure most of the above properties during the same test on the same test specimen. Data from these tests are needed to confirm our correlation and modeling work.

In this paper we will review the work we have accomplished during the past year in three areas: pore and bulk compressibilities and thermal expansions, absolute permeability, and thermal conductivity. Progress on the new multiproperties apparatus will also be reviewed.

ROCK PROPERTIES RESEARCH

Compressibility

Earlier work (Somerton, 1974) has shown that bulk compressibility of reservoir type rocks increases substantially with increased temperature. This has important implications in cases where pore fluid pressure declines in hot or heated reservoir formations. Surface subsidence can be expected to be of greater importance in such cases. Since pore volume compressibility behavior parallels bulk compressibility, substantial contraction of reservoir volume can also be expected when pore pressure decreases. This must be accounted for in material balance calculations.

Measurement of rock compressibility is a difficult and time-consuming procedure. Greenwald (1980) has recently completed a model from which pore volume compressibility may be estimated knowing only some simple properties of the rock. These include mineral composition and elastic moduli of the minerals, porosity, grain size, and a parameter which is related to roundness of the mineral grains. Knowledge of the clay content of the porous rock is also needed to predict the effect of stress on pore volume compressibility.

Agreement between the model and experimental results of pore volume compressibility measurements for three outcrop sandstones is shown in Figure 1.

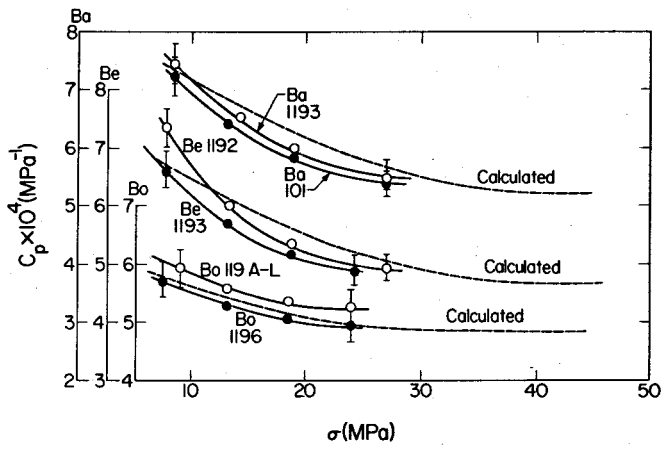

Figure 1. Comparison of model and experimental results of pore volume compressibilities (Greenwald, 1980). [XBL 812-2669]

In general, the agreement between experimental and calculated results is within 10%.

Greenwald (1980) also tested the validity of the Reciprocal Theorem, which states that change in pore volume with respect to confining stress is equal but opposite in sign to the change in bulk volume with respect to pore pressure. Mathematically this states:

$$\left(\frac{\partial V_b}{\partial p_i}\right)_{p_e} = -\left(\frac{\partial V_p}{\partial p_e}\right)_{p_i} .$$

Experimental results shown in Figure 2 for the Berea Sandstone indicate fairly good agreement at higher stress levels, but poorer agreement at lower stress levels.

Tests of the effects of temperature on pore volume compressibility by Greenwald were inconclusive, and further tests on this subject are now in progress. We expect to see a substantial increase in pore volume compressibility with increased temperature.

Thermal Expansion

Earlier work by Somerton and Selim (1961) demonstrated that bulk thermal expansion of dry, unstressed sandstones is very close to that of pure quartz. Quartz, having the largest thermal expansion of the common minerals found in sandstones, seems to dominate the expansion behavior of sandstones with quartz contents as low as 35%. In contrast to quartz crystals, however, most sandstones show substantial irreversible volume changes upon cooling to initial temperature values.

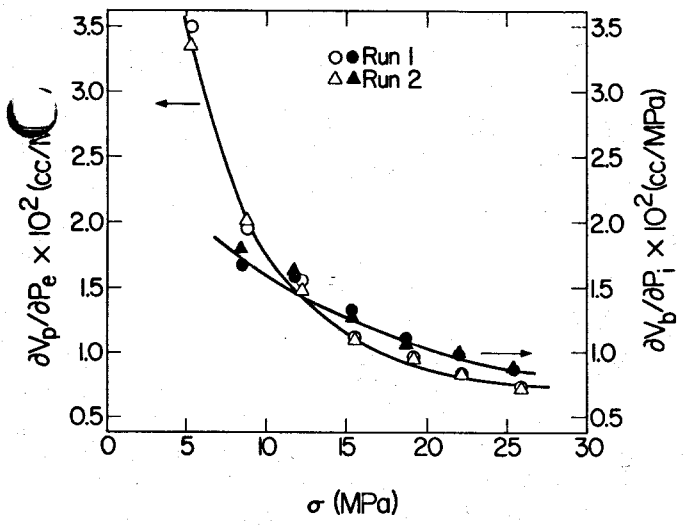

Figure 2. Test of Reciprocal Theorem for Berea Sandstone (Greenwald, 1980). [XBL 812-2670]

Ashqar (1979) has measured bulk thermal expansion of liquid-saturated sandstones under elevated confining and pore pressure conditions. Results of his work on the three sandstones are shown in Figure 3. The thermal expansion of Boise and Bandera Sandstones seem reasonable and give values close to those found for dry, unstressed sandstones. The unusual behavior of Berea, which was rerun giving a similarly shaped curve, is not understood and requires further investigation. All of these tests are currently being rerun with some modifications in the equipment and by a new graduate student. We believe the results are essentially correct but do require verification.

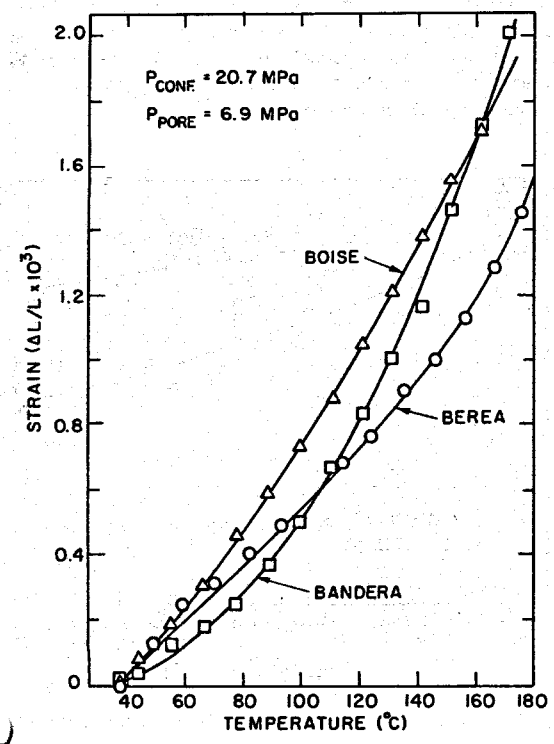

Figure 3. Linear thermal expansions of liquid saturated sandstones (Ashqar, 1979). [XBL 813-5326]

Janah (1980) recently completed a series of tests of the pore volume expansion (contraction) of the three standard sandstones. Results shown in Figure 4 indicate that pore volume contracts with increased temperature for sandstones under stress. The relatively small change in pore volume for all three samples at temperatures up to about 110°C and then the rather sharp increase at higher temperatures are probably related to the basic "looseness" of the structure of these porous rocks, which appears to tighten up at higher temperatures. Porosity seems to have an important effect in that the lower-porosity sample (Bandera) tightens up sooner and shows a sharper change in pore volume with increased temperature.

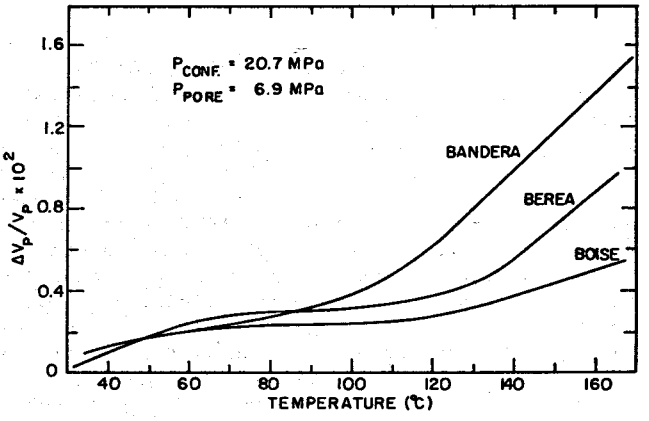

Figure 4. Pore volume contraction with temperature for sandstones. [XBL 809-5874]

Janah also studied the effects of stress level on pore volume thermal contraction and noted that differences in confining stress level had little effect but that increase in pore fluid pressure level had a marked effect, decreasing substantially the pore volume contraction with increased temperature. The latter point is shown for Bandera Sandstone in Figure 5.

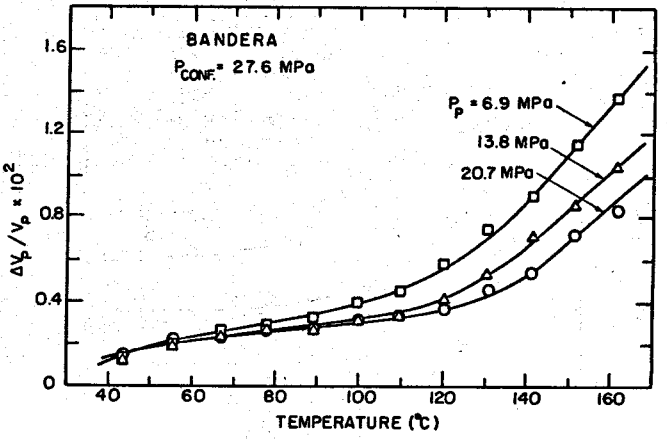

Figure 5. Effect of pore fluid pressure on pore volume contraction of sandstones (Janah, 1980). [XBL 809-5875]

Porosity

On the basis of earlier work, it has been suggested (Somerton, 1980) that porosity of porous rocks under stress would decrease with increased temperature. Subsequent work, discussed above, has confirmed this contention. The combined effects of bulk thermal expansion and pore volume contraction with increased temperature are to decrease porosity by a few percent. Although the amount of decrease with increased temperature is small, the combined effect with decreasing pore fluid pressure could decrease porosity substantially. Further work in progress will test these observations and will provide input data for models of the behavior currently under development.

Fluid Flow Behavior

Wong (1979) has shown that the absolute permeability of sandstones decreases with increased temperature when brine is flowing and the system is at elevated stress levels. Permeability reduction is about 30 to 50% in the range of 25-165°C. The reduction is most pronounced in the lower temperature range, with a tendency to flatten out at higher temperatures. One of the suggested causes of permeability reduction is thermal expansion of mineral grains, with consequent reduction in pore volume when the rock is under confining stress. The permeability-temperature behavior is consistent with a reduction in pore volume with increased temperature, since the small pores and pore necks would be first to close, followed by larger pore volume reductions in the larger pores at higher temperatures.

Wong ran permeability tests during heating of the cores. His results (Fig. 6) were somewhat erratic because it was difficult to control pore pressure with the precision needed in relation to the small pressure differentials across the cores. Okoh (1980) recently completed tests on Berea and Bandera Sandstones in which the temperatures were stabilized at each measuring level. His results showed a lower magnitude of permeability reduction than Wong's, and the results were more consistent, as shown in Figures 7 and 8.

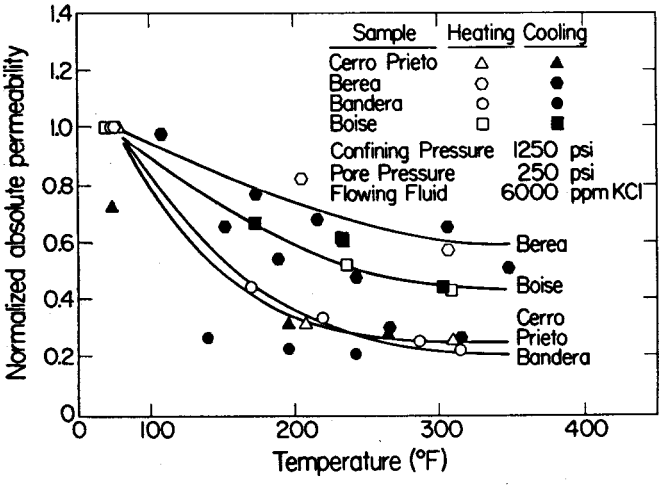

Figure 6. Decrease of permeability with temperature for sandstones, dynamic heating (Wong, 1979). [XBL 812-2671]

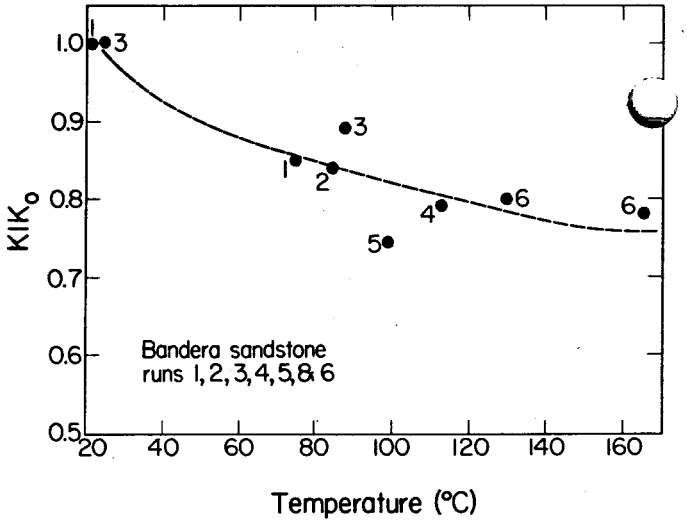

Figure 7. Decrease of permeability with temperature for Bandera samples, stabilized temperature (Okoh, 1980). [XBL 812-2672]

Okoh used Marshall's equation to test the possible order of magnitude of permeability reduction due to thermal expansion of mineral grains under stress. He assumed that pore necks decreased in diameter as a direct consequence of, and in proportion to, thermal expansion of the mineral grains. Some smaller pore necks would close completely at certain temperature levels and would thus cut off some of the flow channels. Using typical pore-size distribution curves and compatible grain-size distributions, he calculated permeability reduction as a function of temperature; the results are shown in Figure 8. Comparing those results with measured values, it is apparent that thermal expansion cannot explain the full magnitude of permeability reduction with increased temperature. This is especially true when considering that calculated values are probably the extreme values which could be expected by this cause.

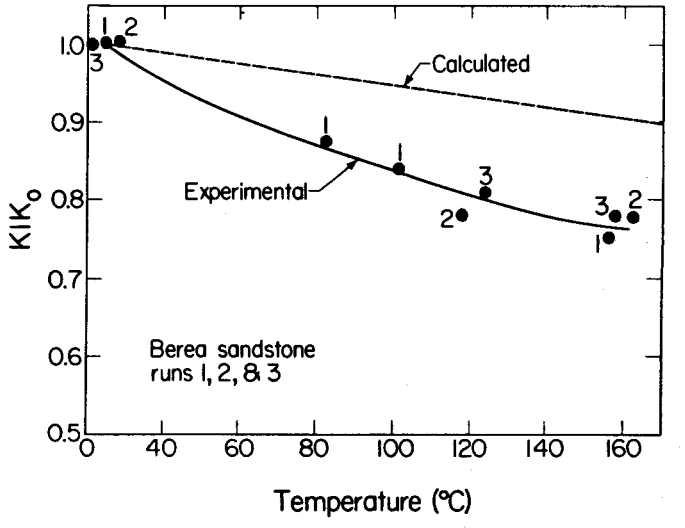

Figure 8. Decrease of permeability with temperature for Berea samples--stabilized temperature measurement and calculated (Okoh, 1980). [XBL 812-2673]

Other causes of permeability reduction include silica dissolution, migration and plugging by fines, and clay swelling. Both Wong and Okoh found increased silicon content in the effluent with increased temperature. Although particulate matter was never observed in the effluent, instantaneous increases in permeability upon reversal of flow direction indicate that migration and subsequent plugging by fines did occur and was probably a major cause of permeability reduction. This was further confirmed by the observations that permeability decrease was more pronounced at higher flow rates and in smaller grain size sandstones. Reduced rates of permeability reduction at higher temperatures are probably due to reduced viscosity and thus reduced carrying capacity of the flowing fluid at elevated temperatures.

In all tests run, there was some restoration of original permeability upon decreasing the temperature, but results were not very consistent. In general, it was noted that greater permanent permeability reduction occurred in the finer grain size cores. Other than this effect, the amount of permanent damage to a core by heating is probably related to the statistical nature of the migration of fines and the plugging process.

Thermal Properties

In our thermal properties study and research program our main effort has been to develop models that will allow thermal behavior of rock-fluid systems to be predicted from other properties of the system which are known or are easy to measure. Reliable thermal properties are difficult to measure, requiring fairly elaborate equipment and substantial amounts of time. Models and correlations have been developed (Somerton, 1973, 1975) which permit estimation of thermal conductivity, thermal diffusivity and specific heat by knowing only the mineral composition of the rock (mainly, the quartz content), the porosity of the rock, and the type and amount of fluid saturation. In addition, a correlation was developed that allows thermal properties at various temperatures to be predicted from known values at a specific base temperature. These correlations give accuracies within ±10% for most rock-fluid systems.

Ghaffari (1980) recently completed his investigation aimed at improving the model so that it would have more general application. Previous models were based on unidirectional heat flow through a cubic packing of spheres flattened at their contact points to give continuously variable porosity. We considered that unidirectional heat flow in the earlier model was probably unrealistic for a three-dimensional system (basically the assumption was made that isothermal surfaces were planes perpendicular to the direction of applied temperature gradient). In addition, the basis for flattening of vertical and horizontal contacts was controlled more by porosity considerations than by heat flow requirements (flattening of vertical contacts, parallel to direction of heat flow, had very little to do with thermal conductance, whereas flattening of horizontal contacts had a major effect on heat flow). And finally, the earlier models applied somewhat unrealistic distributions of wetting and nonwetting phase fluids because of geometric complexities.

Ghaffari attempted to rectify the above difficulties and made good progress. He developed a two-dimensional model with cylindrical coordinates (R and Z) and solved the resulting equations by using a finite-difference technique. To determine the relative flattening between vertical and horizontal contacts, he developed a thermal formation resistivity factor, which bears a reciprocal relationship to the electrical formation resistivity factor, since most of the heat flows in the mineral grains. With the cylindrical coordinate system, he was able to use a more realistic distribution of wetting and nonwetting phase fluids.

Working graphs developed from Ghaffari's work are shown as Figures 9, 10, and 11. Comparing results derived from this work with experimental data showed improved accuracy of the model over a wider range of rock types. The agreement is still not adequate at very low wetting phase saturations, but data in this range are not important in normal applications.

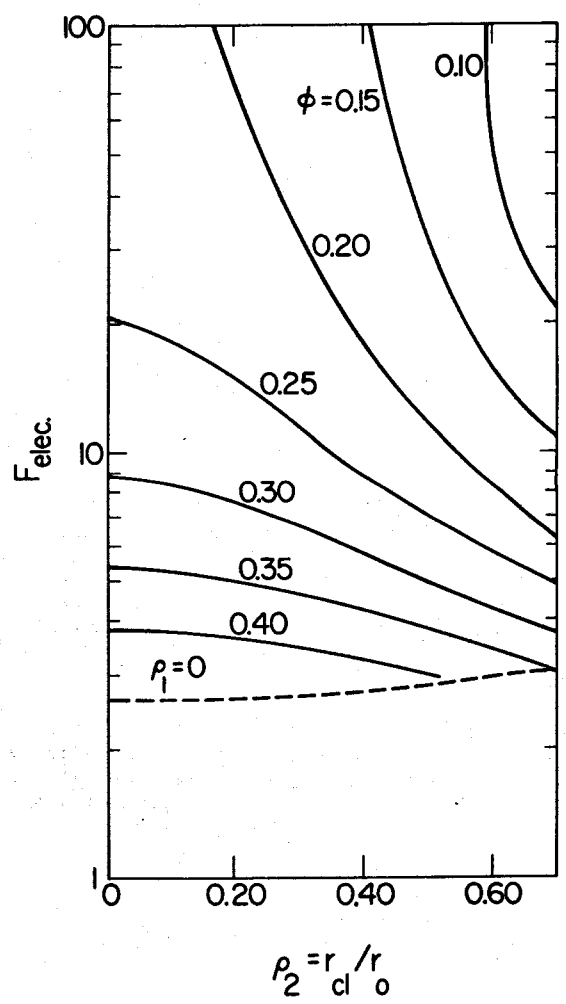

Figure 9. Evaluation of horizontal flattening parameter (Ghaffari, 1980). [XBL 812-2674]

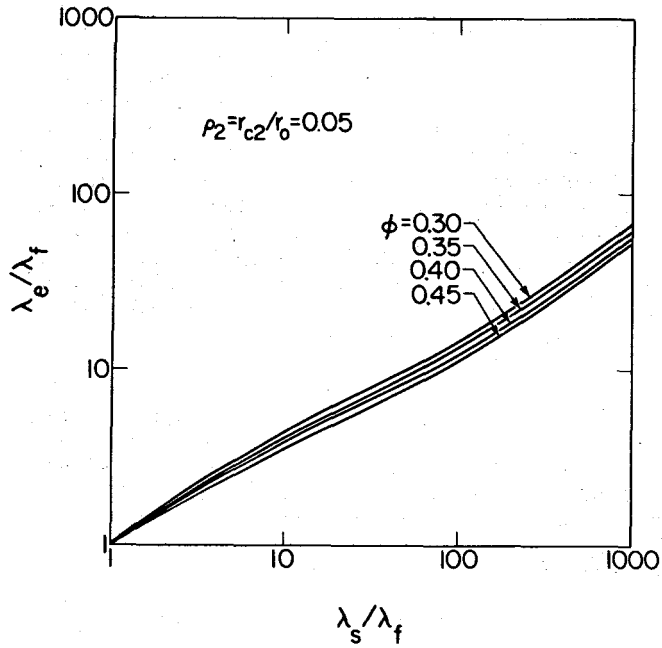

Figure 10. Chart for estimating thermal conductivities of unconsolidated sands (Ghaffari, 1980). [XBL 812-2675]

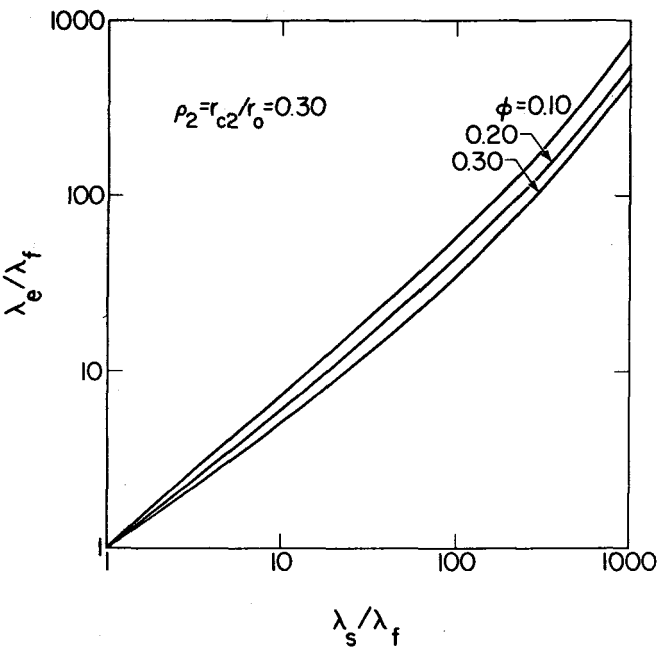

Figure 11. Chart for estimating thermal conductivities of consolidated sandstones (Ghaffari, 1980). [XBL 812-2676]

MULTIPROPERTIES APPARATUS

Measuring Methods

The new multiproperties apparatus has been discussed in detail in earlier reports (Somerton, 1977; Kuo, 1979). The apparatus is designed to permit the measurements of the following properties during the same test on the same test specimen: P- and S-wave velocities, absolute permeability, electrical resistivity factor, pore and bulk compressibilities and thermal expansion, thermal conductivity and thermal diffusivity. Methods of measuring these properties are reviewed briefly in the following paragraphs.

Compressional (P) and shear (S) wave velocities are measured by use of piezoelectric crystals mounted on alumina anvils which are placed on both ends of the cylindrical test specimen. One set of crystals transmits, sequentially, compressional and shear waves, and the other set is used to detect the arrival of the waves at the other end of the test specimen. King (1978) gives details of the design and mounting of the transducer stack. It is important to note that a cooling water circulating system is used around the transducer stack so that the temperature of the crystals will never exceed 150°C. Performance of the crystals deteriorates at temperatures much in excess of this value.

Permeability is measured by pumping brine of desired composition through the core and measuring the pressure drop directly across the core and the temperature of the flowing fluid. The brine is passed through filters external to the cell to remove any particulates which could plug the core. The incoming brine is heated to system temperature as it passes through the test specimen heater and then through holes drilled through the velocity transducer anvils. Disks of porous alundum about one cm thick are mounted between the anvils and the test specimen, their purpose being to distribute the flowing fluid uniformly across the face of the test specimen. The measuring and data acquisition equipment is discussed by Okoh (1980) and Kuo (1979).

Bulk compressibilities and thermal expansion are currently measured by use of strain gauges. Greenwald (1980) and Ashqar (1979) mounted strain gauges directly onto the test specimen. Some difficulties were encountered in isolating the strain gauges from test specimen pore fluids, resulting in shorting of the gauges. In the new apparatus, we plan to mount the strain gauges onto the copper sheathing used to jacket the test specimen. Tests are in progress to make certain that the externally mounted gauges follow the specimen strain. The present strain gauges are limited to operating temperatures of 290°C and will have to be replaced for higher temperature applications.

Pore volume compressibility and thermal contraction are currently measured by a hand-operated precision metering pump with a least count of 0.005 mℓ. This precision is adequate for the test specimen size used in the present work (5 cm dia x 5 cm long). For the new apparatus a precision plunger system actuating an LVDT will be used to measure pore volume changes with temperature and stress. This will greatly simplify data acquisition.

Formation resistivity is measured with a needle electrode located in the cylindrical axis of the test specimen, the outer electrode being the copper sheathing which jackets the core. Accuracy of this method is strongly influenced by the quality of contact between the inner needle electrode

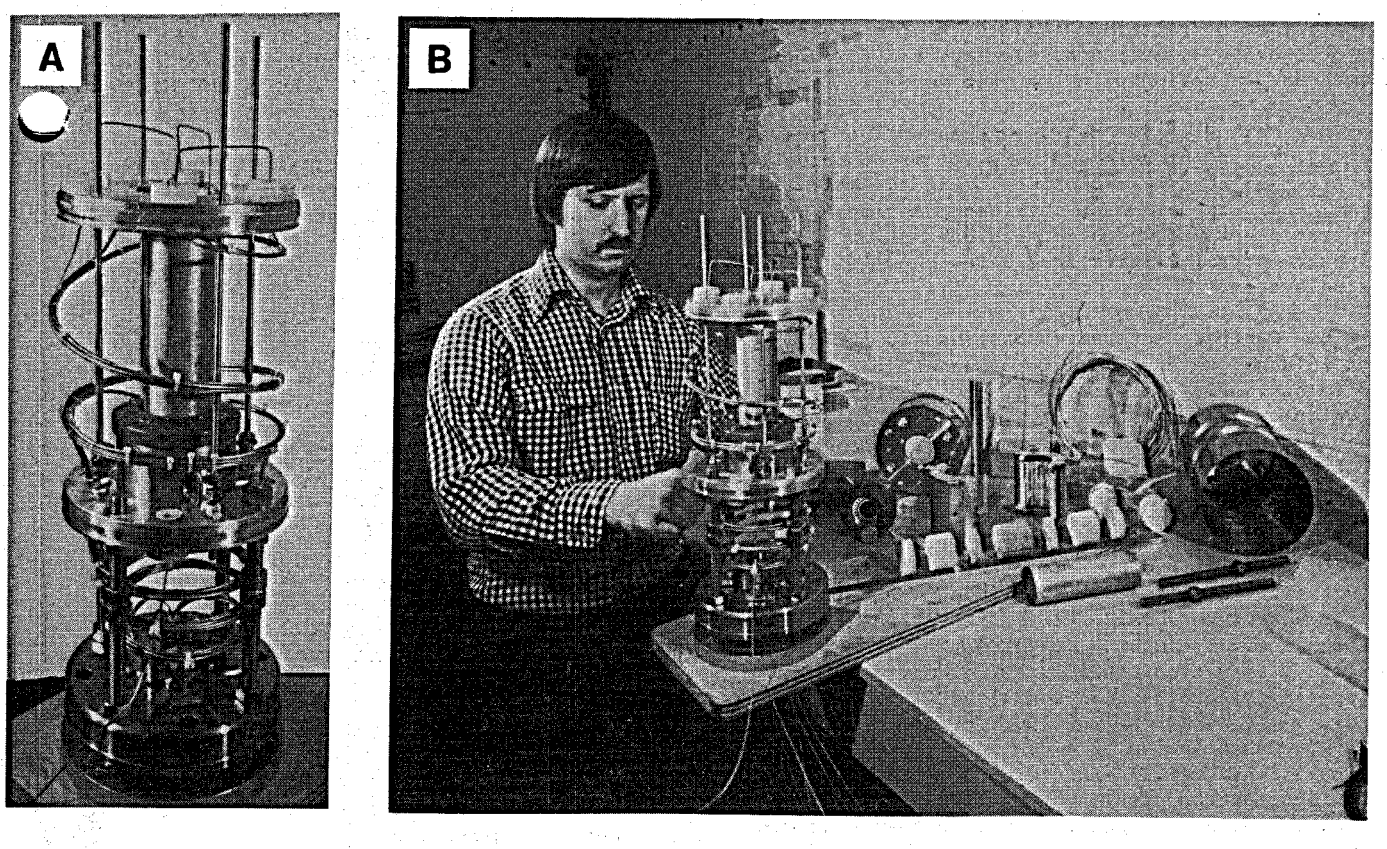

Figure 12. (A) Photograph of multiproperties test assembly. (B) Photograph showing components of apparatus.
[(A) CBB 8011-12857; (B) CBB 8011-12855]

and the test specimen. A high-temperature, electrically conductive cement which has very limited penetration into the pores of the test specimen is used for this purpose.

Thermal conductivity will be measured by use of a needle probe. The probe contains a resistance heating wire and a thermocouple at its tip. Thermal conductivity will be determined from the temperature-time record after a brief heating period. The outer sheathing of the needle probe serves as the inner electrode for the resistivity measurement. The same problem of obtaining good contact between the probe and the test specimen is dealt with by use of a good heat-conducting cement. Thermal diffusivity can also be obtained by recording the temperature differential between the probe thermocouple and a thermocouple located on the outer circumference of the test specimen during a heating cycle. Details of these measurements are given by Kuo (1979).

Apparatus

The assembly for measuring the above rock properties is mounted in a pressure vessel with an interior working space of about 18 cm diameter by 50 [illegible] long. The vessel has a working pressure of 25[illegible]0 psi. Although the vessel is a double closure type to assure high quality, only the top cap will normally be used for assembly mounting.

Photographs of the measuring assembly are shown in Figure 12. Figure 12B shows the various components of the apparatus. The large coiled tubing is used for cooling the velocity transducers. Coiling of the tubing is necessary to allow freedom of axial movement of the test specimen. The apparatus is designed to operate up to a maximum temperature of 400°C.

Argon gas will be used as the pressuring medium. An argon compressor operating in conjunction with a series of solenoid-actuated metering valves will be used to control the confining pressure at constant values or permit it to be changed at constant rates. This part of the system has been designed but not yet constructed.

Initially the apparatus will be operated under manual control and data will be taken on appropriate recorders. When the system has been thoroughly tested, we plan to convert to a computer control-data acquisition system. This has been discussed in detail by Kuo (1979) and is now under further development.

Conclusions

1. Substantial progress has been made in developing methods of measuring a number of physical properties of rock-fluid systems at elevated temperatures and pressures. Data obtained have been

used to test correlations and models of the behavior of these systems. Specifically, the following have been accomplished in the past year.

a. Methods have been developed or improved for the measurement of bulk and pore volume compressibilities and thermal expansions of fluid-saturated rocks, and data have been obtained. A simple model has been developed which permits estimation of pore volume compressibilities from a few known properties of the system.

b. Further tests have confirmed 20-30% reduction in absolute permeability of sandstones subjected to stress in which brine is the flowing fluid. Calculations have shown that thermal expansion of mineral grains can account for part of the permeability reduction but that a large amount of the reduction must be due to silica dissolution with resultant release, migration, and plugging by fines.

c. An improved two-dimensional model of heat flow in multifluid saturated porous media has been developed. This model permits estimation of thermal conductivity knowing only the mineral content, porosity, formation resistivity factor, and the nature and saturations of contained fluids.

2. Construction of a new multiproperties apparatus which will permit measurements of the most important properties of rock-fluid systems during a single test and on the same test specimen is nearing completion.

a. A pressure vessel has been received which will permit measurements at pressures to 25,000 psi and temperatures to 400°C.

b. Test methods have been developed and the test assembly has been constructed. Preliminary testing of the assembly is in progress.

c. The pressure control system has been designed but not yet constructed.

d. Initially, the experiment will be controlled manually and data will be taken on appropriate recorders. When the test system has been proved, we will install a newly designed minicomputer control and data acquisition system.

ACKNOWLEDGEMENTS

The important contributions of several Mechanical Engineering (Petroleum Option) graduate students to this project are hereby acknowledged. These include Anousch Ghaffari and Roy Greenwald (Ph.D. students), Paul Ashquar, Hakim Janah, Wei Kuo and Clement Okoh (M.S. students), and Lester Wong (M. Eng. student).

In addition to Department of Energy funding, other financial support came from Chevron Oil Field Research, Mobil Oil Co., and Getty Oil Co.

REFERENCES CITED

Ashqar, P., 1979. Thermal expansion of porous rocks under stress (M.S. Research Report), Berkeley, University of California, Department of Mechanical Engineering.

Ghaffari, A., 1980. A model for predicting thermal conductivity of rock-fluid systems (Ph.D. thesis). Berkeley, University of California, Department of Mechanical Engineering.

Greenwald, R. F., 1980. Volumetric response of porous media to pressure variations (Ph.D. thesis), Berkeley, University of California, Department of Mechanical Engineering.

Janah, A., 1980. Pore volume variation with temperature for porous rocks under stress (M.S. Research Report), Berkeley, University of California, Department of Mechanical Engineering.

King, M. S., 1978. Some notes on ultrasonic measurements of compressional and shear wave velocities. Saskatoon, University of Saskatchewan, Department of Geological Sciences.

Kuo, W. H., 1979. Microcomputer control system for rock properties experimental apparatus (M.S. Research Report). Berkeley, University of California, Department of Mechanical Engineering.

Okoh, C., 1980. Further studies of the effect of temperature on the flow capacity of rocks under stress (M.S. Research Report). Berkeley, University of California, Department of Mechanical Engineering.

Somerton, W. H., 1973. Thermal properties of hydrocarbon bearing rocks at high temperatures and pressures. Final Report API Research Project 117, Berkeley, University of California.

____, 1974. Deformation moduli of water-bearing formations at elevated temperatures. Calif. Water Resources Center, Contrib. No. 146, Davis, University of California.

____, 1975. Thermal properties of partially liquid saturated rocks at elevated temperatures and pressures. Final Report API Research Project 155, Berkeley, University of California.

____, 1977. Apparatus for measurement of properties and behavior of rock-fluid systems at high temperatures and pressures. Preliminary Report, Petroleum Engineering Laboratories, Berkeley, University of California.

____, 1980. Porous rock-fluid systems at elevated temperatures and pressures. In Recent Trends in Hydrogeology, Denver, Geological Society of America, Special Paper (in press).

Somerton, W. H., and Selim, M., 1961. Additional thermal data for porous rocks: Thermal expansion and heats of reaction. J. Soc. Pet. Engrs., v. 1, no. 4, p. 2490.

Wong, L., 1979. The effects of temperature and pressure on absolute permeability and formation resistivity factor of porous rocks (M. Eng. Research Report). Berkeley, University of California, Department of Mechanical Engineering.

RESULTS OF ALBITE SOLUBILITY MEASUREMENTS AS A FUNCTION OF TEMPERATURE (125-350°C).

J. M. Neil and J. A. Apps

Understanding the solubility of the major rock-forming minerals in low-temperature, hydrothermal environments is important for successful modeling of diagenetic, metasomatic, and metamorphic processes; for predicting the effects of returning cooled, geothermal brines to their reservoirs; or for using aquifers for hot-water storage. Albite, the sodium end-member of the feldspar mineral series, is an ideal candidate for the initial study because it is found in a wide variety of geological environments.

The three previous annual reports have documented the selection and characterization of the albite used in the solubility experiments (Apps and Neil, 1978); the initial solubility experiments at 250°C in 0.1 N NaCl solutions (Neil and Apps, 1979); and the series of solubility experiments at 250°C with pure water and various concentrations of NaCl solutions (0.001 N to 1.0 N) (Neil and Apps, 1980). This report summarizes the results of a series of experiments to measure albite solubility in pure water and in 10^{-3} and 10^{-2} N NaCl solutions with temperature as the experimental variable.

The temperature was raised and lowered in 25°C intervals from 125°C to 350°C along the saturation curve of water. Thus by approaching each sampling temperature from a higher and a lower temperature, the equilibrium at that temperature was approached from oversaturation and undersaturation. The difference in composition between the aqueous samples allows an estimation of the degree to which equilibrium was achieved.

Table 1. Albite Equilibrium Experiments

Run	0 (1 to 20)	0 (21-30)	P	Q	R	S	S*
Starting-maximum-final temperature (°C)	125-350-175	350-150	125-350-125	125-350-325	125-350-125	150-350	350-150
Solution Composition (N NaCl)	0.0	0.0	0.001	0.01	0.01	0.001	0.001
Volume (ml)	850	300+(1)	860	860	860	870	550
Albite charge weight (g)	50.00	(2)	50.20	50.11	51.02	100.00	100.00
Mesh size	-65+100	-65+100	-65+100	-65+100	-65+100	<270	<270
Duration of run (hr)	505.5	246.0	299.5	354	563	988	862
Time before first sample (hr)	96	54	83.5	66	107	244	190
Time between samples (hr)	24	24	12	24	24	48,72(3)	72(4)
Number of samples collected	20	10	21	14	21	20	10
Mass of cemented charge present after run	yes	yes	yes	yes	yes	yes	yes
Analcime present in scale	yes	yes	yes	N.D.	N.D.	N.D.	N.D.
High-temperature reversible loss of chloride ion	no	no	yes	yes	yes	yes	yes
Comments		(5)	(6)	(7)		(8)	(9)

(1) Residual H_2O from 0(1 to 20).
(2) Undisturbed charge from 0(1 to 20).
(3) 144 hr between second 150°C and first 150°C samples.
(4) 168 hr between 150° and 175°C samples.
(5) Vacuumed 300 ml H_2O into autoclave without opening it.
(6) Sampling interval too short.
(7) Small leak at high temperature caused solution loss.
(8) Sample filtered after centrifuging; sampled twice at each temperature.
(9) Sample filtered after centrifuging.

Experimental

The equipment, analytical methods, and experimental procedures have been previously described (Neil and Apps, 1979, 1980). The only significant changes in the experimental procedures were that two experiments were done with an increased charge size (to 100 g) and a smaller particle size (-270 mesh) to increase the surface area. These changes were made to increase the rate of equilibration so that samples below 200°C could achieve equilibrium in realistic times. Filtration of the aqueous sample with a 0.45-μm filter in addition to centrifugation proved to be necessary because of the fineness of the suspended particulates. Table 1 summarizes the experiments of this series.

Results

The results of the chemical analyses for SiO_2, Al^{3+}, Na^+ and Cl^- are plotted as a function of temperature in Figure 1 for the last two experiments (Runs S and Run S*) that were set up to attempt to achieve low-temperature equilibrium. The precision of not only the duplicate samples (Run S, 48 hr; and Run S, 72 hr) but also the second experiment sample (Run S*, 72 hr) are excellent for SiO_2 and Al^{3+}. The exceptions for Run S at 150°C and for Run S* at 350°C may represent sample sensitivity to handling prior to analysis.

The precision of the sodium analyses is not as good as that of the SiO_2 or Al^{3+}, but it is still well within acceptable limits (±10%). The chloride precision is closer to that of silica and aluminum for the low and middle temperature samples. At high temperatures, however, the concentration is very close to the lower limit of the chloride ion selective electrode (Orion Research, 1977), and the precision is degraded.

The high-temperature, reversible loss of chloride ion was unexpected. This phenomenon is illustrated in Figure 2, where the average chloride value for Run S as well as the chloride values for Run S* and Run R (a 10^{-2} N NaCl experiment) are plotted as a function of temperature. The chloride concentrations were checked by silver nitrate titrations using a silver selective electrode as an end-point indicator. Surface area calculations appear to rule out adsorption as the mechanism. A decrease in the sodium concentration is also observed in Figure 1; however, it is not clear whether it is related to the removal of chloride ion. Further study will be required before the mechanism for chloride ion removal from solution is understood.

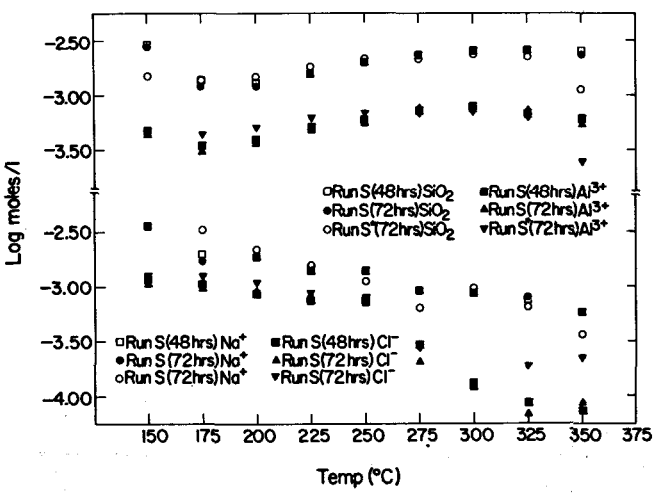

Figure 1. Chemical analyses for SiO_2, Al^{3+}, Na^+, and Cl^- as a function of temperature.
[XBL 8012-2438]

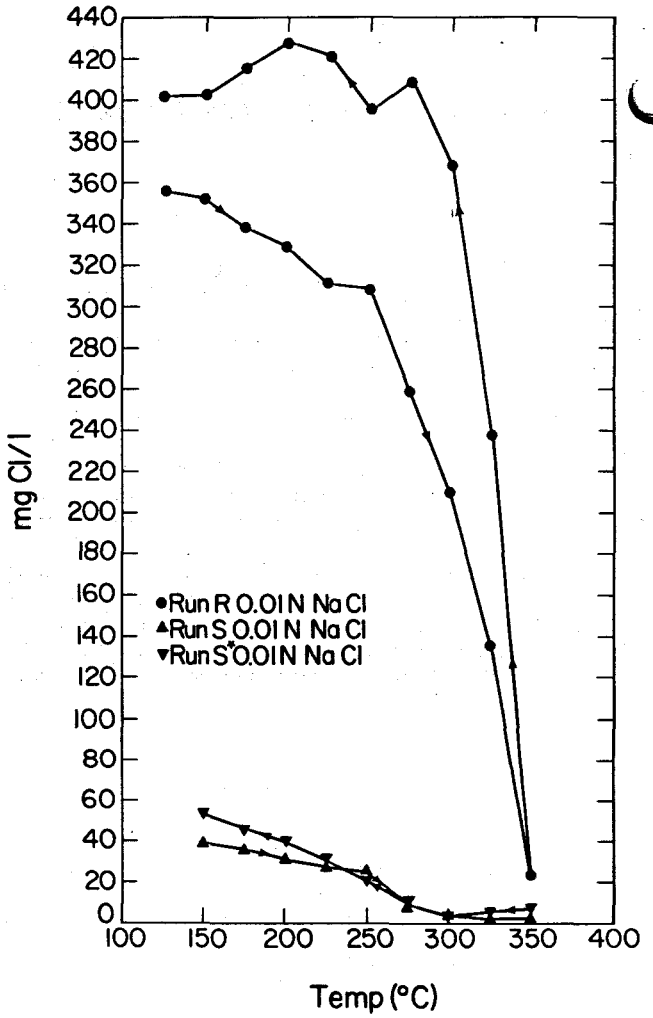

Figure 2. High-temperature, reversible loss of chloride ion plotted as a function of temperature.
[XBL 8012-2439]

The hydrogen ion concentration of the quenched samples is plotted in Figure 3 for Runs S and S*. Considerable difficulty was experienced in measuring the pH of some samples where the pH continued to drift even 50 minutes after starting the pH determination. Measuring the pH of a quenched sample that has not equilibrated internally will require further investigation.

Evaluation of Data

The solubility quotients of albite for the data given in this report have been evaluated, but are not presented here. It appears that the inaccura-

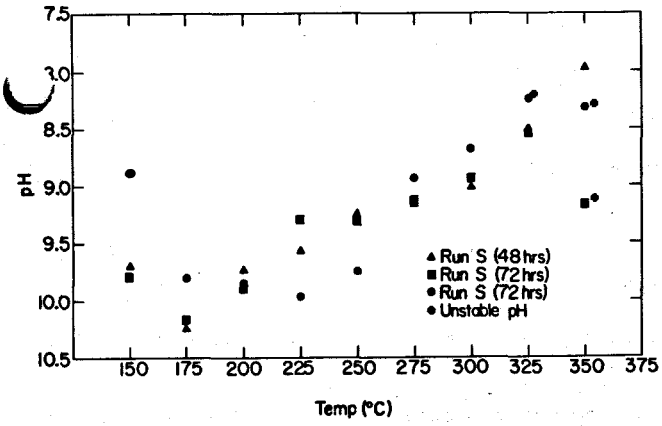

Figure 3. Quench pH as a function of temperature. [XBL 8012-2440]

cies inherent in the existing dissolution constants for aluminum species at elevated temperatures are presently too large for acceptable interpretation. This, together with recurring problems in measuring the pH of quenched samples and the unexplained behavior of the chloride ion in solution, necessitates additional interpretive studies before a final evaluation can be completed.

Conclusions and Future Activities

Current knowledge of aluminum speciation in aqueous solutions at elevated temperatures is contradictory and inconsistent with some phase relations observed in the laboratory experiments reported here and previously. Because such knowledge is critical to the interpretation of the results presented here, studies will be made of aluminum speciation in solution at elevated temperatures by means of a series of diaspore (AlO(OH)) solubility experiments in supporting electrolytes of varying alkalinities.

Further studies will be made to find a means of eliminating pH drift in samples measured at 25°C. A high-temperature pH electrode system will also be fabricated and tested using the current autoclave system. The pH electrode design reported by Niedrach (1980) will be used.

The reversible disappearance of chloride ion from solution at elevated temperatures will be investigated more fully, if time permits, and suitable diagnostic experiments can be conceived.

REFERENCES CITED

Apps, J. A., and Neil, J. M., 1978. Selected albites as candidates for hydrothermal solubility measurements. Berkeley, Lawrence Berkeley Laboratory, LBL-7058, p. 16-19.

Neil, J. M., and Apps, J. A., 1979. Solubility of albite in the aqueous phase at elevated temperatures. Berkeley, Lawrence Berkeley Laboratory, LBL-10349, p. 16-21.

Neil, J. M., and Apps, J. A., 1980. Solubility of low albite in NaCl solutions at 250°C. Berkeley, Lawrence Berkeley Laboratory, LBL-10686, p. 159-165.

Niedrach, L. W., 1980. Oxygen ion-conducting ceramics: A new application in high temperature-high pressure pH sensors. Science, v. 207, p. 120-122.

Orion Research, 1977. Instruction manual, halide electrodes: Model 97-17, model 94-35, model 94-53, and model 96-17. Cambridge, Massachusetts, Orion Research, Inc., 31 p.

THERMODYNAMIC PROPERTIES OF SILICATE LIQUIDS

I. S. E. Carmichael, M. S. Ghiorso, L. K. Moret, M. Rivers, and J. Stebbins

For several years measurements have been made at LBL of properties of silicate liquids as a function of composition and temperature. Although the compositional range of naturally occurring silicate liquids erupted as lavas is large, it is systematic and finite, and experiments can be designed on the basis of simple assumptions to cover the known natural range. This has been done with measurements of density of silicate liquids at 1 bar, in which it was shown that, within the limits of error in the measurement (1-2%), multicomponent silicate liquids mix ideally with respect to volume (Nelson and Carmichael, 1979). On the basis of these results coupled with earlier measurements on the heat capacities (Cp) of silicate liquids (Carmichael et al., 1977), a regular solution model for a 17-component silicate liquid was formulated (Ghiorso and Carmichael, 1980) using experimental equilibria between solid solutions and silicate liquids as a function of pressure and temperature. Experimental results involving only two solid-solution series, the olivines and the plagioclase feldspars, were used to develop the solution model, but nevertheless it correctly showed that liquid immiscibility would be found in high SiO_2 liquid compositions and also in certain lunar lavas. It also predicted partial molar free energies of SiO_2 which were in close agreement with those calculated by other means.

However, it was necessary to develop a computational technique to calculate the compositional limits of the two immiscible liquids, and this has been done recently. The problem is to develop a method which will predict the occurrence of immiscibility and the equilibrium composition of coexisting immiscible phases, given a solution model which expresses Gibbs free energy as a function of temperature, pressure, and composition. Current methods for such calculations (Brown and Skinner, 1974; Barron, 1976) are inadequate in all but the simplest binary and ternary systems. We have pursued a method based upon minimization of the total free energy of mixing in the multiphase, multicomponent system. We have used nonlinear optimization subject to linear constraints, where the function to be minimized is

$$G^{\text{mixing}}_{\text{system}} = \sum_{\phi=1}^{n\phi}\left(RT\sum_{i=1}^{nc} n_i \ln X_i + g^{xs}\right),$$

where $n\phi$ = the number of immiscible phases and nc is the number of components. The linear constraints are

$$\sum_{\phi=1}^{n\phi} n_{i,\phi} = n_{i,\text{total}} \qquad i = 1, nc,$$

$$n_{i,\phi} > 0 \qquad i = 1, nc;\ \phi = 1, n\phi,$$

which express conservation and nonnegativity of mass for each component.

The optimization algorithm we use is the projected gradient method of Gill and Murray (1972), using the program LCMNA from the BKY computer center library SOURCE.

We have tested the method by calculating the phase relations in two ternary solution systems studied by Barron (1976). Our results agree with his and are probably two orders of magnitude more efficient. We have used the technique to study the 10-component regular solution formulation for silicate liquids of Ghiorso and Carmichael (1980). For a bulk composition represented by the residual liquid in a lunar basalt, we predict the coexistence of an FeO-rich, SiO_2-poor liquid with a second liquid which has broadly the composition of basaltic andesite. This is in general agreement with observations made on natural lavas.

Solution models for multicomponent silicate liquids depend in part upon standard state properties of either simple liquid oxides as a function of pressure and temperature or simple compounds. Because of the widespread geological interest in the effect of pressure on the melting temperature of common rock-forming minerals, their fusion curves are often well known to 30 or 40 kbars. With these data it should be possible to compare fusion curves calculated from both liquid and solid thermodynamic properties, and it is to this end that a sustained effort has been made to measure liquid properties.

A series of measurements of the enthalpies and heat capacities of glasses and stable liquids in the $NaAlSi_3O_8$ - $CaAl_2Si_2O_8$ system (abbreviated Ab - An) has been completed. Data for glasses in the temperature range from 840 to 1060 K, and for the liquids between the liquidus and about 1880 K, have been fitted to the linear equations shown in Table 1. The enthalpy results for Ab_{100} and An_{100} glasses agree within a few tenths of one percent with those given by Richet and Bottinga (1980) and Krupka et al. (1979), and the results for stable Ab_{100} liquid are very close to those of Richet and Bottinga in the region where the data overlap.

The heat of fusion of albite can be calculated by combining the data on the enthalpy of the liquid with the heat of vitrification at 985 K reported by Weill et al. (1980) and with the estimation of the thermal properties of crystalline high albite of Helgeson et al. (1978). The derived equation for the enthalpy of fusion as a function of temperature above the melting points (1391 K) is

Table 1. High temperature heat contents of glasses and liquids.

	Regressions of glass data	Regressions of liquid data
Ab_{100}	$H_T - H_{300} = -27.76 + 0.7544T$	$H_T - H_{300} = -44.147 + 0.088872T$
	$N = 6$ $2\sigma = 0.43$	$N = 15$ $2\sigma = 0.72$
$Ab_{75}An_{25}$	$H_T - H_{300} = 29.11 + 0.0770T$	$H_T - H_{300} = -51.422 + 0.094250T$
	$N = 6$ $2\sigma = 0.54$	$N = 6$ $2\sigma = 0.63$
$Ab_{50}An_{50}$	$H_T - H_{300} = -26.46 + 0.07447T$	$H_T - H_{300} = -60.539 + 0.10111T$
	$N = 5$ $2\sigma = 0.43$	$N = 8$ $2\sigma = 0.49$
$Ab_{25}An_{75}$	$H_T - H_{300} = -29.08 + 0.07724T$	$H_T - H_{300} = -67.395 + 0.10641T$
	$N = 5$ $2\sigma = 0.46$	$N = 6$ $2\sigma = 0.46$
An_{100}	$H_T - H_{300} = -30.04 + 0.07784T$	$H_T - H_{300} = -87.72 + 0.1192T$
	$N = 5$ $2\sigma = 0.35$	$N = 9$ $2\sigma = 0.46$

$$\Delta_f H_{Ab,T} = -10081 + 27.172T - 6.95 \times 10^{-3}T^2$$

$$- 15{,}01 \times 10^5 T^{-1} \text{ cal/mol},$$

with $\Delta_f H_{1391} = 13.19$ Kcal/mol. Enthalpy values calculated from the regressions of the data for each intermediate glass composition in the Ab-An system at a temperature such as 985 K are colinear with the values for the end-members within experimental error. This is also true for stable liquids, indicating that within the experimental error, there is no excess heat capacity within the binary. Partial molar heat capacities for Ab and An components are 88.9 and 113.8 cal/mol K, respectively.

The heat of mixing ($\Delta_m H$) of the stable liquids in the Ab-An binary can be calculated by combining the data presented here with the heats of mixing in the glasses determined by solution calorimetry at 985 K. The best approximation may be that $\Delta_m H$ is independent of temperature, with a minimum of about -2 Kcal/mol at about Ab_{50}. The data do, however, permit this value to be reduced in magnitude to about -1 Kcal/mol.

Data on the enthalpies of the liquids can be combined with solid-liquid phase equilibrium data and with recent measurements of $\Delta_m H$ in solid plagioclase measured at 970 K by Charlu et al. (1980). The results of such calculations indicate that for reasonable models of mixing entropies, the enthalpies of mixing for the solid and liquid solutions must be of similar sign and magnitude.

This suggests that a significant change in the heat of mixing in the solid must take place between 970 K (where $\Delta_m H = 1.2$ Kcal/mol) and solidus temperatures. Such a change could be related to the triclinic to monoclinic phase change in albite-rich plagioclase at high temperatures.

REFERENCES CITED

Barron, L. M., 1976. Segregation in ternary solutions. J. Geochem., v. 10, p. 145-154.

Brown, T. H., and Skinner, B. J., 1974. Theoretical prediction of equilibrium phase relations in multicomponent systems. Am. J. Sci., v. 274, p. 961-986.

Carmichael, I. S. E., Nicholls, J., Spera, F. J., Wood, B. J., and Nelson, S. A., 1977. High-temperature properties of silicate liquids: Applications to the equilibration and ascent of basic magma. Phil. Trans. Ry. Soc. Lond., ser. A, v. 286, p. 373-431.

Charlu, T. V., Newton, R. C., and Kleppa, O. J., 1980. Thermochemistry of the high structural state plagioclases. Geochim. Cosmochim. Acta, v. 44, p. 933-941.

Ghiorso, M. S., and Carmichael, I. S. E., 1980. A regular solution model for met-aluminous silicate liquids: Applications to geothermometry immiscibility, and the source regions of basic magmas. Contrib. Mineral Petrol., v. 71, p. 323-342.

Gill, P. E., and Murray, W., 1972. Two methods for the solution of linearly constrained and unconstrained optimization problems. National Physical Laboratory Report DNAC-25.

Helgeson, H. C., Delany, J. M., Nesbitt, H. W. and Bird, D. K., 1978. Summary and critique of the thermodynamic properties of rock-forming minerals. Am. J. Sci, v. 278A, 229 p.

Krupka, K. M., Robie, R. A., and Hemingway, B. S., 1979. High temperature heat capacities of corundum, periclase, anorthite, $CaAl_2Si_2O_8$ glass muscovite, pyrophyllite, $KAlSi_3O_8$ glass, grossular, and $NaAlSi_3Si_3O_8$ glass. Am. Min., v. 64, p. 86-101.

Nelson, S. A., and Carmichael, I. S. E., 1979. Partial molar volumes of oxide components in silicate liquids. Contrib. Mineral Petrol., v. 71, p. 117-124.

Richet, P. and Bottinga, Y., 1980. Heat capacity of liquid silicates: New measurements on $NaAlSi_3O_8$ and $K_2Si_4O_9$. Geochim. Cosmochim. Acta, in press.

Weill, D. F., Hon, R., and Navrotsky, A., 1980. The igneous system $CaMgSi_2O_6$ - $CaAl_2Si_2O_8$ - $NaAlSi_3O_8$: Variations on a classic theme by Bowen. In R. B. Hargraves (ed.), Physics of Magmatic Processes. Princeton University Press, p. 49-92.

CHEMICAL TRANSPORT IN NATURAL SYSTEMS

C. L. Carnahan

Processes occurring in nature can be characterized generally as irreversible changes in which unbalanced forces cause flows of matter, energy, and momentum through open systems. The transport of chemical materials dissolved in groundwater flowing within a porous or fractured rock matrix is such a process, and is affected by spatial and temporal variations of hydraulic potential, chemical potentials, and temperature. In particular, concentrations of dissolved materials are influenced by irreversible processes of convection, diffusion, mechanical dispersion, and spontaneous chemical reactions. It is evident that a complete description of phenomena associated with chemical transport in any natural system should account for the system's irreversibility (or departure from equilibrium) by means of a formalism capable of producing quantitative results which are consistent with experience and the laws of nature. Such a formalism exists in the thermodynamics of irreversible processes, which we are applying to the subject problem.

The thermodynamics of irreversible processes is based on several fundamental assumptions. One of these assumptions states that any flow of mass, energy, or momentum in an irreversible system is, in principle a linear function of all the forces acting on the system; thus flows may be thermodynamically coupled in the sense that a contribution to a given flow may arise from a seemingly unrelated force (Fitts, 1962). A consequence of this assumption (and others) is the prediction of certain relationships between the phenomenological coefficients relating flows to forces; with one important exception, these relationships have been verified experimentally for the processes of interest in our work (Miller, 1960; Miller, 1974). The exception is the set of processes consisting of chemical reactions; it appears that the assumptions of the thermodynamics of irreversible processes do not adequately describe simultaneous chemical reactions and their coupling with each other if the reactions are significantly removed from equilibrium. However, it can be shown that chemical reactions cannot be coupled to flows of mass and energy in most systems of interest to this work (Carnahan, 1976). Moreover, natural hydrogeochemical systems are often in a state very close to chemical equilibrium. For these reasons, we have tentatively retained the phenomenological description of chemical reactions while excluding reaction-reaction coupling. (It is important to distinguish between thermodynamic coupling and ordinary interference between transport processes. In the thermodynamics of irreversible processes, symmetry considerations prohibit coupling between scalar rates of chemical reactions and vector flows of matter and energy. However, chemical reactions can alter local gradients of chemical potentials of reactants and products and thus alter mass flows; this effect is termed interference (Wei, 1966). We are currently investigating the feasibility of replacing the phenomenological description of chemical reactions by a chemical-kinetic formalism for use with reactions which may be significantly removed from equilibrium.

A central concept in the thermodynamics of irreversible processes is the rate of production of entropy by irreversible processes occurring within a volume element of the system of interest; changes of entropy density by convective transport of entropy through a volume element are excluded from the production rate. The entropy production rate has several useful properties. First, when correctly formulated mathematically, it provides the identification of specific flows and forces acting on the system (Denbigh, 1951); these quantities are not always self-evident, and are required for subsequent formulation of the phenomenological equations relating forces and flows. Second, the entropy production rate provides a quantitative measure of the extent of irreversibility in a system; specifically, it is numerically always positive if any irreversible process is occurring, and decreases to zero in the state of thermodynamic equilibrium.

A third useful property of the entropy production rate is related to its behavior in steady-state, nonequilibrium systems. Suppose a nonadiabatic system is acted on by several constrained forces; the system will produce entropy at some fixed, positive rate. If now the constraints are removed from some (but not all) of the forces, the system will progress to a time-invariant state in which the rate of production of entropy will have a local minimum value determined by the magnitudes of the remaining, constrained forces; simultaneously, the

flows conjugate to the unconstrained forces will vanish (Katchalsky and Curran, 1967). (If all constraints are removed, the rate of production of entropy will decrease to zero, all flows will vanish, and the system will then be in a state of thermodynamic equilibrium.) Immediately evident is the possibility of using this minimum property of steady-state systems as an aid in the analysis of complex, multicomponent, reacting, open systems which are in steady states but not at thermodynamic equilibrium, in a manner analogous to the classical minimization of the Gibbs free energy in determining the composition of a closed reacting system which has progressed to an equilibrium state.

Our work this year has focused on the study of steady-state mass transport in the presence of chemical reactions. In particular, one-dimensional, isothermal systems with constant values of chemical potentials at the boundaries and one or two first-order, reversible chemical reactions were investigated. In the formalism of the thermodynamics of irreversible processes, the driving force for diffusional transport of a solute is the negative gradient of the chemical potential of the solute, and the driving force for a chemical reaction is the thermodynamic affinity, which is a linear function of the chemical potentials of the reaction's reactants and products. Mass flows are postulated to be linear functions of all gradients of chemical potentials. Thermodynamic coupling in such a system consists of contributions to the mass flow of a given solute arising from the gradients of the chemical potentials of other solutes. This approach allows study of mass transfer in time-invariant systems which are not in chemical equilibrium, in contrast to the classical approach which assumes equilibrium in all chemical reactions. In the absence of chemical reactions, chemical potentials in one-dimensional, steady-state systems with constant-potential boundaries are linear functions of distance between boundaries; i.e., gradients of chemical potential are consant (or zero). We have found that thermodynamic coupling between mass flows changes only the magnitudes of the gradients, and does not disturb the linearity. The presence of one or more chemical reactions, however, renders the potential distributions nonlinear and may drastically alter the distributions of potentials and mass concentrations. It was found for the systems studied that in the presence of a chemical reaction the chemical potential distributions achieved configurations in the steady state such that the affinity of the reaction was driven toward zero to the largest extent possible within the confines of the system (assuming nonzero values of affinity at the boundaries). This result is consistent with the property of minimum production rate of entropy in the steady state. Furthermore, our modeling studies have shown that the presence of thermodynamic coupling of mass flows in a reacting system can significantly modify values of chemical potentials, mass flows, and chemical reaction rates from values predicted in the absence of coupling. In particular, values of chemical potentials in the state of chemical equilibrium of a reacting system (by definition, when the thermodynamic affinity of the reaction equals zero) may be displaced, by coupling, from values predicted by the methods of classical thermodynamics.

We are currently extending these studies to investigation of the form of the entropy production function generated by an arbitrary number of independent, thermodynamic forces acting on an open, nonisothermal system.

REFERENCES CITED

Carnahan, C. L., 1976. Nonequilibrium thermodynamics of groundwater flow systems: Symmetry properties of phenomenological coefficients and considerations of hydrodynamic dispersion. J. Hydrology, v. 31, p. 25-150.

Denbigh, K. G., 1951. The Thermodynamics of the Steady State. London, Methuen and Co., Ltd., 103 p.

Fitts, D. G., 1962. Nonequilibrium Thermodynamics. New York, McGraw-Hill, 173 p.

Katchalsky, A., and Curran, P. F., 1967. Nonequilibrium Thermodynamics in Biophysics. Cambridge, Mass., Harvard University Press, 248 p.

Miller, D. G., 1960. Thermodynamics of irreversible processes. The experimental verification of the Onsager reciprocal relations. Chemical Reviews, v. 60, p. 15-37.

____, 1974. The Onsager relations: Experimental evidence, in J. J. Delgado Domingos, M. N. R. Nina, and J. H. Whitelaw (eds.), Foundations of Continuum Thermodynamics, London, MacMillan Press, p. 185-214, 215-227.

Wei, J., 1966. Irreversible thermodynamics in engineering. Ind. Eng. Chem. v. 58, no. 10, p. 55-60.

VISCOSITY OF NaCl, KCl, and $CaCl_2$ SOLUTIONS UP TO 350°C AND 50 MPa

S. L. Phillips, H. Ozbek, A. Igbene, and G. Litton

Summarized here are the results of a review of the available data on the viscosity of sodium chloride, potassium chloride, and calcium chloride solutions for the following ranges of geothermal conditions: temperatures up to 350°C, pressures up to 50 MPa, and concentrations up to 5 m (27 wt %) (Lyon and Kolstad, 1974; Phillips et al., 1979). The interest in sodium chloride solutions stems partly from the fact that NaCl is the major dissolved electrolyte in geothermal brines. For example, wells in Baca Location No. 1 in New Mexico contain over 2000 ppm Na and over 3000 ppm Cl; wells in East Mesa, California, have over 700 ppm Na and over 800 ppm Cl; and wells in the Salton Sea area of California have 10,000 to 50,000 ppm Na and 20,000 to 160,000 ppm Cl (Phillips et al., 1980).

Viscosity of a liquid is a measure of the resistance of the liquid to flow; the reciprocal of viscosity is the fluidity. The addition of electrolytes to water either increases or decreases the viscosity of the resulting solution. For example, addition of NaCl, $BaCl_2$, $LaCl_3$, KCl, or $CaCl_2$ increases the viscosity, whereas $CsNO_3$ can decrease the viscosity. The magnitude of the change in viscosity differs for each electrolyte (Phillips et al., 1980).

Data on the change in viscosity of NaCl solutions with temperature, concentration, pressure, and with other dissolved constituents are necessary for calculating fluid volumes when injecting brines. A 139°C (282°F) change in temperature for a 1.11 specific gravity brine will cause an estimated 88.5% decrease in viscosity for a geothermal fluid. This change may be compensated by a decrease in pumping capacity. A note of caution: the temperature change will also cause a decrease in density and thereby increase the fluid volume; this could necessitate an increase in pumping capacity. Thus, on relating the effects of changes in viscosity for predictive modeling, other properties such as density changes need to be considered.

Viscosity data are also used to calculate other properties of solutions, such as kinematic viscosity, and to interpret the structure of electrolyte solutions. In this case, the data are interpreted in terms of ion-water interactions--for example the degree of hydration of dissolved electrolytes whose concentrations exceed about 1 m, such as $LaCl_3$m and of more dilute solutions of other electrolytes, such as NaCl (Spedding and Pikal, 1966).

Correlation Equation for Sodium Chloride Solutions

Over 1500 selected data points were used to develop our correlation; all were initially given equal weight. The form developed is similar to that derived by Vand for colloids and nonelectrolytes with an added exponential term.

$$\frac{\eta}{\eta_w} = 1 + am + bm^2 + cm^3 + dT(1 - e^{km}), \qquad (1)$$

where a = 0.0816, b = 0.0122, c = 0.000 128, d = 0.000 629, k = -0.7, T = temperature (°C), m = molal concentration (g-mol NaCl/Kg H_2O), η = absolute viscosity of NaCl solutions (centipoise), and η_w = viscosity of water (centipoise). In equation (1), the viscosity of water is calculated from

$$\eta_w = \eta_0 \exp\left[\frac{d}{d^*} \sum_{i=0}^{5} \sum_{j=0}^{4} b_{ij}\left(\frac{T^*}{T} - 1\right)^i \left(\frac{d}{d^*} - 1\right)^j\right]$$

with

$$\eta_0 = \left(\frac{T}{T^*}\right)^{1/2} \left[\sum_{k=0}^{3} a_k \left(\frac{T^*}{T}\right)^k\right]^{-1} \qquad (2)$$

(in Pa-s, or 10^3 cP) where T* = 647.27°K and d* = 317.763 kg/m^3. As can be seen, equation (1) reduces to that of water when m = 0, and reduces to polynomial form with a temperature correction term for large values of molality. Equation (1) reproduces the experimental data to an average of better than 2% over the ranges 10-350°C, 1-50 MPa and 0-5 M. See Table 1 for values of η up to 195°C.

The change in viscosity for NaCl solutions has been studied for pressures up to 150 MPa and temperatures to 356°C. Over these ranges the viscosity increases by 1-2%.

Data published by Grimes et al. (1979) on the viscosity of KCl solutions up to 150°C and saturated vapor pressures are given in Table 2. The relative viscosity of KCl solutions is lower than that of NaCl solutions at equivalent molal concentrations and temperatures. Furthermore, the addition of NaCl in the molal ratio 3:1 gives a solution with a relative viscosity higher than that for 4 m KCl but less than that of 4 m NaCl.

Data on the viscosity of $CaCl_2$ solutions up to 90°C were published recently by Gruzdev et al. (1977) and by Goncalves and Kestin (1979). Plots of the relative viscosity of $CaCl_2$ solutions up to 90°C for concentrations between 0.474 and 4.4 m show a flat region over which there is no change in viscosity; at 4.4 m, the relative viscosity decreases over the temperature range 50-90°C. Additionally, the relative viscosity values are higher than those of comparable NaCl solutions by a factor of 1-2. We have correlated the experimental data contained in the International Critical Tables, as well as that published in Gruzdev et al. (1977) and Goncalves and Kestin (1979), for concentrations up

Table 1. The absolute viscosity of NaCl solutions in cp up to 195°C and 5 m concentrations. Pressure = 0.1 MPa.

Temp. (°C)	Density* (kg/m^3)	Molal concentration of NaCl 0	1	2	3	4	5
0	999.557	1.7937	1.9622	2.1758	2.4360	2.7440	3.1013
5	999.676	1.5209	1.6661	1.8485	2.0696	2.3311	2.6343
10	999.428	1.3082	1.4352	1.5931	1.7838	2.0090	2.2698
15	998.850	1.1391	1.2515	1.3899	1.5564	1.7527	1.9799
20	997.976	1.0024	1.1029	1.2255	1.3724	1.5454	1.7454
25	996.833	0.8903	0.9810	1.0905	1.2214	1.3752	1.5529
30	995.446	0.7972	0.8796	0.9783	1.0958	1.2336	1.3929
35	993.838	0.7189	0.7944	0.8840	0.9902	1.1146	1.2583
40	992.025	0.6525	0.7220	0.8038	0.9005	1.0135	1.1440
45	990.025	0.5955	0.6600	0.7351	0.8236	0.9269	1.0460
50	987.581	0.5464	0.6064	0.6757	0.7571	0.8520	0.9614
55	985.512	0.5036	0.5597	0.6240	0.6992	0.7868	0.8877
60	983.021	0.4662	0.5188	0.5787	0.6485	0.7296	0.8230
65	980.383	0.4331	0.4827	0.5387	0.6038	0.6792	0.7661
70	977.605	0.4039	0.4507	0.5033	0.5641	0.6345	0.7155
75	974.694	0.3778	0.4222	0.4717	0.5287	0.5947	0.6705
80	971.653	0.3544	0.3967	0.4434	0.4970	0.5590	0.6301
85	968.487	0.3335	0.3738	0.4179	0.4685	0.5269	0.5939
90	965.197	0.3145	0.3530	0.3950	0.4428	0.4979	0.5611
95	961.786	0.2974	0.3343	0.3741	0.4195	0.4716	0.5314
100	958.257	0.2818	0.3172	0.3552	0.3983	0.4477	0.5044
105	954.610	0.2676	0.3016	0.3379	0.3789	0.4260	0.4798
110	950.847	0.2546	0.2874	0.3221	0.3612	0.4060	0.4573
115	946.968	0.2427	0.2743	0.3076	0.3450	0.3878	0.4366
120	942.974	0.2317	0.2623	0.2943	0.3301	0.3710	0.4177
125	938.866	0.2217	0.2513	0.2820	0.3163	0.3555	0.4002
130	934.644	0.2124	0.2411	0.2707	0.3036	0.3412	0.3840
135	930.309	0.2038	0.2316	0.2602	0.2919	0.3280	0.3691
140	925.861	0.1958	0.2229	0.2505	0.2810	0.3157	0.3552
145	921.301	0.1884	0.2147	0.2415	0.2709	0.3043	0.3424
150	916.629	0.1815	0.2072	0.2331	0.2615	0.2937	0.3304
155	911.846	0.1751	0.2001	0.2253	0.2528	0.2839	0.3193
160	906.953	0.1691	0.1936	0.2180	0.2446	0.2747	0.3089
165	901.950	0.1635	0.1875	0.2112	0.2370	0.2661	0.2992
170	896.839	0.1583	0.1817	0.2048	0.2299	0.2581	0.2902
175	891.622	0.1534	0.1764	0.1989	0.2232	0.2506	0.2817
180	886.298	0.1489	0.1713	0.1933	0.2169	0.2436	0.2737
185	880.871	0.1446	0.1666	0.1880	0.2111	0.2369	0.2663
190	875.341	0.1405	0.1622	0.1831	0.2056	0.2307	0.2592
195	869.711	0.1367	0.1580	0.1785	0.2004	0.2249	0.2526

*Density of pure water.

Table 2. The absolute viscosity of aqueous KCl solutions in cp up to 150°C and 5 m concentrations. Pressure is equal to 0.1 MPA or the vapor pressure, whichever is higher.

Temp. (°C)	Molal concentration of KCl 0.5	1	2	3	4	5
25	0.8989	0.9041	0.9107	0.9234	0.9559	1.0217
30	0.8066	0.8133	0.8243	0.8407	0.8732	0.9321
35	0.7289	0.7368	0.7512	0.7704	0.8026	0.8558
40	0.6630	0.6718	0.6888	0.7100	0.7418	0.7902
45	0.6064	0.6159	0.6349	0.6576	0.6889	0.7331
50	0.5575	0.5675	0.5880	0.6118	0.6425	0.6832
55	0.5149	0.5253	0.5468	0.5715	0.6014	0.6391
60	0.4775	0.4882	0.5106	0.5357	0.5650	0.6000
65	0.4445	0.4553	0.4783	0.5037	0.5323	0.5649
70	0.4152	0.4262	0.4495	0.4750	0.5029	0.5335
75	0.3890	0.4001	0.4237	0.4491	0.4763	0.5050
80	0.3656	0.3766	0.4003	0.4257	0.4521	0.4792
85	0.3445	0.3555	0.3792	0.4043	0.4301	0.4557
90	0.3254	0.3364	0.3600	0.3848	0.4099	0.4342
95	0.3081	0.3190	0.3424	0.3669	0.3913	0.4144
100	0.2923	0.3032	0.3264	0.3504	0.3741	0.3962
105	0.2780	0.2887	0.3116	0.3353	0.3583	0.3794
110	0.2648	0.2755	0.2981	0.3212	0.3436	0.3638
115	0.2528	0.2633	0.2856	0.3082	0.3300	0.3494
120	0.2417	0.2521	0.2740	0.2962	0.3173	0.3360
125	0.2315	0.2418	0.2633	0.2849	0.3054	0.3235
130	0.2221	0.2323	0.2533	0.2745	0.2944	0.3118
135	0.2134	0.2234	0.2441	0.2647	0.2840	0.3010
140	0.2054	0.2153	0.2356	0.2556	0.2744	0.2908
145	0.1980	0.2078	0.2276	0.2471	0.2653	0.2813
150	0.1912	0.2008	0.2202	0.2391	0.2568	0.2724

to 4 m (30 wt %) and temperatures up to 70°C. See Table 3.

Measurements of the viscosity of mixtures of NaCl and $CaCl_2$ over the range 20-90°C and up to 35% concentration show that the viscosity is higher than that of NaCl, even at equal molal concentrations.

Table 3. The relative viscosity of $CaCl_2$ solutions up to 70°C and 3 m concentrations.

Temp. (°C)	Molal Concentration of $CaCl_2$ 0.25	0.5	1	2	3
20	1.069	1.146	1.321	1.785	2.488
25	1.071	1.149	1.328	1.797	2.463
30	1.073	1.152	1.334	1.809	2.477
35	1.074	1.155	1.341	1.823	2.492
40	1.075	1.159	1.348	1.836	2.507
45	1.078	1.163	1.355	1.849	2.523
50	1.079	1.166	1.363	1.860	2.537
55	1.082	1.170	1.371	1.877	2.555
60	1.084	1.175	1.379	1.892	2.570
65	1.086	1.179	1.388	1.907	2.586
70	1.088	1.184	1.397	1.923	2.604

For NaCl/$CaCl_2$ ratios of about 2:1, the viscosity is about 10% higher than for equivalent NaCl solutions; the viscosity is about 25% higher when the molal ratio is 1.

SUMMARY AND CONCLUSIONS

The change in relative viscosity with concentrations differs markedly for $CaCl_2$ solutions as compared with NaCl and KCl solutions. See, for example, Figure 1. In this figure data for $LaCl_3$ obtained from Spedding's paper are plotted for comparative purposes. As can be seen, the curve for $CaCl_2$ has a shape similar to that of $LaCl_3$. The shape of the curve for $LaCl_3$ has been attributed to the highly hydrated La^{+3} ion; it is likely that the rapid increase in viscosity for Ca^{+2} is related also to hydration. Application of the Vand equation might assist in verifying that the large increase in viscosity at concentrations exceeding about 3 m is due to an obstruction of the stream lines in the water solvent by hydrated Ca^{+2} ions. By contrast, KCl is not considered to be highly hydrated in aqueous solutions. Additional information about this approach is found in the publications by Vand (1948), Spedding and Pikal (1966), and Out and Los (1980).

The A coefficient of the Jones-Dole equation is determined by ion-water interactions to form ion-bound water complexes, and by ionic mobilities; the

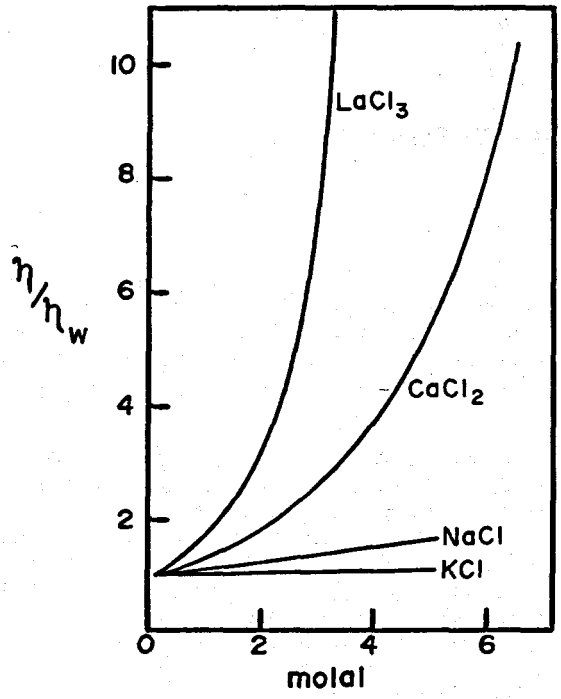

Figure 1. Relative viscosity of KCl, NaCl, $CaCl_2$, and $LaCl_2$ at 20°C. [XBL 808-11239]

A coefficients are calculated from theory for NaCl, KCl, and many other electrolytes. The B coefficient of ions in water shows a strong temperature dependence; the magnitude of B depends on the dissolved salt and resulting ion-water interactions. The dependence of B on temperature has been studied for NaCl, KCl, and other electrolytes (e.g., LiCl) by Out and Los up to 90°C, by Kaminsky (1957) for temperatures between 12.5 and 42.5°C, and by Kay et al. (Out, 1980) for tetraalkylammonium halides between 0 and 65°C. Systematic studies of the D coefficient are mainly those by Out and Los, and at 25°C, by Desnoyers and Perron (1972).

The a, b, and c coefficients in the Vand equation have not been as well studied for aqueous electrolytes such as NaCl. If the first term only is retained, then the Vand equation gives an "excellent representation of the viscosities of many 'strongly hydrated' electrolytes in the region of moderate to high concentrations." The rapidly increasing viscosity with increased concentration is attributed to an "obstruction" effect, due to interference of large hydrated ions with the stream lines in the solvent. See Spedding and Pikal (1966).

LITERATURE CITED

Desnoyers, J. E., and Perron, 1972. The viscosity of aqueous solutions of alkali and tetraalkyl ammonium halides at 25°C. J. Soln. Chem., v. 1, p. 199.

Goncalves, F. A., and Kestin, J., 1979. The viscosity of $CaCl_2$ solutions in the range 20-50°C. Ber. Bunsenges Phys. Chem., v. 83, p. 24.

Grimes, C. E., Kestin, J., and Khalifa, H. E., 1979. The viscosity of aqueous KCl solutions in the temperature range 25-150°C and the pressure range 0-30 MPa. J. Chem. Eng. Data, v. 24, p. 121.

Gruzdev, V. A., Genrikh, V. H., and Shestova, A. I., 1977. Experimental study of viscosity and thermal conductivity of some electrolyte aqueous solutions. Issled. Teplofiz. Svoistv Zhidk. Rastvorov Splavov, p. 20-39.

Kaminsky, M., 1957. Ion-solvent interaction and the viscosity of strong-electrolyte solutions. Discussions Faraday Soc., v. 24, p. 171.

Lyon, R. N., and Kolstad, G. A., 1974. A recommended research program in geothermal chemistry. WASH-1344, Department of Energy, Washington, D. C.

Out, D. J. P., and Los, J. M., 1980. Viscosity of aqueous solutions of univalent electrolytes from 5 to 95°C. J. Soln. Chem., v. 9, p. 19.

Phillips, S. L., Otto, R. J., Ozbek, H., and Tavana, M., 1979. Aqueous solutions database to high temperatures and pressures. NaCl solutions. Berkeley, Lawrence Berkeley Laboratory, LBL-9621.

Phillips, S. L., Ozbek, H., Igbene, A., and Litton, G., 1980. Viscosity of NaCl and other solutions up to 350°C and 50 MPa Pressures. Berkeley, Lawrence Berkeley Laboratory, LBL-11586.

Spedding, F. H., and Pikal, M. J., 1966. Relative viscosities of some aqueous rare earth chlorides at 25°. J. Phys. Chem., v. 70, p. 2430.

Vand, V., 1948. Viscosity of solutions and suspensions, I. Theory. J. Phys. Chem., v. 52, p. 277.

A DATABASE OF CHEMICAL PROPERTIES OF NUCLEAR WASTE ELEMENTS IN AQUEOUS SOLUTIONS

S. L. Phillips and A. Igbene

A program has been initiated at Lawrence Berkeley Laboratory (LBL) to evaluate critically the existing data on the basic properties of nuclear waste elements in order to predict the effects of their long-term isolation in the geologic environment. Included in the program are those elements which are important to studies of the migration, leaching, and treatment of nuclear waste constituents in water. The results of this work will consist not only of tabulated data using an internally consistent set of units, but also of a description of methods useful in calculating data, recommended values for each property and, where necessary, recommendations for additional research (Phillips, 1980).

The results of the work will be made available in two different reports. One will be a critical survey of currently available published data and theory intended to identify significant research gaps and to make recommendations for additional research; the other will be a tabulation of experimental and recommended values for each element and property.

The objective of the program is threefold: (1) to make a critical survey of the currently available published data and theory of the thermodynamic and physical properties of selected nuclear waste elements in order to identify significant research gaps, (2) to tabulate experimental values, theoretical equations, and recommended values for each property and selected waste element; and (3) to utilize modern computer methods for handling bibliographic references and calculating numerical data.

Table 1. The elements and soluble species included in the program.

Uranium and transuranium		Alkali and alkaline earth		Metals		Nonmetals	
Uranium	UO_2^{+2}	Cesium	Cs^+	Technetium	TcO_4^-	Nitrogen	NO_3^-
	UO_2^+				$TcO_4^=$		
	U^{+4}	Strontium	Sr^{+2}		$TcOCl_4^-$	Iodine	IO_3^-
	U^{+3}				Tc^{+4}		I^-
		Radium	Ra^{+2}		Tc^{+3}		
Americium	AmO_2^{+2}					Selenium	SeO_4^-
	AmO_2^+			Thorium	Th^{+4}		SeO_3^{-2}
	Am^{+4}						Se^{-2}
	Am^{+3}			Tin	Sn^{+4}		
					Sn^{+2}	Carbon	CO_3^{-2}
Curium	Cm^{+4}						HCO_3^-
	Cm^{+3}			Nickel	Ni^{+2}		
						Phosphorus	PO_4^{-3}
Neptunium	NpO_2^{+2}			Zirconium	Zr^{+4}		PO_3^{-3}
	NpO_2^+				Zr^{+2}		
	Np^{+4}					Sulfur	SO_4^{-2}
Plutonium	PuO_2^{+2}			Samarium	Sm^{+3}		
	PuO_2^+				Sm^{+2}		
	Pu^{+4}						
	Pu^{+3}			Iron	Fe^{+3}		
					Fe^{+2}		
				Europium	Eu^{+3}		

A number of radionuclides and their properties are needed to predict the effectiveness of nuclear waste handling systems. Priority will be assigned those areas for which the need is greatest and which the data are not readily available (see Table 1 and Benson and Teague, 1980).

The LBL project will cover data relevant to the following three major aspects of nuclear waste handling:

1. Migration, where the solution is in contact with the geologic environment. Parameters relevant to migration include adsorption rate, desorption rate, solubility, diffusion coefficient, dissolved species, composition of the supporting electrolyte, complex dissociation constant, heterogeneous equilibrium constant, pH, and Eh.

2. Leaching, in which solidified nuclear waste material is dissolved by a solution. Typical parameters include solubility, rate of dissolution, surface area, species, diffusion coefficient, diffusion path tortuosity, porosity, permeability, convection, pH, and Eh.

3. Treatment methods to remove long-lived radioactive waste elements from the solutions, mainly plutonium and americium. Selected parameters include solubility, chelate formation constants, and partition equilibrium constants.

Selected elements considered important to waste handling include both those originally present in the waste, and those which may form during the storage period. The work will be limited to the species formed by these elements in aqueous solutions containing the most important ligands, such as hydroxyl, chloride, sulfate, carbonate, phosphate, and organic chelates (see Table 1). Site-specific data is specifically excluded from this work.

In fiscal 1981 work was begun on our first report, which will consist of recommended values for the hydrolysis constants of Pu species (PuO_2^{2+}, PuO_2^{+}, Pu^{4+}, PU^{3+}) to 200°C. Pertinent recent research publications include Cleveland (1970), Allard et al. (1980), Lemire and Tremaine (1980), and Rai et al. (1980).

Besides commonly used methods for measuring complexation constants such as EMF, our work will include a description of methods developed in other fields, but which may have application to the measurement of complexation constants. For example, the rate of complexation might be measured from certain electrochemical reactions according to the following theory for a coupled catalytic chemical reaction (see, for example, Delahay (1954)):

$$OZ + ne \rightarrow R + Z$$

$$R + Z \xrightarrow{k} OZ,$$

where OZ is the electroactive complex. The initial boundary-value problem for a diffusion-controlled electrochemical reaction with a coupled catalytic reaction can be described using Fick's law for a planar electrode:

$$\frac{\partial C_{OZ}}{\partial t} = D_{OZ} \frac{\partial^2 C_{OZ}}{\partial x^2} + kC_R C_Z,$$

$$\frac{\partial C_R}{\partial t} = D_R \frac{\partial^2 C_R}{\partial x^2} - kC_R C_Z.$$

Initially,

$$t = 0,\ 0 < x < \infty:\quad C_{OZ} = C^*_{OZ},\ C_R = 0;$$

then

$$t > 0,\ x \rightarrow \infty:\quad C_{OZ} \rightarrow C^*_{OZ},\ C_R \rightarrow 0$$

$$x = 0:\quad C_{OZ} = 0$$

$$\frac{i}{nFA} = D_{OZ} \frac{\partial C_{OZ}}{\partial x},$$

$$-D_{OZ} \frac{\partial C_{OZ}}{\partial x} = D_R \frac{\partial C_R}{\partial x}.$$

This boundary-value problem may be solved by applying the Laplace transform.

REFERENCES CITED

Allard, B., Kipatsi, H., and Liljenzin, 1980. Expected species of uranium, neptunium and plutonium in neutral aqueous solutions. J. Inorg. Nucl. Chem., v. 42, p. 1015.

Benson, L. V., and Teague, L. S., 1980. A tabulation of thermodynamic data for chemical reactions involving 58 elements common to radioactive waste package systems. Berkeley, Lawrence Berkeley Laboratory, LBL-11448.

Cleveland, J. M., 1970. The Chemistry of Plutonium. New York, Gordon and Breach.

Delahay, P., 1954. New Instrumental Methods in Electrochemistry. New York, Interscience, p. 102.

Lemire, R. J., and Tremaine, P. R., 1980. Uranium and plutonium equilibria in aqueous solutions to 200°C. J. Chem. Eng. Data, v. 25, p. 361.

Phillips, S. L., 1980. A database of chemical properties of nuclear waste elements in aqueous solutions. Berkeley, Lawrence Berkeley Laboratory, LBID-162.

Rai, D., Serne, R. J., and Swanson, J. L., 1980. Solution species of plutonium in the environment. J. Environ. Quality, v. 9, p. 417.

GEOCHEMICAL ASSESSMENT OF FIVE POTENTIAL SITES FOR HYDROTHERMAL MAGMA SYSTEMS

A. F. White

The need for a comparative assessment of potential sites for deep drilling in continental structures was assessed by the Workshop on Continental Drilling for Scientific Purposes, held at Los Alamos, New Mexico. The workshop resulted in a report entitled "Continental Scientific Drilling Program" (National Academy of Sciences, 1979). The report identified major scientific objectives in four areas of study: basement structures and deep continental basins, thermal regimes, mineral resources, and earthquakes. The Department of Energy has a particular interest in thermal regimes because of its commitment to utilization of energy resources and waste disposal. Utilization of geothermal energy, in situ fossil fuel recovery and nuclear waste emplacement in geologic materials are obvious examples.

A proposal to conduct a comparative assessment of five potential hydrothermal-magma sites was prepared and approved by the Department of Energy (DOE), Office of Basic Energy Sciences in November 1979. The four participating DOE laboratories are Los Alamos National Scientific Laboratory (LANSL), Lawrence Berkeley Laboratory (LBL), Lawrence Livermore National Laboratory (LLNL) and Sandia National Laboratory (SNL). The five sites are The Geysers-Clear Lake area, California, Long Valley, California, Salton Trough, California, Roosevelt Hot Springs, Utah, and the Rio Grande rift, New Mexico. Each laboratory was assigned a task of evaluating specific aspects of each site, e.g., geology, geochemistry, geophysics, and energy transport. LBL was assigned the task of geochemical evaluation. Each laboratory also contributed personnel to each of the other tasks. The geochemistry subgroup was chaired by the author. Other members included W. S. Baldridge of LANSL, T. M. Gerlock of SNL, and K. Krauss of LLNL.

CONCLUSIONS REGARDING IMPORTANT GEOCHEMICAL MECHANISMS

Geochemistry of Magma and Associated Lavas

Primary magma sources in the earth's mantle are beyond the reach of present drilling technology. However, magmas that have been introduced into the crust at shallow depth represent possible drilling targets. Whereas geologic and geophysical techniques involving deep drilling can provide information regarding the depth, size, and heat distributions of such magmas, igneous geochemistry is the principal method available for addressing questions concerning the origin and evolution of magmatic systems at a given site. Specific questions involve the origin, coalescence, migration, contamination, emplacement, and crystallization of magma systems. Two of the areas, Long Valley and The Geysers, are inferred to be underlain by a simple large magma chamber. One of the geothermal areas, Roosevelt Hot Springs, may be underlain by such a magma chamber. The remaining two, the Salton Sea geothermal area and the Rio Grande rift, occupy rift settings. The Salton Sea area is located in an oceanic-ridge transform zone and apparently is not underlain by a large magma body. The thermal anomaly is caused by dike injection from small spreading centers. The Rio Grande rift is a major continental rift related to the Basin and Range extensional province. At least one area of the rift, the Valles Caldera, is probably underlain by a large, high-level silicic magma reservoir.

Geochemistry of Hydrothermal Fluids

In general, the data describing the chemistry of hydrothermal fluids have two applications. One application is related to answering scientific questions in related fields. For example, geothermometers can be used to estimate reservoir temperatures. Isotopic data can be employed in estimating age and origin of hydrothermal fluids. Dissolution and aqueous equilibrium constraints can be applied to determine diagenetic changes in secondary permeability and reservoir evolution.

The other application is to use the data to answer basic questions concerning chemical mechanisms and evolution of hydrothermal fluids. For example, the literature indicates that hydrothermal fluids at all sites are high in certain elements, including As, B, Br, F, Cl, and Li. Are these elements derived directly from magmatic sources or from dissolution of reservoir rocks? What is the source of abundant sulfur associated with these solutions? Another major question that can be resolved by drilling is the relationship between hydrothermal solutions and transport and deposition of ore-forming elements.

All five of the proposed sites possess surface and subsurface manifestations of hydrothermal activity to varying degrees. Table 1 is a summary of typical solution compositions associated with each site. Two of the sites, The Geysers and, to a lesser extent, the Valles Caldera, possess vapor-dominated systems. Mercury deposition is associated with The Geysers system, and anomalous heavy metal concentrations occur in the Salton Trough brines.

Geochemistry of Hydrothermal Alteration

Hydrothermal alteration represents the interface between the aqueous and/or vapor geochemistry and the geochemistry of the reservoir rock. Such alteration may be controlled by the development of hydrothermal circulation. In turn, hydrothermal alteration may increase or decrease rock permeability and affect both circulation and convective heat transport. Such hydrothermal alteration records

Table 1. Examples of water compositions associated with geothermal systems in ppm.

	SiO_2	Al	Fe	Mn	As	Ca	Mg	Na	K	Li	NH_4	HCO_3	CO_3	SO_4	Cl	F	Br	NO_3	B	H_2S	pH	Temp.
Geysers-Clear Lake vapor-dominated system[1]	225	14	63	14	--	47	281	12	5	--	1400	0	--	5710	0.5	--	--	--	3.1	--	1.8	100
Geysers-Clear Lake water reflecting serpentization[2]	0.4	0.2	--	--	--	40	0.3	19	11	--	0.19	0	0	0.4	63	0	--	--	0.02	--	11.54	20
Geysers-Clear Lake water reflecting weathering of serpentine[3]	170	0.66	0.22	0.02	--	30	238	162	26	--	--	1258	0.2	6.3	272	--	2	9.2	19	--	6.17	52
Geysers-Clear Lake water from Great Valley sequence[4]	190	--	--	--	--	1.4	58	9140	460	14	303	7390	--	23	11,000	1.1	15	--	293	--	7.2	57
Long Valley thermal water[5]	110	--	--	--	0.74	50	0.6	410	30	2.8	0.40	416	--	96	200	8.4	--	--	10.6	2.3	6.5	79
Long Valley shallow water systems[6]	58	--	--	--	0.02	5.1	5.9	23	40	0.04	0.13	90	0	8.1	5.7	0.5	--	--	0.37	0.1	6.8	11
Rio Grande rift Valles Caldera thermal water[7]	170	--	--	--	--	7.3	13	4800	180	--	--	--	--	1600	2600	16	14	--	26	--	7.7	--
Rio Grande rift groundwater[8]	96	--	--	--	--	160	6.6	510	63	--	--	773	0	290	300	4.4	3.0	--	7.4	--	6.6	--
Roosevelt Hot Springs thermal water[9]	639	1.86	0.016	--	--	31	0.26	2072	403	--	--	25	--	48	3532	--	--	--	--	--	5.0	92
Salton Trough brine[10]	400	--	2000	1370	--	28,800	10	53,000	16,500	210	--	682	--	96	155,000	--	--	--	390	--	5.2	>300
Salton Trough surface water[11]	41	>0.5	>0.3	1	--	435	69	5430	334	12	52	630	--	414	8920	--	9.1	--	62	--	6.33	34

[1] Table 1, White (1970).
[2] Table 2, Barnes and O'Neil (1969).
[3] Seigler Spring, Barnes et al. (1973).
[4] Wilbur Springs (Table 1), Barnes (1970).
[5] 3S/28E-13ES3 (Table 1), Mariner and Wiley (1976).
[6] 2S/28E-25AS1 (Table 1), Mariner and Wiley (1976).
[7] N4 (Table 1), Trainer and Lyford (1979).
[8] H17 (Table 1), Trainer and Lyford (1979).
[9] Sample #3, Parry et al. (1980).
[10] NO2 11D, Helgeson (1968).
[11] Table 1, Muffler and White (1969).

not only the presently active hydrothermal processes but also the past spatial, chemical, and temperature regimes in such systems. Access to such a record by drilling would be important in determining whether hydrothermal alteration reduces permeability sufficiently to cause liquid-dominated hydrothermal systems to evolve into vapor-dominated systems. Spatial distributions of hydrothermal alteration is also important in evaluating geophysical anomalies associated with geothermal sites. Deep drilling also offers an oppportunity to observe alteration assemblages and specific hydrothermal solutions at known temperatures and pressures.

The review of available information and conclusions regarding geochemistry at each site has been published (White, 1980).

RECOMMENDATIONS ON SPECIFIC SITE SELECTION

On the basis of conclusions of the geochemistry and other subgroups (Goff and Waters, 1980; Hardee, 1980; White, 1980), the following recommendations have been made to DOE and the National Academy of Sciences for specific sites in order of preference.

1. Valles Caldera. A scientific drilling program emphasizing features associated with the resurgent dome of the caldera would provide important information in developing an understanding of caldera-forming hydrothermal systems common in continental regimes. The proposed drilling program consists of a deep hole (10 km) sited on the resurgent dome. Technological developments would be required, and a hole of moderate depth (5 km) would be the initial target.

2. The Geysers-Clear Lake Area. Scientific drilling at The Geysers provides a unique opportunity to assess the roots of a major vapor-dominated geothermal system. This uniqueness does limit potential application of the results in liquid-dominated active and fossil geothermal systems. A carefully conceived, comprehensive and extensive drilling program will be required given the structural and geologic complexity of the area.

3. Salton Trough. Available data indicate the presence of intrusions, perhaps as dike swarms at depths of 2-10 km. Scientific drilling in this area would provide valuable information about the roots of an economically important geothermal system associated with an oceanic spreading center, but only limited information on magmatic sources. It is probable that magma targets are small and distributed.

4. Long Valley. Recent data indicate that low-temperature gradients may preclude the existence of magma at depths accessible by drilling. Many of the scientific questions of interest to continental drilling concerning caldera development can be answered by drilling at the Valles Caldera, a more promising target.

5. Roosevelt Hot Springs. The current database is inadequate for direct comparison with the other four sites.

REFERENCES CITED

Barnes, I., and O'Neil, J. R., 1909. The relationship between fluids in some fresh alpine typ ultramafics and possible modern serpentinization. Geol. Soc. America Bull. v. 80, p. 1947-1960.

Barnes, I., Hinkle, M. E., Rapp, J. B., Heropoulos, C., Vaugh, W. W., 1973. Chemical composition of naturally occurring fluids in relation to mercury deposits in part of north-central California. U. S. Geol. Survey Bull. 1382A, 19 p.

Barnes, I., 1970. Metamorphic waters from the Pacific tectonic belt of the west coast of the United States. Science, v. 168, p. 973-975.

Goff, F., and Waters, A., 1980. Continental Scientific Drilling Program--Thermal regimes, geology of five magma-hydrothermal systems. Los Alamos, New Mexico, Los Alamos National Scientific Laboratory, LA 8550-OBES, 99 p.

Hardee, H. C., 1980. Comparative assessment of five potential sites for hydrothermal-magma systems --Energy transport. Sandia National Laboratory, SAND 80-1671, 20 p.

Helgeson, H. C., 1968. Geologic and thermodynamic characteristics of the Salton Sea geothermal system. Am. J. Sci., v. 266, p. 129-166.

Mariner, R. H., and Wiley, L. M., 1976. Geochemistry of thermal waters in Long Valley, Mono County, California. J. Geophys. Res., v. 81, p. 792-800.

Muffler, L. J. P., and White, D. E., 1969. Active metamorphism of the upper Cenozoic sediments in the Salton Sea geothermal field and the Salton trough. Geol. Soc. America Bull., v. 80, p. 137-181.

National Academy of Science, 1979. Continental scientific drilling program. National Academy of Sciences, 210 p.

Parry, W. T., Ballantyne, J. M., Bryant, N. L., Dedolph, R. E., 1980. Geochemistry of hydrothermal alteration of the Roosevelt Hot Springs thermal area, Utah. Geochim. Cosmochim. Acta, v. 44, p. 95-102.

Trainer, F. W., and Lyford, F. P., 1979. Geothermal hydrology in the Rio Grande rift, north central New Mexico, in New Mexico Geol. Soc. Guidebook, 30th Field Conf., Santa Fe County, p. 299-306.

White, A. F., 1980. Comparative assessment of five potential sites for hydrothermal magma systems --Geochemistry. Berkeley, Lawrence Berkeley Laboratory, LBL-11410, UC-60B, 72 p.

White, D. E., 1980. Geochemistry applied to discovery, evaluation, and exploration of geothermal energy resources. U. N. Symp. on Development and Utilization of Geothermal Resources, Pis Proc. Geothermics, Spec. Issue, v. 2, p. 58-80.

DEEP ELECTROMAGNETIC CRUSTAL SOUNDING IN NORTHERN NEVADA

M. J. Wilt, N. E. Goldstein, H. F. Morrison, and J. R. Haught

The Battle Mountain heat-flow high, situated in north-central Nevada, covers several thousand square miles in five counties. This region is characterized by an average heat flow that is twice the continental average and by a number of geothermal anomalies (Fig. 1). Geologically this area is known for its high elevation, frequent earthquakes, fairly recent volcanism, and the presence of numerous thermal springs (Garside and Schilling, 1979). There are also suggestions of continental spreading and abundant evidence of recent faulting (Lachenbruch and Sass, 1977).

The origin and nature of this large region of anomalously high heat flow have not been studied in great detail, although significant work has been done (e.g., Sass et al., 1971; Thompson and Burke, 1974). Seismic evidence from distant earthquakes and nuclear tests has indicated an anomalously shallow crustal section in this region overlying a low-velocity mantle (Hill and Pakiser, 1966; Majer, 1978). There are also indications (from a seismic refraction experiment) of a general upwarp in the mantle surface in this region (Majer, 1978). Magnetotelluric surveys in northern Nevada and Idaho have indicated the presence of low-resistivity zones as shallow as 10 km and at a depth of 15 km throughout the region (Morrison et al., 1979; Stanley et al., 1977). Although the presence of these zones remains unconfirmed by seismic or gravity measurements, it is possible that both of these methods could miss such features if they are relatively thin bodies. It is also conceivable that this low-resistivity zone may not give rise to a seismic or gravity anomaly. Another possibility, however, is that the magnetotelluric data may be distorted by lateral resistivity contrasts or that the anomaly itself could be the manifestation of some source field distortion. As the presence of a deeply buried conductor may have significant importance in helping to explain the anomalous region in northern Nevada, it is important to confirm the presence of such bodies and to learn more about them.

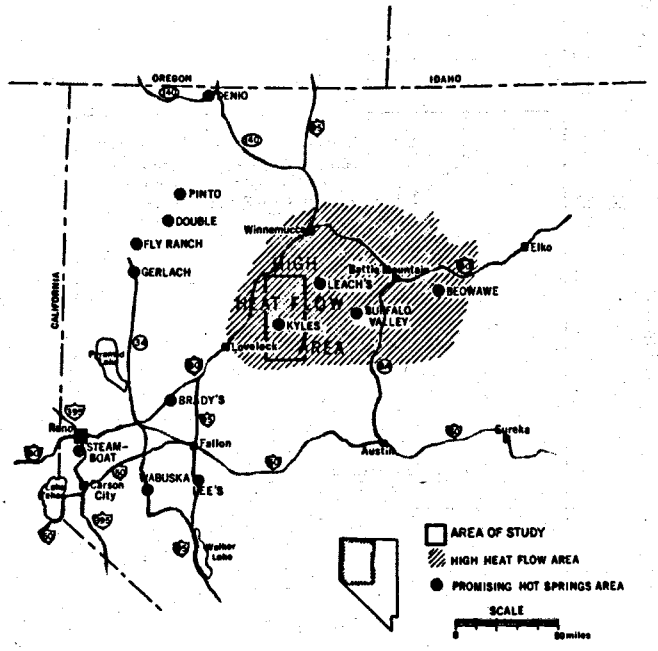

Figure 1. Buena Vista Valley in north central Nevada, field site for experiment. [XBL 813-2785]

To confirm the magnetotelluric results and to map the low-resistivity zones in greater detail, a deep electromagnetic induction sounding experiment was undertaken in north-central Nevada by LBL. The EM method has two distinct advantages for deep exploration when compared to MT. First, with EM the source field is known, and spatial variations in field strength can only be the result of geology, not of source field variations. Second, because the field strength strongly declines with increasing distance from the source, the method is much less sensitive to distant laterally inhomogeneous ground. The EM-60 system, which was originally designed for shallow to intermediate depth geothermal exploration, was used for the experiment. With this system a square-wave current between 0.01 and 1000 Hz is applied to a coil of wire via a motorized generator and a large transistorized switch (Morrison et al., 1978). The total vertical and radial magnetic field is detected at some distance from the loop transmitter, and the incoming data are studied and decomposed on site via Fourier transformation. The resultant field spectra, which include a primary and a secondary (induced) component, are compared to theoretical models to resolve the resistivity of the earth between the transmitter and the receiver. The depth of penetration is approximately equal to the transmitter-receiver separation. For a more detailed system description see Morrison et al. (1978) or Wilt et al. (1980).

Buena Vista Valley in north central Nevada was chosen as the field site for the experiment (Fig. 1). This valley provides an ideal setting for deep electromagnetic sounding measurements; it is long and wide with low relief, vehicular access is good, and the population density is low. In addition, the valley has an active hot springs system, and a significant number of geological and geophysical studies have already been completed (Goldstein et al., 1976).

PROGRESS IN 1980

During 1980 the field system was modified and preliminary field work was conducted. Modifications included a substantial strengthening of the source field and a significant lowering of the noise level

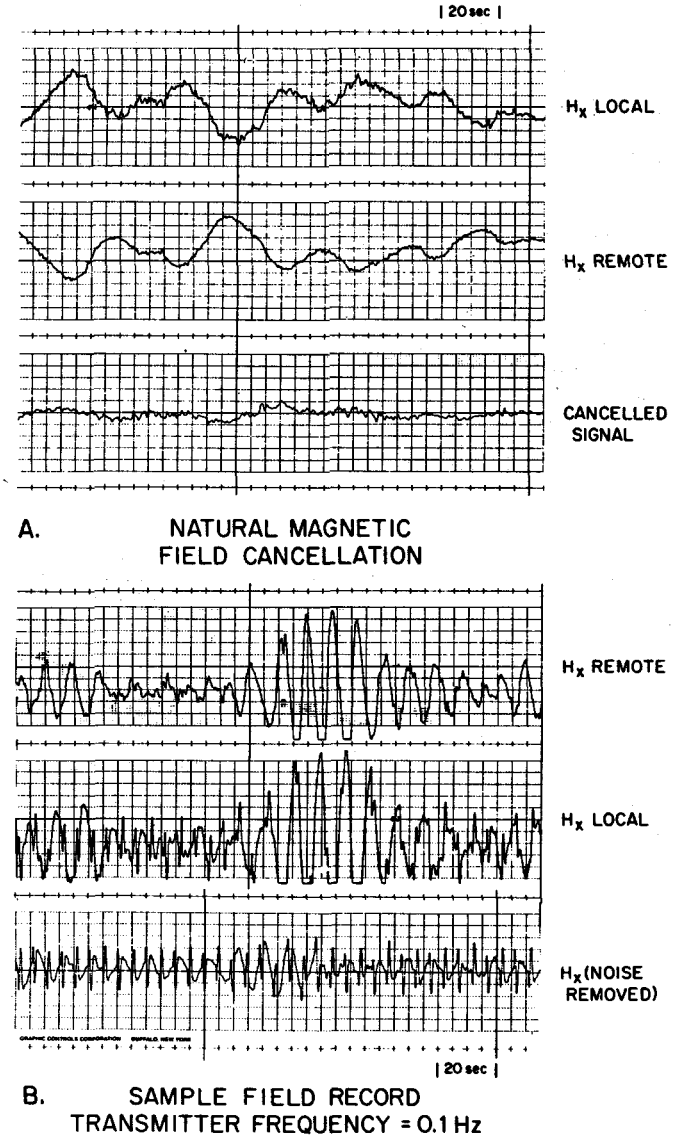

Figure 2. Example of data improvement using the telluric noise-cancellation scheme. (A) Natural geomagnetic signal and initial cancelling at the receiver site with transmitter off. (B) The same system but with transmitter on. [XBL 811-2584]

at the receiver. Both of these modifications were necessary because the transmitter-receiver separations must exceed 15 km to detect a body buried at 15 km and, since the strength of the source field declines as the square of the distance, the signal would be undetectable at the receiver without significant system changes.

To increase the source strength, a square loop 2.5 km on a side was planned for the survey. The loop was made of 30 km of heavy-gauge wire capable of carrying up to 40 A of current. The new loop provided a dipole moment of approximately 1×10^8 MKS, greater than 30 times the source strength used for intermediate-depth exploration. The logistics of laying such a loop in Buena Vista Valley proved considerable. Surveying and wire emplacement required three days for a field crew of four.

To reduce noise at the receiver, two things were done. Natural geomagnetic fields, which constitute noise for this method, were subtracted from the local signal by establishing a remote magnetic detector 100 km from the source and sending the signal via radio telemetry to the receiver. These remote signals, which are free of a dipole-source component, are inverted and subtracted from the local signal prior to switching on the loop current. An example of this procedure is given in Figure 2. Experience with this technique has shown that it can yield a signal-to-noise improvement of up to 20 dB. In addition to the noise cancellation, an HP-9835 on-site computer was added to the system. This device allows greater flexibility in signal processing and allows the evaluation of data segments prior to stacking. The resulting improvement in the quality of data should be significant, and the shortening of post-field processing time should be considerable.

RESULTS FROM FIELD SURVEY

Two weeks of field work were done in Buena Vista Valley in 1980. During this time several intermediate-depth soundings were performed, the distant reference magnetometer was emplaced and tested, the large loop was laid and tested, and preliminary distant sounding measurements were made. An example of one of the intermediate-depth soundings is shown in Figure 3, which consists of plots of ellipticity and tilt angle of the combined

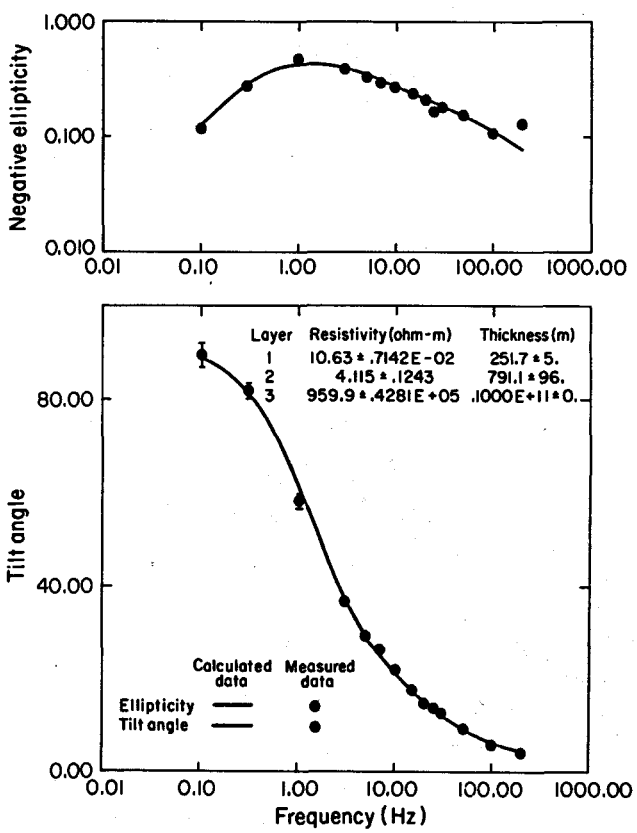

Figure 3. Joint inversion model for sounding BV3, Buena Vista Valley, Nevada. The transmitter-receiver separation is 2 km. [XBL 813-2699]

magnetic field vector as a function of frequency for a site 2 km from the transmitter at the northern end of Buena Vista Valley. A layered model was fit to this data by least-squares inversion, and the results indicate a low-resistivity sedimentary sequence 1 km in thickness overlying resistive basement. These intermediate-depth results are useful in determining the resistivity structure at the upper several kilometers. Distant soundings are not able to determine characteristics of the shallow structure but may be affected by variations within the shallower part of the section.

Preliminary measurements made from the large loop at a source-receiver separation of 20 km showed the problems of accurately measuring such a small magnetic field. The present system was unable to measure these signals with required accuracy even after repeated signal stacking. Geomagnetic noise levels were unusually high during the field experiment, and the noise-cancelling system did not function because of a breakdown in the remote magnetic sensor. In addition we experienced problems with the electronic instruments because of the extreme summer heat.

PLANS FOR 1981

In 1981 we plan a series of shallow and deep soundings in Buena Vista Valley. In light of our recent field experiences, we plan to increase the source strength by a factor of 2, replace heat-sensitive and unreliable instrumentation, and implement a further refinement of the geomagnetic noise-cancelling scheme. The source strength will be increased by the addition of more wire to the loop (the additional wire has been made available from another project). The new instrumentation has been field tested to temperatures in excess of 100°F and performed flawlessly.

To cancel geomagnetic noise, a scheme has been devised which calculates the theoretically invariant transfer tensor between the local and remote geomagnetic fields. Once this is calculated and tested to prove how constant the tensor coefficients are, then the geomagnetic noise may be analytically subtracted from the incoming fields. The expected signal-to-noise improvement is about 40 dB during periods of high natural field activity.

Plans for the field project include the measurement of 18 soundings during the spring of 1981. Of these, 12 are intermediate depth soundings to a maximum transmitter-receiver separation of 3 km, and the remaining six are deep soundings. The six deep soundings will be made from 10 to 30 km from the transmitter.

REFERENCES

Garsick, L. J., and Schilling, J. H., 1979. Thermal waters of Nevada. Nevada Bureau of Mines and Geology, Bulletin 91.

Goldstein, N. E., Beyer, H., Corwin, R., DiSomma, D. E., Majer, E., McEvilly, T. V., Morrison, H. F., Wollenberg, H. A., Grannel, R., 1976. Open File Report, Geoscience studies in Buena Vista Valley, Nevada. Berkeley, Lawrence Berkeley Laboratory, LBL-5913.

Hill, D. P. and Pakiser, L. C., 1966. Crustal structure between the Nevada Test Site and Boise, Idaho, from seismic refraction measurements. Amer. Geophys. Union, Geophysical Monograph 10, p. 391.

Lachenbruch, A. H., and Sass, J. H., 1977. Geothermal setting of the Battle Mountain High. Trans. Am. Geophys. Union, v. 58, no. 12, p. 1237.

Majer, E., 1978. Seismological investigations in geothermal areas (Ph.D. Thesis). University of California, Department of Geology and Geophysics, Berkeley, LBL-7054.

Morrison, H. F., Goldstein, N. E., Hoversten, M., Oppliger, G., and Riveros, C., 1978. Description, field test and data analysis of controlled-source EM system EM-60. Berkeley, Lawrence Berkeley Laboratory, LBL-7088.

Morrison, H. F., Lee, K. H., Oppliger, G., and Dey, A., 1979. Magnetotelluric studies in Grass Valley, Nevada. Berkeley, Lawrence Berkeley Laboratory, LBL-8646.

Sass, J. H., Lachenbruch, A. H., Munroe, R. G., Greene, G. W., Moses, T. H., Jr., 1971. Heat flow in the western United States. J. Geophys. Res., v. 76, p. 6376.

Stanley, W. D., Boehl, J. E., Bostick, F. X., and Smith, H. W., 1977. Geothermal significance of magnetotelluric soundings in the eastern Snake River Plain-Yellowstone region. J. Geophys. Res., v. 82, p. 2501.

Thompson, G. A. and Burke, D. B., 1974. Regional geophysics of the basin and range province. Ann. Rev. of Earth and Planet. Sci., v. 2, p. 213.

Wilt, M., Goldstein, N. E., Stark, M., and Haught, J. R., 1980. An electromagnetic (EM-60) survey in the Panther Canyon area, Grass Valley, Nevada. Berkeley, Lawrence Berkeley Laboratory, LBL-10993.

FEASIBILITY OF SHEAR WAVE VIBRATORS FOR DEEP CRUSTAL STUDIES

S. Coen

The nonlinear inverse-scattering problem has been investigated for a shear wave source on the surface of the earth. The data consist of displacements of the surface measured as a function of time and are used to determine the elastic profile of the earth. The theory has direct applications in exploration seismology and solid-earth geophysics. The data may be provided by the solution of the forward-scattering problem for a known vibrator type and elastic profile of the earth.

An elastic medium is characterized by three parameters, the density, ρ; the shear modulus, μ; and Lamé's constant, λ. In a vertically layered earth model, these are functions only of depth, Z: $\rho(Z)$, $\mu(Z)$, and $\lambda(Z)$, $0 < Z < \infty$. A recent paper by Coen (1980a) presents the solution for the shear modulus profile, $\mu(Z)$, determined uniquely from the static torsional stress beneath the source and the displacement on the surface. The shear modulus, $\mu(Z)$, and density, $\rho(Z)$, profiles are uniquely determined from the reflection coefficient, $S_{12}(\theta\omega)$, due to obliquely incident horizontally polarized shear plane waves (SH plane waves), as shown by Coen (1980b). The reflection coefficient must be available at two angles of incidence, θ_1 and θ_2, and at all frequencies, $0 < \omega < \infty$. The effects of a band-limited response and a finite source are under investigation.

The theory is being extended to include an impulsive SH-wave source and a vibratory torsional SH-wave source. A variety of radiation patterns for arrays of torsional vibrators have been computed and will soon be published (Coen and Yu, 1981). The results show that the shear wave energy from an array of phased torsional vibrators can be directed almost vertically downward despite the fact that the energy from a single torsional vibrator is radiated amost entirely in the lateral direction. Beam-forming is essential to the realization of the necessary improvement in signal-to-noise ratio of the measured reflection events.

A theory is also being developed to reconstruct Lamé's constant, $\lambda(Z)$, as well as the density, $\rho(Z)$, and the shear modulus, $\mu(Z)$. The data consist of surface displacements due to a vibratory SH source mounted on the surface.

The integral equation solution for the scattering of SH-waves in two dimensions has been modified to permit the presence of multiple inhomogeneous scatterers and to include the effect of damping due to the finite Q of earth materials. It has been found that the interaction of laterally separated scatterers is slight for reasonable earth Q's, which indicates that with the proper constraints a one-dimensional inversion theory may be applied to the interpretation of two-dimensional structures. The inclusion of damping permits the modeling of SH-wave scattering by two-dimensional inhomogeneities representing a variety of geothermal reservoir types. For example, The Geysers geothermal area can be represented by a zone of relatively low loss and high rigidity above a zone of higher loss and lower rigidity. These results will be presented in a paper to be submitted for publication (Hall, 1981). The integral equation method has the advantage that the scatterers may be buried very deeply and almost any type of attenuation may be included; however, the machine storage requirement can be restrictively large at times.

The machine storage requirement of the hybrid method is considerably less than that of the integral equation method. The hybrid method uses to advantage the characteristics of the integral equation and finite-element methods. A hybrid-method solution for the forward-scattering problem of SH-waves in two dimensions has been formulated and will be used to model the seismic response of complex deep crustal structures and to design experiments with shear wave sources.

REFERENCES

Coen, S., 1980a. The inverse problem of the shear modulus profile of a layered earth. J. Geophys. Res., in press.

____, 1980b. Inversion of the shear modulus and density profile of a layered earth. J. Geophys. Res., revised.

Coen, S., and Yu, M., 1981. Radiation patterns of torsional vibrators. In preparation.

Hall, R. F., 1981. Applications of an integral equation solution for the scattering of SH waves in two dimensions. In preparation.

APPLIED RESEARCH STUDIES

ENHANCED RECOVERY WITH MOBILITY AND REACTIVE TENSION AGENTS

C. J. Radke and W. H. Somerton

The objectives of the present study are (1) to establish the conditions requisite to tertiary-mode displacement of acidic oils with pH agents and (2) to elucidate the dominant recovery mechanisms and hence permit development of an improved caustic flooding package. The overall project includes studies on restored-state core displacements of Ranger-zone Wilmington oil sands, chemical transport, and emulsion flow and displacement. Earlier summaries of the research are available (Radke and Somerton, 1977, 1978, 1979). Recent progress in the first two areas is highlighted below. More detailed information may be obtained elsewhere (Soo and Radke, 1979; Brown and Radke, 1980; Bunge et al., 1980; deZabala et al., 1980; Lee and Radke, 1980; Rubin and Radke, 1980; Somerton and Radke, 1980).

The accomplishments during this reporting period are listed below.

1. A linear equilibrium displacement model is formulated for alkaline flooding of acid crude oils. In the simplified model, a single acid component of the oil reacts with alkali to produce a water-soluble surfactant. Sensitivity to mobility control is discovered, especially for tertiary alkali flooding. Experimental tertiary alkali floods show agreement with the model calculations.

2. For reservoir rock on which sodium-hydrogen base exchange can occur, even small exchange capacities may result in important chromatographic lag of the alkali at lower pH values. The reversible hydroxide adsorption greatly retards the onset of oil production and reduces the oil cut. To overcome the adsorption delay, alkali flooding should be done at higher pH. Design for optimal pH, based on interfacial tensions, may be annulled by the alkali-rock interactions.

3. Caustic can recover tertiary Ranger-zone oil from Wilmington sands at field temperatures and frontal advance rates. However, because of the high oil viscosity, tertiary recovery with simple alkali requires prolonged flooding. With mobility control and with high pH, tertiary recovery is rapid and substantial. Hence mobility control appears necessary to recover successfully viscous acidic oils with alkali.

4. The fluid state most characteristic of alkali flooding is that in which the alkali aqueous phase is in equilibrium with the oil containing its original acid content. Fluid properties, such as interfacial tension, interfacial viscosity, contact angles, or coalescence kinetics, should be evaluated under this condition. However, screening criteria based on fluid properties alone are insufficient.

5. Caustic reacts slowly with Wilmington sands to generate soluble silicates. The reaction is kinetic controlled and approximately first order in hydroxide concentration. Proper mathematical scaling of the reaction to field scales suggests the possibility of severe alkali consumption, depending on the exact value of the dissolution rate constant.

6. Equilibrium ion-exchange theory is extended to include alkaline precipitation of hardness ions. Both continuous and finite pulse injection are considered. Agreement between theory and experimental data is satisfactory for Wilmington sands and Berea Sandstone.

7. Alkaline preflushes for hardness cation removal prior to low pH micellar or polymer solutions are not attractive if calcium hydroxide is precipitated. The relatively high solubility of calcium hydroxide along with redissolution of the insoluble salt permit large concentrations of calcium ions to occur when low pH solutions contact the precipitated material.

REFERENCES CITED

Brown, J. B., and Radke, C. J., 1980. Area effects in spinning-drop dynamic interfacial tensions. Chem. Eng. Sci., v. 35, p. 1458.

Bunge, A. L., Klein, G., and Radke, C. J., 1980. Divalent ion exchange with alkali. Presented at Fifth SPE International Symposium on Oilfield and Geothermal Chemistry, Stanford, California, May 1980. SPE-8995.

deZabala, E. F., Vislocky, J., Rubin, E., and Radke, C. J., 1980. A chemical theory for linear alkaline flooding. Presented at Fifth SPE International Symposium on Oilfield and Geothermal Chemistry, Stanford, California, May 1980. SPE-8997.

Lee, R., and Radke, C. J., 1980. Interfacial tension and charge of hydrolyzing surfactants. Presented at Second Chemical Congress of the North American Continent, San Francisco, California, August 1980.

Radke, C. J. and Somerton, W. H., 1977. Enhanced recovery with mobility and reactive tension agents. Presented at Third ERDA Symposium on Enhanced Oil and Gas Recovery and Improved Drilling Methods, Tulsa, Oklahoma, v. 1, p. B-5.

____, 1978. Enhanced recovery with mobility and reactive tension agents. Presented at Fourth DOE Symposium on Enhanced Oil and Gas Recovery and Improved Drilling Methods, Tulsa, Oklahoma., v. 1A, p. B-2.

____, 1979. Enhanced recovery with mobility and reactive tension agents. Presented at Fifth Annual DOE Symposium on Enhanced Oil and Gas Recovery and Improved Drilling Methods, Tulsa, Oklahoma, v. 1, p. C-5.

Rubin, E. and Radke, C. J., 1980. Dynamic interfacial tension minima in finite systems. Chem. Eng. Sci. v. 35, p. 1458.

Somerton, W. H., and Radke, C. J., 1980. Role of clays in the enhanced recovery of petroleum. Presented at First Joint SPE/DOE Symposium of Enhanced Oil Recovery, Tulsa, Oklahoma, April 1980. SPE-8845.

Soo, H., and Radke, C. J., 1979. Stable emulsion flow in porous media. Presented at 86th National Meeting of AIChE, Houston, Texas, April 1979.

AN EVALUATION OF NUCLEAR QUADRUPOLE RESONANCE (NQR) TECHNIQUES FOR THE IN-SITU MEASUREMENT OF STRESS/STRAIN IN SALT

E. Schempp, S. M. Klainer, and T. Hirschfeld*

Measurement of the in-situ state of stress underground is one of the more challenging and important problems presented to geoscience and engineering. Accurate knowledge of the stress and the strength of rocks is essential for the design of underground openings and in the study of geotectonic processes. In spite of the fundamental role played by stress, however, techniques and instrumentation for its measurement have developed slowly. Presently available methods are time-consuming and costly. Clearly, in areas where knowledge of sudden buildups or release of stress would be important, such as in earthquake zones and near waste repositories and volcanoes, an improved methodology would be very valuable.

It is the purpose of this research to examine the feasibility of new procedures for determining stress and to develop the instrumentation to permit field evaluation. Several concepts are under study which are based on the microscopic response of crystalline materials to stress and utilize sophisticated notions drawn from experience in solid state physics. Nuclear Quadrupole Resonance (NQR) has been chosen as the method to evaluate. Implementation of this concept requires fundamental research in both physics and instrumentation engineering and requires a synthesis of skills from several disciplines.

Rocks underground are subject to a variety of forces, the most obvious being the lithostatic pressure from the weight of the overburden. Other forces include those from tectonic movements, i.e., horizontal thrusts of the type responsible for uplift, folding, and faulting. Because of strains--dimensional changes arising from stress--a simple vertical pressure will be converted into horizontal forces. In general, therefore, rocks are subjected to a three-dimensional stress which is expressed as a second-rank tensor having six independent elements.

NQR is a radio-frequency spectroscopic technique which, like nuclear magnetic resonance (NMR), uses the nucleus as a small, highly specific, probe of its environment. The technique takes advantage of certain nuclei which possess electric quadrupole moments (those with spin $I \geq 1$) to study the electric fields with which they interact, or more specifically the electric field gradient (EFG) tensor. Modern NQR has recently been discussed more fully by Klainer et al. (1980).

In the studies undertaken as part of this project, the focus has been on determining strain in rock salt, NaCl. NaCl has been selected for evaluation because it represents the simplest, natural system consisting of a single major constituent. In unstrained salt, both the sodium and the chloride ions occupy sites of cubic symmetry which, by very general principles, cannot possess an EFG. Thus the quadrupole coupling is zero. However, when subjected to nonisostatic stress, the crystal will deform to produce noncubic site symmetries at the Cl atom positions, thus giving a small EFG. For example, a compressive stress applied along [100] will make the crystal tetragonal, a stress applied along [110] will make the crystal orthorhombic, etc. Experiments by Marsh and Casabella (1966) indicate that the NQR frequency shift for Cl^{35} in NaCl is on the order of 30 Hz/atm.

NQR AND STRAIN MEASUREMENTS

From the theory of elasticity in linear media stressed below the elastic limit, the strain ε is related to the stress σ by the compliances s, giving Hooke's law in three dimensions as

$$\varepsilon_{ij} = s_{ijk\ell}\sigma_{k\ell} \qquad (1)$$

(where the summation convention is used). Although the $s_{ijk\ell}$ form the components of a fourth-rank tensor and thus consist of 81 separate elements, energy conservation considerations reduce the number to 36 independent elements in the general case and, in the cubic system, which concerns us here, to only three independent components (Nye, 1972). In the nearly universally used matrix notation in which the indices are condensed and summed from 1 to 6,

we have

$$\varepsilon_i = s_{ij}\sigma_j \tag{2}$$

with nonvanishing components in the NaCl class m3m $s_{11} = s_{22} = s_{33}$, $s_{12} = s_{13} = s_{23}$, and $s_{44} = s_{55} = s_{66}$. Measured values of the elastic compliances for NaCl (Nye, 1972) are given in Table 1.

Table 1. Values of the elastic, gradient elastic, and gradient stress tensors for NaCl.

Elastic (10^{-12} cm^2/dyne)				Gradient elastic (10^{15} dyne$^{1/2}$/cm^2)		Gradient stress (10^3 dyne$^{-1/2}$)	
s_{11}	s_{12}	s_{44}		g_{11}	g_{44}	C_{11}	C_{44}
2.21	-0.45	7.83	Na^{23}	2.7	0.95	7.5	7.4
			Cl^{35}	2.9	3.9	8.0	30.8

In this work there are two other tensor properties of crystalline material of considerable importance. One is the EFG tensor V_{ij} which determines the quadrupole interaction, and hence the resonance frequencies. This second-rank tensor is traceless and symmetric (Schempp and Bray, 1970), and thus contains five independent components, three of which can be thought of as determining the orientation of the principal axes, leaving two independent diagonal elements. The parameters of importance to NQR, q and η, are related to the components of the tensor V_{ii} in the coordinate system in which V_{ij} is diagonal, where $eq = V_{zz}$ when the axes are chosen so that $|V_{zz}| > |V_{yy}| > |V_{xx}|$ and

$$\eta = \frac{|V_{xx} - V_{yy}|}{|V_{zz}|},$$

η is dimensionless, satisfying $0 < \eta < 1$; η is known as the "asymmetry parameter."

The other tensor property of interest is the "gradient elastic tensor," $g_{ijk\ell}$, which relates the strain to the EFG via

$$V^o_{ij} - V_{ij} = g_{ijk\ell}\varepsilon_{k\ell}, \tag{3}$$

where V^o_{ij} is the value of the EFG in the absence of strain. For cubic site symmetry, $V^o_{ij} = 0$, giving in matrix notation

$$V_{ij} = g_{ij}\varepsilon_j. \tag{4}$$

Since the g_{ij} constitute a crystal property, they must obey the same invariance under symmetry operations as the elastic coefficients, resulting in a reduction of the 36 elements again to just three in the cubic case, g_{11}, g_{12}, and g_{44}. However, because the V_{ij} tensor is traceless, one can only observe $(g_{11} - g_{12})$ and g_{44}, as can easily be seen by writing out the components, giving

$$g_{12} = -\frac{1}{2}g_{11}. \tag{5}$$

The EFG can be written in terms of the stress by combining equations (1) and (3) (or (2) and (4)) to give

$$V_{ij} = g_{ijk\ell}s_{k\ell mn}\sigma_{mn} = C_{ijmn}\sigma_{mn} \tag{6}$$

where $C_{ijmn} = g_{ijk\ell}s_{k\ell mn}$. The C's may be called the "gradient-stress" tensor (Shulman et al., 1957).

Values of the g's and C's have been measured experimentally by several methods; and although there is some scatter in the data, approximate values can be used to determine the magnitudes to be expected in NaCl (Table 1) (Kanert and Mehring, 1971).

It is possible to calculate the field gradients and NQR frequencies in a few special cases to see the general effects. For this we consider a cubic crystal oriented such that the [100] direction is along X_1, [010] along X_2, etc. These cases are discussed below.

1. The simplest case involves a homogeneous uniaxial stress σ_o applied along [100]

$$\sigma = \sigma_o\begin{pmatrix}1&0&0\\0&0&0\\0&0&0\end{pmatrix} \quad \text{or} \quad V = -\frac{1}{2}C_{11}\sigma_o\begin{pmatrix}-1&0&0\\0&-1&0\\0&0&2\end{pmatrix}.$$

The maximum component of the EFG is thus parallel to the stress direction, [100], giving $q = eV_{zz}$ or

$$e^2qQ_{Cl} = 46 \text{ Hz/atm}, \ \eta = 0,$$

and

$$e^2qQ_{Na} = 55 \text{ Hz/atm}, \ \eta = 0.$$

Since the NQR frequencies are given for the I = 3/2 case by

$$\nu = \frac{1}{2}e^2qQ(1 + \eta^2/3)^{1/2},$$

we obtain, for a uniform stress field of 100 atoms,

$$\nu_{Cl} = 2.3 \text{ kHz},$$

$$\nu_{Na} = 2.8 \text{ kHz}.$$

(These results can be considered accurate only to within a factor of 2. Marsh and Casabella (1966), for example, report equal frequency shifts for both Na and Cl for [100] stress. Accurate determination of the constants during the laboratory phase of the work is a prerequisite for field work.)

2. After carrying out a rotation of the coordinates, the stress tensor becomes

$$\sigma = \sigma_o\begin{pmatrix}1/2&-1/2&0\\-1/2&1/2&0\\0&0&0\end{pmatrix}$$

for a stress applied along [110]. Thus

$$V = \sigma_o \begin{pmatrix} 1/4C_{11} & -1/2C_{44} & 0 \\ -1/2C_{33} & 1/4C_{11} & 0 \\ 0 & 0 & -1/2C_{11} \end{pmatrix}.$$

Introducing the quantities $c = s_{44}/(s_{11} - s_{12})$ and $\gamma = g_{44}/g_{11}$, V can be rewritten as

$$V = \frac{1}{4}\sigma_o C_{11} \begin{pmatrix} 1 & -2\gamma c & 0 \\ -2\gamma c & 1 & 0 \\ 0 & 0 & 2 \end{pmatrix}.$$

This must be diagonalized in order to find the NQR parameters, resulting in

$$V = \frac{1}{4} C_{11}\sigma_o \begin{pmatrix} 1+2\gamma c & & \\ & 1-2\gamma c & \\ & & -2 \end{pmatrix}.$$

For NaCl, using the data in Table 1, we find $c = 2.94$, $\gamma_{Cl} \simeq 1.34$, and $\gamma_{Na} \simeq 0.35$. Since $1 + 2\gamma c > 2$, relabeling the axes gives

$$V_{Cl} = 1.2 \text{ kHz} \begin{pmatrix} -2 & & \\ & -6.88 & \\ & & 8.88 \end{pmatrix},$$

$e^2qQ_{Cl} = 10.3$ Hz/atm, $\eta = 0.55$,
$\nu_{Cl} = 5.2$ kHz/100 atm; and

$$V_{Na} = 1.4 \text{ kHz} \begin{pmatrix} -1.07 & & \\ & -2 & \\ & & 3.07 \end{pmatrix},$$

$e^2qQ_{Na} = 42.2$ Hz/atm, $\eta = 0.30$,
$\nu_{Na} = 2.1$ kHz/100 atm.

For stress applied along [110], the principal axes are along [001], [110], and [$\bar{1}$10].

3. If the stress is applied along the [111] direction, we find

$e^2qQ_{Cl} = 119$ Hz/atm, $\eta = 0$, $\nu_{Cl} = 5.95$ kHz/100 atm,

$e^2qQ_{Na} = 36$ Hz/atm, $\eta = 0$, $\nu_{Na} = 1.80$ kHz/100 atm,

where the z-axis is along [111].

The intensity of the NQR lines depends upon the orientation of the linearly polarized rf exciting field to the axis of the cylindrically symmetric EFG (the $\eta = 0$ case is more complicated). The intensity of the lines is a maximum when the field lies in a plane perpendicular to the symmetry axis (the z-direction) and is zero when the field is parallel to the symmetry axis (Lucken, 1969). This fact must be taken into account when working out the line shapes to be expected for the general homogeneous stress. For example, if the rf field is parallel to the stress direction in the [110] case, the line will not be observed.

The petrofabric in the region of a salt-dome borehole may not present a wholly random orientation of the crystallites. In certain beds, very large "single" crystals with dimensions on the order of a foot or more have been found (Muehlberger, 1959). It is generally accepted that a preferred orientation of crystallites in the final fabric is strongly related to the stress system applied (Kern, 1977). There is some evidence that the [001] axes in halite are preferentially oriented parallel to the principal stress direction, i.e., [001] perpendicular to the axial planes of isoclinal folds in salt domes, which is in agreement with thermodynamic theory for stable crystal orientations under nonhydrostatic stress (Carter and Heard, 1970; Kamb, 1959). Therefore, although a polycrystalline mass may be expected, the crystallites may display a large degree of local order; i.e., a narrow distribution of orientation angles may exist. As a result, the NQR spectra will also have narrower widths than if the orientations are completely random.

In the general case of stresses underground, the stress tensor is not uniaxial, but triaxial, i.e.,

$$\sigma = \begin{pmatrix} \sigma_1 & & \\ & \sigma_2 & \\ & & \sigma_3 \end{pmatrix}.$$

The effect of additional nonzero elements in the stress tensor is generally additive if appropriate care is taken of the signs.

RESONANCE TECHNIQUES

The problem to be addressed is to detect either the sodium or the chlorine quadrupole coupling in sufficient detail to extract the strain/stress information. The quadrupolar coupling will lie in the 1-15 kHz region for stresses up to 300 atm, and the lines will be perhaps 1-5 kHz wide, depending on the degree of crystallite misalignment, the nature of the impurities, dislocations, and other crystal imperfections, and the inhomogeneity of the stress field resulting from the borehole deformation. The three basic approaches are direct detection (pure NQR), quadrupolar perturbed NMR, and double-resonance methods.

Direct Detection

Direct detection of proton NMR signals in the earth's magnetic field (~0.5G) is routinely carried out in magnetometers; the resonant frequency here is about 2.1 kHz. NQR in chlorine will be more difficult because (1) the sensitivity of Cl NMR relative to protons is 4.7×10^{-3}, (2) the magnetometers employ a liquid which has a sharp line in contrast to the broad line from solid NaCl, (3) the proton instrument can be optimized for a single frequency, and (4) line-shape information is not required. Overall, it is likely that the intrinsic Cl S/N ratio will be at least 10^{-5} smaller. Such an experiment would involve a very considerable theoretical and engineering effort to determine its practicality.

Quadrupolar Perturbed NMR

In an NMR experiment a large, reasonably homogeneous magnetic field will have to be provided.

It is assumed that a 1 kG field can be obtained for in-situ measurements, which is a practical requirement. In this case the chlorines will have a Larmor frequency of 0.4 MHz, and the sodiums a frequency of 1.12 MHz, which effects complete separation of the spectra. Since the sodium quadrupolar interaction is in the range of 2 ± 1 kHz, the quadrupole interaction will be small compared to the Zeeman interaction, giving rise to first-order shifts in the NMR transition frequencies. This method has been used to measure the quadrupole frequencies of neighboring shells around Br impurities in doped NaCl (Andersson and Forslind, 1964). The signals could be recorded using standard pulse techniques which detect either the free induction decays (FID) or spin echos, followed by Fourier transforms (Klainer et al., 1980).

Double Resonance

Double-resonance techniques have been developed in recent years which offer enormous increases in sensitivity in the detection of weak NMR and NQR signals. The idea behind these double-resonance techniques is to use the strong signal from one nuclear species to detect a weak signal from another species, where the weakness may arise from low isotopic abundance, low frequency, or long relaxation time. In the case of quadrupole effects in strained NaCl, the problem is the low frequencies of the stress-induced quadrupole coupling constant (QCC).

Of several double-resonance methods, the following can be dismissed as not suitable for the experiments on salt: spin echo double resonance (SEDOR) requires large static magnetic fields, and thus offers no advantage over conventional resonance methods; double resonance in the rotating frame (DRRF) suffers from the same defect; double resonance in the laboratory frame (DRLF) is not generally suitable for detection of quadrupole interactions below 200 kHz, and in any case often renders details of the line shapes unobservable; double resonance via the solid-state effect (DRSSE) presents similar problems.

This leaves two applicable methods, spin-mixing by level crossing (DRLC) and continuous coupling (DRRC), which are closely related (Koo, 1970; Hahn et al., 1972; Edmonds, 1977). Continuous coupling requires magnetic field cycling and a three-step experimental cycle: polarization, irradiation, and detection. The sample is initially placed in a large magnetic field, H_o, long enough for both sets of spins (the A and the R) to reach equilibrium with the lattice temperature, T_L. The time is set by the longest T_1 in the sample; T_1 (Na) ≈ 12 s in salt. The magnetic field should be as large as practicable, about 1 kG for a field instrument or 10 kG in the laboratory.

The sample is now removed bodily from the magnetic field, or the field is switched rigorously off in as short a time as possible, ≲ 1 s. During this time, the Zeeman splitting of the A spins (Na^{23}) collapses, and in so doing crosses over the quadrupole energy levels of the R spins (Cl^{35} Cl^{37}). The R spins thus become partially polarized by energy exchange and now reside in a zero applied field.

Immediately after the H_o field becomes zero, a continuous rf field at frequency ω_r is applied for a time necessary to saturate the R spins (3-5 s). At the completion of this irradiation, the magnetic field H_o is switched back on again and the A spin magnetization measured by applying a single $\pi/2$ pulse and observing the FID. This cycle is repeated for different values of ω_R until the region of interest is covered--in the case of Cl in salt, 2-10 kHz. Before the start of each new cycle, a saturation comb of $\pi/2$ pulses for the A spins initializes the polarization in that system.

The sensitivity of the method depends on the number of R system "spin flips" which occur during the R-irradiation phase. This will depend upon the number of Cl transitions excited within the bandwidth of the ω_R pulse. The sensitivity can be very high, particularly for the spin 3/2 case (Edmonds, 1977). Double resonance by continuous coupling has had considerable success in detecting QCC's in deuterium, ^2H, at natural abundance (Edmonds and Mailer, 1977), and this problem presents many of the same features found in the salt problem.

The foregoing discussion suggests that the two most promising approaches are quadrupolar perturbed NMR and double resonance by continuous coupling (DRCC). Both schemes present some difficulties, but they do not seem insurmountable. Among the difficulties are these: (1) A magnetic field produced by a coil generates heat because of ohmic losses; a cooling system capable of dissipating a few kilowatts will have to be provided. (2) For DRCC it will be necessary to turn the magnetic field off and on in short times, less than about 1 s, and this requires careful engineering design. (3) Any magnetic field generated in a borehole will fall off in intensity with penetration depth, and thus only the nuclei in an annulus not more than 1 cm wide can be effective in the same field. The resulting field inhomogeneity makes a more complex NMR signal and decreases the line widths of the FID and echo, thus requiring fast electronics. (4) Field inhomogeneity limits the amount of material which can be sampled at any one time; this can be partially compensated for by making an oval-shaped rf coil, perhaps 1/10 of the borehole circumference as its small diameter and up to about 60 cm long. This would encompass a volume of about 2 liters (4 kg of salt). (5) The last problem is the intrinsic overlap of the Na^{23}, Cl^{35}, and Cl^{37} (and possibly ^1H) signals in the spectrum, if DRCC is used. This factor, plus the dependence of line shapes on the stress field, the orientation of the crystals, and the orientation of the rf exciting field to both of the foregoing, means that it is unlikely that there will be any simple one-to-one correspondence between visually recognizable features in the spectrum and the stresses. However, mathematical treatments of the spectra, e.g., Fourier transforms, together with a sufficient laboratory database, make it possible to process the input information in the computer and output a value directly related to stress. Thus field measurements could be related to the stress by reference to model spectra obtained from careful laboratory measurements. All of the five listed difficulties appear to have readily implementable solutions.

A good deal of laboratory experimental work needs to be done. This includes developing the conditions to optimize the sensitivity of the instrument, making careful measurements of the values of the gradient-stress constants, verifying the line-shape calculations, and observing whether important parameters vary significantly with temperature. A means of going from the NQR measurements back to the (unknown) stress state will have to be developed. Later experiments will examine the case of extremely high stresses where nonlinear effects, e.g., plastic flow, begin to appear. Finally, details of the borehole configuration will be added to the database. This work will be done with funds from ONWI.

In fiscal 1981, research should be implemented on Al-containing minerals in order to locate lines, optimize their S/N ratios, and make measurements of their shifts under stress.

*Lawrence Livermore National Laboratory, Livermore, California.

REFERENCES CITED

Andersson, L. O., and Forslind, E., 1964. NMR measurements of field gradients at I^{127} nuclei surrounding a substitutional Rb ion in a KI crystal. Arkiv Fysik v. 28, p. 49-64.

Carter, N. L., and Heard, H. C., 1970. Temperature and rate dependent deformation of halite. Am. J. Sci., v. 269, p. 193-249.

Edmonds, D. T., 1977. Nuclear quadrupole double resonance. Phys. Reports, v. C29, p. 233-290.

Edmonds, D. T., and Mailer, J. P. G., 1977. The sensitive detection of deuterium quadrupole resonance. J. Mag. Resonance, v. 26, p. 93-99.

Hahn, E. L., Koo, J. C., and Hsieh, Y., 1972. Pure nuclear quadrupole resonance of naturally abundant O^{17} in organic solids. Chem. Phys. Letters, v. 13, p. 563-566.

Kamb, W. B., 1959. Theory of preferred crystal orientation developed by crystallization under stress. J. Geology, v. 67, p. 153-170.

Kanert, O., and Mehring, M., 1971. Static Quadrupole Effects in Disordered Cubic Solids. In P. Diehl, E. Fluck, and R. Kosfeld (eds.), NMP Basic Principles and Programs (Vol. 3). New York, Springer-Verlag.

Kern, H., 1977. Preferred orientation of experimentally deformed limestone marble, quartzite, and rock salt at different temperatures and states of stress. Tectonophysics, v. 39, p. 103-120.

Klainer, S. M., Hirschfeld, T. B., and Marino, R. A., 1980. In A. Marshall (ed.), Fourier transform nuclear quadrupole resonance spectroscopy, Fourier, Hadamard, and Hilbert Transforms in Chemistry. Plenum Press, New York (in press).

Koo, J. C., 1970. Low field nuclear quadrupole resonance spectroscopy (Ph.D. Thesis). Berkeley, University of California, Department of Physics.

Lucken, E. A. C., 1969. Nuclear Quadrupole Coupling Constants. New York, Academic Press.

Marsh, J. L., Jr., and Casabella, P. A., 1966. Gradient-elastic tensor in sodium chloride and sodium bromide. Phys. Rev., v. 150, p. 546-551.

Muehlberger, W. R., 1959. Internal structure of the Grand Saline Salt Dome, Van Zandt County, Texas. Univ. Texas Bus. Econ. Geology Report, Inv. 38, 18 p.

Nye, J. F., 1972. Physical Properties of Crystals. Oxford, Clarendon Press.

Schempp, E., and Bray, P. J., 1970. Nuclear quadrupole resonance spectroscopy. In H. Eyring, W. Jost, and D. Henderson (eds.), Physical Chemistry, an Advanced Treatise (Vol. 4). Academic Press, New York.

Shulman, R. G., Wyluda, B. J., and Anderson, P. W., 1957. Nuclear magnetic resonance in semiconductors. II. Quadrupole broadening of nuclear magnetic resonance lines by elastic axial deformation. Phys. Rev., v. 107, p. 953-958.

THE USE OF FLUORIMETRIC TECHNIQUES IN TRACE ANALYSIS

S. M. Klainer, D. L. Perry, H. R. Bowman, and T. Hirschfeld*

The ability to rapidly and conveniently determine small quantities of uranium in geomedia such as groundwater and minerals is desirable from several standpoints. With the recent emphasis on the need to have a more complete understanding of the migration of radioactive materials through soils and various types of mineral deposits (especially around nuclear waste repositories), it would be highly advantageous to have the capability of analyzing a large number of samples rapidly. The field of hydrogeochemical exploration for uranium also infers the need for the routine analysis of a large number of samples in order to detect the presence of minute amounts of uranium. Finally, an accurate and precise determination of uranium trace levels in geologic surroundings is important for conducting basic geophysical research in such areas as radiometric age dating and terrestrial heat-flow phenomena.

RESEARCH ACTIVITIES IN 1980

The method of uranium analysis (Perry et al., 1981) developed by members of the Geosciences Group at Lawrence Berkeley Laboratory (LBL) in collaboration with colleagues from the Chemical Analysis and Development Department at Lawrence Livermore National Laboratory affords a simple, cheap sample that can be easily prepared in any laboratory using readily obtainable reagents. Its detection limit for uranium that surpasses that presently demonstrated for other techniques. The analytical scheme involves a precipitation procedure and subsequent sample preparation patterned after methods used by other investigators in their study of other metal-ion systems such as the lanthanide ions (Miller et al., 1977; Wright et al., 1978, 1979). Present techniques utilize solution-precipitated calcium fluoride to coprecipitate uranium (in the form of the most solution-stable species, the uranyl ion, UO_2^{2+}), which is then air-calcined at elevated temperatures. The coprecipitated uranium is then spectroscopically monitored by laser-induced fluorescence excitation (LIFE). The technique has detected uranium in solution at a concentration of 10^{-12} M, or 2.38×10^{-4} ppb. A delayed fluorescence technique has been employed to decrease prompt fluorescence interferences and general light scattering. A spectrum (30:1 signal:noise ratio) of uranium coprecipitated with CaF_2 from a solution containing 10^{-12} M uranium is shown in Figure 1; this spectrum was obtained using chopped excitation and boxcar integration. Its extrapolated sensitivity is 10^{-14} M uranium. Research in this program at LBL has centered on the coprecipitation of uranium in calcium fluoride matrices and the experimental parameters (such as calcination temperature and time, initial uranium concentration in solution, and interfering cations and anions) that affect the concomitant spectra of the samples. Instrumentation used to obtain the spectra has also been designed, interfaced, and its performance optimized. Detection limits, extent of the coprecipitation of the uranium in calcium fluoride, and selectivity of the technique have been studied, along with the application of the technique to actual uranium-containing groundwater samples.

To assure the integrity of an underground nuclear waste disposal site, it will be necessary to maintain analytical surveillance of the site, its underground environment, and groundwater in its vicinity. Proper surveillance should ideally sample the whole spatial distribution around the site. It is difficult, however, to make such surveillance compatible with the desired lack of physical access to the site, its environmentally inhospitable nature, and the general unwillingness to bury large quantities of superreliable, expensive instruments along with the waste.

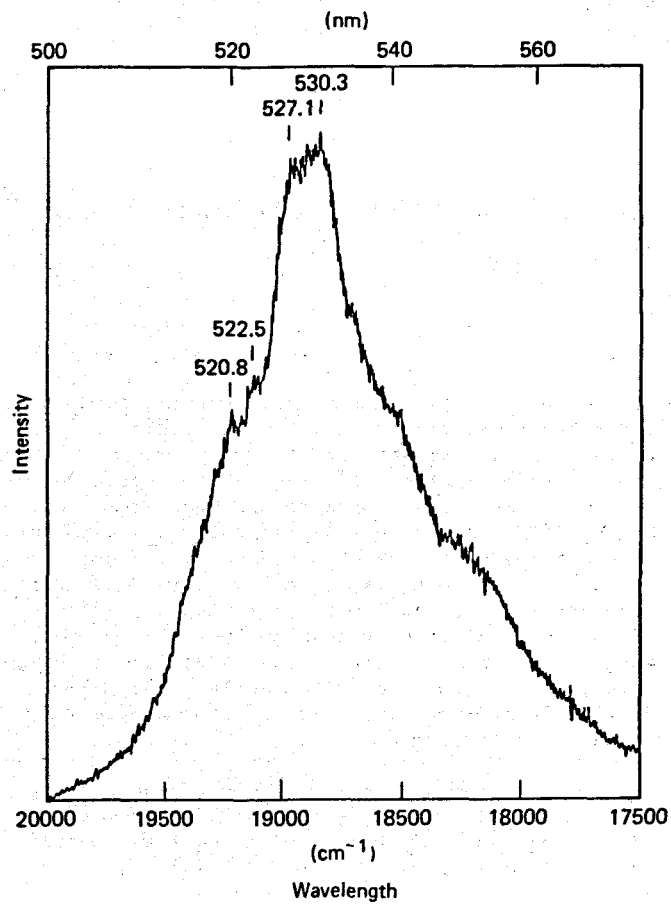

Figure 1. Fluorescence spectrum of uranium coprecipitated with CaF_2 from a solution of 10^{-12} molar UO_2^{2+}. [XBL 812-8255]

Here the alternative to collecting samples is to use long-distance, communications type fiber optics wire in the repository along with the waste package. This allows remote analysis of the repository from a convenient topside location, which is a considerable step forward. Special optical couplers are used to interface a laboratory-type laser-excited fluorescence spectrometer to a fiber, which may be as long as 1 km and whose other end extends down into the repository. Light arriving from the spectrometer triggers fluorescence in the sample, part of which travels back along the fiber and is coupled in the laboratory to appropriate detection and readout electronics. Switching networks are available to use a network of fibers to analyze a great many locations from a single monitoring instrument, with only small additional expense for fibers. The fibers are extremely radiation- and pressure-resistant, and they have a good resistance to temperature and chemicals which may be further improved by using special fiber types at the far end.

Laboratory demonstrations using fibers several hundred meters in length have demonstrated ppb sensitivity with good quantitative response, and a number of such devices have been built. In particular, a number of optical configurations having successively higher optical efficiencies and signal levels have been explored. For naturally nonfluorescent samples, both fluorescence and chemical selectivity can be introduced by using selective reagent coatings on the fiber tip. These ion-specific "optrodes" are designed around nonconsumable reagents, and produce not only higher selectivity but better signals as well.

*Lawrence Livermore National Laboratory, Livermore, California.

REFERENCES CITED

Miller, M. P., Tallant, D. R., Gustafson, F. J., and Wright, J. C., 1977. Spectroscopic system for the study of fluorescent lanthanide probe ions in solids. Anal. Chem., v. 49, p. 1471-1482.

Perry, D. L., Klainer, S. M., Bowman, H. R., Milanovich, F. P., Hirschfeld, T., and Miller, S., 1981. Detection of ultra-trace levels of uranium in aqueous samples by laser induced fluorescence spectrometry. Anal. Chem., (in press).

Wright, J. C., and Gustafson, F. J., 1978. Ultra trace inorganic ion determination by laser excited fluorescence. Anal. Chem., v. 50, p. 1147A-1160A.

Wright, J. C., and Johnston, M. V., 1979. Trace analysis of nonfluorescent ions by associative clustering with a fluorescent probe. Anal. Chem., v. 51, p. 1774-1780.

THE DEVELOPMENT OF ADVANCED MASS SPECTROMETRIC TECHNIQUES

M. Michel and W. R. Keyes

Preliminary work in using the isotope separator (a 5-foot radius mass spectrometer with 40 kev accelerating voltage) to determine the isotope ratios of naturally occurring uranium in groundwaters indicated considerable variation in the $^{238}U/^{235}U$ ratio of a natural standard from run to run. Since the variation in the $^{234}U/^{238}U$ ratio in groundwaters was to be the subject of a research program funded by the Office of Nuclear Waste Isolation, the variation obtained with the standard became of great concern. Because no previous work with individual ion counting had been done with this machine, a source of instrumental error was suspected. The present work was aimed at achieving the capability of measuring such isotope ratios in samples of uranium of 1 ng or less with a precision of approximately 2% in the ratio $^{234}U/^{238}U$.

Because the work on $^{234}U/^{238}U$ disequilibrium does not require high precision in the isotope ratios being measured, the original work was begun using a Bendix Spiraltron (T.M.) solid-state electron-multiplier detector in the ion-counting mode to achieve the sensitivity required for small samples. This device was chosen because of its small size, so that the standard collector box of the isotope separator (which enters and leaves the vacuum system on a differentially pumped probe) could be used to mount the detector, allowing easy withdrawal and reinsertion of the detector without affecting the main vacuum.

It was realized that the small size of this detector carries with it a possible disadvantage--namely, a possible sensitivity-versus-position function that could be sensitive to small shifts in beam position, making it hard to achieve good precision when voltage-stepping through a mass spectrum. This lack of precision could come from the difficulty in adjusting the stepping system so that each successive beam is placed exactly in register with the detector without error. Although the errors in alignment are likely to be small, they may be a problem if the detector sensitivity varies rapidly with position, a situation almost certain to be the case for this detector because of the small size of the sensitive area and the physical inhomogeneity of the surface conformation. In addition, any failure to achieve exactly the same ion-intensity distribution for different mass beams would also introduce a possible mass-ratio error. This can happen in several ways, the most likely of which is failure to maintain the correct ratios between the accelerating voltage and the lens potentials as the accelerating voltage is stepped from one mass number to another. The more commonly observed mass-

dependent response due to different velocities of the different mass beams is not a serious problem because we operate in the ion-counting mode, that differences in gain of the multiplier are of little consequence if the pulse discriminator is properly set. Such setting requires a pulse-height distribution with a well-defined maximum separated from electronic noise, a situation normally difficult to achieve with solid-state multipliers because of the low gain per stage and correspondingly low conversion gain. However, the 40-kV particles from the isotope-separator beam give enough secondary electrons per ion (> 10) to assure the necessary pulse distribution.

Initial measurement of isotope ratios with natural uranium did demonstrate larger-than-expected errors and a bias toward low values of the ratio of $^{238}U/^{235}U$. (These measurements were made under conditions in which the environmentally occurring enriched ^{235}U (Michel, 1981) was not expected to be observable.) The bias exhibited an asymmetric distribution, but with the most probable ratio still near the correct value.

After much searching for the cause, it was found that the accelerating voltage and lens potentials are slightly modulated (at the level of a few parts in 10^4) with an alternating voltage, in some cases both at line and radio frequencies. The net effect of these modulations is to widen the beam so that it is at least as large as the sensitive area of the multiplier and makes the data even more sensitive to the alignment problems discussed above.

Reduction of the modulation levels has the desired effect of reducing both the absolute statistical error in isotope ratios and the asymmetry of the data distribution about the known value. It had been observed earlier that there is a limit to improving the data by decreasing the size of ion-source exit hole; that limit is now assumed to be due to the remaining modulation, which makes further exit-hole reduction ineffective in reducing the beam width. The precision attainable is still not as good as one would expect from statistics alone. (Remember that we must include both beam-intensity statistics and sampling statistics from stepwise cycling through the mass spectrum. This introduces another error if, as is usually the case, the beam intensity is not perfectly constant.) However, we are not far from the kinds of errors common in work with thermal ion sources without correcting for isotope fractionation in the ion source. A rather extensive set of data from a natural uranium sample near the size of our real samples (2 ng) gives a ratio of $^{238}U/^{235}U = 137.7 \pm 0.3$. The accepted ratio is 137.88 ± 0.14 (errors estimated) (Shields, 1960; Cowan and Adler, 1976).

It is clear that the multiplier is still limiting the precision under conditions of large beam intensities, but for measurement of the $^{234}U/^{238}U$ ratio we will generally be limited by statistics because of the small dynamic range of the detector-amplifier system in use, since it is impossible to measure the large ^{238}U beams necessary to get ^{234}U beams of arbitrarily large size without serious coincidence problems. At present, we can obtain precisions of 1-2% on samples well below 1 ng in an hour or two of data collection with intensities at the ^{234}U isotope position of a few counts per second.

REFERENCES CITED

Cowan, G. A., and Adler, H. H., 1976. The variability of the natural abundance of ^{235}U. Geochim. Cosmochim. Acta, v. 40, p. 1487-1490.

Michel, M. C., 1981. Mass spectromatic determination of $^{234}U/^{238}U$ disequilibrium, in Earth Sciences Division Annual Report 1980. Berkeley, Lawrence Berkeley Laboratory, LBL-12100.

Shields, W. R., 1960. Comparison of Belgian Congo and synthetic "normal" samples. Report #8, U. S. National Bureau of Standards Meeting of the Advisory Committee, May 17-18, 1960, 37 p.

SORPTIVE DIFFUSION IN CLAY GELS

C. J. Radke

The purpose of this project is to devise and verify experimentally a quantitative model for the diffusion of ions in aqueous smectite gels under conditions appropriate for nuclear waste isolation. Some clays, such as montmorillonite, swell upon contact with water and thus provide a sealant through which water cannot readily convect. Radionuclide movement is slowed to diffusion rates only. In addition, the exchange capacity of montmorillonite clay is large for typical radionuclides, so that ion migration rates are slowed even further. Engineered clay barriers can provide complete and reliable protection against harmful isotropic release. However, to design the amount and configuration of such backfill material requires a correct model for predicting sorptive diffusion rates of radionuclides in clay gels.

Work this year centered on simple experiments for diffusion of cesium into a bentonite (Belle Fourche) clay gel. The cesium uptake rate into the clay is monitored from concentration changes in a well-stirred tank. Atomic absorption spectrophotometry is used to determine the transient ion concentrations. In addition to the one-sided diffusion cell measurements, the cesium-sodium ion-exchange isotherm for the disaggregated clay is determined by the static method; the bulk-diffusion coefficient of cesium chloride, D, is determined with a standard diaphragm cell; and the tortuosity, τ, of the gel is determined from electrical conductivity experiments.

The simplest model for the unsteady, one-dimensional ion concentration profiles, c(t, x), can be written as follows:

$$1 + \left(\frac{1-\varepsilon}{\varepsilon}\right)\frac{dn}{dc}\,\frac{\partial c}{\partial t} = \frac{D}{\tau^2}\,\frac{\partial^2 c}{\partial x^2}\,, \qquad (1)$$

where ε is the gel porosity and n(c) is the exchange isotherm. Inherent in equation (1) is the assumption that ion-exchange rates are fast compared to diffusion rates so that the sorption process is in local equilibrium. An analytic solution to equation (1) and to the coupled transient in material balance in the stirred tank is straightforward, and permits calculation of the cesium uptake rate by the gel.

Comparison between the theoretical predictions and preliminary experimental results shows cesium diffusion rates up to an order of magnitude lower than expected. One is tempted to introduce an effective diffusion coefficient in the gel to account for hindered migration in between the clay particle platelets. However, an alternate explanation is provided by geometric arrangement of clay particles in the gel. The exact structure of montmorillonite gels is unknown, but it is generally agreed that individual platelets organize into packets (von Olphen, 1977; Cebula et al., 1979). Such oriented structures may present mass-transfer resistances not described by the oversimplified packed-bed model of equation (1).

Our current work focuses on refining and extending the diffusion measurements and in determining the microstructures of clay gels. Results of this study to date demonstrate that engineered clay barriers for nuclear waste isolation are more effective than simple calculations suggest.

REFERENCES CITED

Cebula, D. J., Thomas, R. K., Middleton, S., Ottewill, R. H., and White, J. W., 1979. Neutron diffraction from clay water systems. Clay and Clay Minerals, v. 27, p. 39.

van Olphen, H., 1977. An Introduction to Clay Colloid Chemistry (2nd ed.). New York, John Wiley.

ADVANCES IN FOSSIL ENERGY: COAL MINE VENTILATION SYSTEMS

M. McPherson and M. Hood

The past 30 years have seen a complete revolution in the scale and techniques of mine ventilation planning throughout Eastern and Western Europe, Africa, and, more recently, Australia. From the earlier intuitive estimates and rule-of-thumb methods have developed sophisticated computer-based procedures that are now established as a necessary and integral part of mine planning. Figure 1 illustrates one such organized procedure applicable to both the planning of a new mine and the continued development of an existing undertaking.

The necessity for meticulous planning of the underground environment in those areas of the world has arisen from four separate but interrelated factors:

1. The intensification of mechanized mineral mining methods, particularly in coal mines, produces greater comminution of the rock and exacerbates problems of dust, gas, heat, and humidity.

2. There is a continuing trend toward fewer but larger mines. Continuity of production at working faces becomes of ever greater importance, and downtime due to failure of any part of the mine infrastructure is unacceptable.

3. In some areas mines are becoming deeper, again giving rise to additional hazards.

4. Improved medical knowledge and techniques of diagnosis, coupled with sociological developments, have sharpened public awareness to the longer-term dangers to health that arise from industrial environments. Consequently, mines must continue to operate under increasingly stringent legislation governing permissible threshold values of air pollutants.

All of these trends are evident within the United States, yet, with a few exceptions, there have been no comparable advances in the application of modern mine ventilation planning techniques. In contrast with most mining companies overseas, where a qualified ventilation staff is a vital (and perhaps mandatory) part of the production team, only a minority of American mining enterprises have considered it necessary to employ full-time mine environmental engineers.

There are several reasons for the shortfall in U. S. mine ventilation planning. First of all, coal mines in this country are relatively shallow and reserves plentiful. Hence, "in seam" mining using the room-and-pillar system of extraction continues to be the predominant method of working. This type of mining layout provides many routes for air to follow, and low-pressure fans have, in the main, been capable of providing the required airflows. Unfortunately, the numerous leakage paths available between intake and return airways give poor overall ventilating efficiency. The usual reaction to a deteriorating ventilation system has been to install more and larger fans. With low-resistance layouts and relatively low-cost electricity, this "brute force" approach has been adequate for many companies. However, for any given mine, the operating cost for the main fans is proportional to the cube of the total airflow. Hence, doubling the airflow increases the ventilation costs by a factor of eight. Furthermore, the operating cost is also proportional to the product of fan pressure, p, and fan airflow, Q (cost varies with p x Q). As a mine develops, its resistance to airflow, and hence required fan pressure, increases. Additional leakage caused by the extended workings and enhanced by the higher pressures results in a rise in the total airflow necessary. Thus, as both p and Q increase, the ventilation cost accelerates

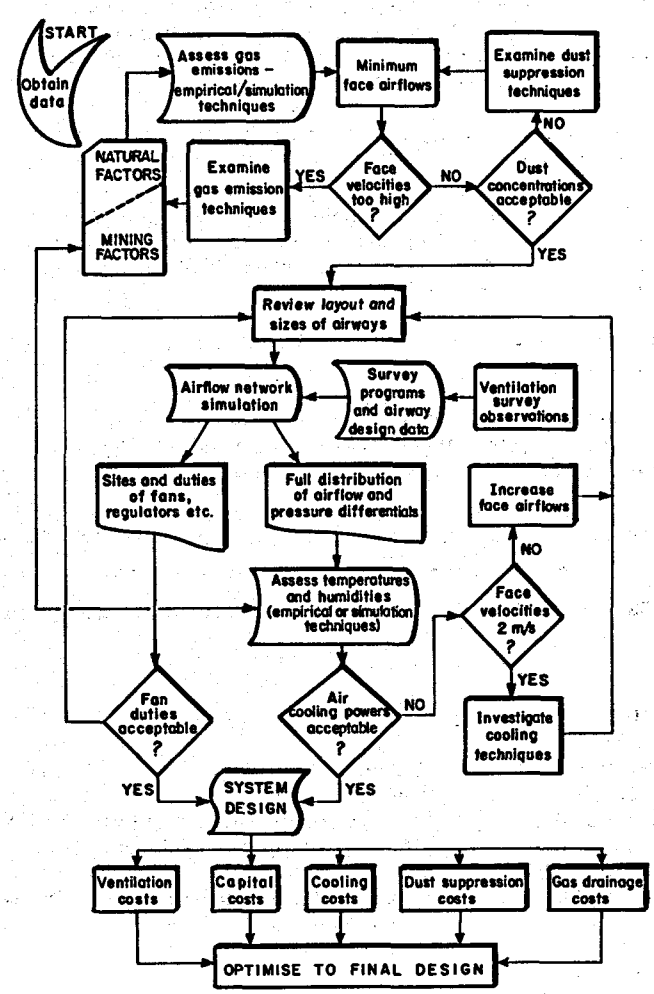

Figure 1. Ventilation planning scheme.

[XBL 792-8265]

rapidly. It is this effect that, despite detailed planning, is facing several large European mines with premature closure unless current research can provide a more economic system of ventilation. Although the situation in the United States is not so critical, the trend is clear. The four fans to be installed at Jim Walters Resources' Tuscaloosa County mines will have a combined and continuing operating cost approaching $2 million per year.

The Second International Mine Ventilation Congress, held in Reno, Nevada, during November 1979, highlighted the extent to which the United States has fallen behind in the science and application of mine ventilation techniques. Through the 1980s more and more companies will find that detailed and continuous mine environmental planning is not only an economic necessity but also a prerequisite to safe mineral extraction. Accelerated research and development is needed now to provide the tools, guidelines, and techniques that will be increasingly required by mine environmental engineers.

The present investigation seeks to determine those areas of coal mine ventilation in which research and development is most needed. The initial stages of the study have involved (1) a classification of literature in the field of mine environmental engineering over the past 5 years and (2) a series of interviews with individuals in industry, state organizations, and academic institutions who are working in this area.

The work already completed, coupled with overseas experience relevant to American mining, has enabled a preliminary classification of research areas to be mapped out. Those areas with particular impact on the planning and economics of mine ventilation systems will be investigated between October 1980 and September 1981.

CLASSIFICATION OF AREAS OF RESEARCH IN MINE VENTILATION

The work conducted thus far has led to the following preliminary classification of research areas in coal mine ventilation.

Systems Analysis of the Mine Environment

The underground environment is a complex system governed by a large number of dependent and independent variables. These may be classified in several ways with respect to their effect on the overall environmental system. One such classification is illustrated by Table 1. The primary purposes of a disciplined system-analysis approach are: (1) to encourage an organized planning procedure; (2) to avoid solving any one environmental problem at the expense of another (the history of mine ventilation is littered with the consequences of such occurrences); and (3) to conduct optimization and sensitivity exercises in order to determine the stability and economics of any given design. Furthermore, an organized planning procedure provides an invaluable guide for the personnel structure of a mine ventilation department. An investigation is needed into the organizational and managerial facets of mine ventilation applicable to American mines.

Ventilation Network Analysis

The core of mine ventilation planning are those techniques concerned with predicting airflow patterns in mine ventilation systems. Known by the generic term "ventilation network analysis," such methods are used to investigate the effects of airway layout and geometry and the best sites and duties required of the fans.

Because of the large number of nonlinear equations that need to be solved, physical or numerical modeling techniques must be employed to handle total mine configurations. The pneumatic, hydraulic, and electrical ventilation analogs of the 1950s have largely been superceded by digital-simulation techniques. All routine ventilation network analyses carried out by the National Coal Board (U.K.) since 1965 (some 3000 exercises per year) have been by digital computer.

Within the United States there has been a proliferation of network-analysis programs, many of which would seem to be more suitable for research purposes than for practical use in industry. The successful programs are those with a simple, well-

Table 1. Factors which affect mine environmental hazards.

NATURAL FACTORS +	MINING FACTORS →	HAZARD ←	SPECIFIC CONTROL TECHNIQUES (if required) +	AIRFLOW CONTROL
Depth				
Geology				Main fans
Permeabilities	Methods of working	Dust	Dust suppression	Booster fans
Porosities	Mining layout			Auxiliary ventilation
Gas content	Rate of mineral production	Gas emissions	Gas drainage	Natural ventilation
Virgin rock temperature	Mineral clearance system			Regulators
Rock thermal parameters	Type, size, and siting of machinery	Temperature and humidity	Air/water cooling	Doors, seals, packs
Wetness of workings				
Age of airways				Size, lining, and layout of airways
Surface climate				

structured but flexible input and an output that is direct, to the point, and easy to interpret.

Ventilation network (VNET) programs currently available require mainframe computers. Further research is required to produce programs that include graphic in/output, that can be run on modern minicomputers, and that will accept practical-sized networks. Such a development would facilitate considerably the routine industrial usage of a VNET package.

Ventilation Systems (Economics, Efficiency, Effectiveness)

The success of any ventilation system design must be measured in terms of economics (the operating cost of the system), efficiency (the fraction of total airflow that is usefully employed), and effectiveness (the quality control of the mine air with particular regard to dust, gas concentration, temperature, and humidity).

Some current mine ventilation systems that have evolved with little or no rational planning can be made less costly, more efficient, and more effective by fairly simple measures. All too often, however, years of neglect in basic ventilation planning can be put right only by the expenditure of large sums of money.

Ventilation costs rise both with respect to the volumes of airflow required and the fan pressures necessary to produce those airflows. There are three basic methods of reducing operating costs for any given mining layout:

1. The use of booster fans to control air pressure differentials, leakage, and hence total airflows. Booster fans at present are not permitted in U. S. coal mines, although this is not the case in coal mines elsewhere in the world. Research into the safety and the potential economic impacts of this legislation is required.

2. The "through system" of ventilation with intake and return surface connections at opposite ends of the mine take.

3. Controlled recirculation of air in working areas of the mine. Despite traditional reaction against this method, reflected by current legislation, major research projects in the U. K. and South Africa are proving the increase in safety as well as reduced costs provided by controlled recirculation, particularly in gassy, dusty, or hot conditions.

Any one of these three techniques may provide dramatic savings in ventilation operating costs. There is, however, no one method that is applicable in all cases. Further research is required to isolate and quantify the governing variables and to establish reliable ground rules for ventilation planners.

District Ventilation Systems

The conventional intake and return "side" of working area (the U system) guarantees maximum leakage and a poor ventilating efficiency. Geometrical layouts that would simultaneously reduce both leakage and resistance to airflow should be investigated for longwall and room-and-pillar workings in American mines.

It is suggested that the concept of "neutral" airways as a legislative requirement for conveyor haulages be reviewed in the light of modern flame-resistant belting. Rather than being regarded as a safeguard against the spread of a conveyor fire, the poor ventilation in neutral airways is, in itself, a condition that would be unacceptable in other mining countries.

Auxiliary Ventilation

The use of brattice cloths for the coursing of air in short headings is practiced in coal mines in India, Australia, and South Africa, as well as the United States. It has, however, many disadvantages. Not only does it give rise to poor ventilation control in the headings, but it also adds heavy resistance to the mine ventilation system in its most sensitive areas, increasing leakage and minimizing the airflows that reach the working districts. Quantified investigations are suggested for the application of auxiliary fan and duct systems, including overlap, duct manifold, and controlled recirculation techniques. The last technique is giving excellent results in the U. K. at the present time.

Ventilation Surveying

The primary data required for the network analysis of an existing mine are obtained from measurements of airflows and frictional pressure drops in each branch of the network. A number of techniques are available for taking such measurements, depending upon the mine geometry and the magnitude of the values. Research is required to establish criteria on which mine ventilation personnel can choose survey techniques appropriate to particular conditions.

Empirical friction factors may often have to be employed for airways that are difficult or impossible to survey. The published design data are based on work carried out more than 50 years ago and have little relevance to modern, machine-mined airways. There is an urgent need for this information to be updated by means of a series of precise surveys covering a range of roadway linings.

Environmental Monitoring and Control

The maintenance of airflow and quality with regard to gas concentrations is enforced by statute, and measurements by hand-held instruments must be made at prescribed places and times. Control of the underground environment is greatly enhanced by the additional provision of continuous monitors with local and remote recording/indication and fitted with audiovisual alarms for abnormal conditions. The primary parameters to be monitored in coal mines are methane concentration and air velocity with additional transducers for pressure differentials, dust, temperature/humidity (where relevant), smoke, and carbon monoxide for the early indication of spontaneous combustion. Conventional machine monitors may be employed to track the performance of

the ventilation plant. The continued development of environmental monitoring systems should be encouraged.

The combination of integrated monitoring systems, fan-control devices, automated regulators, and process computers offers the possibility of automatic control of the underground environment. This is being pursued currently in a number of countries, including the United States. Here again, the research should be encouraged and consolidated with the emphasis on practical application.

Dust

This health hazard, more than any other, has received considerable attention throughout the past decade. Prompted by the 1969 Federal Coal Mine Health and Safety Act, a great deal of research and development has been devoted to means of meeting the 2 mg/m^3 dust standard. The result has been the evolution of such devices as spray curtains and machine-mounted filtration systems. Particular problems exist on longwall faces. Although research on dust prevention, suppression, and filtration should continue, more fundamental studies should be instigated into the dust-carrying characteristics of airflow with regard to flow regime, impaction, particle size, and density.

Hydrological studies and investigations into the effect of water on shales and interstitial clays would provide data of value on the choice of sites suitable for water infusion.

Methane

The migration of natural gas toward mine workings is governed by (1) the gas pressure within the strata, (2) the adsorptive characteristics of the rocks, and (3) the permeability of the source and carrier beds. The first two of these parameters can be quantified by field and laboratory tests, but rock permeability is a tensor quantity that varies both with position and time as the mine workings are developed. The permeability of coal itself is dependent not only upon current mechanical stress but also upon the stress history of the seam. It is for these reasons that the prediction of methane emission levels and the design of methane drainage schemes have been highly empirical exercises. Further concentrated research of both a fundamental as well as an applied nature is required into the retention of gas within the rock mass, the mechanism of its release, and its subsequent migration through the strata. The successful exploitation of some of the nation's deeper coal reserves will be dependent upon handling methane gas emissions. The potential for the collection and use of the method as an energy source already is being explored, and this research should be encouraged and continued.

Heat and Humidity

Although high temperatures and humidities are not considered to be a problem in the majority of the relatively shallow American coal mines, the British experience of the past 10 years provides a cautionary case study. Research in the U. K. in 1970 on the prediction and control of mine heat was regarded by many as premature and unnecessary. Only a decade later, some British mines are faced with curtailment of production because of heat problems; air and water cooler units are being installed, and the decade of research is proving its worth. The heat problem has arisen not simply because of increased depth but mainly as a result of the additional power supplied to mechanized equipment. The problem is certainly one to be faced here in the U. S., and it is likely that the heat problem will grow most rapidly in association with longwall faces. The impact on ventilation economics is considerable, and the whole strategy of airflow planning must be reviewed when air/water cooling systems are considered.

The research and development programs required are extensive, varying from the design of cooling plants suitable for American mines, through the distribution systems of the cooling media, to the optimization of ventilating and cooling-plant capacity. A considerable overlap exists between these programs and the design of certain types of nuclear waste repositories.

Spontaneous Combustion

Past research in several countries has shed light on those factors that cause certain coal seams to be more subject to spontaneous heating than others. Of importance are such factors as air and coal moisture balance, pyritic content, and incubation times. However, the practical means of dealing with the problem still varies from attempts at complete ventilation of the zones at the risk of completely sealing them, the latter coupled with pressure-control techniques. Much of the problem can be avoided at the earliest stages of mine ventilation design by planning the system to avoid hazardous pressure differentials across waste or pillared areas and to minimize leakage paths. Research is needed into ventilation systems designed specifically for mines subject to spontaneous combustion.

Other Areas

The above summary includes those fields of research that have been discussed during interviews or that are topics of current and ongoing investigations in the United States and/or overseas. There are, however, numerous other areas within the general realm of mine environmental engineering that should also be considered for research funding. These include mine fires, explosions, drainage and inundations of water, noise, mine illumination, rescue techniques, ground vibration, radiation, and the surface environment.

AQUIFER THERMAL ENERGY STORAGE STUDIES AT LBL IN 1980

C. F. Tsang, T. A. Buscheck, and C. Doughty

The 1980 Aquifer Thermal Energy Storage (ATES) project at Lawrence Berkeley Laboratory (LBL) includes four main tasks: (1) to solicit appropriate articles and to edit them for a quarterly International ATES Newsletter; (2) to perform ATES generic studies; (3) to carry out field-specific planning and simulation studies; and (4) to improve modeling techniques. This article describes the accomplishments and status of each of these four tasks.

INTERNATIONAL ATES NEWSLETTER

The International ATES Newsletter is published regularly on a quarterly basis. Much enthusiasm, both in the United States and abroad, is evident from the many contributions to and requests for this publication. Our current mailing list includes over 300 subscribers, representing researchers, developers, and program managers in 16 countries including China and Japan. Vibrant exchange of information and ideas becomes possible through this Newsletter, and we are able to keep in touch with researchers and developers at the forefront of this new technology.

Since the initiation of this newsletter in 1978, a number of methods have evolved that utilize underground containments other than natural aquifers for storage. These include storage in buried pipes, shallow man-made aquifers, rock caverns, and natural or man-made lakes. The common factor among these methods of aquifer and nonaquifer storage is their application to long-term or seasonal storage. In light of this expanding methodology, and at the suggestion of the U. S. Department of Energy and the Pacific Northwest Laboratory, we have formally broadened the scope of the Newsletter to include all types of seasonal thermal energy storage. Reflecting this, beginning with the September 1980 issue, the name of the newsletter has been changed to the Seasonal Thermal Energy Storage (STES) Newsletter.

ATES GENERIC STUDIES

Generic studies during 1980 emphasize the understanding of the energy recovery factor (i.e., the ratio of energy recovered to energy stored) as a function of aquifer properties and storage parameters. The goal is to arrive at optimal choices of aquifer and storage arrangements. Dimensionless parameter groups that will be useful in the planning and design of practical projects are being studied and validated.

So far in our studies we have neglected buoyancy flow. This is the case for low-permeability aquifers or for storage of low-temperature water. Nellstrom et al. (1981) recently studied the problem, and from their work a criterion may be used to verify the applicability of this assumption. On the other hand, the results obtained for the functional dependence of the recovery factor may still be true for cases of significant buoyancy flow.

Since many computations have to be made for a study of functional dependence, a simple numerical model is used (Doughty et al., 1981). Besides assuming no buoyant flow, this model also assumes a steady-state fluid flow field in a laterally infinite, uniform aquifer. The recovery factor is calculated for a series of values of aquifer thickness, storage volume, aquifer and aquitard thermal conductivity, caprock thickness, cycle time period, velocity-dependent dispersion, and the number of cycles. In all cases, equal volumes of fluid are injected and produced. Some of the results are shown in Figures 1-4.

Figure 1 shows the energy recovery factor as a function of thermal radius, R_{th}, and aquifer thickness, H. Here R_{th} is defined as the radius that would be reached by the hot water at the end of the injection period if the thermal front were perfectly sharp, i.e., if there were no heat conduction. Each broken line traces the recovery factor for a given fluid volume. There is an optimal value of

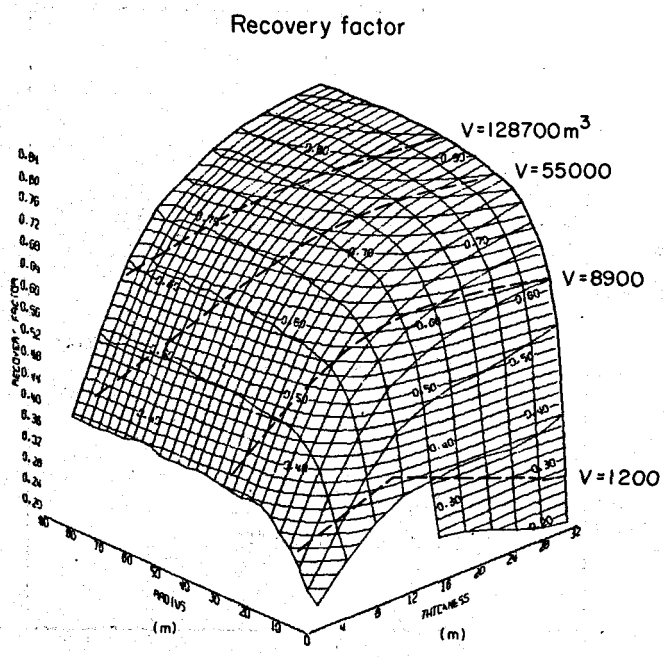

Figure 1. The recovery factor as a function of aquifer thickness and thermal radius. The latter is defined as the radius that would be reached by the hot water at the end of the injection period if there were no heat conduction. [XBL 806-7223]

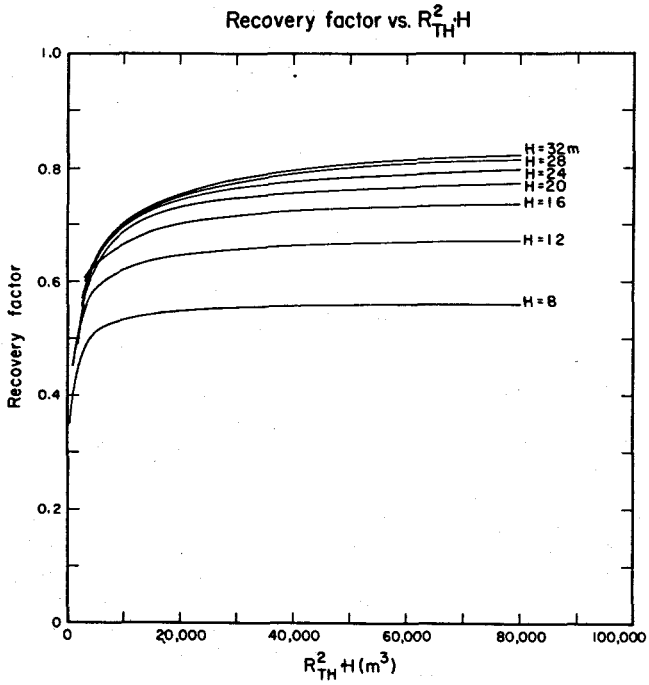

Figure 2. The recovery factor as a function of storage volume, implicitly given by $R_{th}^2 H$.
[XBL 803-6871]

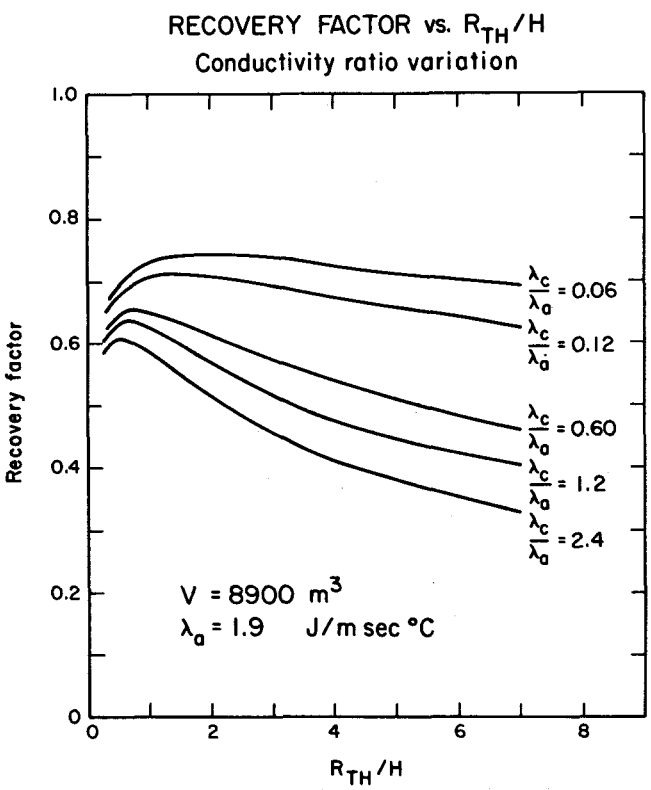

Figure 3. The recovery factor as a function of aspect ratio, i.e., thermal radius over aquifer thickness (R_{th}/H). [XBL 803-6873]

aspect ratio, R_{th}/H, which yields the maximum recovery factor for each volume. Generally, the recovery factor is a much more sensitive function for small values of R_{th} and H than for large values. Figure 2 shows the recovery factor as a function of volume for a series of values of H. The recovery factor increases rapidly at first, then levels off. Figure 3 shows the recovery factor as a function of R_{th}/H for a series of aquitard to aquifer thermal conductivity ratios. As this ratio decreases, the aspect ratio which yields the maximum recovery factor increases. Figure 4 shows the energy recovery factor as a function of the time period of a single injection-storage-production-rest cycle for several different injected volumes. The aquifer thickness for each volume is such that the aspect ratio is optimal. Lines labeled "a" show the results for a cycle with no storage or rest period; i.e., production begins as soon as injection ends. In this figure, injection and production periods are equal. We have found that varying the relative injection and production periods for a given storage period has only a minor effect on recovery factor. Lines labeled "b" show the results for a cycle with equal injection, storage, production, and rest periods. Lines labeled "c" show the results for the hypothetical cycle that is half storage and half rest period, the hot water being instantly injected and later instantly produced. This represents the limit of very short periods of injection and production.

A paper is being prepared (Doughty et al., 1981) which describes the detailed results of this work. Included in the paper will be systematic graphs of the recovery factor as a function of key dimensionless parameters and examples of their use for practical field applications. Plans for further calculations include the incorporation of gravity effects.

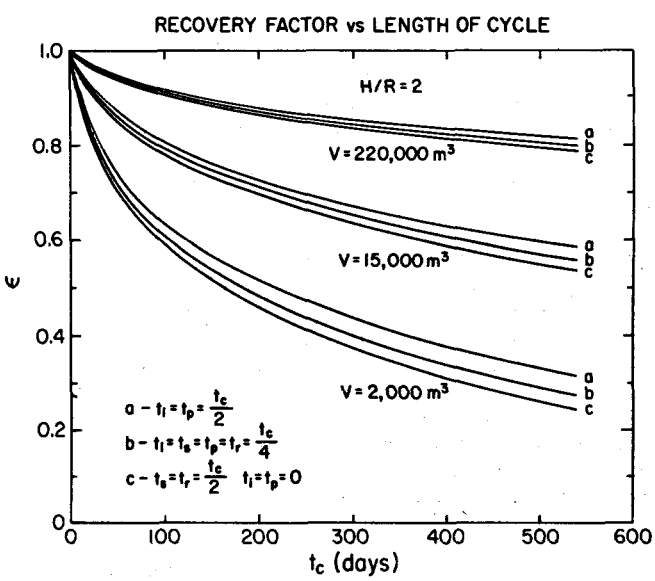

Figure 4. The recovery factor as a function of cycle length (t_{cycle}). [XBL 807-1385]

FIELD-SPECIFIC PLANNING AND SIMULATION STUDIES

During the early part of fiscal 1980, the simulation of the 1978-1979 two-cycle Auburn field experiments (Molz et al., 1980) with the LBL numerical model CCC was completed (Tsang et al., 1980). Observed and calculated recovery factors are within 2% of each other, and the production temperatures are reproduced within 2°C. No adjustable parameter was used. One may conclude (1) that we understand the physical processes involved in the ATES system at the Auburn field site, thus giving us confidence in dealing with confined aquifers of a similar type, and (2) that the LBL numerical model CCC is a satisfactory code that may be useful for further applications.

Cooperation with Auburn University is continuing in the planning and design of the next series of experiments. Several parameter-variation calculations were made to study the results to be expected for different arrangements. Figure 5 shows the effect of partial penetration of the injection-production well into an aquifer with the Auburn field parameters. Note that if the well penetrates the full thickness of the aquifer, the production temperature (solid line) drops steadily with time from the injection temperature of 55°C and the recovery factor, ε, is 69%. In contrast, when the well is producing water from only the upper half of the aquifer, the decrease in production temperature (broken line) during the initial production period is much slower and ε is increased from 69% to 73%. This may be of significant interest, since in most applications decreases in production temperature should be minimized over the main part of the production period. In anticipation of the next series of Auburn experiments, in which water will be stored at 90°C, we performed a series of calculations for that temperature. Figure 6 shows the production temperatures for two such cases. The solid line shows the production temperature obtained when water is injected into and produced from the middle third of the aquifer thickness, as it was during the Auburn experiments. The broken line shows the

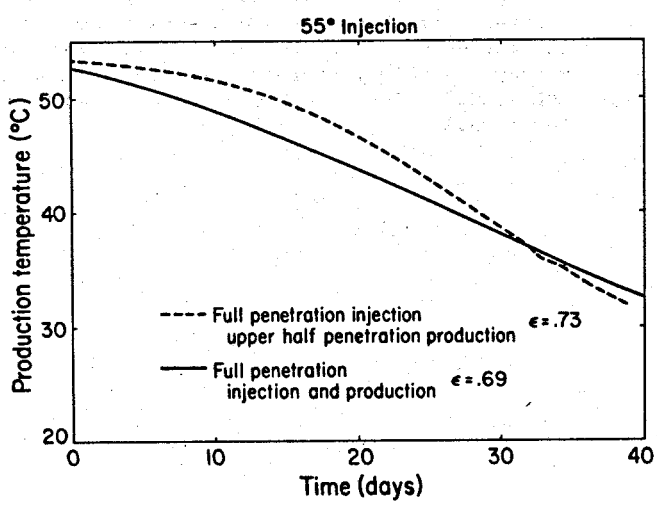

Figure 5. Production temperature vs. time for the storage of 55°C water for two well-penetration arrangements (ε is the energy recovery factor). [XBL 808-7282]

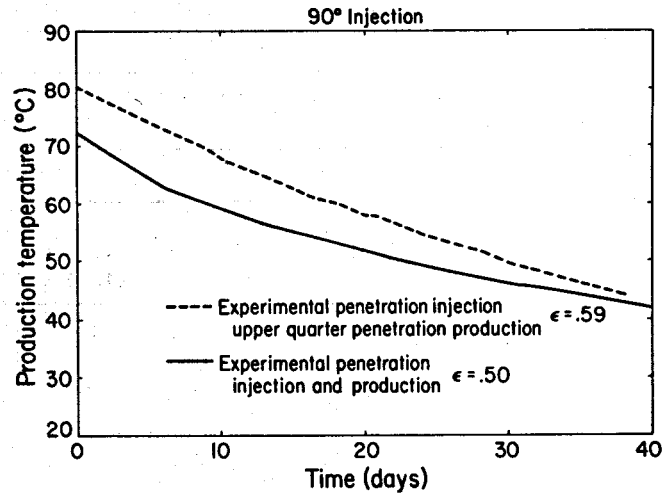

Figure 6. Production temperature vs. time for the storage of 90°C water for two well-penetration arrangements (ε is the energy recovery factor). [XBL 808-7281]

production temperatures when the water is produced from the upper quarter of the aquifer. As one might expect, the recovery factors are lower than those for the 55°C cases because of the higher buoyancy flow associated with the higher temperature.

Table 1 shows the recovery factors for a suite of cases involving injection temperatures and three values of aquifer permeability that were simulated using CCC. In all cases, storage volume is assumed to be 55,000 m^3, thickness of the aquifer is 21 m, and permeability of the aquitard is 10^{-5} that of the aquifer. The Auburn experiment corresponds to a permeability of 52 darcys. This table represents a substantial amount of computation, including different cycle periods and different penetration arrangements. The variation of the recovery factor is clearly seen. Details of these studies are presented and discussed in a paper under preparation (Buscheck et al., 1981).

NUMERICAL MODEL IMPROVEMENTS

The LBL numerical model CCC (conduction-convection-consolidation) that we have been using over the years for aquifer thermal storage studies is one of the best validated and most realistic codes available. However, it is specialized to the simulation of a water-saturated medium. Another numerical model, also developed at LBL, is able to calculate saturated-unsaturated isothermal flows. This code, TRUST (TRansient flow in Unsaturated and SaTurated porous media), is based on the same numerical scheme as CCC. We have initiated work to combine the two codes to develop a numerical model that will simulate nonisothermal flows in unsaturated-saturated media. The resulting improved model will be useful not only in saturated aquifer storage but also in shallower, unsaturated storage systems. Much attention to the latter has been given by the Europeans, but interest is increasing among U. S. researchers as well. A careful modeling study is needed to show the feasibility of such a concept.

Table 1. Summary table of energy recovery factors for different storage temperatures T_{inj} and different aquifer permeability values K_a (calculated with numerical model CCC).

K_a (D)	T_{inj} (°C) 35	55	70	90
15	0.69	0.68		0.68
		0.57		0.34
	0.67	(1/2) 0.62	0.46	(1/2) 0.42
				(1/3) 0.44
52		(60+60+60)		(60+60+60)
		0.65		0.42
		(60+120+60)		(1/2) 0.51
		0.55		
		0.31	0.24	
175		(1/2) 0.39	(1/2) 0.31	
		(1/3) 0.41	(1/3) 0.34	

Unless otherwise indicated, the total time for the injection-storage-production cycle ($t_{inj} + t_{store} + t_{prod}$) amounts to (90 + 90 + 90) days.

(1/2) or (1/3) indicates production from the upper half or upper third of the aquifer thickness.

Ambient aquifer temperature is 20°C.

CONCLUSIONS

Substantial work has been done in 1980. The major conclusions are:

1. From the many comments that have been received, it is clear that the quarterly Newsletter is an effective means of information exchange among workers in aquifer energy storage world-wide. We believe that it has played a major part in promoting the development of this field both in the U. S. and other parts of the world.

2. A better understanding of the energy recovery factor as a function of various aquifer properties and storage conditions has been obtained. We are developing a number of key parameter groups which may prove to be of great help in experimental design and industrial applications.

3. The success of simulating Auburn experiments has given us considerable confidence in numerical model CCC. Further validation against an aquifer storage system of a different type will be useful to verify its range of applicability. This model should be used in the planning of future experiments and in the prediction of observations. Appropriate arrangements should be made for those in industry to learn how to use this model.

4. The improvements of the numerical model CCC to simulate nonisothermal unsaturated flow will result in a code that may soon prove to be very useful.

ACKNOWLEDGEMENTS

We wish to extend our appreciation for the continued cooperation and assistance of our colleagues, G. Hellstrom, D. Mangold, and J. Wang.

REFERENCES CITED

Buscheck, T., Doughty, C., and Tsang, C. F., 1981. Aquifer thermal energy storage--A parameter study. In preparation.

Doughty, C., Hellstrom, G., Claesson, J., and Tsang, C. F., 1981. A study of ATES thermal behavior using a steady flow model. Berkeley, Lawrence Berkeley Laboratory, LBL-11029.

Hellstrom, G., Tsang, C. F. and Claesson, J., 1981. Heat storage in aquifers: Buoyancy flow and thermal stratification problems. Berkeley, Lawrence Berkeley Laboratory, LBL-11059. (To be submitted to J. of Geophys. Research.)

Molz, F. J., Parr, A. D., Andersen, P. F., 1980. Experimental study of the storage of thermal energy in confined aquifers. Auburn, Alabama, Water Resources Institute, Auburn University.

Tsang, C. F., Buscheck, T., and Doughty, C., 1980. Aquifer thermal energy storage--A numerical simulation of Auburn University field experiments. Berkeley, Lawrence Berkeley Laboratory, LBL-10210. (Submitted to J. Water Resources Research.)

IRIDIUM IN SPRING WATERS AND SUMMIT CRATER LAKE OF MT. HOOD, OREGON

H. Bowman, H. Wollenberg, F. Asaro, and R. G. Bowen*

During a hydrogeochemical study of the Mt. Hood volcano in Oregon, the platinum-group element iridium was detected in three out of approximately thirty natural water sources on or near the mountain. Prior to this study iridium had apparently not been detected in terrestrial waters. The element iridium is of special interest because of its apparent association with the Cretaceous-Tertiary boundary on a world-wide basis (Alvarez et al., 1980). The present study (described in detail by Wollenberg et al., 1979) was part of a program to assess the geothermal potential of Mt. Hood, and was carried out under the direction of the Oregon Department of Geology and Mineral Industries with support from the U. S. Department of Energy.

SETTING

Mt. Hood is located 80 km east of Portland, Oregon, along the linear trend of most of the Cascade volcanoes of California, Oregon, and Washington. The geologic setting of Mt. Hood was described in detail by Wise (1969). The mountain is a composite andesitic stratovolcano, mainly Pleistocene in age, rising approximately 2500 m above the surrounding terrain. Its eruptive history is similar to that of many other Cascade volcanoes. The most recent major eruption took place about 220 years ago. At that time a series of hot avalanches cascaded down the west and east sides of the mountain, carrying incandescent debris several miles downslope into the adjacent valleys. Mt. Hood today has 90-95°C fumaroles near its summit, a partially frozen summit crater lake, and a warm spring area, Swim Springs, on its south flank.

SAMPLING

During this study over 40 water samples were collected and filtered in the field and analyzed at Lawrence Berkeley Laboratory (LBL) by x-ray fluorescence and neutron activation analysis (NAA). The locations of the water sources containing iridium are shown in Figure 1. The warm spring area was sampled at different times of the year to test for seasonal chemical variation.

SAMPLE PREPARATION AND ANALYSES

A 500-ml water sample is evaporated to dryness in a cleaned Nalgene container at a temperature of 60-80°C. The residue from the bottom of the container is used as an abrasive to scrape residue from the walls (with a toothbrush). The total residue is then weighed. A 100-mg sample of the residue is mixed with 50 mg of cellulose binder, and the mixture is compressed into a pill 1.00 cm in diameter at a pressure of about 25,000 psi. In the normal NAA regime each pill is encapsulated in polyethylene foil and irradiated with standards for 10-18 minutes in the small U.C. Berkeley research reactor at a flux of about 2×10^{11} n/s-cm^2. All pills are essentially the same size, and the standards and unknowns are rotated in such a way that all samples receive exactly the same neutron dose. After irradiation each sample is counted twice, and 11 elements are measured in these counts. Several weeks later the pills are removed from the polyethelene wrappers and rewrapped in 0.001-in. aluminum foil (99.9999% pure). These samples and a multielement standard, Standard Pottery (Perlman and Asaro, 1971), are irradiated for 8 hr at a flux of about 2.7×10^{13} n/s-cm^2. They are counted at about 1 week and 4 weeks after the irradiation with a 1-cc intrinsic Ge gamma-ray detector and again at about 3 weeks after the irradiation with a 7-cc intrinsic Ge detector. The sensitivity for measurement of iridium with the 7-cc detector is about 0.5 to 1 ppb in the evaporated residue, which leads to sensitivities of about 10^{-13} g Ir/g H_2O in water containing a few parts in 10,000 of residue.

If iridium is chemically removed from water or from its evaporated residue (either before or after a neutron irradiation), better sensitivities can be obtained. This procedure, however, introduces an uncertainty related to the efficiency of the chemical separation. In post-irradiation chemistry, for example, there can be an uncertainty as to the extent of equilibrium between iridium in the unknown and in the carrier used to determine the chemical

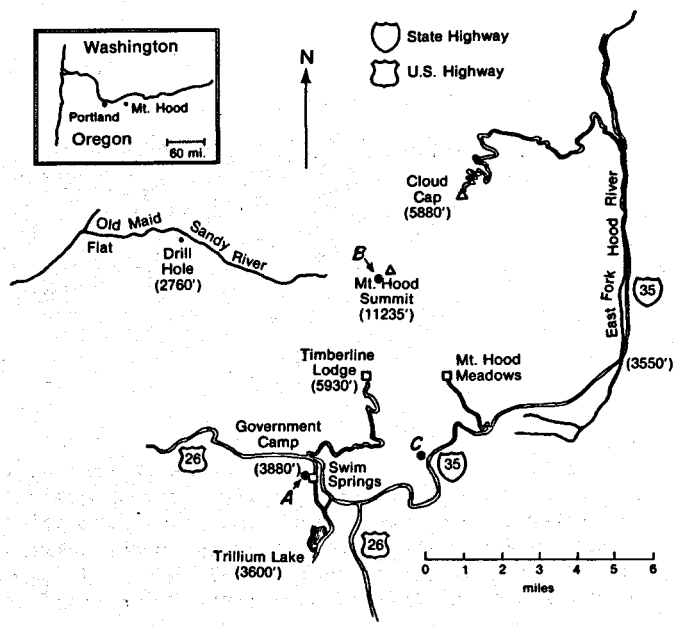

Figure 1. Map of the Mt. Hood area showing the location of water sources which contain iridium. A, Swim Springs; B, Summit crater lake fumarole area; C, Fe-rich cold spring. [XBL 784-644]

efficiency. In order to avoid these uncertainties and still improve the sensitivity, we employed an NAA measurement technique used to obtain a limit on the amount of iridium in sea water (Alvarez et al., 1980). In this procedure a 128-cc Li-doped Ge detector is used to count the 316 and 468 Kev gamma rays of 74.17-day ^{192}Ir for several days some months after the irradiation. There is a substantial background radiation from the continuous Bremstrahlung radiation of 14.28-day ^{32}P. This radiation arises from the $^{31}P(n,\gamma)^{32}P$ reaction and (with smaller neutron cross section) from the reaction $^{32}S(n,p)^{32}P$. As long as ^{32}P is contributing a predominant part of the background, the longer one waits before counting a sample the better will be the background counting statistics (in the Ir peak region) for a given length of count. For one sample of Mt. Hood water, MH-43, a preliminary count of 1502 min was made 33 days after the irradiation. From this count it was estimated that the most efficient analysis would be made 2 months later, and a 7086-min count was made 94 days after the irradiation. The results are summarized in Table 1, and part of the gamma spectrum of the 7086-min count is shown in Figure 2. The best value for the iridium abundance in the residue was 0.074 ± 0.007 ppb, which corresponds to an abundance of 55 ± 5 x 10^{-15} g Ir/g water.

RESULTS

Iridium was first detected in a high-iron-content cold spring on the southern flank of Mt. Hood (location C in Fig. 1). It was then detected in Swim Springs in the samples collected in February and October of 1978 and in a sample obtained in the summer of 1977 from the summit crater lake (location B).

Table 1. Iridium abundance data for Mt. Hood water sample MH-43A (location A, Fig. 1, collected on October 5, 1978).

	Parts-per-billion iridium in evaporated residue 316 kev	468 kev
Normal NAA regime (7-cc Ge detector)		
28 days after irradiation (60-min count)	< 1.8	< 5
Special NAA counting regime (128-cc Ge-Li detector):		
33 days after irradiation (1502-min count)	0.064 ± 0.032	0.061 ± 0.039
94 days after irradiation (7086-min count)	0.077 ± 0.009	0.072 ± 0.014

Best abundance of iridium in residue = 0.074 ± 0.007 ppb.
Abundance of evaporated residue = 7.49 x 10^{-4} g residue/g H_2O.
Abundance of iridium in water = (55 ± 5) x 10^{-15} g Ir/g H_2O.

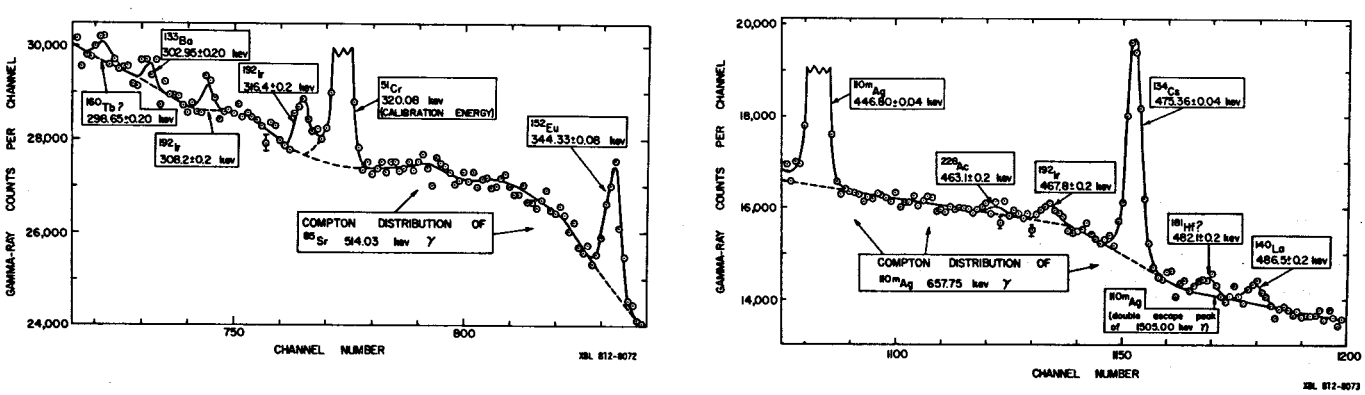

Figure 2. Partial gamma-ray spectrum of the neutron irradiated evaporated residue from Mt. Hood water sample MH-43A. Length of gamma ray count equals 7086 min (94 days after the irradiation). The spectrum was taken with a 128-cc Ge-Li detector. The iridium abundance is (55 ± 5) x 10^{-15} g Ir/g H_2O. This neutron irradiation was the second one done on the sample, and it was made to take advantage of recent improvements in iridium measurement techniques. Ag was an impurity introduced by a sample holder in the counting of the sample after the first irradiation. ^{51}Cr arose from a minute Cr impurity introduced into the sample by a tool-steel die in the sample preparation procedure. ^{140}La was a decay product from the fission of ^{235}U in the sample during neutron irradiation. ^{228}Ac was a natural radioactivity in equilibrium with ^{232}Th, and its gamma rays were part of the background in the lead-lined counting chamber. Ba, Cs, Eu, Ir, and Sr radioactivities and possibly those of Hf and Tb were due to the presence of those elements in the water. [left, XBL 812-8072, right, XBL 812-8073]

The results for seven of the best determined chemical elements in waters from five separate orifices in the Swim Springs area are shown in Figure 3 and the location of the orifices in Figure 4. The plots of six of these elements against sodium concentrations suggest a linear correlation between the elemental abundances. These results, along with water temperature data, suggest that at least two separate water sources are mixed together in differing proportions to produce the spring waters in the warm spring area.

Iridium contents are shown in Table 2. The iridium concentration in one of the warm spring orifices varied from 7 x 10^{-12} g/g in the winter sampling period to 5.5 x 10^{-14} g/g in a sample collected in the following October. The average major-element content of this spring water varied about 20% for the same period, with the higher concentrations also occurring during the winter.

Iridium was also detected in the summit crater lake at the level of 4 x 10^{-13} g/g in a sample collected August 30, 1977, and was found to be less than 1 x 10^{-13} g/g in a sample collected on October 10, 1978.

The presence of iridium in the waters associated with the volcano raises the question of the iridium content of the volcanic rock. However, the presence of iridium above the detectability limit (0.003 ppm) was not detected by standard neutron

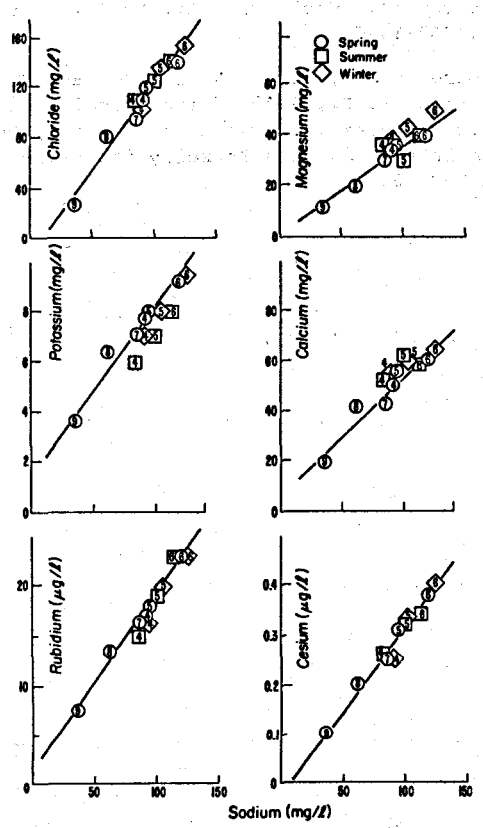

Figure 3. Chemical variations in Swim Springs waters. Numbers are keyed to orifice locations in Figure 4. [XBL 789-2699]

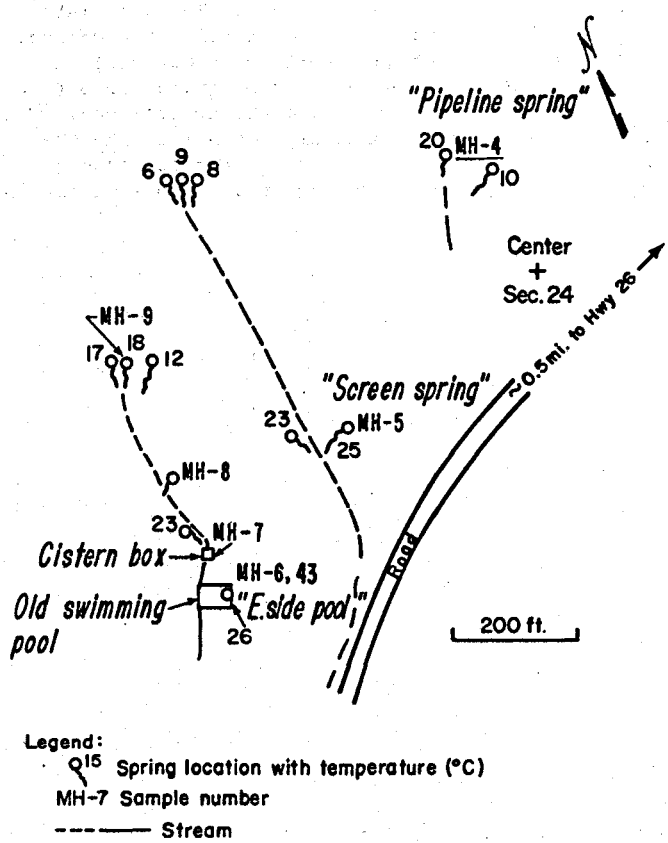

Figure 4. The distribution of water sources at Swim Springs. [XBL 788-2660A]

Table 2. Iridium abundances in Mt. Hood waters.

Location	Date	Iridium (g/g)
A. Swim Spring, orifice	February 22, 1978	7 x 10^{-12}
	October 5, 1978	5.5 x 10^{-14}
B. Lake, summit crater fumarole area	August 30, 1977	4 x 10^{-13}
	October 10, 1978	< 1 x 10^{-13}
C. Fe-rich cold spring	June 2, 1977	3.1 x 10^{-13}

activation analyses of rock samples collected from the summit fumarole or from elsewhere on the mountain (Wollenberg et al., 1979). Special counting procedures similar to those described above should improve significantly our sensitivity for detecting iridium in these rock samples.

CONCLUSIONS

Iridium, one of the platinum-group elements, has been detected for the first time in terrestrial water sources. During the hydrogeochemical study of Mt. Hood, Oregon, iridium was detected in the summit crater lake and in both a warm and cold spring on the southern flank of the volcano. The platinum-group elements are generally associated with basic to ultrabasic igneous terranes. Therefore, it is surprising to find iridium associated with a volcano composed predominantly of andesite. The seasonal variation (February to October) in iridium abundance was found to be quite large ($>10^2$) in water from one of the warm spring orifices. This iridium variation is probably not related to the seasonal variations in major-element abundances detected in this warm spring area. Those variations are relatively small (<20%), and are probably due to dilution effects that occur during the spring and summer thaw of the snow pack.

REFERENCES CITED

Alvarez, L. W., Alvarez, W., Asaro, F., and Michel, H. V., 1980. Extraterrestrial cause for the Cretaceous-Tertiary extinction. Science, v. 208, p. 1095-1108.

Perlman, I., and Asaro, F., 1971. Pottery analysis by neutron activation. In R. H. Brill (ed.), Science and Archaeology. Cambridge, Mass., MIT Press, p. 182-195.

Wise, W. S., 1969. Geology and petrology of the Mt. Hood area: A study of High Cascade volcanism. Geol. Soc. Am. Bull., v. 80, p. 969-1006.

Wollenberg, H. A., Bowen, R. G., Bowman, H. R., and Strisower, B., 1979. Geochemical studies of rocks, water, and gases at Mt. Hood, Oregon. Berkeley, Lawrence Berkeley Laboratory, LBL-7092.

GEOTHERMAL ENERGY DEVELOPMENT

The Earth Sciences Division program in Geothermal Energy Development began in 1973 in response to the national goal of developing alternative energy sources for electrical and nonelectrical applications. The program initially consisted of an exploration assessment of sites in northern Nevada for a proposed demonstration plant; development of a binary-fluid conversion process for high-temperature, low-salinity brines; and various geochemical studies related to brine chemistry, scaling, and corrosion. An additional support project, the National Geothermal Information Resource (GRID), was begun for the purpose of compiling a data bank on topics related to geothermal energy.

Many of these general programs continue in modified or expanded form and others have been added in recent years. Most have been funded by the U. S. Department of Energy (DOE), Division of Geothermal Energy; the Water and Power Resources Service (formerly the Bureau of Reclamation) has contracted with Lawrence Berkeley Laboratory (LBL) for site-specific studies. This section of the Annual Report summarizes our current activities in three principal areas of geothermal research: (1) Geothermal Exploration Technology, (2) Reservoir Engineering, and (3) Geothermal Energy Conversion Technology.

Exploration Technology projects deal with generic research designed to improve our ability to locate and define a geothermal reservoir using surface techniques, mainly geophysical. Historically, our emphasis has been on electrical, electromagnetic, and seismic techniques because of the expertise available to us at the University of California, Berkeley, and because of the need to develop these techniques to the point where they can be better used by industry.

During 1980 the electrical-electromagnetic research was directed toward improving data acquisition, survey procedures, and interpretation techniques. In magnetotellurics we have been concerned mainly with developing better interpretation methods. In controlled-source electromagnetics we have been investigating the practical advantages of frequency- and time-domain methods and the differences between them. Our frequency-domain system, the EM-60, was operated at several geothermal prospects in Nevada to demonstrate to industry the feasibility and cost effectiveness of EM soundings and to define subsurface structures at the sites. The Automatic Seismic Processor (ASP), under development since 1978, was completed and operated successfully at The Geysers. This device was designed for rapid, cost-effective microearthquake monitoring and analysis in geothermal exploration.

In Reservoir Engineering studies, the greatest part of our effort at LBL has been on modeling heat and mass transfer of multicomponent, multiphase fluids through geologic media. This work improves our capability of understanding the behavior of geothermal reservoirs under different production/reinjection conditions and should lead to better reservoir management. The code SHAFT79 was used to obtain a performance match with the

geothermal reservoir at Serrazzano, Italy, and to provide production forecasts to 1990. Another major interest has been in well testing to determine reservoir parameters. In this regard, we have coupled our two-phase reservoir code (SHAFT79) with codes to simulate two-phase transient and steady-state flow in a wellbore.

LBL has developed a combined pressure-temperature-flow tool, a field data acquisition system, and software to interpret pressure transient data. This technology has direct application to lower-temperature resources (< 200°C) which have great potential for nonelectrical applications.

Finally, LBL's Reservoir Engineering program also supports research at specific reservoirs for which case history data are being assembled and analyzed. LBL directs for DOE a Mexican/American cooperative study of the Cerro Prieto, Baja California, geothermal field. The elements of this study are geology-hydrology, geochemistry, geophysics, and reservoir testing and modeling. We have also provided advice on reinjection. LBL also assists DOE in evaluating reservoir data for the Valles Caldera, New Mexico, the site of a 50-MW demonstration plant.

Geothermal Energy Conversion Technology projects develop basic data and analytical tools in heat exchange and thermodynamics needed for the development of moderate-temperature geothermal resources. Through the Binary Fluid Experiment, we are obtaining laboratory-quality data on heat-transfer film coefficients of various candidate hydrocarbon working fluids, and a DOE/Electric Power Research Institute heat-exchanger test will provide a verification of the data under field conditions. A study of fluid properties is under way that seeks to provide the best available thermodynamic and transport data on brines and working fluids. The 500-kW direct-contact heat-exchange pilot plant was completed at East Mesa, California, and testing begun. Our computer code GEOTHM was used to study the relationship of working-fluid composition and resource temperatures for economically optimized binary cycle power plants.

This work was supported by the Assistant Secretary for Conservation and Renewable Energy, Office of Renewable Technology, Division of Geothermal and Hydropower Technologies of the U. S. Department of Energy under Contract No. W-7405-ENG-48.

EXPLORATION TECHNOLOGY

ADVANCES IN ELECTRICAL AND ELECTROMAGNETIC EXPLORATION TECHNIQUES

Overview

H. F. Morrison

The objective of this program is to develop and test improved electrical and electromagnetic techniques and systems for geothermal exploration. Following our development of very successful dc resistivity, electromagnetic (EM-60), and remote reference magnetotelluric systems, the emphasis at Lawrence Berkeley Laboratory (LBL) has shifted toward improving data acquisition, survey systems, and interpretation techniques. For example, a new, general-purpose, in-field data-acquisition and processing system was assembled and successfully tested in fiscal 1980. This system, which comprises a Hewlett-Packard desk-top computer, a Nicolet Explorer III digital oscilloscope and an analog multiplexer of our design, is more flexible and powerful than the multichannel microprocessor developed at LBL in 1978 and currently used by various groups. The new system can either stand alone or interface with the existing digital signal processor to expand its capability for power-spectral averaging, in-field graphics, gain and filter control, and in-field modeling.

Other major activities in progress during fiscal 1980 have included:

1. Fundamental studies of electromagnetic response of the ground for magnetic dipole sources.

2. Development of improved, high-speed, cost-effective algorithms for numerical modeling.

3. Studies of direct inversion schemes for two-dimensional models.

4. Study of topographic effects in magnetotellurics.

5. Field experiments with the new, remote-reference noise-calcellation scheme for the controlled-source electromagnetic prospecting system.

In the sections that follow, we present summaries of a few of our pertinent studies.

Controlled-source electromagnetic interpretation based on a tilted dipole source

J. R. Haught

One problem encountered when deep EM induction surveys are made in hilly or mountainous regions is the lack of a large enough flat area in which to place the source, a loop of wire in our system. Normally the source is placed on as flat a spot as possible so as to produce a vertical moment. If the source is placed on an irregular or sloping surface, the moment will not be vertical, and the fields from the source become more complex than if the dipole is vertical. In fact, the fields measured some distance away cannot be converted to the equivalent fields from a vertical source by means of a simple analytical rotation of the tilt angle. The reason is that the tilted source is a combination of vertical and horizontal dipoles. The horizontal dipole distorts the otherwise axially symmetric fields of the vertical dipole, and interpretation requires not only a knowledge of the relative horizontal and vertical separation between the receiver and the transmitter but also the inclination of the source and the angle between the receiver and the inclined direction of the source.

Figures 1 and 2 are examples of the effect of a tilted dipole on the radial field amplitude and ellipticity for a two-layer model. The radial field is affected throughout the frequency range, with the largest deviations from a vertical dipole field occurring at both high and low frequencies. In these frequency ranges the field from the vertical dipole falls to zero, but the horizontal dipole fields asymptotically approach a constant value,

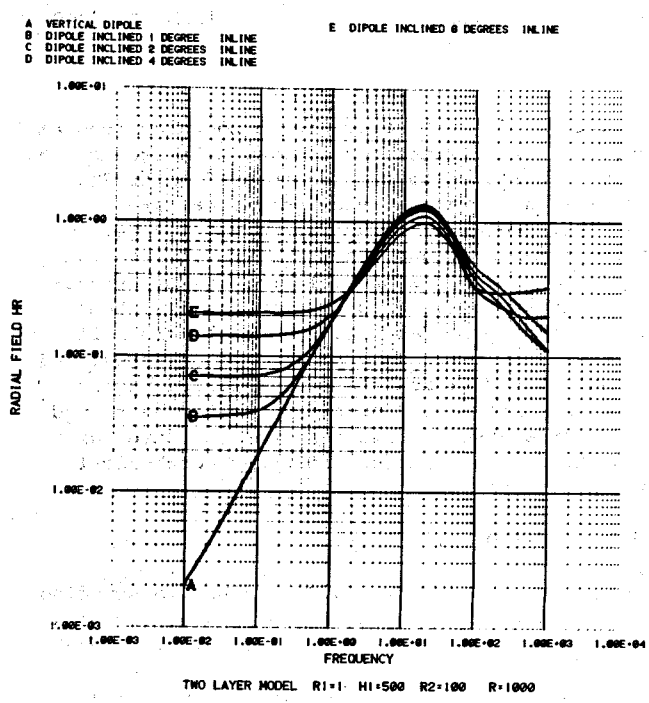

Figure 1. Radial field amplitude. [XBL 811-7809]

thus producing the behavior shown in Figure 1. Figure 2 shows that the fields from a tilted dipole are not equivalent to the fields from a vertical dipole as measured by means of a receiver whose vertical measurement axis is tilted. Another way of stating this effect is to note that the ellipticity of the polarization ellipse from a vertical dipole is insensitive to receiver orientation, whereas the ellipticity from a tilted source is very sensitive to tilt.

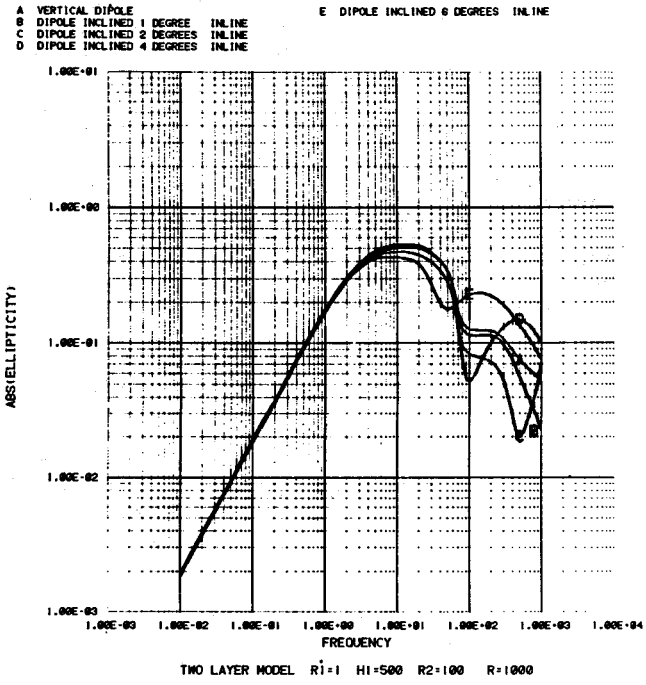

Figure 2. Ellipticity. [XBL 811-7808]

During 1980 we have written a computer program to account for a tilted source over a layered earth, and have applied it to the interpretation of EM field data taken in the McCoy geothermal area, Nevada (Dey and Ward, 1970; Ryu et al., 1970). This program has allowed us to interpret data that were previously uninterpretable because of irregularities in terrain. This program has also been used to reinterpret data which, though originally modeled with an assumed vertical dipole source, had given an interpretation that we suspected was in error. The interpretation derived from the tilted dipole source gave results that agreed better with results at nearby stations and other geophysical data.

REFERENCES CITED

Dey, A., and Ward, S. H., 1970. Inductive sounding of a layered earth with a horizontal magnetic dipole. Geophysics, v. 35, no. 4, p. 660-703.

Ryu, J., Morrison, H. F., and Ward, S. H., 1970. Electromagnetic fields about a loop source of current. Geophysics, v. 35, no. 5, p. 862-896.

Transient field responses

G. M. Hoversten

Quantitative interpretation of electromagnetic prospecting systems has led to elegant mathematical algorithms for computing the fields over layered and inhomogeneous earth models from a variety of transmitters. Often these solutions make it difficult to understand the basic electromagnetic phenomena, hence making the geophysicist's initial interpretation rather abstract or mechanical. Continuing discussions of the relative merits of time- and frequency-domain systems are often based on limiting or asymptotic forms for the solutions, and rarely have the solutions been analyzed in terms of the basic physics of the governing Maxwell's equations. Pridemore (1978) has made a thorough study of frequency-dependent electric fields in a one-layered earth overlying a half-space, and Lewis and Lee (1978) and Nabighian (1979) have studied the transient electric fields in a half-space. These studies have been very useful in explaining the fields observed on the surface in terms of the currents induced in the half-space.

As part of a larger study of time- and frequency-domain electromagnetic systems, we have developed algorithms for calculating the time-domain electric fields in layered half-spaces. The solutions are obtained first in the frequency domain following the methods described in Morrison et al. (1969) and are then transformed to the time domain for a variety of source waveforms. The solutions are completely general, including displacement currents: for the horizontal loop source, they include a variable loop radius.

Apart from our general interest in finding a sound physical interpretation of the fields measured on the surface over layered models, we have found the solutions for the electric field, E, in the ground very helpful in understanding the response of inhomogeneities in a layered half-space. In situations involving significant current channeling, the phase of the current at the inhomogeneity is useful in understanding the phases of the secondary fields at the surface.

An example of the induced electric field within a three-layer model is presented in Figure 1. Here the direction of E is positive into the plane of the figure, with the transmitter loop, radius 56.4 m, to the left of the cross section. The layer resistivities from the top down are ρ_1 = 50 ohm-m, ρ_2 = 1 ohm-m, ρ_3 = 50 ohm-m. The times shown are in milliseconds after the turnoff of the positive section of a square wave with alternating polarity period of 1 s.

As can be seen in Figure 1, the electric field develops a ring pattern with a central E_{max}. Once E_{max} propagates to the conductive layer, it is trapped and moves out from the transmitter horizontally. By using the right-hand rule of magnetic fields about a current element, one can easily understand the observed magnetic fields at a given surface position as a function of time.

This is only one example of many models considered in the frequency and time domain. The results are interesting even on a purely academic level, but implications are far-reaching for understanding the behavior of transient EM effects.

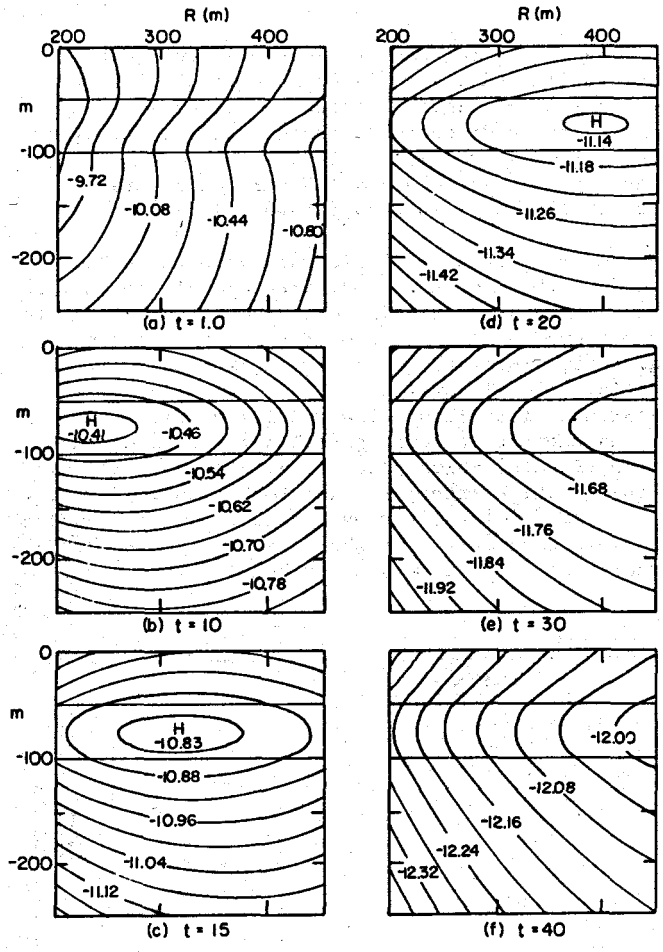

Figure 1. Induced electric field within model C. [XBL 809-11933]

REFERENCES CITED

Lewis, R., and Lee, T., 1978. The transient electric fields about a loop on a half-space. Bull. Aust. Soc. Explor. Geophys., v. 9, no. 4, p. 173-177.

Morrison, H. F., Phillips, R. S., and O'Brien, D. P., 1969. Quantitative interpretation of transient electromagnetic fields over a layered half-space. Geophys. Prosp., v. 17, p. 82-101.

Nabighian, M. N., 1979. Quasi-static transient response of a conductivity half-space--An approximate representation. Geophysics, v. 44 no. 10, p. 1700-1705.

Pridmore, D. F., 1978. Three-dimensional modeling of electric and electromagnetic data using the finite element method (Ph.D. dissertation). Salt Lake City, University of Utah, Dept. of Geophysics.

Approximation of magnetotelluric topographic effects by the solution of Laplace's equation

E. C. Mozley

A magnetotelluric impedance tensor may be calculated from the response of the earth to a plane wave electromagnetic source normally incident at the surface. The total field response of an inhomogeneous earth is due to the combined effects of channeling currents which are nonsolenoidal in nature and induction currents which are characterized by closed current loops. This phenomenon has been investigated through the use of eigenfunction techniques on thin-sheet electromagnetic scattering problems (Annan, 1974).

The general vector solutions of Maxwell's equations, constrained by the boundary conditions, are difficult to compute. However, when the electromagnetic scattering problem involves embedded inhomogeneities or topographic features which have small dimensions on the scale of a wavelength of the surrounding earth, then the resulting perturbations of the field components are predominantly due to the quasi-static channeling of currents into or around these structures. Therefore, the resulting secondary fields may be approximated by the solution of Laplace's equation.

Oppliger (1981) has developed a numerical solution of Laplace's equation which is based on the method of moments (Harrington, 1968). An arbitrary topographic surface is modeled by a finite number of cells, each with a constant slope and surface charge density. To solve this scalar problem for the charge distribution, the evaluation of a linear set of integral equations is required. The field perturbations due to the irregular surface are then calculated from this charge distribution.

A simple two-dimensional model of a smoothed triangular ridge with a slope of 30 degrees was first used. An approximately uniform current source perpendicular to the strike of the ridge was obtained by placing a point source at a distance equal to several model dimensions away from the ridge axis. The ridge generated an anomalous static electric field mode in magnetotelluric measurements. On the crest of the ridge, the current density was less than that of the half-space which resulted in a 38% decrease in the electric field perpendicular to the ridge. The current density increased at the base of the ridge as a result of current channeling into this conducting structure, producing a 36% increase in the perpendicular electric field at this point.

Magnetotelluric data measured in a region of extreme relief (Goldstein and Mozley, 1978), was used to evaluate the magnitude of the topographically induced bias in field data. The digital topographic data from this region was used to construct a parameterized surface of 1600 cells for the static modeling program. The resulting electric fields are calculated at the surface of each cell. The problem was solved for both an E-W and N-S current-source polarization. The results indicated that electric fields may be biased in excess

of 20% in regions of extreme relief. As a general rule, the electric fields are biased downward (decreased) in the vicinity of topographic high points and are biased upward (increased) in low areas located at the base of sloping terrain.

REFERENCES CITED

Annan, A. P., 1974. The equivalent source method for electromagnetic scattering analysis and its geophysical application (Ph.D. dissertation). Memorial University of New Foundland.

Goldstein, N. E., and E. C. Mozley, 1978. A telluric-magnetotelluric survey at Mt. Hood, Oregon. Berkeley, Lawrence Berkeley Laboratory, LBL-7050.

Harrington, R. F., 1968. Field computation by moment methods. New York, Macmillan.

Oppliger, G., 1981. Topographic effects in DC electric potential and magnetic field methods (Ph.D. dissertation). Berkeley, University of California, Dept. of Engineering Geoscience. In preparation.

The utilization of magnetotelluric polar diagrams in a volcanic environment

E. C. Mozley

The magnetotelluric impedance tensor components have a complex spatial relationship when measured in the vicinity of a three-dimensional conductivity distribution. The ability to interpret these data is enhanced when the dependence on the angle of rotation of the tensor (θ) is considered. This dependence on the direction may be graphically demonstrated through the use of polar diagrams of the impedance tensor $\bar{Z}$ and the geomagnetic transfer function $\bar{A}$;

$$Z_{xy}(\theta) = Z_{xy}\cos^2(\theta) + (Z_{yy} - Z_{xx})\sin(\theta)\cos(\theta) + Z_{yx}\sin^2(\theta),$$

$$A_{zu}(\theta) = A_{zy}\cos(\theta) - A_{zx}\sin(\theta),$$

$$\text{apparent resistivity} = 0.2TZ_{xy}(\theta)^2,$$

$$T = \text{period (s)},$$

$$\text{tipper} = A_{zy}(\theta),$$

where $|A_{zy}(\theta)|$ has a maximum in the direction of geological strike for the case of a two-dimensional earth. This scheme provides a useful data-compression technique, since the amplitude of all six complex components may be considered in terms of only three polar diagrams. The various components are related by the following relations:

$$|Z_{xy}(\theta)| = |Z_{yx}(\theta + \pi/2)|,$$

$$|Z_{xx}(\theta)| = |Z_{yy}(\theta + \pi/2)|,$$

$$|A_{zx}(\theta)| = |A_{zx}(\theta + \pi/2)|.$$

The polar diagrams of magnetotelluric data have had limited use as interpretational aids in the literature. These diagrams have been used to describe three-dimensional magnetotelluric modeling results (Reddy, 1977), and in at least one case the polar representation has been utilized to display magnetotelluric field data (Thayer, 1975).

In 1977 magnetotelluric data were collected around the base of Mt. Hood, a stratovolcano on the Cascade mountain range in northern Oregon (Goldstein and Mozley, 1978). Because of physical and financial constraints, the spatial sampling was limited both in regional coverage and in separation between measurement locations. The resulting sparce data set was subject to both spatial aliasing and truncation effects, which placed limitations on the use of quantitative interpretation techniques. However, by utilizing polar diagrams, as shown in Figures 1 and 2, it became evident that there exists a three-dimensional conductivity distribution with lateral

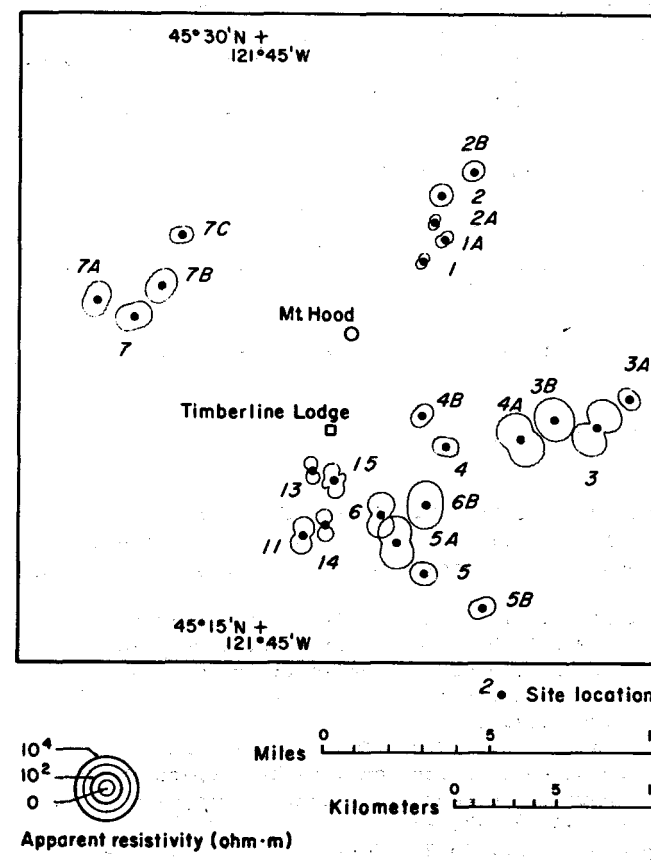

Figure 1. Band averaged from 1.0 to 0.1 Hz. [XBL 805-7053]

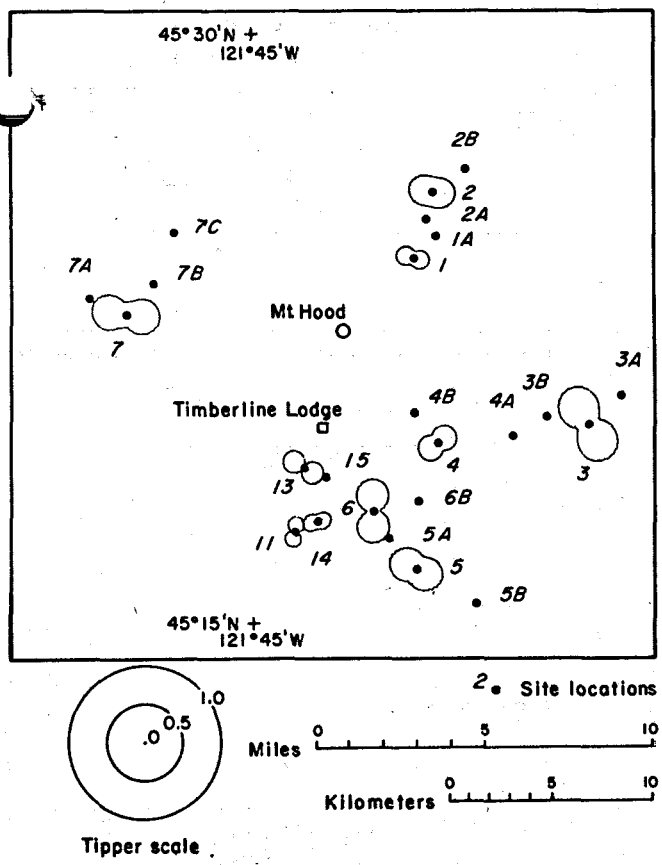

Figure 2. Band averaged from 1.0 to 0.1 Hz.
[XBL 805-7056]

variations on the order of the dimensions of the survey. In the south-southeastern portion of the survey area, significant lateral variations in conductivity occur on a scale equal to the distance between measurement sites. In this example, the polar diagrams provided a useful qualitative tool to determine the dimensionality and scale of conductivity distributions from an insufficient data set available in a complex geologic environment.

REFERENCES CITED

Goldstein, N. E., and Mozley, E. C., 1978. A telluric-magnetotellurics survey at Mt. Hood, Oregon. Berkeley, Lawrence Berkeley Laboratory, LBL-7050.

Reddy, I. K., Rankin, D., and Phillips, R. J., 1977. Three-dimensional modeling in magnetotelluric and magnetic variational sounding. Geophys. J. Roy. Astr. Soc., v. 51, p. 313-325.

Thayer, R. E., 1975. Telluric-magnetotelluric investigations of regional geothermal processes in Iceland (Ph.D. dissertation). Providence, Rhode Island, Brown University, Dept. of Geological Sciences.

ELECTROMAGNETIC INDUCTION SOUNDING AT GEOTHERMAL PROSPECTS IN NEVADA

M. J. Wilt, M. Stark, N. E. Goldstein, and J. R. Haught

~~As part of a joint Department of Energy/Industry geothermal case studies program for the Northern Basin and Range province, Lawrence Berkeley Laboratory (LBL) has conducted~~ controlled-source electromagnetic sounding surveys were conducted with the ~~its~~ newly developed EM-60 system over three promising geothermal targets in northern Nevada. ~~The objectives of these studies were to demonstrate to industry the feasibility and cost effectiveness of EM soundings and to better define the electrical structure for the purpose of reservoir delineation.~~

~~PROGRESS IN 1980~~

~~Three regions in north-central Nevada were chosen for study with the EM-60 system (Fig. 1).~~ These are (1) Panther Canyon, an area in the southeastern portion of Grass Valley; (2) the Soda Lake thermal area, located near Fallon, Nevada; and (3) the McCoy geothermal region, located some 30 miles west of Austin in central Nevada. Significant findings from each survey are summarized, ~~below~~

Panther Canyon

The Panther Canyon geothermal anomaly was first discovered by shallow heat-flow drilling and reconnaissance geophysics (Beyer, 1977; Sass et al., 1977). These studies outlined an oval-shaped 3-km^2 region of higher than normal heat flow associated with a region of low resistivity (Fig. 2). Subsequently, dipole-dipole resistivity data were taken for detailing purposes, and two-dimensional modeling of these results indicated an irregularly shaped conductive body associated with the thermal anomaly. To investigate this anomaly further and to test the EM method in a region of complex structure, the EM-60 system was utilized for a short survey over the thermal anomaly. The study consisted of three frequency-domain soundings from a single horizontal-loop transmitter using a 100-m-diameter loop (Wilt et al., 1980). Receivers were placed 0.5 to 1.5 km from the loop to permit a detailed look from the near surface to a maximum depth of 1.5 km.

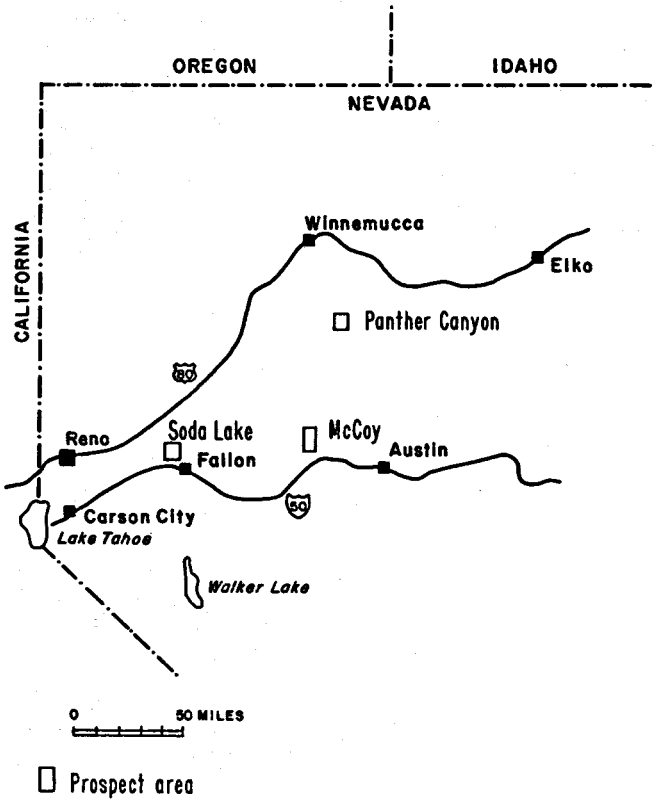

Figure 1. Prospect location map for the three EM-60 surveys conducted in 1979 by LBL. [XBL 802-6771]

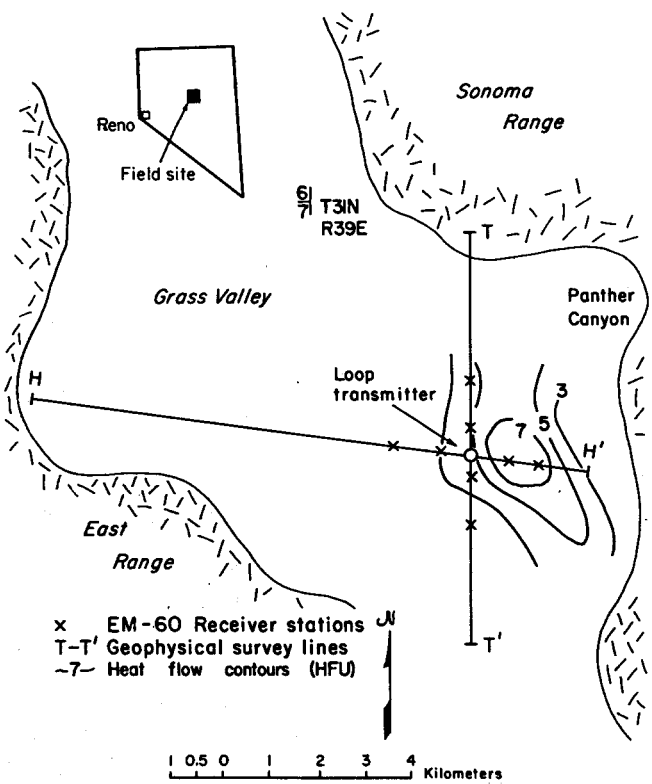

Figure 2. Survey location map of Panther Canyon area, Grass Valley, Nevada. [XBL 804-7050]

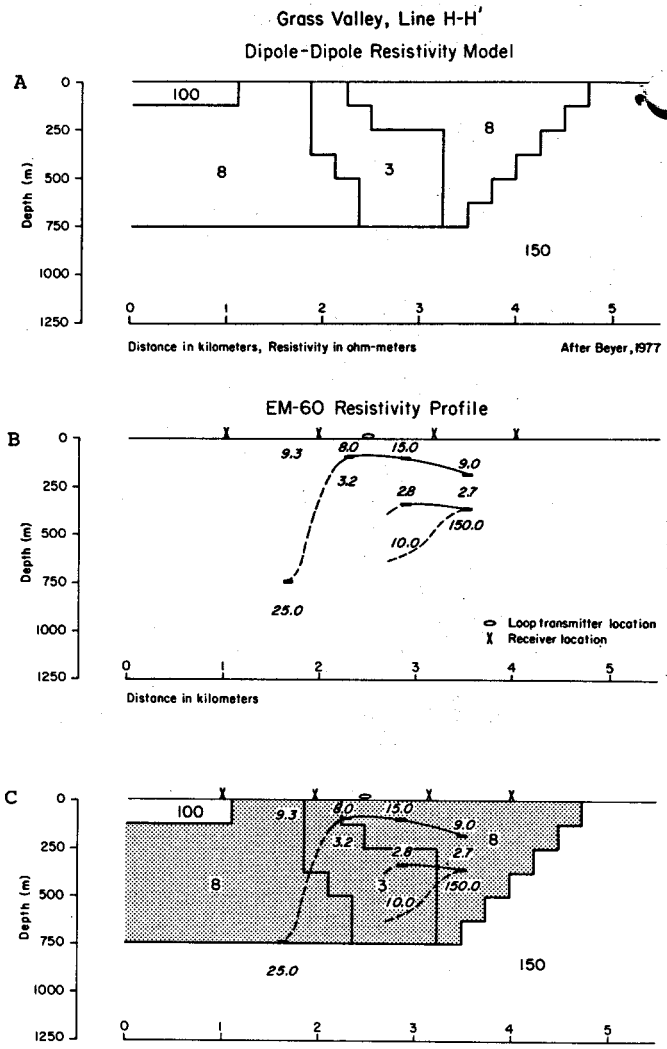

Figure 3. Resistivity cross section over line H-H' in Panther Canyon. (A) Two-dimensional dipole-dipole resistivity model. (B) Profile of one-dimensional EM-60 electromagnetic soundings. (C) Comparison of parts (A) and (B). [XBL 804-7051]

Figure 3 is a cross section of interpreted EM soundings taken in an E-W profile over the Panther Canyon anomaly. Also shown is the independent two-dimensional dipole-dipole resistivity model (Beyer, 1977). Comparison reveals a remarkable correspondence between the two models as to depth and position of the conductive body. Both methods adequately resolve the boundaries and resistivity of the conductive body associated wtih the thermal anomaly and the configuration of resistive basement. The two methods, however, differ significantly in the manner of field deployment and data interpretation. The dipole-dipole survey required 80 field-crew days, whereas the EM-60 survey took less than 24. The dc resistivity data cover an area about 50% larger, but far more labor was required to achieve coverage comparable to that of the EM survey. Interpretation techniques for dipole-dipole data are so far better able to handle complex geology, and the data allow better resolution of resistive bedrock. However, because EM requires

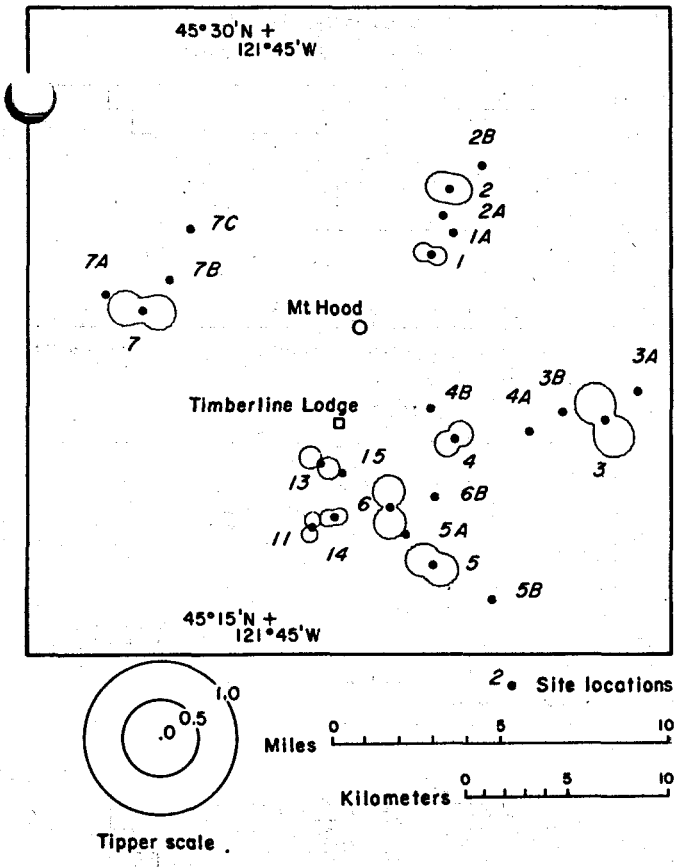

Figure 2. Band averaged from 1.0 to 0.1 Hz. [XBL 805-7056]

variations on the order of the dimensions of the survey. In the south-southeastern portion of the survey area, significant lateral variations in conductivity occur on a scale equal to the distance between measurement sites. In this example, the polar diagrams provided a useful qualitative tool to determine the dimensionality and scale of conductivity distributions from an insufficient data set available in a complex geologic environment.

REFERENCES CITED

Goldstein, N. E., and Mozley, E. C., 1978. A telluric-magnetotellurics survey at Mt. Hood, Oregon. Berkeley, Lawrence Berkeley Laboratory, LBL-7050.

Reddy, I. K., Rankin, D., and Phillips, R. J., 1977. Three-dimensional modeling in magnetotelluric and magnetic variational sounding. Geophys. J. Roy. Astr. Soc., v. 51, p. 313-325.

Thayer, R. E., 1975. Telluric-magnetotelluric investigations of regional geothermal processes in Iceland (Ph.D. dissertation). Providence, Rhode Island, Brown University, Dept. of Geological Sciences.

ELECTROMAGNETIC INDUCTION SOUNDING AT GEOTHERMAL PROSPECTS IN NEVADA

M. J. Wilt, M. Stark, N. E. Goldstein, and J. R. Haught

As part of a joint Department of Energy/Industry geothermal case studies program for the Northern Basin and Range province, Lawrence Berkeley Laboratory (LBL) has conducted controlled-source electromagnetic sounding surveys with its newly developed EM-60 system over three promising geothermal targets in northern Nevada. The objectives of these studies were to demonstrate to industry the feasibility and cost effectiveness of EM soundings and to better define the electrical structure for the purpose of reservoir delineation.

PROGRESS IN 1980

Three regions in north-central Nevada were chosen for study with the EM-60 system (Fig. 1). These are (1) Panther Canyon, an area in the southeastern portion of Grass Valley; (2) the Soda Lake thermal area, located near Fallon, Nevada; and (3) the McCoy geothermal region, located some 30 miles west of Austin in central Nevada. Significant findings from each survey are summarized below.

Panther Canyon

The Panther Canyon geothermal anomaly was first discovered by shallow heat-flow drilling and reconnaissance geophysics (Beyer, 1977; Sass et al., 1977). These studies outlined an oval-shaped 3-km^2 region of higher than normal heat flow associated with a region of low resistivity (Fig. 2). Subsequently, dipole-dipole resistivity data were taken for detailing purposes, and two-dimensional modeling of these results indicated an irregularly shaped conductive body associated with the thermal anomaly. To investigate this anomaly further and to test the EM method in a region of complex structure, the EM-60 system was utilized for a short survey over the thermal anomaly. The study consisted of three frequency-domain soundings from a single horizontal-loop transmitter using a 100-m-diameter loop (Wilt et al., 1980). Receivers were placed 0.5 to 1.5 km from the loop to permit a detailed look from the near surface to a maximum depth of 1.5 km.

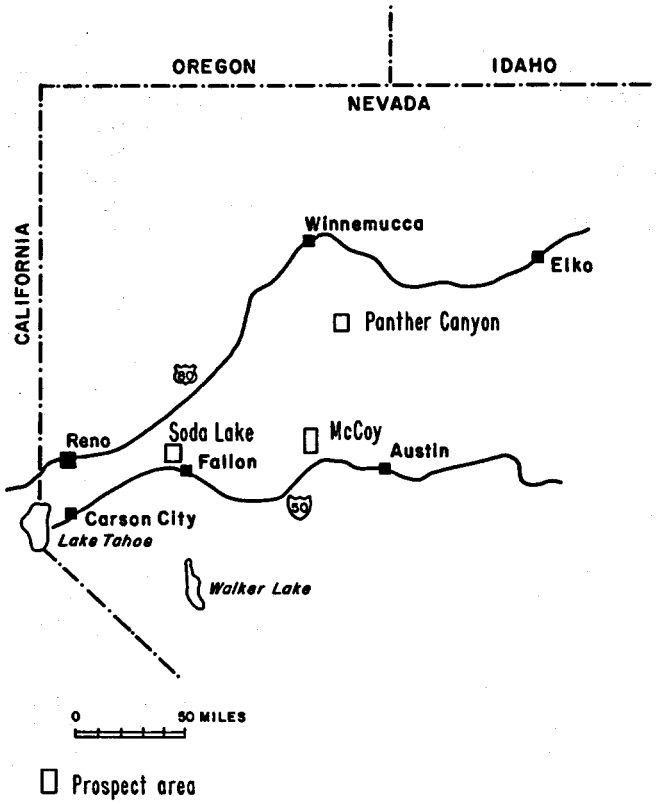

Figure 1. Prospect location map for the three EM-60 surveys conducted in 1979 by LBL. [XBL 802-6771]

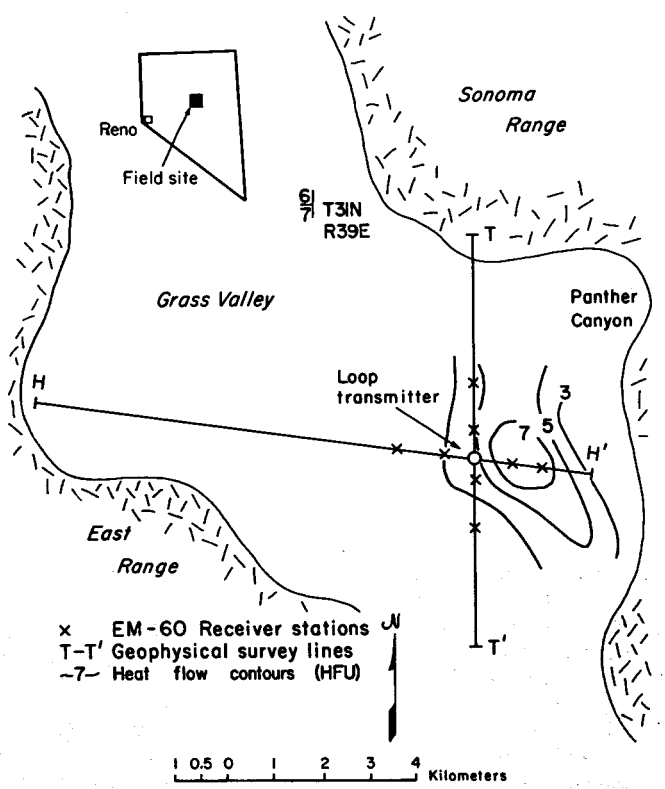

Figure 2. Survey location map of Panther Canyon area, Grass Valley, Nevada. [XBL 804-7050]

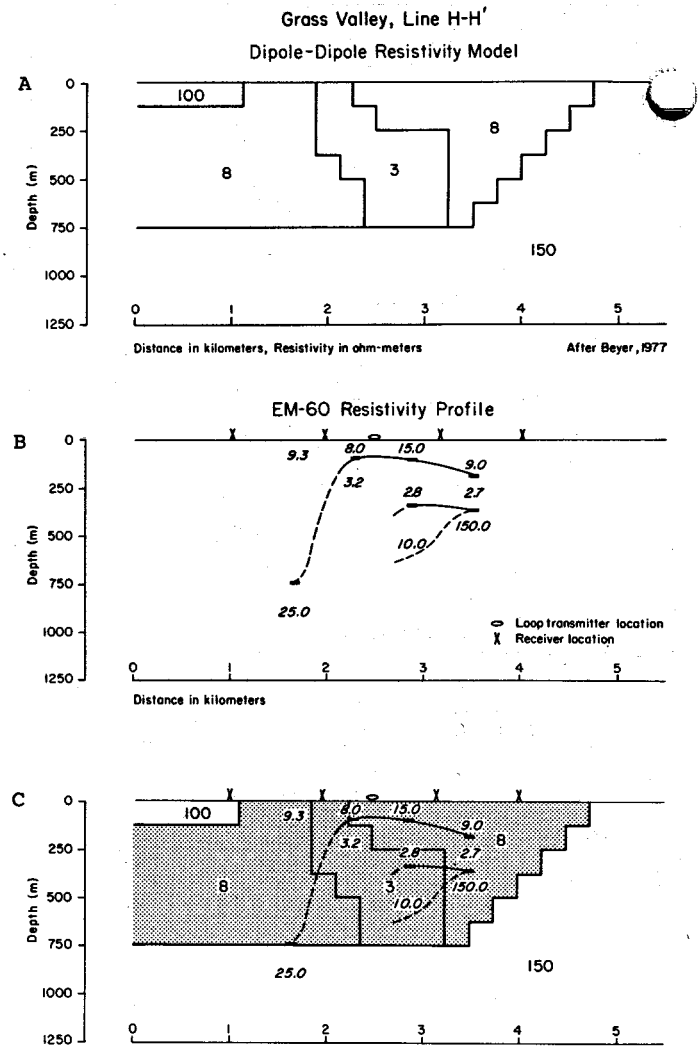

Figure 3. Resistivity cross section over line H-H' in Panther Canyon. (A) Two-dimensional dipole-dipole resistivity model. (B) Profile of one-dimensional EM-60 electromagnetic soundings. (C) Comparison of parts (A) and (B). [XBL 804-7051]

Figure 3 is a cross section of interpreted EM soundings taken in an E-W profile over the Panther Canyon anomaly. Also shown is the independent two-dimensional dipole-dipole resistivity model (Beyer, 1977). Comparison reveals a remarkable correspondence between the two models as to depth and position of the conductive body. Both methods adequately resolve the boundaries and resistivity of the conductive body associated wtih the thermal anomaly and the configuration of resistive basement. The two methods, however, differ significantly in the manner of field deployment and data interpretation. The dipole-dipole survey required 80 field-crew days, whereas the EM-60 survey took less than 24. The dc resistivity data cover an area about 50% larger, but far more labor was required to achieve coverage comparable to that of the EM survey. Interpretation techniques for dipole-dipole data are so far better able to handle complex geology, and the data allow better resolution of resistive bedrock. However, because EM requires

much shorter transmitter-receiver separations than dc resistivity electrode separations for the same depth of exploration, the effects of lateral inhomogeneities are expected to be less important for EM interpretations. The two cross sections suggest that even in regions of two- and three-dimensional geology, EM data will adequately resolve major features without severe distortion.

Soda Lakes

A 13-station EM-60 survey was performed at the Soda Lake thermal anomaly. The Soda Lake area is located at the southeastern margin of the Carson sink, a major drainage basin in central Nevada and much of the Pleistocene geology and near-surface hummocky topography are related to the recent withdrawal of Pleistocene Lake Lahonton (Garside and Schilling, 1979). A shallow source of hot water located 5 km north of Soda Lake (Fig. 4) was accidentally found during the drilling of water wells. Subsequent shallow and deep drilling have indicated that the shallow thermal regime is probably fault controlled, but the deep source of hot fluids is as yet unknown.

Dipole-dipole resistivity and MT sounding data were both acquired from Chevron Resources, Inc., holder of the geothermal leases. These data revealed four resistivity layers: (1) a 10-ohm-m surface layer 300 m or less in thickness, (2) a 2-ohm-m second layer extending to 1 or 1.5 km, (3) a more resistive third layer extending to at least 10 km, underlain by (4) a 1-ohm-m substrate. Deeper drilling indicated that the surface layer is dominated by sand-rich sediments, the second by shale and clays, and the third by volcanic and volcaniclastic formations. Highest temperatures were found in the second clay-rich horizon.

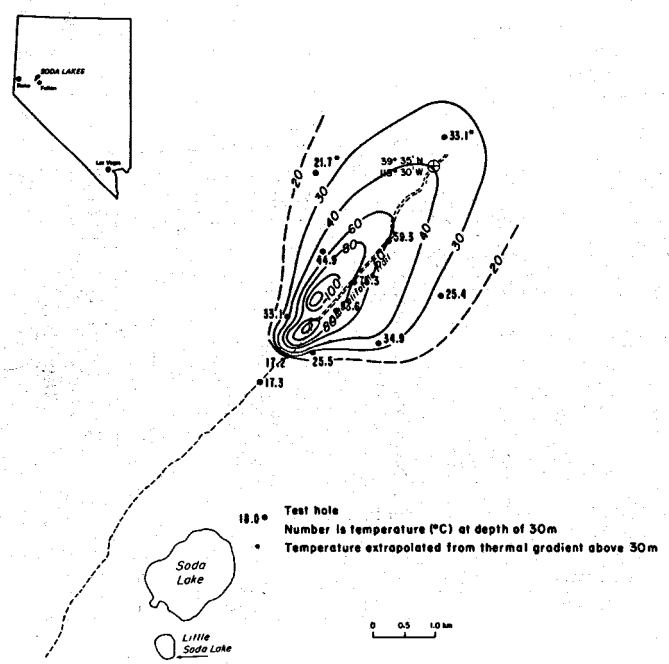

Figure 4. Location map and shallow temperature survey results. [XBL 804-7049]

Thirteen EM-60 soundings were measured over the Soda Lake area in a 6-day period in July 1979. Transmitter-receiver separations were extended to 3 km in an effort to map the surface of the lowermost resistive formation. For these deeper soundings, a noise-canceling scheme was used that subtracts geomagnetic noise signals from total magnetic fields in order to resolve transmitted signals at frequencies below 0.1 Hz (Wilt et al., 1979). This scheme proved particularly important, since lower-frequency information was critical for the resolution of the deeper horizons and the level of natural geomagnetic noise was particularly high (Stark et al, 1980). For those soundings, the lowest frequency that could be used in the presence of geomagnetic noise was reduced from 0.1 to 0.05 Hz.

Figure 5 is a composite profile of EM-60 layered-model inversions, layered models obtained from existing MT data and drillhole information. The figure indicates close agreement between MT and EM interpretations; the EM data gave the best definition of near-surface features, whereas the MT

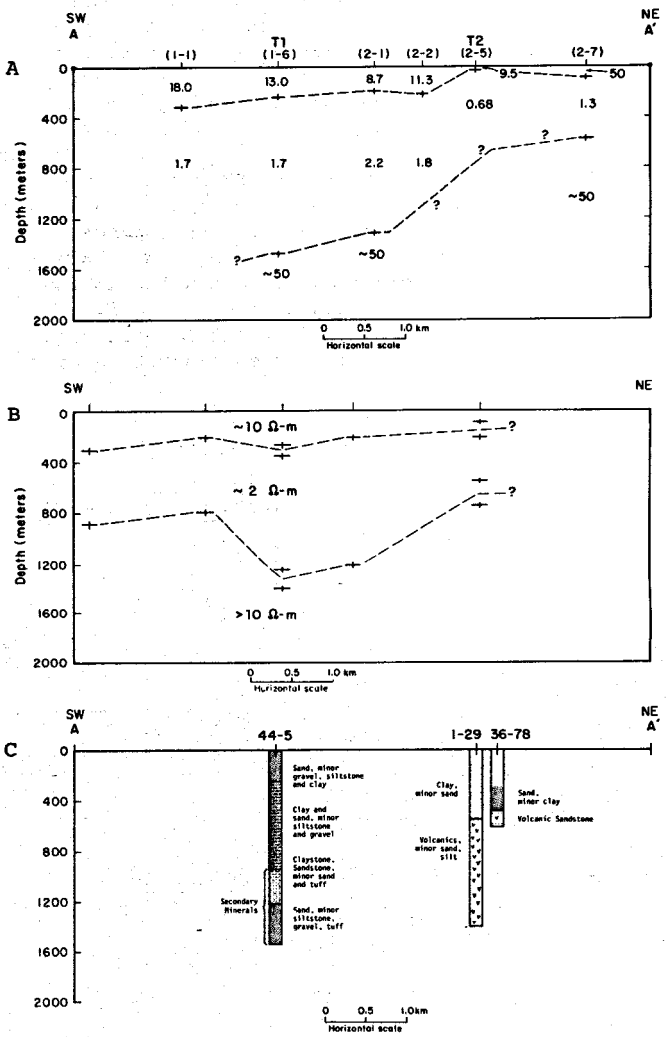

Figure 5. (A) Interpreted EM resistivity cross section, Line A-A'. (B) Interpreted MT resistivity cross section, Line A-A'. (C) Generalized lithologic logs for three wells along Line A-A'. [XBL 806-7204]

gave the best definition of deeper horizons. Both methods were able to detect the confining "basement" layer, located at depths of 1 to 2 km. EM-60 data indicate that the thermal anomaly is associated with a shallowing of the conductive second layer and a vertical offset in the resistive third layer. These offsets are associated with NW-SE faulting that allows hot fluids to rise and mix with the local shallow groundwater.

McCoy

The McCoy Geothermal area is located in a remote mountainous region of central Nevada. The terrain in this area provided new challenges to the system (Wilt et al., 1980). We soon learned that we would have to develop an interpretation scheme that would account for the elevation differences between transmitter and receiver and for the fact that the dipole moment could not be assumed to be vertical, as in flat terrain.

The temperature gradient anomaly map (Fig. 6) indicates an almost 200-km^2 area of higher than normal temperature gradients associated with the thermal anomaly. At the time of the survey, almost no other geophysical information was available. The EM-60 survey consisted of 19 soundings from three transmitters at separations ranging to 4 km.

The interpreted north-south EM resistivity profile shown in Figure 7 indicates that a shallow conductive body is associated with the southern thermal gradient maximum. Well logs from a 765-m drillhole indicate an influx of warm water in the depth interval corresponding to the conductive formation (Olson et al., 1979). The EM data also indicate the possibility of a deep conductive body

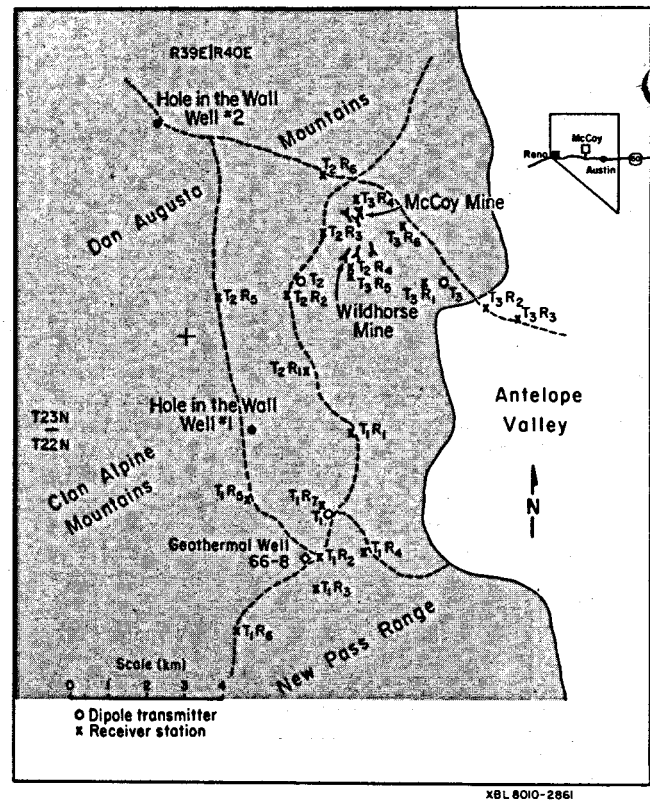

Figure 6. Survey location map of McCoy Prospect, Nevada. [XBL 8010-2861]

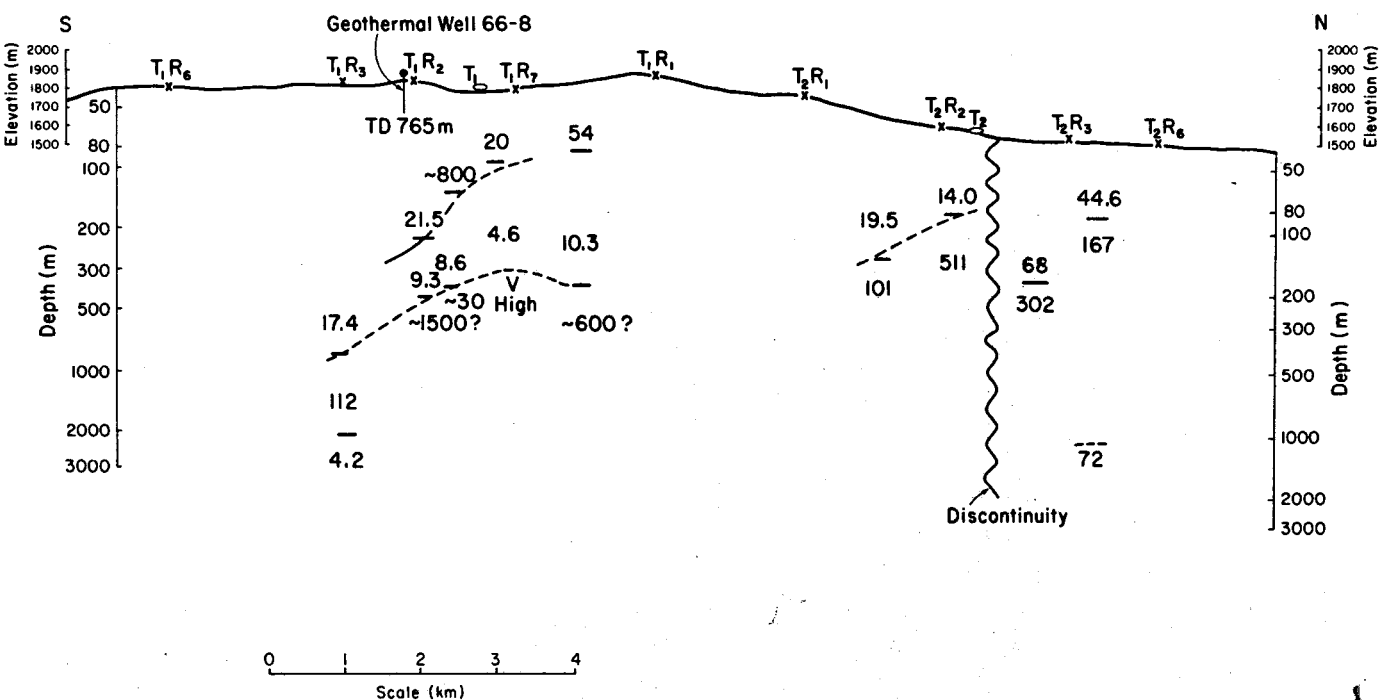

Figure 7. Profile of EM-60 layered-model inversions over the McCoy Prospect. [XBL 8010-2859]

at a depth of about 2 km associated with the southern heat-flow high. At the northern end of the profile, the section is considerably more resistive, with no conductive anomaly indicated at depth. The increase in resistivity can be correlated with the absence of surficial volcanics and a drop in elevation. At present the southern area appears more promising for future geothermal development.

CONCLUSIONS

For the three EM-60 surveys performed in Nevada, the method was found to be fast, efficient, and suitable for unusual field situations and rough terrain. High quality data and good depth of penetration were routinely obtained in Nevada. Shortcomings of the method include the insensitivity of measurements to resistive formations and the inadequacy of available interpretative software, which allows only one-dimensional modeling. Two-dimensional modeling on a routine basis may be feasible in the near future.

REFERENCES CITED

Beyer, J. H., 1977. Telluric and dc resistivity techniques applied to the geophysical investigation of basin and range geothermal systems, Part III: The analysis of data from Grass Valley, Nevada. Berkeley, Lawrence Berkeley Laboratory, LBL-6325, 115 p.

Garside, L. J., and Schilling, J. H., 1979. Thermal waters of Nevada. Nevada Bureau Mines and Geology, Bulletin 91.

Olson, H. J., Dellechaie, F., Pilkington, H.D., and Lange A., 1979. The McCoy geothermal prospect status report of a possible new discovery in Churchill and Lander Counties, Nevada. In Expanding the Geothermal Resources Council (Vol. 3), Transactions from Geothermal Resources Council, p. 515-519.

Sass, J. H., Siagos, J. P., Wollenberg, H. A., Munroe, R. J., DiSomma, D., and Lachenbruch, A. H., 1977. Application of heat flow techniques to geothermal energy exploration. Leach Hot Springs, Grass Valley, Nevada. Berkeley, Lawrence Berkeley Laboratory, LBL-6809. (USGS Open File Report in preparation.)

Stark, M., Wilt, M., Haught, J. R., and Goldstein, N. E., 1980. Controlled source electromagnetic survey at Soda Lakes geothermal area, Nevada. Berkeley, Lawrence Berkeley Laboratory, LBL-11221, 93p.

Wilt, M., Goldstein, N., and Haught, J. R., 1980. An electromagnetic EM-60 survey in Panther Canyon area, Grass Valley, Nevada. Berkeley, Lawrence Berkeley Laboratory, LBL-10993, 95p.

Wilt, M., Goldstein, N. E., Haught, J. R., and Stark, M., 1979. Controlled-source electromagnetic measurements at geothermal sites in Nevada. In Geothermal Energy Development, excerpt from Earth Sciences Division Annual Report 1979. Berkeley, Lawrence Berkeley Laboratory, LBL-11236, p. 11-15.

Wilt, M., Haught, J. R., and Goldstein, N. E., 1980. An electromagnetic survey at the McCoy geothermal prospect, Nevada. Berkeley, Lawrence Berkeley Laboratory, LBL-12012, 109 p.

AUTOMATED SEISMIC PROCESSOR

T. V. McEvilly, E. L. Majer, J. Bartschi, J. Heinsen, and R. O'Connell

The Automated Seismic Processor (ASP) was conceived and designed for rapid, cost-effective microearthquake monitoring and analysis in geothermal exploration. The impetus for the development of the ASP was the desire to simplify routine microearthquake data acquisition and reduction, and enhance the cost-effectiveness of such investigations. Processing data from a large number of events, as encountered in applying seismic techniques to geothermal exploration, was found to be time-consuming, labor-intensive, and thus far more expensive than desired (McEvilly et al., 1978, 1979), a situation which effectively eliminated state-of-the-art microearthquake surveys from the arsenal of geothermal exploration technology.

A two-channel prototype system was completed in the fall of 1978, and a 16-channel ASP was built the following year (Fig. 1). The ASP is a self-contained, micro processor-based (RCA 1802), parallel-processing computer. It is a low-power, 16-bit system, consuming about one watt per channel. Each data channel is monitored by a microcomputer (WORKER) which detects and times the P- and S-waves and does initial processing of the data. This processing includes calculation of amplitudes and a measure of quality for P- and S-waves, P-wave first motion, and S minus P (S - P) time. Each computer also windows the P- and S-waves, depending on the S - P time, and performs a Fast Fourier Transform (FFT) on the data. The spectra are then fit for D.C. level, corner frequency, and high-frequency slope. This information, collected by each WORKER detecting the event, is sent to a central microcomputer (the BOSS) for final processing.

The BOSS evaluates the incoming data on the basis of user-specified criteria for the minimum number of recording stations in a specified time window and on the basis of quality. If these criteria are not met, there is no further processing and the WORKERS are released to search for another

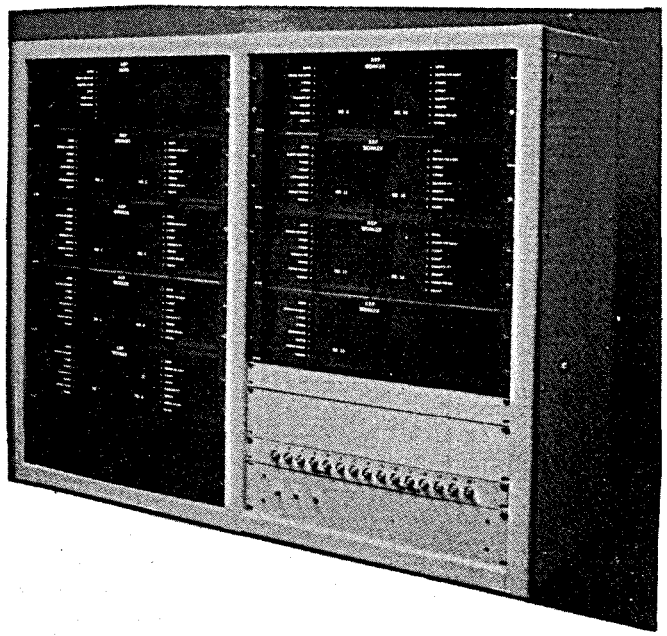

Figure 1. The ASP in field-ready condition. Total power consumption is less than 15 watts. Panels are standard 19 inch width. [CBB 803-3236]

event. If no event is detected, further processing continues according to pre-set instructions from the user. At present, the following operations can be performed in the BOSS (Fig. 2):

1. Debug. All data from WORKERS are printed out.

2. Event count. Lists the number of events from turn-on which have met occurrence criteria; number of events which have S - P times between 0-1 s, 1-2 s, 2-3 s, and > 3 s; average P and S amplitudes; and the station which received the first P-wave.

3, b-Values. Calculates and lists the cumulative and interval b-values using average P- and S-wave amplitudes.

4. Location. Calculates and prints the hypocenter coordinates, time, and residuals for each event. Also gives for each station, the distance to event, azimuth, take-off angle, P residual and S residual.

5. FFT raw data. Calculates and lists for each station the following parameters of the P- and S-waves: corner frequency, long-period level, and high-frequency roll-off slope.

6. FFT processed data. Calculates and lists for each station the moment, source radius, displacement, stress drop, and high-frequency slope using the corner frequency, long-period level, and high-frequency slope (Brunes' model).

7. Average value of FFT-processed data for P- and S-waves.

The first field test of the ASP was carried out at The Geysers geothermal field in northern California. During approximately 20 days of operation, over 550 events were processed. As this was the first actual field test of the system, our principal aim was to detect system software prob that could not be located in laboratory testing, rather than a comprehensive study of stress release in The Geysers production region. After comparing the results of the ASP with results obtained from the simultaneously tape recorded data, it was seen that the automatic detection and processing system was performing satisfactorily in all areas.

Future Activities

Our current plans are to conduct a detailed microearthquake survey at the Cerro Prieto geothermal field in the Salton Trough. A second ASP is being built which will be used for monitoring acoustic emissions at the Climax Stock nuclear waste repository at the Nevada Test Site (Majer et al., 1981).

We are also planning to make improvements in the ASP system. One problem is the loss of events during the time the computer is processing and printing results. If many stations record an event and full printing and processing is carried out, printout time via the thermal printer may be as long as 7 min. Moreover, because the floating-point arithmetic done by the RCA package is relatively slow, the total effective dead-time between events could be as long as 10 min, although in practice the dead-time rarely exceeds 2 to 3 min. To solve this problem a tape cassette recording system is being interfaced with ASP to cut the output time to less than 20 s. Also planned is the inclusion of an arithmetic processor chip to replace the software floating-point arithmetic package. With these two improvements, maximum dead-time between events will be reduced to less than one minute.

We also plan to interface the WORKER to a more powerful Boss computer--HP-85, 9835, or LSI-11 computer. This will allow more sophisticated processing, such as fault-plane solutions using moment-tensor analysis and frequency-wave number processing for noise studies. Also planned is a more advanced location program which will use a velocity-gradient model rather than the half-space model now being used.

REFERENCES CITED

Majer, E. L., McEvilly, T. V., and King, M. S., 1981. Monitoring an underground repository with modern seismological methods. Submitted to Int. J. Rock Mech. (in press).

McEvilly, T. V., Majer, E. L., Bartschi, J., and Heinsen, J., 1978. Geothermal seismic field system development, in Geothermal Exploration Technology Annual Report, Berkeley, Lawrence Berkeley Laboratory, LBL-8603.

McEvilly, T. V., Majer, E. L., Bartschi, J., Heinsen, J., and O'Connell, R., 1979. Automated seismic processor, in Geothermal Ener Development Annual Report. Berkeley, Lawrence Berkeley Laboratory, LBL-11236.

```
*****************
***** EVENT *****
*****************

DAY  HR  MIN  SEC
321  17   54   32

***** DEBUG PRINTOUT (RAW DATA)

P MESSAGE:
 WORKER        PT         PA         PQ
 +10000+01  +59492+05  +32524+04  +18000+02
 +20000+01  +59492+05  +17158+04  +38998+02
 +30000+01  +59492+05  +19558+04  +20000+02
 +40000+01  +59472+05  +38048+04  +16000+02

Q MESSAGE:
 WORKER        PP
 +10000+01  +19299+03
 +20000+01  -62000+02
 +30000+01  +68996+02
 +40000+01  +90000+01

F MESSAGE:
 WORKER       PSL        PF0        PLP        PEX        PGI        PGF
 +10000+01  +64000+02  +13000+02  +25412+05  -50000+01  +10000+01  +26410+05
 +20000+01  +64000+02  +24000+02  +27878+05  -70000+01  +20000+01  +11296+05
 +30000+01  +64000+02  +26000+02  +26760+05  -70000+01  +30000+01  +14844+05
 +40000+01  +64000+02  +28000+02  +28648+05  -50000+01  +20000+01  +32134+05

S MESSAGE:
 WORKER        ST         DT         SA         SQ
 +10000+01  +59736+05  +24398+03  +43544+04  +25000+02
 +20000+01  +59700+05  +21600+03  +29704+04  +66992+02
 +30000+01  +59700+05  +21298+03  +32294+04  +34000+02
 +40000+01  +59696+05  +22098+03  +39276+04  +16000+02

G MESSAGE:
 WORKER       SSL        SF0        SLP        SEX        SGI        SGF
 +10000+01  +12000+03  +34000+02  +17390+05  -40000+01  +30000+01  +15458+05
 +20000+01  +12000+03  +36000+02  +25746+05  -50000+01  +20000+01  +22690+05
 +30000+01  +12000+03  +36998+02  +25184+05  -50000+01  +30000+01  +28230+05
 +40000+01  +12000+03  +38998+02  +17664+05  -40000+01  +30000+01  +20266+05


***** EVENT COUNT
TOTAL EVENTS = +20000+01

   DTAV       PAAV       SAAV       PT1
 +22550+01  +26822+04  +36208+04  +40000+01

   NDT0       NDT1       NDT2       NDT3
 +14665-38  +14665-38  +20000+01  +14665-38


***** RUNNING B-VALUES

    NBT        BP        BPC        BS        BSC
 +20000+01  +50020+03  +50020+03  +64248+03  +64248+03


***** LOCATION ORIGIN DATA *****

   EVENT TIME      - DELTA
DAY  HR  MIN  SEC    (SEC)
321  17   54   32  -01.897

     X0         Y0         Z0      RMS(PRES)  RMS(SRES)
 +48132+01  +18786+01  +93776+01  +20091-00  +57307+00


STATION RESULTS
 STATION     HYPO RAD    AZIMUTH    IO ANGLE     P RES      S RES
 +10000+01  +10347+02  +34040+03  +25000+02  -20174-00  +00000+00
 +20000+01  +10049+02  +93624+02  +21072+02  -15228-00  +60057+00
 +30000+01  +10156+02  +11633+02  +22586+02  -16366-00  +54419+00
 +40000+01  +94544+01  +22952+03  +72920+01  -26335-00  +00000+00


***** POLARITY
 STATION    (+) UP/(-) DN
 +10000+01  +19299+03
 +20000+01  -62000+02
 +30000+01  +68996+02
 +40000+01  +90000+01


***** FFT P RAW DATA
 STATION     F0 (HZ)      LPL       GAMMA
 +10000+01  +10156+02  +99281+00  +18061+01
 +20000+01  +10748+02  +27220-00  +23446+01
 +30000+01  +20312+02  +26136-00  +34530+01
 +40000+01  +15624+02  +80671+00  +29806+01


***** FFT S RAW DATA
 STATION     F0 (HZ)      LPL       GAMMA
 +10000+01  +13200+02  +13580+01  +34718+01
 +20000+01  +14062+02  +10059+01  +26924+01
 +30000+01  +14452+02  +98382+00  +38616+01
 +40000+01  +15233+02  +13093+01  +36184+01


***** FFT P STATION DATA
 STATION      MOMENT      RADIUS     STR D      DISPL      GAMMA
            (DYNE*CM)     (CM)      (BARS)      (CM)
 +10000+01  +41940+21  +10332+05  +29702+02  +17664+01  +18061+01
 +20000+01  +11168+21  +99296+04  +49916+02  +16037+01  +23446+01
 +30000+01  +10816+21  +91664+04  +61568+02  +18259+01  +34530+01
 +40000+01  +31128+21  +11916+05  +80512+02  +31040+01  +29806+01


***** FFT S STATION DATA
 STATION      MOMENT      RADIUS     STR D      DISPL      GAMMA
            (DYNE*CM)     (CM)      (BARS)      (CM)
 +10000+01  +11680+21  +82464+04  +91144+02  +24318+01  +34718+01
 +20000+01  +83984+20  +77880+04  +77796+02  +19604+01  +26924+01
 +30000+01  +83824+20  +75776+04  +83488+02  +20468+01  +38616+01
 +40000+01  +10842+21  +71888+04  +12768+03  +29698+01  +36184+01


***** FFT P AVERAGE DATA
   PFNUM      MOMENT      RADIUS     STR D      DISPL      GAMMA
            (DYNE*CM)     (CM)      (BARS)      (CM)
 +40000+01  +23768+21  +12336+05  +55444+02  +20750+01  +26460+01


***** FFT S AVERAGE DATA
   SFNUM      MOMENT      RADIUS     STR D      DISPL      GAMMA
            (DYNE*CM)     (CM)      (BARS)      (CM)
 +40000+01  +90872+20  +77884+04  +95032+02  +23522+01  +34110+01

*
```

Figure 2. An example of printout received after each earthquake. PT = arrival time (in machine counts 100/sec) of P-wave; PA = P-wave amplitude, PQ = P-wave quality, i.e., (PA/LTA = PQ) where LTA = long-term average (4096 points) prior to trigger; PP = polarity of P-wave, + = up, - = down; magnitude of PP = quality of polarity estimate; PSL = P-wave spectral length; PFO = frequency value of corner frequency; PLP and PEX are mantissa and exponent of long period level; PGI and PGF are integer and fraction of frequency exponent for high frequency slope; ST = S-time; DT = S-P time; SA = S-wave amplitude; SQ = S-quality; SSL = S-wave spectral length; SFO, SLP, SEX, SGI, and SGF are the same as PFO, PLP, PEX, PGI, and PGF, except for S-wave. All other values are labeled and self-explanatory. This printout is for the DEBUG mode and lists the most complete output data set. [XBL 812-2644]

ADVANCES IN MAGNETOTELLURIC SURVEY TECHNIQUES AND DATA INTERPRETATION

W. M. Goubau, J. Clarke, and R. F. Miracky

Nine new magnetotelluric soundings have been made along a line south of the Cerro Prieto Power Plant. The new data define a southern boundary for the main steam production zone. The new data for apparent resistivities and the tipper are consistent with findings of the 1978 and 1979 surveys that suggested a zone of high resistivity near the power plant. To facilitate the interpretation of the data in terms of two-dimensional models, we developed a new method for determining a regional strike direction. The regional strike is about N 30° W (magnetic) which is roughly parallel to the Cucapa Mountains to the west and the Imperial Valley fault to the east.

PROGRESS IN FISCAL 1980

Figure 1 shows the sites of the magnetotelluric soundings performed in 1978, 1979, and 1980. They form roughly four lines: DD', EE', FF', and GG'. The soundings were all performed with the remote reference technique (Goubau, et al., 1978; Gamble, 1978; Gamble et al., 1979a, b, c, d, 1980), using dc SQUID magnetometers. Data were acquired over the frequency range 10^{-3} Hz to 40 Hz. For frequencies above 10^{-2} Hz the data were processed in the field with our DEC LSI-11 computer (Clarke et al., 1979). The long-period information was stored digitally on a Gould data logger operating at a sampling rate of 1 Hz. These data were subsequently processed by the LSI-11 at the end of the survey.

To present the results of a survey as clearly as possible, one must define a coordinate system that obviates as much as possible any lateral symmetry in the conductivity profiles. In the past we have simply oriented our coordinate axes so that one axis is parallel to a major fault or mountain range. However, this is not always a reliable estimate of the subsurface symmetry. This year we developed a new method for determining a regional strike direction that is based on data obtained at a number of locations. The method works as follows. If the conductivity has two-dimensional symmetry, one can rotate the coordinate system into an orientation for which the diagonal elements of the impedance tensor, Z_{xx} and Z_{yy}, are identically zero. Operationally, this is done by finding the angle that minimizes $|Z_{xx}|^2 + |Z_{yy}|^2$, or equivalently, maximizes $|Z_{xy}|^2 + |Z_{yx}|^2$. The rotation angle is (ideally) independent of frequency. If the impedance tensor $\underline{\underline{Z}}$ is affected by noise and/or the influence of three-dimensional conductivity structures, the values of Z_{xx} and Z_{yy} will not be zero in the rotated coordinates, and the rotation angle will, in general, depend on frequency. Thus, an estimate of the strike direction from a single station and a single frequency may not be meaningful. To minimize the influence of local three-dimensional structure on the determination of the strike, we incorporate the results of a number of stations within the region of interest and the information at all frequencies by finding the angle that minimizes

$$B(\theta) = \sum_i \left[|Z_{xx_i}|^2 + |Z_{yy_i}|^2 \right] W_i , \qquad (1)$$

where the summation is over all frequencies and stations, and W_i is a function that weights the statistical significance of each term. The weighting function has the form $W_i = f(t)/\sigma_i$, where σ_i is the variance in the estimate of $|Z_{xx_i}|^2 + |Z_{yy_i}|^2$ associated with random errors, and $f(t)$ is an adjustable function of the period t that scales roughly with skin depth. In practice, the choice of f(t) has little influence on the computed rotation angles, as we will demonstrate below. The rotation angle, θ_z, determined from the impedances, is given by

$$\theta_z = \frac{1}{4} \tan^{-1} \left\{ \frac{2 \sum_i \text{Real}\,(Z_{xy_i} + Z_{yx_i})(Z^*_{yy_i} - Z^*_{xx_i})\, W_i}{\sum_i \left[\left(|Z_{xy_i}| + |Z_{yx_i}| \right)^2 - \left(|Z_{yy_i}|^2 - |Z_{xx_i}| \right)^2 \right] W_i} \right\} . \qquad (2)$$

To test the validity of regional strike estimated from equation (2) we make an independent estimate of the strike using the tipper $\bar{T}$, which we can express as the relationship between vertical and horizontal magnetic fields:

$$H_z = T_x H_x + T_y H_y .$$

The orientation of the regional strike for the tipper is the angle that minimizes:

$$A(\theta) = \sum_i W_i |T_{x_i}(\theta)|^2 .$$

The angle is given by

$$\theta_T = \frac{1}{2} \tan^{-1} \left\{ \frac{\sum_i 2\,\text{Real}\,(T_{x_i} T^*_{y_i})\, W_i}{\sum_i \left(|T_{x_i}|^2 - |T_{y_i}|^2 \right) W_i} \right\} . \qquad (3)$$

We investigated the stability of our regional magnetotelluric strike determination by comparing the orientations found with different functions of the period as weights and by comparing results obtained at the stations on different lines. We calculated the regional strike for the stations on line DD' with four different weighting functions:

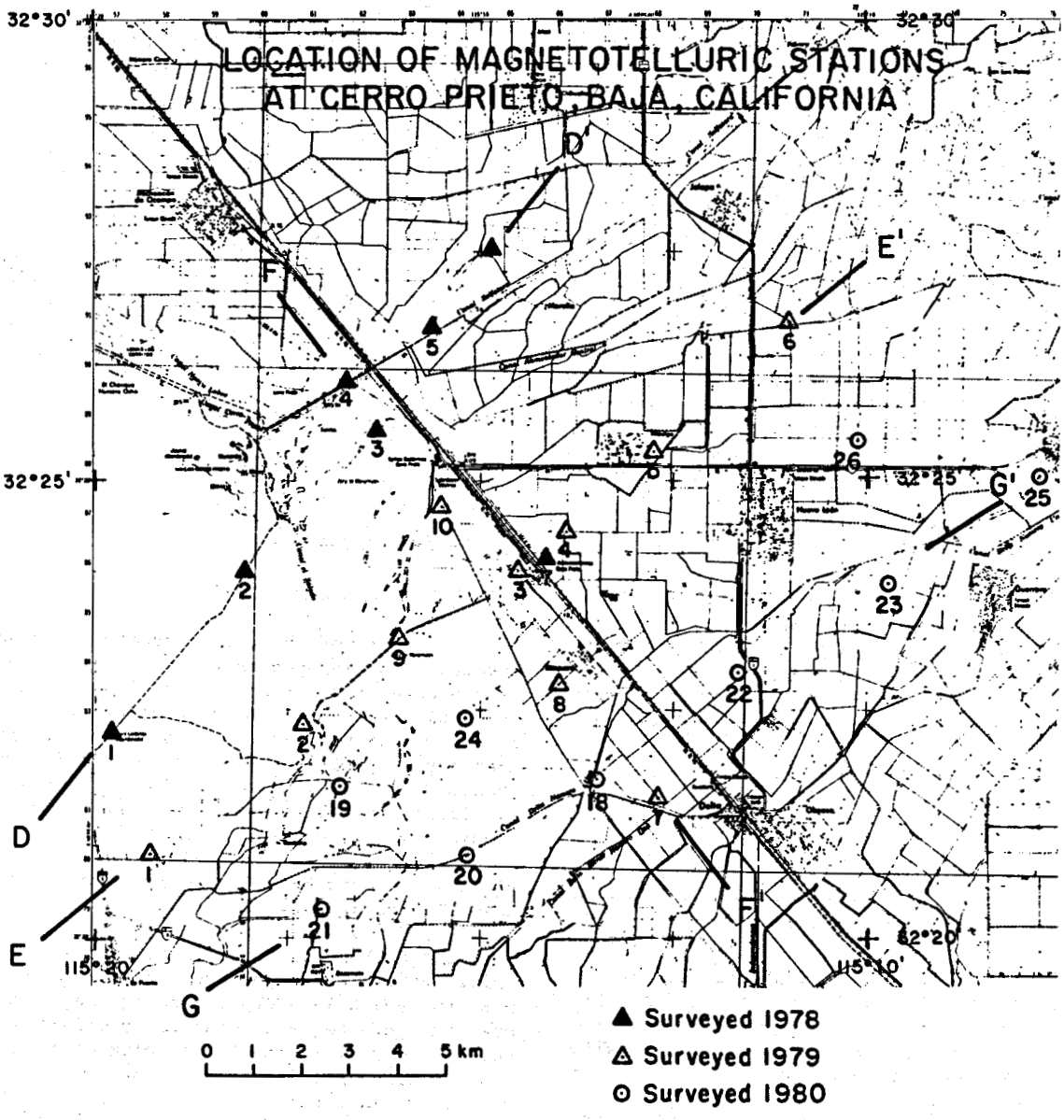

Figure 1. Location of magnetotelluric stations at Cerro Prieto, Baja, California. [XBL 799-11498]

$f(t) = 1$, $t^{1/2}$, t, and $t^{3/2}$. The strike determinations from $\underset{\approx}{Z}$ and $\vec{T}$ with these weights are given in Table 1. They are remarkably consistent. Despite the fact that the relative weights of the long and short periods are varied by more than 10^6, the variation in the tipper estimate of strike varies by only ± 0.4° while the impedance strike varies by ± 2.3°. The mean disagreement between the impedance and tipper strikes is 1.4°. This is comparable to the uncertainty in the orientation of the telluric lines.

This agreement between the $\underset{\approx}{Z}$ and $\vec{T}$ determinations of strike indicates that the structure along DD' might be well matched by a two-dimensional model.

Table 1. Regional strike on line DD' estimated with different weighting functions.

Function of period	Strike from Z	Strike from T
t^0	-32.3°	-30.6°
$t^{1/2}$	-30.0°	-30.1°
t	-28.4°	-29.8°
$t^{3/2}$	-27.8°	-30.2°

However, to ensure that a two-dimensional model is appropriate, one must confirm that the component of $\vec{T}$ in the strike direction and the diagonal components of $\tilde{Z}$ are small in the coordinate system aligned with the regional strike. This is the case for line DD', along which the magnitudes and phases of the off-diagonal components of $\tilde{Z}$ and the magnitude and phase of T_y have been closely matched by a two-dimensional model (Gamble et al., 1980).

A two-dimensional model is not appropriate for the other two lines. Table 2 lists the strike determined along the three lines with the same weighting function f(t) = t. On line EE' the $\tilde{Z}$ and $\vec{T}$ strikes disagree by more than 10° and on FF', by 3.2°. While this may not seem to be a significant discrepancy, it is larger than any of the discrepancies on line DD' for any weight in Table 1. Thus, we feel that any discrepancy between the strikes, as determined from $\tilde{Z}$ and $\vec{T}$ and which is unambiguously larger than the location of the telluric lines, would indicate that a two-dimensional model of the earth will be insufficient.

Table 2. Regional strikes on different lines with f(t) = t.

Line	Z strike	T strike
DD'	-28.4°	-29.8°
EE'	-27.9°	-17.3°
FF'	-25.5°	-22.3°

On the other hand, we see that the regional strike as determined from $\tilde{Z}$ is essentially identical on all three lines: -27.0° ± 1.5°. All of the regional strikes determined from the impedance with the different weights and station locations fall in the range 28.9° ± 3.4°. This confirms both our impression that there is a relatively well-defined regional strike in the Cerro Prieto area and our assertion that a stable regional strike can be determined by a regional calculation based on the measured values of $\tilde{Z}$, even though there are significant deviations from a two-dimensional structure.

Figures 2 and 3 show contour maps of T_x and T_y at 1 Hz, where the axes have been rotated to conform to the regional strike of N 30° W (magnetic). T_x (Fig. 2) is the tipper magnitude where the magnetic field (H_x) is aligned parallel to regional strike. If the region were strictly two-dimensional, T_x would be small (approach zero) everywhere. Its deviation from values < 0.1 clearly indicates a three-dimensional structure. A pronounced effect occurs close to the power plant (Station 3, 1979). There is also the suggestion that a northeast-trending structure occurs between lines E and G. T_y (Fig. 3) is the tipper magnitude where the magnetic field (H_y) is aligned perpendicular to regional strike. If the region were strictly two-dimensional, contours of T_y would run parallel to regional strike, which they do by and large. However, it is clear that a three-dimensional structure is present.

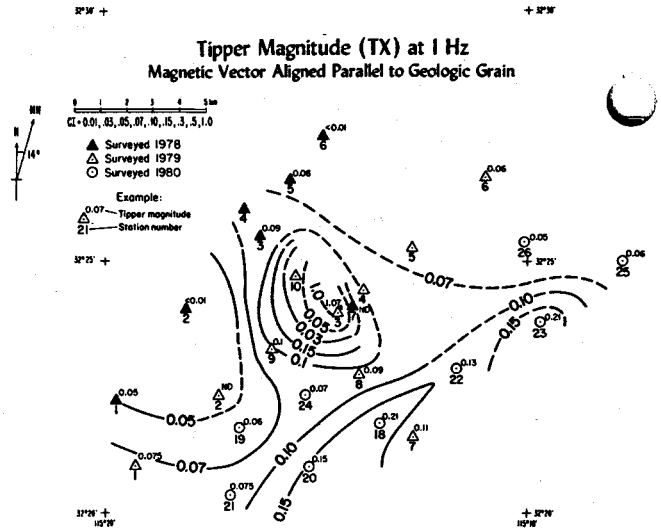

Figure 2. Tipper T_x. [XBL-7910-13038A]

PROPOSED RESEARCH FOR 1981

The state-of-the-art of remote reference magnetotellurics is such that random errors inherent in the data acquisition are now much smaller than uncertainties in the interpretation of the measurements. Thus, we plan to investigate new schemes that may simplify the solution of the inverse problem. In particular, we wish to investigate the possibility of using measurements of magnetic field gradients, together with magnetotellurics, to get a more direct determination of the derivatives of the electric and magnetic fields that enter into Maxwell's equations.

The SQUID magnetometers have worked quite reliably. However, the great progress made over the past two years in SQUID technology may improve the slew rate of the magnetometers by orders of magnitude and may eliminate the problem of flux jumps that at times still exist with our current systems. We plan to investigate the possibility of incorporating such new SQUIDS into our MT system.

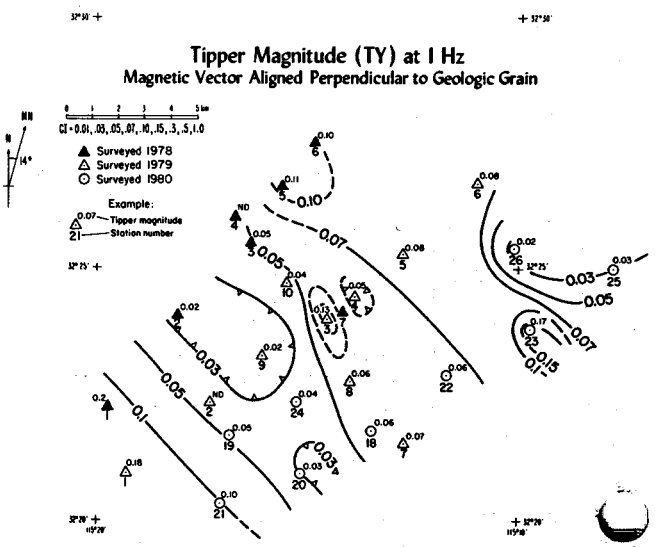

Figure 3. Tipper T_y. [XBL-7910-13039A]

REFERENCES CITED

Clarke, J., Gamble, T. D., Goubau, W. M., Koch, R., and Miracky, R., 1979. Field processing of magnetotelluric data. In Earth Sciences Division Annual Report 1979. Berkeley, Lawrence Berkeley Laboratory, LBL-10686.

Gamble, T. D., 1978. Remote reference magnetotellurics with SQUID (Ph.D. dissertation). Berkeley, University of California. Lawrence Berkeley Laboratory, LBL-8062.

Gamble, T. D., Goubau, W. M., Goldstein, N. E., and Clarke, J., 1979a. Referenced magnetotellurics at Cerro Prieto. In Proc. First Symp. on the Cerro Prieto Geothermal Field, Baja California, Mexico, September 1978, Berkeley, Lawrence Berkeley Laboratory, LBL-7098.

_____, 1979b. Magnetotelluric survey at Cerro Prieto. In Earth Sciences Division Annual Report 1978. Berkeley, Lawrence Berkeley Laboratory, LBL-8648, p. 41-42.

Gamble, T. D., Goubau, W. M., and Clarke, J., 1979c. Magnetotellurics with a remote magnetic reference. Geophysics, v. 44, no. 1, p. 53-68.

_____, 1979d. Error analysis for remote reference magnetotellurics. Geophysics, v. 44, no. 5, p. 959-968.

Gamble, T. D., Goubau, W. M., Goldstein, N. E., Miracky, R., Stark, M., and Clarke, J., 1980. Magnetotelluric studies at Cerro Prieto. In Proc., Second Symp. on the Cerro Prieto Geothermal Field, Baja California, Mexico, October 1979. Mexicali, Comision Federal de Electricidad.

Goubau, W. M., Gamble, T. D., and Clarke, J., 1978. Magnetotelluric data analysis: Removal of bias. Geophysics, v. 43, no. 6, p. 1157-1166.

RESERVOIR ENGINEERING

ADVANCES IN RESERVOIR MODELING

Overview

K. Pruess

Geothermal reservoirs are very complex systems. In the process of exploration and field development, large amounts of data are assembled. These data provide information on rock formations, geometry of the system, composition and thermodynamic state of the fluids, and other important characteristics. In order to develop a geothermal reservoir in a rational way, it is necessary to construct a "model" which integrates all the diverse pieces of information into a unified picture. A model is basically a simplified mental analog of a complex system which makes the system and its behavior readily accessible to the human mind. Besides containing a description of the system (the data base), a model also includes assumptions about the important physical and chemical processes which occur in the natural state or during exploitation. Quantitative (numerical) models can help to answer some of the basic reservoir engineering questions such as: What are the reserves of fluid and heat? What level of power production can a reservoir support? How long will it last? What is the optimal way of producing a reservoir?

In fiscal 1980 a major effort was made to improve existing modeling capabilities and to encourage industry to apply the numerical models developed at Lawrence Berkeley Laboratory (LBL). Over 50 participants from research laboratories and private companies attended a workshop at LBL which was designed to instruct in the use and application of several numerical reservoir simulation models developed at LBL. These models are applicable to a broad range of reservoir simulation and well-test problems in geothermal reservoirs and aquifers. They are now being distributed to the engineering community by the National Energy Software Center in Argonne, Illinois. LBL advised the Department of Energy on design and implementation of a project for comparison and validation of geothermal reservoir simulators. This effort was undertaken to improve acceptance and application of this powerful methodology throughout the industry.

Various applications of numerical simulation were made, among them a major field case study for the vapor-dominated geothermal reservoir at Serrazzano, Italy. This work demonstrated for the first time the feasibility of detailed field-wide performance simulation and history matching. Besides representing actual field situations, modeling can also be used as a "laboratory" for exploring physical mechanisms operating in different types of geothermal reservoirs. An example of this kind of study is reported below for a reservoir of the East Mesa type.

Work continued to enhance the scope of our models and to make them more realistic and applicable to "real world" situations. Of particular importance in this regard is the ongoing development of equation-of-state packages for compositional systems in which the fluid consists of a mixture of water and various noncondensible gases. A computer model for the system water/CO_2 is nearing completion.

The following contributions illustrate accomplishments in reservoir modeling. They focus on the main areas of work and are not intended to be

exhaustive. A more complete account of advances in reservoir modeling in fiscal 1980 is contained in the references at the end of this annual report.

Performance matching and prediction for the Serrazzano geothermal reservoir by means of numerical simulation

K. Pruess, O. Weres, and R. Schroeder

Experience in the petroleum industry has shown that detailed, quantitative reservoir models can aid in developing more efficient production schemes. Computer models of oil and gas reservoirs, usually referred to as "numerical simulators," have gained widespread acceptance and application in the industry during the past decade.

It is believed that similar techniques could greatly enhance our understanding of geothermal reservoirs and thereby contribute to improved reservoir management. The recovery of geothermal energy is inherently more complex than the production of oil and gas. Whereas oil and gas are saleable commodities, geothermal fluids are not. They merely serve to transport subterranean heat to the ground surface, most of which was stored in permeable rock masses. The objective of geothermal production is to recover that heat in the most efficient way.

In the past, geothermal reservoir simulation has been applied mostly to well tests, hypothetical model problems, and idealized (one- or two-dimensional) models of actual reservoirs. The only study of a realistic three-dimensional reservoir model was carried out by Morris and Campbell (1979) for the liquid-dominated East Mesa KGRA, which is currently being developed for production. No detailed realistic simulation has ever been made for a producing vapor-dominated system.

The primary objective of the Serrazzano study was to demonstrate the feasibility of a detailed numerical simulation of a geologically accurate geothermal reservoir model. Serrazzano was chosen as a case study for developing and evaluating the methodology for two reasons: (1) detailed production data and much geological and hydrological information is available for the reservoir, and (2) for environmental reasons surface disposal of produced brines is no longer acceptable in Italy, and numerical studies are needed to aid in developing an appropriate injection program.

THE SIMULATOR SHAFT79

The numerical simulations were carried out with a computer program called SHAFT79. This program computes fluid and heat flow in a porous medium, including vaporization and condensation phenomena, using state-of-the-art mathematical and numerical techniques. SHAFT79 was developed at LBL as a flexible tool for geothermal reservoir engineering. The source code is publicly available from the National Energy Software Center*, and a detailed manual was written to assist interested users (Pruess and Schroeder, 1980).

THE RESERVOIR MODEL

Serrazzano geothermal reservoir is one of the distinct zones of the extensive geothermal areas near Larderello in Central Tuscany, Italy. Natural manifestations and utilization of steam and hot water from shallow holes in this region have occurred for centuries. Deep drilling was begun after 1930, and since 1939 electric power has been generated at Serrazzano from geothermal steam. Present electric power output at Serrazzano is approximately 40 MWe.

Our initial attempts at modeling the natural pre-exploitation state of the reservoir were abandoned when it became apparent that the almost complete lack of data would leave us with a multitude of rather meaningless parameter choices. Subsequently, an effort was made to model the period from 1959 to 1975, for which a much better definition of thermodynamic conditions in the reservoir is available.

The model of Serrazzano reservoir is based on field measurements of temperatures and pressures, laboratory data for core samples, and available geological and hydrological information. The reservoir is represented by a fully three-dimensional, geologically accurate model and production from 19 wells for a 15.5-year period from 1959 to 1975 has been simulated in detail. By means of appropriate parameter adjustments, chiefly with respect to permeability and pore water distribution, it was possible to obtain reasonable agreement between simulated and observed reservoir performance. Details of the trial-and-error simulation procedure and the resulting reservoir model are given in Pruess et al. (1980a, b).

In brief, the reservoir has a steam cap overlying a boiling aquifer. The steam cap is centered in region I (Fig. 1), which contains a pronounced structural high and most of the older wells. The pore water is confined to the margins (regions III and VI, Fig. 1), and is immobile because of the low liquid saturation. As the reservoir is produced, the water boils in place to provide the steam flowing to the wells. The boiling occurs rather uniformly throughout the two-phase regions. Simulated results are extremely sensitive to the permeability distribution. Table 1 shows the permeabilities for the various reservoir regions as determined in the simulation. Figure 2 compares observed reservoir pressures for January 1975 with those obtained after 15.5 years of simulation. There is good agreement in overall patterns, but in quantitative terms simulated pressures decline somewhat less rapidly than field pressures. Pressure response and permeability distribution determined from the simulation provide evidence that some steam reaches the main well field through fractures from depth.

Additional simulations were carried out to examine whether the somewhat more rapid pressure decline in the field could be a consequence of delayed thermal equilibration between rock masses of low permeability and localized permeable regions,

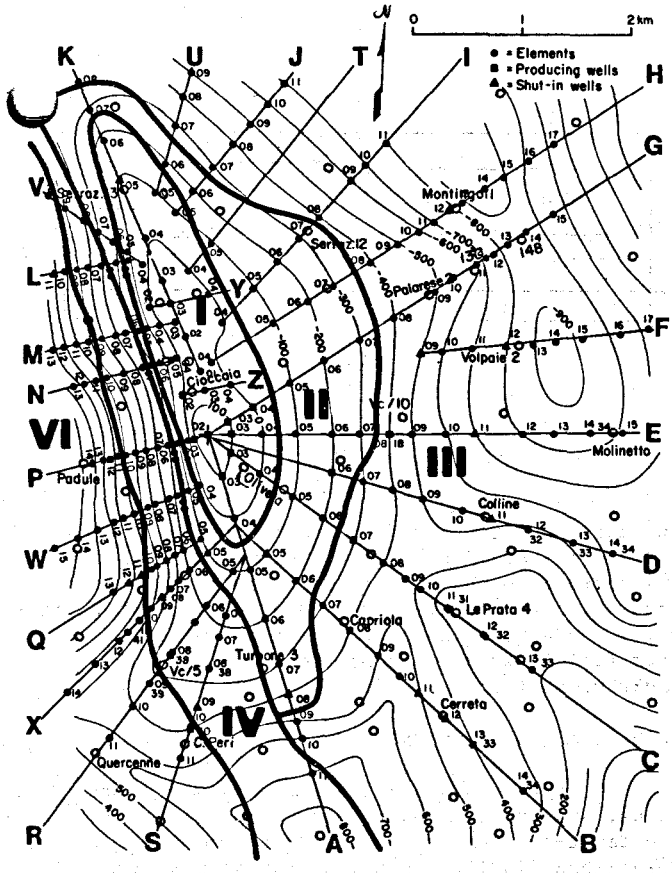

Figure 1. Areal map of Serrazzano geothermal reservoir. Light contours show caprock elevations; heavy contours show boundaries of zones with different permeabilities. Straight lines are geological cross sections for construction of computational grid. [XBL 797-7591B]

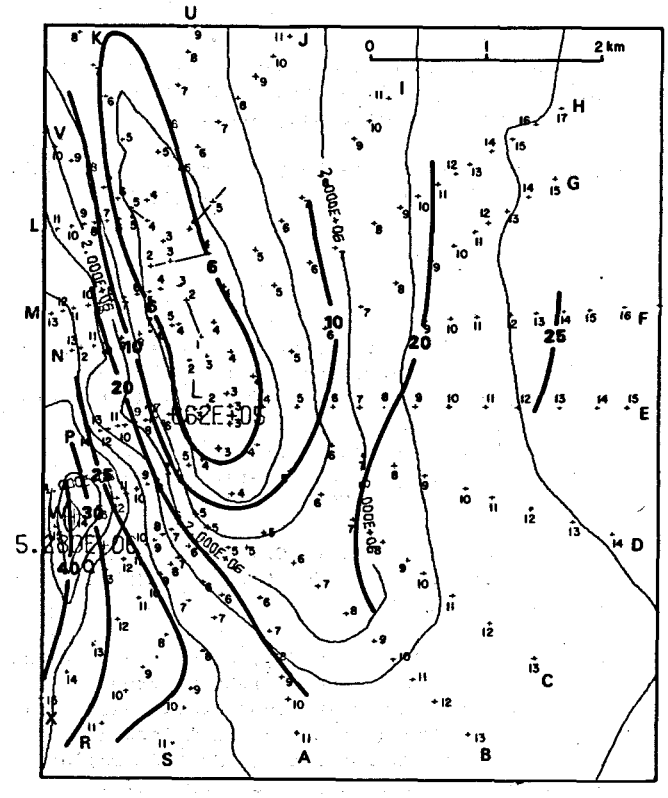

Figure 2. Pressure distribution for January 1975. The thick contours are based on field observations (units: bars), whereas the thin contours are simulated results (units: Pascals). The simulated results refer to the lowest layer of the reservoir model. Simulated vertical pressure variations are small ≈ 1 bar). Pressure increments between contour lines are 5 x 10^5 Pascals = 5 bars. [XBL 807-1401B]

Table 1. Permeability distribution zones as defined in Figure 1; zone V is a deep boiling aquifer underlying the reservoir.

Zone	Permeability (milliDarcy)
I	4000
II	90
III	85
IV	25
V	85
VI	40

where boiling causes a decline of temperatures and pressures. It was found that a typical length of impermeable regions of 100-200 m, corresponding to volumes of 1-8 x 10^6 m^3, would generate the additional temperature and pressure decline needed to make simulated results agree quantitatively with field observations. Impermeable regions of this size are compatible with geological evidence and with the fact that of 37 wells drilled in Serrazzano only 19 are productive.

The model of Serrazzano reservoir as developed in the simulation, was also used to forecast production on a well-by-well basis through 1990 and to assess effects of injecting spent condensate. We predict an overall decline in production rate of 22% from 1975 to 1990. Injection effects are predicted to be negligible because of the small amount of available condensate.

CONCLUSIONS

The modeling work has demonstrated the feasibility of field-wide distributed parameter simulations of vapor-dominated geothermal reservoirs in geologically accurate geometry. The simulation results in a self-consistent reservoir model which integrates much of the field data and provides a reasonable match of the observed field performance. Production forecasting and analysis of injection effects has also been demonstrated.

The methodology developed in this study can be applied to other two-phase reservoirs, and should prove valuable in the design of production/injection schemes for enhanced energy recovery.

ACKNOWLEDGEMENTS

We thank our Italian colleagues G. Neri and R. Marconcini for providing field data and suggestions during the course of this study.

* National Energy Software Center, Argonne National Laboratory, 9700 South Cass Avenue, Argonne, Illinois 60439.

REFERENCES CITED

Morris, C. W., and Campbell, D. A., 1979. Geothermal reservoir energy recovery: A three-dimensional simulation study of the East Mesa field. Presented at the 54th Annual Fall Technical Conference and Exhibition of the Society of Petroleum Engineers, Las Vegas, Nevada, September 1979. SPE-8229.

Pruess, K., and Schroeder, R. C., 1980. Shaft79 user's manual. Berkeley, Lawrence Berkeley Laboratory, LBL-10861.

Pruess, K., Weres, O., Schroeder, R. C., Marconcini, R., and Neri, G., 1980a. History match simulation of Serrazzano geothermal reservoir. Presented at the 55th Annual Fall Technical Conference and Exhibition of the SPE, Dallas, Texas, September 21-24, 1980. SPE-9276. LBL-10657.

____, 1980b. Performance matching and prediction for Serrazzano geothermal reservoir by means of numerical simulation. Paper presented at Second DOE/ENEL Workshop for Cooperative Research in Geothermal Energy, Berkeley, California, October 20-24, 1980. Berkeley, Lawrence Berkeley Laboratory, LBL-11555

Heat and mass transfer in a fault-controlled geothermal reservoir charged at constant pressure

K. P. Goyal and T. N. Narasimhan

Studies of liquid-dominated geothermal systems such as Wairakei (Grindley, 1965), Broadlands (Grindley, 1970), Long Valley (Rinehart and Ross, 1964), Imperial Valley (Elders et al., 1972), Cerro Prieto (Puente and de la Pena, 1978), and Ahuachapan (Ward and Jacobs, 1971) suggest that geothermal anomalies are intimately associated with a specific pattern of faulting. For example, at East Mesa in the Imperial Valley of California, the Mesa fault is believed to act as a conduit for the hot fluids rising up from depth (Combs and Hadley, 1977). Bailey (1977) has hypothesized that the East Mesa geothermal reservoir is recharged by hot waters from the fault at the intersection with an aquifer of sufficient horizontal permeability. The two-dimensional conceptual model of such a system is shown in Figure 1. The fault is considered to be a vertically oriented region of highly fractured material with finite width $2y_e'$. (Dimensional variables are denoted by a prime, and nondimensional variables without a prime.) It extends downward

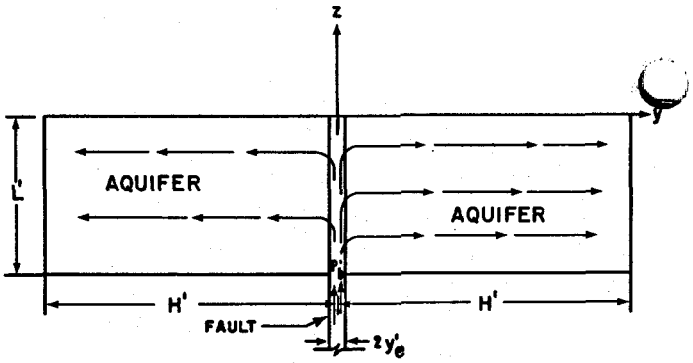

Figure 1. Conceptual model of a liquid-dominated geothermal reservoir. [XBL 7812-2200A]

through the interbedded sediments of the reservoir for a distance of L' into the basement rock. At the surface, both the reservoir and the fault are assumed to be overlain by a thin, impermeable, thermally conducting caprock. The depth of the reservoir (L') is assumed to be much larger than the fault width ($2y_e'$).

RESULTS AND DISCUSSIONS

The governing equations, the boundary conditions, and the related results from the study of the fault-aquifer system are discussed in Goyal and Narasimhan (1981). It may be noted from Figure 1 that three scales of physical length are used to define the system: semifault width (y_e'); reservoir depth (L'); and reservoir width (H'). Thus the temperature field can be obtained for regions very close to the fault, near the fault, and far from the fault (Goyal and Narasimhan, 1981). In this summary, however, we shall confine ourselves to the discussion of some of the more important results.

Table 1 shows the range of various nondimensional parameters used in this study. The meaning and the physical significance of each of these parameters are described in detail in Goyal and Narasimhan (1981). Parameter d, listed in the first column, defines the location of the far-field boundary or, alternatively, the half-width of the aquifer, H', and is equal to d/y_e times the depth of the reservoir, L'. The value of d is obtained by integrating the parabolic energy equation in the aquifer until the solution at the far edge is within 0.5% of the real condition. This approximation provides an engineering estimate of the boundary location. At this point the convection of energy in the y'-direction is very small compared to vertical conduction. The nondimensional parameter, P_b, is the ratio of the actual pressure specified at the fault inlet in excess of the hydrostatic pressure to the reference convection pressure. The Rayleigh number, R, listed in the third column, is the ratio of heat transfer due to convection to that due to conduction under reference conditions. Large values of R suggest that the heat transfer due to convection is far greater than that due to conduction. In this regard, one may expect that fluid particles moving through the system will tend to behave isothermally unless affected by cooling associated with a relatively cold boundary. The

parameter τ (the overheat ratio) is defined as the ratio of the maximum temperature difference across the system to the reference temperature. The nondimensional semifault width, y_e, is defined as the ratio of the half-fault width, y_e', to the depth of the reservoir, L'. As expected, y_e is very small. It may be observed from Table 1 that increases in P_b, R, and y_e will increase d, which means that a larger aquifer is needed for the transition to the conduction-temperature profile when the parameter is increased. In physical terms, this result implies that the hot isothermal portions of the aquifer, maintained by horizontal convection effects, will be more extensive in systems of relatively larger fault-inlet pressure, permeability, and fault size.

Table 1. Values of d for different sets of parameters.

d	P_b	R	τ	y_e
0.32	0.5	500	1	0.025
0.41	1	500	1	0.025
0.49	1.5	500	1	0.025
0.56	2	500	1	0.025
0.255	1	250	1	0.025
0.53	1	750	1	0.025
0.64	1	1000	1	0.025
0.96	1	500	1	0.05
0.41	1	500	2	0.025

Figure 2 shows the vertical velocity, W, in the fault at various depths for different inlet pressures. It may be noted that an increase in the inlet pressure leads to an increase in the vertical

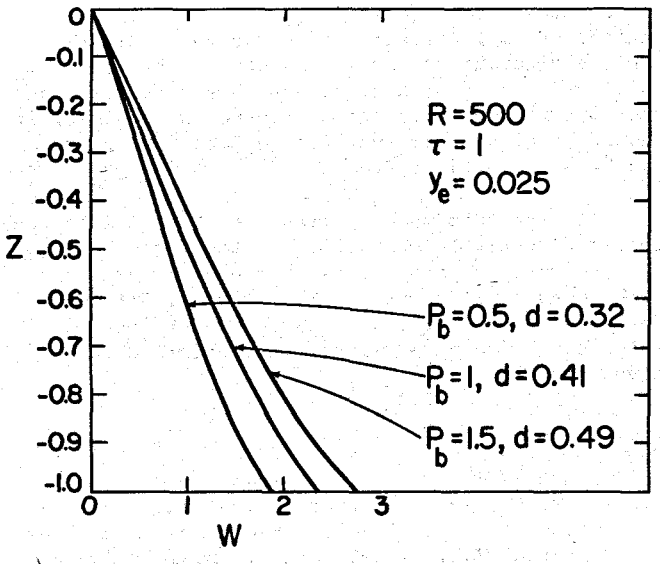

Figure 2. Vertical velocity distributions along the depth of the fault for different fault inlet pressures. [XBL 8011-2369]

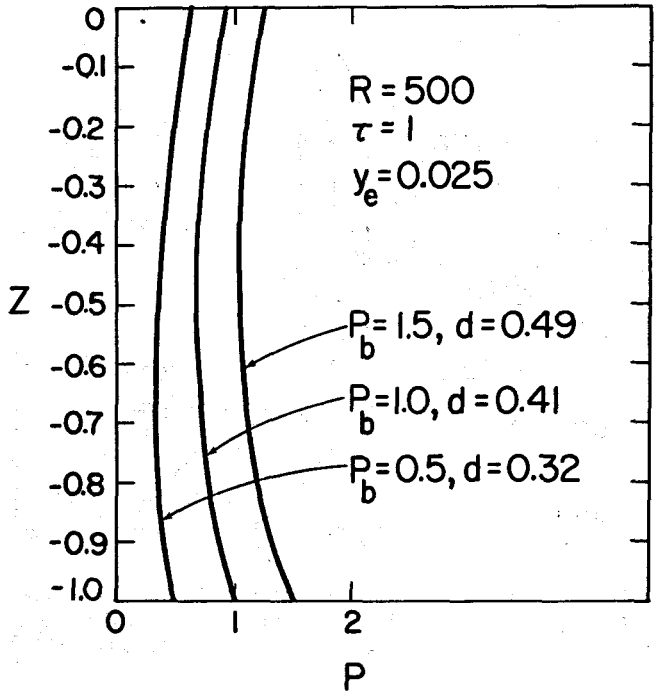

Figure 3. Fault overpressure versus depth for various values of P_b. [XBL 8011-2370]

velocity. It is consistent with the commonly held notion that one would require higher pressure to push more mass into the system. The vertical velocity vanishes at the top of the fault as a result of the impermeable boundary assumption. All the water is forced into the aquifer before it can reach the upper region of the fault. Figure 3 is a plot of fault overpressure, P, versus depth for different values of P_b. As one may expect, the overall fault pressures increase for an increased inlet pressure, P_b. It may be noted that the fault pressures decrease upward and then increase toward the top of the fault. This increase toward the top is caused by the stagnation point at z = 0.

The horizontal velocity in the aquifer at various depths is shown in Figure 4 for different inlet pressures. As expected, horizontal aquifer velocities increase for an increased inlet pressure. The trend of the curves is similar to the overpressure curves in Figure 3. The larger velocities at the top of the aquifer are associated with the relatively higher horizontal pressure gradients there. Figure 5 shows the variations of the aquifer temperature with depth at several horizons. The curve $\hat{y} = 1$ represents the far end of the aquifer, which is located at d/y_e times its depth. It can be seen that temperature in the aquifer decreases with increasing distance from the fault, since heat is lost to the cold upper boundary. It may be noted that at $\hat{y} = 0.1$, half of the aquifer is at least within 80% of the high temperature value. Finally, the effect of two different specified boundary conditions on d is shown in Figure 6. It may be noted that d increases linearly with M (Goyal and Kassoy, 1980), but not so much with P_b. One would expect this in light of the fact that convection--a direct function of velocity--would be enhanced more by a velocity increase than by an equivalent pressure

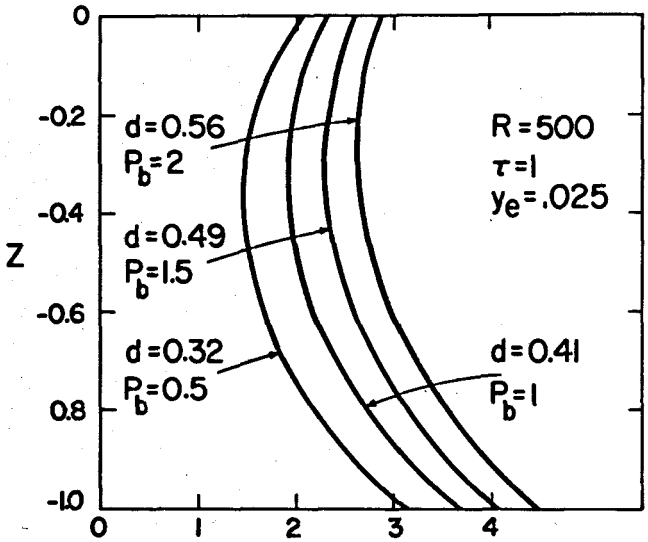

Figure 4. Horizontal liquid velocity in the aquifer along the depth of the reservoir for different values of P_b. [XBL 8011-2371]

increase. Thus it suggests that the extent of the isothermal region in the aquifer is greater when the inlet velocity is doubled than when inlet pressure is doubled. A detailed discussion of the effects of the various parameters listed in Table 1 on the pressures, velocities, temperatures, and temperature gradients in the fault-aquifer system is given in Goyal and Narasimhan (1981).

CONCLUSIONS

A quasi-analytic solution is obtained for a liquid-dominated geothermal system with a specified pressure at the fault inlet. We have investigated the effects of various parameters, such as fault inlet pressure, Rayleigh number, overheat ratio, and fault width, on the thermodynamics and fluid mechanics of the system. We observe that the temperatures in the near-fault regions are maintained

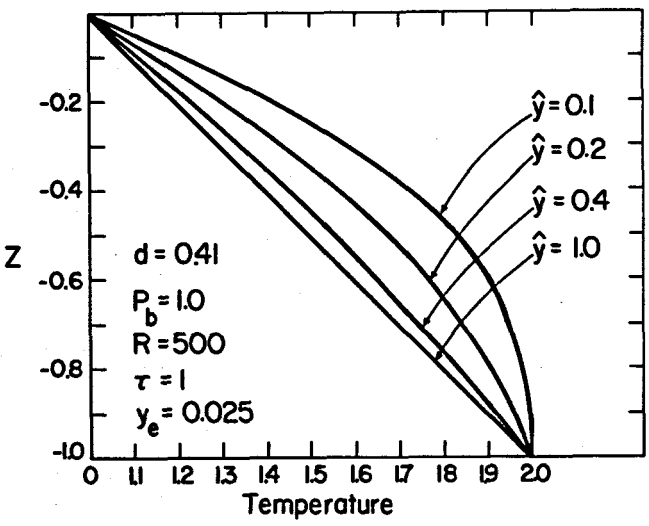

Figure 5. Temperatures in the aquifer at different horizons and depths. [XBL 8011-2372]

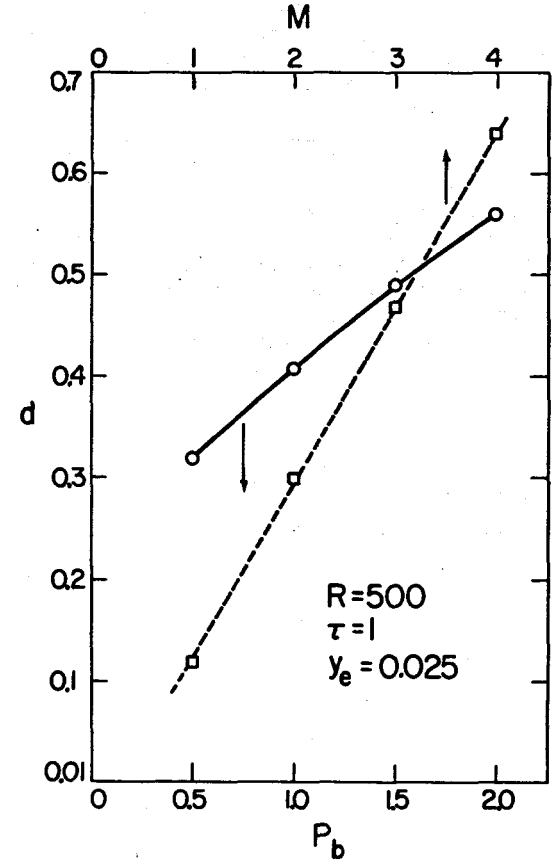

Figure 6. A comparison between the plots of M versus d and P_b versus d (data of M vs d from Goyal and Kassoy, 1980). [XBL 8011-2367]

at the high value shown for the lower boundary. A hypothetical well in these formations would encounter a zero vertical temperature gradient regime associated with a purely horizontal flow. In contrast, conventional wisdom suggests that the observations of small vertical temperature gradients implies vigorous vertical convection. Although it is clear on theoretical grounds that vertical convection will generate nearly isothermal regimes, it should be clear that specific geologic structure can have a similar influence.

The concepts used to generate the model can be tested directly by comparison of the field data and the theoretical prediction. Current measurement techniques provide surface heat flux distributions, downhole temperature, and pressure distributions which can be compared with values obtained in a given model.

REFERENCES CITED

Bailey, T. P., 1977. A hydrological and subsurface study of Imperial Valley geothermal anomalies, Imperial Valley, California. Boulder, University of Colorado, Geological Sciences Department, 101 p.

Combs, J., and Hadley, D., 1977. Microearthquake investigation of the Mesa geothermal anomaly, Imperial Valley, California. Geophysics, v. 42, no. 1, p. 17-33.

Elders, W. A., Rex, R. W., Meidav, T., Robinson, P. T., and Biehler, S., 1972. Crustal spreading in southern California. Science, v. 178, p. 15-24.

Goyal, K. P., and Kassoy, D. R., 1980. Fault zone controlled charging of a liquid-dominated geothermal reservoir. J. Geophys. Research, v. 85(B4), p. 1867-1875.

Goyal, K. P., and Narasimhan, T. N., 1981. Constant pressure charging of a liquid-dominated geothermal reservoir. Berkeley, Lawrence Berkeley Laboratory, LBL-11836. In preparation.

Grindley, G. W., 1965. The geology, structure, and exploitation of the Wairakei geothermal field, Taupo, New Zealand. N. Z. Geol. Surv. Bull., v. 75, 141 p.

____, 1970. Subsurface structures and relation to steam production in the Broadlands geothermal field, New Zealand. In Geothermics: Proceedings of the United Nations Symposium on the Development and Utilization of Geothermal Resources, Special Issue, v. 2, part 1, p. 248-261, Pisa, Italy, Instituto Internazionale per le Richerche Geotermiche.

Puente, C. I., and de la Pena, A. L., 1978. Geology of the Cerro Prieto geothermal field. In Proc., First Symposium on the Cerro Prieto Geothermal Field, Baja California, Mexico. Berkeley, Lawrence Berkeley Laboratory, LBL-7098, p. 17-40.

Rinehart, C. D., and Ross, D. C. 1964. Geology and mineral deposits of the Mount Morrison quadrangle, Sierra Nevada, California. U. S. Geol. Surv. Prof. Pap. 385, p. 106.

Ward, P. L., and Jacobs, K. H., 1971. Microearthquakes in the Ahuachapan geothermal field, El Salvador, Central America. Science, v. 173, p. 328-330.

Thermodynamic models for geothermal and geopressured fluids

E. R. Iglesias

Hydropressured geothermal reservoirs often contain, in addition to dissolved nonvolatile salts, significant amounts of noncondensible gases, chiefly CO_2. The saline brines in the geopressured-geothermal formations of the Gulf Coast are believed to be saturated with dissolved methane and lesser volatile hydrocarbons. For the gas concentrations involved, the thermophysical properties of the hydrothermal fluids differ considerably from those of pure water, and therefore cannot be estimated from steam tables. These properties are important when computing fluid and heat transport in hydrothermal reservoirs and wellbores. Therefore, the ability to predict the thermophysical properties of hydrothermal mixtures is paramount in reservoir engineering studies of reservoir and wellbore performance. In response to this need, I have developed models that describe the thermophysical properties of water-carbon dioxide and of water-methane mixtures pertinent to reservoir engineering studies.

WATER-CARBON DIOXIDE SYSTEM

Attempts have been made (e.g., Sutton, 1976; Grant, 1977; Iglesias, 1979) to describe the properties of H_2O-CO_2 mixtures for geothermal reservoir engineering purposes. These models include a series of ad hoc approximations which result in significant inaccuracies outside a fairly restricted range of pressures, temperatures, and compositions.

Three quantities--namely, the activity coefficients of water and of carbon dioxide, and H_{21}, the thermodynamic equivalent of Henry's Law constant--are central for any model describing accurately the thermophysical properties of H_2O-CO_2 mixtures. These parameters, which are intimately related to the solubility, were determined by processing published experimental data (Iglesias, 1980a). Data reduction was achieved by improved equations which describe phase equilibrium of carbon dioxide and water.

Results of this work were subsequently applied to the development of a model for the thermophysical properties of water-carbon dioxide mixtures (Iglesias, 1980b). This model accounts for mixture nonidealities not considered in previous work.

Solubility of CO_2 in Water

This issue has been investigated by several authors. However, significant discrepancies exist for temperatures exceeding 100°C. These discrepancies have resulted, in part, from inappropriate assumptions about the equations of phase equilibria used to reduce the experimental data. A review of the literature indicated that the problem was in computing the fugacity and activity coefficients.

My approach to the problem was to improve upon the Krichevsky-Illinskaya equilibrium equation used by Malinin (1974) in his work on CO_2 solubility. Elaborating upon this, I derived γ_2, the CO_2 activity coefficient, from a Redlich-Kister expansion of the binary mixture's excess Gibbs energy and the relation of γ_2 with the excess partial Gibbs energy (e.g., Prausnitz, 1969). Neglecting terms of order higher than cubic in the expansion, the activity coefficient is expressed in terms of two parameters: (A/RT) and (B/RT). The extra parameter gained over the Krichevsky-Illinskaya formulation substantially improves data reproducibility with the new equilibrium equation.

A further advantage was achieved over previous efforts by deriving the CO_2 fugacity coefficient from the formulation of De Santis et al. (1974). De Santis and his co-workers developed a pressure-explicit equation-of-state applicable to mixtures of polar gases. The fugacity coefficients derived

in this manner reflect the molecular interactions taking place in the gaseous mixture. This is a considerable advance over previous formulations using the Lewis fugacity rule, especially at high temperatures (T > 100°C), where the fraction of steam in the gas phase increases rapidly with increasing temperature.

Values of H_{21}, (A/RT), and (B/RT) were obtained by reducing the data of Takenouchi and Kennedy (1964) and of Malinin (1974) via the new equilibrium equation. Figure 1 shows the raw and smoothed results obtained for H_{21}, and compares them with previous smoothed results. The questionable quality of the 110°C isotherm of Takenouchi and Kennedy (1964) renders the corresponding value of H_{21} inconclusive. The remaining results indicate that Malinin's smoothed values underestimate H_{21} for $T \geq 250$°C. High temperature heats of solution were also computed from H_{21}.

The main contributions of this work are (1) to provide an upgraded model for the solubility of CO_2 in water, which could be used to reduce new experimental data as they become available and (2) to provide reliable high-temperature values of H_{21} and of the Redlich-Kister coefficients.

Thermophysical Properties for Geothermal Uses

The thermodynamic model described here was developed mainly as an "equation-of-state" package in geothermal reservoir and wellbore numerical simulators.

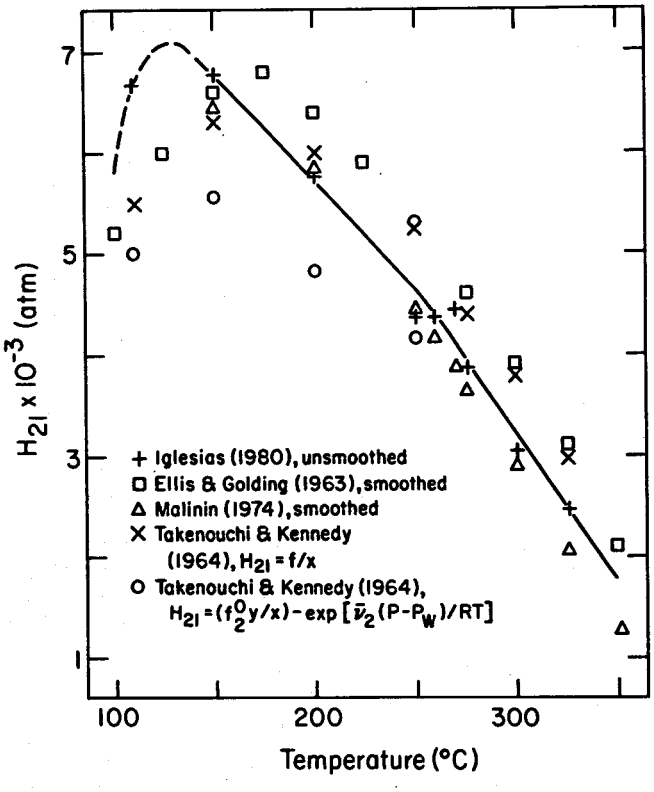

Figure 1. High-temperature solubility constant of CO_2 in water: (+) computed values; (-) recommended smoothed results. For comparison, smoothed results from other authors are also shown. [XBL 8011-6462]

For these applications, the model was required to predict accurately the properties of H_2O-CO_2 mixtures over wide ranges of temperature (in excess of 100°C to near the critical point of water), pressure (to about 200 bars), and compositions (up to several CO_2 wt%). Within this range of parameters, the H_2O-CO_2 system may consist of a compressed solution, a liquid solution in equilibrium with a gas mixture, and a "superheated" gas mixture.

The properties of the gas mixtures, including fugacity coefficients, partial and total molar enthalpies, and internal energies, are derived from the equation-of-state of De Santis et al. (1974). This equation gives the gas pressure in terms of the temperature, total molar volume, and mole fraction of each component in the gas mixture.

For the liquid phase, the partial molar volume corresponding to water and carbon dioxide are estimated by the pure liquid water molar volume and by the infinite dilution molar volume of Malinin (1974), respectively. The total molar volume is then computed from these and from the mole fractions of each component in the solution. The liquid molar enthalpies were derived from excess functions. These excess functions were formulated in terms of H_{21}, the Redlich-Kister coefficients, and the heat of solution, obtained from Malinin (1974), and in terms of the pure liquid water molar enthalpy.

Phase equilibrium is handled by the modified Krichevsky-Illinskaya equation, and supplemented by a conventional fugacity equation for the water component. Pressure effects on phase equilibrium are accounted for by Poynting correction factors.

A number of subroutines have been developed and tested to compute the various thermodynamic and auxiliary variables involved in the model. Currently an "equation-of-state" numerical package is being developed on the basis of these routines. In its present configuration, the package's input variables are pressure, temperature, and molar volume of the mixture. The output variables include: enthalpy and composition of the mixture; (volumetric) gas saturation; and enthalpies, molar volumes, and compositions of the gas and liquid phase.

The main contribution of this work is a model for the thermophysical properties of water-carbon dioxide mixtures which is reliable over the ranges of temperature, pressure, and composition of interest for geothermal reservoir engineering purposes.

WATER-METHANE SYSTEM

The geopressured formations of the United States Gulf Coast are being probed for methane recovery feasibility. One critical variable is the amount of methane actually dissolved in the pore brines. Sampling and subsequent analysis of these geopressured fluids is therefore important for the economic assessment of the resource.

Owing to difficulties experienced in the field with currently available downhole fluid samplers, interest has recently arisen to develop new samplers designed especially for geopressured environments.

Knowledge of the thermophysical and chemical properties of water-methane, and water-methane-sodium chloride fluid mixtures can be advantageous in downhole fluid sampler design, delineating sampler recovery strategies, and developing fluid transfer from the sampler to other containers adequate for subsequent analysis of the fluid.

A Simple Model for Geopressured Fluids

I have developed a simple model to estimate chemical and thermophysical properties of geopressured fluids, and have applied this model in computing and discussing bottomhole-, wellhead-, and sampler-related quantities (Iglesias, 1980C). The following paragraphs highlight the model and some results.

With the exception of a Setschenow correction for methane solubility in NaCl solutions, I neglected the complications posed by the presence of dissolved solids and considered a system composed only of water and methane. This approach is appropriate for engineering purposes.

In the present model, the contributions of methane to the liquid- and gas-phase molar volumes are estimated from a correlation (Brelvi and O'Connell, 1972), and from the ideal gas law, respectively. The corresponding quantities for liquid water and steam are estimated from the steam table equations as given by the International Formulation Committee (1967).

Methane solubility is computed from an empirical correlation (Haas, 1978), which assumes that steam exists in the gas phase at its saturated pressure. A Setschenow-type factor is used to correct methane solubility for salinity.

Applications to Geopressured Fluids Sampling and Production.

Expected bottomhole and wellhead conditions (Fig. 2, Table 1) in geopressured wells of the Gulf Coast were estimated using the model described above. The thermodynamic transformations undergone by the hydrothermal fluids when the closed sampler and wellhead lubricator are cooled to near ambient temperatures were also assessed (Figs. 3 and 4).

The main contributions of this work include a discussion of the combined effects of depth and salinity on the in situ methane content, estimates of wellhead pressures, compositions and gas saturations in relation to well depth, an assessment of the differential pressures acting upon the sampler's walls, and recommendation of a procedure for safe recovery of the sampler from the wellhead lubricator.

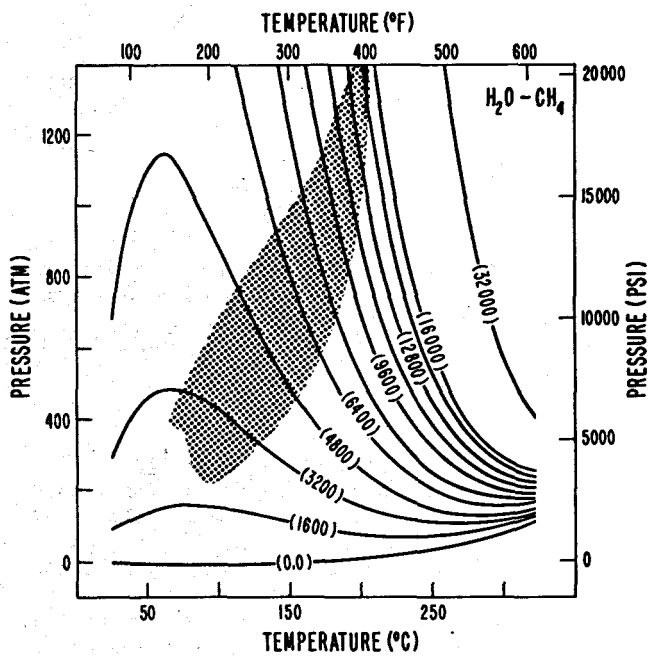

Figure 2. Solubility curves for the H_2O-CH_4 system. Molal and (ppm) methane concentrations are indicated. The shaded area represents, approximately, the range of pressure and temperature covered by the geopressured formations of the Gulf Coast in the United States. [XBL 8011-6407A]

Table 1. Bottomhole-wellhead relations.

z(m)	P_B (atm)	T_B (°C)	T_W (°C)	λ_W (%)	λ_W (ppm)	P_W (atm)	S_W (%)	x_W (%)	Y_W (%)	r_W (%)
6000	1400	200	200	1.555	14,029	846	1.64	1.19	98.19	76.0
6000	1400	200	150	1.555	14,029	834	3.53	0.72	99.44	45.9
3600	800	150	150	0.704	6,297	460	1.51	0.51	98.98	72.9
3600	800	150	100	0.704	6,297	454	2.40	0.37	99.78	52.0

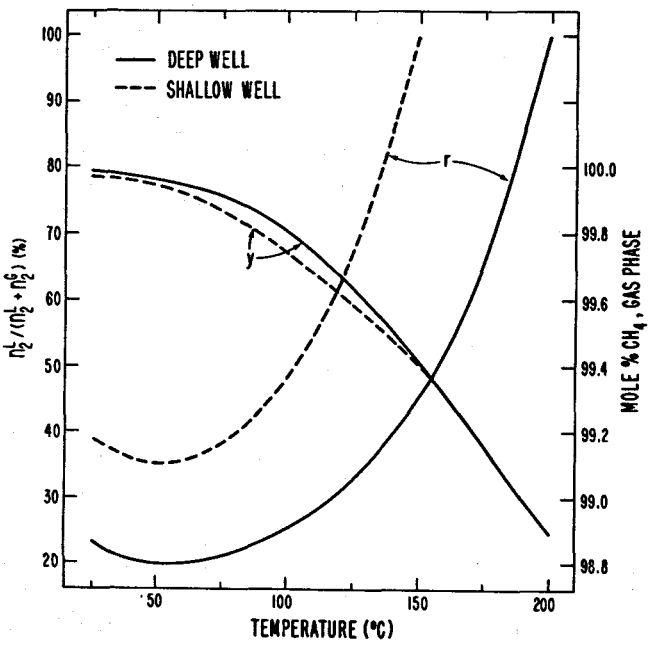

Figure 3. Fraction of total methane in solution and gas phase methane mole fraction responses to sampler cooling for two well depths.
[XBL 8011-6410]

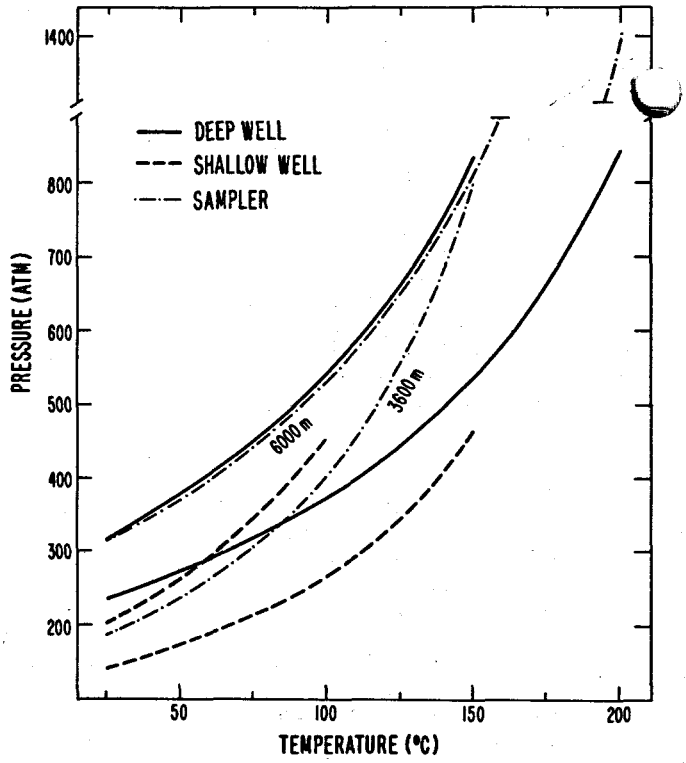

Figure 4. Fluid pressure versus temperature for the (closed) lubricator. Two curves, corresponding to two different assumed values for the steady-state wellhead temperature, are shown for each well depth. For comparison, the P-T curves corresponding to the sampler fluid for each well depth are also shown.
[XBL 8011-6413]

REFERENCES CITED

Brelvi, S. W., and O'Connell, J. P., 1972. Corresponding states correlations for liquid compressibility and partial molal volumes of gases at infinite dilution in liquids. Am. Inst. of Chem. Eng. J., v. 18, p. 1239-1243.

De Santis, R., Breedveld, G. J. F., and Prausnitz, J. M., 1974. Thermodynamic properties of aqueous gas mixtures at advanced pressures. Ind. Eng. Chem. Process Des. Develop., v. 13, p. 374-377.

Grant, M. A., 1977. Broadlands: A gas dominated geothermal field. Geothermics, v. 6, no. 9, p. 9-29.

Haas, J. L., 1978. An empirical equation with tables of smoothed solubilities of methane in water and aqueous sodium chloride solutions up to 25 weight percent, 360°C and 138 MPa. U. S. Geological Survey Open File Report No. 78-1004.

Iglesias, E. R., and Schroeder, R. C., 1979. Properties of H_2O-CO_2 mixtures for geothermal reservoir and wellbore simulators. In Earth Sciences Division Annual Report 1979, Berkeley, Lawrence Berkeley Laboratory, LBL-10686, p. 95-98.

Iglesias, E. R., 1980a. The system H_2O-CO_2 revisited: A reevaluation of the high-temperature CO_2 solubility. In preparation.

____, 1980b. Thermophysical properties of water-carbon dioxide mixtures for geothermal applications. In preparation.

____, 1980c. Sampling geopressured fluids: From bottomhole to wellhead and beyond. (An abridged version of this paper has been presented at the Sixth Annual Geothermal Reservoir Engineering Workshop, Stanford University, Dec. 1980.)

International Formulation Committee of the Sixth International Conference on the Properties of Steam, 1967. A formulation of the thermodynamic properties of ordinary water substance. IFC Secretariat, Verein Deutscher Ingenieure, Duesseldorf, Prinz-Georg-Strasse 77/79.

Malinin, S. D., 1974. Thermodynamics of the H_2O-CO_2 system. Geochim. Int., v. 11, p. 1060-1085.

Prausnitz, J. M., 1969. Molecular thermodynamics of fluid phase equilibria. Englewood Cliffs, New Jersey, Prentice Hall.

Sutton, F. M., 1976. Pressure-temperature curves for a two-phase mixture of water and carbon dioxide. New Zealand J. Sci., v. 20, p. 297-301.

Takenouchi, S., and Kennedy, G. C., 1964. The binary system H_2O-CO_2 at high temperatures and pressures. Am. J. Sci., v. 262, p. 1055-1074.

ADVANCES IN TRANSIENT WELL-TEST ANALYSIS TECHNIQUES

Overview

C. W. Miller

Pressure transient data analysis is an important method of measuring in-situ reservoir properties. However, these well-test analysis methods that were developed in the petroleum and hydrology literature must be modified to include the effects of two-phase and nonisothermal flow in the reservoir. Lawrence Berkeley Laboratory has continued its effort to improve the design and analysis techniques of well tests in geothermal fields. In fiscal 1980 the emphasis was on developing quasi-analytic and numerical models germane to this effort.

The next article describes a quasi-analytic model that was developed to solve the equations governing mass conservation, energy conservation, and Darcy's law. The model showed that the plot of the pressure vs. log (time) approaches a straight line for a constant rate flow test at late times even when the fluid in the reservoir is two-phase. It is possible to measure the slope of that line to obtain the transmissivity of the reservoir.

The quasi-analytic method, however, fails to take into account wellbore effects. Wellbore storage can last for several hours during a geothermal well test as a result of the high compressibility of the two-phase steam-water mixture in the bore. Thus, the development of a transient two-phase wellbore model continued. The friction factor was input as an empirical correlation and the slip between the phases was included. The slip model was input in a manner that allowed modeling of the shut-in of a well where the two phases separate. The existing wellbore model can be coupled with a two-phase reservoir simulator so that well tests of two-phase reservoirs can be designed and analyzed.

Testing geothermal wells requires instrumentation that can withstand high temperatures for prolonged times. An interference test (versus a production test) usually requires that the pressure response from several production wells be considered. The numerical program ANALYZE is one method of handling the multiproduction and observation wells with variable flow rates. ANALYZE is a history-matching program based on the Theis solution that varies the reservoir parameters and the position of hydrological barriers to give the best fit of the observed pressure data.

Future work in this area includes an effort to combine these three problems--two-phase reservoir modeling, transient wellbore modeling, and variable flow rate analysis--in the development of a two-phase well-test program.

An analysis of two-phase production and injection tests

M. J. O'Sullivan and K. Pruess

By introducing a similarity variable, $r/\sqrt{t}$, a quasi-analytical method can be used to calculate the flow induced either by injecting cold water into or by producing of fluid from a hot-water, or boiling, geothermal reservoir. O'Sullivan (1980) has described the application of the method to the analysis of constant-rate production tests. O'Sullivan and Pruess (1980) have considered the injection problem. An outline of the method and results is presented here.

The constant-flow-rate well test is one of the most common methods for determining the properties of petroleum or groundwater reservoirs. In this test, when the pressure drop is plotted against the logarithm of time, the resulting curve becomes asymptotic to a straight line after a short initial period. The mobility-thickness product for the reservoir can be obtained from the slope of this line, and the reservoir compressibility can be calculated from the intercept. The analysis of this test is based on the Theis curve solution, which assumes that the fluid density and viscosity and the formation compressibility and permeability are independent of pressure. In a geothermal reservoir, the fluid is often boiling or near boiling, and the flow induced by a constant-rate well test is not isothermal. The flow may be either a two-phase mixture of steam and water with a varying liquid saturation or a near-boiling liquid which flashes to steam during the test. In either case, the fluid density and viscosity change quite significantly. Also, the compressibility of the reservoir is dominated by the rate at which water condenses or evaporates. Grant (1978) has shown that the effective compressibility for a two-phase fluid is 100 to 1000 times larger than for liquid water and 10 to 100 times larger than for superheated steam. The formation compressibility is commonly of the same order of magnitude as for liquid water (Grant, 1978) and therefore is negligible compared to the two-phase fluid compressibility. The mobility-thickness product for the reservoir is affected by permeability reduction factors for two-phase flow. These factors change as the saturation of the fluid changes, leading to a total mobility which may vary significantly during the progress of the well test.

Because of the complex properties of boiling water, the Theis solution is generally not applicable to the analysis of geothermal well tests. In the special case where both the flow rate and the resulting pressure drops are small, Grant (1978), Grant and Sorey (1979), and Garg (1980), deduced that the pressure versus log (time) curve is approximately linear and showed how to calculate an effective compressibility and mobility-thickness product.

Moench and Atkinson (1978) and Moench (1979) considered the special case of very dry steam and showed that the governing equations can be approximated by a linear diffusion equation in p^2 (pressure squared). Sorey et al. (1980) recently compared well test results obtained with a numerical simulator developed by Zyvoloski et al. (1979) and a quasi-analytic procedure developed by Grant (1979). Their results show that nonlinear effects are important in some tests and, even when pressure depends approximately linearly on log (time), it is not obvious what fluid properties (density, viscosity, relative permeability, etc.) should be used to deduce the formation permeability from the drawdown curve.

When water is injected into a groundwater reservoir, the pressure buildup also follows the well-known Theis curve. The Theis curve analysis assumes that the flow is isothermal and therefore the physical properties of the injected fluid are the same as the reservoir fluid. In a geothermal reservoir, the fluid may be hot water at temperatures in the range 150-250°C or a mixture of steam and water at even higher temperatures. In either case, the physical properties of the reservoir fluid differ significantly from those of the injected fluid with a temperature of 10-100°C. For example, the density, viscosity, and compressibility of 100°C water differ from the 250°C values by approximately 24%, 100%, and 50%, respectively. The contrast is even greater for a two-phase mixture, with order-of-magnitude differences between the liquid and two-phase values (Grant, 1978).

One of the more important aspects of the present work is comparing the results obtained from the quasi-analytical similarity method to results from the SHAFT79 geothermal reservoir simulator.

The injection problem is particularly difficult for numerical simulators to handle, since it involves the propagation of sharp fronts in the reservoir. There is a "hydrodynamic" front where the fluid in the reservoir first starts to move significantly and, trailing behind it, a "thermal front" where the fluid cools down to the injection temperature. Earlier, Pruess and Schroeder (1979) demonstrated the ability of the SHAFT79 program to model injection tests. One purpose here is to demonstrate the usefulness of the similarity method for analyzing either production or injection tests and to confirm the accuracy of SHAFT79 by comparing results obtained with the two methods.

BASIC EQUATIONS AND THE SIMILARITY METHOD

The basic equations solved (see O'Sullivan (1980) and Grant (1978) for details) represent conservation of mass, conservation of energy, and Darcy's Law. These equations take the form of partial differential equations in radial distance, r, and time, t, which must be solved together with suitable initial conditions and boundary conditions. In the problems considered here, a constant mass flow rate is specified at r = 0, an idealized zero radius well; it is assumed that the initially uniform constant pressure and enthalpy persist at large enough distances from the well. For the injection case, the enthalpy at the well is also prescribed.

Following the standard similarity technique a variable, $\eta = r/\sqrt{t}$, is introduced, and the original partial differential equations can be rewritten as ordinary differential equations for the production problem:

$$\eta \frac{dQ_m}{d\eta} = F_Q , \tag{1}$$

$$\eta \frac{dh}{d\eta} = F_h , \tag{2}$$

$$\eta \frac{dp}{d\eta} = F_p . \tag{3}$$

Here Q_m is mass flow rate, h is mixture enthalpy, and p is pressure; while F_Q, F_h, and F_p are complex functions of η, Q_m, h, and p (see O'Sullivan (1980) for details). The nonlinear ordinary differential equations are then solved numerically.

NUMERICAL PROCEDURE

For single-phase injection problems or any production problems, the numerical procedure follows that of O'Sullivan (1980). A logarithmic scale is introduced by solving in terms of z, where $z = \log \eta$. Then equation (1) is numerically integrated for Q_m starting from $Q_m = Q_o$ at $\eta = 0$ and using estimated values for $p(\eta)$ and $h(\eta)$. Next, equation (3) updates $p(\eta)$ using the newly calculated values for $Q_m(h)$ and the boundary condition $p \to p_o$ as $\eta \to \infty$. Finally, in the production case, a difference approximation of equation (2) is solved directly, for injection, a difference approximation of equation (2) is solved by inverting a tridiagonal matrix, using the latest values for $p(\eta)$ and $Q(\eta)$ and the boundary conditions $h \to h_1$ as $\eta \to 0$ and $h \to h_o$ as $\eta \to \infty$. These steps are then repeated until convergence is obtained. For single-phase flow the process works very well with convergence to within a very small tolerance requiring only 5-10 iterations on crude initial estimates. However, the above process does not work for two-phase injection problems. Instead, an inverse procedure is adopted where the position, say η_c, of the condensing front is specified and the corresponding injection rate, Q_o, required to produce it is calculated.

RESULTS

The reservoir parameters (Table 1) are those of Sorey et al. (1980) and O'Sullivan (1980) for a production well test problem. Two injection cases are reported here--a single-phase problem for injecting 100°C water into a 231°C reservoir, and a second problem for injecting 100°C water into a reservoir of 233°C with an initial liquid saturation of 0.80. The pressure and temperature responses are shown in Figure 1; the flow rate buildup and saturation profile are shown in Figure 2. The agreement with SHAFT79 results is good. Naturally, the discrete nature of the SHAFT79 simulator tends to smear the sharp thermal front but it gives a reasonable estimate of its position. There were some differences in the steam table approximations used between SHAFT79 and the similarity technique; therefore, exact correspondence cannot be expected. The results show a dual straight-line pressure drop

corresponding to the Theis curves for cold and hot water, respectively. Also, the very high effective compressibility of the two-phase fluid is evident from the much later pressure buildup.

Table 1. Reservoir data.

Porosity	ϕ =	0.15
Rock density	ρ_r =	2000 kg/m^3
Rock specific heat	C_r =	1.0 kJ/kg-K
Permeability	k =	0.24 x 10^{-12}/m^2
Initial pressure	p_o =	3.0 MPa
Initial enthalpy	h_o =	1.0 MJ/kg or 1.0158 MJ/kg
Injection rate	Q_o =	0.4036 kg/s
Injection enthalpy	h_1 =	0.4154 MJ/kg

Only one production problem is reported here, for a medium pressure reservoir with parameters identical to those in the injection problem (Table 1). The pressure drawdown curves for this problem for several initial liquid saturations are given in Figure 3. These curves show that the p versus log (time) plot does not give a straight line for two-phase or flashing flow. In the range of practical interest (say $10^4 < t/r^2 < 10^6$) the curvature is not large, especially for the low liquid saturation cases, but variations in k/ν_t do occur. The results show that k/ν_t changes significantly during the course of the test for high initial liquid saturations. In such cases, therefore, the initial values p_o and h_o give a value of k/ν_t (approximately the same as that at $t/r^2 = 1$), which is not representative of the slope of the drawdown curve. Also, the values of the obtained k/ν_t vary significantly with the value of the initial enthalpy.

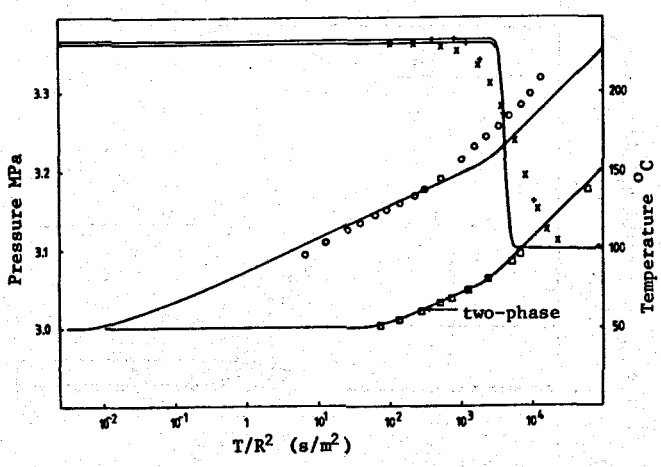

Figure 1. Pressure and temperature profiles. The temperature profiles for the hot-water and two-phase reservoirs are coincident after cooling commences. SHAFT79 results are shown as o for pressure and x for temperature for the hot-water reservoir and □ for pressure and + for temperature for the boiling reservoir. [XBL 812-2650]

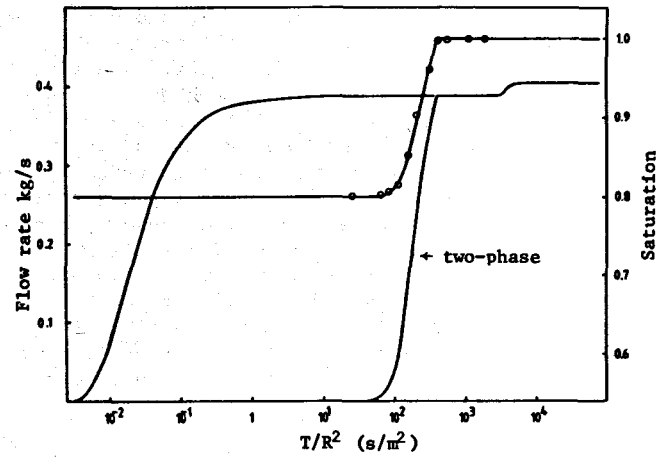

Figure 2. Flow rate and liquid saturation profiles. The flow rate curves coincide after cooling commences. SHAFT79 results are shown as o. [XBL 812-2649]

A simple independent calculation shows that for the Corey permeability reduction factors k/ν_t is a highly nonlinear function of saturation for any particular pressure, attaining a minimum value near $S_\ell = 0.5$ (O'Sullivan, 1980). Therefore, the pressure decline is most rapid for tests where the initial saturation value is near 0.5-0.6. The results shown in Figure 3 are for the Corey-type relative permeability functions, where $S_{\ell r} = 0.3$ and $S_{vr} = 0.05$. Other relative permeability functions give a different shape for the equivalent curves (for example, a different location of the minimum) and lead to different pressure drawdown curves.

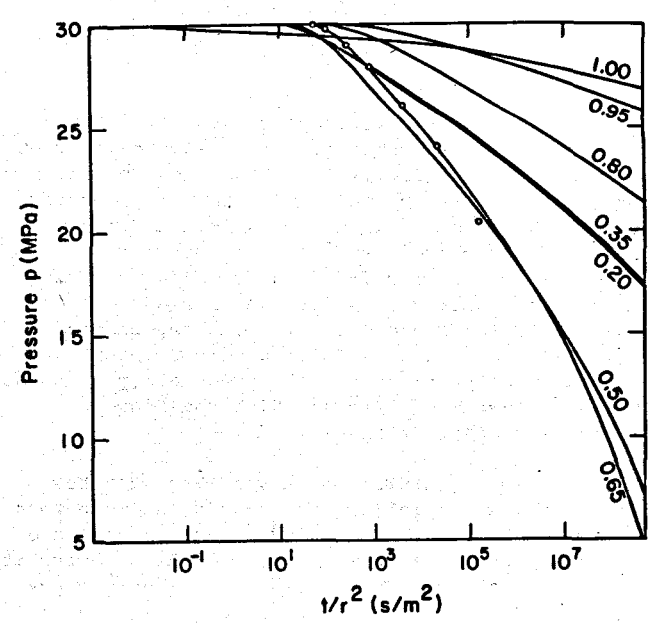

Figure 3. Pressure drawdown curves for the production problem. Curves are labeled with initial liquid saturation values. Results from numerical simulation (SHAFT79) shown as o. [XBL 804-7010]

The flow rate buildup curves are shown in Figure 4. The two-phase curves are all similar but the flashing flow curve is quite different. The flow rate builds up much more quickly, since the liquid water is more dense. When the water flashes, the density decrease caused by boiling must be accompanied in the two-phase region by an increase in the mass flow exceeding that in the single-phase region. Since the final flow rate in the two-phase region is fixed by its value Q_o as $r \to 0$ (or $t/r^2 \to \infty$), the flow rate in the liquid region must remain below Q_o. The size of the jump in flow rate that accompanies flashing depends on the initial state of the reservoir. A colder reservoir takes longer to flash and a larger flow rate builds up before boiling occurs.

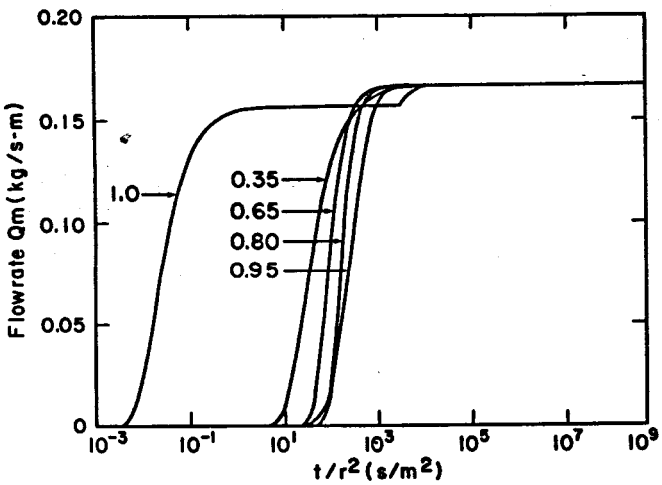

Figure 4. Discharge build-up curves for the production problem. Curves are labeled with initial liquid saturation values. [XBL 804-7012]

The most difficult problem in analyzing the pressure drawdown curves is estimating the correct value of ν_t. For low-liquid saturation conditions, the initial values p_o and h_o can be used to calculate ν_t, but for medium and high initial liquid saturations this procedure is not satisfactory. The changes in saturation and flowing enthalpy during the course of the test are shown in Figures 5 and 6. The results in Figure 6 confirm the asymptotic analysis presented in O'Sullivan (1980), that the flowing enthalpy rises to an approximately constant level at a value of t/r^2 at which the flow rate, Q_m, reaches its constant final value.

The liquid saturation curves (Fig. 5) show that only low initial liquid saturations lead to a "drying out" of the reservoir. Even for the case $S_{\ell o} = 0.5$, the reservoir runs out of heat before it runs out of fluid. This difference in very long-term behavior (either drying out or cooling off) is dependent on both the initial saturation and the relative permeability functions. Further calculations will determine the effect of varying the relative permeability functions on this and other aspects of the results.

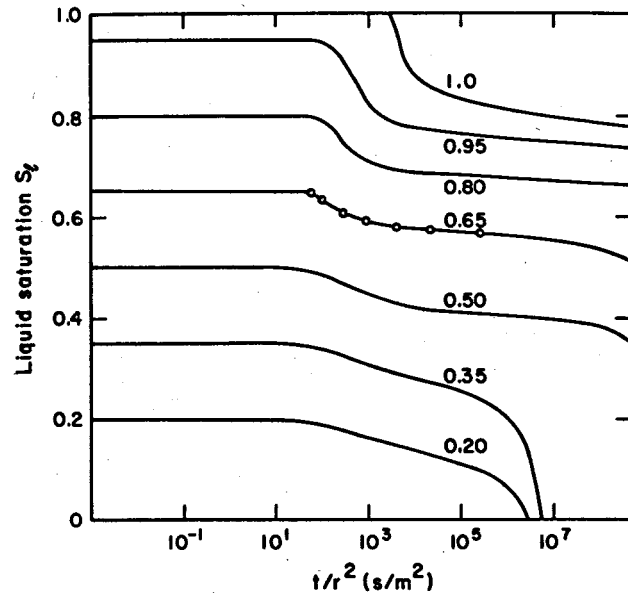

Figure 5. Liquid saturation response curves for the production problem. Curves are labeled with initial liquid saturations. Results from numerical simulation (SHAFT79) are shown as o. [XBL 804-7013]

Calculated results based on the numerical simulator SHAFT79 for the single case $S_{\ell o} = 0.65$ are shown in Figures 3 and 5. These results were obtained using the same grid as Sorey et al. (1980), and show that, in spite of discretization errors, the numerical simulation agrees well with the similarity solution. The last point plotted on Figure 1 at $t/r^2 \approx 10^5$ is a well block pressure with t/r^2 calculated from the procedure suggested by Garg (1980) with r = 0.56 x block radius.

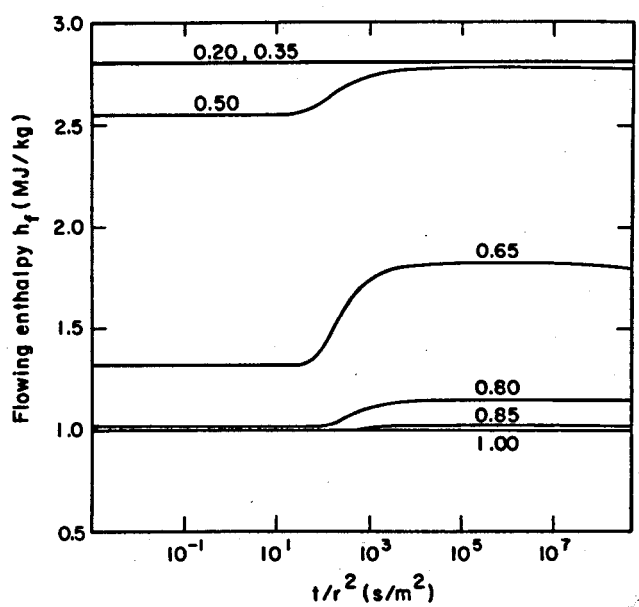

Figure 6. Flowing enthalpy response curves for the production problem. Curves are labeled with initial liquid saturations. [XBL 804-7014]

CONCLUSIONS

The similarity method presented here provides a very powerful method for analyzing constant-flow rate geothermal well tests. Because of its accuracy, the solution method provides a means of checking the results obtained by standard reservoir simulation methods; thus, they can be used with confidence for analyzing constant-flow-rate well-test results, and other well-test results, such as buildup tests and multiple flow rate tests, for which the similarity method does not work.

The solution method also enables the ready analysis of single-phase geothermal injection tests. With more effort, (owing to the trial and error procedure required), injection tests for two-phase or dry-steam reservoirs can also be analyzed. The limited results obtained to date indicate that the SHAFT79 program is a useful tool for analyzing such tests and is much more flexible than the similarity method in terms of the types of tests, such as multiple-rate, to which it can be applied.

The simplicity of the similarity method enables lengthy (real time) calculations to be made very quickly; therefore, the similarity method provides a useful tool for parameter testing and for applying field data to investigate theoretical problems, such as the form of the relative permeability functions.

REFERENCES CITED

Garg, S. K., 1980. Pressure transient analysis for two-phase (liquid/water/steam) geothermal reservoirs. Soc. Petroleum Engin. J., v. 20, no. 3, p. 206-214.

Grant, M. A., 1978. Two-phase linear geothermal pressure transients: A comparison with single-phase transients. New Zealand J. Sci., v. 21, p. 355-364.

Grant, M. A., 1979. Quasi-analytic solutions for two-phase flow near a discharging well. Report No. 86, Applied Mathematics Division, D.S.I.R., Wellington, New Zealand.

Grant, M. A., and Sorey, M. L., The compressibility and hydraulic diffusivity of a water-steam flow. Water Resources Research, v. 15, no. 3, p. 684-86.

Moench, A. F., 1979. Radial steam flow in two-phase geothermal reservoirs--Comparison of analytical and finite-difference solutions for transient pressure drawdown. Presented at California Regional Meeting Society of Petroleum Engineers of AIME, Ventura, California, April 18-20, 1979, SPE-7959.

Moench, A. F., and Atkinson, P. G., 1978. Transient pressure analysis in geothermal steam reservoirs with an immobile vaporizing liquid phase. Geothermics, v. 7, no. 2-4, p. 253-264.

O'Sullivan, M. J., 1980. A similarity method for geothermal well test analysis. Berkeley, Lawrence Berkeley Laboratory, LBL-10968. (To be published in Water Resources Research.)

O'Sullivan, M. J., and Pruess, K., 1980. Analysis of injection testing of geothermal reservoirs. In Proceedings of the Annual Meeting, Geothermal Resources Council, Salt Lake City, Utah, Sept. 9-11, 1980. Berkeley, Lawrence Berkeley Laboratory, LBL-10985.

Pruess, K., and Schroeder, R. C., 1979. Geothermal reservoir simulations with SHAFT79, Proceedings of the Fifth Annual Workshop on Geothermal Reservoir Engineering, Stanford University, Dec. 12-14, p. 183-188.

Sorey, M. L., Grant, M. A., and Bradford, E., 1980. Nonlinear effects in two-phase flow to wells in geothermal reservoirs, Water Resources Research, v. 16, no. 4, p. 767-777.

Zyvoloski, G. A., O'Sullivan, M. J., and Krol, D. E., 1979. Finite difference techniques for modeling geothermal reservoirs, Num. Anal. Meth. Geomech., v. 3, p. 355-366.

Modeling of wellbore dynamics

C. W. Miller

WELBORE is a numerical model for simulating one-dimensional two-phase transient flow in a wellbore. Although models of steady-state one-dimensional two-phase flow and transient energy flow in the wellbore have been reported in the literature, work on a transient two-phase momentum and energy flow model is limited. A transient model aids in understanding the wellbore flow during a well test. It is needed to study the interaction of fluid flow in the wellbore and the reservoir when transients in the bore are still important. A transient model can also determine the sandface flowrate during a well test when wellbore storage is important.

The development of the WELBORE program has been reported in previous years. A description of the numerical model is given in Miller (1979). However, the model assumed no slip between the phases, the friction factor was kept at a constant value, and the wellbore model was connected only to a liquid-filled reservior. Although slip between the phases is an important effect that must be considered, it was still possible to investigate the effect in the bore of nonuniform pressure transients that occur with time when a flowrate change is made at wellhead on the downhole pressure change. It was also possible to study the effect of the nonisothermal changes in the bore on the expected drawdown. This work was completed and previously reported by Miller (1979b).

ACTIVITIES IN 1980

The major work in 1980 consisted of updating the WELBORE model, which included slip between the phases and the friction factor as an empirical correlation, and connecting the wellbore model to an already developed two-phase flow reservoir model. In addition, the code was reformatted for broader accessibility to other members of the reservoir

community, and a user's manual was written for the code. The wellbore model with the single-phase reservoir flow model was made available to other users. An effort was begun to include a second component as CO_2 in the wellbore model. However, this work was postponed until a complete CO_2 water-steam equation-of-state package was available.

The addition of slip between the phases required a major change in the transient model formulation. Initially, the flow of the two-phase mixture was written in terms of an average mass velocity. An attempt was made to include the slip term by continuing to write all terms in the momentum and energy equations comprised of this mass averaged velocity plus an additional expression to account for the slip effect. Such a method fails to allow for an accurate physical representation of the flow. To correct this problem, all terms in the overall momentum and energy equations (except the transient terms $\partial e/\partial t$ and $\partial(\rho v)/\partial t$, where e is the specific energy, ρv is the mass flowrate per unit area, and t is the time) were written separately for each phase. Thus the contribution of each phase to the energy or momentum transport could be written into or out of a finite control volume. Specifically, the convection of energy out of a control volume by the liquid phase is $(\rho v)_\ell(1 - \alpha)e_\ell$ where ℓ denotes liquid and $(1 - \alpha)$ is the volume saturation of the liquid phase. Using this method it is possible to calculate the separation of the phases when the well is shut in.

The slip between the phases was determined by an empirical correlation. The flow regime map summarized by Orkiszewski (1967) gave the types of flow (bubble, slug, transition, mist) as a function of average velocity and quality. The slip in each phase was then specified. The exact expressions are given in Miller (1980a).

The friction factor was that given by Chisolm (1973). It is not written as a function of flow regime but as a function of quality and the friction factor that would exist if the fluid flow were all liquid. This empirical correlation was chosen because it was based on experiments with a steam-water mixture flowing vertically in a pipe at flowrates comparable to those found in a geothermal well. Most friction-factor correlations in the available steady-state geothermal flow models are based on oil-gas or water-air flow. It was felt that a correlation based on a steam-water experiment might better be able to model the flow in a geothermal well.

Since any transient model can be used to model the steady-state flow, the measured pressure profile in a well has been compared to the numerical calculation of that profile using WELBORE. Figure 1 shows such a comparison for well M-91 at the Cerro Prieto field. For this case, the conditions at the wellhead were input to the program, and the resultant pressure profile and downhole conditions were calculated. It is not the intent to develop a wellbore model with different options for friction factor and slip, thereby allowing the user to choose the model that best fits the data. This model, along with the selected empirical correlations, has been checked against a couple of cases in which the

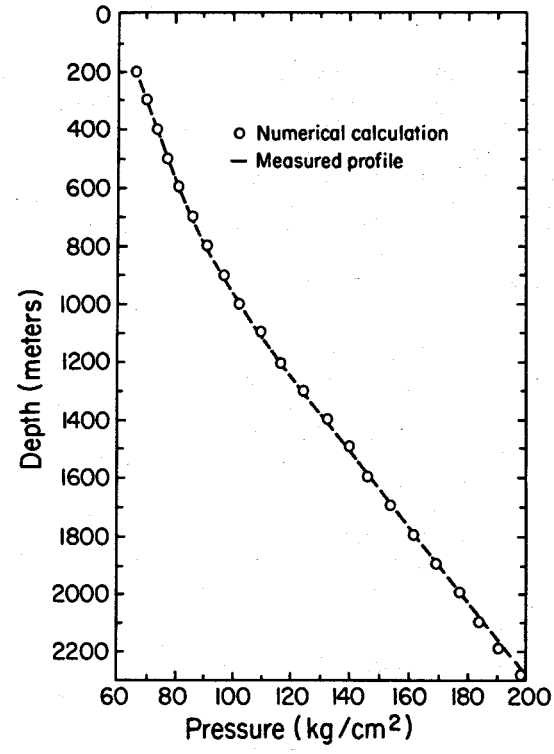

Figure 1. Pressure profile in M-91 at Cerro Prieto field. (Measured profile provided by Comisión Federal de Electricidad de México.) [XBL 8011-6421]

pressure profile was measured and has given good agreement. The program will be updated when better correlations become available.

The WELBORE program was also modified for easier use by other researchers. Several options were added that allow calculations for different boundary conditions. At the wellhead, it is possible to specify mass or volume flowrate or to give the wellhead pressure. Downhole, one can specify the reservoir flow that enters the bore by using the reservoir flow calculations or by just giving the downhole pressure as a function of time. Initial conditions that are still needed are the mass flowrate, downhole or reservoir pressure, and energy. One option includes the heat transfer from the bore to the surrounding rock.

The users' manual written by Miller (1980b) provides four examples that illustrate the problems which could be solved. Figures 2-4 show results from three of those problems. Figure 2 is a plot of both the wellhead and downhole pressure change with time for two drawdown cases where the fluid is flashing in the bore. The flowrate changes in the liquid phase reservoir were calculated along with the changes in the bore. The figure shows the pressure drop to be larger at wellhead than downhole, occurring when a flowrate increase is first made. Also illustrated here is the large difference between wellhead and downhole pressure changes: even at later times, after the flowrate change has been made, the slope of the pressure change with time at wellhead is not equal to that downhole. Over the time of these calculations, wellbore storage is

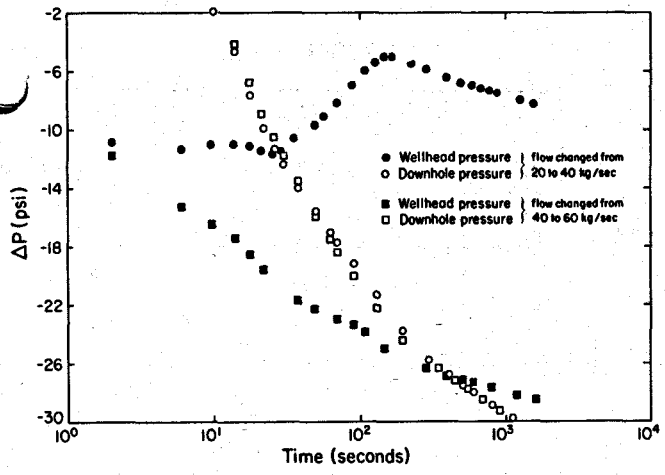

Figure 2. Comparison of wellhead and downhole pressure transients for two drawdown cases. [XBL 8011-6418]

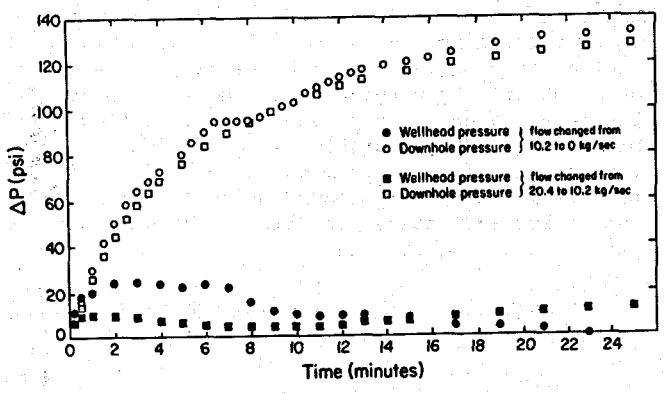

Figure 3. Comparison of wellhead and downhole pressure transients for two different buildup cases. In one case the well is shut in. [XBL 8011-6419]

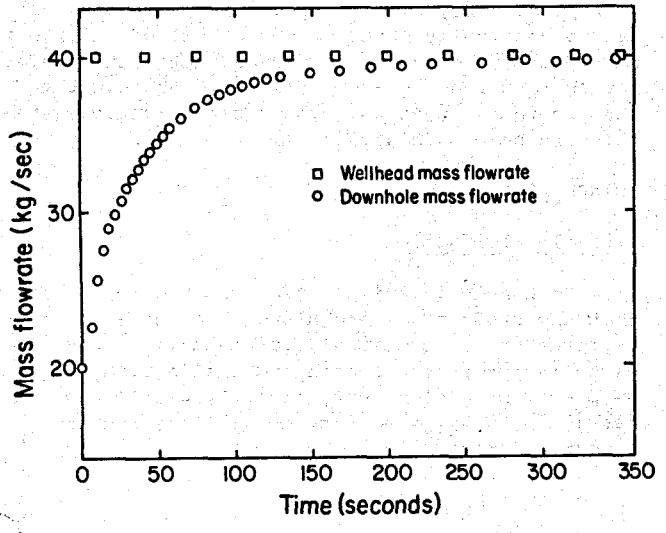

Figure 4. Calculation of sandface flowrate given the wellhead flowrate and downhole pressure. [XBL-8011-6420]

still important; therefore, a steady-state flow model would be inadequate to model the wellbore flow. (A steady-state flow model must naturally assume that the mass flow into the bore is equal to the mass flow out of it.)

Figure 3 illustrates the different pressure buildup curves that can occur when the well is actually shut in and when the flowrate is just decreased but not shut off. Because the convection terms are written separately for each phase, the program calculates the actual separation of the steam and liquid water in the bore when the well is completely shut in. However, this calculation requires a correlation for the slip between the phases, when the liquid phase is falling and only the steam phase is rising. Empirical correlations are available for this case. A slip factor approximating the size in the bubble regime was used. How this slip factor influences the results will be investigated. In any case, a slight leveling off of the pressure rise will occur during the buildup (Fig. 3). This effect results from the pressure that rises too fast in the bore when the two phases are separating out, causing the fluid to flow back into the reservoir. This calculation can be done only with a transient model.

Figure 4 shows the calculation of the sandface flowrate when a step change is made in the flowrate at wellhead. For this calculation the downhole pressure, together with the wellhead flowrate, was specified. In addition, WELBORE calculates the sandface flowrate. For this case, wellbore storage is considered complete in 14 minutes, based on criteria established in the petroleum field. This criteria, however, ignores nonisothermal effects. The program ANALYZE (Benson and McEdwards, 1980) can determine the reservoir parameters of the actual sandface flowrate. ANALYZE is a history-matching program designed to analyze interference or production data, using the actual sandface mass flowrate.

As noted above, an additional improvement is the integration of the wellbore calculation with the two-phase reservoir model of Zyvoloski and O'Sullivan (1979). The energy, momentum, and mass equations have been coupled in a manner whereby the reservoir sandface pressure is applied in the wellbore flow calculation, and the resultant flow between the reservoir and wellbore is applied in the reservoir calculation. A time-step limitation exists: large time steps are not needed to calculate the changes in the bore, since in most cases the calculations of interest involve only those events that occur during a well test. It is also easier to use a layered reservoir model when the calculation is explicit. Detailed calculations of how the wellbore flow affects a two-phase reservoir test have not been made.

FUTURE PLANS

Several problems can be investigated now that the program WELBORE includes slip between the phases and is connected to a two-phase reservoir. A layered two-phase reservoir model interacting with the wellbore is proposed, following which the injection of water into the reservoir will be studied. Also, the modeling of drawdown and buildup tests of a two-

phase reservoir is proposed to determine what provides the best measurement of reservoir conditions. Moreover, the deliverability of a well reservoir system deserves investigation to determine possible flowrates. The program will eventually be updated to include a second component.

REFERENCES CITED

Benson, S. M., and McEdwards, D., 1980. ANALYZE users' manual. Berkeley, Lawrence Berkeley Laboratory, LBL 10907.

Chisholm, D., 1973. Pressure gradients due to friction during the flow of evaporating two-phase mixtures in smooth tubes and channels. Int. J. Heat Mass Transf., v. 16, p. 347-358.

Miller, C. W., 1979. Numerical model of transient two-phase flow in a wellbore. Berkeley, Lawrence Berkeley Laboratory, LBL-9056.

____, 1980a. Wellbore storage effects in geothermal wells. Dallas, Soc. Petroleum Engin. J., v. 26, p. 555-566.

____, 1980b. WELBORE users' manual. Berkeley, Lawrence Berkeley Laboratory, LBL-10910.

Orkiszewski, J., 1967. Predicting two-phase pressure drops in vertical pipe. J. Petroleum Tech., June, p. 289.

Zyvoloski, G. A., and O'Sullivan, M. J., 1979. Finite difference techniques for modeling geothermal reservoirs. Int. J. for Num. and Analy. Methods in Geomech., v. 3, p. 355-366.

ANALYZE

S. M. Benson

ANALYZE is a history-matching program designed for pressure transient analysis of well tests in single-phase fluid-saturated reservoirs. Both interference tests and production tests can be analyzed to yield reservoir transmissivity (kh/μ), storativity (ϕch), and hydrologic boundaries. An analytic solution calculates the pressure drawdown-buildup in an idealized reservoir system. Figure 1 shows schematically the basic reservoir-well model assumed by computational algorithm. The reservoir is assumed to be an isothermal, isotropic, homogeneous, porous medium of constant thickness and infinite areal extent. The production well is modeled as a line source which fully penetrates the reservoir thickness. The flow into the well is assumed to be purely radial and uniformly distributed over the height of the well (gravity effects neglected).

The unique feature of the matching program is an analytic solution which calculates drawdown-buildup caused by arbitrarily variable flow rates from one or more production wells. Flow rates are modeled by superposition of consecutive "production pulses." The flow rate within any "production pulse" may be constant or vary linearly with time.

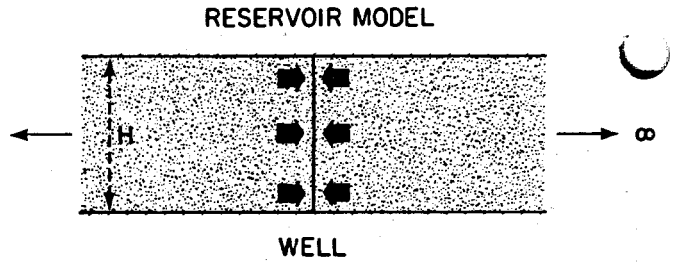

Figure 1. Schematic of the well-reservoir system. [XBL 813-2722]

Any variable flow rate history can be modeled to the desired accuracy by a series of sequential straight lines, each of the appropriate duration and inclination.

The implementation of this technique allows the simultaneous analysis of pressure data for up to 20 observation wells, each influenced by the production (and/or injection) of as many as 20 wells with arbitrarily varying flow rates. Pressure data can be analyzed for the reservoir properties, transmissivity (kh/μ), storativity (ϕch), and a single vertical linear reservoir boundary. If the ϕch product is known for production well analysis, a skin value indicative of wellbore damage or enhancement may also be obtained.

A nonlinear least-squares matching routine minimizes

$$\chi^2 = \frac{1}{N} \sum_{n=1}^{N} \left(\frac{\Delta p_{calc} - \Delta p_{obs}}{\Delta p_{obs}} \right)^2, \qquad (1)$$

where N = # of observation wells, Δp_{calc} = calculated pressure change, and Δp_{obs} = observed pressure change which is functionally dependent on the reservoir parameters, well configuration, and flow rates. By systematically changing the specified reservoir parameters, the χ^2 sum is reduced until the minimization requirements are satisfied. At this time, the program assumes that the correct reservoir parameters have been attained.

METHODOLOGY

Variable Flow Rate

To handle a variable flow rate, q(t), we assume that any production rate history can be adequately represented by sequential, straight-line segments, each of appropriate length and inclination (Fig. 2). We prescribe q(t) to vary linearly within each interval τ_k to τ_{k+1}; so for the kth line segment, q_k can be written

$$q_k = A_k + B_k (\tau - \tau_k). \qquad (2)$$

The drawdown, $\Delta p_k(t)$, caused by a variable production rate q_k is given by the line source solution (Carslaw and Jaeger, 1959):

$$\Delta P_k(t) = \frac{\mu}{4\pi kh} \int_{\tau_k}^{\tau_{k+1}} \frac{q(t)}{t-\tau} \exp\left(\frac{-r^2}{4\eta(t-\tau)}\right) d\tau. \quad (3)$$

Since q(t) is known from equation (2), the integration of equation (3) may be carried out. A closed-form solution of this integration is available and a full development is given in Benson and McEdwards (1980) and McEdwards (1981). The solution is

$$\Delta P(k) = \frac{\mu}{4\pi kh}\Big\{[A_k + B_k(t-\tau_k)(1+U_k)][W(U_k) - W(U_{k+1})] - B_k[(t-\tau_k)\exp(-U_k) - (t-\tau_{k+1})\exp(-U_{k+1})]\Big\}, \quad (4)$$

where

$$U_k = \frac{\mu\phi c r^2}{4k(t-\tau_k)}, \quad U_{k+1} = \frac{\mu\phi c r^2}{4k(t-\tau_{k+1})}, \text{ and}$$

$$W(U) = \int_U^\infty \frac{\exp(-y)}{y}\, dy.$$

The pressure response of one well is calculated by summing the pressure response of each production pulse.

Multiple Production Wells

To calculate the pressure response caused by several production-injection wells, the drawdown-buildup attributable to each well is calculated and then summed. Each production well may have an arbitrary set of unique flow rate data. Equation (4) and the principle of superposition form the basis for all pressure calculations in ANALYZE. With the above equations, multiple wells with variable flow rates and reservoir boundaries can be rigorously accounted for in the pressure calculations.

Hydrologic Boundaries

A single, fully penetrating linear hydrologic boundary can be modeled using the method of images. Briefly stated, a boundary may be viewed and modeled as a line of bilateral symmetry about which image production wells are arranged in one-to-one symmetric correspondence with real production wells (Fig. 3). To model an impermeable boundary, each image well is assigned a flow rate record identical to its symmetrically located real well. This results in zero pressure gradients perpendicular to the line of symmetry at the line of symmetry. A constant potential boundary is modeled using image wells whose production-injection records are identical to their symmetric counterparts but are of opposite sign (production versus injection). This situation results in zero pressure changes along the line of symmetry which is the necessary mathematical condition for a constant potential boundary of infinite horizontal extent. The image wells that model a boundary contribute an additional component to the calculated pressure change, which is parametrically dependent on the values of kh/μ and ϕch. Thus, for each iteration in which a boundary is being searched for, there are four parameters that can be changed: kh/μ, ϕch, r_{image}, and α.

Production Well Skin Effect

The calculated pressure response in a production well may also include an additional component due to the skin effect. The skin effect is defined as the steady-state pressure change due to an annular zone of enhancement or damage around the wellbore (Beals, 1966). The component of pressure change due to the skin is expressed in equation (5), where s is the skin value

$$\Delta P_{skin} = s\,\frac{q\mu}{2\pi kh}. \quad (5)$$

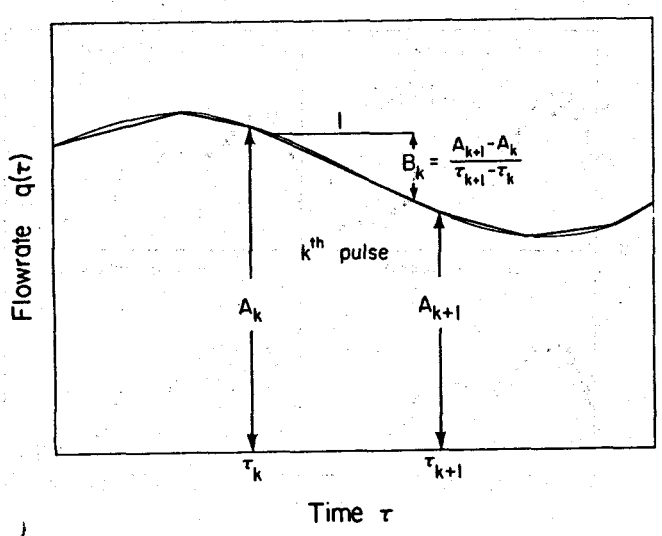

Figure 2. Pulse representation of a variable flow rate. [XBL 792-485]

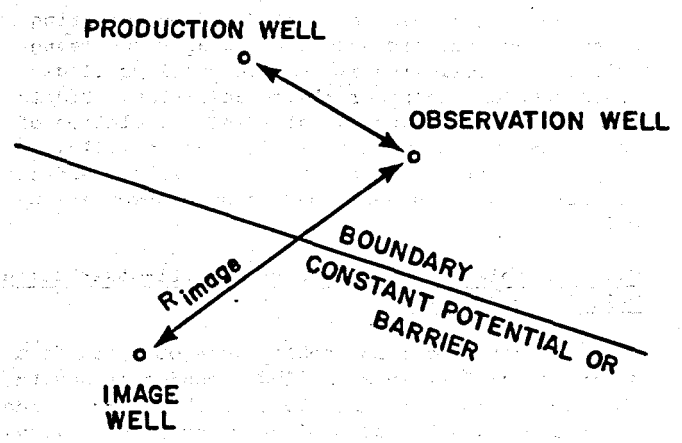

Figure 3. Schematic of image well locations for modeling hydrologic boundaries. [XBL 813-2186]

A positive skin value is indicative of wellbore damage; a negative skin value is an indication of wellbore enhancement.

Least Squares Minimization

The scalar χ^2 measures the agreement of the calculated pressure response with the observed pressure response. The analysis technique aims to determine the reservoir parameters, for which χ^2 is the smallest, by changing the initial parameter values to those values which interactively reduce the value of χ^2. The minimization process uses the least-squares program LSQVMT, a nonlinear fitting routine. For a more complete discussion of the minimization algorithm, see Beals (1966).

A simplified expression of the minimization statistic is shown in equation (6)

$$\chi^2 = \frac{1}{N} \sum_{n=1}^{N} \left(\frac{\Delta P_c(n) - \Delta P_o(n)}{\Delta P_o(n)} \right)^2 . \qquad (6)$$

This formulation has an advantage over a logarithmic minimization statistic because both positive and negative pressure changes can be considered simultaneously. This allows the combination of injection and production data in a single analysis. The difference between the calculated and observed pressure is normalized to the observed pressure change in order to give equal weight to all pressure data, regardless of the absolute magnitude of the response. The equal-weight feature is also implicit in conventional type curve matching. The sum of the difference between the observed and calculated points is averaged over the total data points in the analysis. This averaging allows comparison of results from several analyses with differing numbers of observation points. The absolute magnitude of χ^2 is not the only determinant for success of a particular analysis. The absolute magnitude of χ^2 is a function of the accuracy of the data and the values of the reservoir parameters. Beals (1966) discusses the minimization procedure in detail.

SAMPLE PROBLEMS

The program has been validated by comparing it to numerous analytic models (McEdwards and Tsang, 1977). The following two sample problems illustrate some of the program's capabilities. Sample problem 1 demonstrates a full-field simulation of an injection test with four observation wells. Sample problem 2 analyzes the interference effects of four production wells on a single observation well.

Sample Problem 1. Variable Rate Multi-observation Well-Injection Test

The data for this problem were obtained from an injection test in a shallow groundwater aquifer. The aquifer is approximately 20 m thick and bounded above and below by clays of very low permeability. An array of observation wells were drilled to monitor the effects of injection (Fig. 4) and to obtain estimates of reservoir permeability, porosity, and compressibility. Many difficulties were encountered

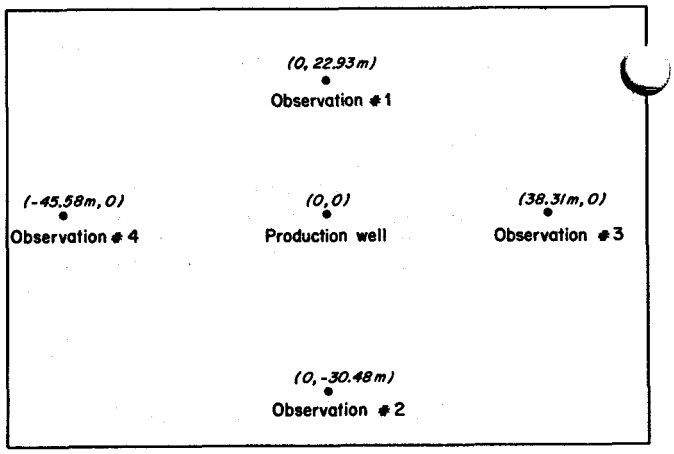

Figure 4. Well location for sample problem 1. [XBL 805-946]

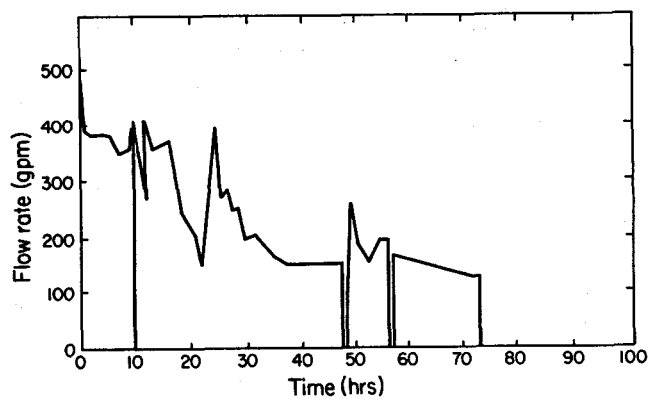

Figure 5. Flow rate history for the injection well in sample problem 1. [XBL 813-2723]

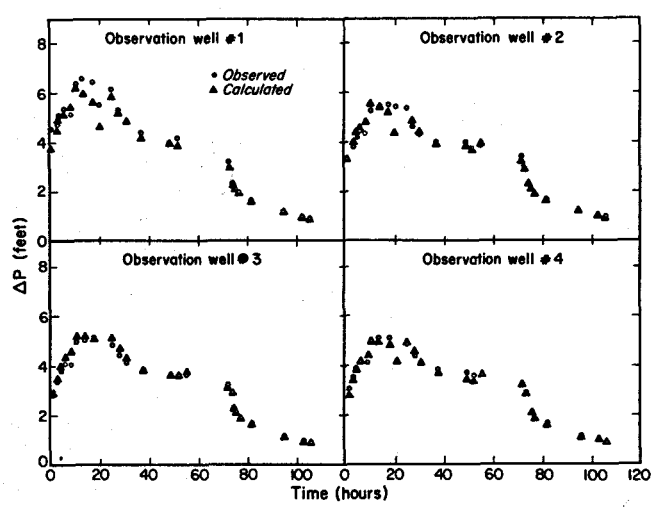

Figure 6. Match of observed and calculated water level data for sample problem 1. [XBL 805-947]

during the test, resulting in a highly variable flow rate (Fig. 5).

Interference data from each well were analyzed individually and initial estimates of the reservoir parameters were input for the full-field analysis. The match of observed and calculated pressure data is shown in Figure 6. For this problem, $kh/\mu = 8.21 \times 10^{-7}$ $m^3/Pa\text{-}s$, $\phi ch = 1.72 \times 10^{-7}$ m/Pa, d = 239 m, and α = 3 degrees (the angle to a line which is perpendicular to a boundary).

Sample Problem 2. Multiple Production Well Interference Test

The following data were obtained from a high-temperature, single-phase liquid reservoir used for electrical power generation. The reservoir is a sedimentary deposit of sands, clays, and shales. The total reservoir thickness is not precisely known, but the central part of the reservoir is believed to be at least 100 m thick. The wells tested range in depth from 2000-3000 m and have open intervals of 100-200 m. This interference test was conducted with four production wells that were being developed for the first time. Therefore, flow rates were gradually stepped up to the maximum rate, held constant for several days, then reduced to a slow bleed. An accurate account of the production schedule was maintained for each well. The flow rate of each production well and the pressure response at the observation well are shown in Figure 7.

The comparison of the calculated and real pressure drops is shown in Figure 8. Although not perfect, the fit is acceptable. Separate analyses of both the drawdown and buildup data were to determine if a reservoir boundary was influencing the pressure drops. Similar values of kH/μ and ϕch were obtained for both the drawdown and buildup data, indicating that no boundary was influencing the pressure response.

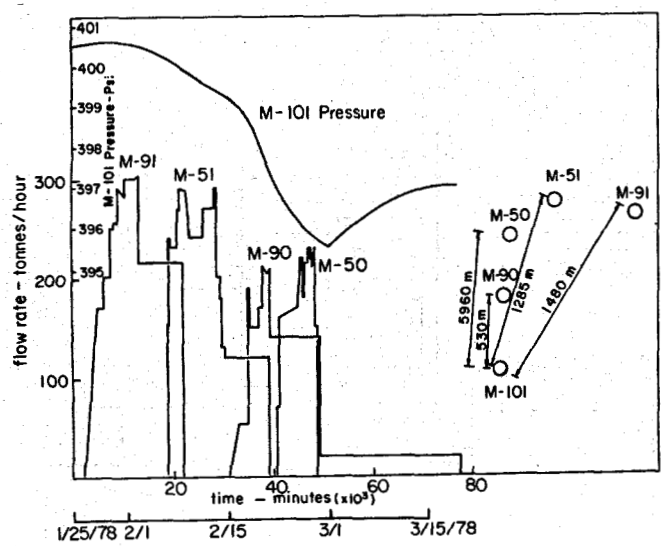

Figure 7. Flow rate and pressure data for sample problem 2. [XBL 792-7383]

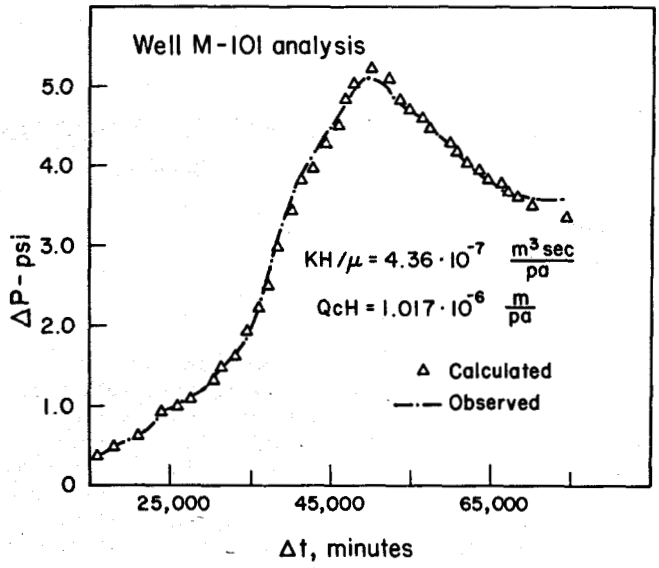

Figure 8. Match of calculated and observed pressure drops for sample problem 2. [XBL 786-1097]

REFERENCES CITED

Beals, E., 1966. VARMIT, a computer program for variable metric minimization, No. E4, BKY-VARMIT, Berkeley, Computer Center Library, Lawrence Berkeley Laboratory.

____, 1966. LSQVMT, a computer program for non-linear least-squares procedure, No. E2, BKY-LSQVMT. Berkeley, Computer Center Library, Lawrence Berkeley Laboratory.

Carslaw, H. S., and Jaeger, J. C., 1959. Conduction of heat in solids (2nd ed.). New York, Oxford University Press, p. 258-262.

McEdwards, D. G. and Tsang, C. F., 1977. Variable rate multiple well testing analysis. In Proceedings, Invitational Well Testing Symposium, Berkeley, California, October 19-21, 1977. Berkeley, Lawrence Berkeley Laboratory, LBL-7027.

McEdwards, D. G., 1981. Multiwell variable rate well test analysis (Ph.D. dissertation). Berkeley, Lawrence Berkeley Laboratory, LBL-9459.

McEdwards, D. G., and Benson, S. M., 1981. User's manual for ANALYZE--A variable-rate, multiple-well, least-squares matching routine for well-test analysis. Berkeley, Lawrence Berkeley Laboratory, LBL-10907.

ADVANCES IN THE DEVELOPMENT OF TRANSIENT WELL-TESTING EQUIPMENT

Overview

S. M. Benson

The Geothermal Group of the Earth Sciences Division has been involved in geothermal well testing since 1975. Experience indicates that the effects of high temperatures and of temperature changes on the behavior of downhole instrumentation have limited the use of conventional well-testing equipment developed by the petroleum and groundwater industries. Consequently, several alternatives to conventional well-testing equipment have been explored. Among these was a downhole chamber and capillary-tube system (Sperry Sun Pressure Transmission System) which uses nitrogen gas or helium to transmit downhole pressure transient data to the surface. This method has the advantage that no downhole electronics or transducers are required and that a continuous surface read-out of downhole pressure is possible (Narasimhan et al., 1978). The disadvantage of this system, not identified until it had been used in the field on numerous occasions, is that temperature changes which take place along the length of the capillary tubing obscure transmission of the downhole pressure response to the surface (Miller and Haney, 1978; Miller, 1980). This causes pressure-transient data obtained by this method to be inaccurate and unsuitable for conventional well-test analysis.

Recognizing the need for reliable instruments suitable for geothermal environments, Lawrence Berkeley Laboratory (LBL) has developed a suite of low (110°C) and moderate (200°C) temperature well-testing equipment. Emphasis has been placed on using off-the-shelf components and transducers that have been developed by various industries for a variety of high-temperature, high-pressure applications. The components have been combined into instrumentation packages which provide the measurement of key downhole quantities for determining the physical parameters of geothermal reservoirs (i.e., pressure, temperature, and flow as a function of depth and time).

Geothermal reservoirs are unique in so far as they occur in geologically complex environments. Typically, a wellbore in a geothermal reservoir will intersect several dominant producing strata or fractures. Wellbore flow surveys (spinner surveys) are required to locate these fractures and/or dominant production zones. Spinner surveys have also been used to determine the flash depth in a wellbore. Temperature profiles in the wellbore are necessary to identify convective and conductive thermal regimes within the reservoir and wellbore. Pressure surveys, in conjunction with temperature surveys, are used to determine whether the reservoir fluid is a single-phase liquid (steam) or a two-phase mixture of steam and water.

Pressure-transient testing is the most accurate and commonly used method of obtaining estimates of the in-situ reservoir transmissivity and storativity. Pressure-transient data analysis is also used to determine the properties of the near-wellbore reservoir formation. Since the temperature of the fluid in the wellbore varies with depth and may change during the test, it is essential to have downhole-pressure data to obtain accurate pressure-transient data. Wellhead data are inadequate because of temperature changes along the wellbore and at the wellhead.

Well-test instrumentation that is suitable for geothermal application must be stable and provide repeatable data throughout a wide temperature range (ideally 80-315°C). It is not sufficient to have components which provide accurate data at a single temperature; nonisothermal temperature-dependent behavior of the components must be correctable. The use of microcomputers has tremendous potential in the development of these tools because it allows for the automatic real-time correction of nonlinear and linear, nonisothermal, temperature-dependent transducer properties. For this reason, and because of the flexibility to be gained in the storage, manipulation, and processing of data, LBL has developed a data acquisition system centered around a DEC LSI 11 microcomputer.

A schematic of the computerized data acquisition system is shown in Figure 1. The system itself is applicable to any type of instrumentation which has an electronic output, be it a frequency, resistance, or voltage signal. The signals from the tools are multiplexed and input to the appropriate measurement device by a scanner. The microprocessor reads the signal from the selected device, either

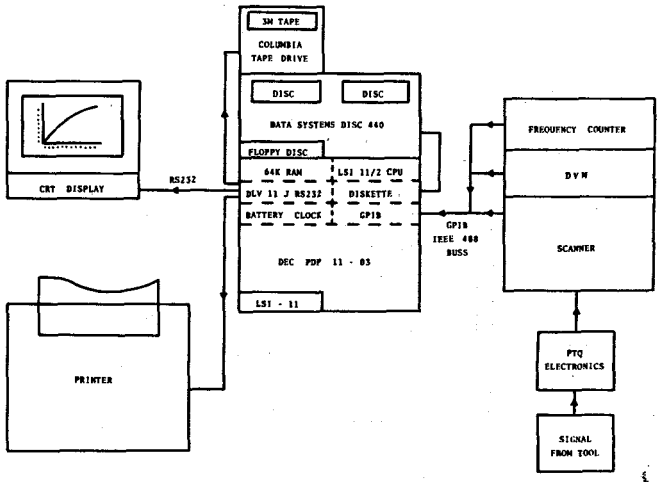

Figure 1. Schematic of computerized data acquisition system. [XBL 812-2665]

the digital volt meter or a frequency counter. The data are then processed, displayed, stored, and printed out. The system is extremely flexible; it is applicable to various types of well-testing activities and is controlled by a real-time operator. Because the LSI 11 can be operated in a foreground/background mode, it can be programmed with data acquisition as its first priority, but real-time data analysis can take place concurrently.

This system has been used for several applications, two of which are summarized below. The article entitled "The LBL PTQ Tool" discusses a wellbore-flow survey and pressure-transient well-testing tool. The PTQ tool simultaneously measures downhole pressure, temperature, and fluid velocity at temperatures up to 200°C. In addition to storing the data, the microcomputer is used to calculate the temperature correction of the signal from a strain-gauge pressure transducer. Temperature data, measured by an RTD (Resistance Temperature Device) are calculated with a spline curve fit to factory specifications for the transducer. The next article, "A Downhole Pressure/Temperature Probe for Low Temperature Application," discusses how the system is used in conjunction with an interference/production test monitoring system for applications up to 107°C.

Tremendous advances have taken place in the design and availability of instrumentation and components suitable for geothermal application. Instruments for obtaining pressure-transient data with a high degree of accuracy and resolution and with real-time surface read-out are now available for applications in downhole environments up to 200°C. There are, however, two major obstacles to the development of instruments which will function at temperatures greater than 200°C, but both are being worked on by various private companies. The first is that electronic pressure transducers with the desired accuracy and resolution are not available for use at temperatures higher than 200°C. It must be emphasized that it is important not only that the transducer be operable at these higher temperatures, but that the transducer remain stable when the temperature changes.

The second obstacle is the lack of electronic components which are operable and stable above 200°C. At the present time, Sandia National Laboratory is developing a variety of electronic components, including a downhole multiplexer which will be rated for continuous use to 275°C (Veneruso, 1980). The advantage of having a high-temperature multiplexer is that it allows instruments which usually would be run on a multiconductor cable to be run on a single-conductor cable. There are several advantages to using single-conductor cable, the most important being that single-conductor cable rated for continuous use at 300°C is available from commercial suppliers.

In coming years, effort will be concentrated on modifying the instruments now in use so that they will perform reliably at temperatures up to 315°C. As part of this effort, we are making a passive temperature tool which will be rated for continuous use up to 300°C. A spinner tool, developed by LBL, has also been modified so that there are no electronic limitations to operating the tool at 300°C. Nonelectrical difficulty may arise at these high temperatures, but they should be identified during field testing. Pressure transducers suitable for this type of application are being laboratory tested to determine how the output of the transducer is affected by elevated temperatures and by temperature changes. When a suitable transducer is identified, it can be incorporated into a downhole pressure probe. The use of microcomputers will prove to be invaluable now that real-time calibration of various types of components is possible. Such calibration allows for increased flexibility in that transducers which have nonlinear temperature-dependent behavior may still be suitable, since such behavior can be corrected by appropriate computer calculations.

REFERENCES CITED

Miller, C. W., 1980. Correcting surface pressure to reflect downhole pressure changes measured with a fluid-filled capillary tube. J. Petrol. Tech., v. 32, p. 2020-2022.

Miller, C. W., and Haney, J., 1978. Response of pressure changes in a fluid-filled capillary tube. Berkeley, Lawrence Berkeley Laboratory, LBL-8883.

Narasimhan, T. N., Schroeder, R. C., Goranson, C. B., and Benson, S. M., 1978. Results of reservoir engineering tests, 1977, East Mesa, California. Berkeley, Lawrence Berkeley Laboratory, LBL-7091.

Veneruso, A. F., Simpson, R. S., and Arnold, C. (eds.), 1980. High Temperature Electronics and Instrumentation Seminar Proceedings, December 3-4, 1979. Albuquerque, New Mexico, Sandia National Laboratory, SAND80-0834C.

The LBL combined PTQ tool

S. M. Benson, C. Goranson, R. Solbau, and A. Biocca

Until recently, technology and methodology for geothermal well testing borrowed heavily from the oil and gas industry. But increased knowledge and experience have shown that well-testing requirements, though similar, are not the same. Both the unique hydrogeologic nature of geothermal reservoirs and the effect of high temperatures on transient well-testing equipment must be considered in the design of transient testing instrumentation for geothermal applications.

Geothermal wells are typically completed with an open interval of several hundred to thousands of feet over which permeability may be highly variable. For instance, there may be more than one dominant production zone within a single well. Thus, detailed flow vs. depth profiles are essential to correct interpretation of pressure transient data. Multiphase wellbore flow can also lead to misinterpretation of pressure transient data and wellbore surveys. Temperature, pressure, and fluid velocity measurements are required to determine the saturation profile of a well.

A moderate temperature (< 200°C) well-test tool specifically for geothermal applications has been developed at Lawrence Berkeley Laboratory (LBL). Three downhole parameters--pressure, temperature, and flow--are measured simultaneously. Off-the-shelf components were used in the downhole transducer assembly. The surface electronics that convert the analog signal to a digital display consists of a digital voltmeter, frequency counter, scanner, and microprocessor.

LBL COMBINED PTQ TOOL

The LBL PTQ tool was designed for simultaneous measurement of pressure (P), temperature (T) and flow (Q) in geothermal environments of moderate temperature (< 200°C). A combined-function tool has several advantages over single-function tools: fewer trips are required in and out of the well; simultaneous capture of all three types of data ensures uniform conditions for all parameters in a single test run; and synthesis of data is much simplified. The components of this tool are off-the-shelf transducers developed by industry for various moderate-to-high temperature environments. The components of the tool are a Bell and Howell (EL-1000-4) strain gauge, a resistance-temperature detector (RTD), and a modified Kuster flowmeter. The tool has no active electronics downhole, which eliminates the problems that arise in temperature-sensitive components.

The CEC-1000-4 temperature-compensated, sputtered strain gauge pressure transducer has a full-scale output of approximately 30 mV. Transducers are available with full-scale pressure ratings of 2500, 5000, and 10,000 psia. The rated accuracy of the transducers at 80°F is 0.25% of the full-scale reading. For the 2500 psia transducer this is 6.25 psi, which is more accurate than required for transient well testing. The resolution of the transducer has not been tested because the calibration system, a deadweight tester, is only accurate to 1 psi. The resolution is better than 1 psi and probably as good as 0.2 psi throughout the compensated temperature range.

The CEC-1000-4 2500 psia transducer is temperature compensated between 80 and 400°F. However, the accuracy of the transducer, in its factory configuration, is temperature-dependent. With increased temperature, both the full-scale mV output and the null voltage of the transducer change. These thermal effects are expressed in terms of the change in the reading as a function of the full-scale reading per °F:

Full scale output	30.538 mV
Pressure range	2500 psia
Temperature compensation	80-400°F
Zero shift	0.006% FR/°F
Full-scale sensitivity shift	0.001% FR/F
Excitation voltage	10 volts

Although the full-scale output shift and zero shift are a very small percent of the full-scale reading, the accuracy is strongly affected when a 320°F (80 - 400°F) temperature change takes place. For instance, with the transducer at its full-scale reading (2500 psi), an 8 psi sensitivity shift and a -48 psi zero shift are incurred for a 320°F temperature change.

$$\text{Pressure} = \text{FSP} \times \frac{10}{\text{EP}} \times \frac{\text{PP}}{\text{FSMV} + \frac{\text{SENSV}}{100} \times \text{FSMV}\ (T - 80°\text{F})} - \frac{\text{Zeros}}{100} \times \text{FSP}(T - 80°\text{C}), \quad (1)$$

where FSP = pressure range, PP = mV signal out, EP = excitation voltage, FSMV = full-scale mV output, SENSV = full-scale sensitivity shift per °F, Zeros = zero shift per °F. With the simple calculation, shown in Equation 1, the effects of the zero shift and the full-scale sensitivity shift can be corrected. Then, the rated accuracy of 0.25% FR can be obtained through the compensated temperature range.

The temperature transducer is a platinum RTD in a three-wire configuration whose accuracy is calibration-dependent. Based on a two-segment linear calibration, an accuracy of 1°C is obtained throughout the temperature range of the combined tool (10-200°C). Greater accuracy can be obtained using spline-curve fitting techniques; however, for initial testing of the tool, the 1°C accuracy was sufficient. The RTD is for both pressure transducer temperature correction and wellbore fluid temperature.

A modified Kuster spinner tool operates as the downhole flow meter. A magnetic reed switch located near a magnet emplaced in the rotating shaft induces a frequency proportional to the fluid velocity. The frequency signal is read at the surface by a frequency counter. Readings are reliable for a fluid velocity greater than 0.25 ft/s.

The complete tool is less than 4 feet in length and has a 2-in. O.D. (without centralizers and collars). In its combined configuration, it has been run on a 20,000 ft long seven-conductor cable. A modified seven-conductor cable head connects the tool to the cable. The spinner can be run separately on a single-conductor cable.

PRESSURE TRANSDUCER CALIBRATION

The pressure transducer was calibrated with a deadweight tester and an oven. It was necessary to immerse the transducer in oil during calibration because a small differential temperature between the pressure diaphragm and the temperature-compensating resistors can cause large errors in the pressure output. The transducer was calibrated at three temperatures: 80°F, 212°F, and 320°F. The calibration at six different pressures as a function of temperature are shown in Table 1. As can be seen, the 0.25% FR rating is obtained for all pressures and temperatures. Pressure resolution was measured by adding a 1-psi load at each calibration point. A more precise calibration can be performed if the nonlinearity of the zero-shift coefficient and the sensitivity-shift coefficient are measured and included in the computer correction. However, an absolute accuracy of 0.25% FR is adequate for most transient well-testing applications.

Table 1. Pressure transducer calibration, CEC 1000-4.

DWT*	80°F	212°F	320°F
Atm	12	15	10
539	540	544	541
1039	1045	1046	1044
1539	1542	1546	1545
2039	2039	2045	2044
2514	2514	2516	2516

*Deadweight tester

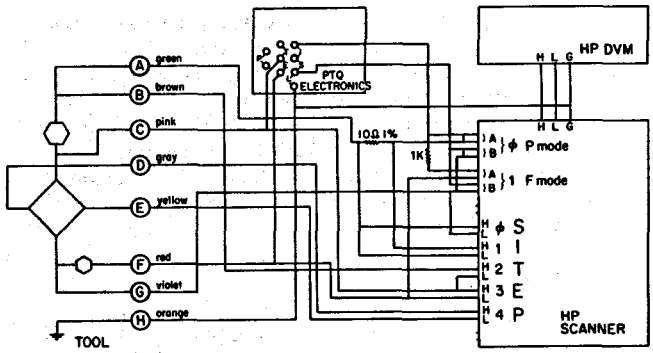

Figure 1. Wiring diagram and surface electronics for the PTQ tool. [XBL 813-2764]

SURFACE ELECTRONICS AND DATA ACQUISITION

The major obstacle in developing the present system was finding a means to supply a constant 10-v excitation to the pressure transducer. Six wires were needed to supply the voltage, regulate the voltage, and measure the transducer output. Figure 1 shows the wiring configuration. Voltage is supplied through legs A and B in the diagram. Leg A has a resistor in it which enables measurement of the current to the tool; moreover, leaks in the tool can be so detected. Legs C and F are measured to control the excitation voltage at the pressure transducer. The pressure reading is obtained from legs D and E.

The seventh leg of the seven-conductor cable provides the measurement of two additional quantities--temperature and flow. The temperature is calculated from the resistance through legs B and C. The change in resistance of the cable is measured on leg F. The frequency signal from the flow meter is transmitted to the surface on leg F.

The power supply (Fig. 1) serves two functions. First, it is designed to supply a constant 10 volts to the pressure transducer. Second, in case of computer failure, the power supply can act as a backup device from which raw pressure data (mV) and raw temperature data (ohms) can be read.

The signals from the pressure transducer and the thermistor are measured by a digital voltmeter. A frequency counter measures the signal from the flow meter.

An LSI 11 microprocessor controls the data sampling interval, storage, processing, and display. FORTRAN programs have been written which accept operational commands from the field operator. A CRT displays real-time data. A TI printer prints out data at operator-specified intervals. Table 2 shows a printout of typical test data. Data are also stored on a floppy disc which can store up to 3920 records. Depending on the time interval selected for data storage, a single disk can store between ten hours (10-s sampling) to several months (1-h sampling) of data.

The LSI 11 operating system can be programmed in a background-foreground mode. For example, this allows the computer to be programmed for the data acquisition as its highest priority. Graphic display of data or data analysis can be performed concurrently without interfering with the primary function of the system.

FIELD APPLICATION

The LBL PTQ tool has been operated in the field on several occasions. In one test, a series of pretransient testing surveys were run on a moderate-temperature geothermal well in the Imperial Valley, California. The operating environment for the surface equipment was harsh (ambient temperatures 110-120°F) and dust-laden. The dust particles caused no noticeable problems with the equipment. The high ambient temperature, however, caused equipment failure several times. This problem was resolved by maintaining the operating environment at temperatures less than 90°F.

Table 2. Printout of typical test data.

Time	P	T	Q	Tp	Pp	Ep	Ip	Sp
12:06:30	2020.3	110.4	0	2.8732	24.687	10.0033	19.930	13.1070
13:06:40	2020.5	110.4	0	2.8732	24.689	10.0034	19.930	13.1071
13:06:50	2020.6	110.4	0	2.8732	24.691	10.0034	19.930	13.1071
13:07:00	2020.6	110.4	0	2.8731	24.690	10.0034	19.930	13.1070
13:07:10	2020.8	110.4	0	2.8731	24.693	10.0034	19.930	13.1070
13:07:20	2020.8	110.4	0	2.8732	24.693	10.0034	19.929	13.1070
13:07:30	2021.0	110.5	0	2.8733	24.695	10.0033	19.929	13.1071
13:07:40	2020.9	110.5	0	2.8734	24.694	10.0032	19.929	13.1072
13:07:50	2020.2	110.5	0	2.8735	24.685	10.0031	19.929	13.1071

Three flowing surveys were run to determine pre-test conditions: a pressure log, temperature log, and spinner log. The flowing temperature log and the pressure log are shown in Figure 2. Both the temperature and pressure gradients are typical of a flowing single-phase liquid brine well. The spinner profile (Fig. 3) shows two distinct production zones, one from 4700-4750 ft and one from 5000-5100 ft.

FUTURE DEVELOPMENT

With our current equipment, the greatest disadvantage of the combined function tool is the need for a seven-conductor cable. A 200°C multiplexer, developed by Sandia National Laboratory, is being made for use with the LBL PTQ tool. This will allow the tool to be run on a standard single-conductor cable.

CONCLUSIONS

The well-test equipment described in this paper was designed to measure the three essential quantities for transient analysis of geothermal wells--pressure, temperature, and flow. Off-the-shelf, moderate-temperature components have been combined to make a practical and available testing device. A microprocessor allows for an enormous amount of versatility in choosing the type, amount, and quality of data. The system has been field tested in two geothermal wells under severe operating conditions and has demonstrated that the sophisticated measurement devices (such as DVM and frequency counter) can withstand a field-type operating environment.

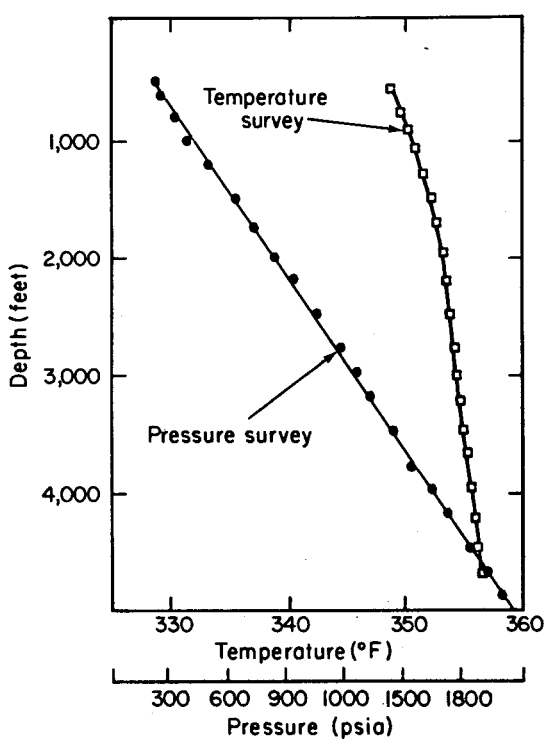

Figure 2. Temperature and pressure profile of a geothermal well. [XBL 8010-2249]

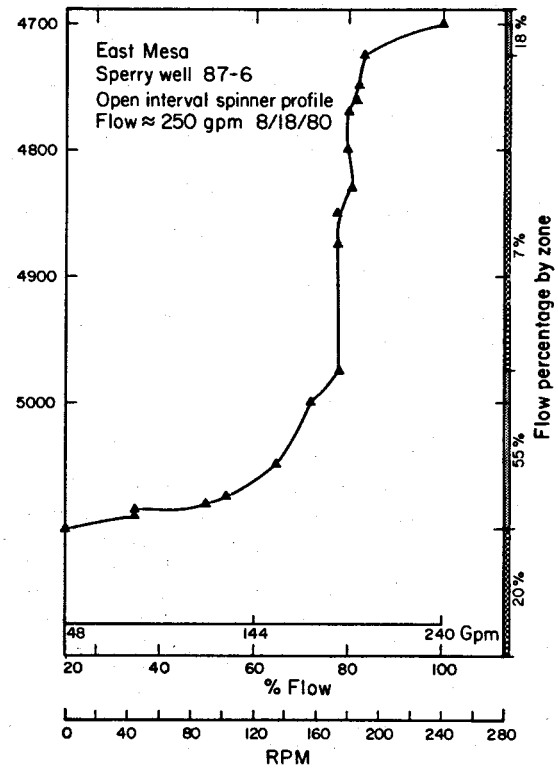

Figure 3. Spinner survey of a geothermal well. [XBL 8010-2247]

This discussion has addressed the computer equipment in conjunction with a single downhole pressure-temperature-flow device. However, such application utilizes only a few of the available channels on the scanner. Additional surface, or other downhole, measurements can be performed with the proper choice of equipment. Surface flow rates, instrumentation of interference wells, wellhead temperature, wellhead pressure, and numerous other measurements can be obtained, processed, and stored by the computer.

The computer allows for both simple and complicated data processing, including but not limited to nonlinear data calibration, stored or calculated orifice flow calculations with nonlinear orifice coefficients, complicated data analysis methods, and equation of state calculations.

A downhole pressure/temperature probe for low-temperature geothermal applications

S. M. Benson, R. Solbau, C. Goranson, and B. Galbraith

Downhole pressure transient test data are invaluable in evaluating geothermal production wells. Temperature changes in the wellbore and two-phase wellbore flow make wellhead pressure and temperature data unsuitable for standard pressure transient data analysis. The development of instrumentation for well testing in high temperature geothermal reservoirs has been hindered by the lack of high temperature transducers and electronics.

But many geothermal reservoirs of less than 150°C are also being developed for nonelectrical applications, thereby creating a need for reliable, low-cost, low- to moderate-temperature instrumentation. Unfortunately, the high cost of the probes currently available for moderate-temperature applications has limited their use. Responding to such a need, Lawrence Berkeley Laboratory (LBL) has developed and fabricated a series of relatively low cost well-testing instruments which use off-the-shelf components.

THE LBL PRESSURE PROBE

LBL has developed a low-temperature downhole pressure probe that is rated for temperatures up to 107°C. The pressure transducer is a relatively inexpensive high-precision quartz-crystal transducer manufactured by Paroscientific Inc. We have used the same transducer as a wellhead pressure gauge in interference tests. The probe contains a thermistor temperature transducer for measuring downhole temperature. The pressure probe has also been used for interference testing in nonartesian wells. The high resolution of the transducer makes it ideally suited for measuring small water level changes (1 mm) in observation wells.

DOWNHOLE INSTRUMENT PACKAGE

The downhole instrument package includes a Paroscientific 400 or 900 psi digiquartz pressure transducer. The transducer is shock-mounted and connected to a pressure port with a stainless steel capillary tool. The capillary is filled with a high-viscosity fluorosilicon fluid that is stable to 550°F. This protects the pressure port of the transducer from brine contamination. The pressure transducer is rated for continuous use at temperatures up to 107°C and has a resolution of 0.001 psi under field conditions.

The temperature element is a YSI 44011 thermistor. It is isolated from the fluid by 1/8-in.-O.D. stainless steel tubing. The thermistor has a resolution of 0.2°C and a response time of 1 s in liquids. A perforated protective housing encloses the temperature probe.

The housing for the combined tool is 9 in. in length and 2.73 in. in diameter. The housing is constructed of stainless steel. Presently, the probe requires a four-conductor cable with which it is connected via an LBL-designed cablehead. The cablehead has a length of 13 in. and a 1.5-in. O.D.

In its present configuration the quartz transducers are not temperature-compensated throughout the operable temperature range. A recent study showed that the accuracy as a function of temperature was 0.0003 psi/°C for both the 400- and 900-psi transducers (Wearn and Larson, 1980). Since the temperature is measured downhole, it should be possible to correct the transducer output for this temperature dependence. However, as a result of the small temperature sensitivity of the transducer, the temperature correction has not been necessary.

SURFACE EQUIPMENT

The Paroscientific digiquartz transducer can be operated without signal amplification for hard-wired links of up to 1 km. If the transducer is to run at a great depth in the well or at large horizontal distances to the recording van, a line driver is required to amplify the signal. LBL has designed and fabricated a line driver that provides power to the transducer from a 12-V automotive battery and transmits the frequency signal for distances up to 2.5 km on a two-conductor wire.

There are two data acquisition system alternatives. One system uses the Paroscientific model 600 digiquartz computer and a Hewlett Packard 5150A thermal printer. Pressure data can be measured and recorded at intervals ranging from 1 s to 2 hours. One computer is required for each pressure transducer, and the thermal printer can be multiplexed to accept data from two pressure transducers. The advantage of this system is that all components are off-the-shelf items. However, to expand the system requires the purchase of another computer for each transducer.

Another alternative is a central data-acquisition system that is easily expandable to include any number of transducers (Galbraith, 1980). LBL has designed and fabricated a data-acquisition system that can be used in a variety of field operations. The data acquisition system is built around a DEC LSI-1/2 microprocessor. Signals from the line drivers are read by a Hewlett Packard 5328A frequency counter. The measured frequency signals are then sent to the microcomputer where they are converted to pressure. The pressure data are then displayed on a CRT, stored on a random-access floppy disc, printed, and graphically displayed. Another advantage is that all measurements are recorded against a single clock, eliminating the need for clock synchronization.

FIELD APPLICATION

The downhole probes have operated successfully in several geothermal applications (Benson, 1980). More recently, a downhole probe was used in a production well test in Klamath Falls, Oregon. One probe was placed at a 700-ft depth, 400 ft below a shaft driver pump. A second probe was placed at a 100-ft depth in an observation well located 1000 ft from the production well. During the production test, the well flowed at a rate of 60 gpm. The fluid-discharge temperature was approximately 180°F. A pressure buildup after two hours of pumping is shown in Figure 1. The observation well showed no response due to the pumped well.

FUTURE DEVELOPMENT

The instrumentation package described here contains a very high-precision quartz pressure transducer ideally suited to small pressure changes. However, this degree of precision is not required when large pressure changes occur. As an alternative to the quartz crystal pressure gauge, temperature-compensated strain gauges are a possibility. When combined with microprocessor

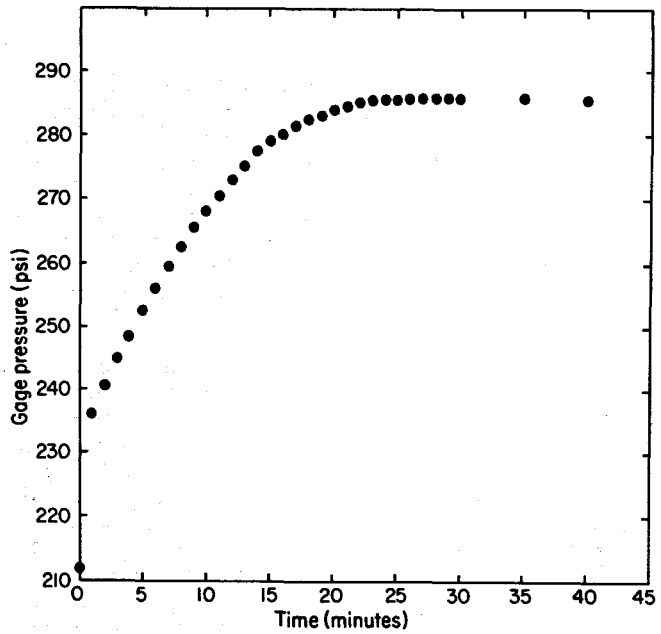

Figure 1. Pressure buildup in City Well 2, Klamath Falls, Oregon. [XBL 812-2652]

capability and/or single-application microprocessor chips, these transducers can provide a practical, cost-effective, and accurate alternative in geothermal applications (Benson, 1981).

REFERENCES CITED

Benson, S., 1981. The LBL combined PTQ tool, in Earth Sciences Division Annual Report 1980 (this volume). Berkeley, Lawrence Berkeley Laboratory, LBL-12100.

Benson, S., Goranson, C., and Schroeder, R., 1980. Evaluation of City Well 1, Klamath Falls, Oregon. Berkeley, Lawrence Berkeley Laboratory, LBL-10848.

Galbraith, R. et al., 1980. A low temperature reservoir interference test data acquisition system developed by Lawrence Berkeley Laboratory, Berkeley, Lawrence Berkeley Laboratory, LBID-317.

Wearn, R. B., and Larson, N. G., 1980. The Parascientific transducer, measurement of its drifts and sensitivities. Seattle, University of Washington, Applied Physics Laboratory, APL-UW 8011.

INJECTION INTO A FRACTURED GEOTHERMAL RESERVOIR

G. S. Bodvarsson and C. F. Tsang

At present, reinjection is a minor factor in the development of a geothermal field. Reinjection tests and small-scale wastewater reinjection have been carried out at several fields, e.g., East Mesa, The Geysers, Ahuachapan, and Otake. The limited use of reinjection can probably be attributed to the uncertainty whether premature intrusion of the injected cold water into the production region would cause a drastic reduction of production temperature. Various studies of reinjection into porous medium systems were made to address this problem (Tsang et al., 1978). It is also generally believed that if fractures are present in the geothermal reservoir, these fractures act as fast conduits for the cold, injected water to reach the production area even earlier than expected. Since all geothermal reservoirs are fractured to some exent, the effect of fractures must be understood.

To date, nonisothermal flow through fractured media has received relatively minor attention in the literature. Earlier work includes studies by Romm (1966), Bodvarsson (1969), Kasameyer and Schroeder (1976), and O'Neill (1978).

In our study we have used a well-validated numerical model that was developed recently at Lawrence Berkeley Laboratory (LBL) to make a study of hydrothermal flow in a porous medium with a few major fractures. Detailed calculations of flows in and around each fracture are made to obtain an understanding of the phenomenon. Our objective is to study the movement of the thermal (cold water) front through the fractures relative to its movement in the porous medium during injection. This would help to answer the key question of the influence of fractures on the time of cold-water breakthrough at the production area.

PROBLEM AND APPROACH

The work summarized here has focused upon an injection well that penetrates a geothermal reservoir at 300°C and having equally spaced, infinite horizontal fractures. Cold water at 100°C is injected and is allowed to enter both the formation and the fractures through the injection well bore. The temperature dependence of viscosity and density is considered, but gravity is neglected. Thus, due to symmetry, only a horizontal section of the geological geometry involving one fracture in an insulated porous medium is included in the calculations (Fig. 1). Of course, such calculations are also applicable to a single-fracture problem in which heat transfer to the caprock or bedrock is negligible.

For this study we used the three-dimensional simulator, CCC (conduction-convection-consolidation), developed at LBL. Details of the model and its validations are given by Lippmann et al. (1977), Bodvarsson et al. (1979, 1980), and Tsang et al. (1979).

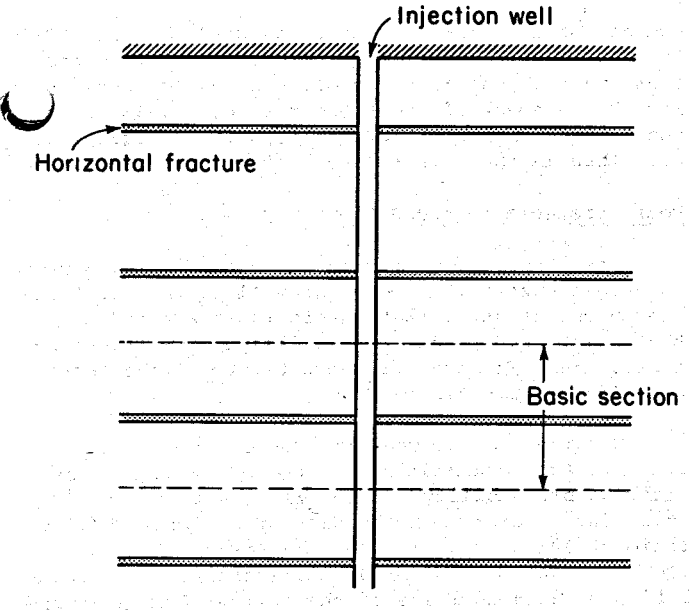

Figure 1. Schematic diagram showing the geometry of the problem and the basic section studied.
[XBL 805-7081]

CALCULATIONS AND RESULTS

Using the basic symmetry section shown in Figure 1, we consider the injection of 100°C water into a 300°C geothermal reservoir (Fig. 2). Our numerical studies consider only the lower half of the system, from fracture to lower boundary (Fig. 2), divided into 144 elements. Vertically, it is divided into six layers of varying thicknesses, from the thinnest near the fracture to the thickest far away from it. Horizontally, very fine elements are assumed near the injection well, increasing in width as a function of increasing distance from the well. An 8-in. wellbore is assumed for the injection well.

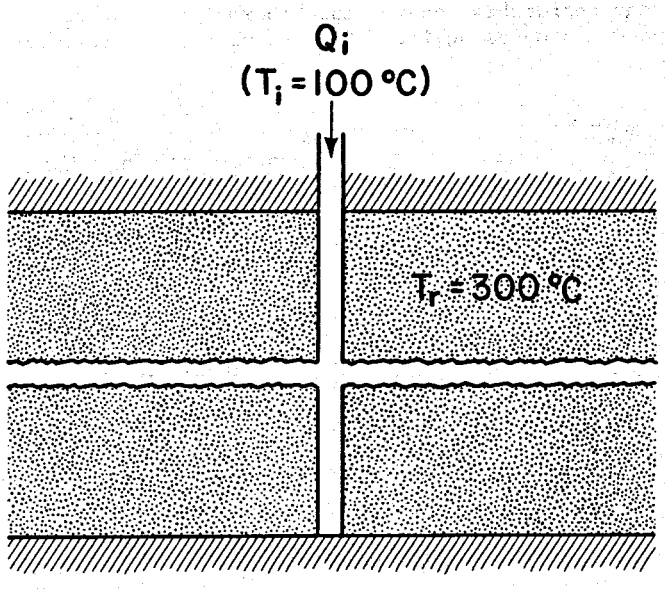

Figure 2. Injection of 100°C water into a 300°C geothermal reservoir, corresponding to the basic section shown in Figure 1. Because of symmetry, only the lower half is modeled numerically.
[XBL 806-1340]

The results are presented below in two categories: (1) rock impermeable to fluid flow and (2) rock permeable to fluid flow. Table 1 summarizes important parameter values in the computer simulations.

Table 1. Parameters used in the numerical study.

	Rock matrix	Fracture
Thermal conductivity (J/m-s-°C)	0.1-5.0	0.65
Heat capacity of solids (J/kg-°C)	1000	1000
Heat capacity of fluid (J/kg-°C)	4200	4200
Density of solids (kg/m^3)	2650	2650
Permeability (m^2)	$0\text{-}1 \times 10^{-13}$	1×10^{-10}
Specific storage (m^{-1})	5×10^{-5}	1×10^{-6}
Porosity (-)	0.01	0.40
Fracture aperture (m)	5×10^{-4}	
Fracture spacing (m)	10.0	

Rock Impermeable to Fluid Flow

Water at 100°C is injected at a constant rate into a 300°C reservoir with an "infinite" horizontal fracture. The "infinite" horizontal fracture is simulated by a large enough radial mesh such that no pressure or temperature changes were observed in the elements farthest away from the well at any time during the simulation. In this first case, the rock was assumed to be impermeable, but heat transfer by conduction was allowed between the fracture and the rock medium. Heat within the fracture was transported by both thermal conduction and convection. Several values of thermal conductivity were used to study that effect, but all other parameters remained the same.

Figure 3 shows the location of the thermal front represented by the 200°C temperature contour after 1.2 days of injection for three of the cases (thermal conductivity 0.1, 1.0, and 5.0 J/s-m-°C). The figure shows, as one would expect, that the higher the thermal conductivity of the rock, the less distance the thermal front advances radially along the fracture and the more it penetrates the impermeable rock medium. It is clear that, even with conduction alone, a substantial retardation is observed in the advancement of the front along the fracture.

Figure 4 shows the cumulative areal velocity of the thermal front versus the thermal conductivity of the rock matrix for two values of time. The curves indicate that there may be an exponential relationship between the thermal conductivity and the areal velocity of the front.

Figure 4 also shows that the cumulative areal velocity of the thermal front is not independent of

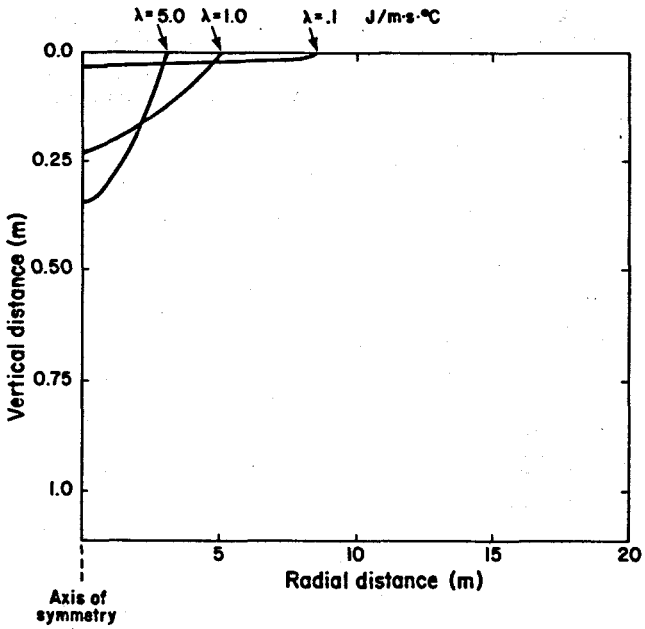

Figure 3. The position of the thermal front (the 200°C contour) at t = 1.2 days for different values of thermal conductivity. Case of zero rock permeability. [XBL 806-1335]

time (or equavalently the thermal front location) as one would expect from a simple radial flow system. O'Neill (1978) also found this to be true for the one-dimensional case. This behavior can be explained when one considers the surface area of the fracture, through which conductive heat loss takes place as a function of time. During injection, the

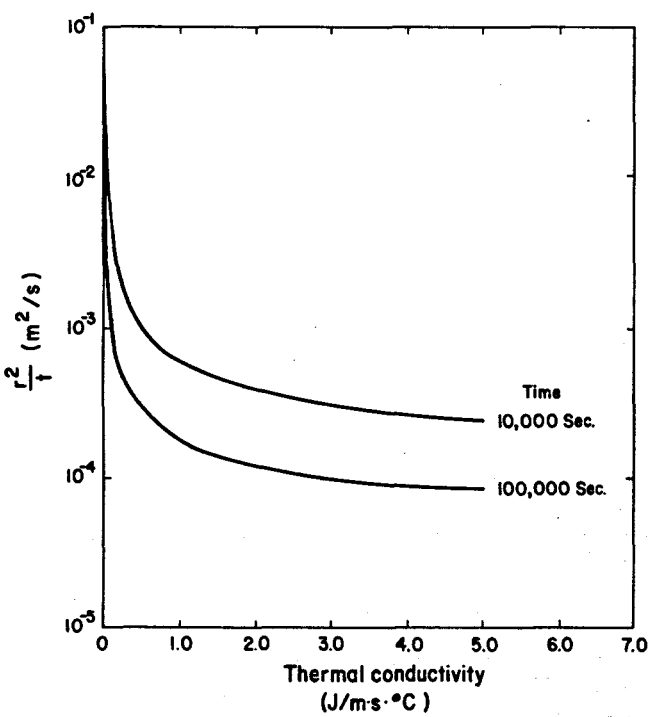

Figure 4. Thermal front cumulative areal velocity in the fracture as represented by R^2/t, where R is the radial position of the thermal front (at 200°C). [XBL 806-1336]

contact area between the injected cold water and the fracture rock surfaces increases with time and consequently heat transfer also increases, retarding the movement of the thermal front. This phenomenon is of course much more drastic in the radial case than in the linear case.

Rock Permeable to Fluid Flow

When the rock medium is permeable, the injected water penetrates the medium as well as the fracture. The amount of water that enters the fracture and the formation depends on their respective transmissibilities. The thermal conductivity of the rock was fixed at 2.0 J/m-s-°C.

Varying the permeability ratio between the fracture and rock medium, we studied several cases with the permeability of the fracture set at 10^{-10} m^2 or 100 darcies. In the first run a permeability ratio of 10^4 was used; i.e., the permeability of the rock was 10^{-14} m^2 or 10 millidarcies. The cumulative areal velocities of the thermal fronts in the fracture and the rock for this case are shown in Figure 5. For a simple constant-injection-rate radial-flow system, the areal velocity again is expected to be a constant. This figure shows that the areal velocity of the thermal front in the fracture is more than one order of magnitude greater than in the rock at early times. As injection continues, the speed of the fracture thermal front decreases exponentially but begins to level off after about 10 days of injection. The rapid decrease in the areal speed of the thermal front in the fracture with time can be explained by the increasing thermal conduction and convection between the fracture and the rock medium.

The areal velocity of the thermal front in the rock, on the other hand, increases as injection proceeds, probably due to cooling effects from the fracture fluids. However, when the rock thermal front approaches the fracture thermal front, its speed decreases again. After that, the fronts move

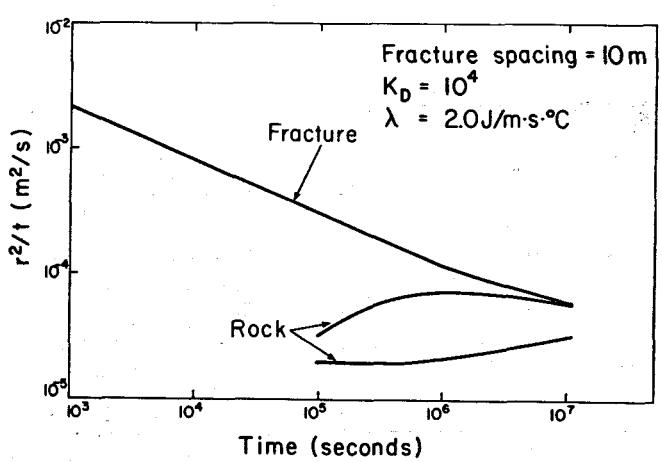

Figure 5. Thermal front cumulative areal velocity. Two curves are shown for the thermal front velocity in the rock. The upper one corresponds to a constant vertical distance of 0.1 m from the horizontal fracture and the lower curve to 3.3 m from the fracture. [XBL 805-941]

at virtually the same speed at all times. The lack of data for the areal velocity in the rock at early times is due to the space discretization used in the study. We have defined the thermal front as the 200°C isotherm; and, at early times, the first rock elements have not cooled down sufficiently to allow accurate determination of the location of the 200°C isotherm.

The most interesting characteristic of the curves shown in Figure 5 is the convergence of the different curves to each other, which means that the thermal front in the rock will catch up with the thermal front in the fracture, and eventually they will advance together. Further studies will be made to confirm this result.

In the second run, we decreased the permeability ratio to 10^3. The results are basically similar to the results of the case shown in Figure 5, but the areal speed of the thermal front is less at all times, due to the increased permeability of the rock. Consequently, there is a relatively lower flow rate along the fracture. Figure 6 shows, in this case, the contour of the thermal front in the system at a number of times. At early times, the thermal front in the fracture is well ahead of the one in the rock. Eventually, however, the two fronts almost coincide. In this case, it is of interest to note that at only 23 m from the injection well, the thermal front in the rock has almost caught up with the front in the fracture.

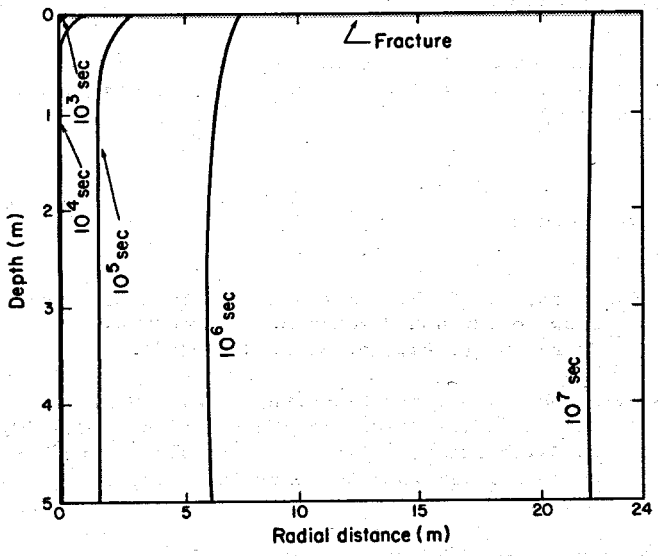

Figure 6. Contours of thermal front (200°C isotherm) at different times for a permeability ratio of 10^3. [XBL 805-7080]

ANALYTICAL WORK

In order to verify our numerical results, an analytical study was performed. Lauwerier (1955) solved analytically the problem of the effect of thermal conduction on the movement of the thermal front in a horizontal layer. In his model, Lauwerier assumed a steady linear fluid flow in a horizontal layer of thickness h, bounded by impermeable, thermally conductive medium on both sides. Gringarten and Sauty (1975) adopted Lauwerier's solution for radial flow and obtained the following expression for the fluid temperature in the horizontal layer:

$$\frac{T_o - T_w}{T_o - T_i} = \mathrm{erfc}\left[\frac{(\rho_w C_w)^2}{K_R \rho_R C_R}\left(\frac{q^2}{\pi r^2}\right)\left(t - \frac{\rho_a C_a}{\rho_w C_w}\frac{h\pi r^2}{q}\right)\right]^{-1/2} . \quad (1)$$

All of the parameters in equation 1 are defined in Table 2.

Table 2. Parameters used in analytical work.

Density of solids, ρ_S	2650 kg/m^3
Heat capacity of solids, C_S	1000 J/kg-°C
Density of water, ρ_W	800 kg/m^3
Heat capacity of water, C_W	4200 J/kg-°C
Thermal conductivity of rock, K_R	0.001-100-J/m-s-°C
Density of rock, ρ_R	2500kg/m^3
Heat capacity of rock, C_R	800 J/kg-°C
Fracture aperture, h	0.001 m
Flowrate, q	1.25×10^{-4} m^3/s
Porosity, ϕ	0.40

By defining the thermal front as

$$T_w = \frac{1}{2}(T_i + T_o), \quad (2)$$

one can derive an expression for the advancement of the thermal front:

$$t_{TF} = \frac{\rho_a C_a}{\rho_w C_w}\left(\frac{\pi h r^2}{q}\right) + (4.34)\frac{K_R \rho_R C_R}{(\rho_w C_w)^2}\left(\frac{\pi r^2}{q}\right)^2 . \quad (3)$$

The first term on the right side of equation 3 denotes the advancement of the thermal front in a fracture when no conductive medium is present (Bodvarsson, 1969). The second term on the right side of this equation denotes the effect of thermal conduction on the movement of the thermal front along the fracture.

Using the parameters shown in Table 2, the curves shown in Figure 7 were generated. Figure 7 shows that at early times the thermal front advances along the fracture at a constant rate corresponding to the first term in equation 3. Later on, however, the areal velocity movement of the thermal front along the fracture rapidly decreases due to the effect of conductive heat transfer from the rock to the fracture fluids. The higher the thermal conductivity, the sooner the curve divides from the mother curve. It is of interest to note that, for

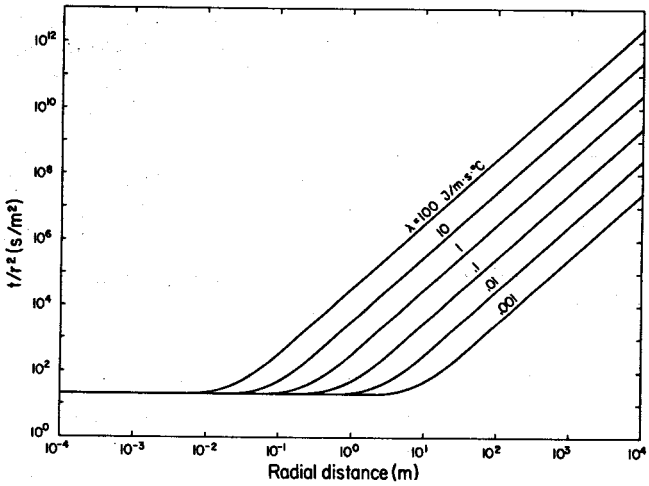

Figure 7. Areal velocity of the thermal front in the fracture based on Lauweriers (6) model.
[XBL 809-2773]

a reasonable value of the thermal conductivity (2.0 J/m-s-°C), the areal velocity of the thermal front in the fracture at a radial distance of 100 m is only about 10^{-7} m^2/s. This corresponds well with results from our numerical studies. Figure 8 shows the effects of the fracture porosity on the movement of the thermal front in the case of thermal conductivity of $\lambda = 10^3$/m-s-°C. As the figure shows, the porosity of the fracture does not significantly affect the areal velocity of the thermal front at any time.

SUMMARY AND DISCUSSION

We have studied the movement of the thermal front (200°C isotherm) when 100°C water is injected into a 300°C reservoir containing equally-spaced, horizontal fractures. Two basic problems were studied using the numerical simulator CCC: first, the effect of heat conduction on the movement of the thermal front through horizontal fractures in impermeable rocks, and second, injection into a permeable reservoir with horizontal fractures.

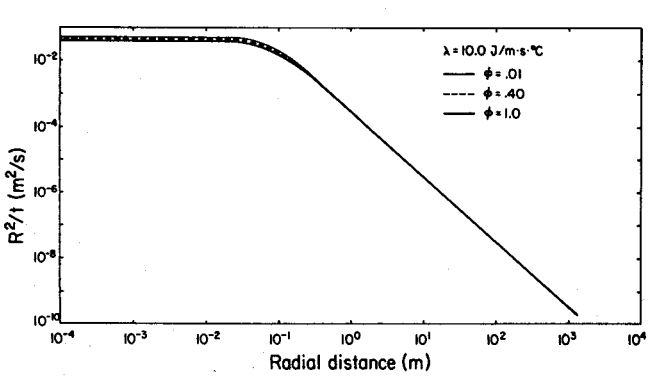

Figure 8. The effects of fracture porosity on the movement of the thermal front in the fracture.
[XBL 809-2771]

When cold water is injected into a fracture in impermeable rocks, heat transfer by conduction from the rock medium to the fracture will heat the water and thus retard the movement of the thermal front in the fracture. The larger the coefficient of thermal conduction of the rock, the more the advancement of the front will be retarded. If no thermal conduction takes place, the thermal front in the fracture will advance at a constant rate (R^2/t).

When cold water is injected through a well, intersecting horizontal fractures in a permeable medium, both convective and conductive heat transfer take place, with the injection fluid permeating into the rock medium from the fractures. The results indicate that, although the thermal front in the fracture advances at a much higher rate than the one in the rock at early times, it slows down rapidly as injection proceeds, and eventually the two fronts coincide and advance together. In other words, at some distance away from the injection well, the thermal front will be uniform over the thickness of the reservoir and the system will behave as if the fracture does not exist. This distance depends on many factors such as the permeability ratio between the fracture and the rock medium, the fracture spacing, the thermal conductivity of the rock and the aperture and porosity of the fractures.

The results presented in this paper form an important basis for understanding a fractured permeable system with production and injection wells.

ACKNOWLEDGMENT

The authors express their gratitude to Dr. Marcelo Lippman for his valuable suggestions during this study.

REFERENCES

Bodvarsson, G., 1969. On the temperature of water flowing through fractures. J. Geophys. Research, v. 74, no. 8, p. 1987-1992.

Bodvarsson, G. S., and Lippmann, M. J., 1979. Recent modifications of the numerical code CCC, in Earth Sciences Division Annual Report 1979. Berkeley, Lawrence Berkeley Laboratory, LBL-10795.

Bodvarsson, G. S., and Lippmann, M. J., 1980. The numerical simulator CCC. Proceedings, Workshop on Numerical Modeling of Thermohydrological Flow in Fractured Rock Masses, Lawrence Berkeley Laboratory, February 19-20, LBL-11566.

Gringarten, A. C., and Sauty, J. P., 1975. A theoretical study of heat extraction from aquifers with uniform regional flow. J. Geophys. Research, v. 80, no. 5, p. 4956-4962.

Kasameyer, P. W., and Schroeder, R. C., 1976. Thermal depletion of a geothermal reservoir with both fracture and pore permeability. Livermore, Lawrence Livermore Laboratory, UCRL-77323.

Lauwerier, H. A., 1955. The transport of heat in an oil layer caused by the injection of hot fluid. Appl. Sci. Research, Section A, v. 5, p. 145-151.

Lippman, M. J., Tsang, C. F., and Witherspoon, P. A., 1977. Analysis of the response of geothermal reservoirs under injection and production procedures. Presented at the 47th Annual California Regional Meeting SPE-AIME, Bakersfield, California, April. SPE-6537.

O'Neill, K., 1978. The transient three-dimensional transport of liquid and heat in fractured porous media (Ph.D. dissertation). Princeton, New Jersey, Princeton University.

Romm, E. S., 1966. On one case of heat transfer in fractured rock. All-Union Institute for Scientific Research and Geological Exporation for Petroleum, U.S.S.R., Preprint.

Tsang, C. F., Bodvarsson, G. S., Lippmann, M. J., and Rivera R., J., 1980. Some aspects of the response of geothermal reservoirs to brine reinjection with application to the Cerro Prieto field. Geothermics, v. 9, no. 1/2, p. 213-220.

Tsang, C. F., Buscheck, T., and Doughty, C., 1979. Aquifer thermal energy storage, a numerical simulation of Auburn University field experiments. Berkeley, Lawrence Berkeley Laboratory, LBL-10210, 44 p. Submitted to Water Resources Research.

LBL STUDY OF THE VALLES CALDERA GEOTHERMAL RESERVOIR

Overview

C. F. Tsang

A 50-MW geothermal power plant is currently being designed for the Baca site in the Valles Caldera, New Mexico, as a joint venture of the Department of Energy (DOE), Union Oil Company, and the Public Service Company of New Mexico. To date, over 20 wells have been drilled at the site, and the data from these wells indicate the presence of a high-temperature, liquid-dominated geothermal reservoir. Lawrence Berkeley Laboratory is currently acting as a technical advisor to the DOE Geothermal Demonstration Project Office for the development and utilization of this geothermal resource. Our work includes technical evaluation of work statements, data compilations and analyses, technical reports and conclusions, as well as participation in meetings to review power plant design. Furthermore, we are to study the thermohydraulics of the geothermal reservoir at the Baca site using state-of-the-art modeling techniques.

It is important to the developers and the financial community that reliable estimates be made of the mass of hot water (capacity) within a geothermal reservoir and the length of time (longevity) the reservoir can supply steam for a power plant at a given rate. Although many modeling and other techniques have been developed for making these estimates, their reliability is yet to be proved in a large-scale experiment such as the demonstration project at the Baca site. Our approach therefore, is to model this reservoir and to estimate its capacity and longevity at several key stages of the project. At each progressive stage, we will make use of the best information available to evaluate and revise our estimates. From these efforts we hope to determine the reliability of the modeling capabilities currently available to the geothermal industry and the accuracy of the estimates.

Such a program is being carried out by a multidisciplinary group of LBL geologists, geophysicists, reservoir engineers, geochemists, and mechanical engineers. We work together in assimilating, analyzing, and understanding the available data, the construction of an appropriate geological model, and the modeling of the geothermal reservoir under a given exploitation scenario. A preliminary reservoir capacity study was made last fiscal year. In the current fiscal year, the major results of the work have been the development of a geological and geophysical model, and a sensitivity study of the longevity of the Baca geothermal reservoir.

Development of a geological and geophysical model of the Valles Caldera geothermal reservoir

S. Vonder Haar and M. J. Wilt

The geological and geophysical model of the Baca field and the surrounding portions of the Valles Caldera was refined during 1980. New ideas on the role of fault-controlled fracturing and details of the stratigraphy permit better definition of the reservoir. This new geological model is used for computerized reservoir simulation (Bodvarsson et al., 1980).

GEOLOGY

The Baca geothermal area occurs at the intersection of two major tectonic features--the NS-trending Rio Grande graben and the NE-SW-trending Quaternary volcanic lineament that extends into Arizona (Fig. 1) (Bailey and Smith, 1978). Well locations are shown in Figure 2, which also indicates the rugged topography that makes geophysical field studies and subsequent interpretations relatively difficult.

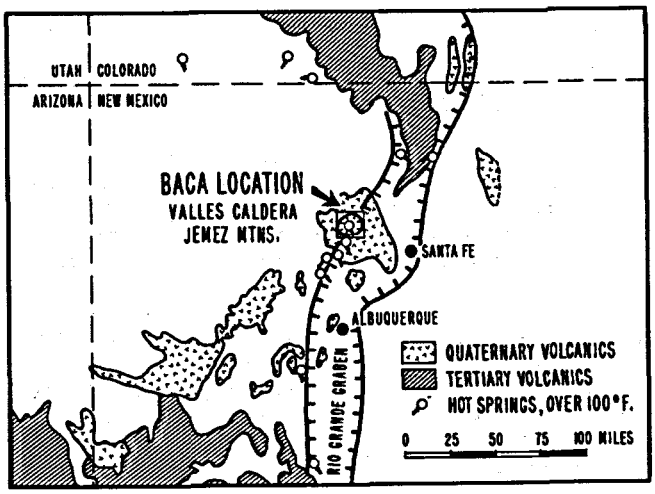

Figure 1. Location map of the Baca geothermal field in north-central New Mexico. [XBL 807-7259]

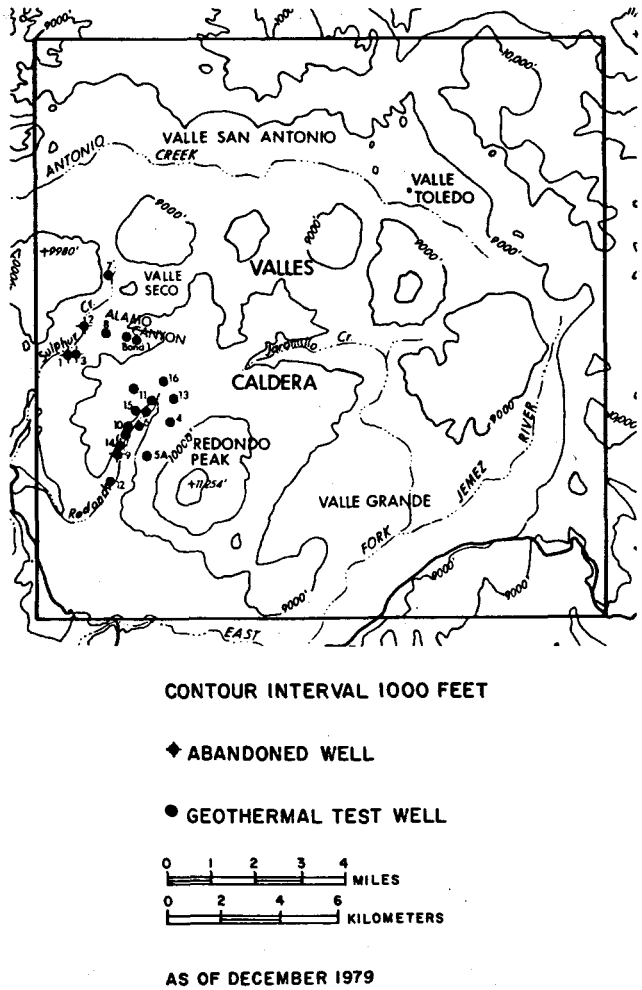

Figure 2. Well location map for the Baca field in Redondo Creek Canyon of Valles Caldera. [XBL 799-11549A]

Stratigraphy for the Baca area has been well defined from borehole cuttings and is summarized in Figure 3 and Table 1. We propose the following five-layer model for computerized reservoir simulations. Layer 1: Caldera fill, Redondo Creek Rhyolite, and the upper portion of the Bandelier Tuff down to a chosen temperature horizon corresponding to the top of the reservoir. Layer 2: the lower segment of the Bandelier Tuff, which is the major fracture-controlled reservoir, as determined by Union Oil geologists. Layer 3: Paliza Canyon volcanics, a fractured reservoir unit. Layer 4: the mixed Tertiary sands and older shales, sandstones, and limestones (this layer is potentially a major production reservoir and is probably a significant storage reservoir). Layer 5: presumed to be the granite basement but may also include highly metamorphosed sedimentary units.

Some downhole geophysical logs suggest that this five-layer model could be further subdivided. In well Baca-13 at a depth of 4880 ft, there is a shift in the SP and conductivity curves that may indicate a temperature or mineral zonation within the Bandelier reservoir. An SP and resistivity shift in well Baca-18 at a depth of 1285 ft could represent a hydrothermally densified zone or a thermal imprint during tuff emplacement within the Bandelier caprock. Epidote, pyrite, and wairakite are hydrothermally precipitated minerals found in the Baca wells that should eventually provide details on the thermal history (Lambert and Epstein, 1980).

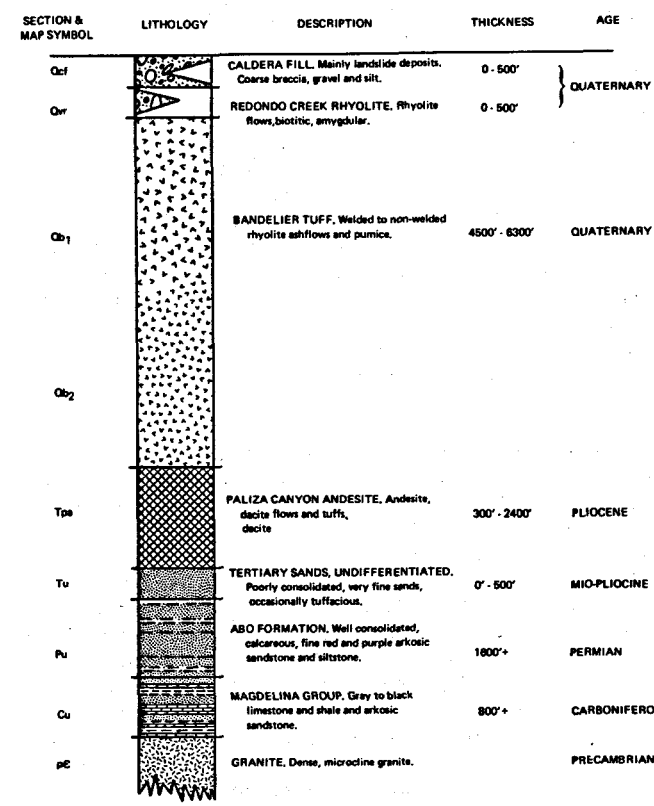

Figure 3. Generalized stratigraphic section in the Baca area based on wellcutting analysis (after Union, 1978). [XBL 799-2904]

Table 1. Data for BACA geological Model

Well	Elevation above sea level (ft)	Total depth (ft)	°F at 3000' ASL*	°F at 6200' ASL	Difference in °F 3000-6200' ASL	First 450°F ft ASL	Top of Base of caprock ft ASL	Top of Paliza Canyon ft ASL	Top of sedimentary units (TU, PU, PC) ft ASL	Bandelier caprock thickness (ft)	Bandelier reservoir thickness (ft)	Paliza Canyon thickness (ft)
B-4	9318	6376	590	490	100	7350	7300	3338	< 2942	2018	3962	----
B-5A	9290	6973	320 @ 3400'	290	30	----	7300	2690	< 2317	1990	4610	----
B-6	8726	4810	540+ @ 4000'	440	100+	5910	6500	< 3916	< 3912	2226	----	----
B-7	8724	5532	465 @ 3300'	390	75	5480	6200	No Tp	5424	2524	776	----
B-8	8631	4384	570+ @ 4400'	480	90+	6750	6300	No Tp	5531	2331	769	----
B-9	8640	5303	----	---	---	----	----	----	----	----	----	----
B-10	8734	6001	520	445	75	6080	5800	3515	2805	2934	2285	710
B-11	9065	6931	570	485	85	6200	6100	3625	2500	2965	2475	1125
B-12	8429	9212	470	355	115	3920	6075	1969	854	2354	4106	1115
B-13	9292	8228	515	460	55	6410	6300	3580	1202	2992	2720	2378
B-14	8605	6824	470	320	150	3310	4900	2805	2465	3705	2095	340
B-15	9117	5505	540 @ 3800'	490	50+	6600	6520	3900	< 3612	2597	2620	----
B-16	9622	7002	570	435	135	6090	6250	4062	2742	3372	2188	1320
Bond 1	8700	3675	---	350 @ 5820'	---	----	----	----	----	----	----	----
B-1	8420	2560	---	---	---	----	----	----	----	----	----	----
B-2	8480	4726	---	415 @ 6920'	---	----	----	----	----	----	----	----
B-3	8420	2200	---	390 @ 6620'	---	----	----	----	----	----	----	----
B-17	9361	6255?	---	233?	---	----	----	----	----	----	----	----
B-18	8735	5280?	348 @ 3485?	280?	68+	----	6535?	----	----	2200?	----	----
B-19	9119	5619?	---	----	---	---	----	----	----	----	----	----

* Above sea level.
Source: Union, 1978.

To understand the reservoir geometry, various contour maps (Fig. 4) and cross sections (Fig. 5) have been made from well data provided by Union Oil (1978). The temperature map (Fig. 4) indicates that well 5A is abruptly cut off from the main producing wells to the north. This is a strong suggestion of a fault. Figure 6 is a three-dimensional view of several prominent horizons found in the Baca reservoir. This figure indicates that the Baca field has a slightly domal upper surface, the base of the Bandelier caprock, that is underlain by Paliza volcanic and sedimentary units. In the southern half of the field, the reservoir center dips gently to south-southwest. The absence of Paliza volcanics in wells Baca-7 and Baca-8 indicate that the reservoir to the northeast consists of Bandelier underlain by sedimentary units. Further well testing is needed to clarify the role of this important stratigraphic discontinuity on reservoir productivity.

GEOPHYSICS

Thermal models for the Valles Caldera by Kolstad and McGretchin (1978) predicted that the top of the original magma chamber may have been within 5 km of the surface 1.1 million years ago and may have extended outside the ring fracture zone. Our interpretation of existing geophysical data cannot confirm the present-day existence of a magma chamber at Baca. Gravity data indicate a 40-50 mgal gravity minimum over the Valles Caldera, but this is more logically explained by a great thickness of caldera fill and lighter volcanic units rather than a deep, extensive magma chamber. Preliminary modeling of this gravity, using densities and layer boundaries from well logs, indicates a thickness of up to 5 km of caldera fill, volcanics, and older sediments. The gravity data also indicate major NE-SW faulting immediately west of Redondo

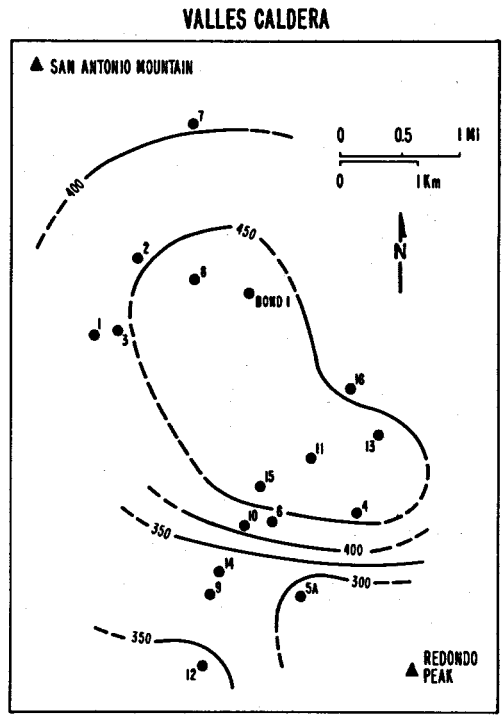

Figure 4. Temperature in °F at 6200 ft above sea level within the Baca reservoir from downhole temperature logs. Note the high-temperature zone centered around well 11. [XBL 807-7243]

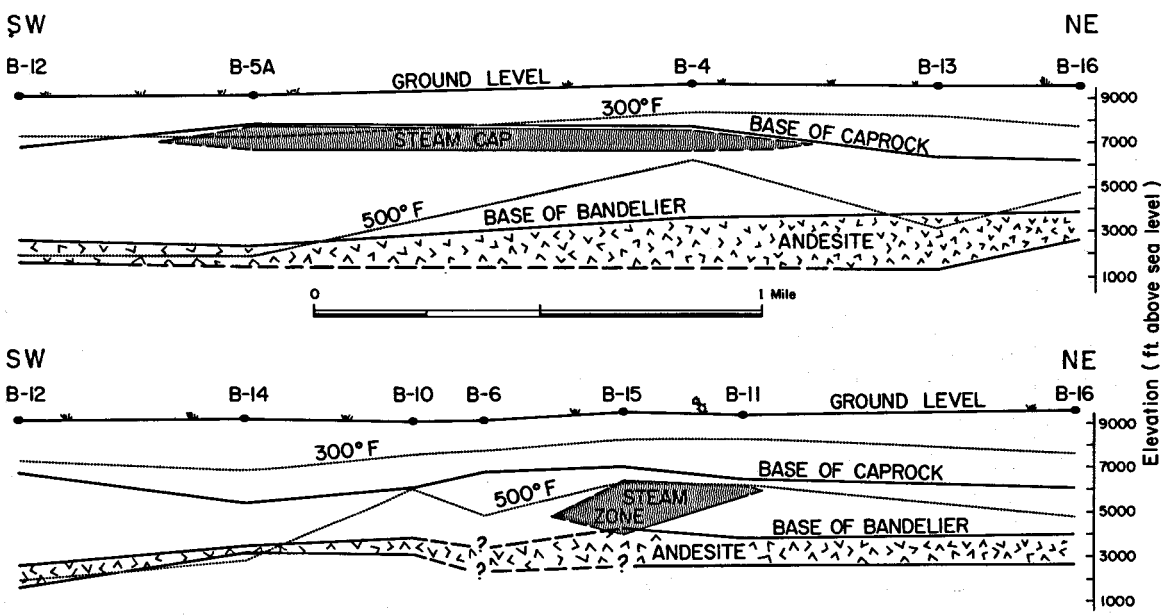

Figure 5. Stratigraphic cross section in the Baca reservoir showing the possible steam cap and steam zone. See Figure 2 for well locations. [XBL 7912-13472]

Peak and show evidence of normal faulting near Redondo Border, which lies west of the producing field at Redondo Creek. Gravity measurements therefore provide some definition to the Redondo Creek graben.

Geophysical data are used to define the areal extent of the reservoir and to determine the controlling structure. Telluric profile and magnetotelluric sounding measurements performed by Geonomics (1976) are very helpful in establishing boundaries to the geothermal field and in locating areas of low resistivity related to fracturing. Figure 7 shows the location of two telluric profile lines. Figure 8 shows the results of measurements along one of these lines. As defined by telluric profile measurements, the maximum N-S extent of the reservoir is 5-6 km. Shallow temperature data correlate well with these boundaries, beginning near station 12 and extending to station 29 (Fig. 7). The two low-frequency telluric profile plots, which are sensitive to the rock units buried as deeply as 5 km, indicate that the region between stations 20 and 26 has the lowest resistivities at depth. This area corresponds to the zone of best steam production in the Redondo Creek area. Telluric profiles D-D' and H-H' (Fig. 7) both suggest the presence of a discontinuity east of the Bond-1 well that may indicate a western boundary to the reservoir. A similar discontinuity is evident along profile G-G' (Fig. 7), along which we can place an eastern boundary to the reservoir. These data then indicate four possible reservoir boundary crossings, which is certainly inadequate for outlining the total extent of the field but does provide constraints for any reservoir models.

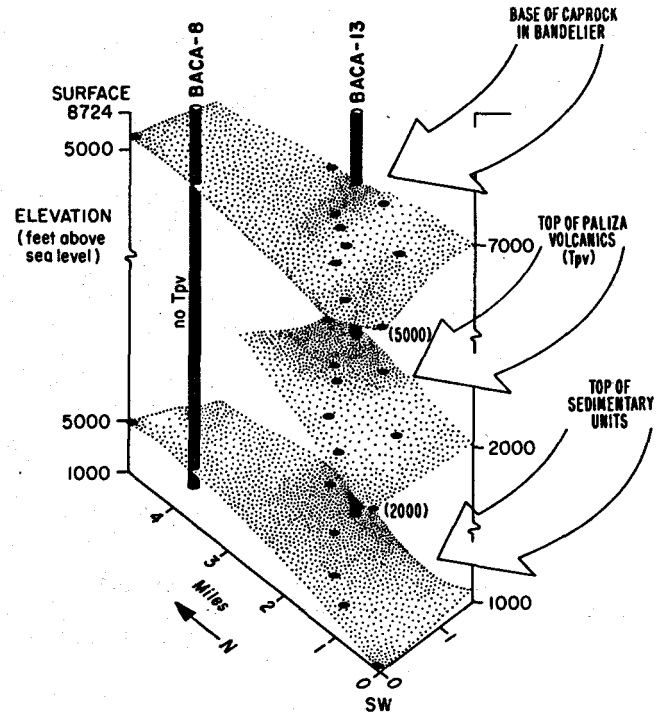

Figure 6. A three-dimensional computer model of key surfaces in the Baca field useful for reservoir simulation. Baca wells 8 and 13 shown as location marker, other wells shown by black dots. Note the absence of Paliza volcanics in the northwestern portion of the field near well 8 and the relatively uniform dip of 20° to the south-southeast of each of the surfaces. [XBL 8011-6424]

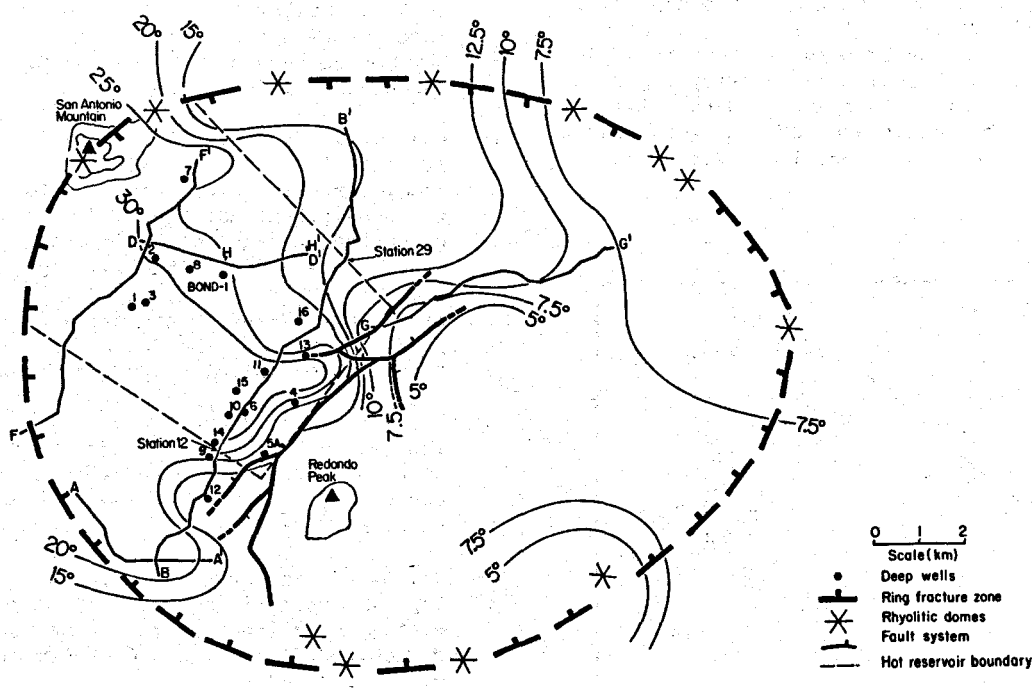

Figure 7. Base map of the Valles Caldera showing shallow temperature gradients (°C/100 ft), geophysical survey lines (e.g., A-A'), specific faults, and the estimated hot reservoir boundary. [XBL 7912-13349]

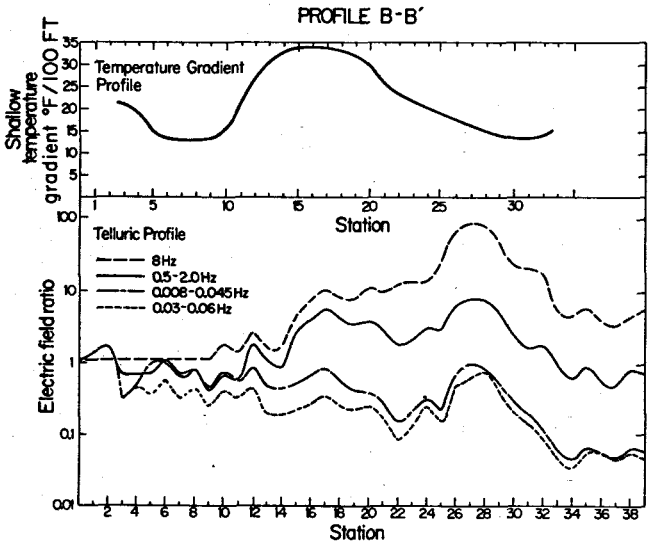

Figure 8. Shallow temperature gradients and telluric profiles along survey line B-B'. [XBL 7912-13350]

Magnetotelluric soundings taken in Redondo Creek, Alamo Canyon, and Sulfur Creek indicate that the regions of low resistivity at depth are very localized and that the Baca region in general has high resistivity. Low-resistivity zones at depth have been identified near well 13 in Redondo Canyon, in Sulfur Creek, and in Valle Seco. Station coverage is inadequate, however, to map the dimensions of these zones accurately. One-dimensional models of the MT sounding data in Redondo Creek generally show a three-layer section (Fig. 9). The top layer is low-resistivity Caldera fill, which is locally very low near zones of hydrothermal alteration. At 300 m or so in depth, the high-resistivity upper portions of the Bandalier Tuff are evident. Resistivities for some soundings are 500 ohm-m or more in this unit, indicating low porosities. Within the lower unit of tuff, several soundings have located anomalously low resistivity, beginning at about 1 km in depth. This deep low-resistivity zone in Redondo Creek is very localized and corresponds remarkably with one area of good steam production. Beneath the Bandalier Tuff, MT soundings generally indicate a slightly less resistive formation 100-200 ohm-m, which corresponds to Mesozoic rocks and perhaps to Precambrian basement.

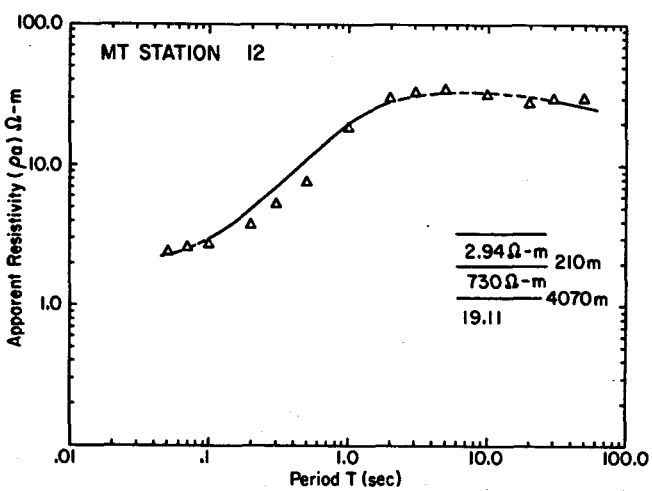

Figure 9. Sample layer model inversion of a magnetotelluric sounding at Baca. [XBL 812-2619]

PLANS FOR 1981

All available data will be used to develop several possible reservoir models for simulation studies. In addition to the 40-km^2 model that we have been using, we will investigate (1) a region defined by the ring fracture zone, (2) an area extending 5 km to the north and northeast from well Baca-13, and (3) the "proven reservoir" centered around well Baca-4, 15, 11, and 13. All of these models will satisfy constraints provided from geological and geophysical data.

Additional two-dimensional modeling will be done with magnetotelluric and gravity data in an effort to provide more information relating to the boundaries of the deep low-resistivity zone in Redondo Creek. Finally, well log information will be used in providing resistivity and density for modeling studies.

REFERENCES CITED

Bailey, R. A., and Smith, R. L., 1978. Volcanic geology of the Jemez Mountains, New Mexico. In J. W. Hawley (ed.), Guidebook to Rio Grande Rift in New Mexico and Colorado, Circular 163, New Mexico Bureau of Mines and Mineral Resources, p. 184-196.

Bodvarsson, G. S., Vonder Haar, S., Wilt, M., and Tsang, C. F., 1980. Preliminary estimation of the reservoir capacity and the longevity of the Baca geothermal field, New Mexico. Paper presented at SPE-AIME Conference, Dallas, Sept. 21-24, 1980, SPE-8273, 6 p.

Geonomics, Inc., 1976. Magnetotelluric-telluric profile survey of the Valles Caldera prospect. Private geophysical study for Union Oil Company.

Kolstad, C. D., and McGretchin, T. R., 1978. Thermal evolution models for the Valles Caldera with reference to a hot-dry-rock geothermal experiment. J. Volcan. and Geotherm. Research, v. 3, p. 197-218.

Lambert, S. J., and Epstein, S., 1980. Stable isotope investigations of an active geothermal system in Valles Caldera, Jemez Mountains, New Mexico. J. Volcan. and Geotherm. Research, v. 8, p. 111-129.

Union Oil Company and Public Service Company of New Mexico, 1978. Geothermal demonstration power plant; v. II, Technical and management proposal to DOE; Program Opportunity EG-77-N-021717.

Longevity of the Baca geothermal reservoir—A sensitivity study

G. S. Bodvarsson and C. F. Tsang

The Baca geothermal reservoir is located in the Valles Caldera, New Mexico, about 55 miles north of Albuquerque. The Union Oil Company of California and the Public Service Company of New Mexico are developing the field. To date, over 20 geothermal wells have been drilled in the Valles Caldera, varying in depth from 2000 to over 9000 ft (Union Oil et al., 1978). Six of the wells have been drilled in the Sulfur Creek area, the remainder along Redondo Creek (Fig. 1).

In an earlier investigation, studies were made of the reservoir capacity and longevity. The reservoir capacity was estimated by volumetric calculations using existing geological, geophysical, and well data. The longevity of the field was calculated based on a power output of 50 MWe, by a two-phase numerical simulator (SHAFT79).

The purpose of the present study is to determine the sensitivity of our longevity estimates to the mesh and the relative permeability curves used in the simulations.

PREVIOUS WORK

Reservoir Capacity

As reported by Bodvarsson et al. (1979), we have estimated the volume of hot water contained in the reservoir (reservoir capacity). The parameters needed to calculate the reservoir capacity are the areal extent of the hot water zone and the average thickness and porosity of the reservoir. The areal extent of the hot-water zone was estimated from geological information, well data, and shallow thermal-gradient contours. These data are supported by geophysical data. Figure 1 shows the estimated areal extent of the Baca Reservoir (broken lines). An average porosity-thickness product (ϕH) was estimated to be 100 ft (Union Oil et al., 1978). Consequently, a reservoir capacity of 2.2×10^{-12} lb of hot fluids was obtained.

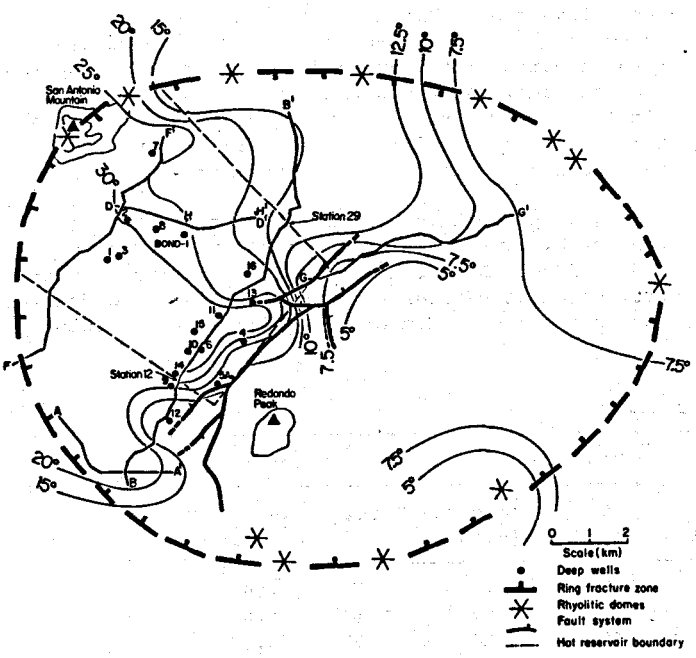

Figure 1. Base map of the Valles Caldera showing shallow temperature gradients (°F/100 ft), geophysical survey lines (e.g., A-A'), specific faults, and the estimated hot reservoir boundary (Grant, 1977; Union Oil et al., 1978; Counsil and Ramey, 1979). [XBL 7912-13349]

Reservoir Longevity

The longevity of the Baca field was studied using the two-phase simulator SHAFT79 (Pruess et al., 1979). The reservoir was simulated by a basic rectangular mesh with overall dimensions corresponding to the estimates given above (Fig. 2). For reasons of symmetry, we modeled only half of the system. Instead of simulating individual wells, the fluid was produced uniformly over one node representing half the well field (assumed to be 1 km^2). The parameters used in the simulations were:

Constant flow rate	Q_t = 330 kg/s
Rock heat capacity	C_v = 950 J/kg-°C
Permeability thickness	kH = 6000 mD-ft
Thermal conductivity	λ = 2.0 J/s-m-°C
Porosity thickness	ϕH = 100 ft
Initial pressure	P_i = 110 bars
Initial temperature	T_i = 300°C

The relative permeability equations were given by Corey (Faust and Mercer, 1979) (Table 1). The residual liquid and steam saturations were fixed at 0.30 and 0.05, respectively.

We studied five cases using a constant mass flow rate. The value was based upon the amount of steam theoretically required for a 50 MWe power plant and a constant value of the mass fraction of steam in the separators (Union Oil et al., 1978). Five cases were studied: a bounded reservoir, an infinite reservoir, and three injection cases. Each case was run until the pressure in the production node dropped below the designed wellhead pressure of 10 bars (Union Oil et al., 1978). The longevity

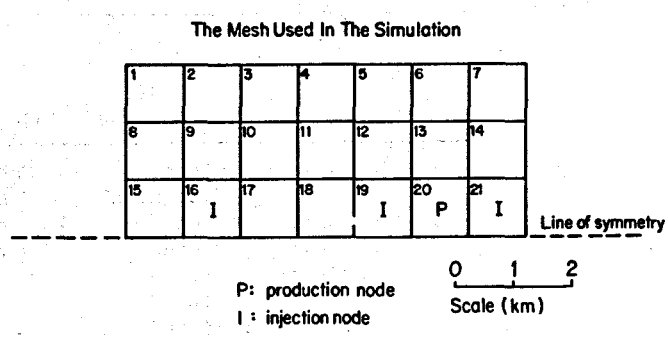

Figure 2. The mesh used in the longevity study for "closed" reservoir cases. [XBL 7912-13354]

Table 1. Relative permeability equations (plots are shown in Figure 4).

Corey's curves:

$$k_{rw} = \begin{cases} [S^*]^4 & S < S_{rw} \\ 0 & S \geq S_{rw} \end{cases}$$

$$k_{rs} = \begin{cases} [1 - S^*]^2 & S > S_{rs} \\ 0 & S \leq S_{rs} \end{cases}$$

$$\text{where } S^* = \frac{1 - S_{rw} - S}{1 - S_{rw} - S_{rs}}$$

Grant's curves:

$$k_{re} = \begin{cases} [S^*]^4 & S < S_{rw} \\ 0 & S \geq S_{rw} \end{cases}$$

$$k_{rs} = 1. - k_{rw}$$

Counsil and Ramey's curves:

$$k_{rw} = \begin{cases} 1 - \frac{S}{0.30} & S < 0.30 \\ 0 & S \geq 0.30 \end{cases}$$

$$k_{rs} = \begin{cases} \frac{S - 0.20}{0.80} & S > 0.20 \\ 0 & S \leq 0.20 \end{cases}$$

of the field was in each case defined as the time it took to reach the pressure of 10 bars. The results are given in Table 2.

Sensitivity Study

Two important factors must be considered when modeling two-phase flow in geothermal reservoirs--the mesh-dependence of the results, and the degree of dependence by the results on the specified relative permeability curves. We conducted a brief study to determine the sensitivity of our results to these factors.

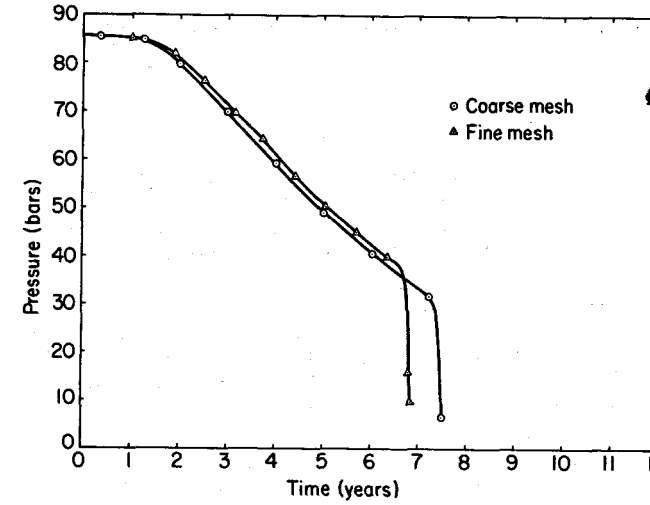

Figure 3. Mesh dependence: pressure behavior in production node. [XBL 807-7248]

For this purpose, a new, finer mesh was constructed to determine the sensitivity of the results to the mesh in the simulations. The fine mesh consists of 81 elements, each element having a volume four times smaller than the corresponding element in earlier simulations (Fig. 2). The production element, however, remained the same size. Using the fine mesh, we studied the case of a constant mass flow rate with closed reservoir boundaries (case 1). Figure 3 compares the fine and coarse mesh results for the pressure behavior in the production node. Although the two curves are quite similar at early times, the curve corresponding to the fine mesh is shifted about 2 bars above the curve corresponding to the coarse mesh.

To explain this behavior, let's consider the fine mesh. The nodes adjacent to the production node undergo phase transition (to a two-phase condition) at an earlier time than the larger nodes in the coarse mesh. Consequently, steam flows into

Table 2. Summary of cases and primary results.

				Conditions at the end of the run			
Case	Flow rate	Boundary conditions	Injection	Time (yr)	Pressure (bars)	Temp. °C	Vapor satuation
1	Constant	Closed	None	7.4	10	237	1.0
2	Constant	"Infinite"	None	9.6	10	214	1.0
3	Constant	Closed	4 km to NW	12.9	10	180	0.99
4	Constant	Closed	1 km to NW	13.7	10	180	0.91
5	Constant	Closed	1 km to NE	14.0	10	180	0.87
6	Variable	Closed	None	25	10	214	1.0
7	Variable	Semi-infinite	None	26	10	213	1.0
8	Variable	"Infinite"	None	35	10	185	1.0
9	Variable	Bounded with a fault	None	50	10	180	0.48

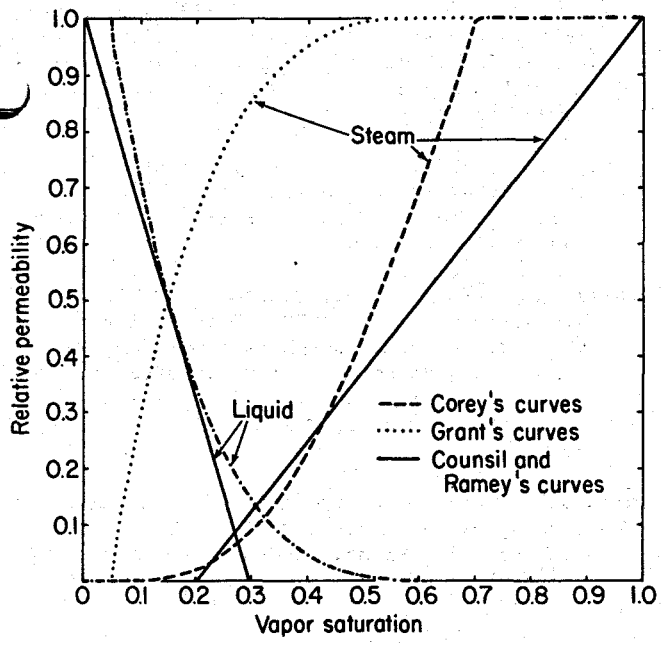

Figure 4. Relative permeability curves used in the study. [XBL 807-7250]

the production node at an earlier time. This implies that for fine mesh less boiling is required in the production node at any given time, resulting in a smaller pressure drop; however, the higher steam flow into the production node causes higher vapor saturation at any given time in the node, so that superheated conditions are reached earlier. Therefore, in terms of longevity, the coarser mesh gives results that are slightly more optimistic (increased longevity).

To study the effects of the relative permeability curves on our results, we used curves suggested

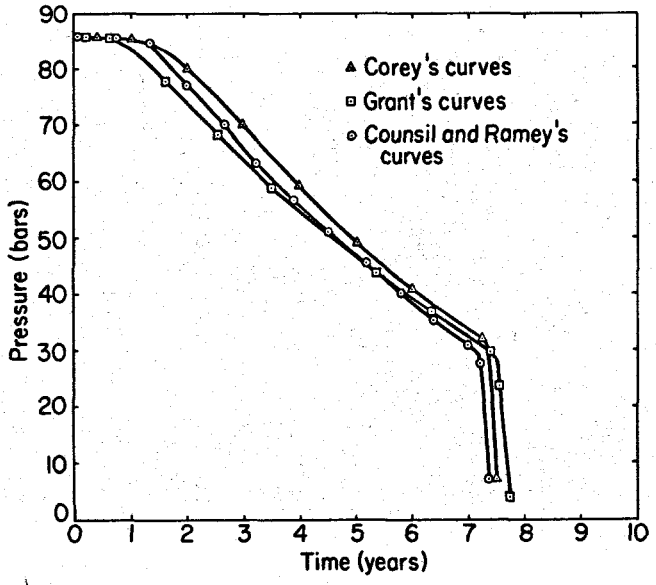

Figure 5. Effects of relative permeability curves. [XBL 807-7249]

by Counsil and Ramey (1979) and Grant (1977), in addition to the Corey curves. The curves by Counsil and Ramey are based on experimental results over a small range of vapor saturation ($0.20 < S < 0.30$). For our simulation studies, these data were linearly extrapolated over the full range of saturation. The curves developed by Grant (1977) are based on data from the Wairakei geothermal field. The liquid relative permeability corresponds to the fourth order Corey equations, but the steam phase is considerably more mobile. The mathematical expressions for the curves in this study are given in Table 1; the curves are illustrated in Figure 4.

Figure 5 shows pressure behavior at the production node for case 1 and different relative permeability curves. The figure shows that longevity (the time when pressure falls below 10 bars) is essentially unaffected by a specific relative permeability curve. The pressure plots based on Counsil and Ramey's curves lie at all times below those results based on Corey's equations. This is expected, since the mobilities of the steam and the liquid are generally less for Counsil and Ramey's curves. At early times, the pressure behavior based on Grant's curves is less than in the case of Corey's curves because more steam is produced; consequently, more boiling occurs in the production node. One must remember that the mass ratio of steam and liquid produced depends on the relative permeability curves. In the case that uses Grant's curves, however, the longevity is slightly higher because of the much more mobile steam phase.

In addition to the runs shown in Figure 5, a couple of runs were made using modifications to Counsil and Ramey's. In the first run, the steam was made immobile at a vapor saturation of 0.60, but the relative permeability of the steam increased linearly, becoming fully mobile at a vapor saturation of 1.0. The results agreed very closely with the original run based on Counsil and Ramey's curves, indicating that the steam relative permeability curve may not be very important for this problem.

In the second case, the residual water saturations were fixed at 0.60 and the curves were again linearly extrapolated to become fully mobile at a vapor saturation of 0.0. In this case, the longevity increased to almost nine years. The increased mobility of the water phase causes considerably more liquid to enter the production node; consequently, the longevity increases.

The effects of the relative permeability curves on longevity were studied in relation to a variable mass flow rate. Counsil and Ramey's curves were used. The results were compared to those results based on Corey's curves. The results compared quite well--a longevity of 23 years was obtained for the Counsil and Ramey case, compared to 25 years for the Corey case (Grant, 1977).

CONCLUSIONS

In studying the sensitivity of our longevity estimates, we have found that the results are mesh-dependent to some degree and that the longevity values obtained by using the coarse mesh may be

slightly optimistic. A brief study, using relative permeability curves suggested by Counsil and Ramey and by Grant, seems to indicate that the results are not very sensitive to the particular relative permeability curves chosen. The key factor is the mobility of the liquid phase. The longevity may increase considerably if relative permeability curves are employed where the liquid phase is more mobile than in the curves that we have used.

REFERENCES CITED

Bodvarsson, G. S., Vonder Haar, S., Wilt, M., and Tsang, C. F., 1979. Preliminary estimation of the reservoir capacity and longevity of the Baca geothermal field, New Mexico. Earth Sciences Division Annual Report 1979, Berkeley, Lawrence Berkeley Laboratory, LBL-10686.

Counsil, F. R., and Ramey, H. J., 1979. Drainage relative permeabilities obtained from steam-water boiling flow and external gas drive experiments. Transactions, Geothermal Resources Council, v. 3, p. 141-143.

Faust, C. R., and Mercer, J. W., 1979. Geothermal reservoir simulation--numerical solution techniques for liquid- and vapor-dominated hydrothermal systems. Water Resources Research, v. 15, no. 1, p. 31-46.

Grant, M. A., 1977. Permeability reduction factors at Wairakei. Paper presented at AIChE-ASME Heat Transfer Conference, Salt Lake City, Utah, August 15-17, 1977.

Pruess, K., Zerzan, J. H., Schroeder, R. C., and Witherspoon, P. A., 1979. Description of the three-dimensional two-phase simulator SHAFT78 for use in geothermal reservoir studies. Paper presented at meeting of Society of Petroleum Engineering, Denver, Colorado, February 1-2, 1979.

Union Oil Company of California and Public Service Company of New Mexico, 1978. Geothermal Demonstration Plant. Technical and Management Proposal to DOE.

RESERVOIR EVALUATION OF KLAMATH FALLS, OREGON

M. T. O'Brien and S. M. Benson

Research activities in fiscal 1980 focused on a detailed geologic study of three wells in the Klamath Falls known geothermal resource area (KGRA), in south central Oregon.

Extensive use of the low-temperature geothermal resource is ongoing in the Klamath Falls area (Fig. 1). The resource is used for small-scale industrial and domestic use. More than 400 wells with a temperature range of 100-235°F (38-112°C) are extracting heat from the reservoir, using a downhole heat-exchanger system. In 1979 the city of Klamath Falls began a city-wide district heating project. Phase I includes heating 14 government buildings and approximately 100 residences. A supply of approximately 700 gpm of 220°F geothermal fluid is required (U.S.G.S., 1978; Benson et al., 1979) to meet the peak heating load. Based on the success of Phase I and the feasibility of pumping more fluid from the reservoir, the project will be expanded to heat the entire downtown district. Expanded use of the reservoir will require an accurate prediction of long-term effects of pumping large quantities of fluid from the reservoir. Estimating the potential fluid flow from the reservoir, requires construction of a geohydrologic model of the geothermal reservoir. One necessary step is to describe the subsurface geology. The research activities for fiscal 1980 concentrated on the lithology, mineralization, and preparation of a generalized geologic cross section.

This study focused on the portion of the KGRA within the city of Klamath Falls and did not include the geothermal area of Olene Gap and Klamath Hills (see Fig. 1). Complete results are reported in O'Brien et al. (1981). Here, the lithology and previous well tests are summarized.

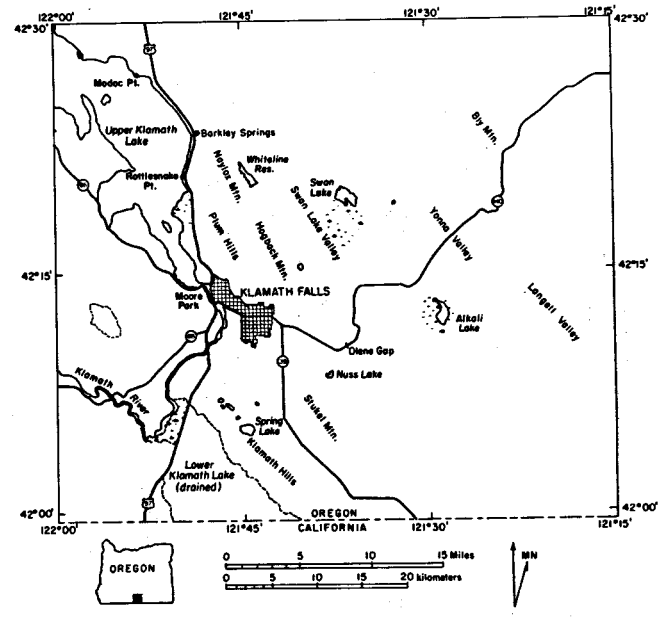

Figure 1. Klamath Falls area and major geographical features, south-central Oregon.

[XBL 8012-6569]

GEOLOGY

The Klamath Falls KGRA is part of the horst and graben structure of the Basin and Range province. Large grabens form Upper and Lower Klamath Lake basins and Swan Lake-Langell Valleys. They are flanked by steeply dipping, normal faults striking N25-35W. Other fault systems of lesser importance trend north-south and northeast-southwest. The dip is nearly vertical in places such as Rattlesnake Point. Offset ranges up to 1000-1600 feet (300-500 m). The city geothermal area occurs adjacent to the fault margin of an uplifted block, east of the Upper Klamath Lake graben. The regional geology has been described by Peterson and MacIntyre (1970) and more recently, Sammel (1980) has reported on the hydrogeology.

Three dominant rock units crop out in the Klamath Falls area: a basaltic flow sequence(s), white tuff and tuffaceous siltstone, and volcanic sediments including basaltic breccia. The basaltic flow(s) are medium grey, vitreous, and aphanitic to fine-grained crystalline. They may include andesitic flows. Some outcrops are massive and include plagioclase phenocrysts up to 4 mm in length. Many locations have basaltic flows that are vesicular to scoriaceous. Jointing is widespread and is present in flows south of and along the east shore of Upper Klamath Lake. The white to buff tuffaceous unit(s) are vitreous with black inclusions (hornblende?) and glass shards. The tuff is very fine grained and readily breaks down to clay sized grains. It is very porous and poorly to moderately consolidated. Often the tuff is underlain by volcanic sediments and basaltic breccia and has a few thin units of interbedded basaltic pebbles or lapilli. The volcanic sediments include basic volcanic flow fragments, tuff, silt- and claystone, and minor amounts of lapilli, scoria, and breccia. Some sediment shows alteration and reworking. The basaltic breccia within the sediments is composed of angular to subangular basaltic cobbles to boulders 10 cm to 0.5 m. The matrix is light grey to buff to yellow with evidence of alteration. The breccia occurs below basaltic flows, for example, at Plum Hills and the ridge east of Barkley Springs. Often a baked contact occurs between the breccia and overlying basaltic flow.

It is difficult to establish stratigraphic relationship among these three units. The basaltic flow units are often topographically above the white tuff. However, most of the basaltic outcrops occur along fault blocks. At Moore Park, south of Upper Klamath Lake, the basalt flow is in contact with the tuff, and there are stringers of basaltic fragments, lapilli, and breccia into the tuff. Both the tuff and basalt indicate a 20-30° dip to the west, based on flow planes in the basalt and stringers in the tuff, suggesting simultaneous deposition.

The stratigraphic section mapped by Peterson and McIntyre (1970) for the Klamath Falls area includes these rock units and dates them as Pliocene Holocene. The oldest unit in the immediate KGRA a Pliocene lacustrine and fluviatile tuffaceous siltstone unit with sandstone ashy diatomite, basaltic tuff and breccias, and a few thin basalt flows interbedded. This unit crops out south of Upper Klamath Lake in the vicinity of Moore Park and east of Plum Hills. Peterson and McIntyre map Plio-Pleistocene basaltic flows and pyroclastics forming the ridges east of Upper Klamath Lake (Naylox Mountain and Hogback Mountain). Pleistocene basalt flows occur west of Swan Lake Valley, and Pleistocene-Holocene units include basaltic tuff, fluvial terraces and lacustrine deposits, and Quarternary alluvial and diatomacious deposits. Many of these units are in fault contact with each other.

Peterson and McIntyre apply no names to these units; however, Newcomb (1958) mapped the lacustrine and fluvial tuffaceous siltstone with interbedded sediment as the Yonna Formation of Pliocene age. Sammel (1980) and others take exception to this formation name because of the lack of formaion boundaries and clear definition of the rock sequence that makes up the unit.

Rocks older than the Pliocene lacustrine siltstone do not crop out in the Klamath Falls area. However, they are present in drill cuttings from some of the geothermal wells.

SUBSURFACE LITHOLOGY

Detailed study of cuttings and drillers' logs were completed for three wells in the city area of the geothermal field (well location shown on Fig. 2). Samples for city wells 1 and 2 (KF 1 and 2) were collected in 10-ft intervals, whereas samples for YMCA-2 well were taken "when the rock-type changed," as indicated by the driller. All samples were examined under an optic microscope, and selected samples were analyzed by x-ray diffractometer and petrographic thin section. Lithologic columns were prepared on the basis of these analyses.

Inherent in rock samples from well cuttings is the potential of downhole contamination. Frequently, ten to twenty percent of a sample has the same lithology as the sampling interval above and could represent contamination, or a small proportion of the lithology is two-tenths into the sampling interval. However, the first occurrence of a rock type in well cuttings is probably reliable and consistent with downhole lithology. Another limitation of well cuttings is the lack of information on fractures and the types of contacts between lithologies. These limitations must be kept in mind when interpreting the lithologic columns.

Lithology of Well KF-1

Well KF-1 is located (see Fig. 2) in the southeast quarter of S 28, T 38S, and R 9E. It is drilled at an elevation of 4191 ft (1278 m) to a depth of 360 ft (110 m), penetrating fine-grained volcanic detritus and andesitic-basaltic flows. The lithology is illustrated in Figure 3. The first one hundred feet is claystone, silicious tuff, and tuffaceous sediment. Thin flows of andesitic-basaltic composition occur at 100-110 ft, 250-260 ft and 290-350 ft (30-33 m, 76-80 m, and 88-107 m) depths. Betweeen the volcanic flows are tuffaceous sediments with volcanic fragments and glassy shards. A volcanic breccia, occuring at 350-360 ft (107-110 m) depth is scoriaceous and vitreous, with vein fillings of silica, calcite, and zeolites.

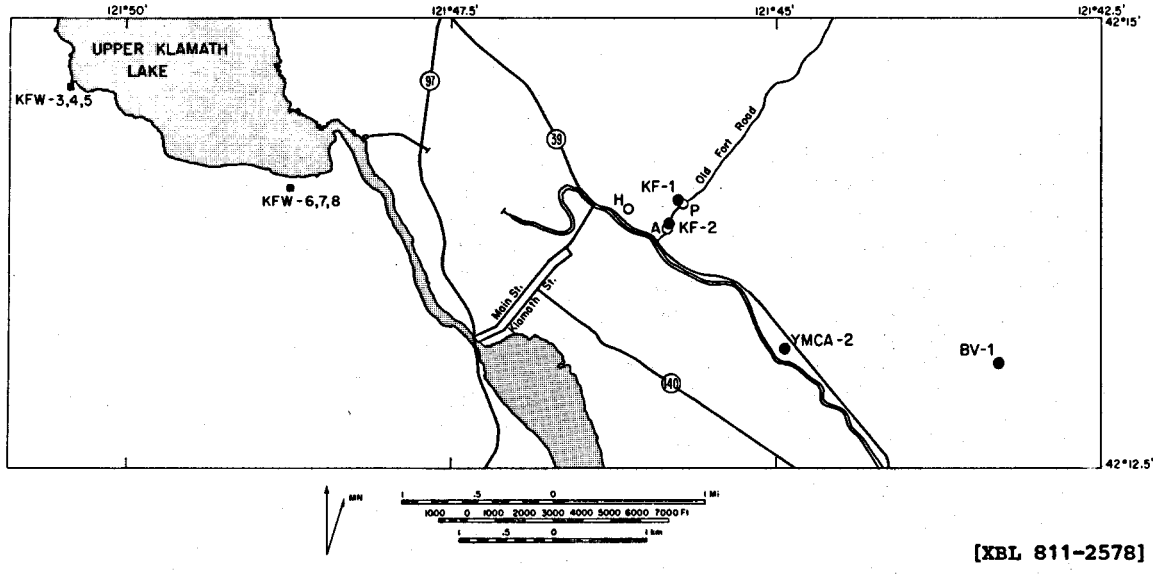

[XBL 811-2578]

Figure 2. Detail of well locations.

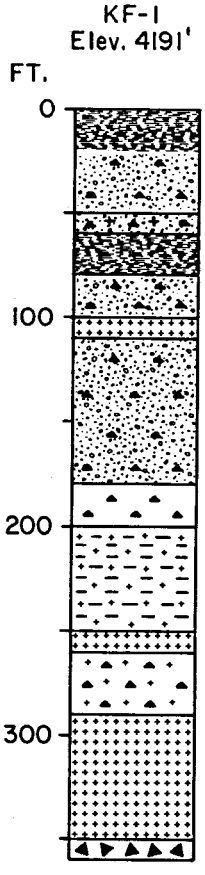

Light gray cherty claystone, white siliceous claystone (reworked ash?).

White siliceous tuff, very fine grained, poorly indurated, trace lithic grains.

Lithic micro-graywacke with cherty claystone fragments.

Gray siltstone and silty claystone.
Buff to gray tuffaceous sediment, increasing volcanic fragments in lower portion.
Basic volcanic fragments, aphanitic, vugs, pyrite.

Buff to brown tuffaceous sediment, vitreous luster, poorly indurated, trace volcanic fragments, black glassy phenocrysts (150-160').

White tuff, with black glassy shards, tuff welded in lower portion.

Basic volcanic sediments, fine grained, vitreous luster, rounded grains in siliceous matrix.

Dark gray basic volcanic fragments, aphanitic, moderately hard.
Volcanic graywacke, dark gray angular to subrounded inclusions, some pyrite, vein filling matrix light gray, vitreous luster, chalcopyrite/marcasite (280').

Gray basic volcanic fragments, aphanitic, massive, hard, trace amounts of veination (300-320'), few euhedral pyrite (320-340').

Red basic volcanic breccia, scoriaceous, subangular, 1-3 mm aphanitic basaltic inclusions, red aphanitic matrix, vitreous luster, many vugs sometimes filled with silica, zeolites, calcite and/or pyrite.

Figure 3. Lithologic column for Klamath Falls City Well #1 (KF-1 on location map Fig. 2). Rock description based on drillers' cuttings. [XBL-806-7164]

Lithology of KF-2 Well

Well KF-2 is located 840 ft (260 m), southwest KF-1 in the same quarter section (Fig. 2). It penetrates lithologies of similar thicknesses and extends to a depth of 880 ft (268 m) (Fig. 4). The sequence includes claystone, tuffaceous and volcanic sediments, basaltic-andesitic flows, and ash.

Gray and buff to brown clay and claystone occur in the first 100-ft interval. White tuff fragments occur within the clay at 50-80 ft (15-24 m) depth. The tuff is vitreous, massive, and well indurated with black inclusions. The inclusions are so small (0.003 mm) that it is not clear whether they are crystal or glass. Diatoms are present in the claystone at 60 ft (18 m) depth, occur in all units to a depth of 140-150 ft (43-46 m), and may occur below this unit.

Below the clay units are black andesitic-basaltic fragments, probably representing flow sequences at 100-140 ft, 300-360 ft, and 520-540 ft (30-43 m, 90-110 m, and 160-164 m) intervals and with a small portion of diatomaceous clay and tuffaceous sediment, possibly interbedded material. Red basic volcanic fragments occur at the 250-260 ft (76-80 m) interval. They are aphanitic and vitreous with black glassy inclusions/phenocrysts. These fragments are similar to the red volcanic lapilli in KF #1 at the 350-360 ft (107-110 m) interval. A very pure andesitic-basaltic volcanic sequence occurs at 280 ft (85 m) depth and extends to a depth of 360 ft (110 m). It is black, massive, and vitreous with few inclusions/phenocrysts.

Below the thick volcanic unit ia a series of volcanic sediment, silt ash, "micro-graywacke," claystone, and basaltic fragments from 360 ft (110 m) to a depth of 660 ft (200 m). The unit looks like volcanic detritus, ash, and reworked flow fragments representing a period of deposition between volcanic flows.

At the 830-ft depth, a thin grey vitreous tuff, with basaltic-andesitic fragments, extends to the total depth of the well. The base of this unit is not known because sampling ends at 880 ft (268 m) depth. There is some mineralization and calcitic cementation. Moderate effervescence occurs in the samples from 140 ft (43 m) to the total depth of the well. The mineralization and cementation are associated with clay and siltstones and with vein and vug-filling in the volcanic fragments.

Lithology of YMCA-2 Well

The YMCA-2 well is located approximately 1 mile south-southeast of the KF-1 and 2 wells. The well is 1410 ft (430 m) deep; however, rock cuttings were collected only when the lithology changed and to a depth of 1079 ft (329 m). Petrographic thin sections were prepared from several samples. However, due to the fine-grained texture and high glass content, it is very difficult to estimate the composition of the rock.

The lithology of YMCA-2 well, shown in Figure 5, varies from silt to claystone and from volcanic sediment to basaltic-andesitic flows. It differs from wells KF-1 and KF-2 in that there is less alteration of the rock, and the first basaltic-andesitic flow, at a depth of 860 ft (262 m), is several hundred feet deeper than the KF-1 and KF-2 wells.

The upper units are a sequence of tuffaceous sediments and vitreous tuff. Below the tuffaceous sediment is a 50-ft (15 m) transition sequence of volcanic detritus above the volcanic flow unit(s). From 857 ft (261 m) to the depth of the well (1079 ft, 329 m), andesitic-basaltic volcanic fragments occur. They are dark gray; aphanitic, massive with few glassy inclusions; silica, pyrite, and opaline vein filling; and some vugs. It is evident from petrographic thin sections that 80-90% of the volcanic material is feldspar and 10-20% is glass, towards the mafic end in composition.

Within the 912- to 1070-ft (278-326 m) interval, a small percentage of red scoriaceous volcanic fragments occur with elongated black glassy and white opaline inclusions. The last sample, the 1070- to 1077-ft (326-238 m) interval, represents a dark-gray andesite flow unit with gray and red aphanitic volcanic fragments. Examination of the drillers' log suggests that flow units may occur throughout the depth of the well.

One problem has been that the drillers' cuttings and the petrographic thin sections are very fine grained, and it is difficult to identify minerals and to obtain an accurate estimate of feldspar composition. Therefore, these limitations must be kept in mind in interpreting this lithologic column. Using extinction angles of combined Carlsbad and albite twins, the feldspar composition is estimated as andesine-labradorite and the volcanics as andesite. However, basalt may be present in different horizons within this and other flow sequences.

TEMPERATURE PROFILES

Temperature profiles were measured in KF-2 and YMCA-2 and are compared to the lithology in Figures 5 and 6. In city well KF-2, the temperature remained almost constant at 195°F (91°C) from 250 to 800 ft (76-244 m) depth. The initial thermal gradient was high and a maximum temperature of 206°F (97°C) was reached at a depth of 200 ft (60 m) where a lost circulation zone was penetrated. The lost circulation zone (LC) occurs in a unit of andesitic-basaltic fragments, probably a volcanic flow sequence(s). The upper boundary of the LC zone corresponds with the upper contact of the rock unit, and the base of the zone shows no response to the lithology because the flow sequence extends below the zone. However, the base of the LC zone may occur along a volcanic flow boundary or along a fracture plane. The nearly constant temperature from 360 ft to 800 ft is probably caused by the flow of fluid down the wellbore from about 360 ft and into the formation at 850 ft.

In the YMCA-2 well the temperature reading begins at a depth of 500 ft (150 m) and the profile extends from 800 ft (244 m) to the total depth of the well (Fig. 5). The gradient increases uniformly from 100°F (38°C) to 155°F (68°C). There is little influence of the change of lithology on the temperature profile and no major lost circulation zone was penetrated.

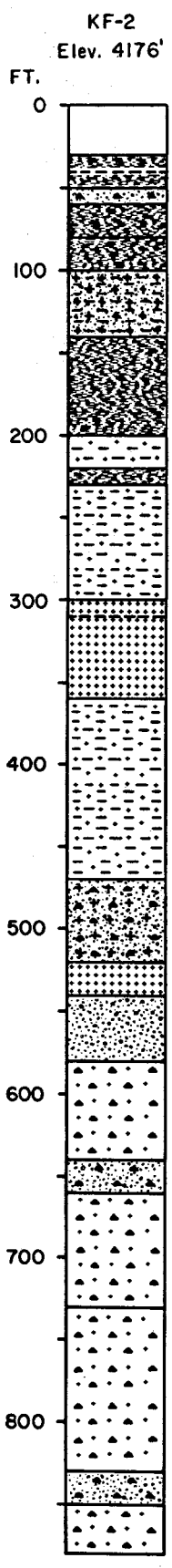

No sample.

Buff-brown clay with few glassy-pumice fragments, unconsolidated.

Light gray clay, vitreous, glassy, lithic frag. moderate consolidation.

Brown ash with white tuff fragments.

Gray vitreous claystone, poorly indurated, with white tuff fragments.

Massive gray claystone, moderate to well indurated, conchoidal fracture.

Black basic volcanic fragments, with gray tuffaceous sediment and gray claystone with diatoms, Stephanodiscus sp. 100-110, 120-130 ft.

Gray to brown calcitic silty claystone with basic volcanic fragments. Claystone is poor to moderately well indurated, vitreous, effervescent, with few glassy fragments.
- 180-190' trace amount volcanic lapilli
- 190-200' first occurrence pyrite, euhedral, 2 mm, vein filling.

Dark gray basic volcanic fragments and gray silty calcitic claystone with trace amounts of white tuff fragments, diatoms.

Gray calcitic silty claystone, with basic volcanic fragments, tuff, pyrite.

Gray basic volcanic fragments with calcitic claystone and pyrite, silica and pyrite veination, trace rhyolitic tuff and porcelain fragments.
- 252' gray siliceous tuff
- 250-260' red volcanic fragments with black glassy inclusions
- 270-280' possible baked contact.

Salt and pepper basic volcanic fragments with clear, white and black microphenocrysts.

Black basic volcanic fragments, angular, massive, vitreous luster.

Gray volcanic silty sediment, unconsolidated to poorly consolidated, with calcitic matrix, few volcanic fragments with inclusions, few white tuff fragments.
- 450-460' first occurrence marcasite/chalcopyrite (?)

Volcanic fragments and ash in siliceous and calcitic matrix, a "micro-graywacke."
- 480-490' first occurrence of green mineral
- 510-520' pyrite and chalcopyrite (?) phenocrysts, 2.0 mm.

Black aphanitic basic volcanic frag., vitreous, white glassy "powder" on surface, some glassy shards.
- 520-530' euhedral pyrite crystals, 2-4.0 mm
- 530-540' subhedral calcite, 1-2 mm; euhedral pyrite 1-3 mm; red cinders, 1-2 mm.

Gray volcanic ash-silty claystone, first occurrence zeolite 540-550'
- 570-580' first occurrence Fe oxide, illite (?)

Unconsolidated volcanic sediment with black basic volcanic fragments and vitreous tuff with inclusions.

Red scoriaceous tuff with glassy inclusions and basic volcanic fragments; 650-660' zeolite, euhedral.

Gray basic volcanic fragments, vitric, aphanitic, massive, with white glassy "powder" on surface.
- 660-670' zeolite, 0.25-0.75 mm
- 670-680' black glassy fragments, obsidian (?)
- 680-690' white milky to green mineral; first occurrence
- 700-710' red tuffaceous frag., vitreous; white and black glassy inclusions
- 720-730' pyrite associated with volcanic fragments.

Gray basic volcanic fragments with varied texture: aphanitic and massive to vesicular, micro-phenocrysts, white aphanitic to opaline vug filling, pyrite.
- 760-770' white tuffaceous and red tuffaceous fragments
- 780-790' subrounded volcanic fragments old surface (?)
- 820-820' Fe oxide vein filling, illite (?).

Gray vitreous tuffaceous fragments with vitreous black and white inclusions with volcanic ash and silt, basic volcanic fragments and white tuffaceous fragments.

Light to dark gray basic volcanic fragments, vitreous, aphanitic, massive, subangular to subrounded, often with vitreous inclusions, red tuffaceous fragments, moderate effervescence.

Figure 4. Lithologic column for Klamath Falls City Well #2 (KF-2 on location map Fig. 2). Rock description based on drillers' cuttings. [XBL-806-7165]

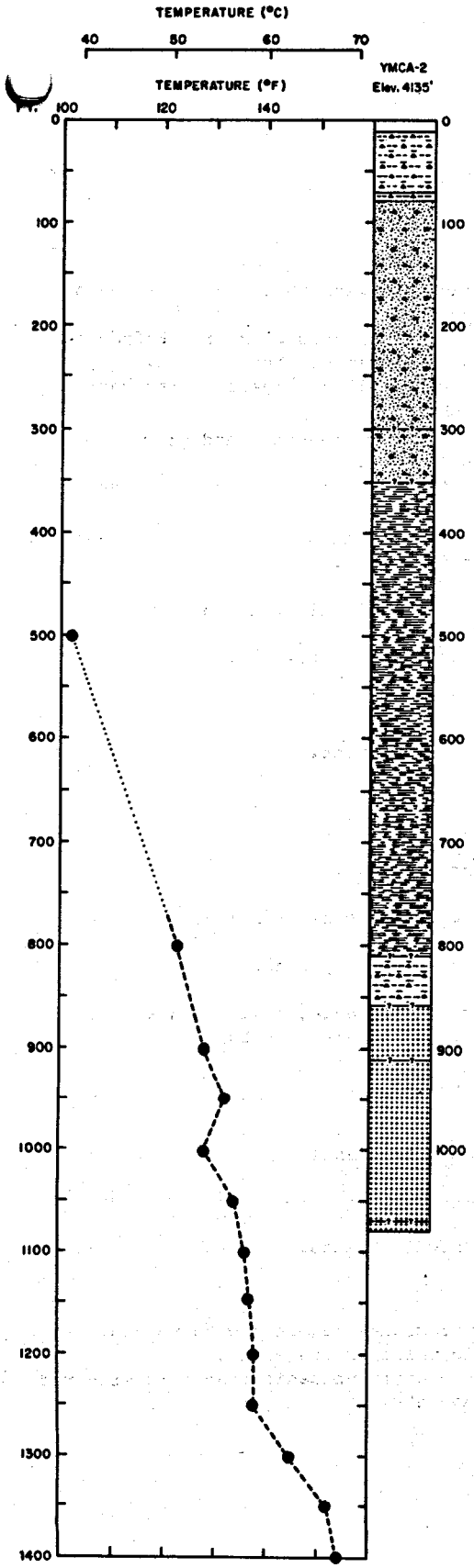

Brown silty soil with volcanic detritus.
Buff tuffaceous sediments with glassy shards.

Gray tuffaceous sediment, massive, moderate induration with glassy shards.

Light gray vitreous tuff with black glassy inclusions, massive, moderate induration, mainly feldspathic, andesine/labradorite, trace mica, pyroxene; diatoms: Stephanodiscus sp., Melosira granulata.

Light-medium gray vitreous tuff with lithic, black glassy and andesitic inclusions, aphanitic, massive, moderately well indurated, opaline to cryptocrystalline quartz, andesine/labradorite, trace magnetite; diatoms: Stephanodiscus sp., Melosira granulata, Cymbella sp.

Light gray clay, tuffaceous, vitreous, few glassy and lithic inclusions, poor to moderate induration.

Gray volcanic sediment, white vitreous tuff with glassy inclusions, gray porceleinite, dark gray basic volcanic fragments.
Dark gray to black vitreous basic volcanic fragments, aphanitic, massive, opaline vein filling, pyrite.

Dark gray volcanic fragments, vitreous, aphanitic, massive, silica-opaline vug filling, with trace white vitreous tuff, pyrite, biotite and magnetite.

Dark gray andesite fragments with gray and red basic volcanic fragments, aphanitic, massive to vesicular, andesine/labradorite, some vugs filled with silica-opaline.

Figure 5. Lithologic column and temperature profile for YMCA-2 well. Rock description based on rock cuttings and petrographic thin sections.
[XBL-806-7166A]

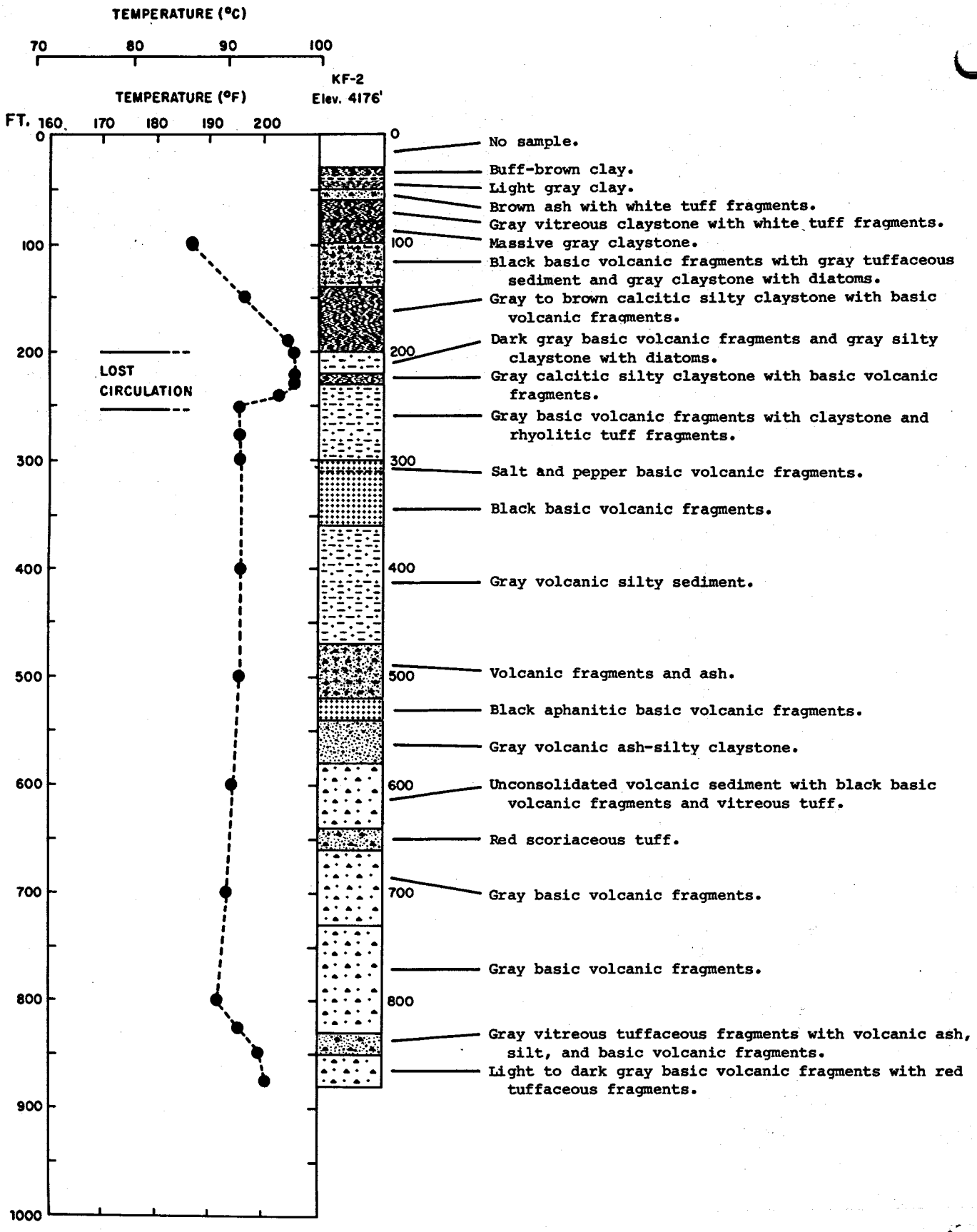

Figure 6. Temperature profile and lithology for Klamath Falls City Well #2. [XBL-813-2763]

PUMP TESTS

Pump tests were conducted in the three wells gain information about reservoir continuity and permeability. Well casing and flow characteristics are tabulated in Table 1.

Table 1. Well completion and flow characteristics.

Well	KF-1	KF-2	KF-2	YMCA-2
Casing size (in.)	12	12	12	9-5/8
Cased depth (ft)	300	360*	0-195 200-240	980
Open interval (ft)	300-360	360-900	195-240	980-1400
Flow rate (gpm)	700	60	900	300
Transmissivity (mD-ft/cP)	7.25×10^6			1.1×10^6

* Perforated from 195 to 240 ft after temperature is taken.

KF-1 was pump tested in September 1979 by pumping for a total of 15 hr. A maximum flow rate of 700 gpm (44 liter/s) was held constant for a period of 7.5 hr with a drawdown of 70 ft (21 m). The discharge temperature of the brine was 218°F (104°C). Three observation wells were monitored during the pump test at a distance of 1500 ft (460 m), 1000 ft (300 m), and 150 ft (46 m). Rapid pressure drops indicated a high degree of hydraulic continuity throughout several distinct lithologic units. Analysis of the test data indicate very high reservoir permeability.

KF-2 was pump tested in February 1980. During the time of this pump test, the well was cased to 360 ft (110 m). A flow rate of about 60 gpm (4 liters/s), with 170 ft (52 m) of drawdown, was obtained. The discharge temperature of the brine was 185°F (85°C). Several observation wells were monitored during the pump test, but no pressure change was observed. Since the flow rate out of the well was so small, no information about reservoir continuity could be gained. On the basis of a thermal anomaly in the temperature profile (see Fig. 6), the interval between 195 and 240 ft (61-73 m) was identified as a potential production zone. The well was then perforated in this zone and pump tested. A flow rate of about 900 gpm (57 liter/s) with 212°F (100°C) brine was reported (Derrah, 1979).

YMCA-2 was pump tested in August 1979 by pumping for approximately 20 hr. A maximum rate of 300 gpm (19 liters/s) with 180 ft (55 m) of drawdown was maintained for 4.5 hr. The brine discharge temperature was about 146°F (63°C). An observation well, 500 ft (152 m) from the production well, was monitored during the pump test. Pressure data analysis from the observation well indicates a reservoir permeability of about 1 darcy. However, without a detailed spinner survey of the wellbore, it is not possible to determine if the production is uniform over the open interval of the well.

DISCUSSION

Several factors are important in interpreting the geology of the Klamath Falls geothermal field. The KGRA is located in an area of active faulting, mostly near vertical normal faults. There are three fault systems trending NW-SE, N-S, and NNE-SSW. The predominant rock units are andesitic-basaltic volcanics, tuff and tuffaceous siltstones, and volcanic sediments. The units vary in thickness and distribution, sometimes interbedded and in fault contact. Jointing is present in surface outcrops of some volcanic flow sequences. Consequently, without detailed field mapping, it is difficult to correlate the rock units, even over a short geographical distance.

Comparing the lithologic columns, temperature profiles, and well tests, indicates that lithology and change in rock type have little effect on the reservoir and flow within the city area of the KGRA. Instead, flow properties appear to be controlled more by regional structure, fault systems, and fracture planes. Because the nature and location of these flow surfaces cannot be accurately described by drillers' cuttings, well logs and core sections and further well testing will be required to assess the hydrogeology of the Klamath Falls KGRA.

ACKNOWLEDGMENTS

We wish to acknowledge the assistance of Edward A. Sammel of the U.S. Geological Survey, Norman V. Peterson of Oregon Department of Geology and Mineral Industries, and John W. Lund of Oregon Institute of Technology, for their willingness to discuss the geology and reservoir characteristics of the Klamath Falls KGRA. Appreciation is due many individuals in the Klamath Falls and Oregon government agencies and to well owners for their cooperation in developing information on the geothermal field. Finally, special thanks to Margot Harding and Marilee Bailey for their fine drafting of the figures.

REFERENCES CITED

Benson, S., Goranson, C., and Schroeder, R. C., 1979. Evaluation of City Well 1, Klamath Falls, Oregon. Earth Sciences Division Annual Report 1979, Berkeley, Lawrence Berkeley Laboratory, LBL-10686, p. 69-76.

Newcomb, R. C., 1958. Yonna Formation of the Klamath River basin, Oregon. Northwest Science, v. 32, no. 2, p. 41-48.

O'Brien, M. T., Benson, S. M., and Goranson, C. B., 1981. Subsurface geology of three geothermal wells, Klamath Falls, Oregon. Berkeley, Lawrence Berkeley Laboratory, LBL-11240, in preparation.

Peterson, N. V. and McIntyre, J. R., 1970. The reconnaissance geology and mineral resources of eastern Klamath County and western Lake County, Oregon. Oregon Dept. Geol. Min. Ind. Bul. 66, 70 p.

Sammel, E. A., 1980. Hydrogeologic appraisal of the Klamath Falls geothermal area, Oregon. U. S. G. S. Prof. Paper 1044-G, 45 p.

U. S. Geological Survey, 1978. Geothermal Hydrology and Geochemistry of Klamath Falls, Oregon, Urban Area. Final Report for USGS Contract #14-08-0001-6-791.

SUBSURFACE HYDROGEOLOGY OF THE SUSANVILLE, CALIFORNIA, GEOTHERMAL RESOURCE

S. M. Benson and M. Bodvarsson

The Susanville geothermal anomaly is located in northeastern California, at the foot of the Sierra Nevada. The presence of several shallow hot-water wells and a natural hot spring initially identified this area as a prospective site for the development of geothermal energy. More recently, increased fossil fuel costs and the high price of transporting liquified natural gas to Susanville and the surrounding area stimulated interest in developing the resource for a city-wide space heating program. Since late 1978, the Water and Power Resources Service and the Earth Sciences Division of Lawrence Berkeley Laboratory (LBL) have collaborated on a geothermal resource evaluation project at Susanville. As part of this project, 12 deep and 5 shallow temperature-gradient holes were drilled, subsurface geologic and geophysical data were analyzed, and a well test was conducted. The results of the well test have been discussed in several reports (Benson et al., 1979, 1980). This article summarizes the subsurface geology and geophysical logs.

GEOLOGIC SETTING

The city of Susanville is located at the intersection of three major physiographic provinces: the Modoc Plateau, the Sierra Nevada, and the Basin and Range province (see Fig. 1). Plio-Pleistocene volcanic rocks form a dissected plateau north and west of the city. These volcanics have been identified (U. S. Bureau of Reclamation, 1976a) as members of the Warner Basalt, a collective unit of petrographically and structurally similar lavas found throughout the Modoc Plateau. South of Susanville lie the Jurassic-Cretaceous quartz monzonite and quartz diorite of the Sierra batholith. Extending east and southeast from Susanville is the graben-like structure of Honey Lake Valley, filled in part by Pleistocene sediments of extinct Lake Lahontan.

The Susanville geothermal exploratory wells penetrated Holocene alluvium and Pleistocene Lake Lahontan sediments, interbedded with Plio-Pleistocene basalts and andesites. These same lithologic units are penetrated by water wells in the Susanville-Johnsonville area and typically provide good yields of groundwater. The amounts of water produced from either the basalt or the sediments are not well understood (Rudser, 1978). Meteoric water permeates through fractures and joints in the basalt and along vesicular and scoriaceous zones at the top and bottom of the basalt units. The Lake Lahontan sediments thicken to the east of Susanville. To the south, they interface with coarser, near-shore Lahontan deposits. These near-shore deposits crop out along the base of Diamond Ridge.

The geologic relationships formed between rock units of the three major intersecting provinces are too complex to be discussed in detail here. We can comment, however, on stratigraphic and structural characteristics of the potential Susanville geothermal area, based on observations made from lithologic and geophysical well bore logs.

Geothermal Wells in the City of Susanville

Twenty-three temperature gradient holes and wells have been drilled in the city of Susanville to date. Five temperature gradient holes were drilled and four (TG-1, TG-17, TG-18, TG-19) were completed to a target depth of 46 m for preliminary resource identification. Between 1977 and 1980, the Water and Power Resources Service drilled twelve exploratory holes (Suzy 1 through Suzy 11 and Suzy 9A), with depths of 135 m to 640 m, in an attempt to outline the areal extent of the geothermal anomaly. Standard heat flow completions were used for most of the wells (Benson et al., 1980). Six older wells, five drilled in the 1920s and one drilled in the early 1960s, are also present. Well locations are shown in Figure 2.

Lithologic well logs compiled during drilling are available in another report, as are the geophysical well logs prepared in part by a commercial logging company (for wells Suzy 2 and 3) and a government well logging service (Benson et al., 1980). The standard suite recorded by the government service was as follows: SP, caliper, resistivity, neutron, gamma-gamma ray, natural gamma ray, and temperature (SP, caliper, and resistivity were not run in the cased holes). The suite recorded in Suzy 2 and 3 was slightly different. With the

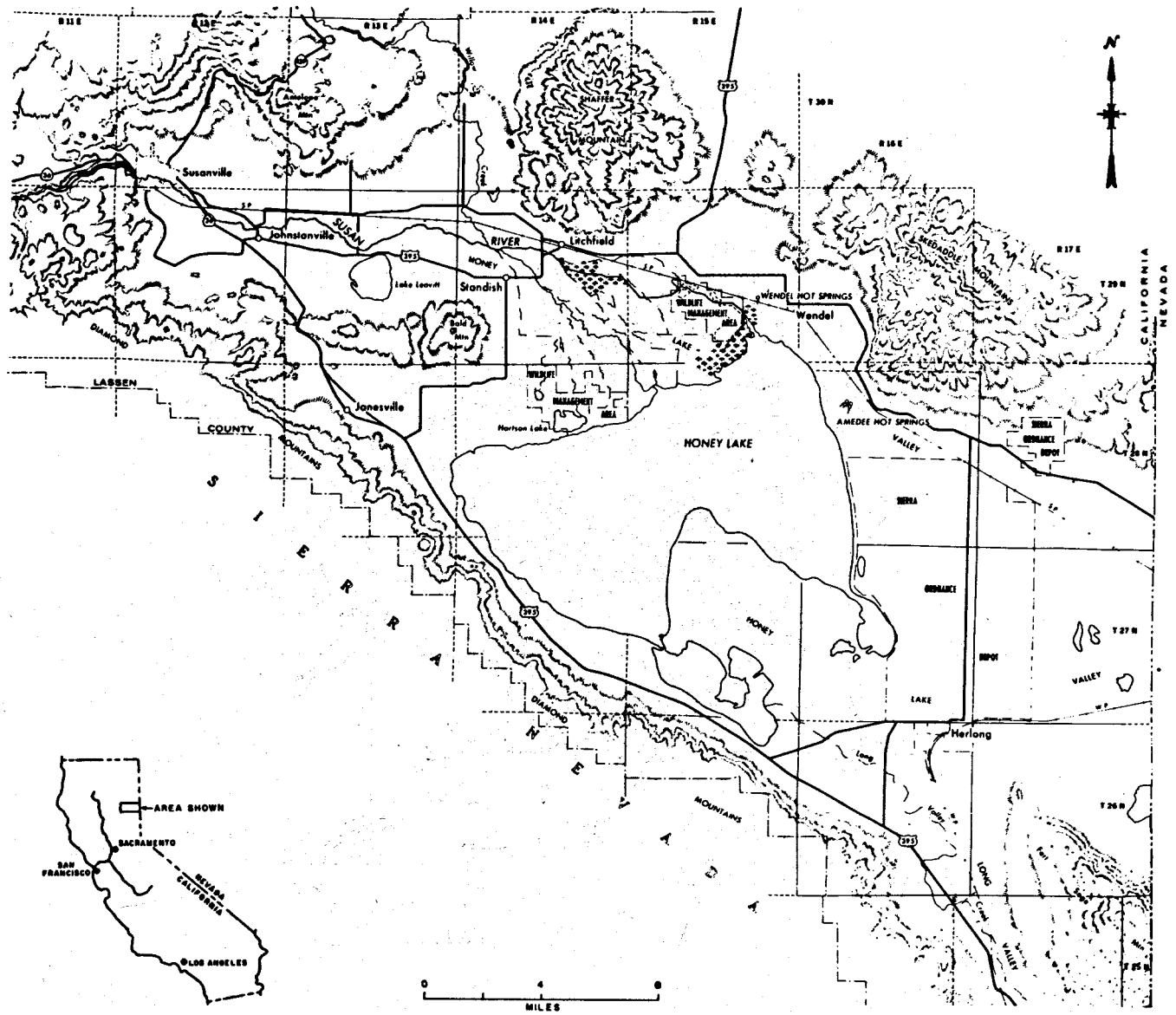

Figure 1. Location map of Susanville Geothermal Anomaly (U. S. Bureau of Reclamation, 1976a). [XBL 813-2697]

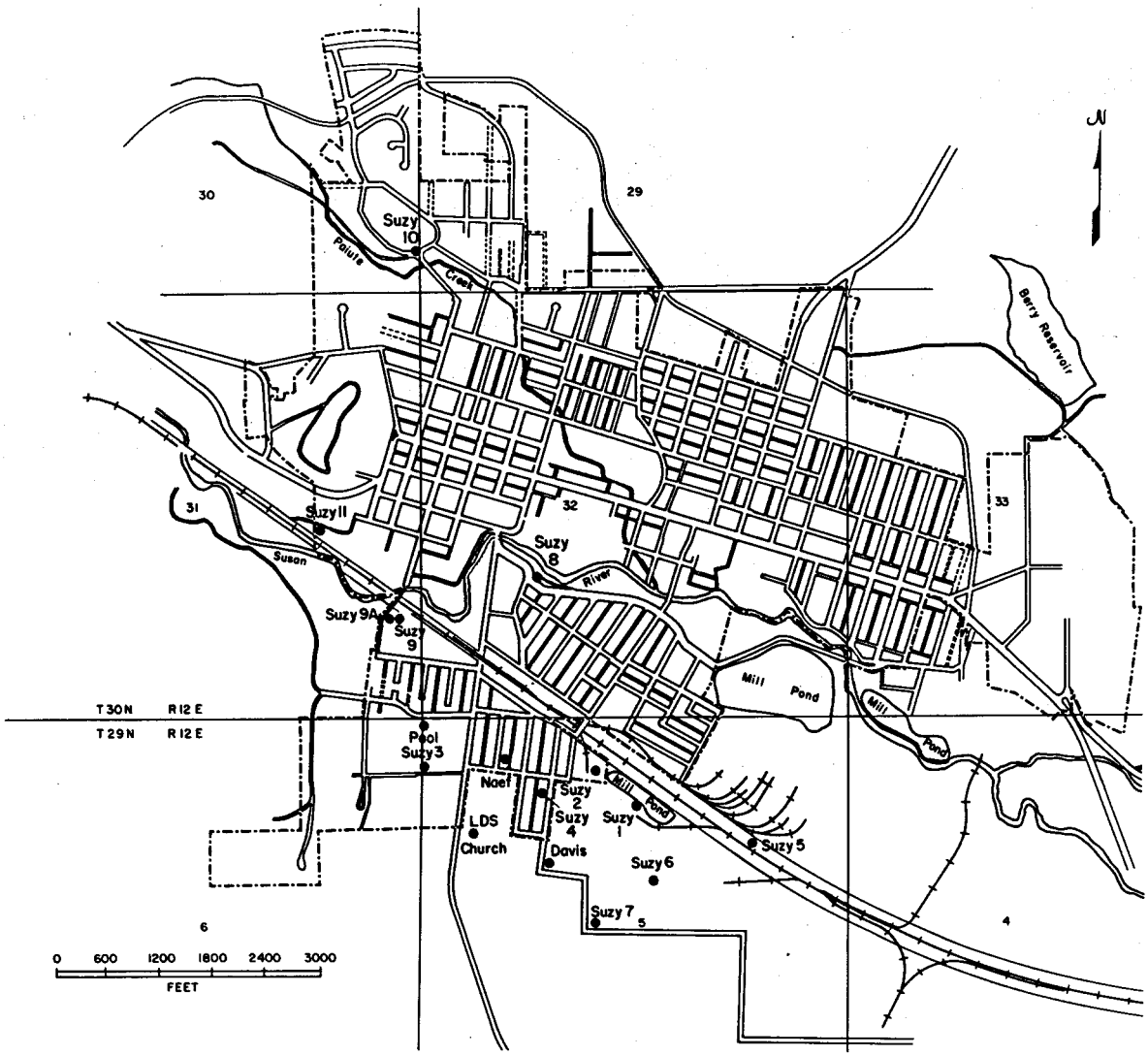

Figure 2. Location map of wells drilled to date in Susanville. [XBL 801-6767]

exception of the Naef well, geophysical well logs were not run in the wells drilled prior to this investigation (the Naef, Davis, L.D.S. Church, Lassen Lumber and Box #2, and Wirth wells), and little information is available on total depths and well completion.

Interpretation of Subsurface Logs

Two basalt beds were identified as marker units on the natural gamma ray logs. Correlations between wells drilled in these two units inferred the structural relationships of the lithologic units penetrated. One of the basalt beds is typically penetrated within the first 30 m of drilling. The second bed is encountered between 90 and 150 m. The basalt beds are absent or ill-defined on the Suzy 3 natural gamma well log. The upper basalt bed is not evident, and there is a poorly defined basalt bed between 40 and 70 m. In Suzy 9, 9A, and 11, the upper basalt bed is present, but the lower bed is andesite rather than basalt.

On the basis of the gamma ray log correlations, the Susanville geothermal prospect has been divided into five structural units (Fig. 3). Cross sections have been constructed to illustrate the structural relationships between the various units (Figs. 4 and 5). The Susanville wells typically penetrate 3-5 m of recent Holocene alluvial deposits, 6-20 m of basalt, 90-120 m of interbedded Lake Lahontan sediments and Pleistocene basalt lenses, and 30+ m of Plio-Pleistocene basalt (Benson et al., 1980).

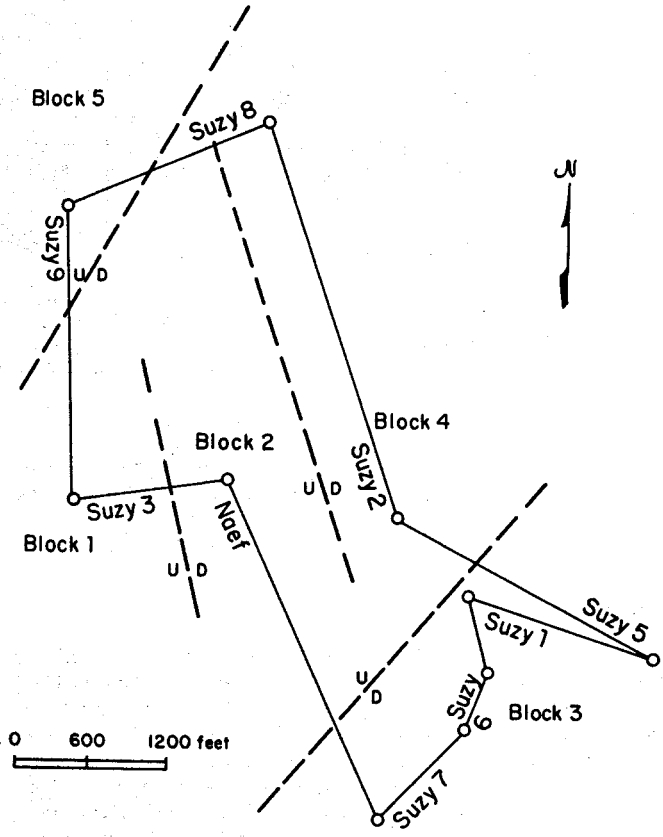

Figure 3. Division of the Susanville geothermal prospect into five structural units.
[XBL 806-7210]

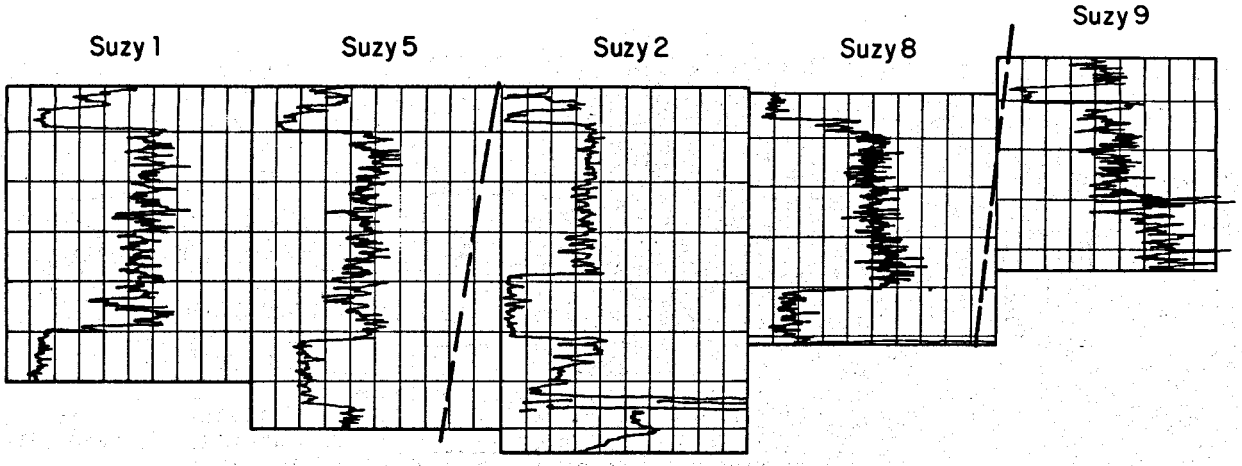

Figure 4. Cross sections showing relationships between various structural units, as indicated by the natural gamma logs. [XBL 806-7211]

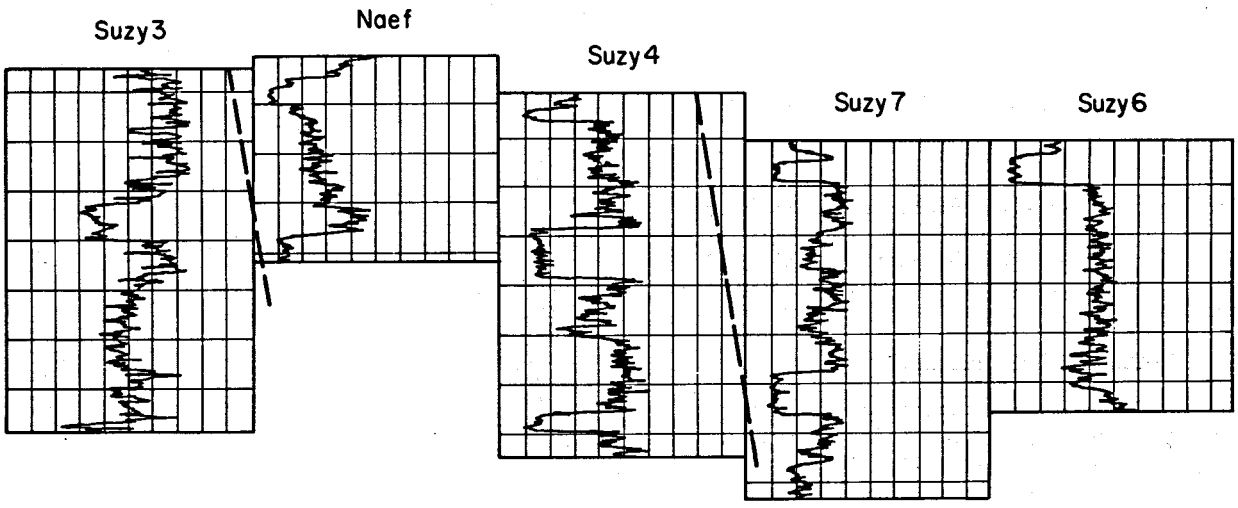

Figure 5. Cross sections showing relationships between various structural units, as indicated by the natural gamma logs. [XBL 806-7209]

Petrologic Studies

The Water and Power Resources Service obtained core samples from several of the wells. Several of the cores from the basaltic units had fracture planes and vugs which were filled with hydrothermal mineral deposits. These deposits were primarily composed of zeolitic minerals and carbonates. The fracture plane mineral deposits from well Suzy 9A were analyzed to determine what type of hydrothermal mineralization had taken place and, specifically, what type of zeolites were present. Correlation of zeolite species with different thermal regimes provides valuable information about the thermal history of the resource. Three distinct zones of mineralization were identified.

Figure 6 shows a thin section of the fracture-coating hydrothermal deposit of the Suzy 9 core. From the outer surface to the rock substrate, the three zones are:

1. A buff-gray, fine-grained crystalline layer about 1.5 mm thick.

2. A translucent to white coarse grained crystalline layer with large crystals, approximately 3.5 mm thick.

3. A fine-grained, white to gray-white layer about 1 mm thick adjoining the rock surface.

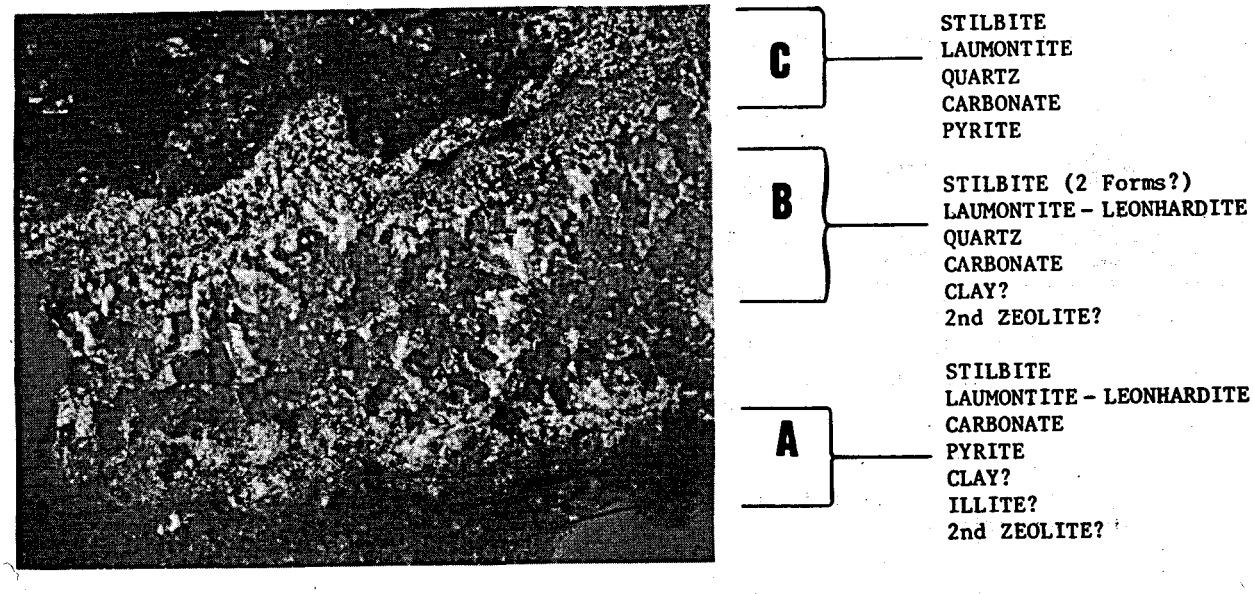

Figure 6. Thin section of the fracture-coating hydrothermal deposit under crossed nichols. [XBB 800-11506]

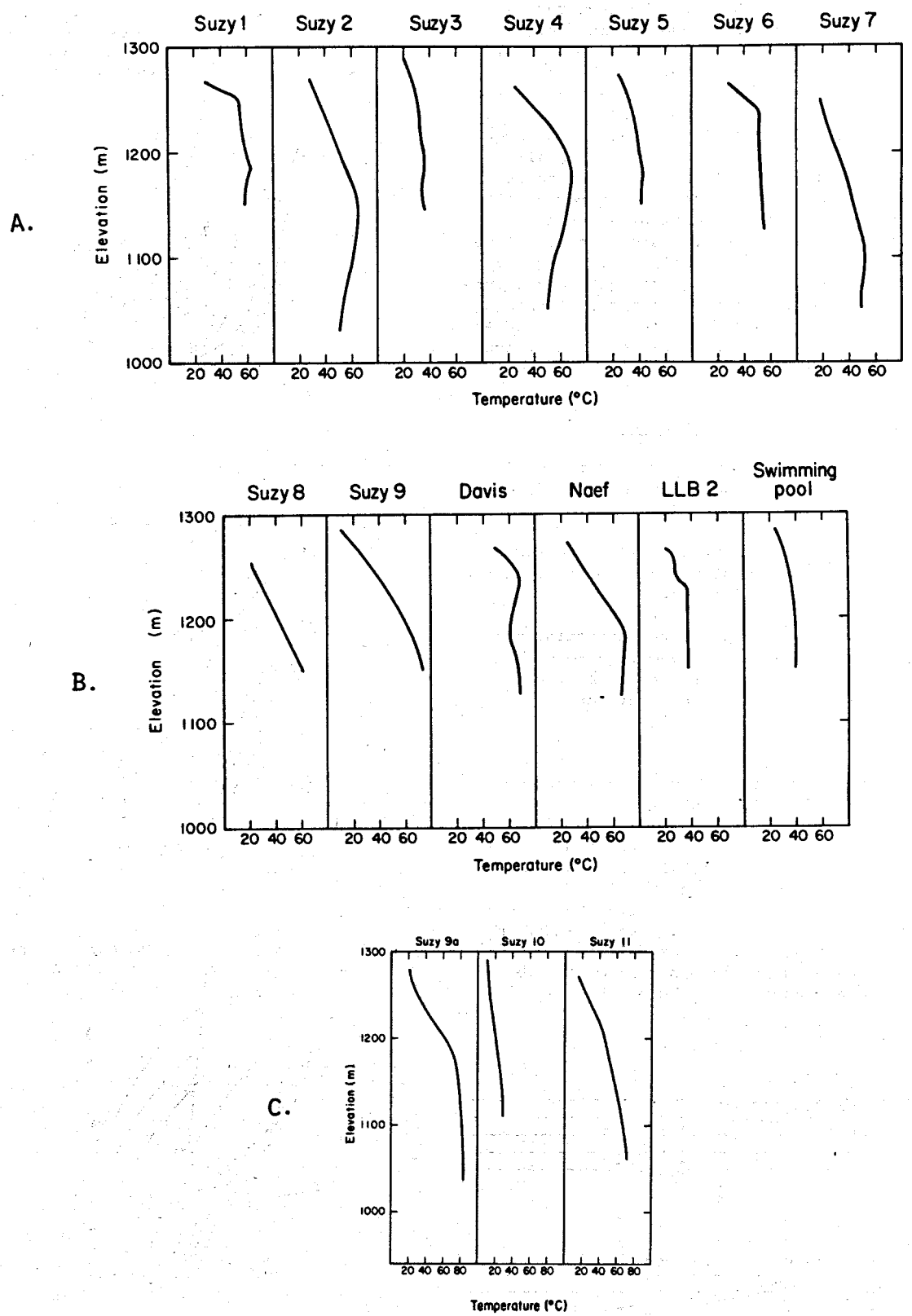

Figure 7. Temperature profiles from wells: (A) Suzy 1 through 7; (B) Suzy 8 and 9, the Davis, Naef, LLB#2, and Swimming Pool wells; and (C) Suzy 9a, 10, and 11. [XBL 8011-6422]

Tómasson and Kristmannsdóttir (1972) have identified temperature and depth zones for zeolites deposited in Icelandic basalts. The temperature zones in order of increasing temperature are: a chabazite zone, a mesolite/scolecite zone, a stilbite zone, and a laumontite zone. If the zeolite temperature sequence is applied to layers A, B, and C, it can be implied that layers A and C reflect a temperature range of 70°-150°C and layer B a range of 70-110°C. The thickness and coarse crystalline form of layer B suggest that the producing solutions were probably present for a much longer period of time than those solutions producing layers A or C. The thickness of the entire fracture plane (zeolite sequence) is quite large (5.5 mm), suggesting that warm solutions have been moving through the fracture plane for a considerable period of time. Although there are uncertainties in the relationship between temperature, solution, and zeolite deposition, the sample indicates that this geothermal system has long been in existence.

Temperature Distribution of the Anomaly

Temperature profiles obtained from the wells are shown in Figure 7. Examination of the temperature logs indicate several trends:

1. The temperature profiles are characteristically similar for wells within each block outlined by the structural study (Fig. 8).

2. In wells with temperature reversals, the maximum temperatures were recorded in a zone immediately above or below the contact between the Lake Lahontan sediments and the lower basalt or andesite unit.

3. Temperatures are generally warmest in Blocks 2, 4, and 5, with maximum temperatures in the wells ranging from 35 to 83°C.

Subsurface temperatures are contoured at three subsurface elevations (1250 m, 1200 m, and 1150 m) in Figure 9. As illustrated, at shallow depths (elev. 1300 m; 50 m below average ground surface), the anomaly is centered around the Davis and Naef wells. At greater depths, the anomaly becomes asymmetrically shaped around a northwest trending axis. The anomaly deepens to the northwest.

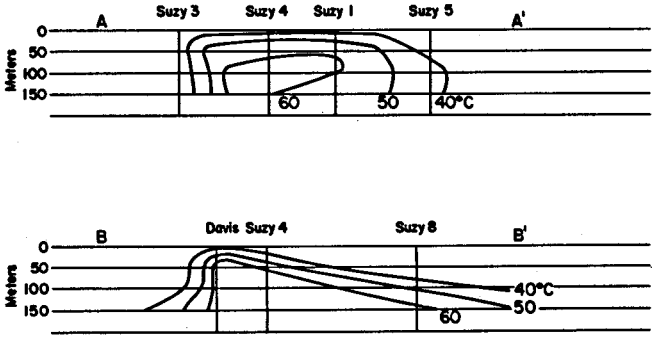

Figure 8. Cross sections of the thermal anomaly. [XBL 796-7511]

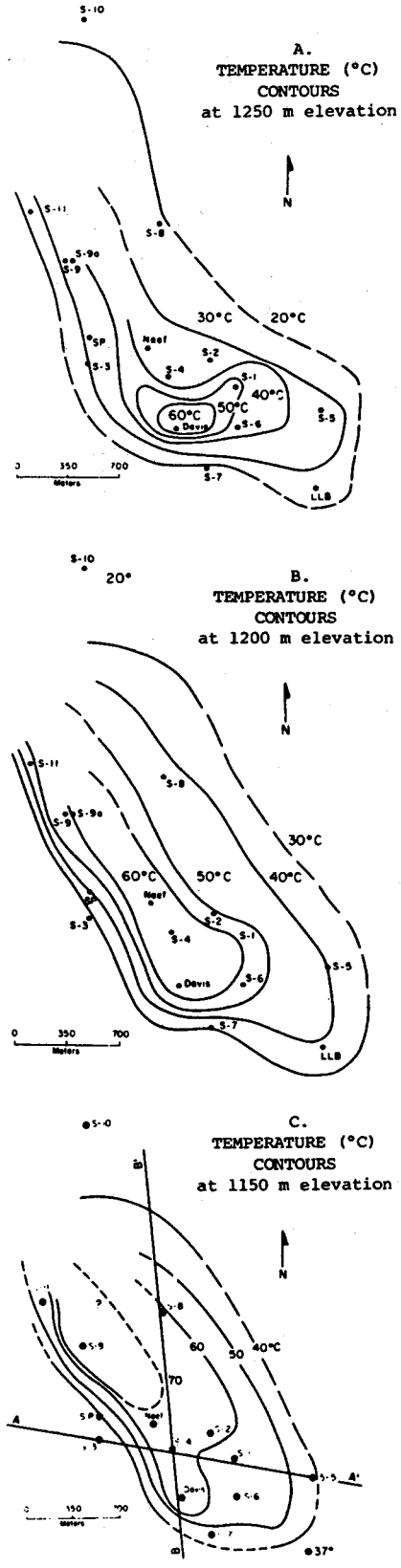

Figure 9. Subsurface temperature contours (A) at 1250 m elevation; (B) at 1200 m elevation; and (C) at 1150 m elevation. [XBL 8011-6423]

The anomaly is sharply bounded to the west, indicating a hydrologic and/or geologic discontinuity; e.g., a fault or a fracture zone. To the east and north, the thermal anomaly gradually abates, while it is more abruptly bounded to the south. Analyses of cores and geophysical data suggest cooler groundwater from shallow saturated strata may be mixing with geothermal fluids in these areas. The asymmetrically shaped thermal anomaly and the noticeable temperature reversals in the southern portion of the field suggest that heated fluids are upwelling along a NW-trending fault, or at the intersection of several faults. They are then dispersed into the reservoir, flowing through the most permeable strata. In the southern portion of the anomaly, the basalt-agglomerate interface appears to be the most permeable.

SUSANVILLE WELL TESTS

From December 10, 1978, to January 8, 1979, the Reservoir Engineering Group at LBL conducted a well test in Susanville (Benson et al., 1979, 1980). Eight observation wells and one production well were monitored. The well test consisted of four segments, the first segment involving the measuring of background data prior to pumping the Davis well.

The second segment of the test consisted of pumping the Davis well at a rate of 250 gpm for a period of 9 days. The well was then shut in, and the pressure build-up was observed. Several days after the Davis well was shut in, the Church well was shut in for twelve hours, then pumped again for several days; shut in for twelve hours, and then pumped continuously for the duration of the test. During the last segment of the test, the Roosevelt swimming pool well was pumped at a rate of 275 gpm for three days and then shut in. Table 1 presents a summary of the values obtained from the well tests and possible indications of reservoir boundaries. Benson et al. (1980) provide a detailed description of the Susanville well test.

Pressure data indicate hydraulic continuity between all of the observation wells and production wells. Preliminary analysis indicates that the reservoir has a permeability on the order of several darcies. Porosity values extracted from the reservoir storativity are ambiguous. However, low storativity values obtained indicate secondary permeability (fracture permeability) may be playing a major role in fluid movement throughout this section of the reservoir.

CONCLUSIONS

The occurrence of the Susanville geothermal anomaly appears to be related to a northwest trending fault and/or the intersection of several faults. Temperature contours and temperature profiles suggest that heated fluids upwell along the fault and are then dispersed into the highly permeable agglomerate-basalt interface and/or permeable zones within the fractured volcanic sequence. The hot water reservoir deepens to the northwest. These higher temperatures indicate that this fluid is less diluted with cool groundwater. Areal confinement of the shallow thermal anomaly has been established for three sides of the resource (west, east, and south). The northwestern boundary of the thermal anomaly has not been completely defined. In the southern portion, the thermal anomaly is vertically confined at or near the agglomerate-basalt interface, as indicated by a temperature reversal. No temperature reversal occurs in the temperature gradient holes in the northern part of the anomaly. However, temperatures are not known at depths below 300 m. The maximum temperature measured, 84°C, was in well Suzy 9A. Petrologic studies of a fracture coating from well Suzy 9 indicate fluids of temperatures betwen 70°C and 150°C have been flowing through the fracture system for some time. This temperature range agrees with the temperature regimes indicated from water samples (U. S. Bureau of Reclamation, 1976b).

Analyses of interference and production test data from the southern portion of the anomaly give high permeability values. Storativity values are low, suggesting a low porosity of the producing strata. This information is consistent with geologic data indicating a fracture-dominated hydrologic system. Wells in the northern portion of the resource have not been sufficiently tested at this time to make estimates of the productivity of these higher-temperature fluids.

Table 1. Summary of well test values and indications of reservoir boundaries.

Observation well	Pumped well	KH/μ	ϕch	Indication of reservoir boundaries
Naef	Church	$3.6 \times 10^{6}\ \frac{mD\text{-}ft}{cp}$	2.3×10^{-4} ft/psi	Barrier boundary
Naef	Davis	$2.3 \times 10^{6}\ \frac{mD\text{-}ft}{cp}$	7.2×10^{-4} ft/psi	Barrier boundary
Naef	Swimming pool	$3.4 \times 10^{6}\ \frac{mD\text{-}ft}{cp}$	3.9×10^{-2} ft/psi	None
Davis	Davis	$7.3 \times 10^{5}\ \frac{mD\text{-}ft}{cp}$	Not obtained	None

REFERENCES CITED

Benson, S., Goranson, C., Haney, J. P., and Schroeder, R. C., 1979. Evaluation of the , Susanville, California, geothermal resource, 1979. Earth Sciences Division Annual Report 1979, Berkeley, Lawrence Berkeley Laboratory, LBL-10686, p. 76-87.

Benson, S., Goranson, C., Noble, J., Schroeder, R., Corrigan, D., and Wollenberg, H., 1980. Evaluation of the Susanville, California geothermal resource. Berkeley, Lawrence Berkeley Laboratory, LBL-11820.

Hay, H. L. , 1977. Geologic occurrence of zeolites, in L. B. Sant, and F. A. Mumpton (eds.), Natural zeolites: Occurrence, properties and use. Elmsford, New York, Pergamon Press.

Rudser, R., 1978. The geology and geothermal potential of Susanville, Lassen County, California (M. S. thesis). Davis, University of Califor[illegible].

Tómasson, J., and Kristmannsdóttir, H., 1972. High temperature alteration minerals and thermal brines, Reykjavík, Iceland. Mineralogy and Petrology, v. 36, p. 123-137.

U. S. Bureau of Reclamation, 1976a. Susanville geothermal investigations: Special report 1976, and Susanville Geothermal Investigations: Supplemental Technical Data - Special Report 1976: Mid-Pacific Region, Sacramento, California.

U. S. Bureau of Reclamation, 1976b. Water quality analysis, inferred geothermal reservoir temperatures and reservoir evaluation test. Mid-Pacific Region, Sacramento, California.

ENERGY UTILIZATION TECHNOLOGY

GEOTHERMAL ENERGY UTILIZATION TECHNOLOGY

R. L. Fulton

The utilization technology portion of the geothermal energy program at Lawrence Berkeley Laboratory (LBL) provides the analytical tools and data required to fully understand the processes by which geothermal energy can be economically developed. Although this development requires accurate economic and technological assessment of the processes used, this information is not always available. The LBL utilization technology project attempts to provide this information, which is an extension of present technology into areas that were not of previous interest. The tools and data developed under this project and other Laboratory resources are then applied to Department of Energy (DOE) sponsored projects that serve as paths to the geothermal industry.

Because the binary-cycle process is expected to be the method chosen to exploit most moderate-temperature hydrothermal resources for electrical energy, most of our utilization technology projects are focused on this process. The Binary Fluid Experiment is providing laboratory-quality data on heat-transfer film coefficients of the various candidate hydrocarbon working fluids, and a DOE/EPRI heat-exchanger test will provide a verification of these data under field conditions. A study of fluid properties is underway that seeks to provide the best available thermodynamic and transport data on brines and working fluids. Direct-contact heat exchange is being investigated because it is expected to improve the economics of second-generation geothermal power plants.

In 1980 the Binary Fluid Experiment concentrated on condensation film coefficients for mixtures of isobutane and isopentane.

The DOE/EPRI field heat-exchanger test was relocated to the DOE Geothermal Component Test Facility at East Mesa, California, and made ready for tests that would start early in fiscal 1981.

The 500-kW Direct-Contact Heat Exchange pilot plant was completed at East Mesa and began an extended test program that will provide both system and subsystem performance data. Alternative methods of hydrocarbon removal from the effluent brine stream of a direct-contact heat exchanger were tested. An approach to the analysis of the direct-contact heat-exchanger performance was developed that takes into account the slight miscibility of the hydrocarbon and brine and provides a new parameter for evaluating the heat-transfer performance.

Our computer code, GEOTHM, was used to study the relationship of working-fluid composition and resource temperature for economically optimized binary-cycle power plants. In addition, a useful characterization parameter for the working fluid and its transposed critical temperature was identified and reported. Members of the LBL staff acted as technical advisers to the DOE project office on both the Baca Geothermal Demonstration Power Plant in New Mexico and the Heber Geothermal Binary Demonstration Power Plant in California's Imperial Valley.

The LBL geothermal utilization technology activities will continue into fiscal 1981 with completion of the Binary Fluid Experiment, the DOE/EPRI field heat exchanger test, and the extended test program for the 500-kW direct-contact pilot plant. Analytical work will be in support of the Heber Geothermal Binary Demonstration Power Plant and will begin an investigation of thermal energy conversion processes for the geopressured resource.

ANALYSIS OF DIRECT-CONTACT HEAT EXCHANGER PERFORMANCE

P. M. Rapier

The U. S. Department of Energy's Division of Geothermal Energy has undertaken a program to delineate and demonstrate the economic advantage of the Direct-Contact Heat Exchange (DCHX) process in power generation. A 500-kW DCHX pilot plant was placed under test at East Mesa in January 1980 by Barber-Nichols Engineering, subcontractor to Lawrence Berkeley Laboratory (LBL). Emphasis has been on accurately testing and modeling DCHX tower performance.

In operating the DCHX tower, the subcontractor overcame some severe startup problems throughout the plant and successfully completed the baseline tests. Computerized heat and mass balances to within 7% were conducted, which showed the instrumentation and calibration to be excellent. Nevertheless, within the DCHX column the available modeling and testing procedures were unable to establish a boiler/preheater interface; directly measure the pinch temperature; utilize the bulk temperature profile, which suggested strong preheater backmixing down to the 12-foot level; or explain why no brine temperatures higher than the two-phase boiling point have been observed. These and other inadequacies indicated the need for an alternative to the univariant three-phase boiling hypothesis, a need which LBL has already addressed by its development of a bivariant two-phase boiling model and an equilibrium flash boiler/preheater combination (Rapier 1978).

1980 ACTIVITIES

Patents Pending

Application was made for letters patent under the United States Department of Energy auspices for an equilibrium flash boiler, comprising the vapor continuous zone, or top section of the 500 kW DCHX tower. In baseline and preliminary tests conducted during 1980, this evaporator has met and exceeded the performance of its predecessors, the volumetric and surface type boilers, with only its essential features having been installed. The advantage of the equilibrium-flash process is that a greater percentage of the boiler feed can be vaporized at a given temperature and pressure than by other processes. (Perry, 1950).

A patent application was also filed for multistage flash degassing of geothermal brine feed to a DCHX unit. By removing CO_2 ahead of the preheater, the tendency for submerged boiling and offgassing with the consequent backmixing can be greatly mitigated and the volumetric efficiency of the tower improved.

Equilibrium Flash Modeling of Heterogeneous Azeotropes

In a major development from Sage and Lacey's (1955) data on the heterogeneous n-butane/water system, LBL has derived the phase diagrams for the IC_4/water system by the principle of corresponding states. Using these reliable mixture properties to replace pure component properties assumed with three-phase boiling models, LBL has developed a multicomponent two-phase boiling model which closely duplicates the observed temperature profiles within the DCHX column.

Figure 1 shows that the process involves three steps: adiabatic mixing, isothermal separating, and isobaric preheating. Although three-phase models predict univariant azeotropic boiling, the observed boiling in the 500-kW plant is two-phase with two degrees of freedom. The bubble point is about 12°F above azeotropic with about 5.8 mole % water in the vapor phase at a pressure of 415 psia. The 12°F departure from azeotropic conditions is classically called the boiling point elevation (BPE) and at constant pressure depends uniquely on composition (McCabe and Smith, 1976). Similarly, the composition of the vapor phase is 1.3 mole % higher in water vapor than azeotropic, which is the cause of the BPE. The BPE of the mixture has been overlooked in previous geothermal investigations.

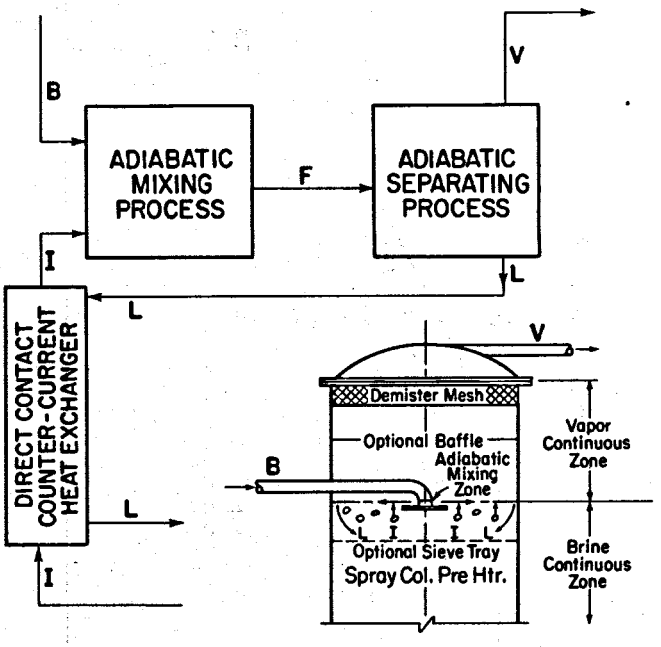

Figure 1. Process block diagram for a direct-contact equilibrium flash boiler/preheater tower. The boiler comprises the vapor continuous zone, including the froth zone; the preheater comprises the brine continuous zone. [XBL 8012-6509]

Adiabatic Feed Mixing Process. This process occurs in the entire froth and splash zone surrounding the hot brine injection nozzle. In the boiler, heat transfer occurs only as a consequence of adiabatic flash mixing and isothermal separation, so that "pinch" temperature differences vanish and the concept of a thermal gradient is superfluous. The best boiler configuration is obtained by using conventional mixing nozzle and flash drum design; staged equilibrium flash theory will yield all the necessary information for multicomponent heat and mass transfer calculations. Volumetric heat transfer coefficients for sizing the boiler mixing zone can be obtained from Figure 2 (Porter 1965) as a function of the total mixing velocity at the brine nozzle. For best efficiency the nozzle velocity should be as high as possible.

Adiabatic Separation of Working-Fluid Vapor and Residual Brine-Rich Liquid. The residual brine leaving the froth zone proceeds by gravity into the brine continuous region of the DCHX column. The working-fluid vapor rises out of the splash zone and is demisted by a woven mesh demister. The working-fluid velocity through a horizontal demister should be for best performance,

$$V_c = 0.32\left(\frac{\rho_L - \rho_G}{\rho_G}\right)^{1/2} \text{ ft/s.}$$

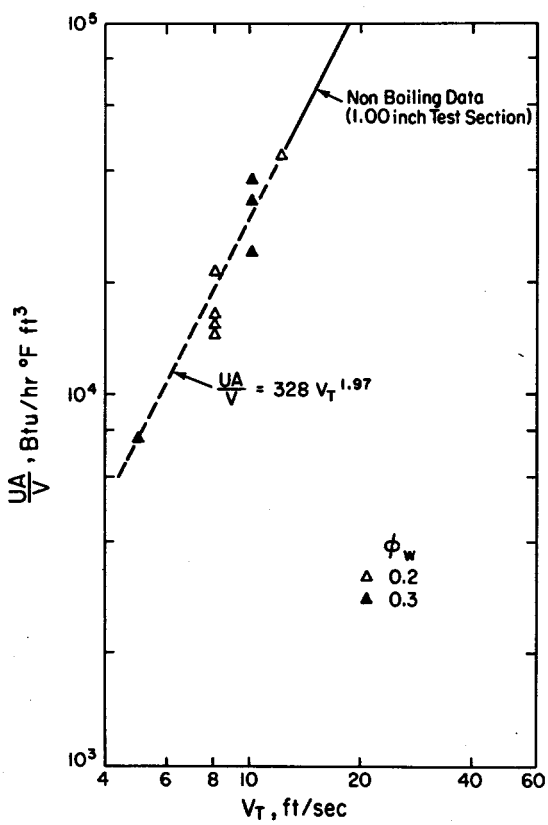

Figure 2. Boiling heat transfer coefficients vs. mixing velocity (Porter, 1965). [XBL 8012-6512]

Countercurrent DCHX Preheater Column. The preheater ideally functions as a countercurrent direct-contact liquid-liquid heat exchanger from the top of the brine continuous zone downward to the exte that it is not disrupted by backmixing. The backmixing can occur as eddies from the brine nozzle above, by submerged boiling and offgassing of noncondensables from the IC_4 distributor below, or by "wake-shedding," as with the Letan-Kehat model (1968). The existence of the countercurrent operation can be validated only by measuring actual temperature differences between the brine and hydrocarbon along the length of the column. Because of the boiler's equilibrium flashmixing operation, these differences will nearly vanish along the preheater/ boiler interface. Consequently, preheater "pinches" derived from models which neglect interfacial backmixing and measured thermal profiles are inappropriate to reflect the actual preheater performance.

LBL is investigating models using the measured bulk mixture temperatures within the preheater for comparing ideal and actual preheater performance. For example, in run #7, since less than half of the 25-ft preheater length is active because of backmixing (compare in Table 1 bulk ΔT/ft, run #7 vs. ideal), the bulk temperature rise per foot is only 27% that of an ideal 25-ft preheater, wherein all backmixing and crossflow effects have been theoretically removed.

From this comparison of the volume ratio of the operating and ideal preheaters we can define the volumetric preheating efficiency E_p as the ratio of the mean respective bulk temperature rises per foot. Thus the measured temperature profile of the column can be quantitatively taken into account.

Data Evaluation

The data of 20 runs of the DCHX unit at East Mesa have been grouped into five averaged sets and analyzed. The results are summarized and presented in Table 1 along with those of three typical runs.

Average #3 of the most stable runs demonstrates a boiling point of 253°F at 415 psia for the working-fluid composition of 5 mole % water and 95% isobutane. The vaporization efficiency, E_v, was 88.67%, the vapor pressure depression, VPL, was 49 psi, and the total boiling point elevation, BPE, was 11.1°F.

These balances which can be solved by the lever principle from the H-X diagram are based upon enthalpies per pound of mixture, as single valued functions of composition, since,

$$dH = Tds + VdP.$$

At constant applied pressure, VdP approaches zero, so that the enthalpy depends only on the boiling point; and the boiling point depends only on composition.

Run #7 from Table 1 is illustrated on the T-X diagram (Fig. 3); at the nozzle, the hot flashing brine at 320.2°F and the preheated IC_4 droplets mixed adiabatically. As the brine flashes down the equilibrium pressure of 414.7 psia, it mixes with and vaporizes all the working fluid and leaves

Table 1. Summary of DCHX performance (runs of 7/22/80 and 7/23/80 at East Mesa).

CODE CHX runs	Av#1 (linear T-L plot)	Av#2	Av#3 (most stable)	Av#4	Av#5	Run#1 (highest Ev)	Run #5 (lowest Ev)	Run #7 (most stable)	Calc. ideal
Temp. °F brine in	319.54	320.1	319.6	319.09	319.38	319.1	319.5	320.2	
Temp. °F brine exit	151.36	154.15	153.13	153.1	152.25	156	155.1	155	
Temp. °F HC in	94.96	97.08	94.5	95.95	95.15	98.5	97.3	93.9	
Temp. °F WF out	252.52	253.45	253.08	252.92	253.23	251.2	256.4	254.2	
psia WF out	415.5	415.95	415.05	415.77	414.6	417.1	415	415	
$p(H_2O)$ psia	31.18	31.68	31.48	31.39	31.56	30.46	33.33	32.10	
$P_{sat}(HC)$ psia	430.29	435.09	432.58	431.92	433.19	424.53	446.3	437.18	
E_v	0.8932	0.8832	0.8867	0.8899	0.8842	0.9108	0.8552	0.8758	0.938
VPL(psi)	45.97	50.82	49.01	47.54	50.15	37.86	64.63	54.28	26.8
BPE °F	10.52	11.45	11.08	10.92	11.23	9.2	14.4	12.2	6.5
Bulk ΔT °F/ft	5.08	4.84	4.92	4.9	4.91	4.45	4.95	5.02	10.3
E_p	0.272	0.26	0.264	0.263	0.263	0.239	0.265	0.269	1
25' Prhtr. U_v BTU/°F-ft^3-hr	4000	3940	3985	4040	4030	3950	3909	3875	
2' Blr. U_v BTU/°F-ft^3-hr	39,100	36,000	38,000	37,400	37,200	45,700	29,400	34,400	
25' Tower U_v BTU/°F-ft^3-hr	6920	6833	6880	7000	6970	6890	6856	6670	
Blr/Prhtr. LMTD °F	11.32	11.45	11.68	11.45	11.49	11.49	11.54	12.07	
Potential flash °F	67.02	66.65	66.52	66.17	66.15	67.9	63.1	66.0	66.5
Brine/HC mass ratio	1.205	1.236	1.211	1.1864	1.2193	1.132	1.236	1.2199	
Brine FR Mlb/hr	103.05	104.36	105.78	103.81	105.67	99.81	104.33	105.75	
HC FR Mlb/hr	85.51	85.48	87.333	87.55	86.66	88.17	84.41	86.69	
Prhtr. ΔH MMbtu/hr	9.847	9.808	10.12	10.064	10.02	9.869	9.81	10.17	9.87
Boiler ΔH Mbtu/hr	7.18	7.20	7.346	7.13	7.29	7.345	7.39	7.33	7.35
DCHX ΔH_T MMbtu/hr	17.03	17.01	17.47	17.42	17.31	17.31	17.21	17.49	17.22

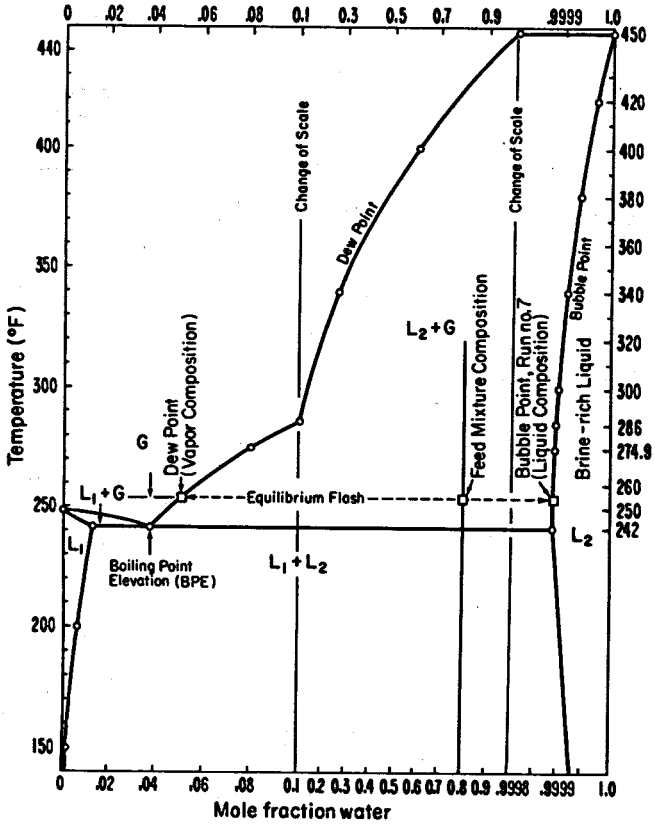

Figure 3. Adiabatic mixing process on T-X phase diagram showing isothermal tie line connecting bubble point and dew point. [XBL 8012-6510]

a residual brine-rich liquid. By conservation of mass, the bulk preheating and mixing process operates along the vertical 0.8 mole fraction water composition line, and the mixture boils continuously at 254.2°F in the two-phase (L_2 + G) region of the phase diagram. At this temperature, azeotropic boiling occurs at 471 psia, so that there exists a 56-psi vapor pressure loss (VPL) in two-phase boiling. This VPL is equivalent thermodynamically to a 12.2°F boiling point elevation (BPE).

As a further illustration, it can be seen from the H-X diagram (Fig. 4), that drawing a straight line from the brine inlet bubble point of 320.2°F through the observed feed mass composition of 55% on the vaporization tie line of 254.2°F and then extrapolating to intersect the IC_4 liquid line yields a temperature of about 254°F for the boiling IC_4-rich phase. Other lines, drawn as shown in the cooler sections of the preheater, solve for the coldest bulk liquid temperature and for the median temperature.

Vaporization Efficiency, E_v

LBL's study of phase equilibria in DCHX operations reveals that the most important criterion for measuring performance and for improving design is the classical steam vaporization efficiency, E_v, defined as the ratio at the vapor exit temperature of the partial pressure actually exerted by the hydrocarbon to its saturation pressure (Perry, 1950).

The baseline tests at design flow boiled off vapors at about 237.0°F, a pressure of 338 psia and a vaporization efficiency of 85%. During July the boiling temperature was increased to 252.1°F at a pressure of 414.7 psia and a vaporization efficiency of 89%. When 340°F brine becomes available from pumping the 6-2 well and when a higher velocity brine nozzle is installed in the DCHX unit, it is expected that the two-phase boiling temperature can be raised to 255°F and the pressure to 450 psia. The vaporization efficiency corresponding to these conditions is 94.88%, which is close to the 95% limit predicted by Carey (1930) and which is the design value that corresponds to the definition phase of the project.

The highest efficiency results in a working fluid having the highest pressure and lowest steam fraction for the temperature. This yields the best operation for the turbine.

FUTURE WORK

1. Parallel developments of two-phase and three-phase boiling models are to be continued during fiscal 1981.

2. Testing of additional devices within the DCHX column will be scheduled to improve overall tower performance and to create modular designs for a 20-ft-diameter column, thereby replacing the plurality of DCHX units otherwise required for commercial size (≥ 50 MWe) installations.

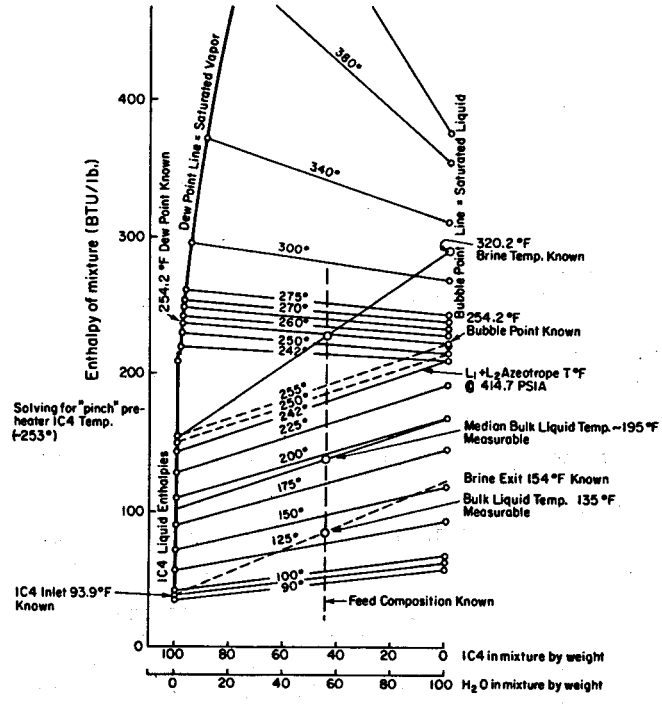

Figure 4. Graphic solution of heat and mass balance for run #7 on enthalpy-composition phase diagram. (Any number of isothermal tie lines may be drawn.) [XBL 8012-6513]

REFERENCES CITED

Grey, J. S., 1930. Vaporization efficiency in steam distillation (Sc.D. thesis). Massachusetts Institute of Technology, Cambridge, Massachusetts.

Letan, R., and Kehat, E., 1968. The mechanism of heat transfer in a spray-column heat exchanger. Am. Inst. Chem. Eng. J., v. 14, no. 3, p. 398-405.

McCabe, W. L., and Smith, J. C., 1976. Unit operations of chemical engineering (3rd edition). New York, McGraw-Hill.

Perry, J. H., 1950. Chemical engineer's handbook (3rd edition). New York, McGraw-Hill, p. 583-585.

Porter, J. W., 1965. Studies in direct-contact heat transfer with application to seawater conversion (Ph.D. dissertation). Berkeley, University of California, Department of Chemical Engineering.

Rapier, P. M., 1978. Proposed design for direct-contact isobutane boiler. Berkeley, Lawrence Berkeley Laboratory, LBL Engineering Note UCID-8029 GT1808, Serial M 5194.

Sage, B. H., and Lacey, W. N., 1955. Some properties of the lighter hydrocarbons, hydrogen sulfide and carbon dioxide. Monogram on API Research Project 37, Section XVIII nButane-Water System. New York, American Petroleum Institute.

BINARY GEOTHERMAL POWER PLANT INVESTIGATION AT LBL

W. L. Pope and P. A. Doyle

This article summarizes the results of geothermal binary Rankine-cycle studies which began in 1979 and continued through 1980. The early work was not presented in the 1979 Annual Report while U.S. Patent protection was being obtained.

Roughly 80% of all commercial electric power generated in the U. S. is produced in simple reheat or combined steam Rankine thermodynamic processes. Key determinants in Rankine-cycle performance are the choices of working fluid and turbine states. A current difficulty in the design of the closed organic "binary" Rankine cycle for geothermal power plants is the selection of the optimum working fluid and turbine states. This difficulty is common to all non-steam Rankine systems under development in the U. S. and elsewhere and is, therefore, a matter of great technical importance to the world power community.

Recent geothermal binary-Rankine-cycle power plant research at Lawrence Berkeley Laboratory (LBL) shows considerable promise toward resolving the difficulties. Our preliminary investigations, described in detail in Pope and Doyle (1980) and summarized in Pope et al. (1980) have been successful in identifying a useful new working-fluid thermodynamic characterization parameter--the fluid's transposed critical temperature (TPCT) line in the anomalous specific heat region above the critical point.

Although the Rankine cycle has been used worldwide for over 100 years and the existence of a fluid's specific heat anomaly has been known for perhaps 50 years, we believe we are the first to identify the importance of working fluid specific heat behavior in the critical region to the performance of optimum Rankine-cycle power plants.

In brief, we have found that when the optimum working-fluid mixture composition is determined for a supercritical, binary-Rankine-cycle power plant, the optimum turbine-inlet state is always in the anomalous specific heat region, very close to the transposed critical temperature line, such that the turbine expansion is dry but with minimum exhaust superheat consistent with the vapor boundary characteristics of the selected mixture system and imposed power plant constraints.

These findings are based upon detailed investigations of geothermal binary-Rankine-cycle power plant conceptualizations assuming the isobutane/isopentane (iC_4/iC_5) system (Pope and Doyle, 1980) and upon recent spot checks of three other two-component hydrocarbon mixture-systems for resource temperatures between 150°C and 220°C.

Figure 1 is a schematic diagram of the simple geothermal binary-Rankine-cycle power plant investigated (Pope and Doyle, 1980), including a list of seven independent variables which characterize the overall thermodynamic performance of the system. The plant assumes conventional shell-and-tube heat exchangers and a forced-draft wet cooling tower. The surface plant is coupled to a simulated hydrothermal resource of infinite lateral extent and fixed depth via frictionless, adiabatic wells. Brine (pure H_2O) is produced at the wellhead as saturated liquid using downhole production pumps driven by electric motors. All spent brine is reinjected. Design heat-transfer coefficients are input constants, and the flow rates per well are specified. All major system parasitic losses are included, and each subsystem is adequately characterized with regard to thermodynamics and economics for the problem at hand.

Although this is about the simplest system configuration we could come up with and yet simulate the "whole potato," a number of technical and financial input assumptions (Pope and Doyle, 1980) which could have influenced our results had to be nulled out. To do this we varied brine unit heat costs, plant subsystem unit costs, and subsystem efficiency

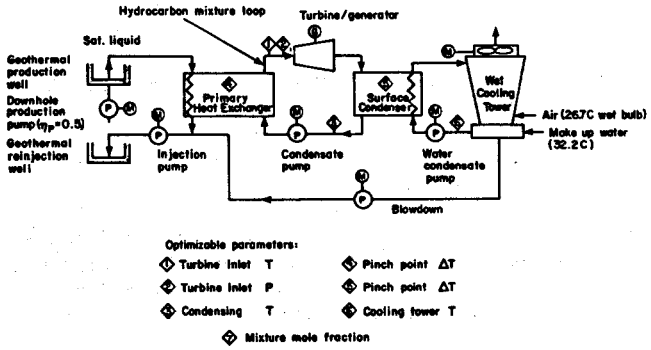

Figure 1. Schematic diagram of the simple geothermal binary-Rankine-Cycle power plant investigated in Pope and Doyle (1980). Also shown is a list of seven independent variables which characterize the overall thermodynamic performance of the system. See Table 1 and Fig. 2 of the above-mentioned report for other details. [XBL 806-1134]

factors over wide limits (up to a factor of 5). All our calculations represent system designs optimized in seven parameters using state-of-the-art techniques (Kestin, 1980, Sec. 8.2.8).

Figure 2 shows our computed optimum isobutane mole fraction for this plant configuration assuming the iC_4/iC_5 mixture-system between resource temperatures of 165°C and 205°C. It can be seen that the optimum isobutane mole fraction is a monotonically decreasing function of resource temperature, as predicted by Starling (1977). This figure also shows, however, that the optimum composition depends upon unit brine costs and assumed constraint conditions. For the same input assumptions, our results agree very well with the Holt/Ghormley study conducted in 1976 for EPRI (Roberts, 1976).

Figure 3 is a schematic diagram of typical computed optimum turbine expansion paths followed for supercritical cycles on pressure-enthalpy coordinates. Note that the optimum turbine-inlet state is <u>always</u> adjacent to the transposed critical line for the optimum mixture composition. The Group A

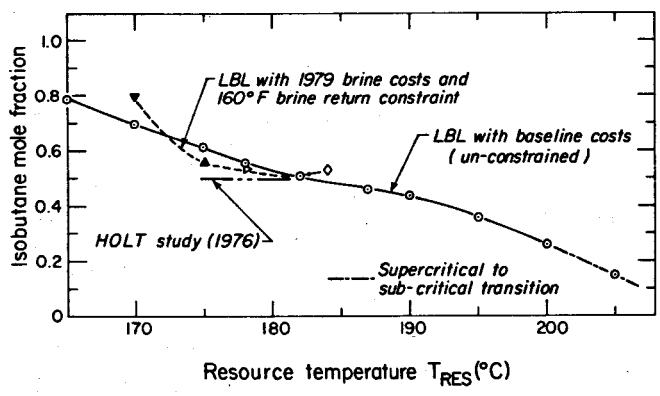

Figure 2. Computed optimum iC_4 mole fraction as a function of resource temperature. The optimum composition also depends on turbine constraints (not shown). [XBL 805-963]

cases represent cycles for which the turbine inlet state was allowed to be anywhere outside the two-phase vapor envelope and the crosshatched region for the selected mixture composition. Because in many instances expansions could proceed into the two-phase zone, the expander dry stage adiabatic efficiency was arbitrarily penalized by 1% for each percent of working-fluid moisture present at stage exhaust conditions. In other words, lacking another basis, we applied Baumann's rule-of-thumb from <u>steam</u> turbine technology.

For the Group B-1 cases, the turbine inlet state was constrained to assume only values of inlet entropy which were greater than the maximum saturated vapor entropy of the selected mixture composition. This constraint ensures only dry turbine expansion (and therefore the above efficiency penalty was not applied) and allows the simulation of designs under practical stage superheat margins on a consistent basis.

The Group B-2 expansion line represents cycles for which the brine return temperature (primary heater exit temperature) was constrained to be greater than or equal to 344K (160°F). This return temperature may apply to binary-Rankine geothermal plants at the Heber resource in the Imperial Valley of California.

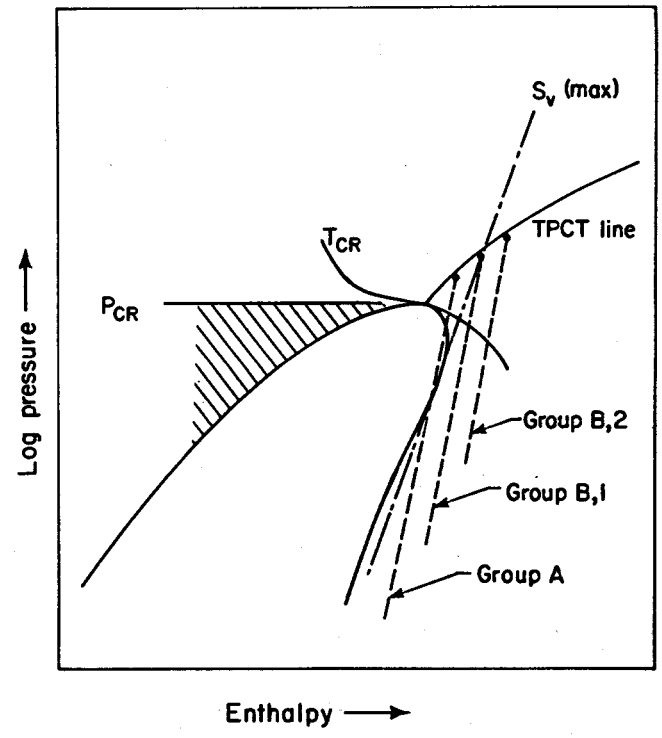

Figure 3. Pressure-enthalpy sketch illustrating typical turbine expansion paths for each constraint group of this study. Turbine inlet states in the two-phase and shaded region were disallowed in all cases. Differences in optimum composition (vapor dome location and shape) were ignored for illustration purposes. [XBL 806-1138]

Figure 4 shows our correlation between the temperature on the TPCT line (at the optimum turbine inlet pressure) and the optimum turbine inlet temperature for busbar cost optimized iC_4/iC_5 mixture binary-Rankine-cycle power plants. The numbers on the curves apply to the circles with the dots, which represent turbine states at various resource temperatures between 170°C and 200°C with Baseline input subsystem assumptions (Pope and Doyle, 1980, Table 1). The other symbols on the plots represent a variety of input subsystem unit cost or efficiency factor assumptions which differ from Baseline Conditions by as much as 500% (Pope and Doyle, 1980, Fig. 2).

It can be noted that the optimum dimensionless turbine inlet temperature is, in all cases, within 1% of the dimensionless transposed critical temperature line for the optimum mixture composition. Note also that the degree of departure of the optimum turbine inlet temperature from the TPCT line is independent of the resource temperature and of all unit cost or subsystem efficiency factor assumptions, and depends only upon the assumed constraint conditions.

Figure 5 shows our correlation between the reduced pressure on the TPCT line (at the optimum turbine inlet temperature) and the optimum reduced turbine inlet pressure. Once again, all points represent a variety of resource temperatures and radically different subsystem unit cost and efficiency factors, but the TPCT line departure depends only upon imposed constraints.

Figures 2 to 5 represent binary-Rankine power plant conceptualizations optimized for minimum cost of energy at the busbar for a variety of <u>input</u> unit cost assumptions.

Could the input cost assumptions somehow <u>create</u> the observed TPCT affinity? We can demonstrate that this is not the case with the following

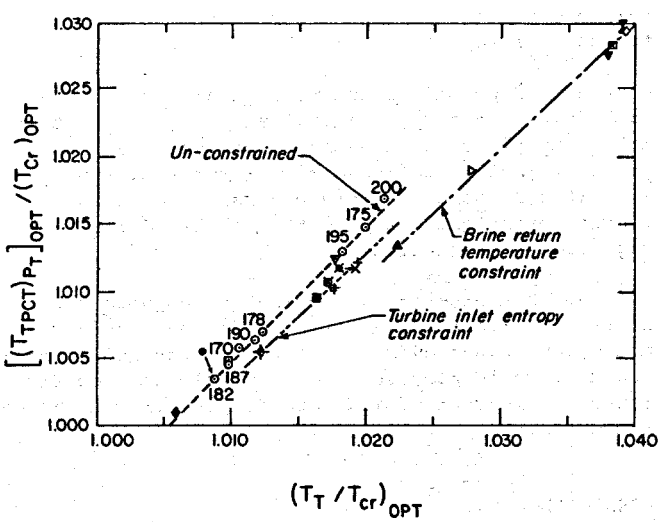

Figure 4. Correlation between the temperature on the TPCT line (at the optimum turbine inlet pressure) and the optimum turbine inlet temperature for busbar cost optimized iC_4/iC_5 mixture geothermal-binary-Rankine-cycle power plants. [XBL 805-965]

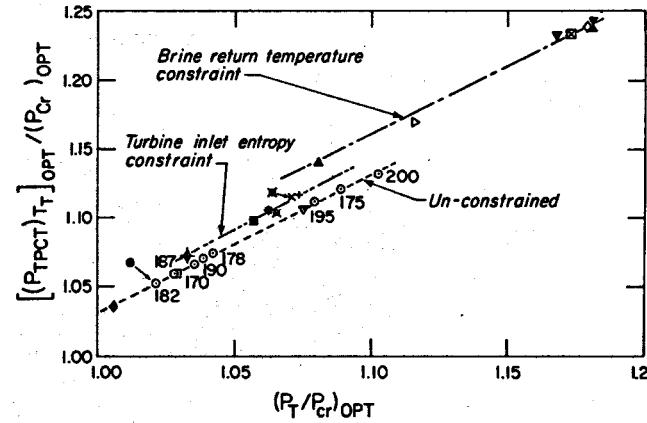

Figure 5. Correlation between the pressure on the TPCT line (at the optimum turbine inlet temperature) and the optimum turbine inlet pressure. [XBL 805-964]

test. After obtaining cost optimum values for the previously described seven independent system parameters (Fig. 1), the pinch point temperature differences of the three nonwork-producing subsystems of the plant are fixed. The systems are then reoptimized in four-parameter, constrained thermodynamic brine "yield" optimizations in which minimum brine mass flow rate is the Design Objective for fixed net system power. In these optimizations, <u>all</u> subsystem costs and financial factors are <u>immaterial</u>.

This test is a useful measure of thermodynamic optimality for geothermal Rankine-cycle power plants, because when the brine flow-rate is minimized the net plant fuel (brine) utilization efficiency is maximized.

In these tests, our computed thermodynamic optimum turbine inlet states fall within 0.1% of the TPCT line of the optimum working-fluid mixtures --that is, to within about the limits of resolution of our existing process simulator. We believe this test provides a <u>sound thermodynamic basis</u> for the preference of the TPCT line for supercritical Rankine-cycle power plants.

Figure 6 illustrates the busbar energy cost-design surface (Design Objective) for an optimized mixture binary-Rankine-cycle power plant. Here, the relative busbar energy cost has been plotted as a function of turbine inlet temperature and pressure. The values of pressure and temperature along the sharp trough--the Global Minimum busbar cost region--are virtually coincident with the transposed critical temperature line of the selected optimum mixture (see Pope and Doyle, 1980, Figs. 10 and 11). The gradually sloping operating region on the left of Figure 6 corresponds to slightly subcritical and slightly supercritical turbine inlet states below the TPCT line, to the right of the critical point in the superheated vapor region on pressure-enthalpy coordinates. (Note that this region would be "steeper" if off-design expander characteristics had been factored in.) The region on the right side of Figure 6, where the busbar energy cost rises

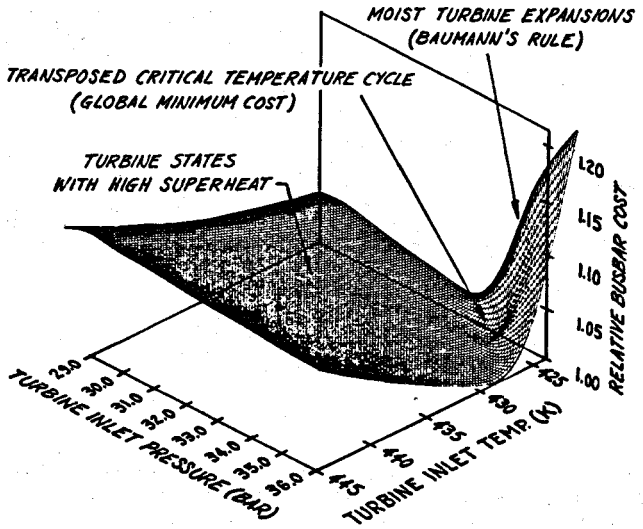

Figure 6. Relative busbar energy cost design surface (Design Objective) for a simple geothermal mixture binary-Rankine-cycle power plant as in Figure 1. [XBL 805-968]

abruptly, corresponds to turbine inlet states immediately above and/or to the left of the TPCT line (on P-h coordinates) which would result in expansion, by one or more exhaust stages, into the two-phase vapor region of the selected optimum mixture. This plot clearly shows the potentially severe system economic penalties associated with reduced turbine efficiency due to wet expansion, and emphasizes the importance of accurate knowledge of the location of the fluid's vapor-saturation boundary. Although superheat at the turbine exhaust is undesirable, expanding into the two-phase vapor dome must be avoided with these "retrograde" fluids if moisture degrades turbine efficiency.

Why are all our optimum cycles supercritical? It can be shown that if the unit fuel cost is very low, there is no economic incentive for high-temperature (pressure) turbine states to increase utilization efficiency in subcritical Rankine cycles and, therefore, no economic advantage from even higher-pressure (efficiency) supercritical cycles.

The input unit fuel cost for the examples presented (Pope and Doyle, 1980) ranged from about 60¢ per million Btu to about $3.00 per million Btu. Under these conditions, the optimum cycle for this plant configuration and hydrocarbon mixture-system between 165°C and 200°C was always a supercritical cycle. We have done a limited number of calculations on the simple binary geothermal cycle that suggest that when the annualized fuel costs are equal to or greater than the annualized plant capital plus operating and maintenance costs, the supercritical cycle is preferred. As we have previously shown, this optimum cycle is always a TPCT Rankine cycle for the geothermal-plant configuration and hydrocarbon-mixture systems investigated. We have strong reason to believe the Transposed Critical Temperature Rankine thermodynamic cycle will be most appropriate for numerous other Rankine process applications other than geothermal, and we urge other investigators to explore this possibility in their work.

Additional system correlations (Pope and Doyle, 1980, Figs. 13, 14) suggest that the TPCT line could be used with other, previously identified, fluid characterization parameters to make consistently good initial selections of working fluids and turbine states. A successful effort in this direction might reduce current geothermal binary cycle initial fluid selection difficulties to the level of a programmable hand calculator and greatly enhance the state of the art. One facet of our current efforts involves developing a system correlation based on process state exergy (Kestin, 1980, Chapter 3).

We have found that the mixing rules in the fluid-properties formulations we are using do not adequately predict the critical-point locus for some hydrocarbon mixtures (Silvester, 1978). For future work, which will concentrate on conditions applicable to the Heber Binary Demonstration Plant, we plan to use new fluid property routines based upon Extended Corresponding States formulations.

A comprehensive patent application based on the foregoing concepts has been filed (Pagano, 1980). This Method Application utilizes the fluid's transposed critical temperature for selecting and operating Rankine process systems. Because the concepts disclosed are new and potentially applicable to a broad variety of Rankine systems and subsystems (turbines, simple cycles, and combined cycle plants for electric power, automotive, and waste heat recovery applications), 31 potential claims were identified.

Major conclusions of this study are:

1. The Transposed Critical Temperature is an important thermodynamic property which should be considered in the selection of working fluids and operating states for geothermal binary-Rankine cycles.

2. A high priority should be placed on the development of a new equation of state for hydrocarbon mixtures. Extended Corresponding States formulations appear promising.

3. Although our study (Pope and Doyle, 1980) was limited to simple binary-Rankine-cycle geothermal power plants with a single mixture system, greatly simplified financial characterization, and a limited resource temperature range, additional recent investigations support much broader potential TPCT applicability.

4. Mixture-binary-Rankine cycles appear to offer significant utilization efficiency and economic advantages over pure fluid cycles and, consequently, could play an important role in electric power development of moderate-temperature geothermal resources.

ACKNOWLEDGEMENT

We acknowledge the valuable contributions to this work from H. S. Pines, L. F. Silvester, and R. L. Fulton of LBL, and encouragement from numerous outside reviewers of our original report (Pope

and Doyle, 1980). Special thanks go to Sheldon R. Meyer of Phillips-Moore and Associates for preparing the patent application.

REFERENCES CITED

Kestin, J. (Editor-in-Chief), 1980. Sourcebook on the production of electricity from geothermal energy. Providence, Rhode Island, Brown University. U. S. Government Printing Office (DOE/RA/4051-1), Washington, D. C. 20402 (Section 8.2, Conceptual design optimization, was prepared by W. L. Pope, P. A. Doyle, H. S. Pines, R. L. Fulton, L. F. Silvester, and J. M. Angevine of the LBL Earth Sciences Division.)

Pagano, R., (Editor). LBL researchers find a key to more efficient power plants. Currents, v. 7, no. 31, 1980. Berkeley, Lawrence Berkeley Laboratory, Public Information Department.

Pope, W. L., and Doyle, P. A., 1980. The transposed critical temperature Rankine thermodynamic cycle (concept). Berkeley, Lawrence Berkeley Laboratory, LBL-10312.

Pope, W. L., Doyle, P. A., Fulton, R. L., and Silvester, L. F., 1980. The importance of the specific heat anomaly in the design of binary Rankine cycle power plants, Presented at the Geothermal Resources Council Annual Meeting, Salt Lake City, Utah, September 9-11, 1980. Berkeley, Lawrence Berkeley Laboratory, LBL-10974.

Starling, K. E., 1977. Conclusion stated at presentation before the Fourth Meeting of the Centers for the Analysis of Thermal-Mechanical Energy Conversion Concepts (CATMEC), Lawrence Berkeley Laboratory, Berkeley, California, January 24-25, 1977.

Roberts, V. W., 1976. Geothermal energy conversion and economics - Case studies. Prepared by Holt/Procon for Electric Power Research Institute, Palo Alto, California, November 1976. EPRI ER-301, Project 580.

Silvester, L. F., 1978. Thermodynamic and transport properties of light hydrocarbons and their binary mixtures. In Earth Sciences Division Annual Report 1978. Berkeley, Lawrence Berkeley Laboratory, LBL-8648.

BINARY FLUID EXPERIMENT IN 1980

B. W. Tleimat, A. D. K. Laird, G. V. Dizon, S. Zhao, H. Rie, and T. Vermeulen

The Binary Fluid Experiment (BFE) was designed to obtain laboratory-quality data to determine heat-transfer film coefficients for heating and condensing certain working fluids proposed for use in binary-cycle geothermal power plants.

The apparatus was designed and constructed to simulate the binary cycle, with steam as the heat source instead of geothermal brine and a throttling valve instead of a turbine. The equipment was built to use a variety of working fluids: pure light hydrocarbons, mixtures of light hydrocarbons, or refrigerants.

In specifying heat-transfer equipment for a process, the designer is usually armed with well-tested information on the performance of similar equipment under similar or identical conditions. However, in unusual applications, such as a binary-cycle geothermal plant using isobutane or a mixture of isobutane and isopentane as the working fluid, reliable data on the transport and thermodynamic properties of the working-fluid at the desired conditions are essential for sizing the heat-transfer equipment. The empirical correlation equations, such as those of Dittus and Boelter, Colburn, Sider and Tate, used to calculate the film coefficient are based on fluid transport properties and give the mean value, or the most probable value, of a large amount of experimental data.

Because of minor and unrecognized variations in conditions, the designer can only be reasonably sure that the performance of the heat exchanger will be within ± 35% of the mean. Consequently, to assure fulfillment of guarantee for a new design, the designer would select a heat-transfer coefficient value at the lower limit, resulting in higher cost of equipment. Lack of data on fluid properties, or lack of reliable data for the desired conditions, make the designer's task difficult at best. This factor is extremely important for the geothermal program, because computer studies (LBL's GEOTHM, for example) indicate that heating the fluid in the supercritical region will result in higher cycle efficiency than heating below the critical point. Moreover, other studies (Pope et al., 1980) indicate that using mixtures of isobutane and isopentane as the working fluid in the loop and heating the fluid close to the pseudocritical line (transposed critical line) will result in high efficiency as well as extend the useful life of the geothermal reservoir. Consequently, the most effective and reliable approach for specifying the heat-transfer equipment is to determine the heat-transfer coefficient at the proposed operating conditions of the plant.

The BFE apparatus was built and installed at the University of California's Richmond Field Station to determine the heat-transfer coefficient for

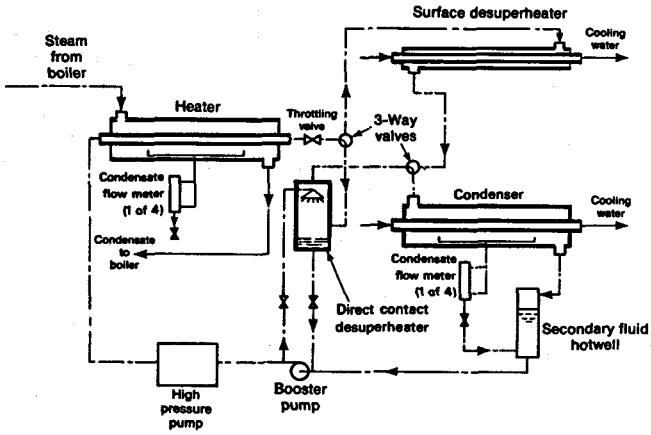

Figure 1. Binary fluid experiment, schematic flow diagram. [XBL 783-7893]

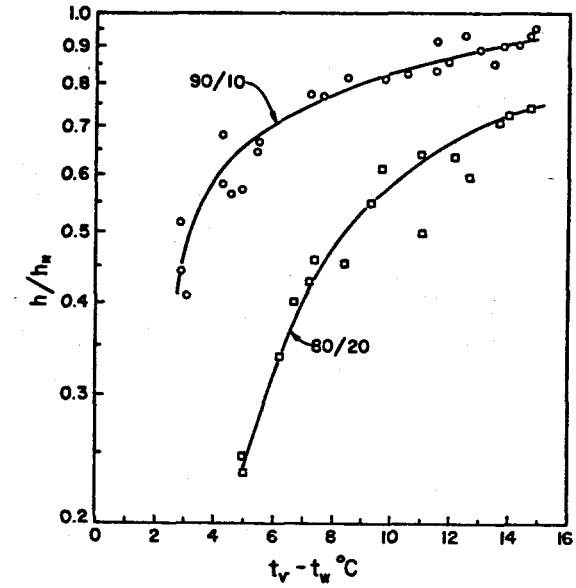

Figure 2. Ratio of film coefficient for mixtures to film coefficient for pure substances (Nusselt correlation) as a function of temperature difference between vapor and outside wall of tube of 90/10 and 80/20 mole % isobutane/isopentane mixtures. [XBL 8010-7357]

working fluids at the proposed conditions of the binary-cycle geothermal power plants. Figure 1 is a simplified schematic diagram of the experiment. A detailed description of the apparatus is given elsewhere (Tleimat et al., 1979b).

ACCOMPLISHMENTS DURING 1980

Data on heating and condensing of 90/10, 80/20, and 70/30 mole % isobutane-isopentane mixtures were obtained and analyzed. The empirical correlation

$$Nu = 0.022 \; Re^{0.82} \; Pr^{0.4},$$

found earlier (Tleimat et al., 1979a) for heating isobutane, gives an excellent fit to the observed film coefficient in heating, when simplified for convenience by using the viscosity and thermal conductivity of pure isobutane in the correlation.

The results for condensation showed that the Nusselt correlation for condensing a pure substance did not fit the results obtained for condensation film coefficients for mixtures. It was found that the condensation film coefficients for mixtures were consistently lower than those for pure isobutane, especially when the temperature difference between the vapor and the wall was relatively low. Condensation data for 90/10 and 80/20 mole % mixtures have been published (Tleimat et al., 1980), including Figures 2 to 6 shown here. Figure 2 shows the ratio of the condensation film coefficient of the mixture to that predicted from the Nusselt correlation for pure isobutane at the same saturation temperature as a function of the temperature difference between the vapor in the condenser shell and the outside wall of the tube. Figures 3 and 4 show the condensation film coefficient for the 90/10 and 80/20 mixtures, respectively, as a function of Reynolds number. Figures 5 and 6 show the dimensionless plots of the data shown on Figures 3 and 4. The solid lines show the Nusselt correlation for pure isobutane with values of transport properties as given by Hanley (1976).

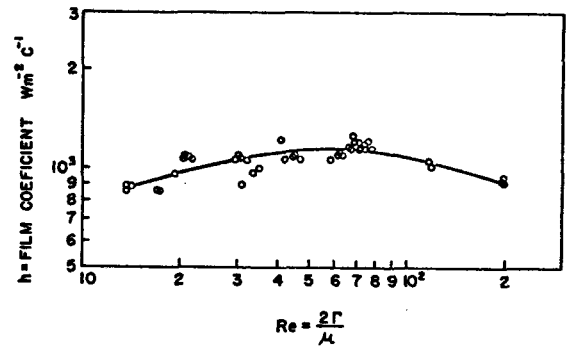

Figure 3. Film coefficient for condensation of 90/10 mole % mixture of isobutane/isopentane on a horizontal tube as a function of Reynolds number. [XBL 8011-12795]

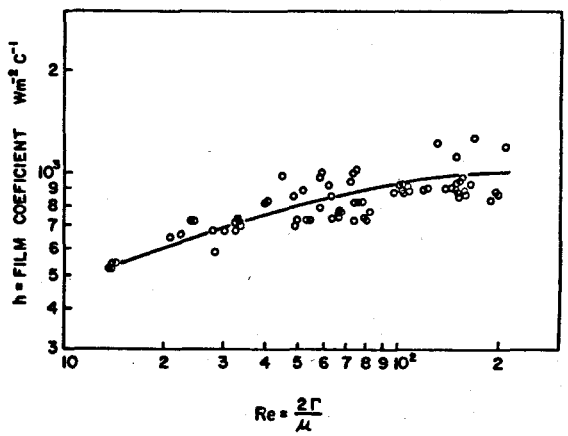

Figure 4. Film coefficient for condensation of 80/20 mole % mixture of isobutane/isopentane on a horizontal tube as a function of Reynolds number. [XBL 8011-12796]

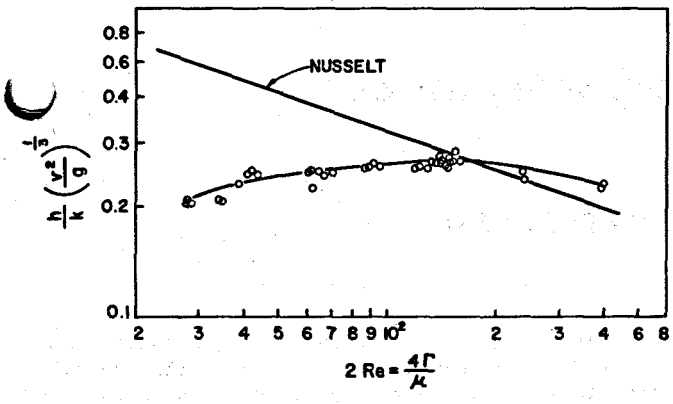

Figure 5. Dimensionless plot of data on condensation of 90/10 mole % mixture of isobutane/isopentane on a horizontal tube. Solid line shows the Nusselt correlation for pure substances. [XBL 8010-7356]

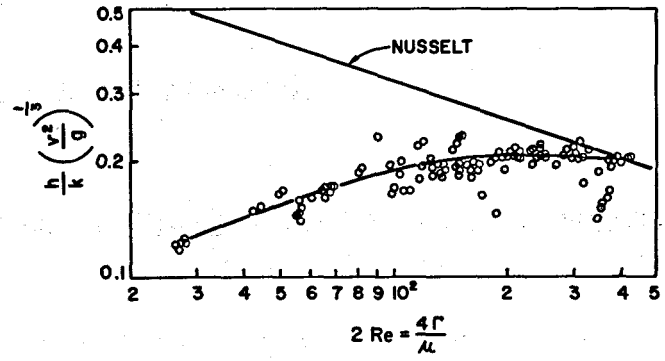

Figure 6. Dimensionless plot of data on condensation of 80/20 mole % mixture of isobutane/isopentane on a horizontal tube. Solid line shows the Nusselt correlation for pure substances. [XBL 8010-7355]

FUTURE PLANS

Data will be obtained on heat-transfer film coefficients for heating and condensing other mixtures of isobutane-isopentane. It is anticipated that data will also be obtained for supercritical heating and condensing of Freon 114 and mixtures of Freon 114 and Freon 115. The data will be used in the design of heat exchangers for the Sperry gravity-head technology program for the development of turbine-driven downhole pumps for the geothermal program.

REFERENCES CITED

Hanley, H. J. M., 1976. Prediction of the viscosity and thermal conductivity of mixtures. Cryogenics, v. 16, no. 11, p. 643-651.

Pope, W. L., Doyle, P. A., Pine, H. S., Fulton, R. L., Silvester, L. F., and Angevine, J. M., 1980. Conceptual design optimization, in J. Kestin (Editor-in-Chief), Sourcebook on the production of electricity from geothermal energy (Section 8.2). Washington, D.C., Department of Energy DOE/RA/28320-2.

Tleimat, B. W., Laird, A. D. K., Hsu, I. C., and Rie, H., 1979a. Baseline data on film coefficient for heating isobutane inside a tube at 4.14 MPa [600 psia]. ASME publication 79-HT-14.

Tleimat, B. W., Laird, A. D. K., Rie, H., Hsu, I. C., Seban, R. A., 1979b. Hydrocarbon heat transfer coefficients: Preliminary isobutane results. Berkeley, Lawrence Berkeley Laboratory, LBL-8645, 45 p.

Tleimat, B. W., Rie, H., Laird, A. D. K., and Zhao, S., 1980. Condensation film coefficients for mixtures of isobutane and isopentane. Presented at the 15th Intersociety Energy Conversion Engineering Conference, Seattle, Washington, August 18-22, 1980.

MEXICAN-AMERICAN COOPERATIVE PROGRAM

OVERVIEW OF THE MEXICAN-AMERICAN COOPERATIVE PROGRAM

M. J. Lippmann and N. E. Goldstein

The Cerro Prieto geothermal field is located about 35 km south of the city of Mexicali in Baja California, Mexico (Fig. 1). Until October 1980, when a 10-MW power plant went on line at Brawley, California, Cerro Prieto was the only liquid-dominated geothermal system generating electric power on a commercial scale in North America.

Production of 75 MWe began in 1973; in April 1979 it was increased to 150 MWe. In May 1981 a 30-MWe lower pressure turbine is scheduled to go into operation. The latest plans of the Comisión Federal de Electricidad (CFE), which manages and operates the field, call for a total production of 620 MWe by 1984. The probable capacity of the Cerro Prieto reservoir is estimated to be about 1100 MWe (Comisión Federal de Electricidad, 1980).

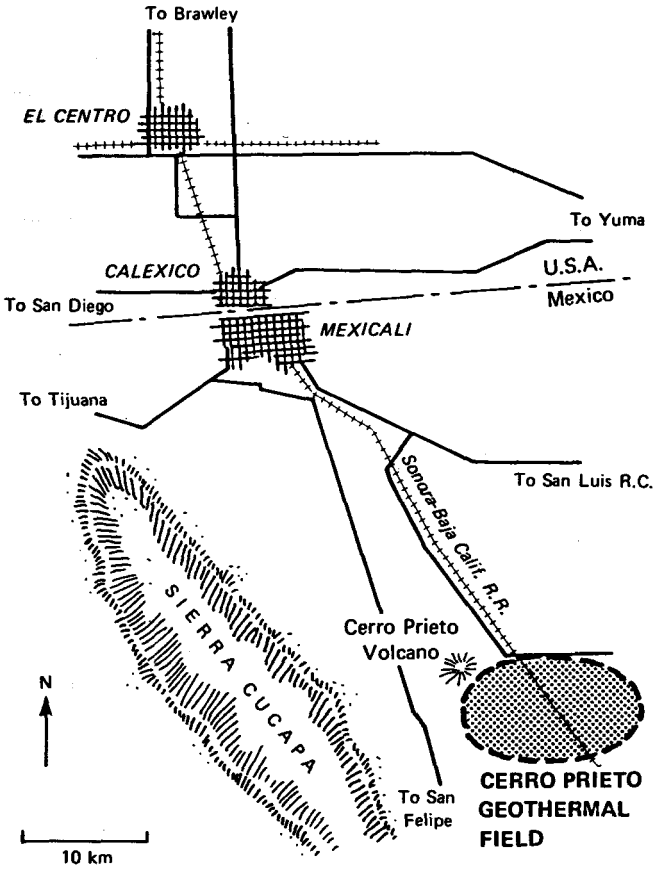

Figure 1. Location map of the Cerro Prieto geothermal field. [XBL 788-10409]

During the winter months, the generation capacity of CFE's system in northern Baja California, which includes Cerro Prieto, exceeds the local needs. Recently, San Diego Gas and Electric of southern California has begun purchasing 20 to 30 MW of that surplus electrical power. The sale of electricity is bound to increase as the development of the Cerro Prieto field continues.

CFE's large development plans are based on a comprehensive exploration effort which began in 1975 and covers not only Cerro Prieto but also other promising areas in the Mexicali Valley. At present, about 75 deep wells have been completed at Cerro Prieto (Figs. 2 and 3). The drilling program has continued with step-out wells in the eastern areas (e.g., M-117 and M-189), exploration wells around the village of Hidalgo (e.g., H-2 and M-172), and new, deeper production wells in the exploited area (e.g., E-1 and E-2).

Lawrence Berkeley Laboratory (LBL), under the direction of the Division of Geothermal Energy of the U.S. Department of Energy (DOE), has been working with CFE in carrying out a cooperative project on Cerro Prieto. These geothermal studies are being performed through a 5-year agreement signed in 1977 between CFE and DOE (Witherspoon et al., 1978).

A number of organizations are cooperating in this project (Table 1). The Earth Sciences Division of LBL is coordinating the U.S. technical activities carried out under the agreement; the Coordinadora Ejecutiva de Cerro Prieto of CFE is coordinating the Mexican participation.

Table 1. Principal organizations cooperating in the Mexican-American project.

<u>Mexico</u>
Comisión Federal de Electricidad (CFE)
Instituto de Investigaciones Eléctricas (IIE)
Dirección General de Estudio del Territorio Nacional (DETENAL)
Centro de Investigación Científica y Educación Superior de Ensenada (CICESE)
Consejo Nacional de Ciencia y Tecnología (CONACYT)
<u>United States</u>
Department of Energy (DOE)
Lawrence Berkeley Laboratory (LBL)
U. S. Geological Survey (USGS)
University of California, Riverside (UCR)

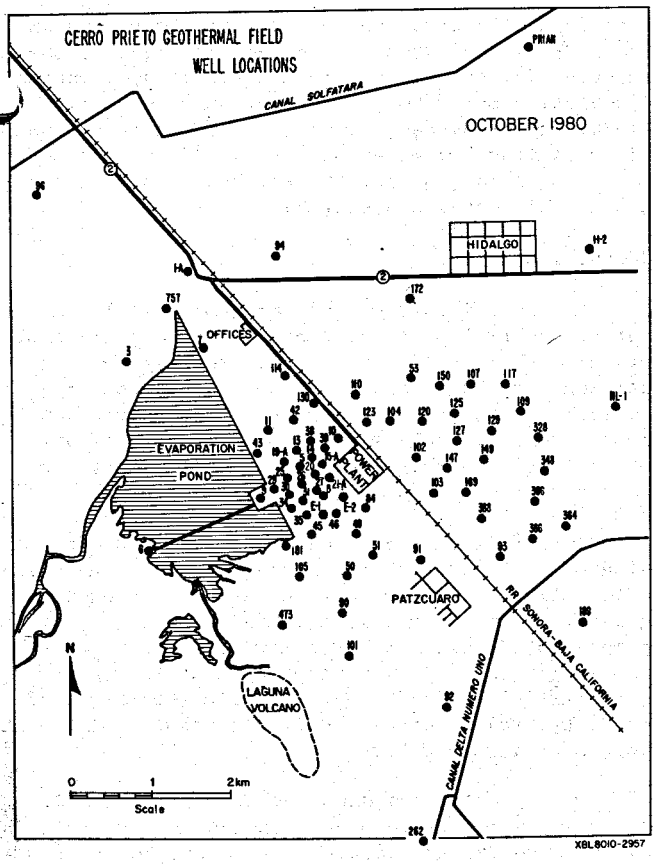

Figure 2. Location of wells at the Cerro Prieto geothermal field (as of October 1980). [XBL 8010-2957]

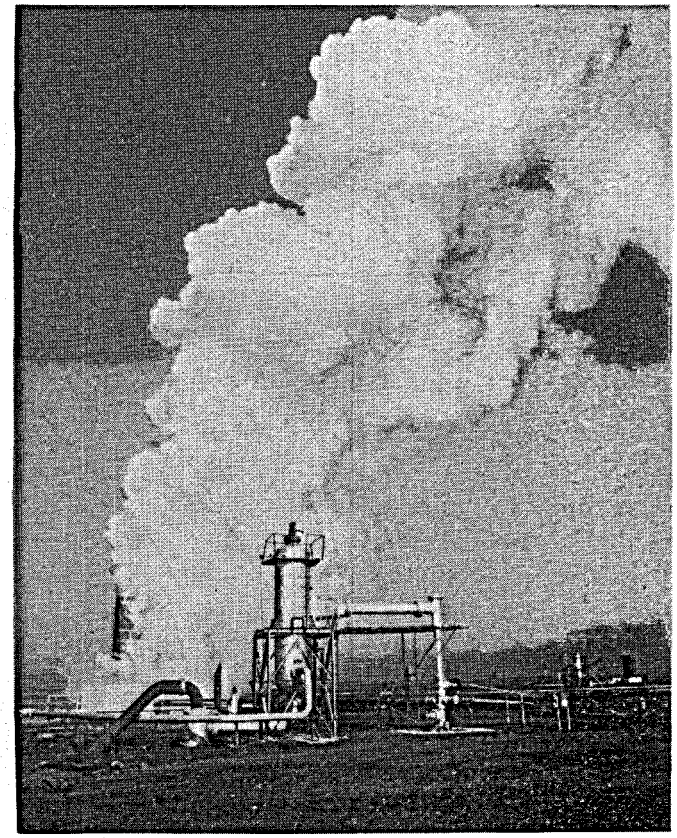

Figure 3. Wellhead installations at one of Cerro Prieto's wells. The produced fluids are being discharged through the silencers, partially hidden by the steam plume. [CBB 782-1495]

The principal objectives of this Mexican-American project are to develop a hydrogeologic model of the Cerro Prieto geothermal system and to study its response to large-scale fluid production and injection. The experiences gained will be extremely useful for planning the development of similar water-dominated geothermal fields in the nearby Imperial Valley, California.

In January 1980 discussions were initiated between DOE/LBL and CFE to extend the Mexican-American cooperative program to include the Los Azufres geothermal field in the state of Michoacán, México. An amendment to the present agreement, which will include Los Azufres, may be signed during the first half of fiscal 1982.

ACTIVITIES DURING FISCAL 1980

Some of the activities and results discussed below are described in further detail elsewhere in this volume. Most of the results obtained in previous years have been published in the proceedings of the first two symposia on Cerro Prieto (Lawrence Berkeley Laboratory, 1978; Comisión Federal de Electricidad, 1981).

Geology

In March 1980 a 3-day internal workshop between DOE and CFE personnel was held in Menlo Park, California (The Vallombrosa Meeting), to exchange the latest data and results on the Cerro Prieto field (Lippmann and Mañon, 1980). The main objective was to develop a hydrogeologic model of the geothermal system.

An updated map of the fault system for the field was drawn on the basis of recent geologic and geophysical studies (Fig. 4). It was decided that the fault interpretation based on well-to-well correlations of the contact between the relatively unconsolidated Unit A and the lithified Unit B is inaccurate. We now understand that this is a gradational thermal metamorphic contact which cuts across lithologies and owes its position to the geometry of subsurface isotherms rather than to faulting. The Cerro Prieto fault, an apparently continuous NW-SE fault traceable from the Gulf of California to the Cerro Prieto volcano, is believed to be merely a boundary fault to the field rather than the conduit for ascending hydrothermal fluids. This conclusion is based partly on the generalization that strike-slip faults do not account for significant fluid flow compared to normal or reverse faults. However, the Cerro Prieto fault does not behave as an impermeable boundary near the surface. It was noted from water-level responses that well M-6 west of the fault is connected to the main production area east of the Cerro Prieto fault. The Volcano fault system, a series of NE-SW faults, is considered to have three main components, Delta, Pátzcuaro, and Hidalgo. It is generally believed that this fracture system acts as the conduit to

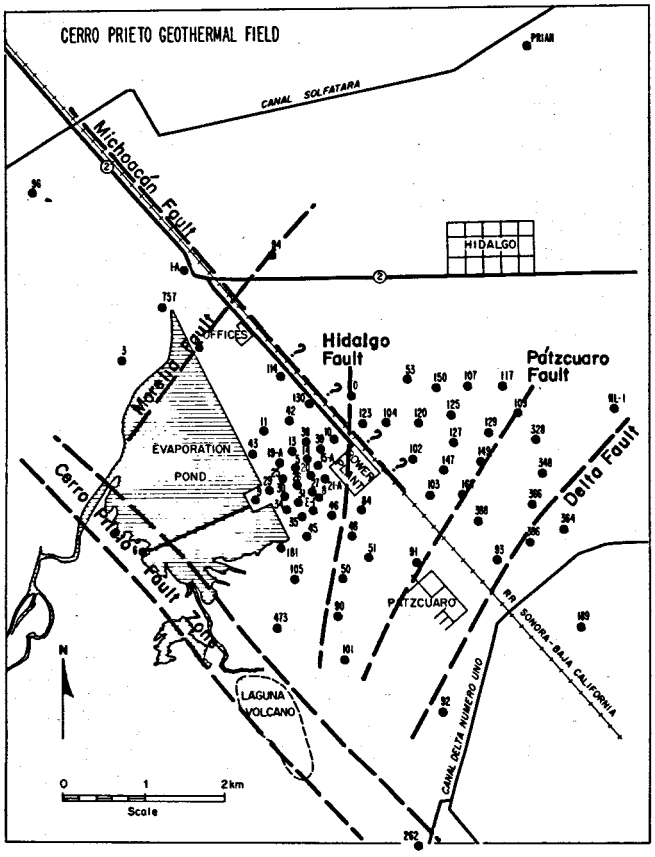

Figure 4. Simplified fault map for Cerro Prieto. [XBL 804-7022A]

fluid flow, especially where it intersects the NW-SE fault system. A new NE-SW fault (Morelia fault) has been discovered north of the main production field. It passes near wells M-7 and M-94. This fault was considered to be part of the northern (leaky) boundary. The Michoacán fault, which parallels the railroad track, is believed to extend northward for an undetermined distance beyond the Morelia fault, and might extend as far south as the village of Delta (near well M-189), which was damaged in June 1980 by a magnitude 6+ earthquake. From interference tests and recent lithological studies, it is clear that the fields on opposite sides of the Michoacán fault, Cerro Prieto I and II, are connected. The hot water is believed to flow in a westerly direction at some depth while cold water from the Colorado River recharges the reservoir from the northeast.

Work done by Lyons and van de Kamp (1980) on the deltaic depositional environment in the field suggests that wells in Cerro Prieto I and II are producing generally from delta-plain sediments. However, it was considered that wells M-6 and S-262 have penetrated prodelta materials.

The mineralogic and petrographic studies on cuttings and cores still continue at the University of California, Riverside. Various methods of geothermometry have been used, including authigenic mineral assemblages and light stable isotopes, to study temperature distribution and rock-fluid interactions in the subsurface. These data have revealed a pattern of mineral zones and isotopic ratios in the rocks which serves to define the shape of the reservoir and to record the pattern of hydrothermal circulation prior to production. Elders et al. (1980) inferred the existence of an elongate plume of convecting hot water which dips 45° to the northeast, is recharged from the northeast, and discharges to the southwest (Fig. 5).

Geophysics

LBL continued a program of geophysical monitoring of the field. Precision gravity, dipole-dipole resistivity surveys, and seismic monitoring were carried out over the area to determine whether subsurface changes in the physical properties of rocks are taking place in response to exploitation of the field. Additional magnetotelluric stations were added to help delineate the field boundary.

During fiscal 1980, CFE continued its exploration of new potential geothermal areas in the Mexicali Valley. Schlumberger resistivity, magnetic, gravity, self potential, and heat flow surveys were completed at Tule Check (northwest of Cerro Prieto), and Schlumberger resistivity and heat flow surveys were carried out at Mesa de Andrade (southeast of Cerro Prieto). However, only the results of the LBL work are discussed here.

During the geophysical presentations and discussions at the Vallombrosa Meeting the following points were raised about the Cerro Prieto area:

1. The positive magnetic and coincident gravity anomalies centered about 6 km northwest of the Cerro Prieto volcano are due to a shallow magnetic basement.

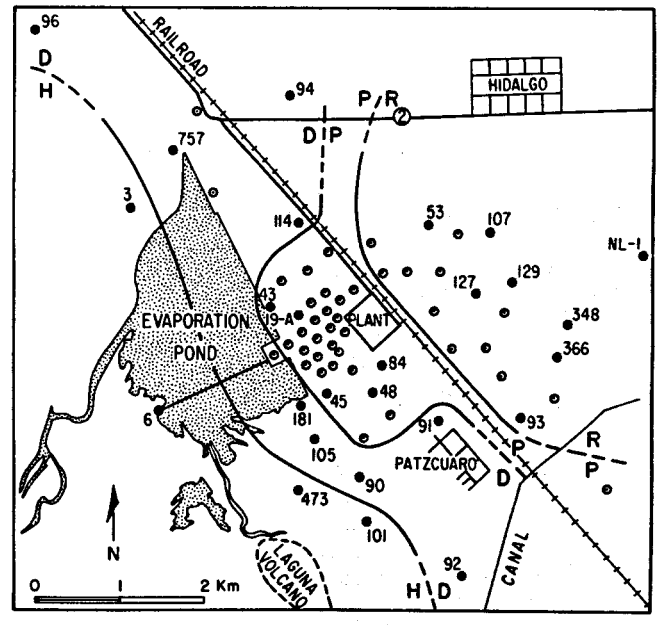

Figure 5. Proposed division of the geothermal field into regions of characteristic flow regime. R, Recharge Zone; P, Thermal Plume Zone; D, Discharge Zone; H, Zone of Horizontal flow (after Elders et al., 1980). [XBL 811-7517]

2. The large, circular, positive magnetic anomaly and the general gravity low south of Nuevo Leon, about 5 km southeast of well M-53, could be caused by a complex of diabase dikes and sills at a depth of roughly 2 km.

3. Coincident gravity and magnetic lows are indicative of thick sedimentary sequences; one such pattern is observed south of the Cerro Prieto volcano, centered on the highway to San Felipe. Seismic reflection data support this interpretation. However, magnetic and seismic evidence obtained between the volcano and Nayarit suggests that volcanic rocks exist above the basement within the sedimentary rocks.

4. Gravity methods seem better than magnetic methods for helping to define the zone of hydrothermal alteration/metamorphism associated with the geothermal field.

5. The "ridge-like" gravity high extending southeastward from well M-96, subparallel to the Cerro Prieto fault and truncated by the Pátzcuaro fault, very likely results from densified shales below the contact between the unconsolidated and consolidated sediments (A/B contact).

6. There is no clear evidence of the simple basement horst purported to underlie the original production area.

7. Both gravity and magnetic data have proved useful in defining major structures in the Mexicali Valley.

8. The large dipolar self-potential anomaly mapped over the field seems to be caused by a combination of fluid flow (electrokinetic effect) and temperature gradient (thermoelectric effect).

9. At Cerro Prieto, where normal resistivities of the saline sediments are low (1-2 ohm-m), the geothermal field is best correlated with a resistivity high.

10. Resistivity lows near the field could be explained by (a) marine sediments to the west containing saline pore fluids or (b) near-surface thermal manifestations, offset laterally from the reservoir.

11. Detailed interpretation of dc resistivity (dipole-dipole) provides a two-dimensional picture to depths of 2-3 km; parameters of deeper layers are better fixed by means of magnetotelluric interpretation.

Dipole-Dipole Resistivity

A dipole-dipole resistivity survey was repeated in March 1980 over an established E-W line centered over the reservoir region. The measurements were performed in a nearly identical manner to those done in fiscal 1979, and we utilized the same current electrodes and equipment. Current was impressed by means of the LBL 25-kW motor generator, which produces a 40-s square wave pulse of 17-35 A. A dipole length of 1 km was used, and voltages at potential dipoles with separations of up to n = 8 were read using our programmable, multichannel digital receiver. Signals from four potential dipoles were averaged simultaneously; usually four signal cycles were stacked for each measurement and 15-25 measurements were used to obtain an average apparent resistivity. Analysis of the data shows that the standard errors associated with 90% of the data points are less than 2%. However, the accuracy in most apparent resistivity estimates is probably not that good. Repeat measurements made several days apart gave average apparent resistivities that agree to within 4-6%. Telluric noise cancellation was not used.

A comparison of 1979 and 1980 data sets reveals that a change in apparent resistivities has occurred that cannot be attributed merely to measurement error. An analysis of the changes is being deferred until another set of data is obtained in fiscal 1981.

Seismic Monitoring

The five-station seismic network was put back into operation after several months, during which time we modified the three-component geophones to operate in the high temperatures encountered in the 100-m-deep wells. We also found it necessary to replace the hardwire links between stations with a radio telemetry system because the wires were frequently broken by human activities (Fig. 6). Following the earthquake of June 8, 1980, centered 10 km southeast of the field, the aftershock activity became so high (50-100 events per day compared to two events before the earthquake) that routine monitoring and recording of data was not possible with the triggered digital cassette recorder. We therefore set up a visual monitor on one geophone until the number of aftershocks decreased and normal monitoring could resume.

Magnetotellurics

Nine new MT stations were established in fiscal 1980 to obtain more complete coverage on the southern side of the field (Fig. 7). Data were

Figure 6. Checking the radio telemetry system for the induced seismicity network. [CBB 782-2240]

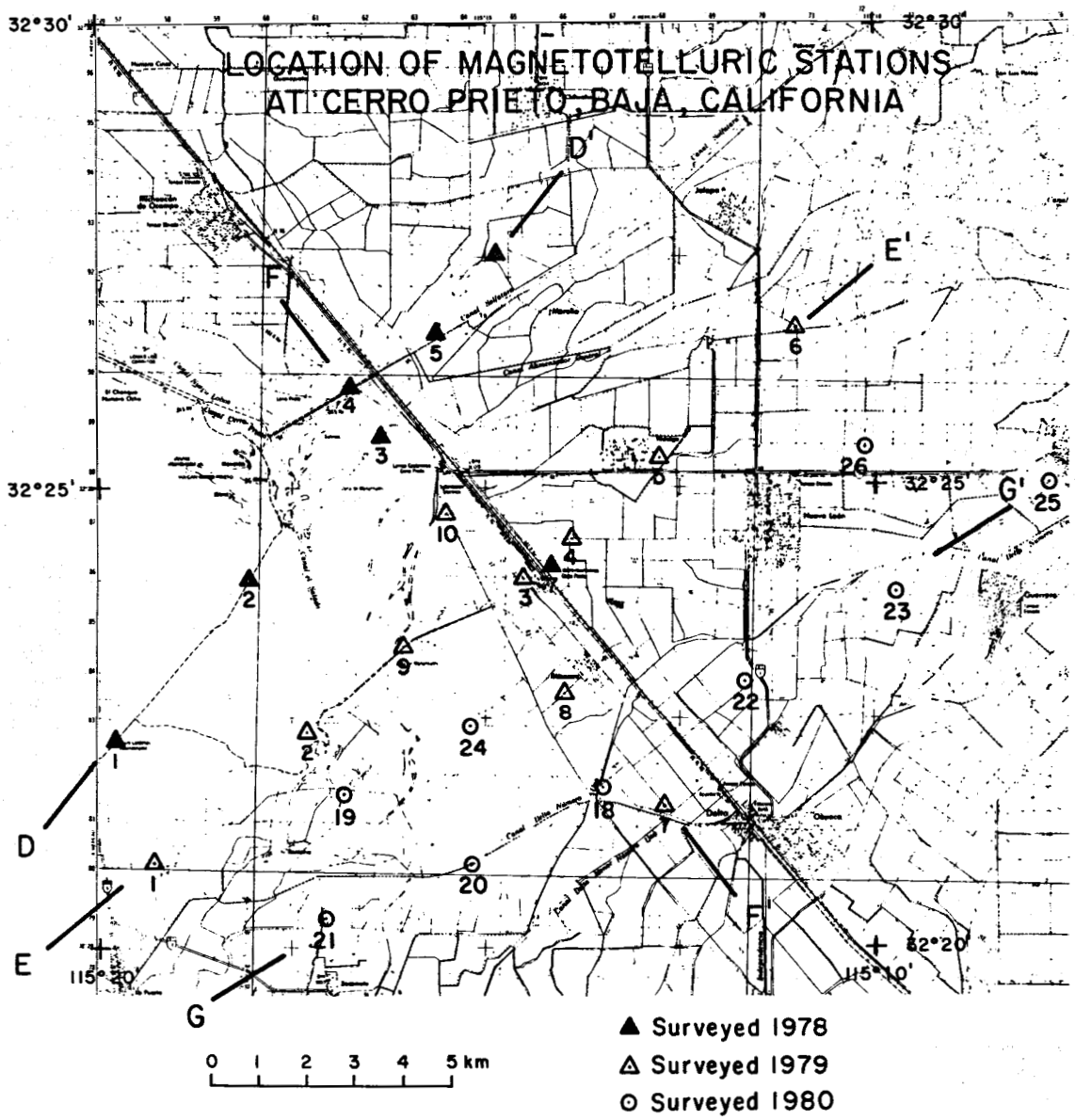

Figure 7. Location of magnetotelluric stations at Cerro Prieto. [XBL 799-11498]

collected over the frequency range from 40 to approximately 0.001 Hz using the reference magnetic technique (Gamble et al., 1979). A discussion on methods of data analysis and results is presented elsewhere in this report (Goubau et al., 1981).

Gravity Survey

Between January and March 1980, the 60 gravity monuments around the field were occupied for the third successive year. Measurements were made in accordance with procedures discussed by Chase et al. (1978) and Grannell et al. (1979). Each station was occupied four times; during each visit four readings were obtained for a total of 16 readings per station. A La Coste and Romberg G-model gravity meter was used in a looping technique in which each station is surveyed between two base-stations no more than 5 hours apart. The data were reduced to observed gravity values using meter calibrations and the appropriate corrections made for both earth tides and instrument drift.

The standard deviations for most of the stations is better than ±10 μgal. This degree of accuracy--the best achieved in the 3 years of measurements--is due to the use of a new spring-mounted transport box which has greatly reduced mechanical vibrations during travel over rough roads. Although no significant gravity variations have been noted yet at any station, small changes in gravity have occurred in two areas; (1) south-southeast of the Cerro Prieto volcano and (2) east of the field near Hidalgo. These changes of approximately 5-10 μgal may not be related to geothermal production; rathe they seem to result from small elevation changes (the free-air correction is 3 μgals/cm) caused by regional tectonics.

Geochemistry

CFE continued studying the chemical variations observed in the fluids produced by the Cerro Prieto wells. Fausto et al. (1981) used the Na/K and Na-K-Ca geothermometers and chloride content to study the direction of water recharge and the physical processes occurring in the reservoir.

The changes with time in enthalpy and chemical composition of geothermal fluids have been interpreted by A. H. Truesdell (U. S. Geological Survey), M. A. Grant (New Zealand), A. Mañon (CFE), and others to indicate two major effects of exploitation on the Cerro Prieto reservoir: (1) Local boiling in the aquifer results from near-well pressure decreases. The zones of local boiling are characterized by fluids with excess enthalpy (steam flow) during expansion into new hot rock and by local quartz deposition and silica-deficient fluids, especially during the period of expansion. (2) The lack of a low-permeability cap on the reservoir allows the influx of cold water from above because of the reduction in pore pressure. This cold water influx is indicated by decreases in chloride, oxygen-18, and other fluid constituents and by chloride-enthalpy slopes characteristic of cold sweep processes.

In fields with tight caprocks, general pressure reduction produces a steam cap, and some shallower wells permanently produce nearly dry steam, a phenomenon not found at Cerro Prieto. Aquifer temperatures away from wells, as indicated by the Na-K-Ca geothermometer, show slow decreases not immediately affected by local boiling or cold water influx. However, after the heat contained in reservoir rocks is exhausted, the inflow of cold water must produce rapid enthalpy declines.

Reinjection

The reinjection of untreated brines at about 165°C into well M-9 continues. CFE, which is in charge of the operation, reports that after an initial reduction (from 40 to about 25 ton/hr), the injection rate has increased to about 80 ton/hr. The monitoring of neighboring production wells detected no changes in wellhead temperature, pressure, or enthalpy caused by the injection operation. The shallow depth of injection (721-864 m in well M-9) could explain why the surrounding producing wells do not show any effects, especially pressure changes (the depth to the producing reservoir in this area is more than 1100 m).

Because of the success of the long-term M-9 injection test, CFE is considering the repair of some older nonproducing wells in the present production area to convert them into injection wells (Comisión Federal de Electricidad, 1980.

Reservoir Engineering

CFE has continued its well-testing program, especially in the eastern part of the Cerro Prieto field. The reservoir permeabilities estimated from the well-test data were on the order of tens of millidarcies.

The LBL pressure-temperature-flow tool was tested with the improved surface equipment during the injection test at well M-9. The pressure and temperature transducers and the surface equipment functioned well up to the hottest temperature encountered in the well (229°C). However, the LBL-modified Kuster flow-tool indicated no flow below the perforated interval and did not recover when it was pulled up the well. During the tests it was observed that the turbine bearings would fail while the hot section of the well was being surveyed (Alonso et al., 1979).

The LBL two-phase computer program SHAFT79 was used in preliminary modeling studies of the field's behavior. Two-dimensional horizontal and vertical lumped-parameter models were developed. Besides being used to obtain pressure and enthalpy histories, these simple models were used to gain insight into the relative permeabilities of steam and water phases for various saturation conditions. The complexity of the models will be increased as a better understanding of the boundary and initial reservoir conditions is obtained.

Field data for mass flow, heat flow, and temperature for each Cerro Prieto well were compiled up to 1977. A computer program AVERAGE was developed to calculate (1) yearly mass flow rates for all the wells, (2) total mass flow from the field each year, (3) annually averaged mass flow rates for the entire field, (4) annually averaged mass flow rates per well per year, (5) total mass flow rates for each month for the entire production zone, (6) cumulative mass produced, (7) monthly averaged mass flow rates, (8) monthly averaged mass flow rates per well, (9) cumulative heat produced, and (10) annnually and monthly averaged enthalpies.

The LBL computer program WELFLO was modified to include the effects of variable well-casing diameters. It will now be possible to compute the bottomhole conditions from available wellhead conditions and develop a reservoir-pressure production history of the field.

Subsidence

A third first-order leveling survey was completed in the area by DETENAL in December 1979. The preliminary results seem to indicate the same trend of localized vertical subsidence and uplifts as were detected by comparing the 1977 and 1978 vertical-control surveys.

This year neither the regional nor the local horizontal-control networks were resurveyed by the U. S. Geological Survey. This field work is planned for January 1981. It is expected to measure significant ground deformations resulting from the large earthquakes of October 1979 and June 1980.

As part of the DOE Geothermal Subsidence Research Program managed by LBL, Terra Tek, Inc. carried out an experimental program to determine the mechanical and physical responses of cores from selected Cerro Prieto wells. Of particular interest were the effects of pore-pressure reduction due to reservoir drawdown on rock compaction and vertical permeability. Abou-Sayed et al. (1981) concluded

that (1) pore pressure reduction will cause substantial compaction and reduction in permeability, (2) some part of the compaction and permeability reduction is not returned upon restoration of pore pressure, and (c) the laboratory-measured vertical permeabilities of less than 1 millidarcy are significantly less than the reservoir permeability of 20 millidarcies or more estimated from well-test data.

Conferences

The Second Symposium on the Cerro Prieto geothermal field was held October 17-19, 1979, in Mexicali, Baja California, Mexico, followed by a field trip to the area. This time the meeting was organized by CFE with the assistance of DOE and LBL. About 250 scientists and engineers from the government, academia, and the private sector attended the symposium. The proceedings of this meeting are being prepared by CFE and are expected to be published in early 1981 (Comisión Federal de Electricidad, 1981).

The English edition of all papers presented during the First Symposium (San Diego, September 1979) was published in Geothermics (v. 8, no. 3/4, 1979; and v. 9, no. 1/2, 1980). The English-Spanish proceedings of this meeting had been issued previously (Lawrence Berkeley Laboratory, 1978).

During this fiscal year, preparations began for the Third Symposium (San Francisco, California, March 24-26, 1981). A bilingual announcement was prepared and mailed out, contracts were signed, and a call for papers issued.

REFERENCES CITED

Abou-Sayed, A. S., Schatz, J. F., and Wolgemuth, K. M., 1981. Compaction and permeability of Cerro Prieto cores: A laboratory evaluation. In Proceedings, Second Symposium on the Cerro Prieto Geothermal Field, Mexicali, Baja California, Mexico, October 17-19, 1979. Mexicali, Comisión Federal de Electricidad.

Alonso E., H., Domínguez A., B., Lippmann, M. J., Molinar C., R., Schroeder, R. C., and Witherspoon, P. A., 1979. Update of reservoir engineering activities at Cerro Prieto. In Proceedings, Fifth Workshop, Geothermal Reservoir Engineering, December 12-14, 1979. Stanford, Stanford University, p. 247-256.

Chase, D. S., Clover, R. C., Grannell, R. B., Leggewie, R. M., Eppink, J., Tarman, D. W., and Goldstein, N. E., 1978. Precision gravity studies at Cerro Prieto. In Proceedings, First Symposium on the Cerro Prieto Geothermal Field, Baja California, Mexico, September 1978. Berkeley, Lawrence Berkeley Laboratory, LBL-7098, p. 249-256.

Comisión Federal de Electricidad, 1980. Estado actual de la geotermia en México. Brochure distributed during the Third OLADE Seminario sobre Desarrollo y Explotación Geotérmica, Mexicali, México, October 13-17, 1980.

Comisión Federal de Electricidad, 1981. Proceedings, Second Symposium on the Cerro Prieto Geothermal Field, Mexicali, Baja California, Mexico. October 17-19, 1979. Mexicali, Comisión Federal de Electricidad.

Elders, W. A., Hoagland, J. R., and Williams, A. E., 1980. Hydrothermal alteration as an indicator of temperature and flow regime in the Cerro Prieto geothermal field of Baja California. Geothermal Resources Council, Trans., v. 4, p. 121-124.

Fausto L., J. J., Sánchez A., A., Jiménez S., M. E., Esquer P., I., and Ulloa H., H., 1981. Hydrothermal geochemistry of the Cerro Prieto geothermal field. In Proceedings, Second Symposium on the Cerro Prieto Geothermal Field, Mexicali, Baja California, Mexico, October 17-19, 1979. Mexicali, Comisión Federal de Electricidad.

Gamble, T. D., Goubau, W. M., and Clarke, J., 1979. Magnetotellurics with a remote magnetic reference. Geophysics, v. 44, no. 1, p. 53-68.

Goubau, W. M., Clarke, J., and Miracky, R. F., 1981. Advances in magnetotelluric survey techniques and data interpretation. In Earth Sciences Division Annual Report 1980. Berkeley, Lawrence Berkeley Laboratory, LBL-12100.

Grannell, R. B., Tarman, D. W., Aronstam, P., Clover, R. C., Leggewie, R. M., Eppink, J., and Kroll, R., 1979. Precision gravity measurements in the Cerro Prieto geothermal area. In Abstracts, Second Symposium on the Cerro Prieto Geothermal Field, Mexicali, Baja California, Mexico, October 17-19, 1979. Mexicali, Comisión Federal de Electricidad, p. 37-39.

Lawrence Berkeley Laboratory, 1978. Proceedings, First Symposium on the Cerro Prieto Geothermal Field, Baja California, Mexico, September 20-22, 1978. Berkeley, Lawrence Berkeley Laboratory, LBL-7098.

Lippmann, M. J., and Mañon M., A., 1980. Minutes of the Cerro Prieto Internal DOE/CFE Workshop Vallombrosa Center, Menlo Park, California, March 10-12, 1980 (unpublished).

Lyons, D. J., and van de Kamp, P. C., 1980. Subsurface geological and geophysical study of the Cerro Prieto geothermal field, Baja California, Mexico. Berkeley, Lawrence Berkeley Laboratory, LBL-10540.

Witherspoon, P. A., Alonso E., H., Lippmann, M. J., Mañon M., M., and Wollenberg, H. A., 1978. Mexican-American Cooperative Program at the Cerro Prieto geothermal field. Berkeley, Lawrence Berkeley Laboratory, LBL-7095.

GEOLOGY OF THE CERRO PRIETO FIELD

S. Vonder Haar and J. H. Howard

A comprehensive effort to understand the geology at Cerro Prieto began in 1977 with the signing of a cooperative agreement between the Comisión Federal de Electricidad de México (CFE) and the U. S. Department of Energy, Division of Geothermal Energy. Results of ongoing studies that include geophysics, geochemistry, well testing, and reservoir engineering are discussed in the proceedings of the first two symposia on the Cerro Prieto geothermal field (Lawrence Berkeley Laboratory, 1979; Comisión Federal de Electricidad, 1981). This article focuses briefly on the tectonic regime of the Cerro Prieto field and on the altered porosity and permeability within the reservoir.

The wedge-shaped region termed the Salton Trough extends southward from the Salton Sea to the Gulf of California geothermal fields (Fig. 1). This region is bounded on the east by the poorly defined Craton Margin Lineament and the Sierra Pinacate volcanics. On the west, the San Felipe basin-bounding fault zone and the combined Elsinore/San Jacinto fault zones form a sharp boundary. Slicing through the trough are the Cerro Prieto and Imperial faults, among others. These major faults may be thought of as hybrids, having features of both San Andreas-style wrench faults and oceanic transform faults. The Cerro Prieto geothermal field is thus localized between major faults in a zone of crustal spreading, most likely at an offset of the landward extension of the East Pacific Rise. The field lies about 5 km southeast of the rhyodacite Cerro Prieto volcano, which has been estimated by paleomagnetic dating as having a maximum age of 110,000 years.

Areas similar to the Cerro Prieto region were investigated in relation to both early rifting phases and transform faulting. In addition to studies of basins in the Gulf of California, the in-situ structural observations along transform fault "A" in the FAMOUS area of the Mid-Atlantic Ridge have provided clear insights into fault style and dynamics (Fig. 2). Geophysical studies and well drilling in the Cerro Prieto region have furnished a model that compares favorably with these analogs if the increasing rate of deltaic sedimentation and the thickening of the continental basement near Cerro Prieto are considered.

The structural framework of the field, derived from interpretation of geophysical studies and subsurface data from well logs, is illustrated in Figure 3. The first-developed producing area of the field is located between the Cerro Prieto and the Michoacán faults, which are approximately 3 km apart and nearly parallel. The high productivity of certain wells, such as M-103 (Alonso et al., 1979), is most likely due to their proximity to the intersection of either the Cerro Prieto or the Michoacán

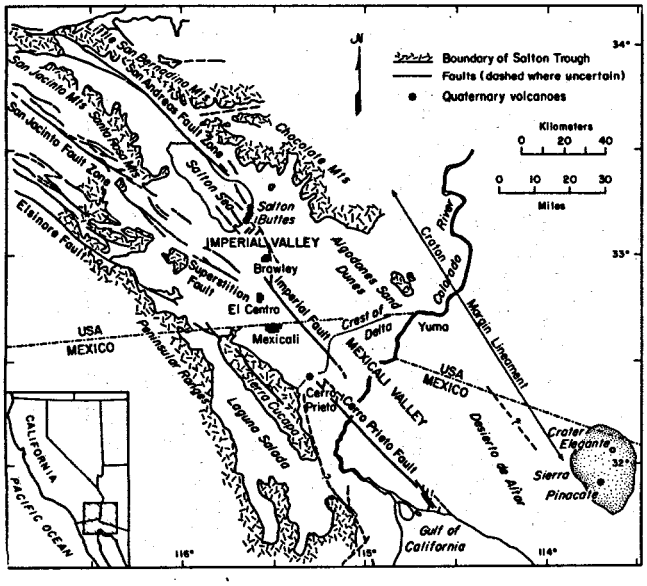

Figure 1. Regional geology of the Cerro Prieto geothermal field. Note the prevalent and long NW-SE trending faults with much shorter intersecting faults of NE-SW trends. [XBL 801-6718]

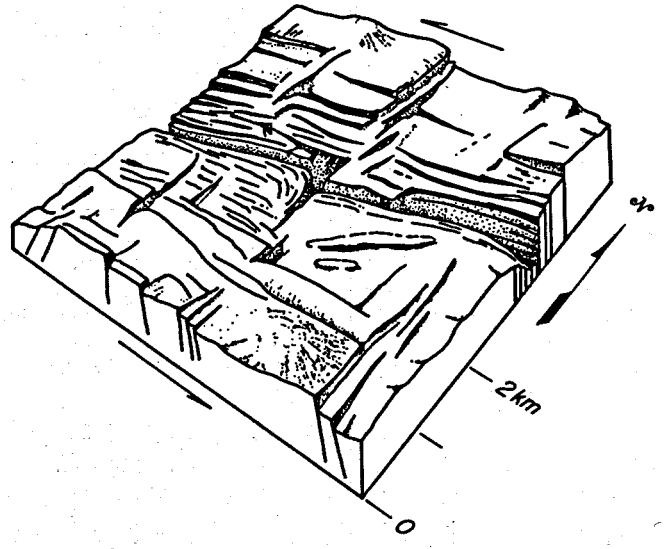

Figure 2. Interpretive block diagram of the oceanic transform fault "A" in the Mid-Atlantic Ridge, showing structural domains. The ramps, cross-faults, and 200-m-wide active zone of strike-slip movement within a 4-km-wide fault trough suggest the possible complexity of faulting along the Cerro Prieto and Imperial faults and within the producing geothermal fields (after Choukroune et al., 1978). [XBL 797-7583]

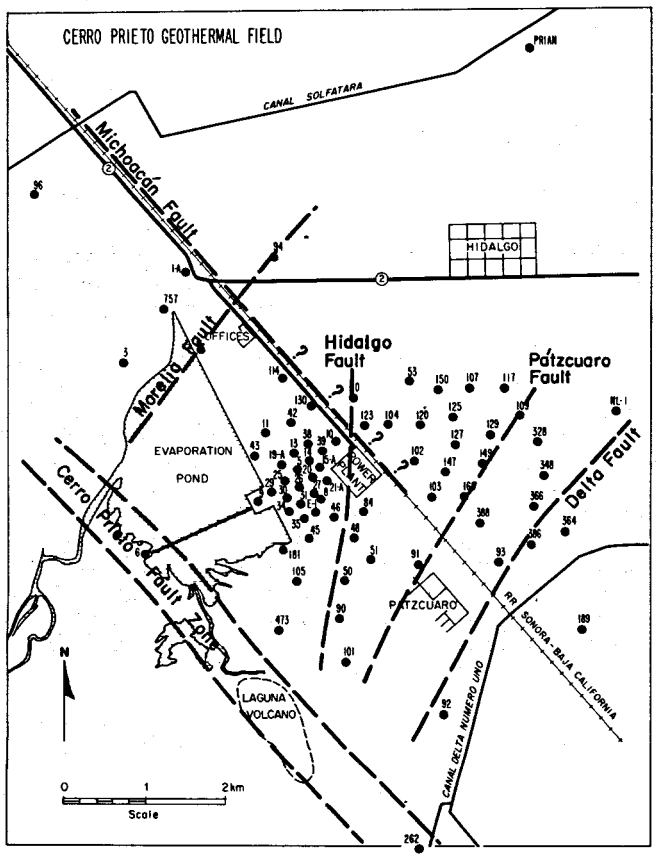

Figure 3. Map of the Cerro Prieto geothermal field with a simplified fault system. [XBL 804-7022A]

fault and the NE-striking set of faults. Such intersections furnish a fracture zone of relatively high permeability that serves as a preferential conduit for convective circulation of geothermal fluids.

Although only the dip-slip component of faulting is evident from well-log correlations, there may also be significant lateral slip in some cases. Vertical offsets range up to several hundred meters. Only a few wells have penetrated the basement rocks, and these indicate a general deepening of the sedimentary section from west to east, with fault blocks bounded by the NW-striking faults displaced progressively downward to the east. Seismic refraction surveys indicate that the depth to the basement east of the Cerro Prieto fault is approximately 5 km. West of the fault the basement refractor (5700 m/s) is at a depth of 1.5-3 km.

The stratigraphic section of Cerro Prieto is divided into three broad units: unconsolidated sediments (silts, clays, sands) that extend from the surface to a depth of approximately 800 m; underlying consolidated sandstones and shales; and granodioritic basement rocks. Within the consolidated sedimentary rocks, there are two principal reservoirs: an upper reservoir from which most of the present production from the field is derived, and a hotter, deeper reservoir where temperatures reach 350°C. The two zones are separated in some locations by approximately 50 m of relatively impermeable shale. From well-log analyses, Lyons and van de Kamp (1980) have identified five classes of

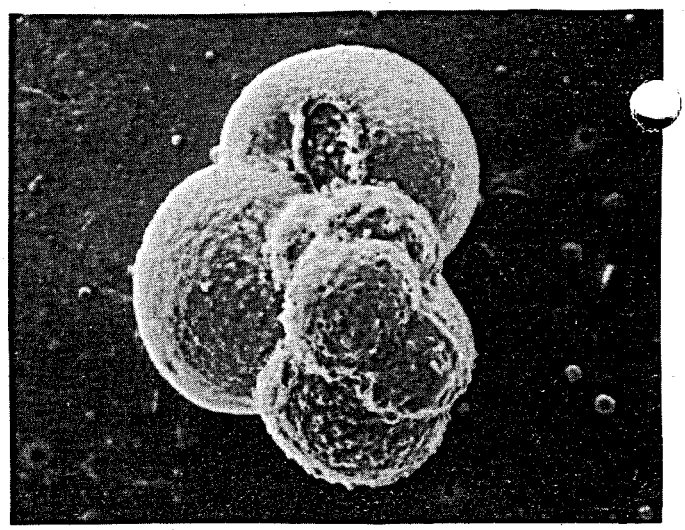

Figure 4. Cassigerinella chipolensis, a mid-Tertiary planktonic microfossil found in Cerro Prieto geothermal well cuttings. Scanning electron micrograph provided by J. L. Lamb, Exxon Production Research; actual diameter of the microfossil is 0.7 mm. [XBB 790-13447]

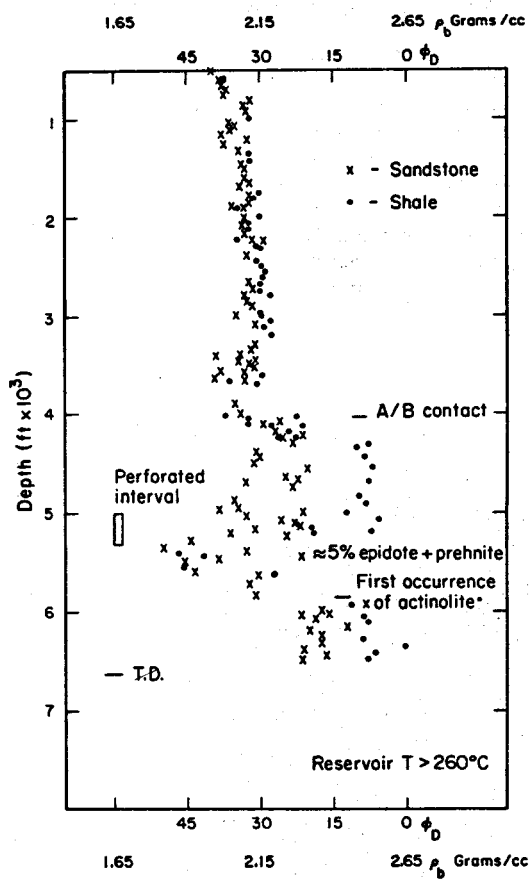

*Mineral data after Elders and others (in press)

Figure 5. Plot of porosity and density versus depth for well M-103 as determined from well logs and cuttings. The high porosity in the perforated interval represents extensive dissolution porosity. [XBL 805-7079]

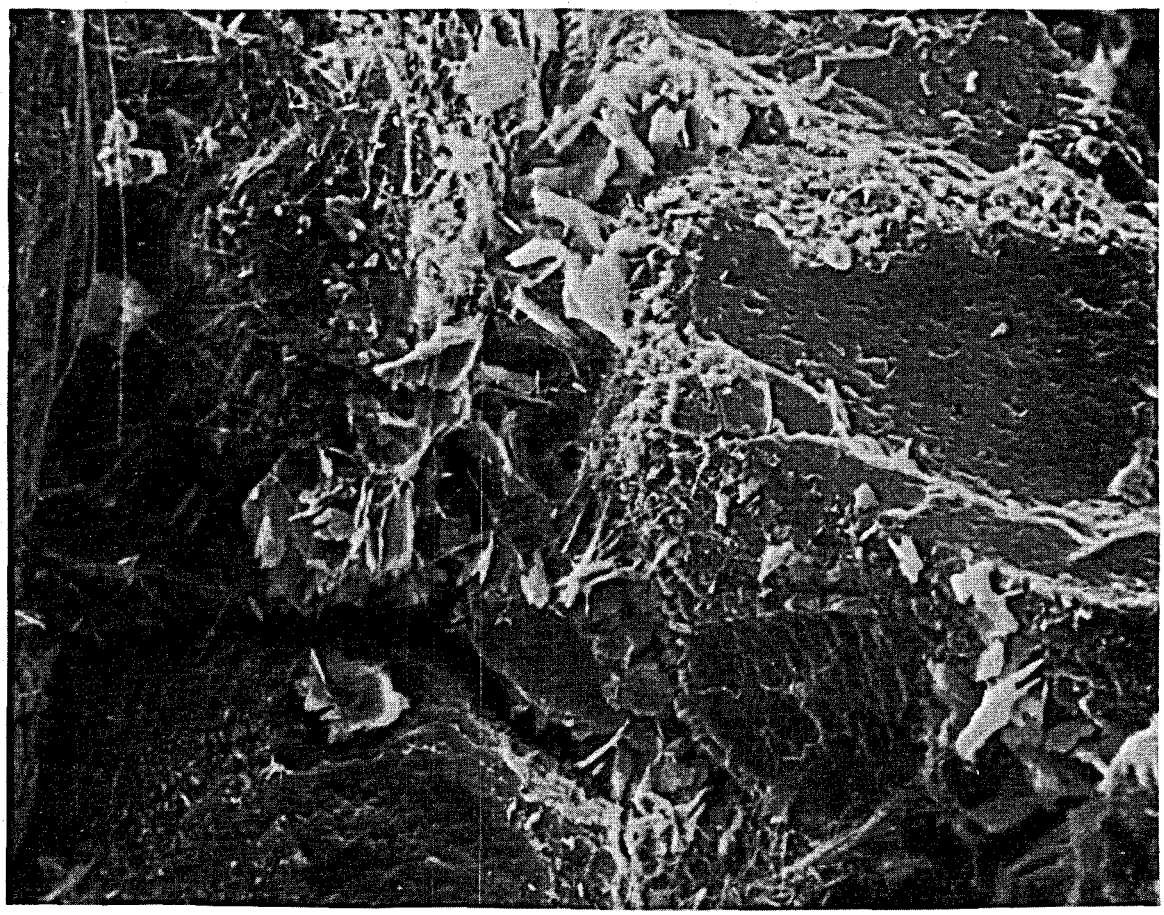

Figure 6. Scanning electron micrograph of a core chip from well NL-1 at 2720 m below the surface; the field of view across the photograph is 40 μm (0.04 mm). This reservoir quartz sandstone lies within the 260°C epidote mineral horizon. Note the hydrothermally precipitated, platy, and needle-shaped clay particles clogging the opening between the sand grains, thus reducing permeability.
[XBB 799-12511]

lithofacies, each with a characteristic lithology and apparent thickness. Present production is limited to the thicker, mixed sand and shale classes representative of a delta plain depositional environment.

Of major importance to the regional stratigraphy was the discovery, in well cuttings from the Cerro Prieto geothermal field, of a planktonic marine microfossil--Cassigerinella chipolensis, a mid-Tertiary foraminifer approximately 15 million years old (Fig. 4). If the presence of this foraminifer is confirmed by more extensive sampling, the current conceptualization of the opening of the Gulf of California and the mid-Tertiary history of the Pacific coast will need to be revised.

Within the deltaic sedimentary rocks of the reservoir, there are diverse porosities and permeabilities. Much of the matrix porosity at depth (as in well M-103 at 5200 ft, Fig. 5) is due to alteration by hot fluids. Scanning electron micrographs (Fig. 6) vividly document the clogging of openings between sand grains by hydrothermally precipitated clays.

The geothermal reservoir is now believed to be recharged by waters primarily from the east and northeast, consisting partly of Colorado River water and partly of sea water whose chemical constituents are concentrated by solar evaporation in coastal lagoons.

From petrographic and mineralogic analyses of well cuttings, four zones of alteration have been recognized by Elders et al. (1980). In order of increasing threshold temperature, these are (1) a diagenetic zone, (2) an illite-chlorite zone (> 150°C), (3) a calc-aluminum silicate zone (> 230°C), and (4) a biotite zone (> 325°C). Diagrams of depths to the first appearance of diagnostic alteration minerals (Fig. 7) illustrate the temperature distributions within the field. The configuration of the alteration-mineral horizons generally conforms to the dome-like pattern of relatively high density and high electrical resistivity associated with the producing field, as indicated by surface geophysical surveys.

Fractures in the reservoir rocks often appear to be sealed by hydrothermal mineralization. Therefore, although fracture permeability undoubtedly plays a role, the secondary matrix porosity due to the solution effects of the geothermal fluids in the sandstone is also a major factor in providing reservoir permeability.

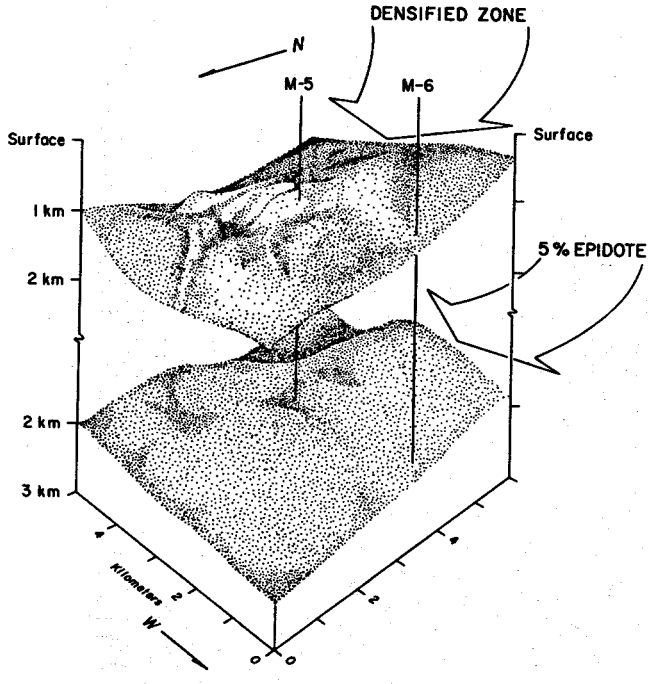

Figure 7. This three-dimensional perspective of the present Cerro Prieto geothermal field indicates an upper densified dome-like surface at approximately 1 km that serves as a low-permeability barrier, partially capping the reservoir. Between the densified zone and the 5% epidote surface is the zone of extensive dissolution porosity with its zone of variable permeability. [XBL 805-7073]

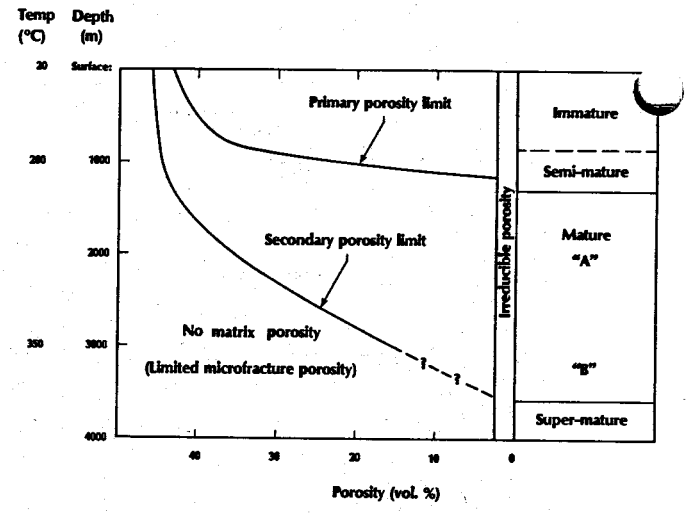

Figure 8. Accelerated porosity alteration in the deltaic quartz sandstone of the Cerro Prieto geothermal field. The immature stage represents mainly mechanical reduction of primary porosity; the semimature stage, mainly chemical reduction of primary porosity. Mature "A" is a zone of predominant carbonate mineral dissolution and mature "B" is of silicate mineral dissolution. Super-mature is a metamorphic zone of very low matrix porosity, yet a key zone for microfracture porosity. [XBL 805-7075]

The main geologic and economic significance of secondary matrix sandstone porosity is that it extends the depth range for effective sandstone porosity 1-3 km below the depth limit for effective primary porosity. Generation and migration of both petroleum and geothermal water occurs mainly below the range of effective primary porosity. The migration and the accumulation sites of geofluids are thus commonly controlled by the distribution of secondary porosity. The distribution of secondary matrix porosity in a productive sandstone formation may not necessarily show a direct relationship with the original depositional layering or burial history and is difficult to predict. However, our detailed geological analyses at Cerro Prieto have met with success. An initial summary of these ideas is shown in Figure 8. This diagram will be refined as more geothermal fields come into operation (such as the Heber and Salton Sea fields north of Cerro Prieto).

REFERENCES CITED

Alonso E., H., Dominguez A., B., Lippmann, M. J., Molinar C., R., Schroeder, R. C., and Witherspoon, P. A., 1979. Update of reservoir engineering activities at Cerro Prieto, in Proceedings, Fifth Workshop on Geothermal Reservoir Engineering, December 11-14, 1979, Stanford, California, Stanford University, SGP-TR-40, p. 247-256.

Choukroune, P., Francheteau, J., and Le Pichon, X., 1978. In situ structural observations along transform fault A in the FAMOUS area, Mid-Atlantic Ridge. Geol. Soc. America Bull., v. 89, p. 1013-1029.

Comisión Federal de Electricidad, 1981. Proceedings, Second Symposium on the Cerro Prieto Geothermal Field, October 17-19, 1979, Mexicali, Baja California, Mexico. Comisión Federal de Electricidad de México.

Elders, W. A., Hoagland, J. R., Vallette, J. N., Williams, A., Barker, C., Collier, P., 1981. A comprehensive study of samples from geothermal reservoirs: Petrology and geochemistry of subsurface and surface samples from the Cerro Prieto geothermal field, Baja California, Mexico. Riverside, University of California (in press).

Lawrence Berkeley Laboratory, 1979. Proceedings, First Symposium on the Cerro Prieto geothermal field, Baja California, Mexico, September 20-22, 1978, San Diego, California. Berkeley, Lawrence Berkeley Laboratory, LBL-7098, 455 p.

Lyons, D. J., and van de Kamp, P. C., 1980. Subsurface geological and geophysical study the Cerro Prieto geothermal field, Baja California, Mexico. Berkeley, Lawrence Berkeley Laboratory, LBL-10540.

ANALYSIS OF CERRO PRIETO PRODUCTION DATA

K. P. Goyal, C. W. Miller, and M. J. Lippmann

As part of the Mexican-American cooperative program, Lawrence Berkeley Laboratory (LBL) has undertaken the analysis of available production data from the Cerro Prieto field in order to generate relevant reservoir parameters to numerically simulate the behavior of this geothermal system. The primary objective of this modeling is to estimate the energy production capacity and longevity of the field under different production and injection scenarios.

A first step in the simulation is to validate the model against the known production history of the field. For that purpose the modeler needs to know the evolution of the field due to exploitation. Since most computer programs are designed to simulate the behavior of the entire geothermal field, they compute physical properties of the fluid in the reservoir itself rather than in the wellbore. Traditionally, routine measurements of the production data are made only at the wellhead. However, sometimes downhole measurements for temperature and pressure are also made, as described by Bermejo et al. (1978).

Our purpose is to analyze the wellhead data to obtain the production history of the field, and to calculate the downhole conditions of some representative production wells.

The following activities were undertaken during fiscal 1980:

1. Production data for mass flow, heat flow, and temperature were compiled for each well during 1973-1977 to obtain the production history of the field.

2. A computer program, AVERAGE, was developed to calculate (a) yearly mass flow rates for all the wells, (b) total mass flow from the field each year, (c) annually averaged mass flow rates for the entire field, (d) annually averaged mass flow rates per well, (e) total mass flow rates for each month for the entire production zone, (f) cumulative mass produced, (g) monthly averaged mass flow rates, (h) heat produced each month and each year from the entire field, (i) cumulative heat produced, and (j) annually and monthly averaged enthalpies.

3. The LBL computer program WELFLO (Miller, 1979) was modified to calculate the bottomhole conditions under single- or two-phase flow, with or without variable well diameter.

The information generated using program AVERAGE was summarized in the form of tables and graphs. Figure 1 shows the cumulative mass produced in the Cerro Prieto field from 1973 to 1977. It may be noted that about 100 million tonnes of fluid was extracted by 1977. Figure 2 shows an average mass flow rate of the field for each month. This plot

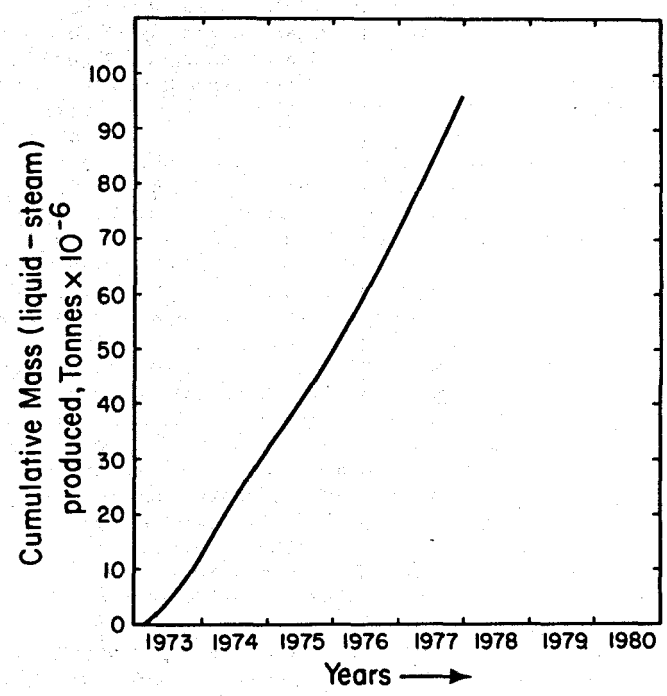

Figure 1. Cumulative mass production in the Cerro Prieto field. [XBL 808-7265]

is quite useful for preparing the input data for the model used to study the reservoir behavior. It may be noted in this figure that the production rate increased sharply during 1973 from about 1000 tons/hr to about 2200 tonnes/hr. This rise is attributed to the fact that more wells were placed into production. The total number of wells increased threefold, from 4 wells in March 1973 to 11 wells in December 1973. Another rise in the mass flow rate during 1976-1977 was also the result of

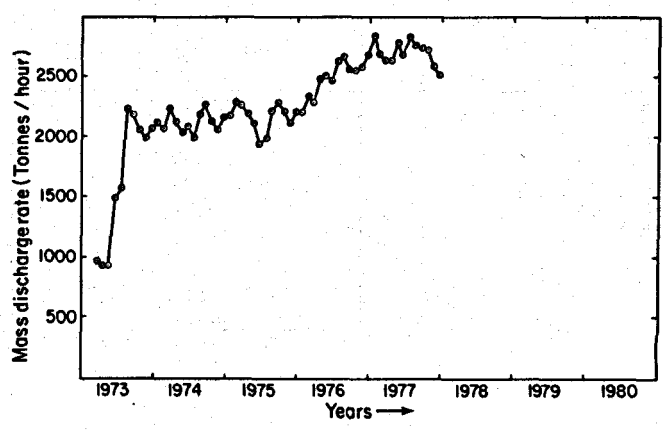

Figure 2. Mass discharge rate from all wells in the Cerro Prieto field. [XBL 808-7266]

an increase in number of production wells. The average number of production wells during 1974-1975 were about 12 compared to 15 during 1976-1977.

Figure 3 shows the cumulative heat produced from the Cerro Prieto field during 1973-1977. About 30 x 10^{12} kcal was extracted from the reservoir by the end of 1977. It is equivalent to an average energy production of about 800 MW. Actual electric power production from the field during this time was only 75 MW. This shows an operating efficiency of about 9% of the produced heat energy. Figure 4 shows the monthly averaged heat discharge for each month up to December 1977. It may be noted that the trends of Figures 3 and 4 for mass and heat extraction are quite similar, as expected. Figure 5 shows a plot of average enthalpy production from the field versus time. Here one may note that the average enthalpy of the field increases up to mid-1975 and decreases thereafter up to 1977. Two factors govern this type of field behavior. First is the addition of new production wells, which, in general, enhances the energy output, as can be seen in Figure 5 up to 1975. Second is the decrease in the enthalpy of the produced fluids resulting from the mixing with the colder waters drawn from the overlying aquifers under the pressure gradient associated with the field exploitation (Truesdell et al., 1978). This factor appears to contribute to the enthalpy decline during 1975-1977. This type of field behavior data is quite useful for a modeler, since it is useful to see whether the model is able to predict a similar enthalpy response.

During the next phase of our study, computer program WELFLO was used and modified to calculate the downhole conditions under both single-phase and two-phase flow. This code is able to calculate pressures, temperatures, velocities, saturations, and enthalpies of each phase as a function of depth.

Wellhead measurements, such as pressures, mass flow rates, and enthalpies, are often susceptible to some error. Thus the downhole conditions predicted by these data may also be in error. To find the effect on downhole conditions, a sensitivity analysis was conducted for wells M-90 and M-91, for which pressure data are available. Flow rates, wellhead pressures, and enthalpies were varied between ±20%, and it was found that the overall pressures in the wells either increased or decreased in

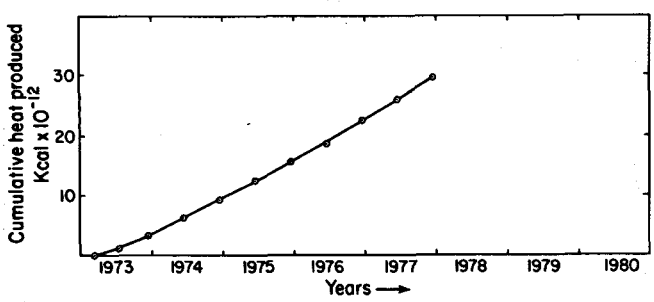

Figure 3. Cumulative heat production from all wells in the Cerro Prieto field. [XBL 808-7270]

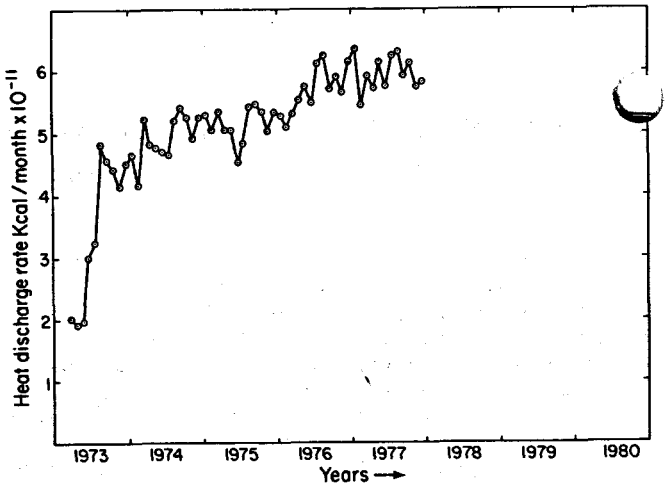

Figure 4. Monthly averaged heat produced from all wells, Cerro Prieto field. [XBL 808-7269]

response to a corresponding pressure change at the wellhead. As expected, an increase in the wellhead enthalpy resulted in lower pressures throughout the well, and vice versa. However, the increase in pressures associated with reduced enthalpies was quite significant for both wells and may be attributed to the presence of only water below certain depths in the wells. On the other hand, a decrease in the wellbore pressures due to increased enthalpy was larger in M-91 compared to that in M-90. This difference may have been caused by the presence of only liquid water in M-91 and steam-water mixture in M-90. It was also noticed that the decrease in the pressures in well M-90 was negligibly small for the enthalpy increase from 5% to 20%, indicating a flow of a two-phase fluid in the well with lower fluid densities. Thus the error toward increasing enthalpy may be comparatively smaller and within acceptable limits if the well were assumed to be filled to its full depth with a two-phase mixture. The effect of flow rate on the pressures was relatively small.

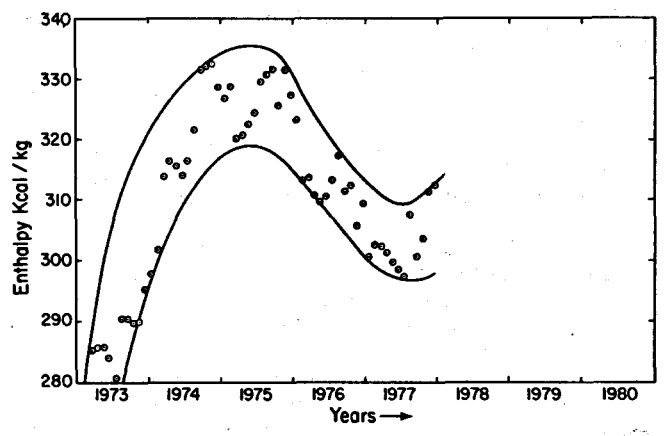

Figure 5. Average enthalpy production from the Cerro Prieto field. [XBL 808-7272]

The effect of well radius on the bottomhole pressures was also studied. It was found that the well radius does affect the downhole pressures considerably. Furthermore, the wells in the Cerro Prieto field were found to have scale deposits. For example, by 1976 more than 2.5 inches of scale had accumulated in well M-30 at a depth of 1500 m. Similar scale deposits were also observed in many other wells in the field. Thus, to obtain reasonable downhole pressures, it is necessary to have a computer program which accounts for variable diameters. The computer program WELFLO, which uses a uniform well diameter, was modified to account for variable diameters. It will now be possible to calculate bottomhole pressures at different times for each well and to develop isobaric maps for the reservoir and to study its pressure changes as the development of the field continues.

The information on the production history of the field and the changes in downhole reservoir conditions will be used to validate the numerical model being developed for the Cerro Prieto geothermal field.

REFERENCES CITED

Bermejo M., F. J., Cortéz A., C., and Aragón A., A., 1978. Physical and thermodynamic changes observed in the Cerro Prieto geothermal reservoir. In Proceedings, First Symposium on the Cerro Prieto Geothermal Field. Berkeley, Lawrence Berkeley Laboratory, LBL-7098, p. 300-332.

Miller, C. W., 1979. Numerical model of transient two-phase flow in a wellbore. Berkeley, Lawrence Berkeley Laboratory, LBL-9056 Rev., 31 p.

Truesdell, A. H., Mañon M., A., Jiménez S., M. E., Sánchez A., A., and Fausto L., J. J., 1978. Geochemical evidence of drawdown in the Cerro Prieto geothermal field. In Proceedings, First Symposium on the Cerro Prieto Geothermal Field. Berkeley, Lawrence Berkeley Laboratory, LBL-7098, p. 130-138.

NUCLEAR WASTE ISOLATION

Although a number of different rock types continue to be considered as potential geologic repository environments for the emplacement of nuclear wastes, the bulk of the Earth Sciences Division's efforts are pointed to research in fractured media with emphasis on hard rock geologies. Such phenomena as mechanical response to thermal loading, fluid flow through fractures, and chemical sorptivity must be investigated to understand their interactions and magnitudes. As this body of knowledge increases, the technical community will develop confidence in valid long-term predictions about the integrity of nuclear waste isolation in hard rock or other repository media. Within the Earth Sciences Division, research continues both on fundamental investigations of geological aspects of fractured media and on experimental and field research projects of a more applied nature.

The Swedish-American Cooperative Program, begun in July 1977, was a first-of-its-kind experiment for fractured rocks. The fundamental questions of how to characterize materials and properties and how to measure them were approached both experimentally and theoretically. The major field-data-gathering portion of this effort was completed at the Stripa mine in Sweden in August 1980. A comprehensive analysis of these field results has begun and will continue for a number of years at Lawrence Berkeley Laboratory and various other organizations under contract to the Department of Energy. Background and preliminary results from some specific experiments conducted at the Stripa site follow in this report. It is expected that these continuing analytical efforts will improve the existing state of knowledge and point to additional experiments and methodologies to characterize a fractured rock mass for the permanent and safe isolation of nuclear wastes.

Other topics under study span the range of theoretical analyses, laboratory studies, literature surveys, and computational simulations. Included in this report are results from studies of the chemical and physical waste-rock reactions that control radionuclide concentrations in geologic environments. A review of current thermomechanical-hydrochemical modeling, a progress report on the continuing theoretical development of a unified chemical transport model to predict the migration of interacting solutes in water-saturated porous or fractured media, an update on groundwater dating techniques based on the disequilibrium between ^{234}U and ^{238}U, and a report on the development and evaluation of geophysical techniques which might be used to monitor the operational integrity of repositories in hard rock are also presented.

This work was supported by (1) the Assistant Secretary for Nuclear Energy, Office of Nuclear Waste Management, Division of Waste Isolation; and (2) the Assistant Secretary for Nuclear Energy, Office of Nuclear Waste Management, Division of Surplus Facilities Management of the U. S. Department of Energy under Contract No. W-7405-ENG-48.

TOPICAL INVESTIGATIONS

A REVIEW OF THE STATE OF THE ART OF THERMOMECHANICAL-HYDROCHEMICAL MODELING OF A HARD-ROCK WASTE REPOSITORY

C. F. Tsang

Recent interest in the possibility of isolating nuclear waste in hard rocks has opened up a major new area of research (Lawrence Berkeley Laboratory, 1978, 1979). The basic idea is to store nuclear waste in repositories emplaced in hard rock formations so that no appreciable radionuclides will escape into the biosphere for hundreds of thousands of years. This presents a problem of major challenge because of the following unanswered questions.

1. How can we define the physical system under study? The characterization of a fractured rock mass is a major problem. Procedures have not yet been developed to represent such a system by an equivalent porous medium with major fractures or some other suitable model. Furthermore, much work is required to determine the parameters describing the fractured rock system by means of a finite number of borehole observations. Studies to date tend to be either completely deterministic (detailed fracture approximation) or completely random (porous medium approximation). A proper understanding, perhaps employing a stochastic approach, is urgently needed.

2. How can we calculate the processes associated with such a system? Four major processes are involved: (a) heating of the rock mass by the nuclear waste, (b) mechanical behavior of the rock, (c) the flow of the fluid in the geological system, and (d) chemical transport and reactions between water, rock, and dissolved radionuclides. There are hopes that some portions of these processes may be uncoupled, but this is by no means certain for all possible systems. In any case, coupled studies must be made to determine the limits of validity of uncoupled modeling. Up to now, various fields such as hydrology, geochemistry, and geothermal energy have, at most, coupled two of the four effects at the same time. To develop a model and to understand the overall process when all four processes are involved is a problem of major proportions.

3. Is it possible to extrapolate our understanding and calculations to the 10^3 - 10^6 years necessary to isolate the waste? What makes the present problem unique is the requirement that modeling has to be extrapolated with sufficient accuracy to times on the order of 10^3 - 10^6 yr, while being validated by only 2-20 yr of experiments. This not only demands very carefully designed models, but also requires including all relevant processes in our modeling, especially those slow processes which may be of little significance in experiments of "short" time span.

USES OF MODELING

The uses of modeling are not limited to simulating what has happened in the past or making predictions for the future. Modeling can also be used

1. To understand key processes. By generic studies, such isolated key factors as borehole stability and convective flow in fractures, can be investigated and an understanding of the processes obtained.

2. To determine sensitivity of key parameters. This will help to establish criteria for the accuracy with which a parameter need be measured in the field or in the laboratory.

3. As a tool for designing experiments. Modeling can be used to determine crucial guidelines concerning the layout of field experiments and the required sensitivity of instrumentation.

4. As a test against field data. Any discrepancy will either point out some error and inaccuracies in the model or, more interestingly, uncover unexpected processes or effects not yet built into the model.

5. As a prediction tool. By simulation, using site-specific conditions, predictions can be made for different scenarios or for later times.

STATE OF THE ART OF NUMERICAL MODELS

No numerical model is currently available that couples simultaneously all four processes: heat transfer, fluid flow, mechanical stress and displacement, and chemical reactions. However, considerable literature exists in the modeling of each of these phenomena. Because of the developments in the related fields of hydrology, petroleum engineering, geothermal energy, and geochemistry, some progress has also been made in the coupling of pairs of these processes. The thermomechanical and thermohydrological models are somewhat more highly developed, mainly for porous media, but much work remains to be done for fractured systems. In contrast, the hydromechanical and hydrochemical models for the waste repository systems are still in an early stage of development. The remainder of this section summarizes the state of the art of thermohydrological, thermomechanical, hydromechanical, and hydrochemical modeling.

Thermohydrological Modeling

Table 1 lists the major thermohydrological models available and their main characteristics. The choice is somewhat arbitrary and emphasizes those in the published literature that could be applied to or may be extended for use with fractured systems. In general, models of porous media models are quite well developed, but, except for the double-porosity models, they were not originally designed for fractured rock systems, hence much work needs to be done to establish their applicability to those systems. All of these models are verified against a few analytical solutions, but more validations should be made, especially against fracture-flow solutions. Only about five of the models listed have been validated against field data. None of the models treat uncertainty in input data or consider statistical distributions of parameters.

Table 1. Some of the major thermohydrological models.

Model	Current developers	Main characteristics
CCC	M. Lippmann, LBL	Flow-heat-consolidation, 3D, IFD, geothermal, aquifer storage, waste isolation
Duguid	J. Duguid, ONWI	Flow, double-porosity, 2D, FE, hydrology
O'Neill	K. O'Neill, CRRE A. Shapiro, Princeton	Flow-heat, double-porosity, 3D, FE, geothermal
GWTHERM	A. Runchal, D & M	Flow-heat-(transport), 2D, IFD, waste isolation
FINI	A. Burgess, Acres	Flow-heat, 2D, FE, waste isolation
CFEST	S. Gupta, BPNL	Flow-heat-solute, 3D, FE, hydrology, waste isolation
SWIFT	S. Pahwa, Intera	Flow-heat-solute-(transport), 3D, FD, waste isolation
Coats	K. Coats, Intercomp	Flow-heat, two-phase, 3D, FD, geothermal, petroleum
Faust-Mercer	C. Faust, J. Mercer, Geotrans	Flow-heat, two-phase, 3D, FD, geothermal
MUSHRM	J. Pritchett, S^3	Flow-heat-solute, two-phase, 3D, FD, geothermal, geopressure
SHAFT79	K. Pruess, LBL	Flow-heat, two-phase, 3D, FD, geothermal, waste isolation

Sources: Brownell et al., 1975; Burgess, 1977; Coats, 1977; Duguid and Lee, 1977; Lippmann et al., 1977; Narasimhan et al., 1977; Rattigan et al., 1977; Dillon et al., 1978; Narasimhan et al., 1978; O'Neill, 1978; Cole and Gupta, 1979; Faust and Mercer, 1979; Pruess and Schroeder, 1979; Runchal et al., 1979; Ayatollahi and Noorishad, 1980; Wang et al., 1980.

Thermomechanical Modeling

Table 2 lists some of the major thermomechanical models available. The boundary-element methods are integral methods, which assume linear behavior. The finite-element and finite-difference methods, on the other hand, treat the system in detail. They can handle complex nonlinear behavior and possibly the coupling of fluid flow, heat transfer, and mechanical responses. Most of the available models are essentially continuous models, even though special provision may be made to incorporate discrete discontinuities. Some of these models have been applied to field data. In general, thermal fields are well simulated although temperature-dependent thermal properties may be needed for accurate modeling. The stress-strain results show the need to incorporate faults or fractures in the calculations. Further work is needed in this area, such as validation of these models for fractured systems and generic studies of borehole stability with the presence of fractures.

Table 2. Some of the major thermomechanical models.[1]

			Capabilities							
Basis of method	Code name	Source of code	2-D	3-D	Thermal	Stress	Nonlinear	Joint	Detailed	Regional
Boundary-element methods	SALT	OWI	X		X	X	X			X
	SALT[2]	University of Minnesota	X		X	X				X
	BASUM	University of Minnesota	X		X	X				X
	EXPAR	University of Minnesota		X	X	X	X			X
	REPOS	University of Minnesota		X	X	X	X			X
	BEH2D	Dames & Moore	X		X	X	X	X	X	X
	DAMBIT	Dames & Moore	X	X	X	X	X	X	X	X
Finite element	FINEL	Dames & Moore/Imperial College	X	X	X	X	X	X	X	X
	DAMSWEL	Dames & Moore/Swansea University	X		X	X	X	X	X	X
	BASFEH	University of Minnesota	X		X				X	X
	RSI/TRANCO	RE/SPEC	X		X		X		X	
	RSI/TEPO	RE/SPEC	X			X	X		X	
	RSI/TEVCO	RE/SPEC	X			X	X		X	
	RSI/NOMOR	RE/SPEC	X			X	X		X	
	CDC/ANSYS	Swanson Analysis Systems	X	X	X	X	X	X	X	
	CDC/MARC	Marc Analysis Research	X	X	X	X	X	X	X	
	Rock structure interaction	Agbabian Associates	X	X		X	X	X	X	
	ADINA, ADINAT	MIT	X	X	X	X	X	X	X	X
	SAP	University of California	X	X		X			X	
	NONSAP	University of California	X	X		X	X		X	
	SANDIA-ADINA	Sandia National Labs	X	X	X	X	X	X	X	X
	JAC	Sandia National Labs	X		X	X	X	X	X	X
	SANCHO	Sandia National Labs	X		X	X	X	X	X	X
	COUPLEFLOW	Sandia National Labs	X		X	X	X		X	
	WULFF	Sandia National Labs	X	X	X	X	X		X	X
	BMINES	U.S. Bureau of Mines	X	X		X	X	X	X	X
	BMINES (Modified)	Sandia National Labs	X	X	X	X	X	X	X	X
	DIFFUS2	University of Minnesota			X					X
Finite difference (explicit)	KO/HEMP	Lawrence Livermore	X	X	X	X	X		X	
	DAMSEL	Dames & Moore	X	X	X	X	X		X	
	STEALTH	Science Applications	X	X	X	X	X	X	X	X
(implicit)	GWTHERM, PORFOW	Analytic & Computational Research, Inc.	Coupled thermal fluid and stress 2-D							

[1] This table was compiled with assistance of G. Hocking, R. Hoffman, A. Runchal, L. Ramspott, T. Butkovich, and R. Krieg.

Hydromechanical Modeling

Currently there are not many coupled fluid-flow and stress-strain models. The major ones are listed in Table 3. Among these, only the model by Ayatollahi and Noorishad is designed for fractured systems. More validations against laboratory or field experiments are needed. Additional and more extensive generic studies are needed to understand the capability of the models, as well as the behavior of the interactions between fluid flow and stress-strain.

Table 3. Coupled hydromechanical models.

Developers	Main characteristics
Sandhu and Wilson (UCB)	FE(variational principle), saturated porous medium, 2D axisymmetric, water incompressible.
Ghaboussi and Wilson (UCB)	FE(variational principle), saturated porous medium, 2D axisymmetric, water compressible.
Ayatollahi and Noorishad (LBL)	FE(variational principle), nonlinear porous medium with fractures, 2D axisymmetric, compressible fluid
Safai and Pinder (Princeton)	FE (Galerkin), saturated-unsaturated porous media 2D axisymmetric

Sources: Sandhu and Wilson, 1969; Ghaboussi and Wilson, 1971; Safai and Pinder, 1979; Ayatollahi et al., 1980. Acknowledgment is also made to J. Noorishad for discussions and assistance in the preparation of this table.

Hydrochemical Modeling

Substantial work has been conducted in chemical modeling in aqueous systems (American Chemical Society, 1979). However, the modeling of coupled chemistry and fluid-flow relevant to nuclear waste isolation problems is still in an early stage. Many factors need to be considered including physical, chemical, and radiological properties of the rock medium and waste form. Also needing study is the dependence of sorption, complexation, dissolution, and precipitation on thermal effects, groundwater flow, and concentration gradient. Table 4 summarizes major coupled hydrochemical models. The models by Ahlstrom et al. and Lichtner and Benson were developed for waste repository studies. Norton's (1979) primarily involved geological processes such as ore deposition and formation of geothermal reservoirs, although his results can be useful for our work. All these models require validation.

Table 4. Hydrochemical models.

Developers	Main characteristics
Ahlstrom, Cole, Washburn et al, (PNL)	Macro-micro transport model, discrete-parcel-random walk algorithm, 1D (2D steady state flow), instantaneous equilibrium, sorption; radioactive decay complexation and precipitation not included.
Rubin and James (USGS)	1D Galerkin method, deterministic, instantaneous equilibrium, ion-exchange, complexation, precipitation.
Lichtner and Benson (LBL)	1D, IFD method, deterministic, instantaneous equilibrium, ion-exchange, complexation, precipitation and radioactive decay.
Norton et al, (U. of Arizona)	ADI-FD method, dissolution precipitation, single-phase heat and mass transport, local thermal equilibrium, irreversible fluid-rock reactions.

Sources: Rubin and James, 1973; Ahlstrom et al., 1977; Norton, 1979; Lichtner and Benson, 1980. Acknowledgment is also made to P. Lichtner for discussions and assistance in the preparation of this table.

Coupled Thermal-Fluid-Stress Modeling

Several groups, including LBL, SAI, and Dames and Moore, are currently attempting to develop models to study coupled thermal, fluid, and stress effects. These models are mainly for two-dimensional systems, are only partially coupled, are still in the development stage, and require careful validation.

RESEARCH NEEDS

To study the thermomechanical and hydrochemical processes around a hard rock repository, it is convenient to discuss three different levels of scale:

1. Canister scale. Here the borehole stability, maximum allowable temperatures, lining or engineered barrier design, and hydrochemistry are the key questions.

2. Repository scale. At this scale, the excavation layout, shaft design, repository stability, and waste choice of backfill material are matters of major concern.

3. Regional scale. Main problems at this scale are the regional groundwater flow, chemical transport and dispersion, and effects of major fractures or faults.

These different scales require different levels of sophistication in the coupled thermomechanical and hydrochemical modeling. The sophistication needed probably decreases from canister scale to regional scale. However, regional scale requires results from repository scale for input, which in turn depend on results from canister scale studies.

Figure 1 illustrates the couplings among the four processes for tight formations which are of interest to us here. First, there is a strong coupling between chemical reactions and fluid flow. The fluid flow transports the chemicals, and any dissolution or precipitation would affect the flow velocity. Because the fluid velocity is proportional to the cube of fracture aperture, a small change in aperture due to precipitation would have a significant effect on fluid flow. This coupling is probably critical at the canister scale, but it is still important at the regional scale, although the process may be much slower and perhaps easier to model.

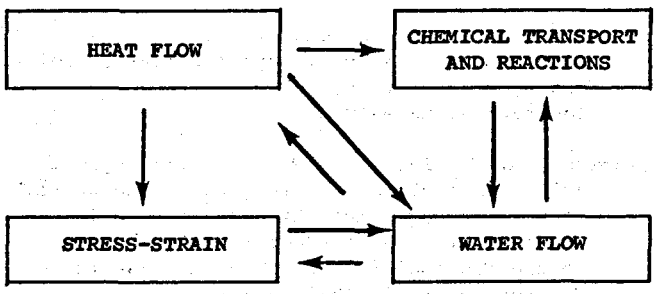

Figure 1. Schematic of couplings.

Between heat and fluid flow, the influence of heating on regional groundwater flow is of major interest. However, the amount of fluid in the hard-rock medium may be small for tight systems, and its effect on the temperature field may be less significant, except near the canister. Similarly, for the interaction between stress-strain in changing the fracture aperture may cause significant flow differences, but the influence network may be smaller, except possibly on the canister scale.

The remaining couplings indicated in Figure 1 are thermal effects on the rates and thermodynamics of chemical reactions and the thermally induced stress-strain phenomena. The reverse influences may be minimal. It is possible, however, that for shale and tuff, stress-strain effects may affect heat flow.

With the above discussion as background and reviewing the present state-of-the-art, we may conclude that our capability of handling these coupled processes is still in an unsatisfactory state. Many times drastic assumptions have to be made to fit the situation to the capability of the available models for site-specific studies. Though a fully-coupled model involving all four processes may not be needed (nor is it possible with current computer capabilities), careful studies should be made to establish the limits of various simplifications. Besides these studies, careful validations of current models for fractured rock systems are of particular importance, especially against field data. We also need their application to improve our understanding of all relevant physical and chemical processes in fractured rock. In this way, we may be able to justify any assumptions we make and have more confidence in our modeling results, especially when extrapolated to 10^3-10^6 yr.

Some Challenging Problems

Some of the challenging problems facing modelers today are listed below.

1. The characterization of fractured rock masses.

2. The determination of parameters from a small number of borehole observations.

3. Modeling of uncertainties; stochastic modeling.

4. Evaluation of effective fracture surface area.

5. Megascopic dispersion phenomena, and determination of dispersive coefficients from field data. (Is the functional form that is usually assumed for dispersion valid for slow velocities?)

6. Geochemistry modeling with ion-exchange, dissolution and precipitation, sorption and complexation.

7. Modeling of jointed rocks.

8. Determination of appropriate scales of simulation.

9. Effects of changes in permeability/connectivity/porosity due to chemical reactions or temperature increase.

10. Effects of system heterogeneity and anisotropy.

11. Modeling long-term geological phenomena.

Many other problems may be listed. These problems not only may require modelers to build numerical models, but also to use them to gain a better understanding of all the processes involved.

CONCLUDING REMARKS

The present paper attempts to answer three questions concerning the state of the art of numerical modeling for nuclear waste repositories. (1) What are the major issues involved? (2) Where are we now? (3) What further research needs to be done? The arguments presented are somewhat subjective but can be used as basis for further discussions. Much work remains to be done in model validation, especially for fractured rock masses, the application of models to the understanding of relevant processes, and the study of the couplings among processes.

With a concerted effort, we would hope in the near future to have a good understanding of all the processes involved to enable development of a reasonably confident long-term prediction of the behavior of a hardrock waste repository.

ACKNOWLEDGEMENTS

Acknowledgements are gratefully made for many useful discussions with many colleagues, especially L. Benson, N. Cook, G. Hocking, R. Hoffman, P. Lichtner, J. Noorishad, A. Runchal, J. Wang, and P. Witherspoon.

REFERENCES CITED

Ahlstrom, S. W., Foote, H. P., Arnett, R. C., Cole, C. R., and Serne, R. J., 1977. Multicomponent mass transport model. Battelle Pacific Northwest Laboratories Report, BNWL-2127.

American Chemical Society, 1979. Chemical modeling in aqueous systems. ACS Symposium Series 93.

Ayatollahi, M., and Noorishad, J., 1980. Coupled analysis of stress and flow in deformable, saturated, fractured porous media. Preprint, Department of Materials Science and Mineral Engineering, University of California, Berkeley, California.

Ayatollahi, M. S., Noorishad, J., and Witherspoon, P. A., 1980. A finite-element method for stress and fluid-flow analysis in fractured rock masses, part I and part II. Berkeley, Lawrence Berkeley Laboratory, LBL-11430.

Brownell, D. H., Garg, S. K., and Pritchett, J. W., 1975. Computer simulation of geothermal reservoirs. Presented at the 45th Annual California Regional Meeting of the Society of Petroleum Engineering of AIME, Ventura, California, SPE-5381.

Burgess, A., 1977. Groundwater movements around a repository, regional groundwater flow analyses. Part 1: Initial conditions. Part 2: Long term residual conditions. KBS Technical Report 54:03, Hagconsult AB, Karnbranslesakerhet, Stockholm, Sweden, October 1977.

Coats, K. H., 1977. Geothermal reservoir modeling. Presented at the 52nd Annual Fall Technical Conference and Exhibition of the Society of Petroleum Engineers of AIME, Denver, Colorado, October 1977. SPE-6892.

Cole, C. R., and Gupta, S. K., 1979. A brief description of the three-dimensional finite element groundwater flow model adapted for waste isolation safety assessment. Battelle Pacific Northwest Laboratory Report, PNL-2652.

Dillon, R. T., Lantz, R. B., and Pahwa, S. B., 1978. Risk methodology for geologic disposal of radioactive waste: The Sandia waste isolation flow and transport (SWIFT) model. Sandia Laboratories, SAND78-1267, NUREG/CR-0424.

Duguid, J. O., and Lee, P. C. Y., 1977. Flow in fractured porous media. Water Resources Research, v. 13, no. 3, p. 558-566.

Faust, C. R., and Mercer, J. W., 1979. Geothermal reservoir simulation. 1: Mathematical models for liquid- and vapor-dominated hydrothermal systems. Water Resources Research, v. 15, no. 1, p. 23-30.

Ghaboussi, J., and Wilson, E. L., 1971. Flow of compressible fluids in porous media. Berkeley, University of California, SESM Report no. 72-12.

Lawrence Berkeley Laboratory, 1978. Proceedings of GAIN symposium, Berkeley, California, July 16-20, 1978. Berkeley, Lawrence Berkeley Laboratory, LBL-7096.

Lawrence Livermore Laboratory, 1979. Proceedings of workshop on thermomechanical modeling for a hardrock waste repository, Berkeley, California, June 25-27, 1979. Livermore, Lawrence Livermore Laboratory, UCAR-10043; Office of Nuclear Waste Isolation Report 98.

Lichtner, P. C., and Benson, L. V., 1980. Development of a multicomponent thermochemical transport model. Berkeley, Lawrence Berkeley Laboratory, LBL-10918.

Lippmann, M. J., Tsang, C. F., and Witherspoon, P. A., 1977. Analysis of the response of geothermal reservoirs under injection and production procedures. Presented at the 47th Annual California Regional Meeting SPE-AIME, Bakersfield, California, April 1977, SPE-6537.

Narasimhan, T. N., and Witherspoon, P. A., 1977. Numerical model for saturated-unsaturated flow in deformable porous media. 1. Theory. Water Resources Research, v. 13, no. 3, p. 657-664.

Narasimhan, T. N., Witherspoon, P. A., and Edwards, A. L., 1978 Numerical model for saturated-unsaturated flow in deformable porous media. 2. The algorithm. Water Resources Research, v. 14, no. 2, p. 255-261.

Norton, D., 1979. Transport phenomena in hydrothermal systems: The redistribution of chemical components around cooling magmas. Bull. Mineral., v. 102, p. 471-486.

O'Neill, K., 1978. The transient three-dimensional transport of liquid and heat in fractured porous media (Ph.D dissertation). Princeton, New Jersey, Princeton University, Department of Civil Engineering.

Pruess, K., and Schroeder, R. C., 1979. Geothermal reservoir simulation with SHAFT79. Paper presented at the 5th Geothermal Reservoir Engineering Workshop, Stanford, California, 1979. Berkeley, Lawrence Berkeley Laboratory LBL-10066.

Ratigan, J. L., Burgess, A. S., Skiba, E. L., and Charlwood, R., 1977. Groundwater movements around a repository, repository domain groundwater flow analyses. Part 1: Permeability perturbations. Part 2: Inflow to repository. Part 3: Thermally induced flow. KBS Technical Report 54:05, Hagconsult AB, Karnbranslesakerhet, Stockholm, Sweden, September 1977.

Rubin, J., and James, R. V., 1973. Water Resources Research, v. 9, no. 5, p. 1332-1356.

Runchal, A., Treger, J., and Segal, G., 1979. Program EP21 (GWTHERM): Two-dimensional fluid flow, heat and mass transport in porous media. Technical Note TN-LA-34. Advanced Technology Group, Dames and Moore, Los Angeles, California.

Safai, N. M., and Pinder, G. F., 1979. Vertical and horizontal land deformation in a desaturating porous medium. Advances in Water Resources, v. 2, p. 19-25.

Sandhu, R. S., and Wilson, E. L., 1969. Finite element analysis of seepage in elastic media. Jour. of Eng. Mech., Division of ASCE, p. 641.

Wang, J. S. Y., Sterbentz, R. A., and Tsang, C. F., 1980. The state-of-the-art of numerical modeling of thermohydrologic flow in fractured rock masses. Berkeley, Lawrence Berkeley Laboratory, LBL-10524.

MONITORING ACOUSTIC EMISSIONS AT THE CLIMAX STOCK REPOSITORY

E. L. Majer, T. V. McEvilly, and D. Hopkins

Lawrence Berkeley Laboratory is monitoring acoustic emission (AE) microseismic (MS) activity related to the emplacement of spent fuel by Lawrence Livermore National Laboratory (LLNL) in the Climax Granite at the Nevada Test Site.

The experiment seeks to develop and evaluate techniques for monitoring the integrity of nuclear waste repositories and to determine the suitability of granite or hard rock as a repository medium. Acoustic emission and microseismic techniques are being employed to study the relation between discrete rock failure and/or stress release relative to thermal effects, radiation degradation, mine geometry, and canister spacing. The scale of the experiment is designed to monitor elastic wave energy in the range 1-10 kHz. These frequencies correspond to fracture generation on the order of meters to a few centimeters in length. Although there may be microfracturing on a much smaller scale, i.e., 100kHz-1MHz, it was felt that these fractures would not be important in determining overall mine integrity.

The spent-fuel experiment is being conducted in granite 430 m beneath the surface. The maximum temperature anticipated in the rock is 100°C. In addition to the AE-MS measurements, LLNL has installed 430 thermocouples, 18 stress meters (vibrating wire), 116 extensometers, and 34 convergence heads in the facility.

1980 ACTIVITIES

The AE-MS experiment began in December 1979 with the emplacement of AE sensors (piezoelectric accelerometers), preamplifiers, and a 15-channel transient waveform analyzer (Fig. 1). The sensors are deployed in a 15-station, three-dimensional array centered on the canister drift which would eventually house the spent fuel and heaters (Figs. 2 and 3). Results from 3 months of monitoring activity prior to heater turn-on and waste emplacement are:

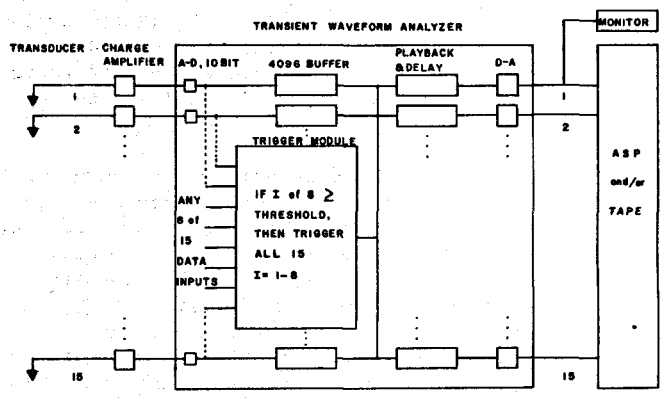

Figure 1. System configuration. The transient waveform analyzer allows a 1000:1 slowdown so that the data can be processed or recorded with microearthquake equipment and techniques. [XBL 8010-12374]

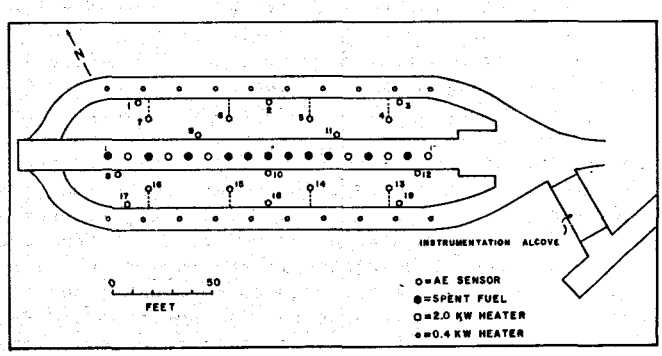

Figure 2. Plan view of climax repository experiment showing canister locations (solid dots in center drift), heater locations, and AE sensors. Heater output is adjusted to the thermal output of the spent fuel canisters. [XBL 8010-12309]

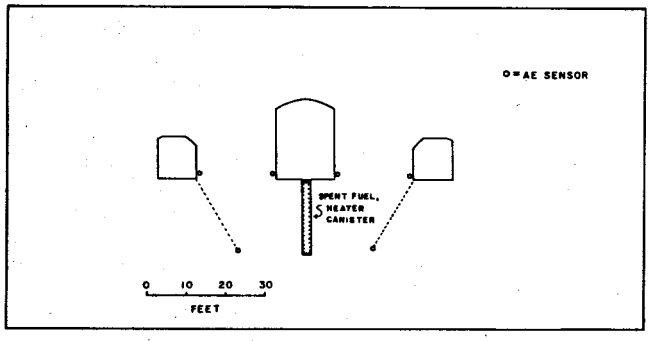

Figure 3. Cross section of climax repository showing downhole location of AE sensors.
[XBL 8010-12310]

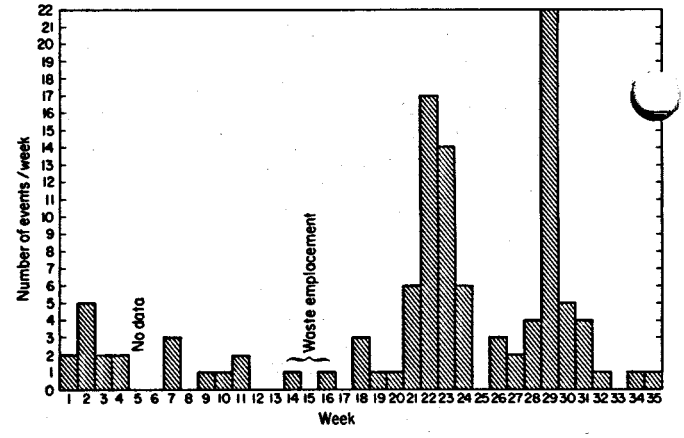

Figure 4. Number of events per week detected before and after waste emplacement. [XBL 813-2724]

1. The repository rock has average P- and S-wave velocities of 5.5 to 5.9 and 3.2 to 3.6 km/s, respectively, for a Poisson's ratio of 0.20 to 0.25; values are typical for granite.

2. The rock on this scale is not homogeneous in velocity and attenuation properties for seismic waves at frequencies between 1 and 10 kHz. Ongoing observations of these properties may offer a means of mapping the progress of fracture zones or zones of alteration. Preliminary findings indicate a Q_p of about 50.

3. Certain discrete seismic events occur within the mine structure that are not associated with the canister area. These events occur at a rate of 1-3 per week and seem to be related to fracturing on the scale of centimeters, presumably in response to stresses induced by mining, drilling, and coring.

4. There was no evidence that strong ground motion within the respository, associated with nearby underground nuclear explosions, induces cracking or otherwise enhances the microfracturing process.

Several weeks prior to waste emplacement and heater turn-on, there was a period of relatively low human activity within the mine. During this time the number of detected events subsided to about one per week. After emplacement, however, the AE-MS activity dropped even further. No events were recorded for 2 weeks. At this time the trigger status (stations at which signals must rise above a minimum level in a specified time window) used three stations in the middle of the array. When the trigger stations were reduced to two central stations the activity detected increased again to 1-3 events/week. After waste emplacement, the detected activity seems to be occurring in two different types of events. The first type is the event with an impulsive onset occurring at the rate of 1-2 per week and located in the rock mass. The second type is the event with an emergent onset occurring in a swarm sequence. Although more difficult to locate, these events seem to occur in the canister drift at shallow depths near canisters 11-15, possibly in the concrete floor of the drift. These events are of roughly equal magnitude, i.e., no dominant event with a foreshock or aftershock sequence, whereas the single impulsive events are distributed in magnitude. Visual identification of cracks in the concrete around the top of the canister and heater holes was made several weeks after emplacement. It is not known whether (1) the concrete cracked before the rock, (2) the rock had developed cracks (although the lack of discrete events at the time would suggest not), or (3) the cracks in the concrete were already there and had opened when heating began. However, the radial pattern of the cracks (i.e., at a 45-degree angle to the canister center line) would suggest a compressive stress due to the heating of the canister.

The emergent-type events were detected for only several weeks--and always near the east end of the canister drift, although the entire drift had been filled with canisters or heaters. After this phase, activity returned to 1-4 events per week. However, for the first time, events were located near the canisters below the canister drift floor, in the rock mass. These events suggest that the rock is beginning to respond to the emplacement of the canister and/or heater turn-on. Figure 4 shows the number of events detected during the length of the experiment.

To date, it seems as if the waste emplacement/heater turn-on has had an effect on AE-MS activity. Although small, the main effect has been on the concrete floor above the canisters. The rock either has not been sufficiently heated to respond on a large scale, or its nature is such that expansion is not manifested in discrete failure events, although several events have been detected near the canisters for the first time. As the experiment continues and rock temperatures increase, it will be easier to determine the importance of thermal stresses to rock fracture and failure.

ACTIVITIES PLANNED FOR FISCAL 1981

A piezoelectric pulser has been installed in AE 13 to provide continuous velocity and attenuation monitoring. Presently the AE-MS data are being recorded on magnetic tape and returned to Berkeley for analysis. However, there is considerable loss of dynamic range and processing capability. Therefore, an Automated Seismic Processor being built will provide on-line detection, source characterization, stress release, and source location.

MULTICOMPONENT THERMOCHEMICAL TRANSPORT MODEL

P. C. Lichtner and L. V. Benson

There is a need in many earth science problems for a comprehensive transport model capable of accurately predicting the migration of interacting solutes in water-saturated porous or fractured media. For example, not until recently has detailed attention been given to the influence of chemical interactions on the potential migration of radionuclides from a high-level nuclear waste repository. The formation of neutral or negatively charged ion pairs which are not easily sorbed, reduction and oxidation reactions, ion-exchange, coprecipitation and precipitation-dissolution reactions could all play an important role in determining the rate of advance of chromotographic fronts of radionuclides should they escape from their original confinement.

Although several sophisticated thermodynamic models are capable of predicting the equilibrium distribution of species resulting from various chemical reactions, the development of models which couple fluid transport processes with chemical interactions is still in its infancy.

This is the second progress report on the continuing theoretical development of a unified chemical transport model. The model assumes a phenomenological description of advective and diffusive/dispersive fluid flow coupled to locally equilibrated chemical reactions describing ion exchange and aqueous complexation. This work generalizes the work of Rubin and James (1973) to include ion-exchange site-competition effects and aqueous complexation.

One objective of this work has been to develop a general theoretical framework from which simplifying assumptions can be made on the basis of sound physical judgement and experience. By precisely formulating the solute-transport problem as a system of partial differential equations which are exact within the stated assumptions, this theory can be used to analyze the validity of various approximations, such as the common use of a linear sorption isotherm description of ion-exchange processes and the intuitively-based zone model widely employed in chromotography.

Two effects of chemical reactions on retardation were studied during this fiscal year. The effect of competition between cations for sorption sites was investigated by examining the movement of concentration isopleths in a one-dimensional model. It was discovered that retardation could be enhanced or diminished relative to that predicted by the customary linear isotherm description depending on whether interference with other fronts was coherent or noncoherent. Coherent interference results when time derivatives of two interfering concentration fronts are of the same sign; noncoherent interference occurs when they are of opposite sign. Noncoherent interference occurs, for example, between a sorbing species and its corresponding desorbing species, resulting in a greater retardation of the sorbing component than expected from calculations employing a linear isotherm.

Sorbing and desorbing interference was further studied in a three-component sorption model in which an anion component was included to balance aqueous charge. Conservation of local aqueous charge and the decoupling of the anion component from the cations allowed the elimination of one of the cations, resulting in a single nonlinear partial differential equation for the remaining cation. This equation is exact within the assumption of local chemical equilibrium and includes all interference effects between the two cations. It should prove useful in studying chromatographic column experiments when nontrace concentrations are present.

The influence of complexation on retardation was shown to result, in the absence of site-competition effects, in a general expression for the retardation factor, defined as the ratio of the average pore velocity v_o to the actual solute velocity, v_{ret}, of the form

$$R = \frac{v_o}{v_{ret}} = 1 + \frac{\rho\alpha}{\phi} K_d, \qquad (1)$$

where the factor α contains the effects of complexation, ρ is the bulk density of the porous medium with porosity ϕ, and K_d is the distribution coefficient obtained in the absence of complexation.

When complexation was introduced into the three-component sorption model between the anion and the sorbing cation with equilibrium coefficient K_{01}, α was found to have the explicit form

$$\alpha = \frac{1 + K_{01}c_+}{1 + K_{01}(c_- + c_+)}, \qquad (2)$$

where c_- is the anion concentration and c_+ the sorbing cation concentration. Thus even for trace amounts of c_+, complexation can be an important factor in solute-migration rates.

This work has demonstrated the feasibility of developing a transport model of chemically interacting solutes in porous media within the restriction of local chemical equilibrium.

REFERENCE CITED

Rubin, J., and R. V. James, 1973. Dispersion-affected transport of reacting solutes in saturated porous media: Galerkin method applied to equilibrium-controlled exchange in unidirectional steady water flow. Water Resources Research, v. 9, p. 1332.

SORPTION MODELING STUDIES AND MEASUREMENTS AT LBL IN 1980 FOR THE PACIFIC NORTHWEST LABORATORIES WRIT PROGRAM

R. J. Silva, A. F. White, and A. W. Yee

This program covers an experimental and theoretical investigation of the principal physical and chemical reactions that control the aqueous concentrations of radionuclides in geologic environments anticipated for terminal waste storage facilities. The goal of the program is to develop a basis for predicting the radionuclide-geologic media interactions that govern migration.

In fiscal 1979 experimental and theoretical efforts were concentrated on a study of the sorption of cesium on the substrates silica and montmorillonite--two representative geologic materials that are widely distributed and frequently coat weathered surfaces--in order to begin to delineate the principal parameters in sorption processes. Cesium sorption isotherms were obtained for the two substrates at 26°C as a function of initial Cs concentration, pH, and $NaCl^-$ supporting electrolyte concentration in batch-type experiments using finely crushed material. Theoretical efforts were aimed at developing and testing an electrolyte-binding electrical double-layer model to predict sorption isotherms. Comparisons of calculated data with experimental data showed that the model was able to simulate the isotherms reasonably well (Silva, 1979).

In fiscal 1980, experimental and theoretical studies of the sorption of Cs on silica and montmorillonite were expanded to include the behavior of UO_2^{++} in contact with the two substrates.

EXPERIMENTAL RESULTS

Solution concentrations were measured at 25°C for UO_2^{++} and Cs^+ in contact with Belle Fourche Clay (montmorillonite) and Min-u-sil (silica) as a function of pH, initial U and Cs concentration, and supporting electrolyte concentration in batch-type experiments using finely ground material (a few microns in diameter). For uranium, the initial UO_2^{++} concentrations were about 10^{-4} M, 10^{-6} M, and 10^{-8} M; pH values were 5, 7, and 9; supporting electrolyte solutions were 10^{-3} M, 10^{-2} M, 10^{-1} M, and 1 M NaCl prepared in the absence of CO_2 and the same solutions containing 10^{-4} M total carbonate. For cesium, the initial concentrations were about 10^{-4} M, 10^{-5} M, 10^{-6} M, 10^{-7} M, and 10^{-9} M; pH values were 5, 6, 7, 8, 9, and 10; supporting electrolyte concentrations were 10^{-3} M, 10^{-2} M, 10^{-1} M, 1 M NaCl, and a synthetic basalt groundwater.

Examples of the results obtained for Cs and Belle Fourche Clay and for Cs and Min-u-sil are shown in Figure 1. Here the logs of the measured K_d values are given as a function of pH (solid points) for several different initial Cs and NaCl concentrations.

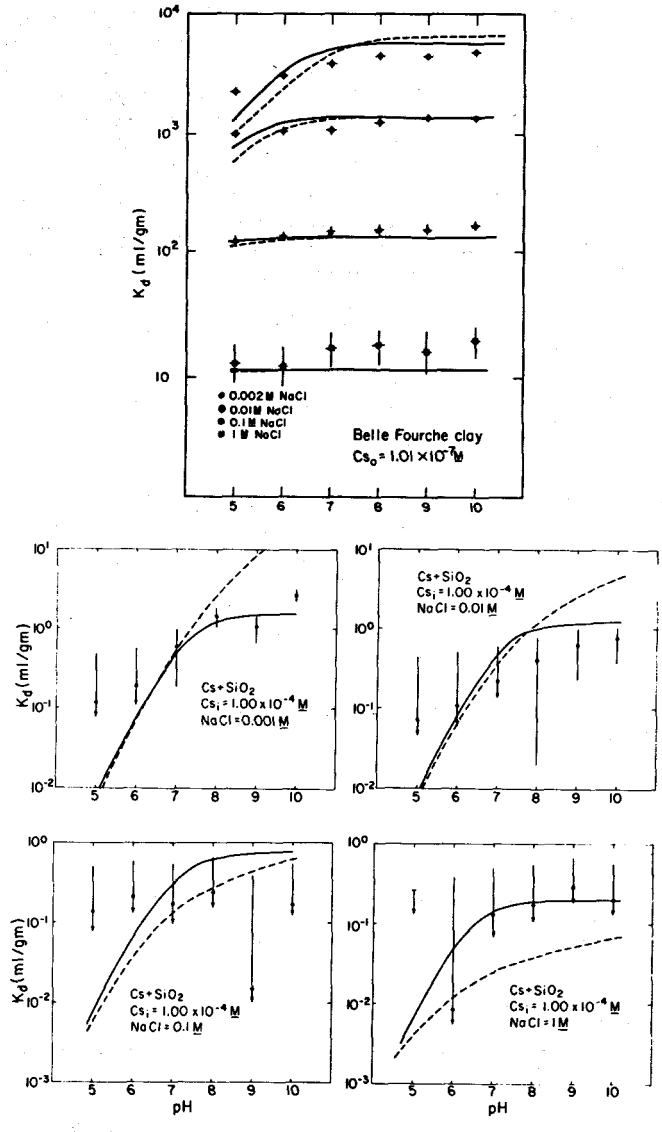

Figure 1. Log Cs distribution coefficient (K_d) versus pH for Belle Fourche Clay and silica. [XBL 8010-2857]

Examples of the results obtained for U and Belle Fourche Clay and for U and Min-u-sil are shown in Figure 2. Since precipitation of uranium hydroxide was expected to occur for the more concentrated U solutions, plots of K_d did not seem appropriate. Instead, the log of the final U solution concentrations are given as a function of pH (solid points) for the different initial U and electrolyte concentrations.

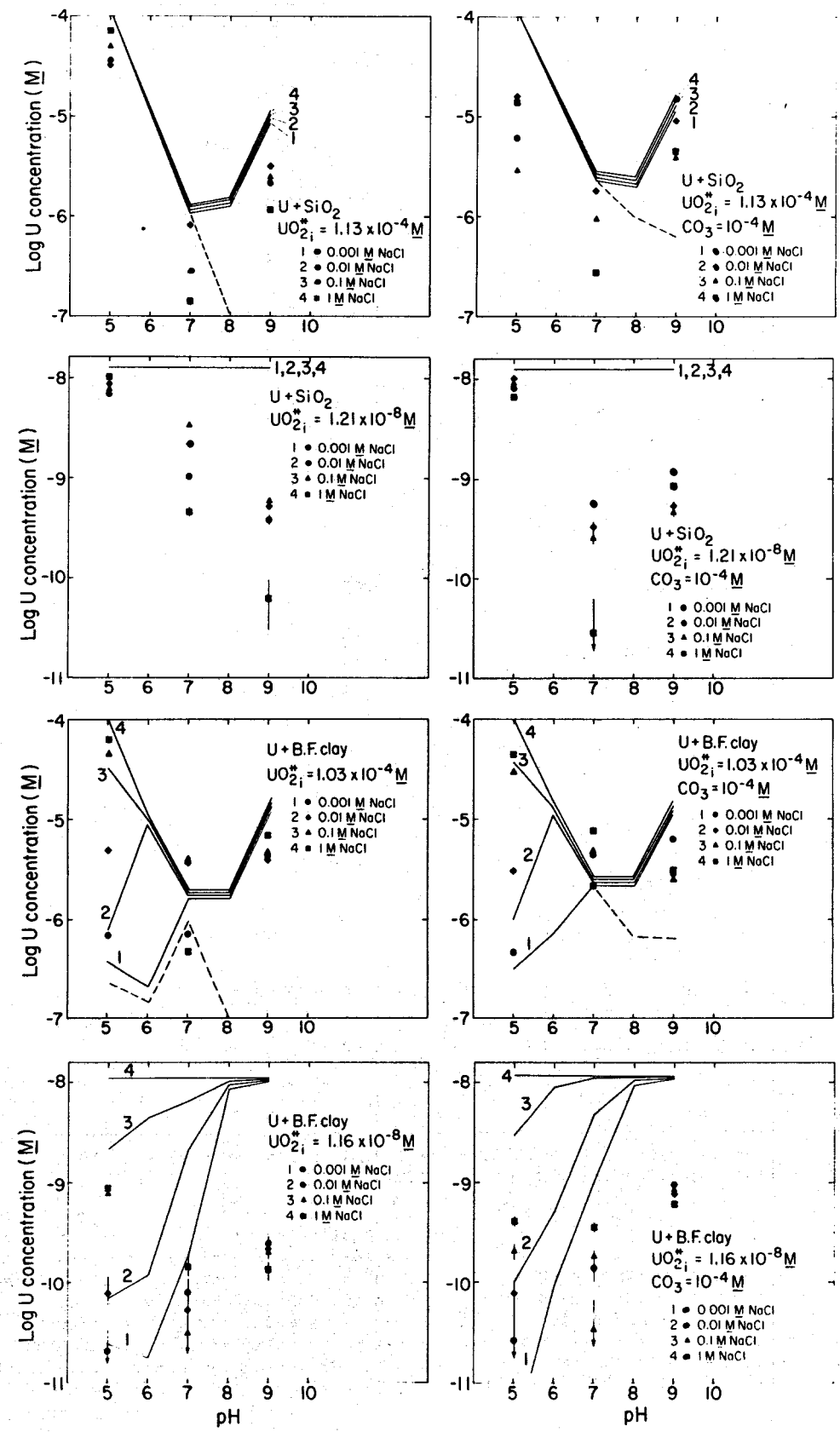

Figure 2. Log uranium solution concentration versus pH for Belle Fourche Clay and silica.
[XBL 813- 2762]

Table 1. Chemical Thermodynamic Data for U and Cs.

Reaction	Log K				
COMPLEXES	(1)	(2)	(3)	(4)	(5)
$UO_2^{2+} + H_2O = UO_2(OH)^+ + H^+$	- 5.50	- 5.78	- 5.90	- 5.78	
$UO_2^{2+} + 2H_2O = UO_2(OH)_2^o + 2H^+$			-10.80	-11.93	
$UO_2^{2+} + 3H_2O = UO_2(OH)_3^- + 3H^+$			-21.0		
$2UO_2^{2+} + H_2O = (UO_2)_2(OH)^{3+} + H^+$			- 4.4		
$2UO_2^{2+} + 2H_2O = (UO_2)_2(OH)_2^{2+} + 2H^+$	- 5.89	- 5.63	- 5.6	- 5.63	
$3UO_2^{2+} + 4H_2O = (UO_2)_3(OH)_4^{2+} + 4H^+$	-12.31		-11.80		
$3UO_2^{2+} + 5H_2O = (UO_2)_3(OH)_5^+ + 5H^+$	-16.46	-15.65	-15.0	-15.65	
$3UO_2^{2+} + 7H_2O = (UO_2)_3(OH)_7^- + 7H^+$				-30.75	
$4UO_2^{2+} + 7H_2O = (UO_2)_4(OH)_7^+ + 7H^+$	-22.76				
$UO_2^{2+} + CO_3^{2-} = UO_2CO_3^o$		10.07			
$UO_2^{2+} + 2CO_3^{2-} = UO_2(CO_3)_2^{2-}$		16.98			
$UO_2^{2+} + 3CO_3^{2-} = UO_2(CO_3)_3^{4-}$		21.40			
$UO_2^{2+} + Cl^- = UO_2Cl^+$		0.24			
$Cs^+ + Cl^- = CsCl^o$					-0.39
PRECIPITATES					
$UO_2^{2+} + H_2O = \gamma - UO_3 + 2H^+$		- 7.69			
$UO_2^{2+} + H_2O = UO_{3(amorph)} + 2H^+$		-10.40			
$UO_2^{2+} + 2H_2O = UO_2(OH)_2 + 2H^+$		- 5.56	- 5.60		
$UO_2^{2+} + 3H_2O = UO_2(OH)_2 \cdot H_2O + 2H^+$		- 5.40			
$UO_2^{2+} + CO_3^{2-} = UO_2CO_3$		14.46			

Source: Smith and Martell (1976), Langmuir (1978), Sylva and Davidson (1979), Allard et al. (1980), Lemire and Tremaine (1980).

COMPUTER SIMULATIONS

Attempts were made to simulate the observed behavior of U and Cs with the two substrates in terms of the known solution chemical thermodynamic data of U and Cs, the measured properties of the substrates, and proposed sorption reactions using a computer program called MINEQL (Silva et al., 1979; Westall et al., 1976).

Briefly stated, MINEQL is designed to accept a list of input components of a solution, e.g., cations and anions, and their analytical concentrations; solve the appropriate set of mass balance and equilibrium constant expressions that describe the specified reactions; and produce a list of the identities and concentrations of all species, solution and solid, formed by the interaction among the components and between them and/or water. Sorption of ions by solid surfaces can be included by writing the reactions as complexation of the ions with surface sites. The surface is treated as a weak acid, SOH, which can dissociate or adsorb ions (e.g., Na^+, Cs^+, UO_2^{++}) in exchange for H^+.

The development of surface charge produces a difference in the activities of ions near the surface and in the bulk solution. Our version of

MINEQL, developed by Davis et al. (1978), incorporates the surface charge corrections through the use of the electrical double-layer model. Activity coefficients of ions in solution are calculated using the Davies equation.

The thermodynamic constants taken from the literature (Smith and Martell, 1976; Langmuir, 1978; Sylva and Davidson, 1979; Allard et al., 1980; Lemire and Tremaine, 1980) for the solution reactions of UO_2^{++} and Cs^+ used in the simulation calculations are given in Table 1. The four different sets of constants for the proposed hydrolysis products of UO_2^{++} produce considerably different calculated values for the solution concentration of U in equilibrium with the solid uranyl hydroxide, particularly at the higher pH values.

The constants for the surface reactions of the solid substrates and other input parameters used in the simulation calculations are given in Table 2. The surface acid dissociation and sodium exchange constants were estimated from surface charge data obtained from acid/base titrations of aqueous sols of the clay and silica containing different amounts of NaCl. The values of the Cs/H and U/H exchange constants were estimated from the sorption data.

Since montmorillonite typically exhibits at least two energetically different exchange sites (frequently designated SOH and TOH) with differing acid dissociation and exchange constants, a two-site model was used for the clay analyses.

An example of the results of the calculations for Cs are shown in Figure 1. The solid curves show the results obtained without including the surface charging effects; the broken curves show results when they were included. The same quality of fit was obtained for the other initial Cs solution concentrations.

Table 2. Reactions and parameters for solid substrates.

Reaction	Log K		
	B. F.	Clay	Min-u-sil
SITES	SOH	TOH	SOH
$SOH = SO^- + H^+$	-4.0	-7.1	-7.4
$SOH + Na^+ = SONa + H^+$	-0.24	-2.9	-6.6
$SOH + Cs^+ = SOCs + H^+$	0.84	-1.8	-5.5
$2SOH + UO_2^{2+} = UO_2(SO)_2 + 2H^+$	2.7	-2.6	-10.0
PARAMETERS			
Sorption site concentration (meq/g)	0.36	0.84	0.021
Surface area (m^2/g)	800		2.52
$K_{Cs/Na} = 12$			
$K_{U/Na} = 1500$			

An example of the results of the calculations for U are shown in Figure 2. The solid curves (number refers to different NaCl concentrations) resulted when the hydrolysis data of Lemire and Tremaine (1980) and the hydroxide solubilities and carbonate complexes of Langmuir (1978) were used; these sets of constants gave the best overall fit of the calculations to the experimental data. For comparison, the broken curves show results of NaCl alone (10^{-2} M) using Langmuir's hydrolysis constants. Only sorption of UO_2^{++} by surface ion-exchange reactions was considered.

DISCUSSION

In general, MINEQL was able to simulate the data for Cs plus clay reasonably well over the entire range of pH, initial Cs concentrations, and electrolyte concentrations, assuming the solution concentration of Cs was controlled only by sorption of Cs^+ by ion-exchange reactions with surface sites. Inclusion of surface charging corrections did not improve the fit. For Cs plus silica, the simulations did not give as good a representation of the experimental data as for Cs plus clay. However, in general, MINEQL predicted the right order of magnitude of K_d versus pH over the range 7-10 for all values of initial Cs concentration and electrolyte concentration, assuming only sorption of Cs^+ ions by surface sites via ion-exchange reactions. Below pH 7, MINEQL consistently underestimated the K_d values by 1 to 2 orders of magnitude. Inclusion of corrections for surface charging produced a much poorer simulation of the experimental data.

MINEQL was able to simulate the final uranium concentrations for UO_2^{++} in contact with the silica and clay to some extent for an initial concentration of 10^{-4} M. For this initial concentration, precipitation of uranyl hydroxide was calculated to occur for pH values greater than about 6 and was the principal control of the solution concentration of U in contact with both the silica and clay for the neutral to alkaline pH region. At a pH value of 5, the results of the calculations indicated that reactions of UO_2^{++} with the surface sites was not a significant process for the control of the uranium solution concentration for the quartz but was important for the clay. For initial UO_2^{++} concentrations of 10^{-6} M and 10^{-8} M, no precipitation and little ion-exchange sorption were calculated to occur and the final U solution concentrations were not expected to decrease appreciably from their initial values at any pH or NaCl concentration for U plus silica. However, 90% or more of the U was lost from solution at pH values of 7 and 9 and smaller amounts at a pH of 5. For UO_2^{++} in contact with the clay at these initial concentrations, the model overestimated the final solution concentrations at the higher pH values and also at a pH of 5 for the higher NaCl concentrations. As with the silica, considerably more U was lost from solution than could be accounted for by ion-exchange reaction of UO_2^{++} with surface sites at all pH values. For both silica and clay, the presence of 10^{-4} M total carbonate appeared to increase only slightly, if at all, the measured U solution concentrations. It should be noted that the final U solution concentrations for the clay differed very little from the values measured for the silica for the three different initial U concentrations at pH values of 7

and 9 though the ion-exchange capacities of the two substrates differed by a factor of about 60. Finally, there appeared to be little affect of NaCl concentration on the measured final U concentration at these pH values in contrast to the behavior expected for ion-exchange reaction.

CONCLUSIONS

1. The solution concentration of Cs in contact with Belle Fourche Clay and silica is controlled primarily by sorption of Cs^{+} by the solid substrates via ion-exchange reactions.

2. For UO_2^{++} in contact with silica, ion-exchange reactions with surface sites do not appear to play a significant role in the control of the U solution concentration at any pH or NaCl concentration. For UO_2^{++} in contact with Belle Fourche clay, ion-exchange reactions are important for controlling the U solution concentrations for pH < 7 but decrease rapidly in importance for pH > 7.

3. For an initial UO_2^{++} concentration of 10^{-4} M, precipitation of uranyl hydroxide appears to control the U solution concentration for pH > 6 for both silica and clay. However, for lower initial concentrations, where precipitation was not expected to occur, large losses of U from solution were found experimentally. This loss does not appear to be due to simple ion-exchange reactions of uranium species with surface sites since there was little dependence on the cation-exchange capacity of the substrates or on NaCl concentrations. There may be yet another mechanism, in addition to simple ion-exchange reactions and the formation of uranyl hydroxide that play a significant role in the control of the solution concentration of uranyl under environmental conditions.

REFERENCES CITED

Allard, B., Kipatsi, H., and Liljenzin, J. O., 19[illegible]. Expected species of uranium, neptunium and plutonium in neutral aqueous solutions. J. Inorg. Nucl. Chem., v. 42, p. 1015-1027.

Davis, J. A., James, R. O., and Leckie, J. O., 1978. Surface ionization and complexation of the oxide/water interface. J. Colloid Interf. Sci. v. 63, no. 3, p. 480-499.

Langmuir, D., 1978. Uranium solution-mineral equilibria at low temperatures with applications to sedimentary ore deposits. Geochim. et Cosmochim. Acta., v. 42, p. 547-569.

Lemire, R. J., and Tremaine, P. R., 1980. U and Pu equilibria in aqueous solutions to 200°C. J. Chem. Eng. Data, v. 25, p. 361-370.

Smith, R. M., and Martell, A. E., 1976. Critical stability constants (v. 4: Inorganic complexes). New York, Plenum Pub. Corp., p. 104.

Silva, R. J., Benson, L. V., Yee, A. W., and Parks, G. A., 1979. Theoretical and experimental evaluation of waste transport in selected rocks. Berkeley, Lawrence Berkeley Laboratory, LBL-9945.

Sylva, R. N., and Davidson, M. R., 1979. The hydrolysis of metal ions. Part 2. Dioxouranium (VI). J. Chem. Soc. p. 465-471.

Westall, J. C., Zachery, I., and Morel, F. M. M., 1976. MINEQL--A computer program for the calculation of chemical equilibrium composition of aqueous solutions. Note No. 18, EPA Grant R803738. Cambridge, Massachusetts, Dept. Civil Engineering, Massachusetts Institute of Technology, 91p.

MASS SPECTROMETRIC DETERMINATION OF $^{234}U/^{238}U$ DISEQUILIBRIUM

M. Michel

OBJECTIVES

The purpose of this program is to develop techniques for dating groundwaters on the basis of the disequilibrium between $^{234}U/^{238}U$. This work has been slowed by the existence of a highly enriched ^{235}U component in the uranium present in ion-exchange resin, as reported previously (Michel and Keyes, 1979). During 1980 this type of material has been shown to occur in varying concentrations in ion-exchange resins produced by several manufacturers over at least a 15-year period. The same or similar material is also observed in other manufactured products, particularly those associated with the plastics industry. Attempts to trace the source of enriched ^{235}U have had low priority. Results to date, in the case of ion-exchange resin, indicate it may be present in the styrene polymer used as the base material for the resin.

A comprehensive effort was initiated to reduce the effect of the ^{235}U contaminant because it interferes with the uranium samples being examined for disequilibrium between ^{234}U and ^{238}U as part of the program to develop methods of dating groundwaters. A chemical separation scheme has been developed which is suitable for mass spectrometric work and which assures minimum exposure of the groundwater sample to possible contamination by natural uranium. The chemical separation method has been tested on synthetic and real groundwater samples and finally used to measure the disequilibrium in the $^{234}U/^{238}U$ ratio in groundwater samples from areas of possible interest as nuclear waste repositories. The reason for developing the mass spectrometric technique was to use the extreme sensitivity of this method to reduce the size of water samples. This is an important consideration, as samples recovered under difficult circumstances (e.g., from deep drill holes) are usually limited in volume.

EXPERIMENTAL RESULTS

Previous work (Michel and Keyes, 1979) indicated that it might be possible to deplete the ion-exchange resins of the ^{235}U contaminant by repeated cycling through, essentially, a blank run of the chemical separation scheme. To determine the size of the reservoir to be depleted, small batches of untreated resin were chemically oxidized with hydrogen peroxide (in sulfuric acid medium) and analyzed for uranium with a ^{233}U isotopic dilution technique. Using this isotope, it is possible to get the isotopic composition of the sample and a quantitative determination of uranium in the same sample. From these experiments it has been found that some natural uranium as well as the enriched ^{235}U were released from the resin. The quantities of each released appear to be independent of the relative amounts present and appear to vary with as yet undetermined differences in column operation techniques. This implies a different site in the resin structure for at least part of the two components. Analysis of several different batches of resin gave amounts varying from 1 to 2 ppb of total uranium, with the ^{235}U enriched by factors of 1.1-1.5. A special batch of resin was prepared by a commercial firm where special care was taken to reduce the uranium and other inorganics to as low an amount as possible. This resin had only 0.78 ppb of uranium but was enriched by a factor of 1.7 in ^{235}U. The higher enrichment of the low uranium sample is consistent with the previous suggestion that the styrene polymer may be the source of the ^{235}U and that the natural uranium came partly from reagents used to convert the polymer to the active resin. The special batch of resin was subjected to extreme cycling through the chemical process, with blank isotopic and chemical analyses being performed at intervals. After an extended series of such treatments, a column was obtained which permits separation of the uranium from groundwaters, thereby introducing sufficiently little enriched ^{235}U as to allow mass spectrometric determination of the $^{234}U/^{238}U$ ratio to be made with negligible error in a sample as small as 1 ng. The amount of ^{234}U in such a sample, if in equilibrium, would be 0.55 pg. Even after depletion of the resin, the amount removed in each cycle is still not reproducible enough to eliminate an occasional higher level of ^{235}U. Because the enriched ^{235}U contains a small amount of ^{234}U (present at higher concentrations relative to ^{235}U than in natural equilibrium uranium), it should be pointed out that any sample of natural equilibrium uranium contaminated by it will have the ^{234}U enriched slightly relative to ^{238}U. Since the $^{234}U/^{235}U$ ratio for a known source, such as the ion-exchange resin, can be determined, correction for this contamination can be made based on the observed increase in the $^{235}U/^{238}U$ ratio. Unfortunately, this increases experimental error because the several isotope ratios used in the correction reduce the precision of the final $^{234}U/^{238}U$ ratio. In addition, if more than one source of enriched ^{235}U contributes, as may well be the case, and if each has a different amount of ^{234}U, the correction becomes impossible to make with any confidence. For this reason it is essential to reduce the ^{235}U effect as much as possible. Fortunately for the purpose of dating groundwater systems, high precision is not required because the interpretation of the data does not lead to precise ages. This is due to the uncertainty surrounding the closed nature of the groundwater system with respect to addition or subtraction of uranium.

It has been recognized by many researchers that no single method of groundwater dating is likely to be convincing by itself, inasmuch as all are likely to suffer from one or more deficiencies in meeting

the hydrogeologic prerequisites for a good age determination. Since each method is likely to depend on different critical parameters, agreement among different methods represents the best verification of the observed age.

MEASUREMENT OF GROUNDWATER SAMPLES

Work has begun on groundwater samples from the Pasco Basin in the state of Washington, a region of successive lava flows separated by sedimentary layers which often contain water. This region, because of its low seismic activity and other practical advantages, has been suggested as a possible waste repository site. At present the data are too fragmentary to reveal age information, but the results to date well illustrate the advantages of the mass spectrometric method developed under this program.

One sample from a deep drill hole piercing the successive lava flows will suffice to illustrate the direction of the research. The groundwater in the well has a total uranium content of 9.5 parts per trillion. A 50-ml sample was processed by treating it with gaseous HCl until 4 M in hydrogen ion. This was followed by treatment with sulfur dioxide gas until just below saturation. After isotopic dilution with ^{233}U, the solution was passed through an ion-exchange column packed with strong base anion-exchange resin, pretreated to be in the chloride form. The eluent was discarded, the column washed with one column volume of 4 M HCl, and the uranium eluted with 0.1 M HCl. For the column chosen, the uranium is quantitatively recovered in about 30 drops of solution. This is reduced to about 40 µl in volume in a closed sub-boiling dry nitrogen flow evaporator, and the resultant solution pipetted into the ion source of the mass spectrometer. The final solution was free of iron or other visible evidence of inorganic ions.

The mass analysis showed the sample to be "enriched" in ^{234}U by a factor of 1.8 over the equilibrium value. The entire sample contained 475 pg of uranium, with the ^{234}U being at about 0.047 pg (approximately 10^8 atoms). A small correction was made for slight contamination by enriched ^{235}U from the column resin. Without this complication, an isotopic ratio could have been measured on a considerably smaller sample with the same precision.

By comparison, determination of the enrichment of ^{234}U by conventional alpha spectrometry, assuming (unrealistically) that essentially zero background counting rates could be achieved, would take approximately 3600 days of counting time to give the same 2-3% precision, or more practically, would require 40 liters of water to make the measurement in 3-4 days of counting. The importance of the kind of sensitivity the mass spectromatic technique affords for difficult-to-recover samples is clear. It is especially easy to see the advantage to be gained when remote samplers of limited volume come into use and can recover uncontaminated deep water samples. The problems with present methods of recovering larger samples is that the samples are likely to be contaminated with foreign materials or diluted by surface waters.

IMPLICATIONS FOR RELATED RESEARCH

The existence of enriched ^{235}U as a contaminant in laboratory materials poses the possibility that this type of impurity could be responsible for undetected errors in published data which are based on isotopic measurements of uranium. In most disequilibrium studies to date, the majority of near-surface or surface waters have been found to be only slightly enriched or depleted in ^{234}U. Those which are depleted are in the minority. Such waters are usually rather high in total uranium concentration, and it is generally easy to obtain samples containing a microgram or more of uranium in a reasonable volume of water. Thus one would not expect the small amounts of ^{235}U found in this work, rarely over a few tens of picograms, to have a serious effect on such data. Because chemical recovery of uranium from large volumes of water is inconvenient, those waters of lowest uranium content generally represent the smallest samples to be counted in the alpha spectrometer, and these may be affected slightly by the presence of a little enriched ^{235}U. In principle, the investigator would be aware of a problem from the observation of a non-natural ratio of $^{235}U/^{238}U$. However, for reasons associated with the nuclear energy levels in ^{231}Th and with the usual practice of counting until a predetermined standard deviation in the precision of the $^{234}U/^{238}U$ ratio is achieved, small enrichments in ^{235}U would probably not be noticed. Thus it is possible that some relatively small fraction of previous measurements overestimate the enrichment or underestimate the depletion of ^{234}U. The magnitude of this error should not be large, and it may not drastically alter the conclusions of any published work.

With respect to the $^{235}U/^{238}U$ ratio itself, there is a paper by Arden (1977) reporting an anomalously high ^{235}U abundance in the more chemically resistant phases of a carbonaceous chondrite. Subsequent attempts by others to confirm this work have been unsuccessful (Chen and Tilton, 1979; Chen and Wasserbug, 1980). Arden used ^{235}U as the isotope dilution spike for quantitative analysis, omitting it, of course, for the main isotopic analyses and spiking a fraction of the sample. He also measured the blank levels of supposedly natural uranium from all sources to be sure the data were not subject to error. These are routinely spiked since the only use is to get quantitative data. Unfortunately, the ^{235}U spike obscures any contamination by enriched ^{235}U in the blank. The net effect of such contamination would be to make the blank appear smaller than it actually is. Furthermore, Arden used a two-stage dissolution technique in order to demonstrate that the chemically resistant phases had the highest enrichment. The samples were first partially dissolved under rather mild conditions with analysis of the resulting uranium in solution. Then the remainder of the sample was dissolved, and the uranium in this fraction also analyzed. The second sample, invariably only a fraction of the total uranium, would be expected to contain, on the average, as much ^{235}U contamination as the first. Thus one would expect the anomaly to be distinctly greater in the more resistant fractions (second sample) and, generally, greater the

smaller the total amount of uranium. This was the case in Arden's data, leading one to suspect that the ^{235}U found to be so widespread in this work may be partially or wholly responsible for the reported isotopic anomaly.

CONCLUSION

An extremely simple ion exchange separation technique has been developed and tested for extracting uranium from groundwaters with purity sufficient for the thermal ion source of the mass spectrometer, i.e., at the level of 0.05 pg or less. The primary interference is from a widely observed industrial source of enriched ^{235}U. Repeated blank runs have demonstrated that the ion exchange resin, which is the most difficult source of ^{235}U enrichment to control, can be depleted and that the performance of the resin slowly improves with time. At present, it is possible to separate the uranium from samples of groundwater containing one nanogram of uranium or more and determine the $^{234}U/^{238}U$ ratio with insignificant error from the ^{235}U source. This corresponds to measurements on 0.05 picograms of ^{234}U, and a usable sensitivity of approximately 1.7×10^{-15} g.

REFERENCES CITED

Arden, J. W., 1977. Isotopic composition of uranium in chondritic meteorites. Nature, v. 269, p. 788.

Chen, J. H., and Tilton, C. R., 1979. Lunar and planetary science X. In Proc, 10th Lunar and Planetary Science Conference, March 19-23, 1979, Part 1, p. 193.

Chen, J. H., and Wasserbug, G. J., 1980. A search for isotopic anomalies in uranium. Geophysical Research Letters, v. 7, no. 4, p. 275-278.

Michel, M. C., and Keyes, W. R., 1979. $^{234}U/^{238}U$ disequilibrium studies. In Earth Sciences Division Annual Report 1979. Berkeley, Lawrence Berkeley Laboratory, LBL-10656, p. 215-217.

PRELIMINARY CHARACTERIZATION AND ASSESSMENT OF THE WELDON SPRING LOW-LEVEL WASTE DISPOSAL SITE

B. Y. Kanehiro, V. Guvanasen, A. Smith, and R. Sterrett

The Weldon Spring Quarry was the site for disposal of low-level radioactive wastes between 1960 and 1969, having been previously used for disposal of TNT-contaminated soils during the 1940s. The quarry occupies an 8.6-acre site 4 miles west of the Weldon Spring Chemical Plant and about 20 miles west of St. Louis (Fig. 1). The location of the quarry with respect to the Missouri River is shown in Figure 2.

This project represents the first phase of the characterization and assessment of the radioactive waste disposal site at Weldon Spring, Missouri, performed by the Lawrence Berkeley Laboratory. The work was done for the Department of Energy as the first part of their Engineering Options Plan for the Weldon Spring site.

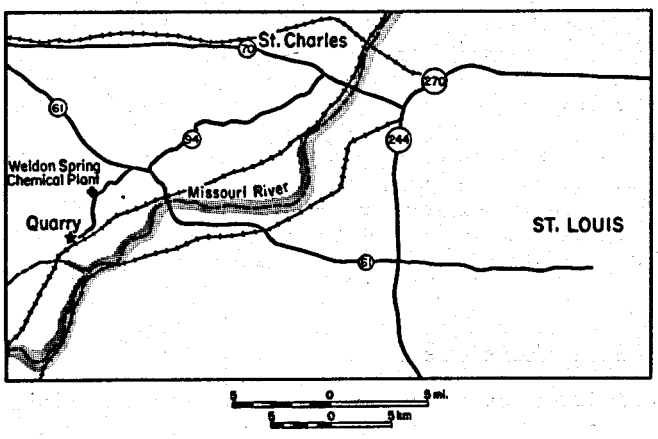

Figure 1. Location map of the Weldon Spring Quarry. [XBL 813-2184]

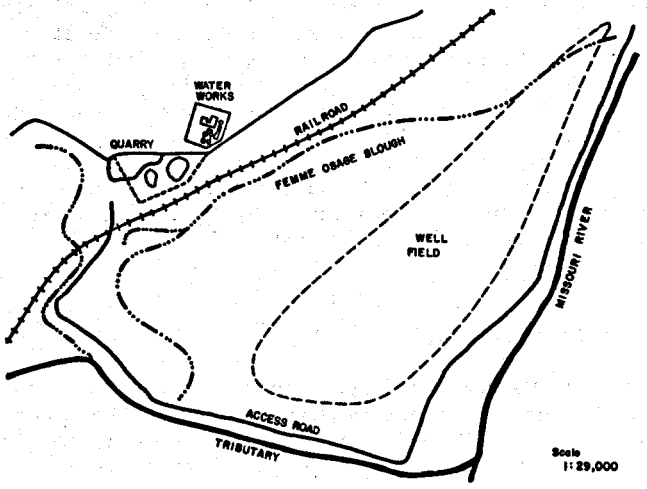

Figure 2. Location of the quarry with respect to the Missouri River. [XBL 813-2185]

Radioactive wastes at the Weldon Spring Quarry site currently pose a number of potential hazards, including: (1) radiation exposure and contamination of trespassers into the quarry; (2) contamination of groundwater, particularly the water pumped from the alluvial well field opposite the quarry across the slough, which supplies drinking water; and (3) contamination of nearby surface waters, particularly the Femme Osage Slough and the Femme Osage Creek.

SCOPE OF WORK

The two main objectives of this study are: (1) to characterize and assess the present situation at the site and (2) to obtain sufficient data for predicting the future of the site under existing conditions as well as possible changing conditions in the future. It is especially desirable that the efficiency of proposed engineering options for the site be determined.

These objectives imply that answers are needed for the following types of questions concerning the site. What type of and how much radioactive material is presently at the site? What are the radionuclide migration paths? When and at what concentrations will the waste arrive at critical points in the migration process? What will the answers be to the above questions if various engineering options are implemented?

Finding the answers to these questions requires a variety of activities: the present location of the migration front of radioactive nuclides must be determined; a model for flow of groundwater and chemical transport must be developed or an existing model modified for the site; and data to provide input parameters for the model must be collected.

For Weldon Spring, this implies that additional information is needed in conjunction with characterizing and assessing present conditions: (1) characterization of the geometry of the site with respect to topography, geology, and hydrologic boundaries; (2) characterization of the hydraulic and chemical properties of the geologic materials found in and around the site, specifically, the permeabilities and storage coefficients, adsorptive properties, dispersivities, and porosities; and (3) the present conditions, including an inventory of radioactive materials at the site and the location of the present migration front of radioactive nuclides and other contaminants.

ACTIVITIES FOR 1980

The Weldon Spring project began in 1979. The 1979 phase was primarily directed toward the assessment of present conditions and some boundary conditions at the site. The 1980 phase was directed toward developing the capability to forecast the future migration of radionuclides from the site. To this end, work was expanded to include material property determinations and numerical model development and modification. A tabulation of work performed follows.

Geologic and Hydrologic

1. Geologic data were accumulated and reviewed to determine boundary conditions.

2. Low-level area photographs were obtained to locate critical terrain features for boundary conditions and sampling locations.

3. A map of fractures and other potential conduits for contaminant migration in the limestone was prepared to better understand both the boundary conditions and the potential material properties of the limestone.

4. Existing wells were cleaned preparatory to geophysical logging.

5. Geophysical logs of the boreholes were run, including borehole television for fracture identification and natural gamma radiation logs. The logs will be used to infer both material properties and boundary conditions.

6. Seventeen new observation wells were drilled outside the quarry to determine the geometry of the geologic formations in the area and to try to gain some information about the location of the present migration front of radioactive nuclides.

7. During the drilling of the new wells, solid samples, taken with a split spoon sampler at intervals from 2.5 to 5 ft, were used to define geometry and material properties.

8. The new wells were surveyed and tied to established benchmarks, and older existing wells were resurveyed. This precision surveying is necessary for accurately determining an isopotential map.

9. An ongoing program of monitoring water levels was initiated. This is imperative for assessing the effects of seasonal variations on the water table.

10. Ten hydraulic tests of the new wells were performed to determine material properties.

11. Based on the results of the hydraulic tests, small-scale tracer tests were run to estimate the porosity and determine a possible order of magnitude value for dispersivity in the limestone.

12. Work is ongoing on the predictive model that will be used to organize all of the field data and do the final forecasting for the site. The model is presently complete enough to be used for the analysis of the pump and tracer test.

Waste Characteristics

1. Existing radiological data were accumulated and reviewed. Information on materials known to have been dumped into the quarry was reviewed.

2. A preliminary radiological survey was conducted, including plans for protection of personnel working at the site.

3. Areas requiring limited access due to high surface radiation levels were delineated.

4. Radiological samples were obtained in order to quantify the volumes and species of radionuclides present.

5. A low-level, helicopter-borne, detailed radiometric survey was performed by EG&G, Idaho. Results of the survey should be available in 1981.

6. Radiological samples were obtained during the drilling of observation wells. Results of analysis will provide information about the location of uranium migration from the site.

Geochemistry

1. An ongoing program was initiated to monitor the groundwater geochemistry in the area.

2. Analysis of groundwater samples is being done for a large range of cations and anions. Such analysis will provide information about the present location of material escaping from the site, i.e., initial conditions.

3. Specific analyses are being done for uranium. This supplies information about initial conditions and possibly the adsorption of uranium on the geological material, i.e., material properties.

CONCLUSIONS

Perhaps the most important finding to date is that uranium has been found outside the quarry both in solid samples of alluvium taken during drilling and in water samples from the wells after completion. Although these wells are close to the quarry walls, approximately 400 ft, the implication is that there is potential for future problems with the municipal wells located down gradient from the quarry. More work must be done to determine the full extent of migration and to collect enough data to predict future migration at the site.

Future work for this project will be directed primarily toward forecasting future migration under present conditions and evaluating proposed engineering options. Included in this work will be the installation of more monitoring wells at greater distances from the quarry, evaluation of far-field boundary conditions and material properties, and the forecasting itself.

SWEDISH-AMERICAN COOPERATIVE PROGRAM

STRIPA HEATER TESTS

T. Chan

To gain a basic understanding of the response of a hard rock mass to thermal loading under conditions similar to those expected in a future geological repository, a series of heater tests have been conducted in a granite body at a depth of 338 m in an abandoned iron-ore mine at Stripa, Sweden, about 150 km west of Stockholm. This work is part of a Swedish-American cooperative program of investigations on radioactive waste disposal initiated in July 1977 between the Lawrence Berkeley Laboratory (LBL) in the U. S. and KBS (the Nuclear Fuel Safety Program) in Sweden (Witherspoon and Degerman, 1978). Cook and Witherspoon (1978) have provided details of the objectives and design of these heater tests.

Heating commenced in June 1978 and lasted for approximately one year. The rock was heavily instrumented to measure the temperature, displacement, and stress fields. Monitoring of the rock response continued for six months after the heaters were deactivated. All field activities were concluded in June 1980 with the completion of in situ post-test calibrations of instrumentation. The status of the project as of June 1980 was reviewed by Chan et al. (1980).

Activities in fiscal 1978 and 1979 were summarized in previous annual reports (Witherspoon et al., 1978; Hood et al., 1980). Major activities during fiscal 1980 included post-test calibration and evaluation of instrumentation, data base preparation, and a limited amount of post-test thermal and thermomechanical analyses.

INSTRUMENTATION RECALIBRATION AND EVALUATION

Instrumentation at Stripa included 389 thermocouples for temperature, 35 rod extensometers for displacement, 30 U. S. Bureau of Mines (USBM) borehole deformation gauges, and 26 IRAD vibrating wire gauges for stress determination (Schrauf et al., 1979). After the heaters had been turned off and monitoring of rock cool-down had been concluded, all instruments were recovered whenever possible and recalibrated. This recovery and recalibration has provided valuable information for evaluating the performance of the various types of instrumentation under prolonged operation in a hot and humid environment.

A problem with the calibration procedure has been identified for thermocouples and is still being analyzed. For extensometers and USBM gauges, good repeatability was obtained between pre-test and post-test calibrations. A major problem with the extensometers was friction in the rods, which could cause step-wise jumps in the measured displacement up to 0.1 mm, according to simulated bench tests. The USBM gauges experienced a high failure rate during operation due to corrosion problems. The reliability was improved after taking remedial measures. Recalibration of IRAD gauges has shown that the calibration parameters apparently vary between gauges and with time, calibration configuration, and preset stress. Further investigation is in progress.

DATA BASE PREPARATION

Data acquisition and display were accomplished using an on-site computer-based system (McEvoy, 1979). "Raw voltage" data from some 750 sensors were collected at a sampling rate of four per hour, digitized, transmitted to the computer and recorded on a magnetic tape. These data tapes were sent to LBL every fortnight for archiving. A parallel data acquisition system consisting of four data loggers provided back-up data.

In anticipation of post-test data analysis, the enormous data base (approximately 50 million measurements) has recently been verified, converted to engineering units, structured, and written onto two standard magnetic tapes, copies of which are available to the nuclear waste storage research community. This is the first time that a comprehensive data base of this type has been released in computer-readable form. The data base preparation includes the following steps: (1) verification of "raw data" recorded on magnetic tapes by demonstrating their nearly perfect cross-correlation with corresponding back-up data recorded by data loggers, (2) correction for voltage error introduced by a hardware problem in the computer-based data acquisition system, (3) compensation for temperature dependency of instrumentation characteristics and conversion to engineering units, (4) verification of procedures in item 2 by statistical test and procedures in item 3 by repeating the calculations on randomly selected data using either a different numerical algorithm or an independently coded computer program based on the same algorithm, and (5) compacting the data by time-averaging and structuring in the order of causality: heater power, temperatures, displacements, and measurements from which stresses can be deduced and written on standard magnetic tapes.

Details of the data verification and processing procedures outlined above, as well as the data, are presented in Chan et al. (1980).

THERMAL ANALYSIS

Prior to conducting the experiments, preliminary calculations were made to guide the design. Because of the tight schedule of the project and

the need to store the complete predicted history of the thermal field in an on-site computer at Stripa for instant graphic comparison with field data, a highly idealized closed-form solution based on the Green's function method was adopted (Chan et al, 1978).

In Figure 1, calculated and measured rock temperatures at several thermocouples, located at various elevations in the vertical hole nearest to the 3.6 kW heater (at 0.4 m radius), have been plotted as a function of time. Although there is general agreement between the closed-form solution (broken curve) and experimental results (asterisks), closer examination of comparison plots such as Figure 1 has revealed that (1) above the planned horizontal heater midplane (z = 0 plane), measured rock temperatures are higher than predicted by the closed-form solution with an isothermal boundary condition, whereas below the midplane, measured temperatures are lower than predicted; and (2) rock temperatures measured above the horizontal midplane are higher than those at equal distances below the midplane. These trends generally hold for all three heater experiments.

Further examination of the field data, along with detailed finite-element calculations, was undertaken to identify the causes of the asymmetry of the vertical temperature profile (Chan et al., 1980). If groundwater convection or steam formation were responsible for the higher rock temperatures above the planned midplane, the vertical asymmetry would be expected to be more pronounced for the 5-kW experiment than for the 3.6-kW experiment because of the higher temperatures and thermal gradients in the former. Comparison of the field data for these two experiments shows that the opposite is true. This has led to the suspicion that the position of the 3.6-kW heater might be in error. When the position was remeasured, it was found that the 3.6-kW heater was indeed installed 10-13 cm above the planned position. Shifting the heater position up 10 cm removes more than 50% of the discrepancies between observed temperatures and the original closed-form solution.

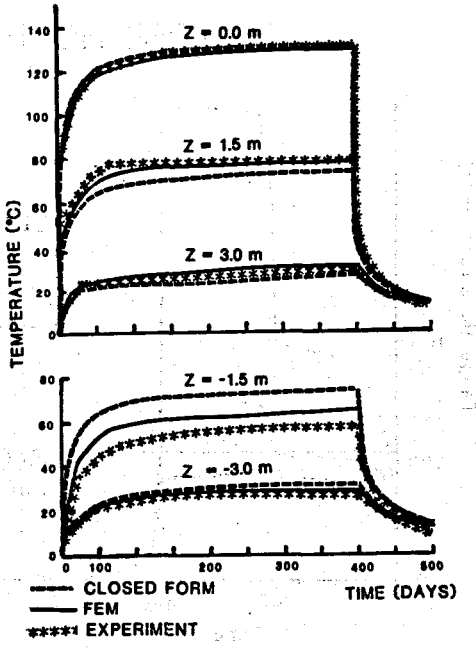

Figure 1. Measured and calculated rock temperatures as a function of time at radial distance 0.4 m from the axis of the 3.6-kW heater and at various elevations. The closed-form solution models the experiment as a finite-length line heater in a semi-infinite medium. The finite-element model (FEM) includes more realistic initial and boundary conditions and accounts for temperature-dependency of the thermal conductivity of Stripa granite.
[XBL 804-9273]

Possible causes for the remaining discrepancies were investigated by nonlinear, finite-element analysis. In the finite-element model, the nonuniform initial temperatures measured in the rock, the convective boundary conditions at the surfaces of the heater hole and the heater and extensometer drifts, and the variation of thermal conductivity of Stripa granite with temperature all were taken into account. The close agreement between the finite-element solution (solid curve) and measured temperatures in Figure 1 demonstrates that conduction is the predominant heat transfer process. Asymmetry in the vertical temperature distribution can be attributed primarily to operating conditions. Minor discrepancies still remain. These may perhaps be related to geological features such as dikes, faults, and joints.

THERMOMECHANICAL ANALYSES

In contrast to the temperature results, the rock displacements differ significantly from the values calculated prior to heater turn-on (lower curve, Figs. 2 and 3) using temperature-independent rock properties (Chan and Cook, 1979). A limited number of laboratory tests of intact small samples of Stripa granite were conducted in parallel with the in situ heater tests (Swan, 1978; Chan et al. (1980). Among the different rock properties, the thermal expansion coefficient varies most rapidly with temperature. Young's modulus and Poisson's ratio are also temperature-dependent at higher temperatures. Finite-element calculations were made to investigate the influence of these temperature-dependent properties on predicted displacements and stresses.

In Figure 2 the measured vertical rock displacement (negative sign indicates expansion) between two anchor points for a vertical extensometer in the 3.6-kW heater test is compared with calculated displacement obtained using both constant and temperature-dependent rock properties. Evidently, considering the temperature dependence of rock properties significantly improves the agreement between calculated and measured displacements during both the heating and cooling periods. However, the displacements calculated with temperature-dependent material properties are somewhat smaller in magnitude than the measured displacements.

A similar plot is shown in Figure 3 for relative horizontal rock displacements between two anchor points at a radial distance of 1 m on oppo-

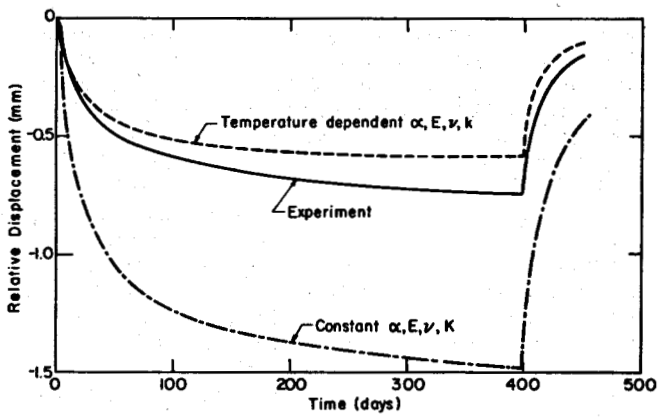

Figure 2. Calculated and measured relative vertical rock displacements between two anchor points 2.24 m above and below the heater midplane for a vertical extensometer at a radial distance of 1 m from the 3.6-kW heater. Displacements calculated using both constant and temperature-dependent properties are shown. Note that displacements calculated with temperature-dependent rock properties are larger in magnitude than measured displacements.

[XBL 801-4611]

site sides of the 3.6-kW heater and about 0.6 m below the bottom of the heater. Although the use of temperature-dependent rock properties again significantly reduces the magnitude of the calculated displacements, the results are still much higher than the measured values, in contrast to the situation for the vertical displacements. One reason may be that the axisymmetric model used is stiffer in the vertical direction and more flexible in the horizontal direction than the real rock structure. Another possibility is that the measured horizontal displacements are unreliable because of their small values (generally less than 0.2 mm) and thus probably contains larger percentage errors. Better agreement between modeled and measured horizontal displacements were obtained for the 5-kW heater test where larger displacements occurred (Chan et al., 1980).

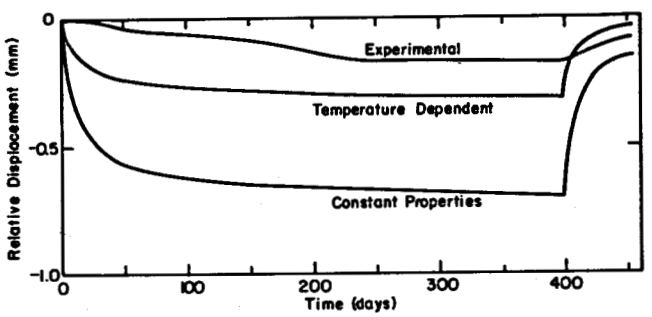

Figure 3. Calculated and measured relative horizontal rock displacements between two anchor points 1 m radial distance on opposite sides of the 3.6-kW heater for a horizontal extensometer 0.6 m below the bottom of the heater. Displacements calculated using both constant and temperature-dependent properties are shown. Note that displacements calculated with temperature-dependent rock properties are smaller in magnitude than measured displacements.

[XBL 803-4906]

Serious decrepitation of the wall-rock has been observed in the 5-kW heater borehole shortly after the peripheral heaters were turned on. According to linear thermoelastic calculations using constant rock properties (Chan and Cook, 1979), the highest compressive stress, i.e., the tangential stress at the heater hole, would have reached a value of 215 MPa before the peripheral heaters were turned on. This calculated tangential stress increases very rapidly after the turn on of the peripheral heaters. A casual comparison of this stress with the uniaxial compressive strength 208 MPa of Stripa granite at 20°C may suggest that the onset of gross borehole failure occurred when the tangential stress exceeds the compressive strength (Hood et al., 1980). Further calculations using temperature-dependent properties (Chan et al., 1980), have shown that the stress at the wall of borehole is very sensitive to the temperature-dependence of the rock properties, as shown in Figure 4. Further work is needed to elucidate the mechanism of this thermomechanical failure because the strength of Stripa granite (Swan, 1978) is also somewhat temperature-dependent and has been measured only to 190°C, where it has decreased to a value of 148 MPa, and gross borehole failure occurred at a temperature estimated to be over 300°C.

CONCLUSIONS

The Stripa heater tests conducted in the past three years have yielded a great wealth of field data on the thermal and thermomechanical behavior

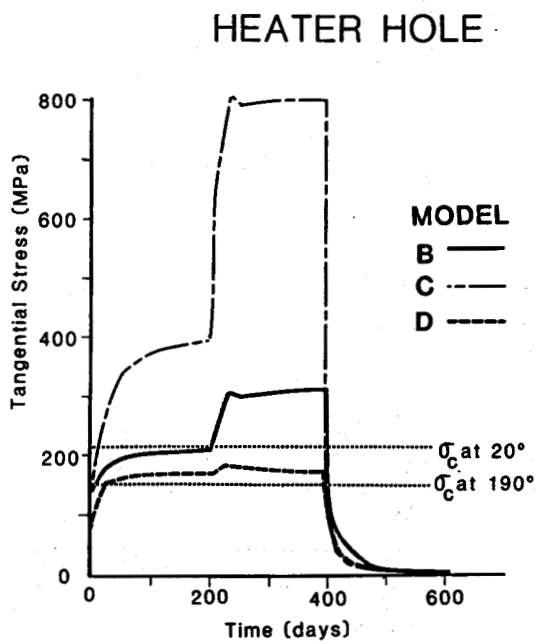

Figure 4. Tangential stress at the wall of the 5-kW heater borehole at midplane level as calculated by three finite-element models: Model B, constant rock properties; Model C, upper-bound curve for temperature-dependent properties determined by laboratory testing; Model D, lower-bound curve for temperature-dependent rock properties determined by laboratory testing. Also shown are values for uniaxial compressive strength, σc, of Stripa granite.

[XBL 803-8961]

of a hard rock mass subjected to heating. Preliminary evaluation of instrumentation has already improved our knowledge of instrumentation requirements for measuring rock temperatures, displacements, and stresses under simulated repository conditions. A limited amount of data analysis by comparison with numerical models has advanced our understanding of the thermomechanics of a hard rock mass. At the same time, it has also demonstrated the complexity of geotechnical problems at elevated temperatures and the need for a concerted effort of field tests, laboratory measurements, numerical modeling, and data analysis.

REFERENCES

Chan, T., Binnall, E., Nelson, P., Stolzman, R., Wan, O., Weaver, C., Ang, K., Braley, J., and McEvoy, M., 1980. Thermal and thermomechanical data from in situ heater experiments at Stripa, Sweden. Berkeley, Lawrence Berkeley Laboratory, LBL-11477 (SAC-29).

Chan, T., and Cook, N. G. W., 1979. Calculated thermally induced displacements and stresses for Stripa heater experiments. Berkeley, Lawrence Berkeley Laboratory, LBL-7061 (SAC-22).

Chan, T., Cook, N. G. W., and Tsang, C. F., 1978. Theoretical temperature fields for heater project at Stripa. Berkeley, Lawrence Berkeley Laboratory, LBL-7082.

Chan, T., Hood, M., and Board, M., 1980. Rock properties and their effect on thermally-induced displacements and stresses. Presented at ASME 1980 Energy Technology Conference and Exhibition, New Orleans, February 1980. Berkeley, Lawrence Berkeley Laboratory, LBL-10517.

Chan, T., Hood, M., and Witherspoon, P. A., 1980. Predicted and measured temperatures, displacements and stresses from the Stripa heater experiments, in Proceedings, Rockstore '80, Stockholm, Sweden, June 23-27, 1980, p. 829-837.

Chan, T., Littlestone, N., and Wan, O., 1980. Thermomechanical modeling and data analysis for heating experiments at Stripa, Sweden, in Proceedings, 21st U. S. Rock Mechanics Symposium, May 28-30, Rolla, Missouri, p. 16-25.

Chan, T., Witherspoon, P. A., and Javandel, I., 1980. Heat transfer in underground heating experiments in granite, Stripa, Sweden, in Proceedings, Symposium on Heat Transfer in Nuclear Waste Disposal (ASME Monograph HTD-Vol. 11), ASME Winter Annual Meeting, Chicago, Illinois, Nov 16-21, F. A. Kulacki and R. W. Lyczkowski, eds., p. 1-8.

Cook, N. G. W., and Witherspoon, P. A., 1978. In situ heating experiments in hard rock: Their objectives and design. Part II. Berkeley, Lawrence Berkeley Laboratory, LBL-7073 (SAC-10).

Hood, M., Chan, T., and Nelson, P., 1980. Thermomechanical experiments at Stripa, in Earth Sciences Division Annual Report 1979. Berkeley, Lawrence Berkeley Laboratory, LBL-10686, p. 196-201.

Hood, M., Carlsson, H., and Nelson P. H., 1980. The application of field data from heater experiments conducted at Stripa, Sweden, to parameters for repository design. Berkeley, Lawrence Berkeley Laboratory, LBL-9392 (SAC-26).

McEvoy, M. B., 1979. Data acquisition, handling, and display for the heater experiments at Stripa. Berkeley, Lawrence Berkeley Laboratory, LBL-7062 (SAC-14).

Schrauf, T. A., Pratt, H., Simonson, E., Hustrulid, W., Nelson, P., DuBois, A., Binnall, W., and Haught, R., 1979. Instrumentation evaluation, calibration and installation for heater tests simulating nuclear waste in crystalline rock, Sweden. Berkeley, Lawrence Berkeley Laboratory, LBL-8313 (SAC-25).

Swan, G., 1978. The mechanical properties of Stripa granite. Berkeley, Lawrence Berkeley Laboratory, LBL-7074 (SAC-03).

Witherspoon, P. A., Cook, N. G. W., and Gale, J. E., 1978. Swedish-American cooperative program on radioactive waste storage in mined caverns in crystalline rock, in Earth Sciences Division Annual Report 1978. Berkeley, Lawrence Berkeley Laboratory, LBL-8648, p. 199-209.

Witherspoon, P. A. and Degerman, O., 1978. Swedish-American cooperative program on radioactive waste storage in mined caverns. Berkeley, Lawrence Berkeley Laboratory, LBL-7049 (SAC-01).

FRACTURE HYDROLOGY STUDIES AT STRIPA—FISCAL 1980

J. Gale, P. Fritz, J. Barker, C. Forster, K. Raven, P. A. Witherspoon, and C. R. Wilson

The overall fracture hydrology program at Stripa has been outlined by Gale and Witherspoon (1979), and the preliminary results from this program have been given in a series of reports and papers: Fritz et al. (1979a, b; 1981), Gale et al. (1979, 1980), Olkiewicz et al. (1979), Witherspoon et al. (1979a, b), Andrews et al. (1980), Forster and Gale (1980a, b), Gale and Raven (1981), Witherspoon et al. (1980a, b) and Gale (1980). Other summary papers and reports, etc., appear in various conference and workshop proceedings.

OVERVIEW OF STRIPA FRACTURE HYDROLOGY PROGRAM

The overall hydrology program at Stripa (Gale and Witherspoon, 1979) is summarized in Figure 1. The five major areas of research are: (1) assessment of directional permeabilities; (2) geochemical and isotope studies; (3) tracer studies; (4) an underground macropermeability experiment to measure rock-mass seepage; and (5) pump tests. The macropermeability experiment is discussed elsewhere in this report. The tracer studies have not been initiated at this time. Thus, this paper deals primarily with the first two parts of the program: assessing directional permeabilities of the Stripa granite and the geochemical and isotope studies.

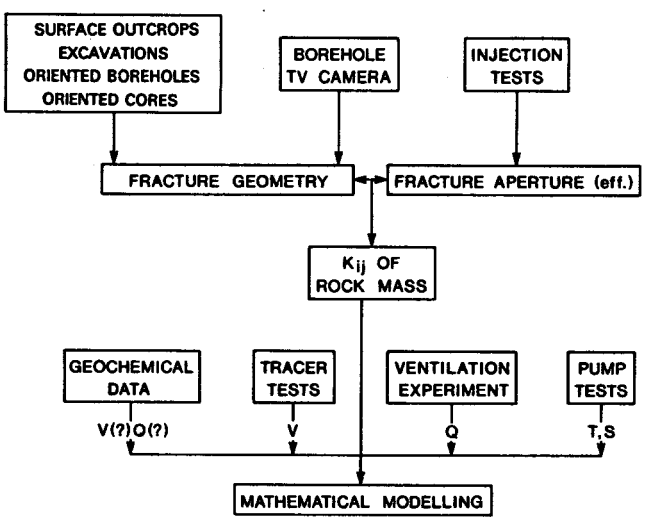

Figure 1. Block diagram of fracture hydrology program at Stripa (Gale and Witherspoon, 1979)
[XBL 7811-2144]

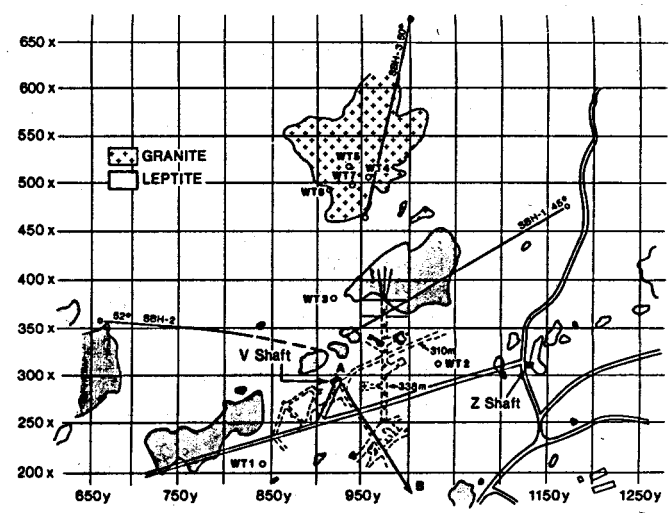

Figure 2. General geology and hydrology borehole locations. Squares are 50 m on a side.
[XBL 804-9434]

Fracture hydrology tests have been performed in both surface and subsurface boreholes. The surface boreholes consist of six water-table wells, WT-1 through WT-6; a pump test well, WT-7; and three long inclined boreholes, SBH-1, SBH-2, and SBH-3 (Fig. 2). SBH-1 is an open, 76-mm diameter, diamond-core hole, 385 m long, that angles downward at 45 degrees, passes over the top of the test excavations, and terminates at approximately the 290-m level. SBH-2, also diamond-cored, was drilled from the west toward the test excavations. This borehole is 365 m long, angles downward at 52 degrees, and terminates in the position shown in Figure 2 at approximately the 290-m level. SBH-3, 315 m long, also diamond-cored, is drilled from the north at an angle of approximately 50 degrees south toward the test excavations, terminating in the position shown. All three inclined surface boreholes were oriented to optimize their intersection with the major fracture sets.

The subsurface hydrology boreholes (Fig. 3) are located at the north end of the test excavat[illegible]. This group of boreholes are all diamond-core hole[illegible] 30 m long and 76 mm in diameter, except R-1 and R-6 which are 40 m long.

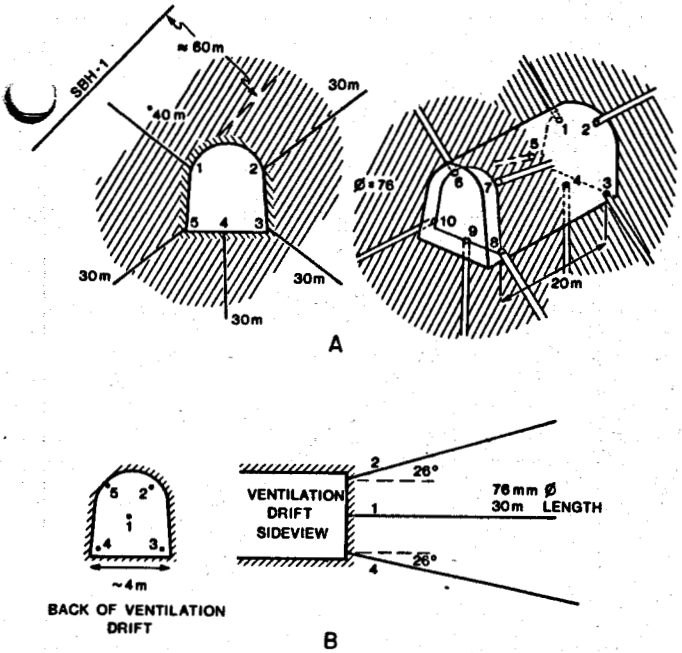

Figure 3. Location and orientation of subsurface hydrology boreholes. [XBL 7811-13108]

ACTIVITIES IN FISCAL 1980

Permeability Measurements and Related Activities

The primary focus of the fracture hydrology program in fiscal 1980 was the tabulation of the fluid pressure and flowrate data from the borehole tests at Stripa. This work has been completed and the data files have been assembled on computer tapes. Partially processed data is being published in a SAC Report (Gale, 1980). The basic test data for the R-4 borehole are shown in Figure 4.

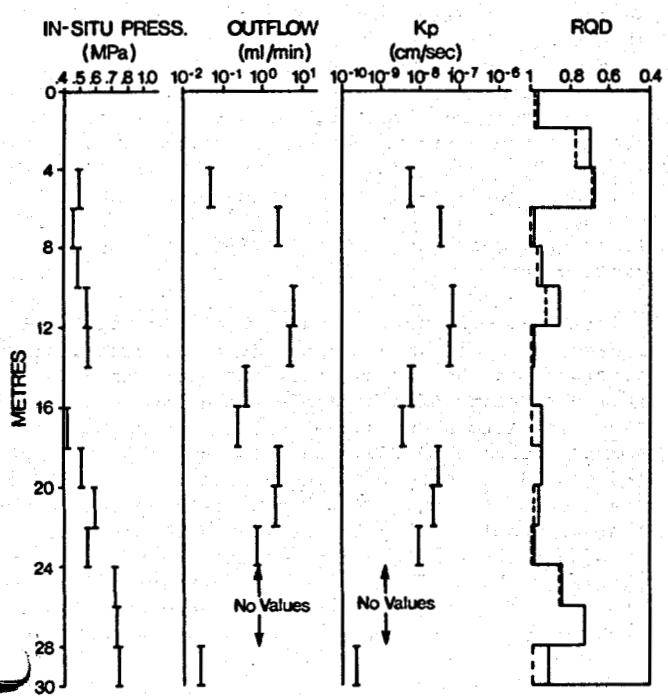

Figure 4. Fluid withdrawal and fracture data from R-4 Borehole (Gale et al., 1979). [XBL 813-2679]

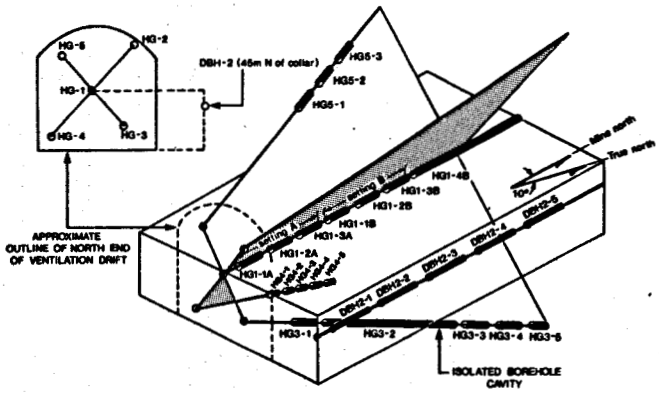

Figure 5. Schematic perspective of borehole installation pattern (Forster and Gale, 1980). [XBL 813-2680]

Results from the field pressure pulse testing program were tabulated and reported in fiscal 1980 (Forster and Gale, 1980). This program consisted of instrumenting five boreholes at the end of the ventilation drift with multiple packer assemblies (Fig. 5). In Figure 5, the solid areas along each borehole represent the open intervals in cavities being tested, and the gaps between the solid areas represent the inflatable packer elements used to isolate the cavities. Both steady-state injection tests and pressure pulse tests were carried out in these cavities. A summary plot of the pressure decay versus time plots are given in Figure 6. The hydraulic conductivity values calculated from steady state tests are given as k_{ss} values with the pressure-time record for the pressure pulse test in the same cavity. As can be seen from the results presented in Figure 6, there does not appear to be any correlation between the range of steady-state hydraulic conductivities and the distribution of pressure-time curves.

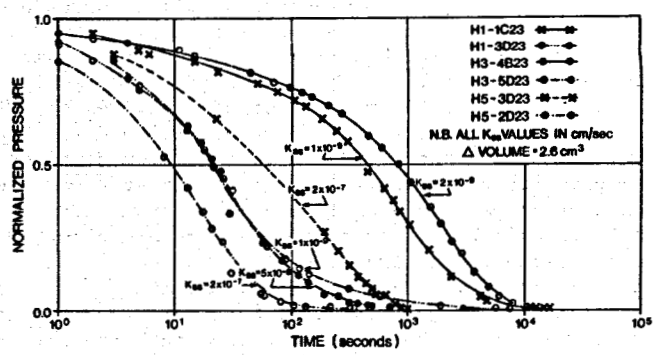

Figure 6. Summary plot of normalized pressure against log time (Forster and Gale, 1980). [XBL 813-2681]

A laboratory study to assess the effects of sample size on the stress-permeability characteristics of natural fractures was completed by Gale and Raven (1981). This experiment included the collection and testing of five samples, 10 cm, 15 cm,

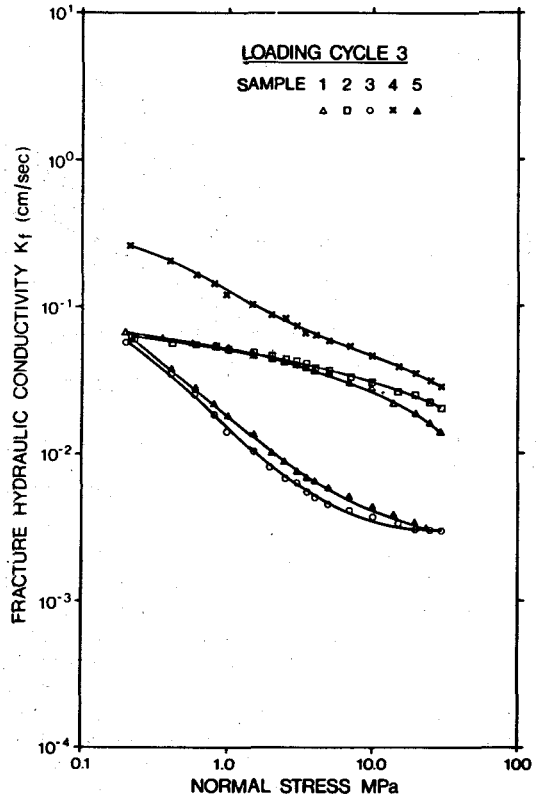

Figure 7. Fracture hydraulic conductivity as a function of normal stress, samples 1-5, loading cycle 3 (Gale and Raven, 1980). [XBL 813-2683]

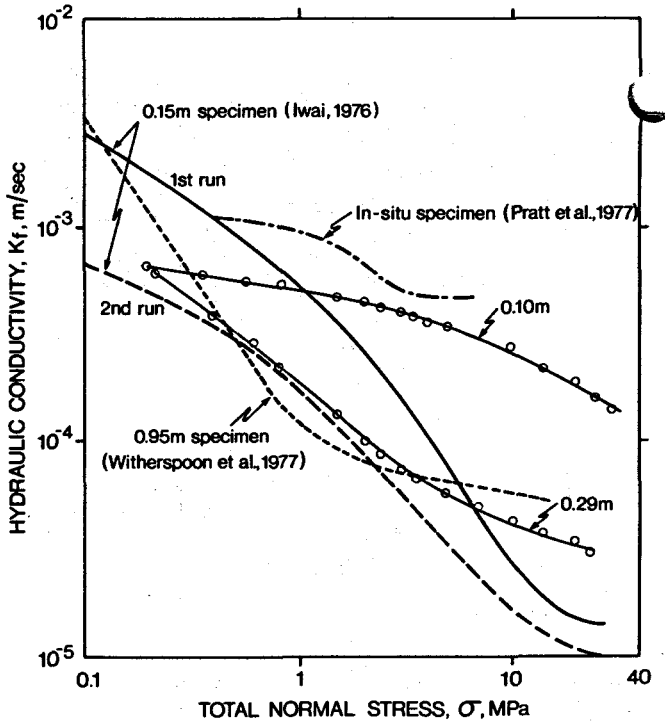

Figure 8. Comparison of the variation of fracture hydraulic conductivity with normal stress, samples 1 and 5 with published data after Witherspoon et al. 1979c (Gale and Raven, 1980). [XBL 813-2684]

20 cm, 25 cm, and 30 cm in diameter, containing natural fractures oriented perpendicular to the core axis. Each sample was subjected to three loading and unloading cycles with flow rates, under radial flow conditions, being measured at given increments of normal stress. Figure 7 is a summary plot of fracture hydraulic conductivity versus normal stress for all five samples. This shows that samples 3 and 5 (the 20-cm and 30-cm diameter samples, respectively) have different stress permeability relationships than samples 1 and 2 (the 10-cm and 15-cm diameter samples, respectively). The 25-cm diameter samples (number 4) gave an anomalous stress-permeability relationship but it is believed that this resulted from damage to the fracture plane during sample preparation. The data for samples 1 and 5, the smallest and largest samples, have been reported in Figure 8. This shows that the apparent size effect reflected in our data is the reverse of that predicted by Witherspoon et al. (1979c).

Geochemical Studies at Stripa

During 1979-1980 the research reported by Fritz et al. (1979b) was continued. Additional water samples from the mine and surrounding area were analyzed. A mineralogical study of the fracture fill material from the research areas in the Stripa mine was conducted. These activities are summarized by Fritz et al. (1980).

Figure 9 indicates that all groundwaters from the Stripa mine fall near the meteoric water line and therefore have not suffered significant evaporation or isotopic exchange with minerals. Evaporation does seem to have significantly influenced many surface and shallow groundwaters in this area. The abundance of ^{2}H and ^{18}O is dependent on the temperature of condensation. Therefore, the depletion observed in deeper groundwaters in both ^{2}H and ^{18}O suggests they were recharged under cooler climates than existed during recharge of shallow groundwater. Figure 10 also indicates that the fractured granite at Stripa contains different water types at different depths. The increase in Cl^{-1} content is paralleled by a decrease in the $^{18}O/^{16}O$ ratio of the groundwater.

It was originally thought that a gradual increase in total dissolved solids (TDS) with depth persisted in the Stripa mine. However, more detailed sampling of a borehole extending from the 410-m level to about 840-m depth suggests that an abrupt increase in TDS occurs in the deepest sample (811-to 838-m depth). Groundwaters from the 330-m level down to about 770-m depth are chemically similar with only a slight increase in TDS with depth. This suggests that a mixing of different water masses may be occurring at depth rather than a simple evolution of groundwater chemistry with depth. Perhaps more saline waters will be encountered at greater depths in this area.

Groundwater samples were collected from the dewatering systems during the full- and time-scale

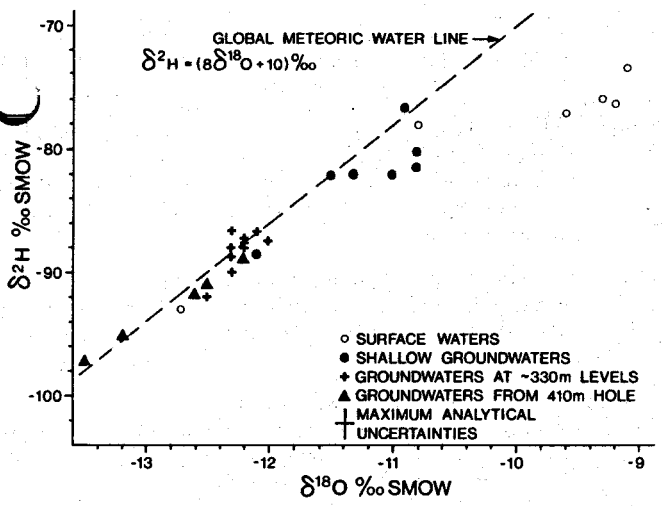

Figure 9. Comparison of $\delta^{18}O$ and $\delta^{2}H$ values of water samples collected from the surface waters, shallow groundwaters and water from the granite at Stripa. Note the closeness to the meteoric water line of all but the surface water samples (Fritz et al., 1979b). [XBL 813-2682]

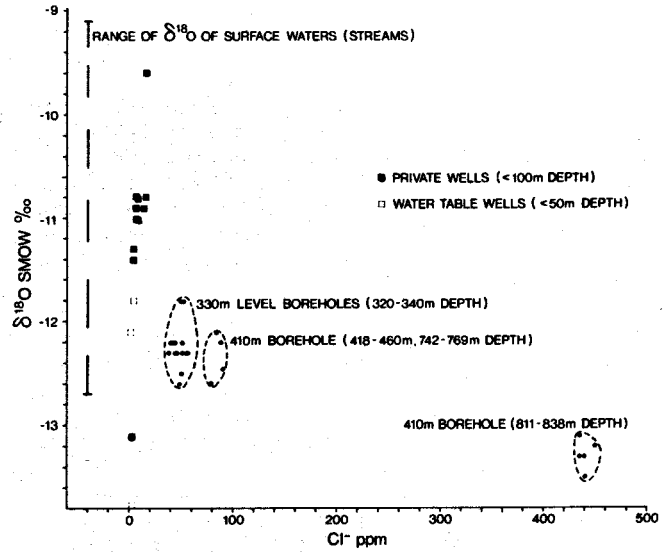

Figure 10. This comparison of Cl^- with $\delta^{18}O$ values shows that in the Stripa granite, different fracture systems carry different types of water. [XBL 813-2685]

heater experiments. Changes in groundwater chemistry due to rock-mass and water temperature increases were only observed in heater boreholes where temperatures in excess of 100°C were encountered.

A pump-packer assembly was used to collect shallow groundwater from SBH-3 (89- to 104-m depth interval). Detailed analyses suggested that shallow groundwater, generally free from drilling fluid contamination, was obtained. The possibility of contamination from shallower groundwaters could not be excluded, however. This emphasizes the usefulness of sampling from excavations where artesian conditions are likely to be encountered, and groundwater contamination is thus minimized.

Table 1 summarizes the estimated ages of groundwaters at the Stripa site. Groundwaters from the 330-m level and the upper parts of the vertical borehole at the 410-m level are a few tens-of-thousands-of-years old while the more saline waters at the 810- to 839-m level in the vertical borehole are probably much older. The interpretations of these age estimates, their uncertainties and interrelations will be addressed in forthcoming publications.

Table 1. Estimated groundwater ages (yr) at the Stripa Test Site.*

	$\delta^{18}O$ ‰ SMOW	$\delta^{13}C$	^{14}C	$^{234}U/^{238}U$ Activity Ratios	$^{234}U/^{238}U$ + Radon	^{226}Ra-^{222}Rn	^{4}He	$^{40}Ar/^{36}Ar$
	(1)		(2)	(3)			(4)	(5)
Shallow < 100 m	-10.9	>10,000 or >25,000	Modern					Increasing age ↓
330-m levels	-12.2		> 20.000		12,000 - 35,000	> 8000	n x 10^4	
410-m borehole (top)	-12.3		> 25.000	> 2.5 x 10^5			n x 10^4	
410-m borehole (bottom)	-13.2		?	> 4 x 10^5		> 8000	n x 10^5	VERY OLD?

* Fritz et al., 1979c.
(1) Lower ^{18}O contents signify lower recharge temperatures provided global atmosphere circulation patterns did not shift.
(2) These age brackets assume insignificant bacterial activities such as methane oxidation.
(3) Closed system evolution without rock-water interaction is assumed.
(4) The estimated values are dependent on uranium/thorium contents of the rocks. Values typical for the Stripa granite were assumed (30-160 ppm).
(5) No age estimates were attempted because no information was available on argon release rates from the rocks.

FUTURE ACTIVITIES--FISCAL YEAR 1981

In fiscal 1981, a detailed analysis of the fracture and borehole packer test data will be undertaken. Emphasis in the fracture analysis will be in determining how well we can characterize the fracture system from borehole and drift mapping. This work should produce a three-dimensional characterization of the fracture system at Stripa as well as the statistics of fracture spacing, length, and orientation.

Once the borehole packer-test data have been analyzed, we will use this data in a classical porous media approach to calculating flow into the ventilation drift. Also, the classical porous media approach will be used to conduct a preliminary three-dimensional numerical model study of the regional flow system around Stripa. This study, with an existing numerical model, will permit calculation of flow lines in an attempt to interpret the isotopic and geochemical data from the Stripa site within a flow system context. Additional model development will be required in order to fully incorporate the complete fracture permeability characteristics into a study of both the local and regional flow systems. Additional modeling work in fiscal 1981 will involve an attempt to simulate the pressure pulse field tests within the context of the fracture system and boundary conditions at the Stripa site.

REFERENCES CITED

Andrews, J. N., Giles, J. S., Kay, R. L. F., Lee, D. J., Osmond, J. K., Cowart, J. B., Fritz, P., Barker, J. F., and Gale, J. E., 1980. Uranium isotopes and age relationships between groundwaters from the granites at Stripa, Sweden. In press.

Forster, C. B., and Gale, J. E., 1980a. A laboratory assessment of the use of borehole pressure transients to measure the permeability of fractured rock masses. Berkeley, Lawrence Berkeley Laboratory, LBL-8674 (SAC-28).

____, 1980b. A field assessment of the use of borehole pressure transients to measure the permeability of fractured rock masses. Berkeley, Lawrence Berkeley Laboratory, LBL-11829, in preparation.

Fritz, P., Barker, J. F., and Gale, J. E., 1979a. Geochemistry and isotope hydrology of groundwaters in the Stripa granite--Results and preliminary interpretation. Berkeley, Lawrence Berkeley Laboratory, LBL-8285 (SAC-12).

____, 1979b. Geochemistry, origin and age of groundwaters at the Stripa (Sweden) test mine, in Proceedings, Scientific Bases for Nuclear Waste Management. Boston, Massachusetts, November 1979, p. 543-552.

Fritz, P., Barker, J. F., Gale, J. E., Andrews, J. N., Kay, R. L. F., Lee, D. J., Cowart, J. B., Osmond, J. K., Payne, B. R., and Witherspoon, P. A., 1979c. Geochemical and isotopic investigation at the Stripa test site (Sweden). International Symposium on the Underground Disposal of Radioactive Wastes Vol. 2, Helsinki, Finland, July 2-6, 1979.

Fritz, P., Barker, J. F., and Gale, J. E., 1980. Summary of geochemical activities at the Stripa test site during FY 1979/80. Berkeley, Lawrence Berkeley Laboratory, LBL-11864, in preparation.

Gale, J. E., 1980. Hydrogeologic data from Stripa testing programs. Berkeley, Lawrence Berkeley Laboratory, Technical Report, SAC report, both in preparation.

Gale, J. E., and Raven, K. G., 1981. Effects of sample size on the stress-permeability relationships of natural fractures. Berkeley, Lawrence Berkeley Laboratory, LBL-11865, in press.

Gale, J. E., and Witherspoon, P. A., 1979. An approach to the fracture hydrology at Stripa--Preliminary results. Berkeley, Lawrence Berkeley Laboratory, LBL-7079 (SAC-15).

Gale, J. E., Quinn, O., Wilson, C., Forster, C., Witherspoon, P. A., and Jacobson, L., 1979. Hydrogeologic characteristics of fractured rocks for waste isolation--The Stripa experience. In Proceedings, Scientific Bases for Nuclear Waste Management, Boston, Massachusetts, November 1979, p. 507-518.

Gale, J. E., Fritz, P., Witherspoon, P. A., Barker, J., and Wilson, C., 1980. Hydrogeological and geochemical characteristics of the Stripa site. In proceedings, Rockstore '80, Stockholm, Sweden, June 23-27, 1980.

Olkiewicz, A., Gale, J. E., Thorpe, R., and Paulsson, B., 1979. The geology and fracture system at Stripa. Berkeley, Lawrence Berkeley Laboratory, LBL-8907 (SAC-21).

Witherspoon, P. A., Gale, J. E., Nelson, P., Doe, T., Thorpe, R., Forster, C., and Paulsson, B., 1979a. Rock mass characterization for storage of nuclear wastes in granite. Fourth Congress, International Society for Rock Mechanics, Montreaux, Switzerland, September 2-9, 1979.

Witherspoon, P. A., Wilson, C., Long, J. C. S., Dubois, A. O., Gale, J. E., and McPherson, M., 1979b. The role of large-scale permeability measurements in fractured rock and their application at Stripa. Berkeley, Lawrence Berkeley Laboratory, LBL-9903.

Witherspoon, P. A., Cook, N. G. W. and Gale, J. E., 1980a. Geologic storage of radioactive waste: Results of field investigations at Stripa, Sweden. Science, in press.

____, 1980b. Progress with field investigations at Stripa. Berkeley, Lawrence Berkeley Laboratory, LBL-10559 (SAC-27).

Witherspoon, P. A., Amick, C. H., Gale, J. E., and Iwai, K., 1979. Observations of a potential size effect in experimental determination of the hydraulic properties of fractures. Berkeley, Lawrence Berkeley Laboratory, LBL-8571 (SAC-17).

STRIPA MACROPERMEABILITY EXPERIMENT

C. R. Wilson

The macropermeability experiment is an attempt to measure the permeability of a large volume of low-permeability, fractured granite. The experiment is being conducted in a 5m x 5m x 33m drift called the ventilation drift at the 335-m level of the Stripa mine in Sweden. Water flow and pressure are being monitored. The experiment began in November 1979, following completion of primary instrumentation, and ended in September 1980.

The primary objective of the experiment is to improve techniques for permeability characterization of large volumes of low permeability rock for regional groundwater studies. In meeting this objective, we expect the results at Stripa to:

1. Measure the hydraulic conductivity of 10^5 to 10^6 m^3 of rock.

2. Confirm analysis of a series of borehole permeability tests.

3. Improve our ability to monitor average in situ water pressures in fractured rock.

4. Evaluate the ventilation technique for flow measurement.

Discussion of the theoretical basis for the experiment and the need for this type of research are presented in earlier papers (Witherspoon et al., 1979, 1980; Long et al., 1980). Some of our more interesting results and interpretations are presented below.

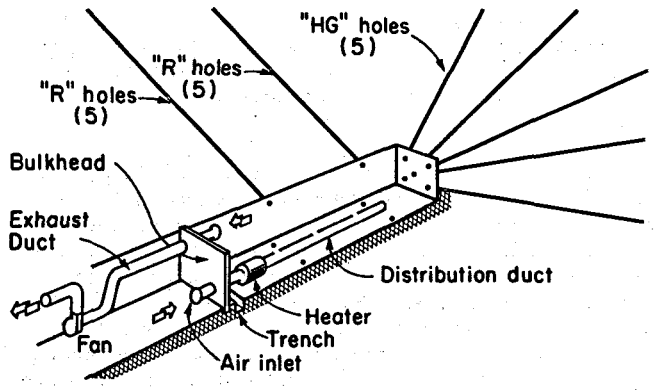

Figure 1. Schematic representation of ventilation drift showing installed equipment and boreholes. [XBL 7910-13004]

A schematic drawing of the experimental setup is presented in Figure 1. Water inflow is measured as the net moisture pickup of the ventilation system inside a sealed portion of the ventilation drift. The ventilation air is heated to improve its moisture carrying capacity and to improve the accuracy of the measurement. Hydraulic gradients are determined by measuring water pressure in 90 isolated intervals of 15 boreholes penetrating the rock mass surrounding the drift. Each isolated interval is about 5 m long, a length intended to include sufficient numbers of open fractures (generally about 15 to 20) within each zone to average the pressure data and to produce a smooth pressure profile, as would be expected in a porous medium.

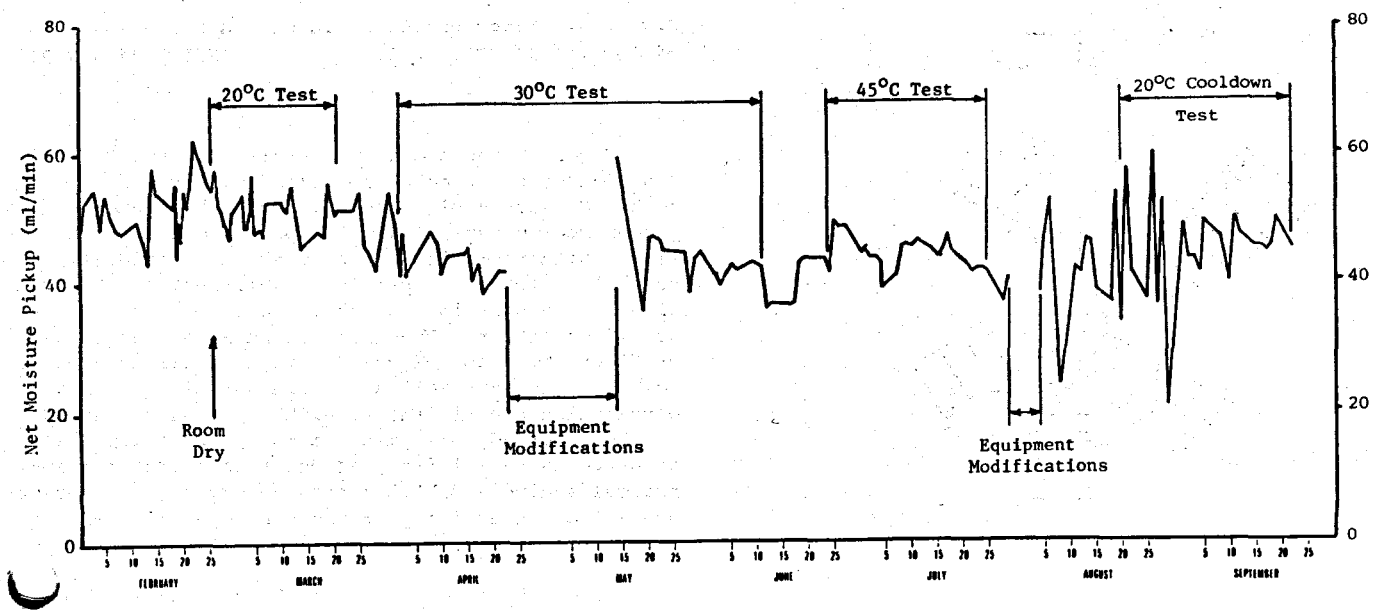

Figure 2. Net moisture pickup by ventilation system for period February 1 through September 30, 1980. [XBL 8011-12709]

Tests were run for three different room temperatures of about 20°C, 30°C, and 45°C, followed by a cooldown test back to 20°C. A room temperature of 20°C most closely reproduces the conditions under which the earlier borehole permeabilty tests were performed. Analysis of the data from these tests is now underway. The two higher temperature tests will provide a higher accuracy of measurement and will permit investigation of temperature effects on the measured groundwater inflow and on the ventilation techniques. Subject to our overall time constraints, an attempt was made to continue all tests until steady state conditions were essentially reached.

Net moisture pickup measurements are shown in Figure 2 for the period February 1 through September 30. Moisture pickup for the 20°C test averaged about 50 ml/min., although the data show considerable scatter due to low measurement accuracy at this low temperature. This first test was actually run at an average room temperature of about 18°C, which was as close to the ambient room temperature of about 15°C as we could operate while still evaporating all the incoming moisture. Water pressures measured in the various isolated zones of the boreholes are shown in Figure 3 for the ten R-holes and Figure 4 for the five HG-holes.

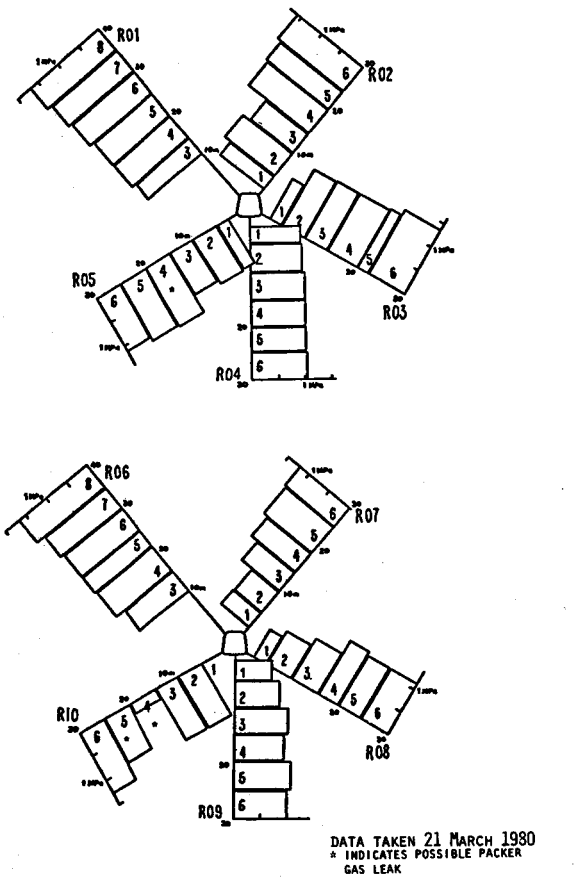

Figure 3. Water pressures in the R-holes measured at end of 20°C test. [XBL 8011-12710]

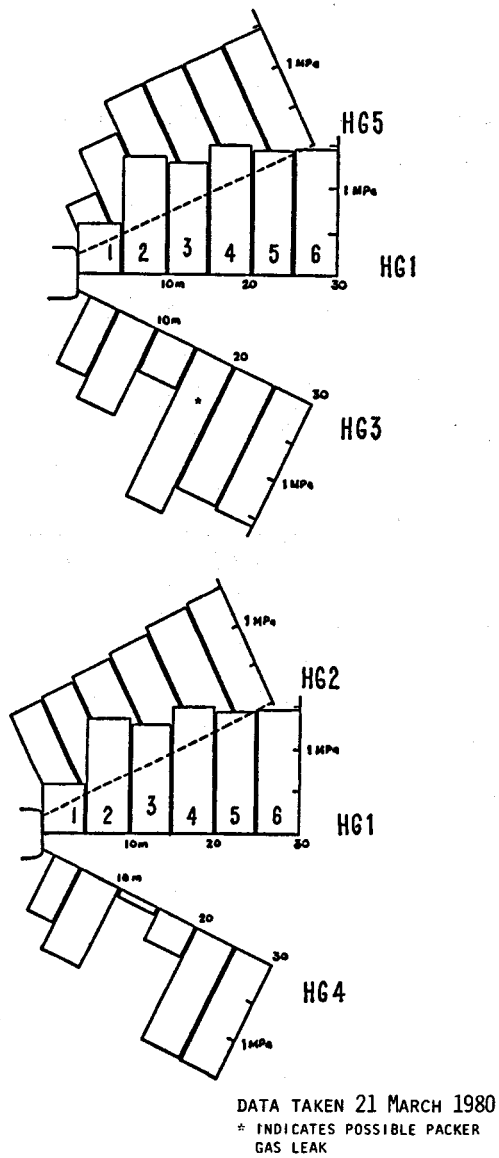

Figure 4. Water pressures in the HG-holes measured at the end of 20°C test. [XBL 8011-12712]

Figure 5 shows a distance-drawdown type semi-log plot of the R-hole pressure data for the 20°C test. On such a plot, purely radial homogeneous porous medium type flow will appear as a straight line. Data from four out of the ten individual boreholes plot as surprisingly well-defined straight lines, with correlation coefficients on the order of 0.9 or better. These are shown as dashed lines on Figure 5. The weighted average of all data points plots very well as a straight line, with a correlation coefficient of 0.98. Assuming that 80% of the observed 50 ml/min net moisture pickup occurred as radial flow, as determined from a theoretical analysis of flow into the drift, the average hydraulic conductivity of the monitored rock mass is about 1.0×10^{-10} m/s.

It may be noted on Figure 5 that the weighted average line and the individual borehole lines would indicate a water head significantly higher than the

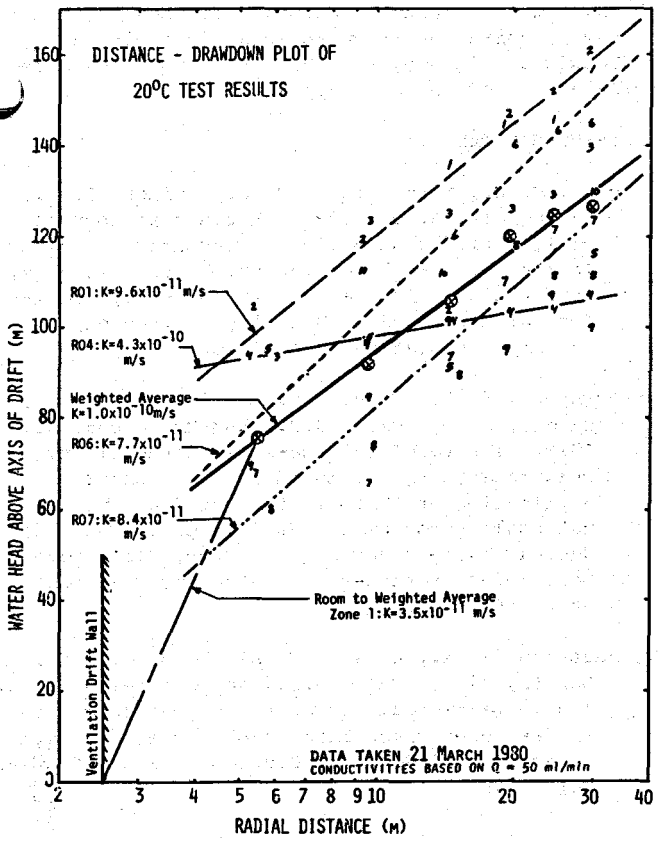

Figure 5. Distance-drawdown plot for 20°C test. [XBL 8011-12708]

actual head if projected to the ventilation drift wall. This indicates that a skin of lower permeability rock exists between the drift wall and the zone 1 measurements. If this skin is assumed to be homogeneous and about 2.5 m thick, its hydraulic conductivity would be about 3.5 x 10^{-11} m/s, or about one-third of the average conductivity of the rock mass. If the skin were thinner, its conductivity would be even smaller.

Heater power was increased on April 2 to raise the room temperature to 30°C for the second constant temperature run. The target room temperature was reached by April 16, but the increase in temperature was accompanied by a decrease in net moisture pickup of the ventilation system of about 16%, dropping from about 50 ml/min under the 20°C test to about 42 ml/min at 30°C. This test was interrupted for about three weeks to modify the equipment to permit a more precise monitoring of net moisture pickup. The heater unit was modified to recirculate air within the room, and the air flow monitor was modified to measure considerably lower air flow rates. Calibration accuracy was improved by replacing the 380-mm diameter air duct with a 165-mm diameter duct. Measurements recommenced for the 30°C run on May 14 and the moisture pickup again stabilized at about 42 ml/min. The 30°C test was concluded on June 10.

Figure 6 shows a distance-drawdown plot of the pressure data for the 30°C test. Comparison with Figure 5 indicates that pressures are generally higher than for the 20°C test, with the greatest increase occurring nearest the drift. The pressures reacted in a manner which tends to compensate for the observed drop in net water inflow, such that the computed rock mass permeability tends to remain stable. Based upon the weighted average values of all pressure data and on an observed net moisture pickup of 42 ml/min., the computed rock mass hydraulic conductivity for the 30°C run is 9.4 x 10^{-11} m/s. Thus, although the drop in observed moisture pickup was on the order of 16%, the compensating increase in water pressure resulted in a drop in computed hydraulic conductivity of only 6%, which is well within experimental error. We interpret this to indicate that the conductivity of the rock mass remained essentially unchanged as the room was heated, while the conductivity of the skin around the drift decreased. It should be noted, however, that the above data and interpretations are all considered preliminary, and may be changed when the complete experimental results become available.

The reasons for the existence of the apparent skin of lower-permeability rock around the drift and for its change in hydraulic conductivity as a function of room temperature are not known. However, it is probably due to thermal expansion of the rock and/or chemical precipitates left in the rock by the evaporating water.

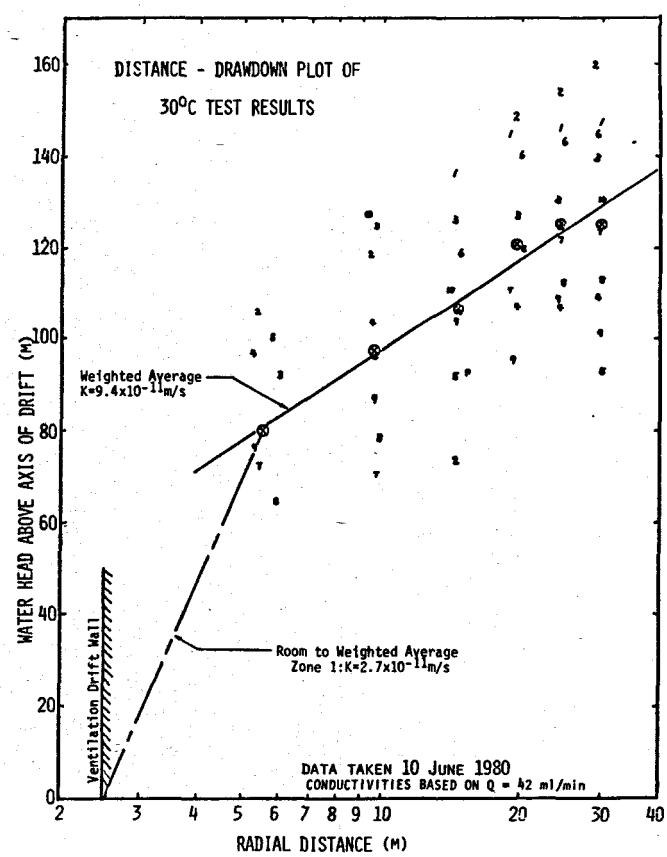

Figure 6. Distance-drawdown plot for 30°C test. [XBL 8011-12711]

After some initial surges due to changing room temperature and fan speed, the net moisture pickup for the 45°C test settled back to about 43 ml/min, which is essentially identical to the 42 ml/min pickup observed at 30°C. It would thus appear that for the limited duration of the 45°C test, the approximately 15°C increase in room temperature did not produce a further decrease in net moisture pickup. Following the 45°C test, the room was cooled as quickly as possible and the 20°C cooldown test was considered to have begun when the room air temperature reached 20°C. The relatively slow but progressive increase in net moisture pickup during this final test, as shown in Figure 2, confirms that the heat added to the room and the rock during earlier tests was indeed responsible for the previously observed decrease in net moisture pickup. Time constraints required ending the cooldown test before it could be determined if the groundwater system had stabilized. The average net moisture pickup as of the end of the cooldown test was about 47 ml/min. Preliminary data analysis for both the 45°C and the 20°C cooldown tests is now underway.

The initial results of the macropermeability experiment show that the ventilation and pressure measurement techniques applied at Stripa can be employed to generate reproduceable results in the measurement of low hydraulic conductivities in large volumes of fractured rock. Our tests have shown, however, that the accuracy of these techniques is quite sensitive to local geologic and hydrolgic conditions, and their use should be carefully evaluated for each application.

REFERENCES CITED

Long, J. C. S., Witherspoon, P. A., Wilson, C. R., and DuBois, A. O., 1981. Large-scale permeability testing at Stripa. Presented at Third Invitational Well Testing Symposium, Berkeley, Lawrence Berkeley Laboratory, Berkeley, California, March 1980. Berkeley, Lawrence Berkeley Laboratory, LBL-12076.

Witherspoon, P. A., Wilson, C. R., Long, J. C. S., DuBois, A. O., Gale, J.E., and McPherson, M., 1979. The role of large-scale permeability measurements in fractured rock and their application at Stripa. Presented at International Symposium on the Scientific Basis for Nuclear Waste Management, Boston, Mass. November, 1979. Berkeley, Lawrence Berkeley Laboratory, LBL-9903.

Witherspoon, P. A., Wilson, C. R., Long, J.C. S., DuBois, A. O., Gale, J.E., and Galbraith, R. M., 1980. Large-scale permeability measurements in fractured crystalline rock. Presented at International Geologic Congress, Paris, France, July 1980.

APPLICATION OF GEOPHYSICAL METHODS AT STRIPA

P. H. Nelson

The geophysical program at Stripa was designed to provide data and interpretations relevant to the rock mechanics and fracture hydrology programs. Borehole logging techniques and the emplacement of ultrasonic transducers around the heater experiments have provided the chief means of investigation. Among the objectives are the mapping of fracture frequency and fracture location, the assessment of geological heterogeneity of the rock mass, and the monitoring of time-dependent changes induced by the heating and cooling of the rock mass during the heater experiments.

Data acquisition terminated in fiscal 1979 with the close of Lawrence Berkeley Laboratory (LBL) field operations at Stripa. What follows is a summary of salient findings made thus far.

RADON TRANSPORT IN GROUNDWATER

Total count gamma ray logs were run in most of the surface and underground boreholes at Stripa (Nelson et al., 1980). Ordinarily, the total count rate measured by a borehole probe simply detects the summed gamma emissions of all isotopes in the three major decay series occurring naturally in rock--potassium, thorium, and uranium. However, at Stripa an unusual circumstance occurs. The groundwater contains sufficient amounts of radon to be observed on the total count gamma-ray log, over and above the gamma contribution from the rock itself. These very unusual, high radon levels occur because: (1) the uranium content in granite is high, between 35 and 40 ppm, (2) the uranium seems to be localized along fractures; and (3) groundwater flow is along fractures in low-porosity rock so that dilution is minimal, and the flow rates are high enough to bring in sufficient radon to be detected.

A simple thin-crack model for radon transport in fractured media is shown in Figure 1 where it is assumed that water flowing radially inward along a fracture enters a borehole, flows upward in the bore, and exits the hole at the collar. If the radon decay rate is λ, then using the parameters defined in Figure 1, the entering concentration at the wellbore is

$$C_o = \frac{E}{\lambda h}\left[1 - \exp\frac{-\lambda h\pi(b^2 - a^2)}{Q}\right].$$

The flow rate and source geometry determine the value of the exponent and hence the dependence of concentration upon flow. If the flow is sufficiently high so that $Q \gg \lambda\pi h(b^2 - a^2)$, then the above equation predicts that C_o decreases inversely with Q, which is contradictory to our observations at Stripa.

If, on the other hand, the flow rate is low enough or the source area large enough that the fluid residence time within the source area is several half-lives or more, so that $Q \ll \lambda\pi h(b^2 - a^2)$, then the exponent can be ignored and $C_o = E/\lambda h$. Under these conditions the entering concentration is independent of flow rate and dependent upon geometry only through the fracture width h. Therefore, we expect the radon concentration in groundwater entering a borehole to be reasonably constant, subject only to local variations in radon emanation and crack aperture.

If radon enters at one fracture intercepting a borehole and moves upward within the water column without diffusion or dispersion, then a single exponential decay with distance z from the source should be observed. The travel time from the entry point to the observation point in a hole of area A is simply Az/Q, so the concentration $C(z) = C_o\exp(-Az/Q)$.

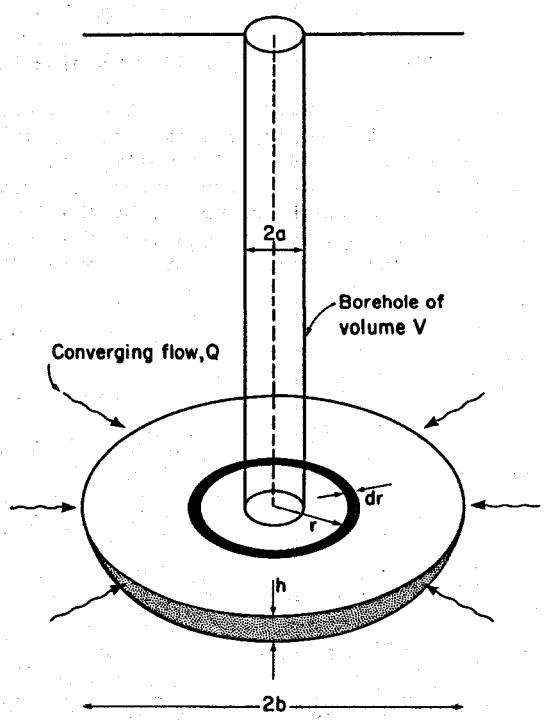

Figure 1. Thin crack model for radon transport. Water flow radially at a rate Q through a thin crack of aperture h into the borehole. The crack contains a circular source area of outer radius b which produces radon atoms at a rate E.

[XBL 802-6794]

Hence, if the logarithm of the concentration, or equivalently the gamma-ray count rate, is plotted against depth, a straight-line fit to the decay will give the flow rate Q if the single-entry no-mixing conditions prevail.

Figure 2 gives an example where this technique is applied to a gamma log from borehole S2, a 40-m angle hole alongside the time-scale drift. A background count rate of 200 counts per second has been subtracted from the logs to remove the counts contributed by the radioelements in rock, the remaining counts contributed by radon daughter products in the water-filled borehole. The three logs, run on three separate dates, show a progressive increase in count rate, attributed to an increased inflow rate over the 1.5-yr time span. The slope of curve 2, which loses half its activity over 9-m length, corresponds to a flow rate of 11.5 liters/day, a rate which was confirmed shortly after with the bucket-and-stop watch method measuring the outflow at the collar.

A more complex example is shown in Figure 3, where the gamma log is shown along with determinations of the activity (approximately 200 cps) in rock core specimens established in the low-background counting facility at LBL. Borehole SBH1 is a slant hole, with the water level at 80-m slant depth. The high count rate above the water level is caused by radon introduced into the wellbore by groundwater infiltrating into the open hole and trickling down the lower side. Water entering the hole gradually releases its radon to the air as it trickles down the hole. Once the radon-charged water reaches the top of the water column, the count rate drops because the water has already released radon to the air, where the solubility is higher.

Spikes and other fluctuations in the log are caused by geological changes, such as the granite-metamorphic contact at 208 m. The metamorphics contain lower uranium and thorium concentrations, as shown both by the single datum and by the lower gamma log response. Within the granite, the count rate exceeds 300 cps, except at depths greater than

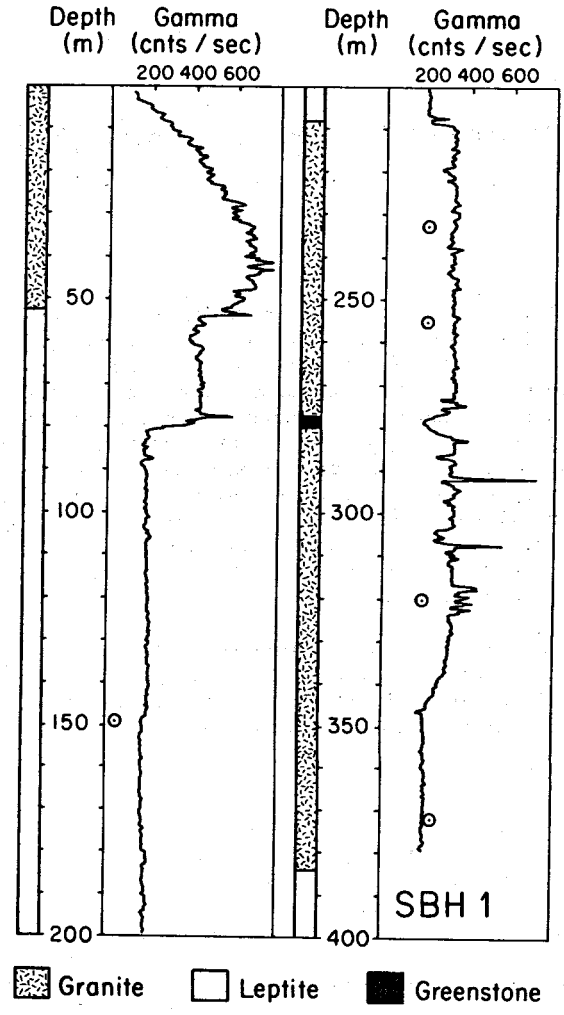

Figure 3. Complete gamma log of hole SBH1, logged in February 1978. The five data points are computed from laboratory spectral gamma analyses of core samples. [XBL 808-7296]

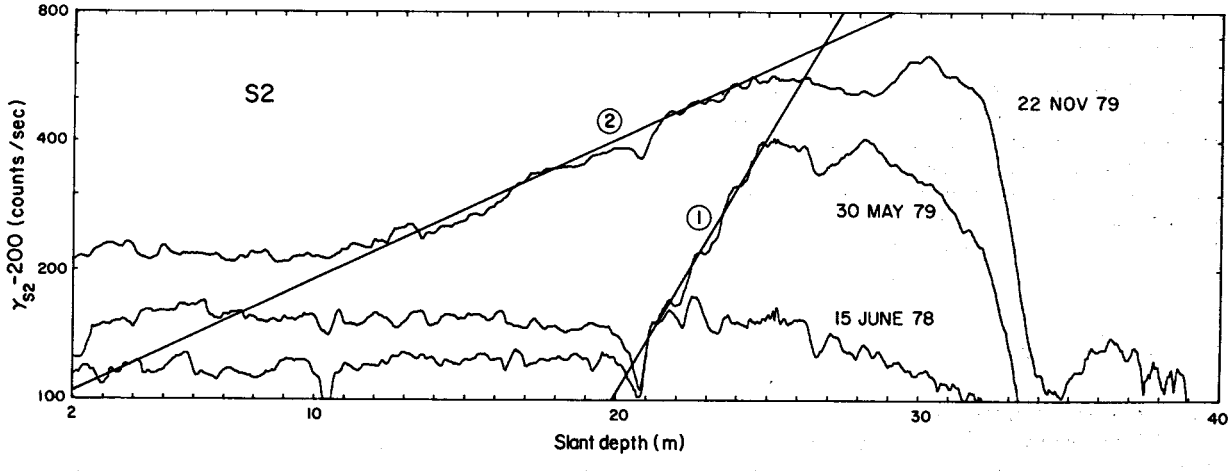

Figure 2. Logarithmic plot of S2 gamma logs for three different dates. The 200 cps background due to the rock and the anomaly at 25 m have been subtracted. The slopes of lines 1 and 2 indicate flows of 3.0 and 11.5 liters/day, respectively. [XBL 802-6791]

345 m, where the count rate drops to the 200 cps level contributed by the rock alone. As a result, the radon-charged groundwater exits the hole between 320 and 345 m, with static conditions below that depth. Because the count rate is relatively constant above the exit zone, the flow rate must be high compared to the radon decay rate. A simple calculation shows that the flow exceeds 1000 liters/day.

Hence, at Stripa, the gamma log serves as a flow profile, locating zones of water entry (or loss) by an increase (or decrease) in the total activity. If mixing within the borehole does not occur, the activity decreases exponentially along the hole away from the entry point, resulting from the steady decay of radon. As we have shown, the rate of radon decay can then be used to estimate the volumetric flow rate.

It is important that the natural radioelement distribution in rock and groundwater at a waste storage site be carefully determined during the site characterization phase. Even with careful baseline studies, one must remain aware that the natural radioactive component of groundwater may change due to changes in the hydrological regime.

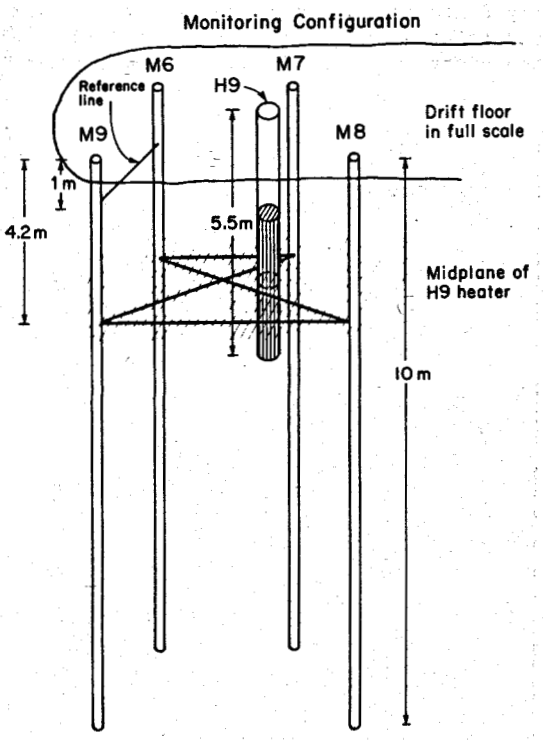

Figure 4. Heater H9 (3.5 kW) is centered in a large borehole 4.2 m below the floor of the underground drift. Only four of the numerous instrumentation boreholes surrounding the heater are shown here. In this configuration sonic transducers in each of the four holes track the sonic wave propagational speed along ray paths in the central plane of the heater. [XBL 7910-13054]

CROSS-HOLE ULTRASONIC INVESTIGATIONS IN HEATED GRANITE

Ultrasonic measurements were made between four vertical holes in the vicinity of the 3.5-kW heater experiment, using the configuration shown in Figure 4. The measurement program involved pairs of transmitting and receiving sondes inserted at 4.2-m depth to obtain data over the ray paths indicated in Figure 4. The sondes were removed and reinserted at regular intervals during the 18-month heater operating time to monitor changes in compressional and shear-wave velocities as the rock mass heated and cooled. Compressional wave arrivals were picked with a precision of ±0.2% on an oscilloscope display.

Preliminary results from the ultrasonic experiment are discussed by Paulsson et al. (1980). Shown in Figure 5 is one of the more dramatic field results: compressional velocities along the four ray paths in the heater mid-plane increase during the first 50-100 days following turn-on of the heater, remain at fairly constant levels for nearly 400 days of operation until the heater is turned off, and then quickly drop. As a check on system consistency, Figure 5 also shows velocities measured along a reference line between two nearby boreholes where the rock is unaffected by temperature or stress increases from the heater.

Although simple in form, the results are an integrated representation of ultrasonic velocity changes along different travel paths, each segment of which responds to different thermal and stress loads. As discussed by Paulsson et al. (1980), how the rock responds at each point along the travel path will depend upon: (1) its composition; (2) the behavior of discontinuities, including the effects of mineralogy and stress-induced fracture closure; (3) the velocity-stress dependence of intact rock; and (4) the in-situ stress state existing prior to heating. Unraveling such dependencies and tying them to changes of rock modulus will represent an important contribution to undertanding the thermal effects induced in the rock mass surrounding the heaters.

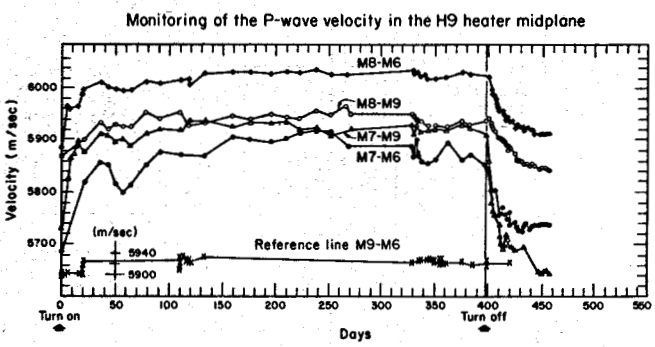

Figure 5. The H9 heater operated at 3600 W for almost 400 days during 1978 and 1979. During this time the transducer array of Figure 4 was used to acquire the velocity changes shown here. The reference line was far enough from the heater that it was unaffected by the heater operation. [XBL 801-6742]

ACOUSTIC EMISSION ACTIVITY

Acoustic emission methods are commonly employed to study the behavior of cracks and crack formation in laboratory samples. We used a simple, single-sensor acoustic emission system to monitor acoustic activity during the cooling of the rock after turn-off of the two full-scale heater experiments (Paulson et al., 1980). Although the lack of multiple sensors made it impossible to locate events, it was possible to track the changes in total emissive activity during cooldown of two similar experimental geometries.

As shown in the equipment diagram of Figure 6, emissive waveforms from either the 3.5- or 5.0-kW heater areas were amplified, band-pass filtered, and sent to an oscilloscope which triggered when the preset threshold level was exceeded by a cycle of the waveform. The resulting pulses were counted for one-minute intervals and recorded on paper tape.

Valid data was acquired during the nighttime hours when there was no human activity in the experimental areas. System constancy was checked at several times during the observation period by dropping a steel ball onto a fixed target in each of the areas. The results suggest no discernable loss in response during the first 475 days of data collection.

Observed results from the 5.0-kW experiment are shown in the histogram plot of Figure 7. Plotted in the figure is the number of 1-min intervals per recording day in which a minimum number of cycles were counted. The 3.5-kW experiment produced very similar results. Both exhibit a sudden rise of activity immediately following turn-off of the heaters, but peak activity does not occur before the passing of several more days. Acoustic emissions then diminished over the next 60 days. This behavior contrasts with the displacement and stress measurements which show a maximum rate of change after turn-off.

Stress and displacement gauges are sensitive primarily to the elastic response of rock, whereas acoustic emissions are usually associated with inelastic material behavior such as crack formation

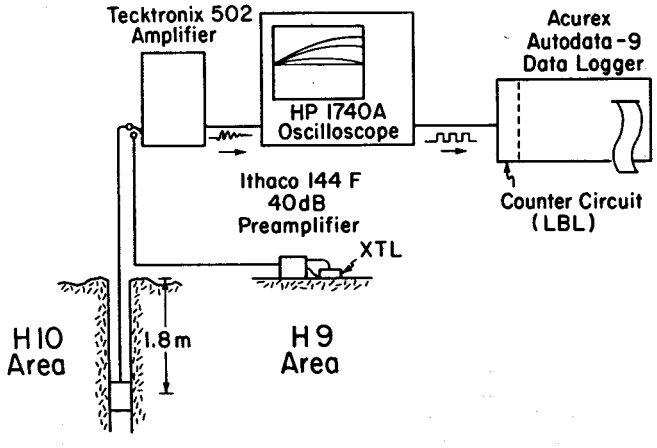

Figure 6. Block diagram of the acoustic emission monitoring system. [XBL 809-2812]

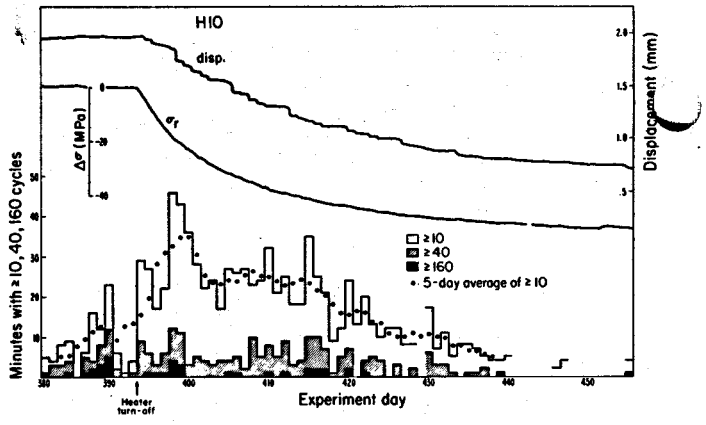

Figure 7. Acoustic emission activity plotted as the number of minutes per overnight recording period in which a minimum number of cycles were counted during the one-minute sampling interval. Also shown are curves for radial stress and displacement for two holes in the H10 heater area. [XBL 809-2806]

or frictional sliding. The magnitudes of rock movements and stress changes associated with acoustic emission events are likely to be less than the sensitivity of the displacement and stress gauges.

To explain the lag of peak acoustic emission activity following heater turn-off, a model was constructed relating the temperature decay rate, and thus the contraction in the rock volume, around the

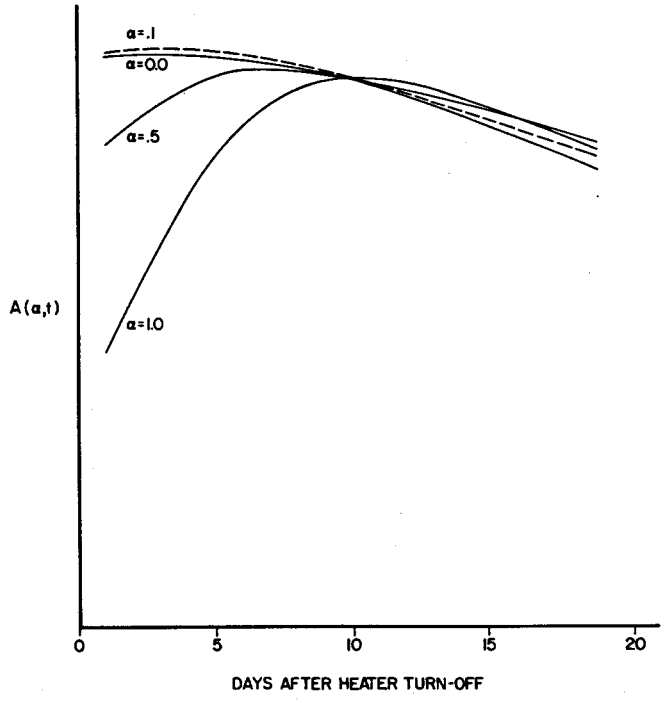

Figure 8. The acoustic emission activity function A (linear scale) computed for turn-off of the 5.0-kW main heater. Curves normalized to the same value of A at day 10 for each alpha value. [XBL 8011-2999]

heater to the acoustic emission activity. The activity detected by the receiver from any one source point is taken to be proportional to the temperature decay at that point modified by the distance from the point to the receiver in order to include the effects of spherical spreading and attenuation of seismic energy. The resulting derived function approximates the recorded acoustic emission data quite well for values of the seismic attenuation coefficient, alpha, of 1.0 (Fig. 8). Lower values of alpha eliminate the ascending portion of the curve, but independent data on Q for the Stripa granite suggest that the higher value for alpha is preferred.

As the Stripa experiment employed only one receiver, the amount of information pertaining to the behavior of rock was limited. A more complete monitoring system for repository sites should at least be capable of locating events and determining their energy. Such a system, described elsewhere in this annual report (see the article in this section by E. Majer), was developed and installed by LBL at the Nevada Test Site waste storage experiment.

ACKNOWLEDGEMENTS

The work of the LBL staff at Stripa who acquired the geophysical data is greatly appreciated. R. Rachiele, A. Smith, and H. Wollenberg contributed to the radon transport analysis. B. Paulsson collected and reduced the ultrasonic data, and R. Rachiele collected and analyzed the acoustic emission results.

REFERENCES CITED

Nelson, P. H., Rachiele, R., Smith, A., 1980. The effect of radon transport in groundwater upon gamma ray borehole logs. Berkeley, Lawrence Berkeley Laboratory, LBL-11180.

Paulsson, B., King, M., and Rachiele, R., 1980. Ultrasonic and acoustic emissions results from the Stripa heater experiments. Berkeley, Lawrence Berkeley Laboratory, LBL-10975.

HYDRAULIC FRACTURING AND OVERCORING IN-SITU STRESS MEASUREMENTS IN A DEEP BOREHOLE AT THE STRIPA TEST SITE

T. Doe

This report summarizes the preliminary results of the in-situ stress measurement program at the Stripa mine in Sweden in fiscal 1980. The Stripa stress measurement program consists of measurements in boreholes drilled from both the surface and underground. During 1980 the stress measurements in a new vertical borehole were completed. The results are complete except for integration of laboratory material properties into the analyses and comparative analysis of the results of the different techniques used. Final analyses of the data will be included in the final report on surface measurements to be completed in March 1981.

The new vertical borehole, SBH-4, is located approximately 700 m north of the LBL-KBS experiments (Fig. 1). SBH-4 was drilled specifically as a stress measurement hole during the summer of 1980. The hole was drilled with an NX conventional double-tube barrel having a hole diameter of 3 in. (76 mm) and a core diameter of 2-1/8 in. (62 mm). The hole was continuously cored, and the core was logged for fractures to help in selection of test zones for the hydraulic fracturing.

During the drilling of the hole two types of measurements were carried out. First, overcoring stress measurements were carried out by the Swedish State Power Board (Statens Vattenfallverk) using their unique deep hole Leeman triaxial cell equipment. Second, hydrologic measurements consisting of single packer, bottom-hole pressure measurements and open hole falling head tests were conducted to provide data on the in-situ water pressures and gross permeabilities of the rock penetrated by the hole. The preliminary results of the overcoring measurements are presented below. However, analyses and results of the pressure measurements and the fracture logging will not be presented until the final report.

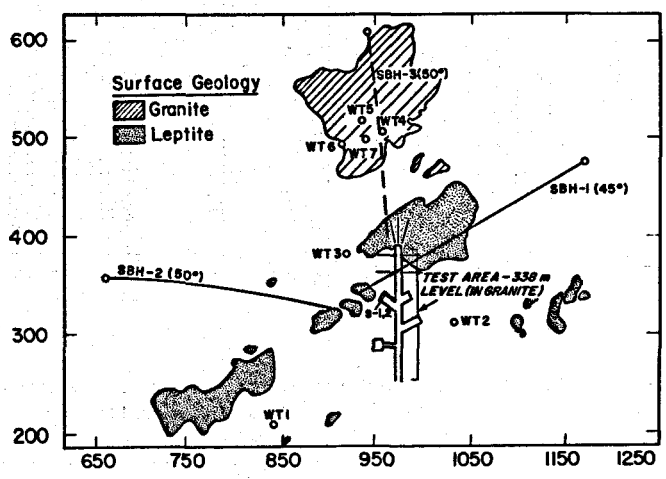

Figure 1. Location of surface boreholes and underground experiment areas at Stripa. SBH-4 is a vertical hole located at the collar of SBH-3.
[XBL 792-7380A]

The drilling of the stress borehole began in late June 1980. The hole was bottomed at a depth of 381 m on September 18, 1980. Since the elevation of the hole is at +29.5 m in the mine system, the bottom of the hole is at 409.5 m or about 60 m below the level of the heater tests. Overcoring measurements were carried out in sets of four every 100 m in the hole. The hydraulic fractures were carried out at intervals of about 50 m, with additional tests below 300 m near the depths of the test facility.

OVERCORING MEASUREMENTS

The procedures used in the overcoring by the Swedish State Power Board are the same as those described in Hiltscher et al. (1979). As with most overcoring techniques, a pilot bore a few decimeters in length is drilled at the end of the main borehole. A strain cell consisting of three strain gage rosettes is cemented to the wall of the pilot hole. After a reading of the strain gage outputs, the strain cell is overcored by a drill with a larger-diameter bit. For the Power Board strain cell, the pilot bore and main borehole diameters are 36 mm and 76 mm, respectively. The change in the strain cell readings after the cell is overcored and brought to the surface are then used to calculate the in-situ stresses using elastic formulae for borehole deformation (Leeman, 1971). The overcoring procedures are shown diagrammatically in Figure 2. Figure 3 shows the strain cell consisting of the three plastic cantilevers with strain gage rosettes hidden within the glue pot at the end.

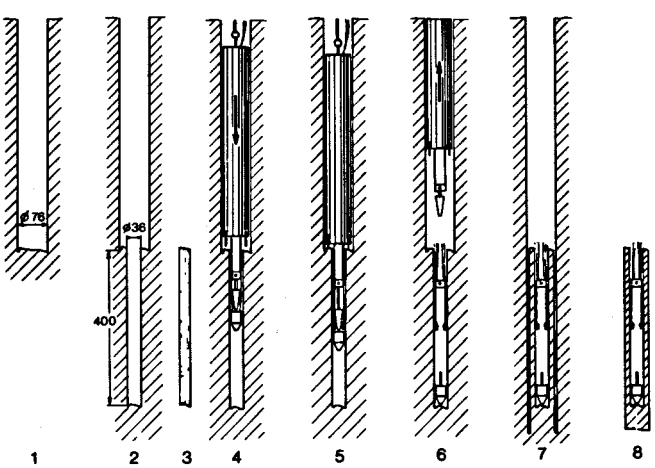

Figure 2. Procedures for overcoring stress measurements. (1) Main 76-mm borehole. (2) Drilling of 38-mm pilot borehole. (3) Appraisal of quality of pilot hole core. (4) Positioning of stress probe before setting gauges. (5) Cementing the gauges, recording initial strains. (6) Release of strain gauge carrier and removal of probe. (7) Overcoring. (8) Removal of overcored gauges and second strain measurement. [XBL-8011-12797]

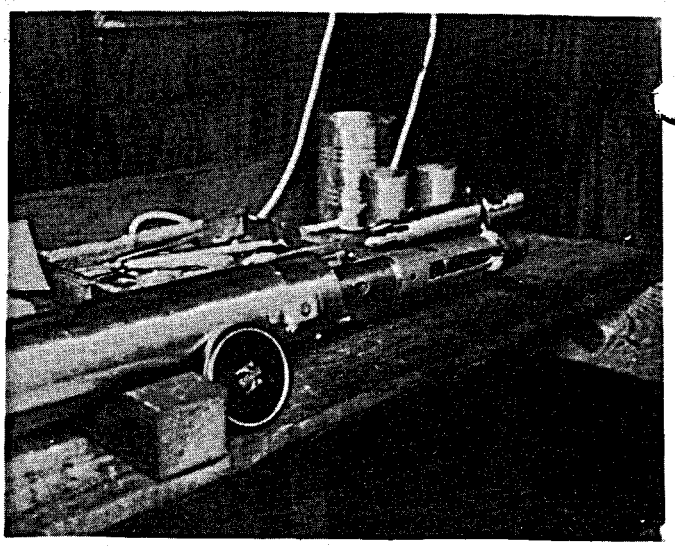

Figure 3. Strain cell and probe used at Stripa. [CBB 809-11093]

OVERCORING RESULTS

Seventeen successful measurements were made in SBH-4 using Leeman overcoring techniques. Stress measurements were performed in groups of four every 100 m of the hole. One additional measurement, performed at 329 m depth, is included with the 300-m level results, where the data are grouped. The orientation data are plotted in equal area projection by depth in Figure 4. Below the first 200 m, the maximum principal stress is within 25 degrees of horizontal with a west to west-northwest orientation.

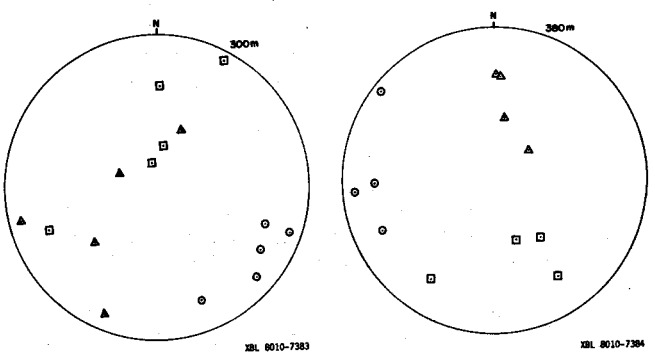

Figure 4. Equal-area plots (upper hemisphere) of deep principal stress orientations from Stripa, SBH-4 overcoring stress measurements. Circles indicate greatest stress; squares, intermediate stress; triangles, least stress. Stress data are grouped by depth range.
[left, XBL-8010-7383; right, XBL 8010-7384]

Plots of the vertical and horizontal stress components are shown against depth in Figure 5. These data are average values of the four to five measurements at their respective depth intervals. It is noteworthy that the vertical stresses measured are in excess of the vertical stress that would be

predicted by the weight of the rock alone. Using the regression lines for the horizontal and vertical stresses, one can interpolate the stress values at the depth of the LBL/KBS heater experiments (348 m in mine coordinates or 318 m depth in SBH-4). These values are a maximum horizontal stress of 3670 psi (25.3 MPa), a minimum horizontal stress of 1650 psi (11.7 MPa), and a vertical stress of 1740 psi (12.0 MPa). The average direction of the maximum principal stress for each depth group is to the northwest, except for the 100-m depth measurements.

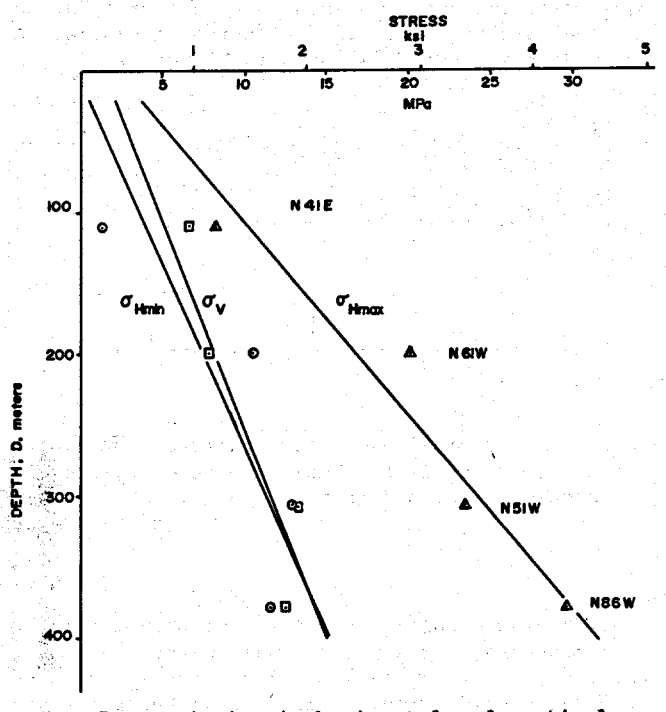

Figure 5. Variation in horizontal and vertical stress magnitudes with depth, SBH-4 overcoring tests. Data points are average values of all measurements in each depth group. Mean orientation of greatest horizontal stress given at right. Triangles indicate maximum horizontal stress; circles, minimum horizontal stress; squares, vertical stress.
[XBL 8010-7391]

HYDRAULIC FRACTURING EQUIPMENT AND PROCEDURES

The hydraulic fracturing of the borehole was performed using a straddle packer assembly consisting of two 2-5/8 in. (67 mm) diameter Lynes packer elements separated by sufficient perforated tubing to give a straddle interval of 2 ft (0.6 m). Mounted above the packer assembly was a watertight housing containing two pressure transducers, one to monitor the pressure in the injection test zone, the other to monitor the packer pressure. Both transducers were strain gage type with pressure rating of 0 to 5000 psi (34 MPa). A nine-conductor electrical cable manufactured by Advanced Cable Co. was used to transmit the signals from the transducers to the surface.

The water for the fracturing was conducted through Hydril 1-in. (25 mm) tubing which had a threaded joint capable of sealing to 10,000 psi (69 MPa). The Hydril tubing also provided the support for the packer assembly for hoisting. The packers were inflated through two 3/16 in. (4.8 mm) Eastman Hytron hydraulic hoses strapped to the Hydril tubing along with the electrical cable. Two hoses were used as a precaution against problems with deflating the packers. Water was used as the packer inflation, and in wells where the water level is depressed--as it is at Stripa due to the drainage effects of the mine--the packers may not completely deflate. The second inflation line could have been used to blow the water out of the inflation line with compressed air had deflation problems occurred.

The pump for the fracturing was a Haskell, air-actuated, hydraulic pump capable of developing a flow of about 8 liters per minute (2 gpm) at 6000 psi (41 MPa). The same pump was used for the inflation of the packers in most tests. The pump was equipped with an air-charged accumulator to dampen the pressure surges of the positive-displacement Haskell pump.

In addition to the pressure transducers downhole, an additional pressure transducer was mounted in the flow manifold on the surface to serve as a backup in the case of electrical failure of the downhole instruments. A Flow Technologies Omniflow turbine flowmeter was also mounted in the flow manifold. The flowmeter was rated for use at 0.25-5.0 gpm (1-20 liters/min).

Data from the pressure transducers and flowmeter were recorded on two time-based strip chart recorders--one recording packer pressure, test zone pressure, and flow rate and the other recording the test zone pressure and manifold pressure. The complete system for the fracturing is shown schematically in Figure 6.

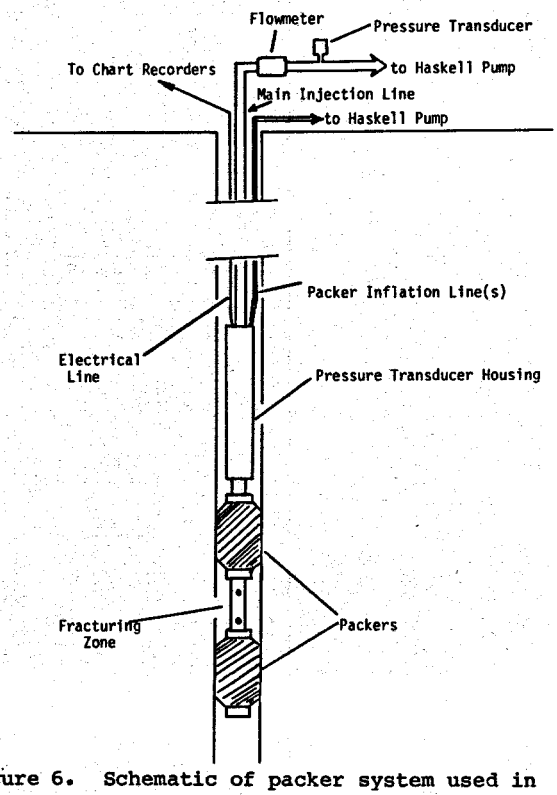

Figure 6. Schematic of packer system used in hydraulic fracturing stress measurements.
[XBL 8010-7386]

During the lowering of the packer assembly into the hole, records were kept of the lengths of each pipe placed in the tube string. The lengths were recorded to the millimeter to assure location of the packers at the desired test zones. The fracture tests were conducted from the top of the hole downward so that the time required to remove the packers would be minimal had problems arisen. Test zones were selected to be free of pre-existing fractures.

Once the packers had been lowered to the desired test zone, the packers were inflated to a pressure exceeding the expected breakdown pressure. For most tests this pressure was about 2500 psi (17 MPa). Originally, we had expected to set the packers at a lower pressure and rely on the pressure increase in the zone between the packers to act on the ends of the packers and increase the pressure of the seal. This interaction of the packer pressure and the injection zone pressure has been observed by most workers engaged in hydraulic fracturing work for stress measurement. We had observed this phenomenon in a 3-in. casing while testing our original system containing packers manufactured by TAM, International. However, after the discovery of leaks in the packers forced us to fall back on a Lynes system, we found the packer pressure was not at all affected by the pressure in the test zone. The packer assembly used in the tests is shown in Figure 7.

Figure 7. Straddle packer system used in Stripa stress measurements. Foreground: upper and lower straddle packers. Background: pressure transducer housing. Hytron tubing on reels and ends of Hyrill rod can be seen in upper right. [CBB 809-11091]

Once the packers were set, the pressure was raised in the test zone at a rate of 2000 psi (14 MPa) per minute until fracturing was indicated by an increase in the pumping rate. As soon as fracturing was felt to have occurred, the manifold was shut in and the pressure was monitored for 2-4 min. This procedure was repeated two to four additional times to observe secondary breakdown pressures and to obtain additional shut-in pressure values. One test, which involved slowly pumping up the test zone to the pressure at which the fracture would just begin to open, was run at each test level to further set the value of the shut-in pressure. A typical test record is shown in Figure 8.

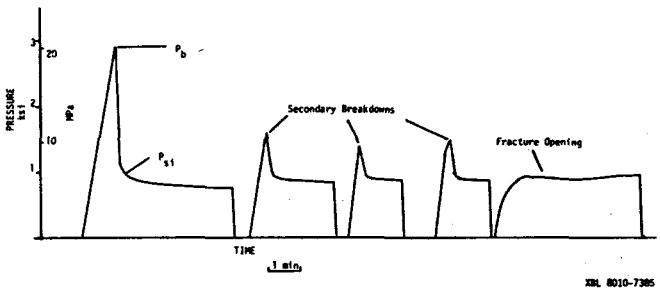

Figure 8. Typical hydraulic fracturing pressure-time record; P_b is breakdown pressure; P_{sj} is shut-in pressure. Record is from TEST 17, 304.9 m. [XBL 8010-7385]

Having completed the fracturing experiment, the pressure on the packers was released at the surface, and the hole was filled with water to speed the packer deflation. Since the packer pressure was being monitored downhole, the release of the packers could clearly by seen by the equilibration of the packer and zone pressure, and damage to the packers from premature hoisting after deflation was easily avoided.

IMPRESSION PACKER EQUIPMENT AND PROCEDURES

Once the fracture experiments were completed, impressions of the test zone were made to determine the orientation of the fractures. The impression packer equipment consisted of a TAM 1-7/8 inch (48 mm) packer element with a removable sleeve coated with a soft rubber capable of extrusion into the fracture under pressure. The packer was placed below a Sperry Sun 1-3/8 in. (35 mm), single-shot, magnetic borehole-survey compass modified to screw directly into the packer end cap. The compass was separated from the packer by 3 ft of nonmagnetic tubing to eliminate any effect the packer might have on the compass. This entire assembly was attached to a wireline and inflated pneumatically through the same Hytron tubing used in the fracturing experiment. The packer was hoisted by a wireline hoist which included a cable counter to assure proper depth of emplacement.

Once the packer sleeve was in place, a film disk was inserted into the camera on the borehole compass, and the timer for the camera was set to record the compass orientation at a time sufficient to allow lowering and inflation of the packer. For

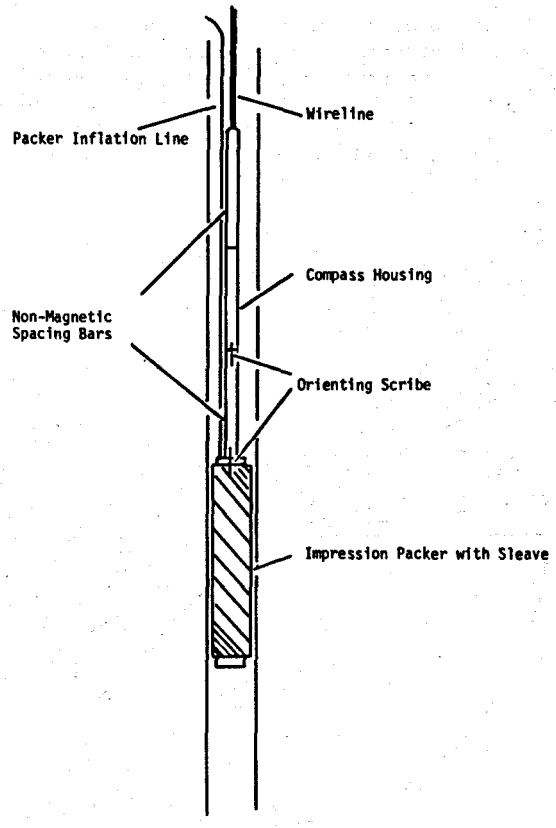

Figure 9. Schematic of wireline impression packer system for fracture orientation. [XBL 8010-7387]

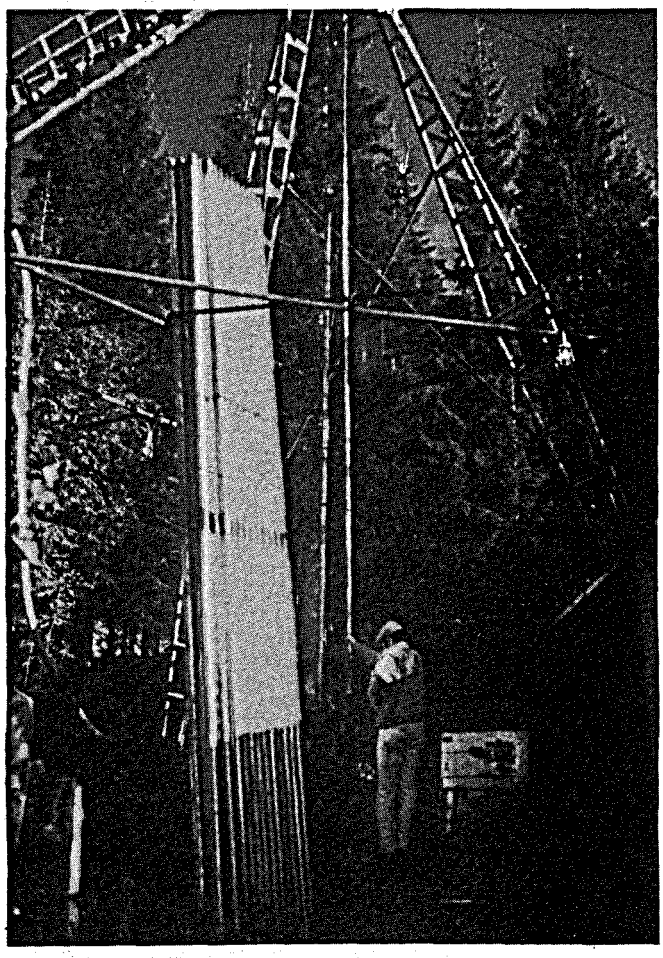

Figure 10. Wireline impression packer system hanging from drill tripod. Impression packer located about one foot (0.3 m) below point where system is being held by M. Moebus. [CBB 809-11089]

the deepest impressions in the hole, this time to exposure was only 45 min, a setting which allowed 15 min for the inflation of the packer. The pressure in the packer was set between the shut-in and the secondary breakdown pressure to assure opening of the fracture and extrusion of the packer rubber into the crack. The packer was left inflated through the exposure of the film disk in the compass for a period of about 30 min. Retrieving the impression packer from the deepest tests took about 25 min, a considerable saving of time over conventional emplacement of packers in rigid tubing. Once the impression system was out of the hole, the film disk was immediately developed and stored. Most of the impression sleeves were used two or three times. As soon as the packer had been retrieved, the impressions from each test were painted on with different colors of paint to avoid confusion between impressions of different tests. The impression system is shown schematically in Figure 9. The system is shown hanging from the tower of the drill rig in Figure 10.

DATA ANALYSIS--FRACTURING TESTS

The stress state was interpreted from the fracturing data using the standard elastic solutions of Haimson (1979)

$$S_{Hmax} = 3\,S_{Hmin} - P_b + T + P,$$

where S_{Hmax} = maximum horizontal principal stress, S_{Hmin} = minimum horizontal principal stress, P_b = first breakdown pressure, T = hydrofracture tensile strength, and P = pore pressure. The minimum horizontal principal stress is equal to the shut-in pressure, which was in turn determined from the sharp break in slope observed in semilog plots of the post-breakdown pressure versus time. The hydrofracture tensile strength was assumed to be 1500 psi. This figure was based on--but slightly lower than--Swan's (1978) Brazilian test data for the Stripa Granite; this downward adjustment is based on the observation that Brazilian test tensile strengths tend to be high compared to hydrofracture tensile strengths. Final calculations of the test results must be made after hydrofracture tensile strength tests are run on the cores from the test zones themselves. Regression lines for the data are shown on the plot of stress versus depth in Figure 11. The vertical stress is calculated using a gradient of 3.73 psi (25.7 kPa) per meter depth, based on the measured density values for Stripa Granite given by Swan (1978).

As shown in the stress-depth plot, the shut-in pressures follow a trend with a slope relatively close to that of the lithostatic gradient but at a somewhat higher stress level. The maximum horizontal stress data follow a similar trend with depth

as the minimum stress data though with somewhat greater scatter. This variability may reflect variations in the tensile strength of the rock which have not yet been taken into account.

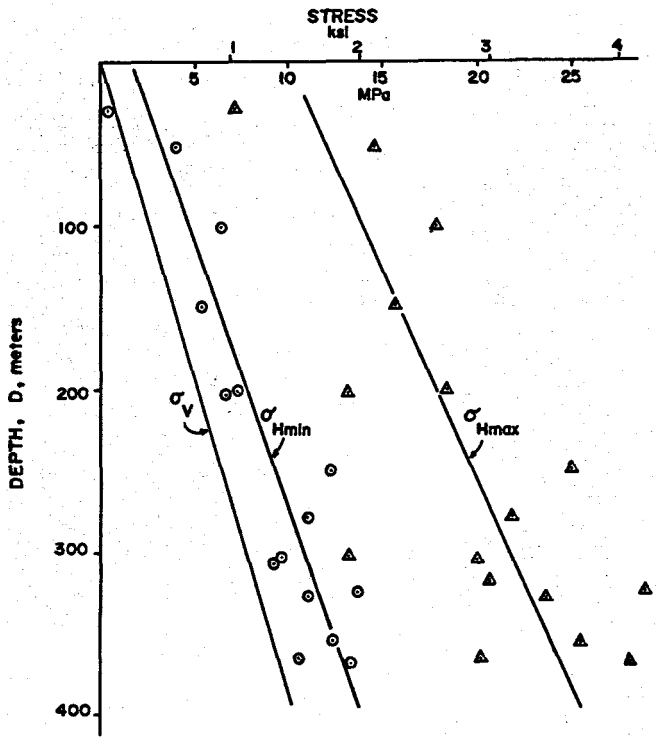

Figure 11. Variation in stress magnitudes with depth as determined by hydraulic fracturing, Stripa, SBH-4. Circles indicate minimum horizontal stress; triangles, maximum horizontal stress. Vertical stress calculated using lithostatic gradient of 3.7 psi (26 kPa) per meter. [XBL 8010-7389]

RESULTS--IMPRESSION PACKER WORK

Successful impressions were obtained for only nine of the tests. Although this is as many impressions as have usually been taken in hydrofracture experiments, a larger number of results would have been more satisfying. The tests without impressions generally appeared to be the result of uneven inflation of the packer with only a fraction of the packer in contact with the borehole. This problem did not appear in the equipment tests at Raymond, California, and seemed to be a greater problem with depth, although successful impressions were obtained for the two deepest SBH-4 tests.

The problem of the uneven inflation of the impression packer might be solved by using elements that are both shorter in length and larger in diameter. Although our original aim in designing the wireline impression packer system was to minimize the size to avoid potential problems caused by getting hung up in the hole, our experience with running the wireline system in high quality rock has given us greater confidence in using larger packers.

Despite the lost impressions, the tests with successful impressions show a reasonably consistent WNW trend to the fracture strikes. The stereographic projection of the fracture planes in Figure 12 shows a set of fractures with a mean strike of N 65 W, with a standard deviation of 28 degrees.

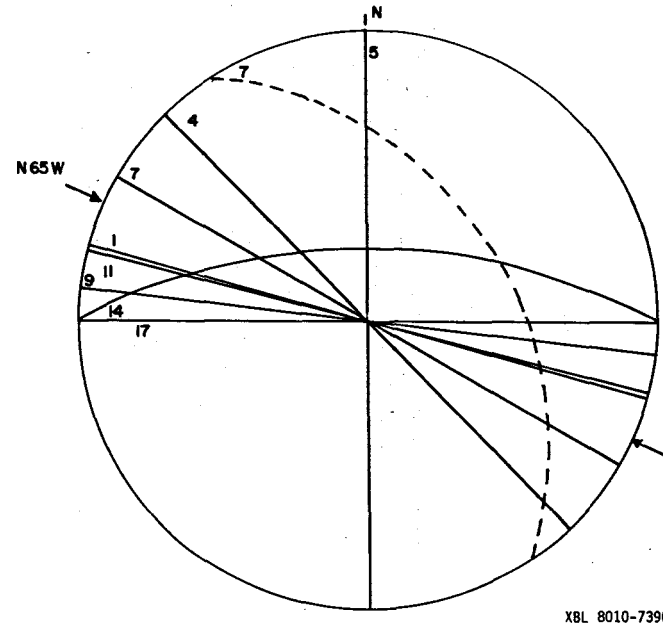

Figure 12. Lower-hemisphere stereographic projection of hydrofracture orientations. [XBL 8010-7390]

STRESS STATE AT STRIPA

Based on the preliminary results of the hydraulic fracturing, the in situ stresses at the level of the LBL-KBS experiments are as follows: The maximum stress at the 345 m level (314 m of hole depth) is about 3230 psi (22.3 MPa) in a N 65 W direction; the minimum horizontal stress is 1620 psi (11.2 MPa); and the vertical stress, calculated from the weight of the overburden, is 1180 psi (8.1 MPa).

REFERENCES CITED

Haimson, B. C., 1978. The hydrofracturing stress measuring method and recent results. Int. J. Rock Mech. Min. Sci., v. 15 p.167-178.

Hiltscher, J., Martna, F., and Strindell, L., 1979. The measurement of triaxial rock stresses in deep boreholes in the design and construction of underground openings. In Proceedings, Fourth Congress of the International Society of Rock Mechanics, v. 1, p. 227-234.

Leeman, E. R., 1971. The CSIR "doorstopper" and triaxial stress measuring instruments. Rock Mechanics, v. 3, p. 25-50.

Swan, G., 1978. The mechanical properties of Stripa granite. Berkeley, Lawrence Berkeley Laboratory, LBL-7074 (SAC-03), 25 p.

MARINE SCIENCES

Environmental aspects of using the oceans as an energy source are being coordinated for the Department of Energy by the Marine Sciences Group of the Earth Sciences Division, Lawrence Berkeley Laboratory (LBL). The technologies being considered are Ocean Thermal Energy Conversion (OTEC), salinity gradients, wave power, tidal power, and ocean currents. At present (November 1980) only OTEC is being funded to a pilot-plant level; the other technologies remain at the feasibility-study level. The Marine Sciences Group acts as lead laboratory for environmental studies, specifically for the OTEC program. As such, LBL is responsible for fundamental research in the tropical oceans, for management of other environmental research groups in the private and public sectors to provide integration of the environmental data, and for insuring compliance with environmental regulations. Research requirements of the OTEC program include collection, analysis, and evaluation of fundamental physical, chemical, biological, and geological oceanographic site and regional data to characterize natural variability. Such studies are used to estimate the energy extractable with minimal or nondetectable environmental change. These studies also provide designers and engineers with the specific environmental conditions required for safe and efficient extraction of the resource.

Thus far, site-specific oceanographic data has been collected in the Gulf of Mexico (two sites), Puerto Rico, Hawaii (two sites), and a regional study in the equatorial South Atlantic. Other potential near-term sites are near Key West, Guam, and the Virgin Islands (Fig. 1). Formal environmental assessments and analyses have been issued for (1) a generic OTEC--1 megawatt plant, (2) programmatic OTEC, and (3) a generic OTEC--10/40 megawatt plant.

This work was supported by the Assistant Secretary for Conservation and Renewable Energy, Office of Solar Power Applications, Ocean Energy Systems Division of the U. S. Department of Energy under Contract No. W-7405-ENG-48.

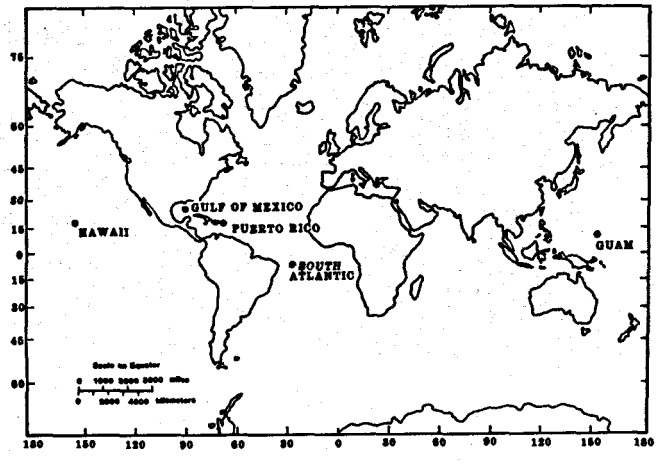

Figure 1. Location of selected sites of interest.
[XBL 8012-13520]

BIOLOGICAL OCEANOGRAPHIC RESEARCH

E. O. Hartwig, C. J. W. Carmiggelt, M. L. Commins, A. T. Jones, and C. Ryan

During the past year the biological oceanography program of the Marine Sciences Group pursued three avenues of research. These are presented below.

SITE DESCRIPTIONS

This was a field effort aimed at providing a biological description of the water masses at potential OTEC sites. The purpose of these studies is to provide information useful to design engineers, environmental engineers, and the scientific oceanographic community. This work was performed by LBL working with local oceanographic institutions such as the University of Hawaii, the University of South Florida, the Rosentiel School of Marine and Atmospheric Science of the University of Miami, and the University of Puerto Rico.

Zooplankton distributions in the upper 1000 m of tropical oceans at OTEC sites vary greatly (Fig. 1). Generally, there is a decrease in zooplankton abundance with depth. In Hawaii, however, there is a subsurface zooplankton abundance maximum. This subsurface maximum also appears in the biomass indicator data (Fig. 2, chlorophyll a, phaeophytin and ATP). The correlation between the two distributions has yet to be proved conclusively. This is partially because in the upper water layers, where organisms are concentrated, their distribution is patchy and their abundance highly variable. These problems may be overcome by extensive sampling over time.

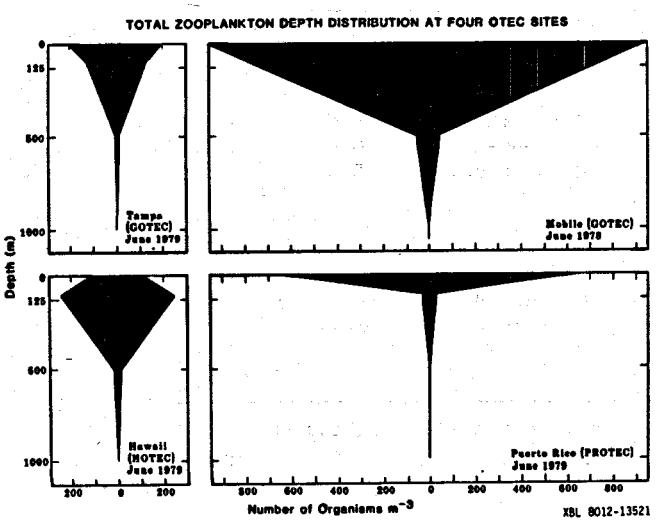

Figure 1. Total zooplankton depth distribution at four OTEC sites. [XBL 8012-13521]

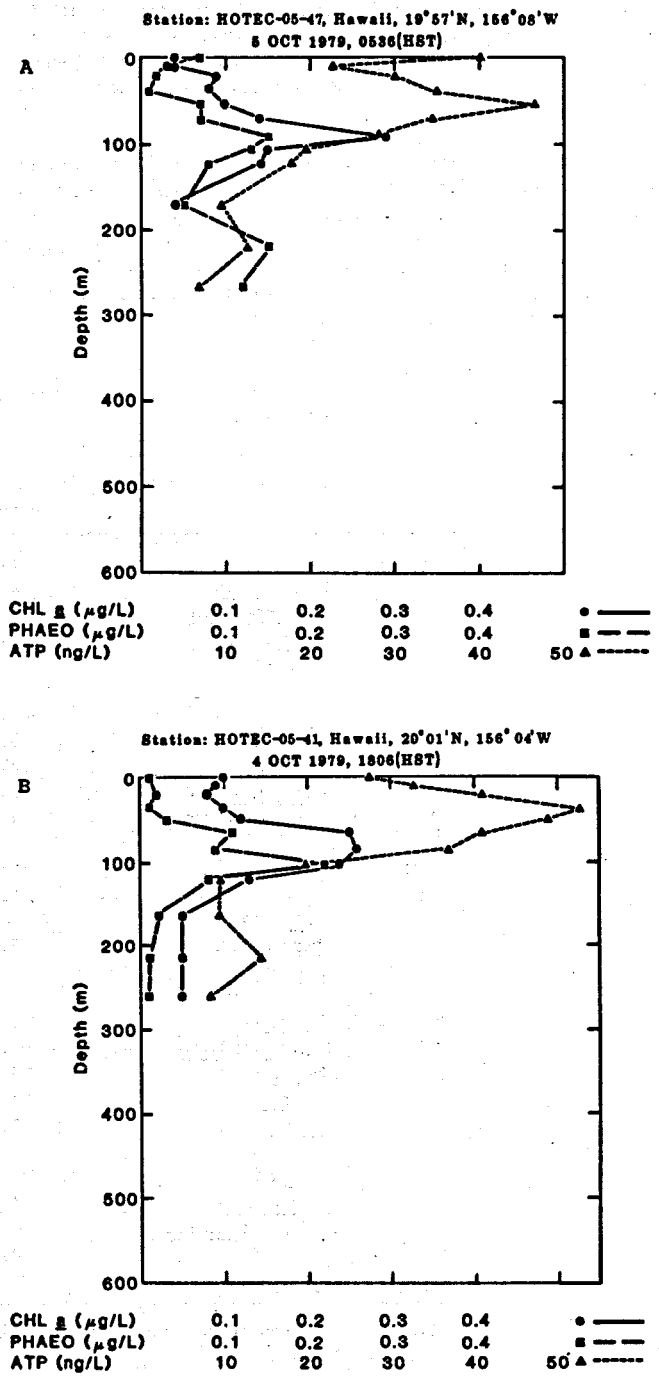

Figure 2. Biomass indicator data. (A) HOTEC site 19°57'N, 156°08'W). (B) HOTEC site (20°01'N, 156°04'W). [A, XBL 8012-13522; B, XBL 8012-13523]

Entrainment and impingement of organisms present a potentially significant impact associated with the operation of an OTEC plant. To assess their importance, the affected communities must be examined. OTEC warm water intakes will entrain organisms from the upper 25 m. This water mass contains a high biomass which varies temporally and spatially. Many zooplankters undergo a diel vertical migration so that their numbers change greatly both with time and with depth. Horizontal variability results from the patchy distribution of zooplankton. These faunal distributions are related to inter- and intraspecific competitive pressures, e.g., predation, feeding, and reproduction. Sampling for zooplankton must, therefore, account for this variability.

OTEC cold water intakes are located at depths of 600-1000 m. These waters contain low densities of organisms whose distribution have yet to be adequately defined because of the problems in sampling at great depths. Data to date indicate no diurnal variability, although we must still address spatial and longer-term temporal variability.

The size of individual zooplankters and the taxonomic composition of the zooplankton community is being investigated to permit a post-deployment assessment of the impact of OTEC on zooplankton. Table 1 shows the variability in taxonomic composition with depth and time of day at the Gulf Coast OTEC site off Tampa Bay (TAM) in Florida.

Taxonomic and distributional studies of micronekton and ichthyoplankton communities were initiated this year at the Puerto Rican OTEC site. The first vertically stratified samplings to 1000 m have been made (November 1980) but are not yet analyzed.

Phytoplankton distributions were examined at the potential OTEC sites using chlorophyll a as the living biomass indicator and phaeopigment as the detrital indicator. ATP (adenosine triphosphate) distributions of total living biomass were then compared to phytoplankton distributions. In Figure 2 the ATP maxima is above the chlorophyll a maxima. This relationship may be the result of changes in the chlorophyll a/ATP ratio in phytoplankton, the presence of a population containing ATP but no chlorophyll a, or both.

Table 1. Taxonomic composition of dominant copepod genera at one Gulf Coast OTEC site.

Sample #	Dominant genera	Percent of total copepods	Percent composition by order		Number of taxa*
TAM 40† (a)	Oncaea	28.6	Calanoids	61.9	30
	Eucalanus	22.6	Cyclopoids	35.7	
	Pleuromamma	17.3	Harpacticoids	0.0	
	Rhincalanus	6.0			
	Conaea	4.8			
TAM 41 (b)	Eucalanus	22.3	Calanoids	60.5	63
	Oncaea	19.8	Cyclopoids	35.7	
	Conaea	12.6	Harpacticoids	0.2	
	Pleuromamma	7.7			
	Clausocalanus	4.8			
TAM 42 (c)	Clausocalanus	21.9	Calanoids	62.3	57
	Oncaea	21.2	Cyclopoids	37.0	
	Oithona	7.0	Harpacticoids	0.5	
	Farranula	6.2			
	Temora	5.7			
TAM 43 (d)	Oncaea	20.3	Calanoids	48.3	42
	Clausocalanus	18.7	Cyclopoids	43.0	
	Temora	14.9	Harpacticoids	0.5	
	Farranula	10.4			
	Oithona	7.0			
TAM 45 (e)	Temora	26.8	Calanoids	75.7	53
	Farranula	11.9	Cyclopoids	23.6	
	Clausocalanus	10.7	Harpacticoids	0.5	
	Oncaea	8.9			
	Undinula	6.8			

* Represents number of species identified plus genera not identified to species level.
† TAM: Gulf Coast OTEC site of Tampa Bay, Florida.

(a) 1000-800 m day
(b) 800-200 m day
(c) 200-0 m day
(d) 25-0 m day
(e) 25-0 m night

ZOOPLANKTON STUDIES

Upper Level (25-0 m) Distribution

The fine-structure distribution of zooplankton within the upper 25 m water column (OTEC warm water entrainment depths) is not known. We recently completed the first vertically-stratified sampling at 5 m intervals from the surface to 25 m. A preliminary look at these samples revealed little difference between the various layers except in the surface layer (neuston) which appeared to contain a higher biomass. Further taxonomic and distributional statistical analysis is being completed.

New Sampling Apparatus

A simplified cod-end (Fig. 3) for zooplankton nets was invented and sufficiently field-tested (Duncan, 1981, in press, patent applied for). Its simplicity of use and effectiveness reduce the time needed to complete a net station. Further simplifications in use of the invention are being field-tested off the southeast coast of Puerto Rico.

Food Web Interrelationships

As part of this study, T. Hopkins of the University of South Florida is examining the gut contents of micronekton. This work concentrates on a couple of well-represented species to use as models for other similar organisms. G. Gunter and J. Steen of the Gulf Coast Research Laboratory (GCRL), Ocean Springs, Mississippi, are concentrating on upper water column zooplankton. The investigation uses both the literature and state-of-the-art techniques in scanning electron microscopy, fluorescence microscopy, and histochemistry to assess the food of zooplankton.

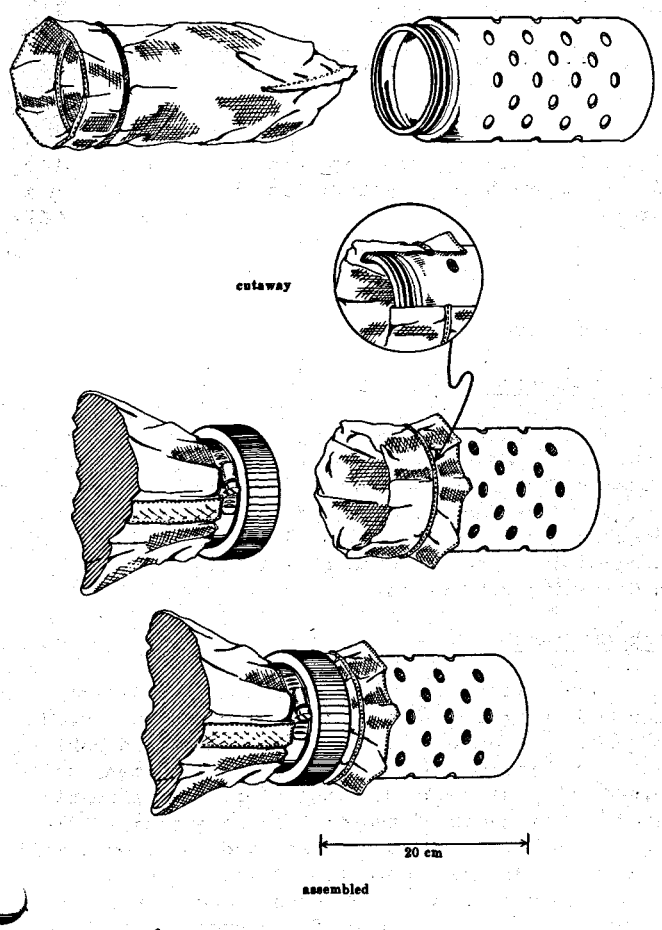

Figure 3. A simplified cod-end for zooplankton nets. [XBL 809-11788]

Diurnal Variability

A series of replicate net tows collected through a 24-hour period was examined by Gunter and Steen of GCRL. Analysis of the number of zooplankters and the taxonomic composition of the samples has been completed. The data are being statistically analyzed for diel variability.

PHYTOPLANKTON STUDIES

Biomass, Numbers and Taxonomy

Methods for analyzing phytoplankton biomass (Estrella and Hartwig, 1980) plus phytoplankton numbers and taxonomy at potential OTEC sites were examined. The distribution and composition of taxonomic groups varied greatly. The major groups were diatoms, dinoflagellates, unidentified nannoplankton (< 5 μm), and unidentified others. This unidentified portion constituted 10% to 70% of the total phytoplankton community. With such a high percentage of unidentified phytoplankters, it will not be possible to assess the effect of OTEC on total phytoplankton species distribution. However, OTEC's effect on taxonomic groups, e.g., diatoms and dinoflagellates, and their size distribution can be assessed.

As a by-product of the phytoplankton studies, the Marine Sciences Group has been investigating preservation and counting methods. Glutaraldehyde, Lugol's iodine, and chromacetic acid preservatives were tested. Chromacetic acid proved to be the poorest preservative both in the quality of preservation (flagella removed, cells distorted) and in the quantity of cells preserved. Gluteraldehyde and Lugol's iodine preserved equally well, but because of the toxic nature of gluteraldehyde, Lugol's iodine is preferred.

Phytoplankton cells are counted using an inverted light microscope after settling of the cells into counting chambers. Random fields of known area are counted and the number corrected for the total area. However, we have found that there is an edge effect in the chamber; reduced numbers are present within two fields of view of the edge. This effect must be accounted for in the final area correction.

Phytoplankton Size Versus Productivity and Percent of Total Phytoplankton Biomass

Data collected and analyzed by Paul Bienfang of the Oceanic Institute, Waiomanalo, Hawaii, conclusively showed the importance of nannoplankton biomass in the tropical waters off Hawaii. Additionally, there was a strong indication that production was nutrient-limited and variations in productivity were not accounted for by variations in phytoplankton biomass. Correlations between dead

phytoplankton and integrated ammonia concentrations and integrated primary production indicated that regenerated nutrients were primarily responsible for observed temporal variability in photosynthesis (Bienfang and Szyper, 1980).

Bioassays

Bioassays were initialed in Hawaii to assess the impact of mixing deep, nutrient-rich water with the near-surface nutrient-depleted waters. The bioassays also looked at the impact of an ammonia (OTEC working fluid) spill on surface waters. Figure 4 shows that the addition of ammonia to water collected at 25 m produces an initial increase in the rate of $H^{14}CO_3^-$ uptake and that the ammonia is preferentially taken up until the ammonia level is reduced below approximately 1.0 µg-atm/liter. When nitrate-rich 800-m water is mixed with 25 m and 100-m water, the same basic response is observed and nitrate is utilized (Fig. 5).

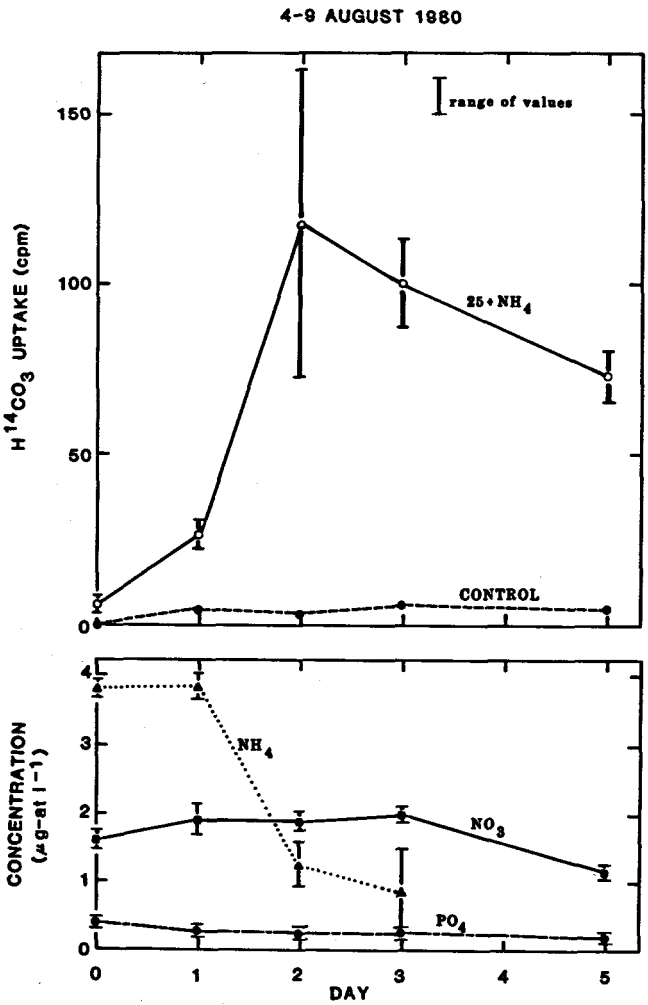

Figure 4. Bioassay showing impact of the addition of ammonia to water collected at 25 m.
[XBL 8012-13524]

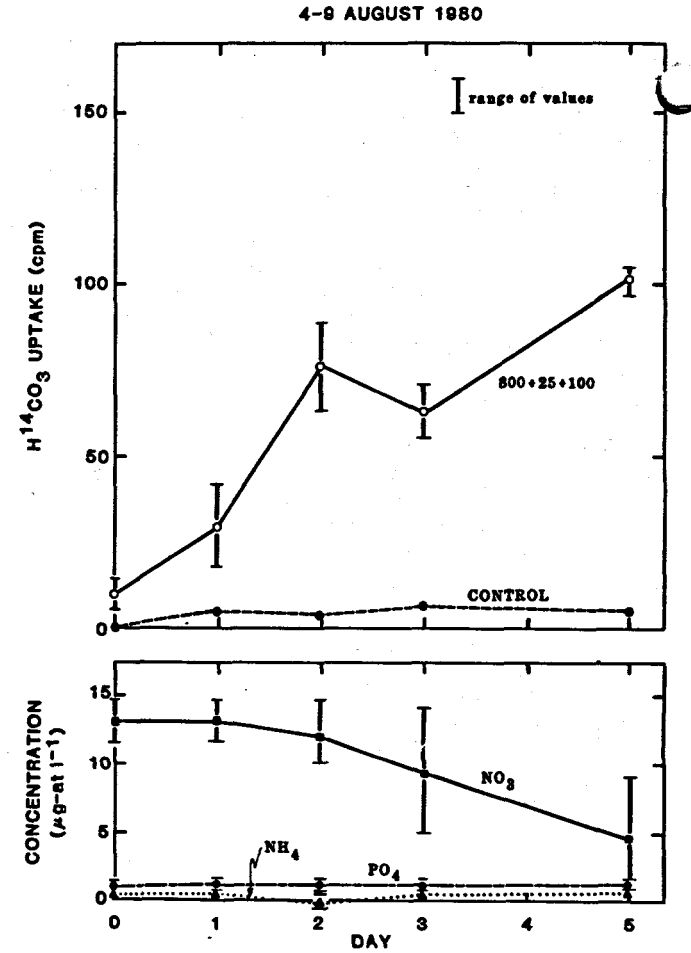

Figure 5. Bioassay showing results of the mixing of nitrate-rich 800 m water with 25 m and 100 m water.
[XBL 8012-13525]

NEKTON STUDIES

Natural History

Nekton (actively swimming organisms such as fish, squid, and marine mammals) at tropical OTEC sites are being investigated. The known natural history about the permanent or seasonal residents (Jones, 1980; Ryan and Jones, 1980; Ryan, 1980) is being used to predict potential interactions with an operating OTEC plant.

Fish Landings

Faunal lists derived from the marine literature and records of commercial fishermen were used to describe the organisms and their detailed habitat. The long-term records of commercial fishermen, maintained by local government agencies, were investigated for evidence of temporal fluctuations in fishing stocks. The record of fish landings from Hawaii began in 1948; the record from Puerto Rico began in 1967. The data shown in Figures 6 and 7 indicate the highly variable nature of commercial fish landings temporally as well as spatially at a site. This variability makes assessing the impact of an

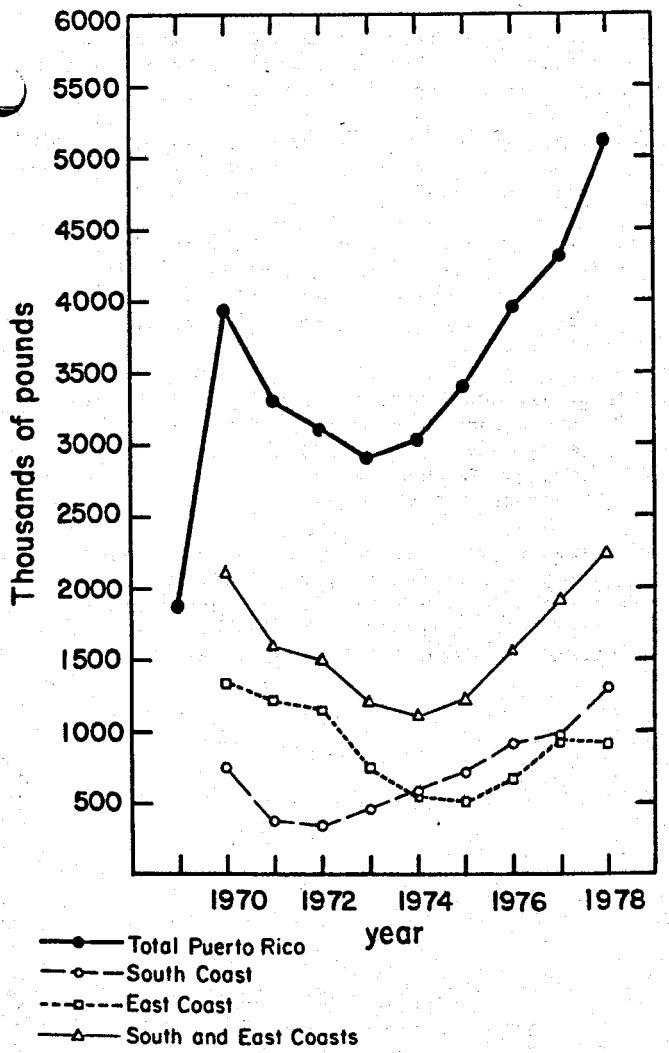

Figure 6. Puerto Rico total commercial fish landings. [XBL 8012-13526]

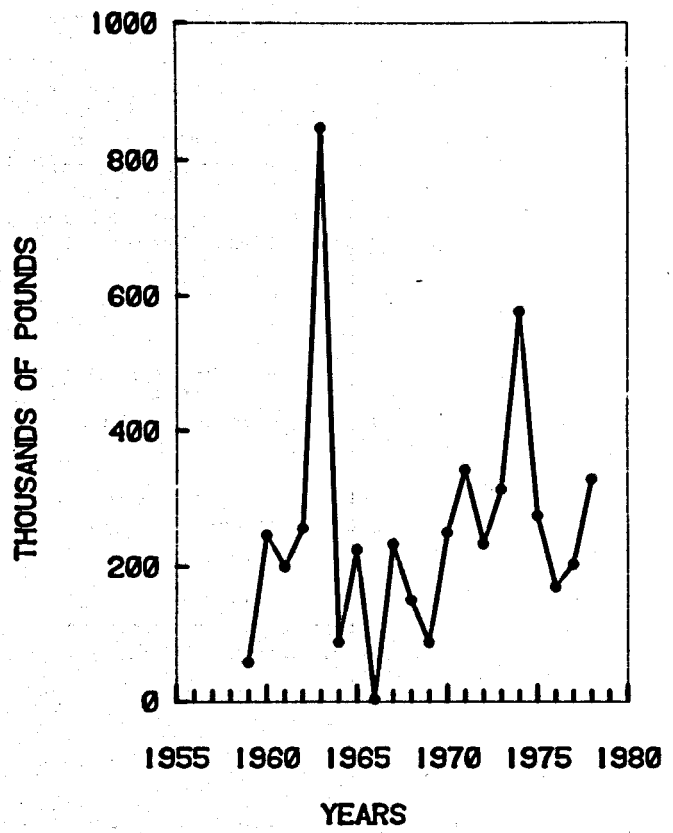

Figure 7. Hawaiian HOTEC-site fish data, totals for all species. [XBL 8010-12208]

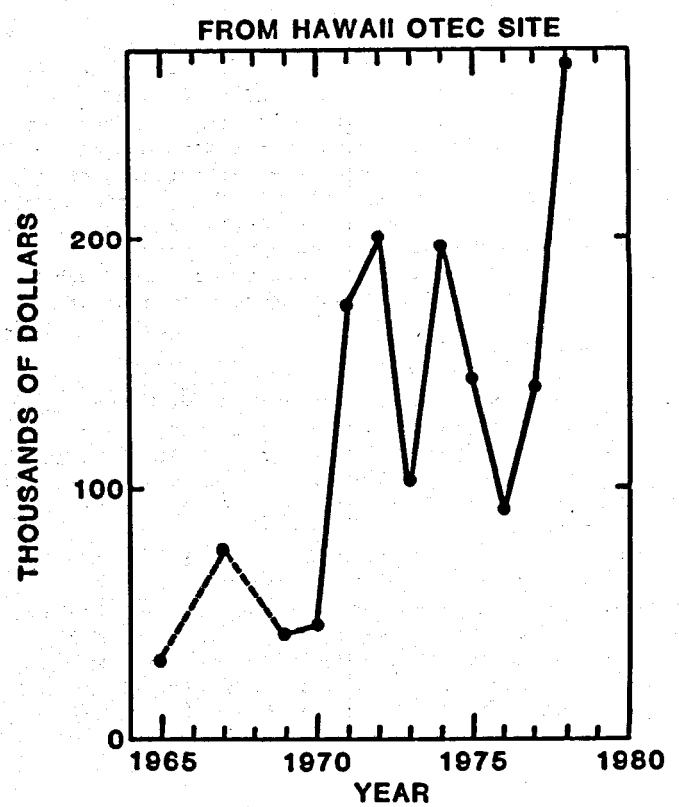

Figure 8. Annual dollar value of commercial fish landings. [XBL 8012-13527]

OTEC plant on nekton difficult. The economic importance to the local community of these landings is, however, substantial (Fig. 8) and must be considered.

In addition to the above fisheries information, the Marine Sciences Group has conducted an extensive literature survey of marine mammals (Payne, 1980).

TOXICITY STUDIES

Chlorine and Ammonia Toxicity

Ammonia is the working fluid of proposed closed-cycle OTEC plants. Chlorine has been the proposed method of controlling biofouling so that the evaporators and condensers of an OTEC plant will operate efficiently. Both chlorine and ammonia are known to be toxic to living organisms. A study of the effect of the leakage and catastrophic spillage of these toxic substances on marine organisms is being conducted at the Gulf Coast Research Laboratory under the direction of A. Venkataramiah.

Research conducted on chlorine and ammonia toxicity has involved controlled laboratory bioassays on several organisms from the tropical oceans. These have included mullet (Mugil cephalus), Sargassum shrimp (Latreutes fucorum), and filefish (Monocanthus hispidus). The results have shown species specific size versus toxicity relationships, as well as behavioral changes at sublethal concentrations. Present bioassays are using an oceanic copepod of the genus Eucalanus (Venkataramiah et al., 1980).

REFERENCES CITED

Bienfang, P., and Szyper, J. P., 1980. Phytoplankton dynamics in oceanic waters off Ke-ahole Point, Hawaii. Berkeley, Lawrence Berkeley Laboratory, LBL-11277.

Duncan, P., 1981. A simplified zooplankton-net cod-end. Berkeley, Lawrence Berkeley Laboratory, LBL-11594.

Estrella, D., and Hartwig, E., 1980. A selected bibliography of chlorophyll a determination methodology. Berkeley, Lawrence Berkeley Laboratory, LBID-266.

Jones, A., 1980. A selected bibliography of Tuna--(Scombridae) from the Hawaiian Islands--a potential OTEC area. Berkeley, Lawrence Berkeley Laboratory, LBID-286.

Payne, S. F., 1980. The marine mammals of the Gulf of Mexico. Berkeley, Lawrence Berkeley Laboratory, LBID-265.

Ryan, C. J., 1980. A selected bibliography of fishes and fisheries at a potential ocean thermal energy conversion site in Puerto Rico. Berkeley, Lawrence Berkeley Laboratory, LBID-252.

Ryan, C. J., and Jones, A. T., 1980. Commercial fishery data from a proposed Ocean Thermal Energy Conversion (OTEC) site in Puerto Rico. Berkeley, Lawrence Berkeley Laboratory, LBL-11926.

Venkataramiah, A., Lakshmi, G. J., Horne, A. J., Wilde, P., and Gunter, G., 1980. Studies on toxicity of OTEC plant components on marine animals from the Gulf of Mexico. Berkeley, Lawrence Berkeley Laboratory, LBID-298.

CHEMICAL OCEANOGRAPHIC RESEARCH

M. S. Q. Hunt, D. J. Estrella, R. Valentine, and A. T. Jones

The chemistry program of the Marine Sciences Group participated in OTEC site characterization, a nutrient preservation study, and a study of the mechanisms of chlorine degradation in sea water; it also initiated a radioactive tracer development program and a program examining the partitioning of trace metals in the water column. The relationship between the distribution of trace elements in the water column and other oceanographic parameters was examined to explore the possibility of using such a relationship to predict trace element concentrations.

SITE CHARACTERIZATION

A year-long study in conjunction with the University of Hawaii and Dr. David Ziemann of Aecos, Inc. at the benchmark OTEC site off the Kona Coast of Hawaii has been completed. Hydrocasts were taken on each of six bimonthly cruises. Two casts to 1000 m taken at approximately noon and two casts at midnight showed the distribution of various parameters over the water column of interest to OTEC. Several chemical parameters were determined, including these nutrients: reactive phosphate, nitrate, silicate and ammonia, and dissolved oxygen. Profiles of phosphate, nitrate, silicate, and dissolved oxygen with depth are shown in Figure 1. Distributions observed were typical of the tropical Pacific Ocean.

Two additional hydrocasts to 300 m provided more detailed information on the euphotic zone. In addition to the chemical parameters measured on the

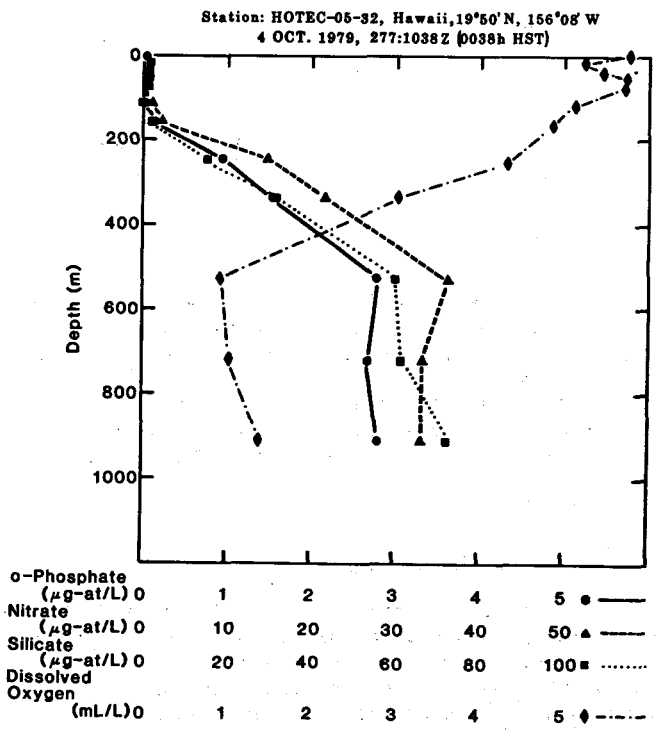

Figure 1. Profiles of phosphate, nitrate, silicate, and dissolved oxygen with depth. [XBL 815-9542]

deep hydrocasts, samples were collected for chlorophyll a, phaeophytin, and adenosine triphosphate, as well as water to be used for ^{14}C uptake experiments for primary productivity. Figure 2 of the preceding article shows typical distributions of the biomass indicators with depth at the Kona Coast (HOTEC) site. Determination of the biomass indicators and primary productivity provides information on the standing stock and photosynthetic activity of the natural phytoplankton. Natural phytoplankton are considered to be extremely sensitive to perturbation and may show an early impact of the operation of an OTEC plant.

NUTRIENT PRESERVATION STUDY

Although the analysis of nutrients is considered routine (Strickland and Parsons, 1972; Grasshoff, 1976), samples must be analyzed rapidly or they degrade. Because it is frequently impossible to analyze samples immediately, a number of preservation techniques have been devised (Fitzgerald and Faust, 1967; Rigler, 1964; American Public Health Association, 1975; Gilmartin, 1967; Jenkins, 1968; Maynard and Hopkins, 1973; Degobbis, 1973). A study was conducted with Dr. John Morse of Rosenstiel School of Marine and Atmospheric Science at the University of Miami (RSMAS) to determine which of the more common preservation techniques was effective. Samples of deep and surface water were collected from the Gulf Stream, filtered immediately, and returned to the laboratory for processing. One subsample of each type of water was analyzed immediately for nitrite, nitrate plus nitrite, ammonium, reactive phosphate, total dissolved phosphate, and silicate. Other subsamples were preserved for analysis after 7, 30, and 60 days using various techniques including three bottle types: glass, polyethylene, and Teflon; two temperatures: frozen and refrigerated; and using either no preservative, acid, or poison: $HgCl_2$ for all nutrients but ammonia, and alkaline phenol for ammonia.

No preservation method was found to be effective for all nutrients; in fact, none were completely effective for any of the nutrients. For nitrate plus nitrite and reactive phosphate, poisoning with $HgCl_2$ and freezing in glass bottles proved to be most effective; for total phosphate and silicate, freezing with $HgCl_2$ in polyethylene worked best. Samples did not have enough nitrite to complete the study, and no method worked well for ammonium.

RADIOACTIVE TRACER STUDY

Radioactive tracer methods have been developed by G. Brass (RSMAS) and R. Dodge (Nova University, Florida) to study oceanic mixing rates at potential OTEC sites. ^{228}Ra was chosen for study because it enters the ocean water primarily from sediments; its half-life of 5.7 yr makes it ideal for studying natural mixing processes with a time constant of less than 25 years.

TRACE METAL PARTITIONING STUDIES

This joint program between Lawrence Berkeley Laboratory (LBL) and Moss Landing Marine Laboratory (MLML) developed and compared methods for sampling and analyzing for dissolved and particulate trace metals in the oceanic water column. The relative distribution of the trace metals in the dissolved and particulate phases, as well as the particle flux, are important for characterizing the oceanic ecosystem and predicting of OTEC-related alterations of the marine environment.

Trace elements frequently are found in the marine environment in extremely low levels--concentrations of less than 1 ppb are not unusual. Because natural levels are so low, sampling must be conducted using ultra-clean techniques. The past year has been spent examining methods of contamination-free sampling that can be used on small craft in areas of the world where clean laboratory conditions are generally unavailable.

An initial study in February 1980 was conducted at a potential OTEC site off St. Croix in the Virgin Islands. Sampling methods included a particle interceptor trap developed by A. Knauer of MLML, large-volume water samplers, and plankton nets.

Samples for dissolved and filterable particles were collected in 30-liter Teflon-lined Go-Flor bottles which had been acid-cleaned and stored in plastic and wood containers until flushing with sea water and use. All metal fittings were removed or covered with clear plastic resin. During sampling, bottles were attached to dacron-sheathed hydrowire wrapped on a winch drum covered with polyethylene, and passed through a stainless steel meter wheel. The bottles entered the water closed in order to avoid surface contamination. After collection, samples were processed in a clean laboratory constructed out of polyethylene sheets, and samples were packaged and returned to shore for analysis. Atomic absorption (AAS) analyses were conducted at MLML by Knauer and M. Gordon, neutron activation analyses (NAA) by F. Asaro and H. Michel of LBL, x-ray fluorescence (XRF) measurements by R. D. Giauque of LBL, and isotopic dilution mass spectrometry (IDMS) by A. R. Flegal at the California Institute of Technology.

Surface water and plankton samples were collected from a rubber raft in acid-cleaned polyethylene bottles and plankton nets at a sufficient distance from the ship to permit relatively uncontaminated samples. The sampling methods being used were found to be largely contamination-free, although a few samples were contaminated.

The four different methods of analysis were complementary, providing sufficient overlap for quality assurance but each expanding the number of elements that could be determined.

This study was the first of its kind off St. Croix. The surface water was found to have some of the lowest values for cadmium (less than one part per trillion) in the world. The surface lead values (less than 8 parts per billion) are the lowest yet reported for the Atlantic. The manganese profile was found to be consistent with those reported for other regions.

As the water off St. Croix appears relatively clean and the reefs surrounding the island are an important natural resource, it will be of great

importance to characterize this environment and protect it from any potential impact of an OTEC plant.

TRACE METAL CORRELATION STUDY

In order to predict the possible impact of an operating OTEC plant on the local biological and chemical species composition, or to predict the efficiency of the OTEC plant itself, it is important to have a good understanding of the ambient water column.

The chemical composition throughout the water column must be known at each potential OTEC site. For some compounds, for example the nutrients, procedures for determination have been standardized (Strickland and Parsons, 1972; Grasshoff, 1976). For others, for instance the trace metals mentioned above, it can be an extremely expensive and difficult procedure, requiring sophisticated sampling and analysis procedures and highly skilled personnel (Patterson and Settle, 1976; Bruland et al., 1979).

Traditionally, elements in sea water have been separated into two categories, the conservative and the nonconservative. Conservancy implies that the ratio of the elemental composition to salinity is constant over the normal oceanographic range (Brewer, 1975; Culkin, 1965; Dittmar, 1884). The major elements, sodium, potassium, chlorine, bromine, etc., are conservative with salinity (Dittmar, 1884; Forchhammer, 1865; Cox, 1965; Culkin and Cox, 1966). The nonconservative elements are the gases, the nutrients, and the nonnutrient trace elements. The profiles of the nutrients, biomass indicators, and dissolved oxygen are related to their biological activity. The concentrations of the nonnutrient gases are dependent largely upon their solubilities. The distribution of a large group of trace elements remains unexplained.

Recently, however, the concentrations of some of these trace elements (e.g., uranium, vanadium, and molybdenum) have been found to correlate with chlorinity; in other words, they are conservative. In addition, a second type of conservancy or correlation--that of trace elements with biologically-controlled chemical species--has been identified. The correlation can be a simple linear relationship between the trace element and another parameter, such as that exhibited by cadmium and phosphate (Bruland et al., 1978). But often the relationship is more complex, the elemental concentration being linearly related to a combination of the concentrations of two or more parameters. Nickel, for example, correlates with a combination of silicate and phosphate (Bruland, 1980).

In light of these correlations, it is reasonable to propose that the concentration of a specific element could be predicted if its relationship to other parameters were known. We have reviewed the literature reporting elemental distributions in sea water and identified the correlations exhibited with the idea of using these correlations to predict trace element concentrations at OTEC sites. For some elements, although detailed profiles have not been determined, a correlation category could be suggested based on the data available. For other elements, no prediction has been made. These were largely elements for which little or no data exists and which are found only in ultra-trace quantities with no reported evidence of biological importance in the context of OTEC operations.

CHLORINE IN SEA WATER

OTEC generating stations propose to use chlorine as a biofouling-control agent. Because of the large amounts of chlorine that would be used, it is essential to understand the fate of this chemical in the marine environment. One degradation mechanism involves the reaction of chlorine (an oxidizing agent) with reducing agents, both organic and inorganic, involving several intermediates, including bromide and ammonia. Chlorine reacts with ammonia (also an OTEC working fluid) and organic amines in seawater to form chloramines (mono-, di-, and trisubstituted); chloramines can then react with bromide (present in seawater in significant quantities) to form bromines, which may be carcinogenic. It therefore is important to examine these reactions.

In a study conducted at LBL (concurrently verified by Trofe, Johnson, and Inman at the University of North Carolina), chloramines have been found to react with bromides at a rate described by

$$r = K[Br]\ [H+]\ [NH_2Cl].$$

Organic amines have been found to react similarly, although not consistently according to this expression. The total oxidant concentration in a seawater-chlorinated effluent mixture decays at an instantaneous rate given by

$$r = \{K_1[Br^-] + K_2\}C,$$

where K_1 = bromide reaction rate constant, K_2 = nonbromide reaction constant, and C = total oxidant concentration.

REFERENCES CITED

American Public Health Association, 1975. Standard methods for the examination of water and wastewater. Washington, D. C. 14th edition, p. 518-534.

Brewer, P. G., 1975. Minor elements in seawater. In J. P. Riley and G. Skirrow (eds.), Chemical Oceanography (2nd ed.). London, Academic Press, p. 415-496.

Bruland, K. W., Knauer, G. A., and Martin, J. H., 1978. Cadmium in northeast Pacific waters. Limnol. Oceanogr., v. 23, p. 618-625.

Bruland, K. W., Franks, R. P., Knauer, G. A., and Martin, J. H., 1979. Sampling and analytical methods for the determination of copper, cadmium, zinc and nickel at the nanogram per liter level in seawater. Anal. Chim. Acta, v. 105, p. 233-245.

Bruland, K. W., 1980. Oceanographic distributions of cadmium, zinc, nickel and copper in the north Pacific, Earth Planet. Sci. Lett., v. 47, p. 176-198.

Cox, R. A., 1965. Physical properties of seawater. In J. P. Riley and G. Shirrow (eds.), Chemical Oceanography (1st ed.). London, Academic Press, p. 73-120.

Culkin, F., 1965. The major constituents of seawater. In J. P. Riley and G. Shirrow (eds.), Chemical Oceanography (1st ed.). London, Academic Press, p. 121-162.

Culkin, F. and Cox, R. A., 1966. Sodium, potassium, magnesium, calcium, and strontium in seawater. Deep-Sea Research, v. 13, p. 789-804.

Degobbis, D., 1973. On the storage of seawater samples for ammonia determination. Limnol. Oceanogr., v. 18, p. 146-150.

Dittmar, W., 1884. Report on the scientific results of the exploring voyage of the HMS Challenger. Physics and Chemistry, v. 1, London, H. M. Stationary Office.

Fitzgerald, G. P., and Faust, S. L., 1967. Effect of water sample preservation methods on the release of phosphorus from algae. Limnol. Oceanogr., v. 12, p. 332-335.

Forchhammer, G., 1865. On the composition of sea water in the different parts of the ocean. Roy. Soc. London, Phil. Trans., v. 155, p. 203-262.

Gilmartin, M., 1967. Changes in inorganic phosphate concentrations occurring during seawater sample storage. Limnol. Oceanogr., v. 8, p. 152-156.

Grasshoff, K., 1976. Methods of seawater analysis, Weinheim, Verlag Chemi, 317 pp.

Jenkins, D., 1968. The differentiation, analysis, and preservation of nitrogen and phosphorus forms in natural waters. In Trace Inorganics in Water, R. G. Gould (ed.), Amer. Chem. Soc. Pub., p. 265-280.

Maynard, V., and Hopkins, T. L., 1973. An evaluation of effects of field and lab procedures on nitrate-nitrite nitrogen. In Advances in automated analysis. Proceedings of Technicon International Congress, New York, June 1972, p. 29-35.

Molinari, R. L., Voituries, B., and Duncan, P., 1981. Observations in the subthermocline undercurrent of the equatorial south Atlantic Ocean, in preparation.

Patterson, C. C., and Settle, D., 1976. The reduction of orders of magnitude errors in lead analysis of biological materials and natural waters by evaluating and controlling the extent and sources of industrial lead contamination introduced during sample collecting, handling and analysis. National Bureau of Standards Special Publication 422, p. 321-351.

Rigler, F. H., 1964. The phosphorus fractions and the turnover time of inorganic phosphorus in different types of lakes. Limnol. Oceanogr., v. 9, p. 511-518.

Strickland, J. D. H., and Parsons, T. R., 1972. A practical handbook of seawater analyses. Ottawa, Fisheries Research Board of Canada Bulletin 167 (2nd ed), 310 pp.

GEOLOGICAL OCEANOGRAPHIC RESEARCH

P. Wilde, J. Oldson, and D. Corrigan

Knowledge of the characteristics of the seabed is extremely important to the success of the ocean energy program from both an engineering and an environmental perspective. All types of proposed OTEC platforms obviously require bottom data for mooring and anchoring, cable and pipeway paths, etc. Plant ships will operate only in regions deeper than the cold water pipe depth, so even these facilities will require bathymetric knowledge.

ARCHIVAL AND PREVIOUS WORK

To insure that all pertinent data from previous investigations are available to engineers, designers, and environmental scientists, thorough archival studies should be done to avoid both costly duplication of effort and mistakes based on unfamiliarity with the professional literature.

For OTEC studies, this review has been initiated with a joint program between the Marine Sciences Group of Lawrence Berkeley Laboratory (LBL) and the Pacific Arctic Branch of Marine Geology at Menlo Park. The archival program is basically the production of regional marine geologic and oceanographic data sheets which serve as a bathymetric planning base plus an index to the marine geologic and oceanographic data for a particular region of OTEC interest. (Table 1 lists the contents of these sheets.) The data sheet for the Hawaiian area (18°-23°N; 154°-159°W) has been completed (Wilde et al., 1980), and the Puerto Rico-Virgin Islands sheet (17°-19°N; 64°-68°W) is in final draft form.

Table 1. Contents of regional data sheets for each region.

Bathymetric base map - 100 m contour interval
List of applicable navigation charts
Geographic features map
Map of geologic samples - repositories indexed
Map of earthquake epicenters
Map of gravity anomalies
Map of magnetic anomalies
Track lines of seismic reflection/refraction with cruises, year and data sources indexed
Monthly maps of sea surface temperature and current drift
Selected profiles of sub-bottom records
List of pertinent references classed by published papers and books, reports and theses
List of sources with addresses and contacts.

Additional material where applicable or available,
- Wave and wind climate (monthly)
- Temperature-salinity-density profiles with water masses
- Map of bottom sediment types and geotechnical data

PALEO-OCEANOGRAPHIC MODELS

In cooperation with the Paleontology Department at the University of California, Berkeley, models are being developed to explain the occurrence of organic-rich sediments at various times in the geologic record. The basis for the model is the progressive ventilation of the ocean by surface wind mixing and by density-driven deep water during glacial episodes (Berry and Wilde, 1978). The intersection of the residual anoxic layer with the ocean floor provides a reducing environment for deposition of organic-rich sediments. Wilde and Berry (1980) developed an extension of their 1978 model to explain the apparent return to anoxic conditions at midwater depths in the Cretaceous as seen in organic-rich layers in cores from the deep-sea drilling project (Schlanger and Jenkyns, 1976; Thiede and van Andel, 1977). The model predicts that after long nonglacial periods, anoxic conditions could redevelop at middepths through a change in the deep water masses from cold oxygen-rich, high-latitude water during glacial times to warmer oxygen-poorer, higher-salinity water formed at middle latitudes. Figure 1 shows the proposed oxygen-depleted zones for the nonglacial case.

To evaluate the time history of the ventilation and calculate the oxygen demand for ventilation, Berry and Wilde (1980) are also attempting to model

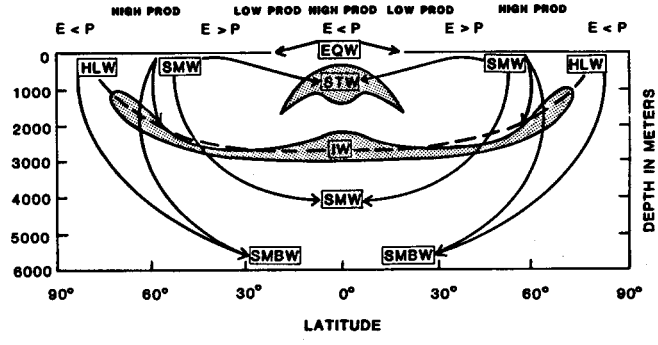

Figure 1. Longitudinal profile for Case A conditions with oxygen-depleted zones shaded. Water designations as follows:

EQW = equatorial water
SSW = shelf sea water
STW = subtropical water
SMW = salinity maximum water
HWLa = high-latitude water for Case A conditions
HWLb = high-latitude water for Case B conditions
IW = intermediate water
SMBW = salinity maximum bottom water
MW = Mediterranean water [XBL 809-11901]

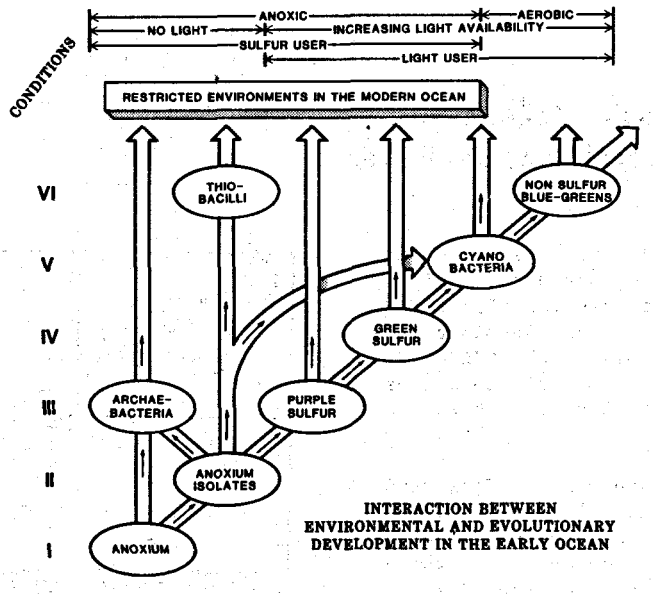

Figure 2. Interaction between environmental and evolutionary development in the early ocean.

Conditions:

I. Outgassing of earth has provided an ocean of sufficient depth to permit fluid water at high temperatures. Atmosphere: high CO_2, methane, and ammonia, cloudy and hot near surface. Oceans: low pH, high CO_2, anoxic with dissolved H_2S, NH_3, and rich in dissolved erosion products. Chemoautotroph Anoxium evolves at outgassing submarine thermal springs.

II. H_2S. Carbon fixing by Anoxium begins. Carbon fixing proceeds--heterotrophes possible; however, autotrophes probably more efficient--and carbon begins to be stored in geologic sinks. Amount of S and CO_2 is diminished in oceans and atmosphere as S and C go into sinks. Cloudiness and temperature gradually reduced. $S_2O_3^{=}/S^{=}$ increases with expansion of autotrophes. Gradient of $S^{=}$ from vents puts environmental pressure on Anoxium isolates to use another energy source.

III. As carbon fixing and storage of C in sinks proceeds, quantity of light reaching ocean surface increases. Anoxium isolates at sea surface develop ability to use light to augment $S^{=}$, occupying niches similar to modern purple bacteria.

IV. Quality of light improves with reduced CO_2 and cloudiness so more low wave-length light available. Green bacterial niche available.

V. Continued scarcity of $S^{=}$ and improved quantity and quality of light gives advantage to near-surface photic organisms. Transition from sulfur to photic organisms developed in cyanobacteria. Biogenic-free O_2 appears in atmosphere.

VI. Oxidation of sulfur compounds by free O_2 eliminates anoxic environments near surface. Pure photic nonsulfur organisms become primary producers. Previous anoxic environments become restricted. Adaptation to existence at anoxic-aerated boundary developed by thiobacilli.

[XBL 8010-12275]

the primitive ocean prior to the evolution of photosynthesis. This model suggests that carbon-fixing by sulfur chemosutotrophes living in the primitive anoxic ocean provided the evolutionary stimulus for the eventual development of photosynthesis as the principle mechanism of primary production. Figure 2 shows the proposed sequence of events that lead to sufficient free oxygen in the atmosphere to initiate ventilation.

REFERENCES CITED

Berry, W. B. N., and Wilde, P., 1978. Progressive ventilation of the oceans--an explanation for the distribution of the Lower Paleozoic black shales. Amer. J. Science, v. 278, p. 257-275.

Berry, W. B. N., and Wilde, P., 1980. Evolutionary and geologic consequences of organic carbon fixing in the primitive anoxic ocean. Berkeley, Lawrence Berkeley Labortatory, LBL-11592. Submitted to Nature.

Schlanger, S. O. and Jenkyns, H. C., 1976. Cretaceous oceanic anoxic events: causes and consequences. Geol. Mijnb., v. 55, p. 179-184.

Thiede, J., and van Andel, T. H., 1977. The paleoenvironment of anaerobic sediments in the Late Mesozoic South Atlantic Ocean. Earth Planet. Sci. Lett., v. 33, p. 301-309.

Wilde, P., Chase, T. E., Normark, W. R., and others, 1980. Oceanographic data off southern Hawaiian Islands. Berkeley, Lawrence Berkeley Laboratory, Pub. 359.

Wilde, P., and Berry, W. B. N., 1980. Progressive ventilation of the oceans--potential for return to anoxic conditions in the post-Paleozoic. Berkeley, Lawrence Berkeley Laboratory, LBL-11544. Submitted to Cretaceous Research.

PHYSICAL OCEANOGRAPHIC RESEARCH

C. P. Duncan, V. Harms, G. Schladow, and T. Weil

Physical oceanographic research performed in the Marine Sciences Group is directed at solving engineering and environmental questions for the OTEC resource. Results directly applicable to the program are disseminated rapidly to the OTEC community and results of wider interest arising out of the programmatic work are published in the professional literature.

The primary physical oceanographic data needed at an OTEC site, once the annual thermal cycle is known, is for local and far-field current data. With such data, the stresses upon an OTEC plant and its moorings can be calculated, the flow of warm water to the plant can be determined, and input for computer models of downstream dispersal of discharge can be provided.

CURRENT METER ARRAYS

Researchers with the Lawrence Berkeley Laboratory (LBL) physical oceanography program have installed arrays of current meters (see Figure 1 schematic) at three sites: (1) off the west coast of Oahu; (2) off the west coast of the island of Hawaii (this array includes a wave-measuring buoy); and (3) off the south coast of Puerto Rico (Figs. 2-4). The arrays have been installed in conjunction with thermal surveys. LBL has begun processing data from these arrays, and the most significant results from these preliminary data are the high speeds seen at the OTEC-1 site off the west coast of the island of Hawaii. Speeds in excess of 100 cm/s, gusting to 150 cm/s (3 knots), at a depth of 56 m were seen for a duration of 10 days within a 28-day observational period in August/September 1980. These speeds are in agreement with the Coast Pilot for the region. Current reversals and high speeds at

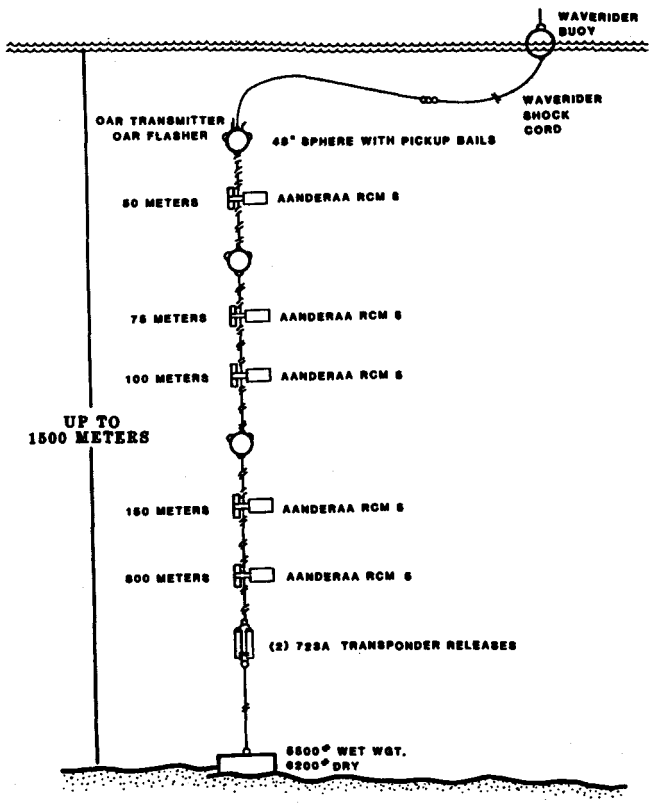

Figure 1. Mooring design for OTEC 1, primary current meter mooring. [XBL 8012-13529]

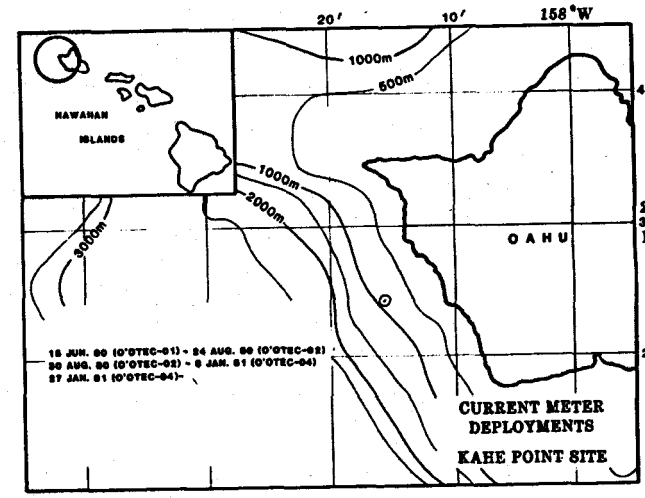

Figure 2. Current meter deployments, Kahe Point site. [XBL 813-8543]

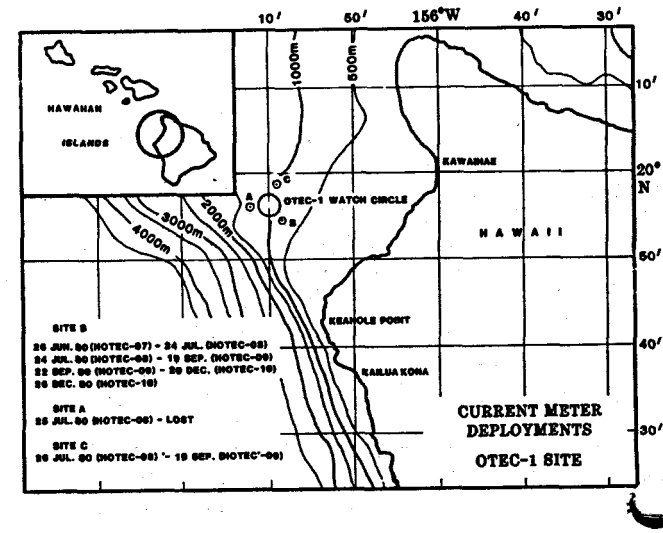

Figure 3. Current meter deployments, OTEC-1 site. [XBL 813-8542]

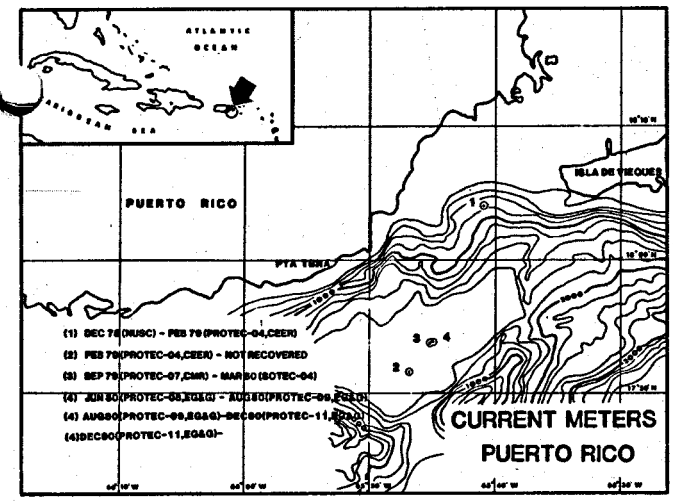

Figure 4. Current meter deployments Puerto Rico site. [XBL 813-8541]

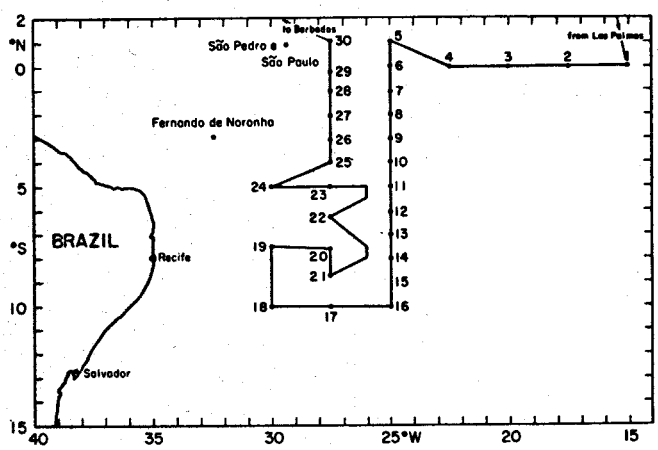

Figure 5. Track chart with station positions, cruise of R. V. Researcher, 21 Feb-7 Mar 1980. [XBL 806-7096]

the OTEC-1 site in the upper 150 m were associated with large (4°C) temperature changes that could affect OTEC operations at this site. Similar temperature changes have not been noted at either the Punta Tuna or Kahe Point sites. At Kahe Point the maximum current recorded between June 1980 and January 1981 was 71.5 cm/s at 100 m below the surface, directed to 335°, parallel to the isobaths. By June 1981 a complete year's data will be available for each site, and a thorough analysis of the data will commence as the LBL field program phases out. At the Puerto Rico site the observed speeds have been less than 40 cm/s, dominantly in a WSW direction between September 1979 and February 1980. Between June and August 1980, however, the direction was reversed.

OTHER RESEARCH BY THE PHYSICAL OCEANOGRAPHY SECTION

A research cruise to the south Atlantic aboard the National Oceanic and Atmospheric Administration (NOAA) Oceanographic Survey Ship O.S.S. Researcher was made in February-March 1980 (Fig. 5). Both chemical and biological observations were made during the cruise. The chemistry of the tropical Atlantic is intimately related to the complex and as yet little-understood system of currents and countercurrents within 10 degrees of the equator. The results of this cruise show definite correlations between the distribution of dissolved nutrient salts in the upper 300 m of the ocean and the velocity field, which are used by Molinari et al. (1981) to describe the South Equatorial Undercurrent.

APPENDIXES

APPENDIX A: PUBLICATIONS

JOURNAL ARTICLES

Benson, L. V., 1978. Fluctuation in the level of pluvial Lake Lahontan during the last 40,000 years. Quaternary Research, v. 9, p. 300-318. (LBL-11185)

Berry, W. B. N., and Wilde, P., 1980. Evolutionary and geologic consequences of organic carbon fixing in the primitive anoxic ocean. (Submitted to Nature.) (LBL-11592)

Bienfang, P. K., and Szyper, J. P., 1980. Phytoplankton dynamics in oceanic waters off Ke-Ahole Point, Hawaii. (Submitted to Deep Sea Research.) (LBL-11277)

Binnall, E. O., 1980. Instrumentation and computer based data acquisition for in-situ rock property measurements. (Submitted to Transactions in Nuclear Science.) (LBL-10532)

Brittain, H. G., and Perry, D. L., 1980. Luminescence spectra of the uranyl ion in two geometrically similar coordination environments, uranyl nitrate hexahydrate and di-U-aquo-bis (dioxodinitratouranium(VI) di-imidazole. (Submitted to the Journal of Physical Chemistry.) (LBL-10542)

Dorn, G. A., 1980. Radiation impedance of torsionally vibrating seismic sources. (Submitted to Geophysics.) (LBL-11843)

Duncan, C. P. and Schladow, S. G., 1980. World surface currents from ship's drift observations. (Submitted to the International Hydrographic Review.) (LBL-11001)

Foglia, M., Iwamoto, F., Harada, M., Chambre, P. L., and Pigford, T. H., 1979. The superposition solution of the transport of a radionuclide chain through a sorbing medium. Transactions of the American Nuclear Society, v. 33, p. 386-387. (LBL-10346)

Ghiorso, M. S., and Carmichael, I. S. E., 1980. A regular solution model for met-aluminous silicate liquids, applications to geothermometry, immiscibility, and the source regions of basic magmas. Contributions to Mineralogy and Petrology, v. 71, p. 323-342. (LBL-9755)

Goyal, K. P., and Kassoy, D. R., 1979. Fault zone controlled charging of a liquid dominated geothermal reservoir. (Submitted to the Journal of Geophysical Research.) (LBL-9327)

Goyal, K. P., and Kassoy, D. R., 1980. A plausible two-dimensional vertical model of the East Mesa geothermal field, California, U.S.A. (Submitted to the Journal of Geophysical Research.) (LBL-10617)

Harada, M., Iwamoto, F., and Pigford, T. H., 1979. Effect of source boundary conditions in predicting the migration of radionuclides through geologic media. Transactions of the American Nuclear Society, v. 33, p. 383-384. (LBL-10339)

Higashi, K., Harada, M., Iwamoto, F., and Pigford, T. H., 1979. Migration behavior of the $^{234}U \rightarrow {}^{230}Th \rightarrow {}^{226}Ra \rightarrow$ decay chain. Transactions of the American Nuclear Society, v. 33, p. 386-387. (LBL-10345)

Hirschfeld, T., and Klainer, S. M., 1980. Short range remote NQR measurements. Journal of Molecular Structure, v. 58, p. 63-77. (LBL-10865)

Javandel, I., and Witherspoon, P. A., 1980. A semi-analytical solution for partial penetration in two-layer aquifers. (Submitted to Water Resources Research.) (LBL-10875).

Lee, K. H., and Morrison, H. F., 1980. A solution for TM-mode plane waves incident on a two-dimensional inhomogeneity. (Submitted to Geophysics.) (LBL-10649)

Lee, K. H., Pridmore, D. F., and Morrison, H. F., 1980. A hybrid three-dimensional electromagnetic modeling scheme. (Submitted to Geophysics.) (LBL-10378)

Lippmann, M. J., and Tsang, C. F., 1980. Ground water use for cooling: Associated aquifer temperature changes. (Submitted to Ground Water.) (LBL-10406)

Luhr, J. F., and Carmichael, I. S. E., 1980. The Colima Volcanic Complex, Mexico, post-caldera andesites from volcano Colima. Contributions to Mineralogy and Petrology, v. 71, p. 343-372. (LBL-10932)

Marino, R. A., Wenk, H. R., and Apps, J. A., 1980. Proposed applications of NQR techniques to the geosciences. Journal of Molecular Structure, v. 58, p. 445-457. (LBL-10866)

Narasimhan, T. N., 1979. On general conservation equations for multiphase systems: I. Averaging procedure. (Letter to the Editor submitted to Advances in Water Resources.) (LBL-10302)

Narasimhan, T. N., Houston, W. N., and Nur, A. M., 1980. The role of pore pressure in deformation in geologic processes. (Submitted to Geology.) (LBL-10637)

Nelson, S. A., and Carmichael, I. S. E., 1979. Partial molar volumes of oxide components in silicate liquids. (Submitted to Contributions to Mineralogy and Petrology.) (LBL-9210)

Neretnieks, I., 1979. Age dating of groundwater in fissured rock: The influence of water volume in micropores. (Submitted to Science.) (LBL-9473)

Noorishad, J., Mehran, M., and Narasimhan, T. N., 1980. A note on the formulation of saturated-unsaturated fluid flow through deformable porous media. (Submitted to Advances in Water Resources.) (LBL-11550)

O'Sullivan, M., 1980. A similarity method for geothermal well test analysis. Submitted to Water Resources Research. (LBL-10968)

Paulsson, B. N. P., and King, M. S., 1980. Between-hole acoustic surveying and monitoring of a granitic rock mass. (Submitted to the International Journal of Rock Mechanics and Mining Science.) (LBL-10483)

Phillips, S. L., Mathur, A. K., and Garrison, W., 1981. Treatment methods for geothermal brines. ASTM Special Technical Publication 717. (LBL-9100)

Pitzer, K. S., and Peiper, J. C., 1979. The activity coefficient of aqueous $NaHCO_3$. (Submitted to the Journal of Physical Chemistry.) (LBL-10298).

Taft, J. L., Taylor, W. R., Hartwig, E. O., and Loftus, R., 1980. Seasonal oxygen depletion in Chesapeake Bay. Estuaries, v. 3, no. 4, p. 242-247. (LBL-12101)

Wilde, P., and Berry, W. B. N., 1980. Progressive ventilation of the oceans--Potential for return to anoxic conditions in the post-paleozoic. (Submitted to Cretaceous Research.) (LBL-11544)

Witherspoon, P. A., Amick, C. H., Gale, J. E., and Iwai, K., 1979. Observations of a potential size-effect in experimental determination of the hydraulic properties of fractures. Water Resources Research, v. 15, no. 5, p. 1142-1146. (LBL-8571; SAC-17)

Witherspoon, P. A., Cook, N. G. W., and Gale, J. E., 1981. Geologic storage of radioactive waste: Results of field investigations at Stripa, Sweden. Science, v. 211, p. 894-900. (LBL-11585)

LBL REPORTS

Alonzo, H. E., Dominguez, B. A., Lippmann, M. J., Molinar, R. O., Schroeder, R. C., and Witherspoon, P. A., 1979. Update of reservoir engineering activities at Cerro Prieto. (LBL-10209; CP-04)

Apps, J. A., Doe, T., Doty, B., Doty, S., Galbraith, R., Kearns, A., Khort, B., Long, J. C. S., Monroe, A. O., Narasimhan, T. N., Nelson, P. H., Wilson, C. R., and Witherspoon, P. A., 1979. Geohydrological studies for nuclear waste isolation at the Hanford Reservation. v. I--Executive summary; v. II--Final report. (LBL-8764)

Aquifer Thermal Energy Storage (ATES) Newsletter, 1979. v. I, no. 4. (PUB-294)

____, 1980. v. II, no. 1-3. (PUB-341)

Aydelotte, R. R., 1980. Transient well testing in two-phase geothermal reservoirs (Intercomp). (LBL-10562; GREMP-08)

Barber-Nichols Engineering Co., 1979. Direct contact heat exchanger 10 kW power loop. Sec. 1--Executive summary; Sec. 2--Test series no. 1.; Sec. 3--Test series no. 2. (LBL-7036)

Benson, L. V., 1980. Paleoclimatic significance of lake level fluctuations in the Lahontan Basin. (LBL-11265)

____, 1980. A tabulation and evaluation of ion exchange data on smectites, certain zeolites, and basalt. Topical Report No. 2, FY 1980 for Rockwell Hanford Operations of Rockwell International. (LBL-9677, Part I)

Benson, L. V., Carnahan, C. L., and Che, M., 1980. A study of rock-water-nuclear waste interactions in the Pasco Basin, Washington. Part II--Preliminary equilibrium-step simulations of basalt diagenesis. (LBL-9677, Part II)

Benson, L. V., and Teague, L. S., 1980. A study of rock-water-nuclear waste interactions in the Pasco Basin, Washington. Part I. (LBL-9677, Part I)

____, 1980. A tabulation of thermodynamic data for chemical reactions involving 58 elements common to radioactive waste package systems. (LBL-11448)

Benson, L. V., Teague, L. S., Molton, C. A., Frisch, C. J., Stolzman, R. A., and Corrigan, D. J., 1979. Distribution and composition of secondary and primary mineral phases in basalts of the Pasco Basin, Washington. July interim report FY 1979 for Rockwell Hanford Operations of Rockwell International. (LBID-068)

Benson, S., Goranson, C., Noble, J., Schroeder, R., Corrigan, D., and Wollenberg, H., 1980. Evaluation of the Susanville, California geothermal resource. (LBL-11187)

Blair, C. K., Harrison, R. F., 1980. Development of an instrument to measure the concentration of noncondensable gases in geothermal discharges. Final Report (Terra Tek, Inc.). (LBL-11499)

Bodvarsson, G. S., O'Sullivan, M. J., and Tsang, C. F., 1980. The sensitivity of geothermal reservoir behavior to relative permeability parameters. (Presented at the Sixth Workshop on Geothermal Reservoir Engineering, Stanford Geothermal Program, Stanford, California, December 16-18, 1980.) (LBL-12040)

Burleigh, R. H., Binnall, E. O., DuBois, A. O., Norgren, D. U., and Ortiz, A. R., 1979. Electrical heaters for thermo-mechanical tests at the Stripa mine. (LBL-7063; SAC-13)

Buscheck, T. E., 1980. Probabilistic simulation of subsurface fluid flow, a study using a numerical scheme (M.S. thesis). (LBL-10711)

Chan, T., and Cook, N. G. W., 1979. Calculated thermally induced displacements and stresses for heater experiments at Stripa, Sweden. Linear thermoelastic models using constant material properties. (LBL-7061; SAC-22)

Chan, T., Binnall, E., Nelson, P., Stolzman, R., Wan, O., Weaver, C., Ang, K., Braley, J., and McEvoy, M., 1980. Thermal and thermomechanical data from in situ heater experiments at Stripa, Sweden. (LBL-11477)

Chan, T., Littlestone, N., and Wan, O., 1979. Thermomechanical modeling and data analysis for heating experiments at Stripa, Sweden. (LBL-10193)

Doe, T. W., and Kanehiro, B. Y., 1980. Radiological, hydrogeological, geochemical, and geophysical assessment of the Weldon Spring Quarry, Missouri, disposal site. (LBID-152)

Doughty, C., McEdwards, D. G., and Tsang, C. F., 1979. Multiple well variable rate well test analysis of data from the Auburn University Thermal Energy Storage Program. (LBL-10194)

Duncan, C. P., 1980. A simplified zooplankton-net cod-end. (LBL-11594)

Earth Sciences Division, 1978. Earth Sciences Division Annual Report 1978. (LBL-8648)

____, 1979. Earth Sciences Division Annual Report 1979. (LBL-10686)

____, 1979. Earth Sciences Division Newsletter. v. 2, no. 1; v. 2, no. 1-2. (PUB-283)

____, 1980. Earth Sciences Division Newsletter. v. 3, no. 1; v. 3, no. 1-2. (PUB-343)

Earth Sciences Division, Marine Sciences Group, 1978. Preliminary data reports for the GOTEC 04, 05, 06 and 07 cruises to the Gulf of Mexico, Mobile and Tampa sites, June 1978 through December 1978. (LBL-9439-9442; GOTEC 04-07)

Estrella, D., and Hartwig, E. O., 1980. A selected bibliography of chlorophyll a determination methodology. (LBID-266)

Frye, D., Davison, A., and Leavitt, K., 1981. Physical oceanographic data from the OTEC Punta Tuna, Puerto Rico site, September 1979-June 1980 (EG&G Environmental Consultants).

Geosciences Annual Report 1978. (Excerpt from the Earth Sciences Division Annual Report 1978, LBL-8648.) (LBL-10349)

Geothermal Energy Development Annual Report 1979. (Excerpt from the Earth Sciences Division, Annual Report 1979, LBL-10686.) (LBL-11236)

Ghaffari, A., 1980. A model for predicting thermal conductivity of rock-fluid systems (Ph.D. thesis). (LBL-11384)

Harada, M., Chambre, P. L., Foglia, M., Higashi, K., Iwamoto, F., Leung, D., Pigford, T. H., and Ting, D., 1980. Migration of radionuclides through sorbing media, analytical solution. (LBL-10500)

Harms, V. W., and Westernik, J. J., 1980. Wave transmission and mooring force characteristics of pipe-tire floating breakwaters. (LBL-11778)

Hlinak, A., Lobach, J., Nichols, K., Olander, R., and Werner, D., 1980. Final design, installation and baseline testing of 500 kW direct-contact pilot plant at East Mesa. (LBL-11153)

Hood, M., Carlsson, H., and Nelson, P. H., 1979. Some results from a field investigation of thermo-mechanical loading of a rock mass when heaters are emplaced in the rock and the application of field data from heater experiments conducted at Stripa, Sweden, to parameters for repository design. (LBL-9392; SAC-26)

Howard, J. H., Goldstein, N. E., and Graf, A. N., 1980. An updated plan for support of research related to geothermal reservoir engineering. (LBL-10807)

Howard, J. H., 1980. Discussion of a procedure for geothermal property appraisal. (LBID-326)

Hsu, I. C. W., 1979. Heat transfer to isobutane flowing inside a horizontal tube at supercritical pressure (Ph.D. thesis). (LBL-10442)

Iglesias, E. R., 1980. Rough estimates of fluid pressures for the design of the LBL downhole geopressured sampler. (LBID-258)

Jones, A. T., 1980. A selected bibliography of tuna (Scombridae) from the Hawaiian Islands, a potential ocean thermal energy conversion area. (LBID-286)

Karamarakar, M., and Cheng, P., 1980. A theoretical assessment of James' method for the determination of geothermal wellbore discharge characteristics. (LBL-11498)

Lamb, D. W., 1980. Cost and schedule for drilling and mining underground test facilities. (LBL-11490)

Lamers, M. D., 1979. Measurement requirements and methods for geothermal reservoir system parameters, an appraisal (Measurement Analysis Corporation). (LBL-9090; GREMP-06)

Langmuir, D., and Herman, J. S., 1980. The mobility of thorium in natural waters at low temperatures. Geochimica et Cosmochimica Acta, v. 44, no. 11, p. 1753-1766. (LBL-12528)

Marine Sciences Group, 1980. Ocean Thermal Energy Conversion Preliminary Data Report for the November 1977 GOTEC 02 cruise to the Gulf of Mexico Mobile Site. (LBL-9437)

Marine Sciences Group, 1980. Ocean Thermal Energy Conversion Preliminary Data Report for the February 1978 GOTEC 03 cruise to the Gulf of Mexico Mobile Site. (LBL-9438)

Marine Sciences Group, 1980. Preliminary data reports for the GOTEC 04, 05, 06 and 07 cruises to the Gulf of Mexico, Mobile and Tampa Sites, June 1978 through December 1978. (LBL-9439-9442; GOTEC 04-07)

McEvoy, M. B., 1979. Data acquisition, handling and display for the heater experiments at Stripa. (LBL-7062; SAC-14)

Michels, D. E., 1980. Deposition of calcium carbonate in porous materials by flashing geothermal fluid (Republic Geothermal Inc.). (LBL-10673; GREMP-09)

Miller, C. W., 1980. Eliminating the wellbore response in transient well test analysis. (Presented at the Sixth Workshop on Geothermal Reservoir Engineering, Stanford Geothermal Program, Stanford University, Stanford, California, December 16-18, 1980.) (LBL-12037)

Miller, I., Dershowitz, W., Jones, K., Myer, L., Roman, K., and Schauer, M., 1980. Simulation of geothermal subsidence (Golder Associates). (LBL-10794 (10571); GSRMP-06)

_____, 1980. Physical properties of compaction. Companion report to simulation of geothermal subsidence (LBL-10571) (Golder Associates). (LBL-10838; GSRMP-07)

_____, 1980. Detailed report on tested models. Companion report to simulation of geothermal subsidence (LBL-10571) (Golder Associates). (LBL-10837; GSRMP-08)

_____, 1980. Case study data base. Companion report 3 to simulation of geothermal subsidence (LBL-10571) (Golder Associates). (LBL-10839; GSRMP-09)

Morse, J. W., and Zullig, J. J., 1980. OTEC, Gulf of Mexico oxygen and nutrient measurements. (LBID-294)

Narasimhan, T. N., 1980. Multidimensional numerical simulation of fluid flow in fractured porous media. (Submitted to Water Resources Research.) (LBL-12087)

News of Geothermal Energy Conversion Technology (GECT) Newsletter, v. II, no. 2, October 1980. (PUB-354)

OTEC, 1979. Ocean thermal energy conversion ecological data report from O.S.S. Researcher in Gulf of Mexico (from data collected July 12-23, 1977). (LBL-8945; GOTEC-01)

Payne, S. F., 1980. The marine mammals of the Gulf of Mexico. A bibliography. (LBID-265)

Pelka, W., 1980. Two well storage systems for combined heating and air-conditioning by groundwater heatpumps in shallow aquifers. (LBL-11302)

Pope, W. L., and Doyle, P. A., 1980. The transposed critical temperature Rankine thermodynamic cycle. (LBL-10312)

Pope, W. L., Doyle, P. A., Pines, H. S., Fulton, R. L., Silvester, L. F., and Angevine, J. M., 1980. Sourcebook on the production of electricity from geothermal energy, conceptual design optimization. (Section 8.2, in Sourcebook on the production of electricity from geothermal energy, Joseph Kestin (ed.), Brown University Press.) (LBL-8685)

Pritchett, J. W., Rice, L. F., and Garg, S. K., 1980. Reservoir simulation studies--Wairakei geothermal field, New Zealand. Final report (Systems, Science and Software). (LBL-11497; GREMP-11)

Pruess, K., and Schroeder, R. C., 1980. SHAFT79 User's Manual. (LBL-10861)

Pruess, K., Schroeder, R. C., Witherspoon, P. A., and Zerzan, J. M., 1979. SHAFT78, A two-phase multidimensional computer program for geothermal reservoir simulation. (LBL-8264)

Pruess, K., Weres, O., Schroeder, R. C., Marconcini, R., and Neri, G., 1980. History match simulation of Serrazzano geothermal reservoir. (LBL-11235)

Rogers, P. S. Z., 1981. Thermodynamics of geothermal fluids (Ph.D. thesis). (LBL-12356)

Rogers, P. S. Z., Bradley, D. J., and Pitzer, K. S., 1981. Densities of aqueous sodium chloride solutions from 75°C to 200°C at 20 Bar. (Submitted to the Journal of Chemical and Engineering Data.) (LBL-12047)

Ryan, C. J., 1980. A selected bibliography of fishes and fisheries at a potential ocean thermal energy conversion site in Puerto Rico. (LBID-252)

Ryan, C. J., and Jones, A. T., 1980. Commerical fishery data from a proposed Ocean Thermal Energy Conversion (OTEC) site in Puerto Rico. (LBL-11926)

Sands, D., 1980. OTEC draft programmatic environmental assessment (EA). (LBL-10511; 2 volumes, in preparation)

Schrauf, T., Pratt, H., Simonson, E., Hustrulid, W., Nelson, P. H., DuBois, A., Binnall, E. P., and Haught, R., 1979. Instrument evaluation, calibration and installation for the heater experiments at Stripa. (LBL-8313; SAC-25)

Seasonal Thermal Energy Storage (STES) Newsletter, 1980. v. II, no. 4. (See Aquifer Thermal Energy Storage Newsletter.) (PUB-341)

____, 1980. v. III, no. 1. (PUB-393)

Silva, R. J., Benson, L. V., Yee, A. W., and Parks, G. A., 1978. Waste isolation safety assessment program. Task 4--Collection and generation of transport data theoretical and experimental evaluation and waste transport in selected rocks. Annual Progress Report, October 1, 1978-September 30, 1979. (LBL-9945)

Snow, D. T., 1979. Packer injection test data from sites on fractured rock. (LBL-10080)

Stark, M., Goldstein, N. E., and Wollenberg, H. A., 1980. Geothermal exploration assessment and interpretation, upper Klamath Lake area, Klamath Basin, Oregon. (LBL-10140)

Stark, M., Wilt, M., Haught, J. R., and Goldstein, N. E., 1980. Controlled-source electromagnetic survey at Soda Lakes geothermal area, Nevada. (LBL-11221)

Steen, J. P., Jr., and Gunter, G., 1980. Zooplankton study at the mobile OTEC site in the northern Gulf of Mexico. (LBID-299)

Sudol, G. A., Harrison, R. F., and Ramey, H. J., Jr., 1979. Annotated research bibliography for geothermal reservoir engineering (Terra Tek, Inc.). (LBL-8664; GREMP-01)

Sullivan, S. M., Sands, M. D., Donat, J. R., Jepsen, P., Smookler, M., and Villa, J. F., 1981. Environmental assessment Ocean Thermal Energy Conversion (OTEC) pilot plants. (LBL-12328)

Teague, L. S., 1980. Secondary minerals found in cores DC2 A1 and DC2 taken from the Grande Ronde Basalt Formation, Pasco Basin, Washington. (LBL-10387)

Thorpe, R. K., 1979. Characterization of discontinuities in the Stripa granite time-scale heater experiment. (LBL-7083; SAC-20)

Tsang, C. F., 1979. Seasonal temperature energy storage in aquifers. Mathematical modeling studies in 1979. (LBL-10208)

Tsang, C. F., 1980. Theoretical studies in long-term thermal energy storage in aquifers. (Presented at the International TNO-Symposium, "Thermal Storage of Solar Energy", Amsterdam, The Netherlands, November 5-6, 1980.) (LBL-11593)

Tsang, C. F., Buscheck, T., and Doughty, C., 1980. Aquifer thermal energy storage--A numerical simulation of Auburn University field experiments. (LBL-10210)

Tsang, C. F., Hopkins, D., and Hellstrom, G., 1980. Aquifer thermal energy storage--A survey. (LBL-10441)

Venkataramiah, A., Lakshmi, G. J., Horne, A. J., Wilde, P., and Gunter, G., 1980. Studies on toxicity of OTEC plant components on marine animals from the Gulf of Mexico. (LBID-298)

Wang, J. S. Y., Tsang, C. F., Cook, N. G. W., and Witherspoon, P. A., 1979. A study of regional temperature and thermohydrological effects of an underground repository for nuclear wastes in hard rock. (LBL-8271)

Weres, O., Yee, A., and Tsao, L., 1980. Kinetics of silica polymerization. (LBL-7033)

White, A. F., Baldridge, W. S., Gerlach, T. M., and Knauss, K., 1980. Comparative assessment of five potential sites for hydrothermal magma systems: Geochemistry. (LBL-11410)

Wilde, P., 1980. Environmental assessment and monitoring program Ocean Thermal Energy Conversion (OTEC). (LBID-254)

Wilt, M., Goldstein, N. E., Stark, M., and Haught, R., 1980. An electromagnetic (EM-60) survey in the Panther Canyon area, Grass Valley, Nevada. (LBL-10993)

Wilt, M., Haught, R., and Goldstein, N. E., 1980. An electromagnetic (EM-60) survey of the McCoy geothermal prospect, Nevada. (LBL-12012)

Witherspoon, P. A., Cook, N. G. W., and Gale, J. E., 1980. Progress with field investigations at Stripa. (LBL-10559; SAC-27)

Witherspoon, P. A., Wang, J. S. Y., Iwai, K., and Gale, J. E., 1980. Validity of cubic law for fluid flow in a deformable rock fracture. (LBL-9557; SAC-23)

Wollenberg, H. A., Strisower, B., Corrigan, D. J., Graf, A. N., O'Brien, M. T., Pratt, H. F., Board, M., and Hustrulid, W., 1979. Search for underground openings for in-situ test facilities in crystalline rock. (rev. Jan. 1980). (LBID-077)

Zais, E. J., and Bodvarsson, G., 1980. Analysis of production decline in geothermal reservoirs. (LBL-11215; GREMP-10)

CONFERENCES AND PROCEEDINGS

Abou-Sayed, A., and Schatz, J. F., 1979. Physical and mechanical properties of core from the Cerro Prieto geothermal field. (Presented at the Second Symposium on the Cerro Prieto Geothermal Field, Mexicali, Mexico, October 17-19, 1979.) (LBL-9564, abstract)

Benson, S. M., Goranson, C. B., Haney, J. P., and Schroeder, R. C., 1979. The status of the resource evaluation at Susanville, California. (Presented at the 1979 Annual Meeting, Geothermal Resources Council, Reno, Nevada, September 24-27, 1979.) (LBL-9469)

Benson, S. M., Goranson, C. B., and Schroeder, R. C., 1980. Evaluation of city well 1, Klamath Falls, Oregon. (Presented at the Symposium on Commercial Uses of Geothermal Energy, Geothermal Resources Council, Boise, Idaho, June 16-18, 1980.) (LBL-10848)

Binnall, E. P., DuBois, A. O., and Lingle, R., 1979. Rock instrumentation problems experienced during in-situ heater tests. (Presented at the International Symposium on the Scientific Basis for Nuclear Waste Management, Materials Research Society, Boston, Massachusetts, November 27-30, 1979.) (LBL-9952)

Bodvarsson, G. S., and Tsang, C. F., 1980. Injection into a fractured geothermal reservoir. (Presented at the 1980 Annual Meeting, Geothermal Resources Council, Salt Lake City, Utah, September 9-11, 1980.) (LBL-10983)

Bodvarsson, G. S., Vonder Haar, S., Wilt, M., and Tsang, C. F., 1980. Preliminary estimation of the reservoir capacity and the longevity of the Baca geothermal field, New Mexico. (Presented at the 55th Annual Technical Conference and Exhibition, Society of Petroleum Engineers of the American Institute of Mining, Metallurgical and Petroleum Engineers, Inc., Dallas, Texas, September 21-24, 1980.) (LBL-10656)

Bunge, A. L., Klein, G., and Radke, C. J., 1980. Divalent ion exchange with alkali. (Presented at the Fifth Society of Petroleum Engineers International Symposium on Oilfield and Geothermal Chemistry, Stanford, California, May 28-30, 1980.) (LBL-10884)

Chan, T., and Javandel, I., 1980. Heat transfer in underground heating experiments in granite, Stripa, Sweden. (Presented at the Technical Session on Heat Transfer in Nuclear Waste Disposal, ASME Winter Annual Meeting, Chicago, Illinois, November 16-21, 1980.) (LBL-10876).

Chan, T., Hood, M., and Board, M., 1980. Rock properties and their effect on thermally induced displacements and stresses. (Presented at the American Society of Mechanical Engineers 1980 Energy Technology Conference and Exhibition, New Orleans, Louisiana, February 3-7, 1980.) (LBL-10517)

Chan, T., Hood, M., and Witherspoon, P. A., 1980. Predicted and measured temperatures, displacements and stresses from the Stripa Heater experiments. (Presented at Rockstore 1980, Special Session on Nuclear Waste Disposal, Stockholm, Sweden, June 23-29, 1980.) (LBL-10358)

Corwin, R. F., and Fitterman, D. V., 1980. Geological interpretation of self-potential data from the Cerro Prieto geothermal field. (Presented at the Second Symposium on the Cerro Prieto Geothermal Field, Mexicali, Baja California, Mexico, October 17-19, 1979.) (LBL-9544; CP-17)

Cotton, M. L., and Vonder Haar, S., 1980. Microfossils from Cerro Prieto geothermal wells, Baja California, Mexico. (Presented at the Second Symposium on the Cerro Prieto Geothermal Field, Mexicali, Baja California, Mexico, October 17-19, 1979.) (LBL-10303; CP-05)

De Boer, J., 1980. Paleomagnetism of the Quaternary Cerro Prieto, Crater Elegante, and Salton Buttes volcanic domes in the northern part of the Gulf of California rhomochasm. (Presented at the Second Symposium on the Cerro Prieto Geothermal Field, Mexicali, Baja California, Mexico, October 17-19, 1979.) (LBL-9547; CP-06)

Earth Sciences Division, 1980. Second DOE-ENEL Workshop for Cooperative Research in Geothermal Energy, October 20-22, 1980, Berkeley, California. (Presented at the Second DOE-ENEL Workshop for Cooperative Research in Geothermal Energy, Berkeley, California, October 20-22, 1980.) (LBL-11555, Program and Abstracts only; proceedings in press)

____, 1981. Abstracts (resumenes) of the Third Symposium on the Cerro Prieto Geothermal Field, Baja California, Mexico, March 24-26, 1981, San Francisco, California. (Sponsored by U.S. Department of Energy, Division of Geothermal Energy, and Comisión Federal de Electricidad.) (LBL-11967)

Earth Sciences Division, Marine Sciences Group, 1979. Appropriate zooplankton sampling methodology for OTEC sites. (Presented at the Conference of the Marine Sciences Group, Earth Sciences Division on Appropriate Zooplankton Sampling Methodology for OTEC Sites, Lawrence Berkeley Laboratory, Berkeley, California, July 9-10, 1979.) (LBL-11979)

Goldstein, N. E., Wilt, M. J., Stark, M., Mozley, E., and Morrison, H. F., 1979. Magnetotelluric and controlled-source electromagnetic studies at Mt. Hood, Oregon. (Presented at the Fall Meeting of the American Geophysical Union, San Francisco, California, December 3-7, 1979.) (LBL-9776, abstract)

Goranson, C. B., and Schroeder, R. C., 1979. Site specific geothermal reservoir engineering activities at Lawrence Berkeley Laboratory. (Presented at the 1979 Annual Meeting, Geothermal Resources Council, Reno, Nevada, September 24-27, 1979.) (LBL-9463)

Goubau, W. M., Stark, M., Gambel, T. D., Goldstein, N. E., and Miracky, R. F., 1979. Magnetotelluric studies at Cerro Prieto. (Presented at the Second Symposium on the Cerro Prieto Geothermal Field, Mexicali, Baja California, Mexico, October 17-19, 1979.) (LBL-9545; CP-09)

Goyal, K. P., and Kassoy, D. R., 1979. Fault zone controlled charging of an aquifer. (Presented at the 18th ASME-AIChE National Heat Transfer Conference, San Diego, California, August 5-8, 1979.) (LBL-9329, abstract)

Goyal, K. P., and Narasimhan, T. N., 1980. Heat and mass transfer in a fault-controlled geothermal reservoir charged at constant pressure. To be presented at the 20th ASME/AIChE Heat Transfer Conference, Milwaukee, Wisconsin, August 2-5, 1981.) (LBL-11802, abstract)

Goyal, K. P., Miller, C. W., and Lippmann, M. J., 1980. Effect of measured wellhead parameters and well scaling on the computed downhole conditions in Cerro Prieto wells. Presented at the Sixth Annual Workshop on Geothermal Reservoir Engineering, Stanford Geothermal Program, Stanford University, Stanford, California, December 16-18, 1980 (LBL-11835)

Grannell, R. B., Tarman, D. W., Aronstam, P., Clover, R. C., Leggewie, R. M., Eppink, J., and Kroll, R., 1979. Precision gravity measurements in the Cerro Prieto geothermal area. (Presented at the Second Symposium on the Cerro Prieto Geothermal Field, Mexicali, Baja California, Mexico, October 17-19, 1979.) (LBL-9551; CP-16)

Guvanasen, V., and Chan, T., 1980. Finite-element solution of coupled heat and fluid flow, solute transport, and thermomechanical deformation in fractured porous media. (Presented at the 1980 American Geophysical Union, Fall Meeting, San Francisco, California, December 8-12, 1980.) (LBL-11528, abstract)

Haney, J. P., Goranson, C. B., Solbau, R., and Schroeder, R. C., 1979. (Presented at the 1979 Annual Meeting, Geothermal Resources Council, Reno, Nevada, September 24-27, 1979.) (LBL-9462)

Harms, V. W., 1979. Floating breakwater performance comparison. (Presented at the 17th International Conference on Coastal Engineering, Sydney, Australia, March 23-29, 1980.) (LBL-9707)

Howard, J. H., 1980. High temperature geothermal reservoir engineering. (Presented at the National Conference on Renewable Energy, Honolulu, Hawaii, December 1980.) (LBL-11347)

Howard, J. H., and Schwarz, W. J., 1979. Status of geothermal reservoir engineering management program (GREMP)--December, 1979. (Presented at the 1979 Annual Meeting, Geothermal Resources Council, Reno, Nevada, September 24-27, 1979.) (LBL-9326)

Iglesias, E. R., and Weres, O., 1980. Theoretical studies of Cerro Prieto brines chemical equilibria. (Presented at the Second Symposium on the Cerro Prieto Geothermal Field, Mexicali, Baja California, Mexico, October 17-19, 1979.) (LBL-9563; CP-07)

Javandel, I., and Chan, T., 1979. Detailed analysis of temperatures from underground heating experiments in granite. (Presented at the fall meeting of the American Geophysical Union, San Francisco, California, December 3-7, 1979.) (LBL-9767, abstract)

Lippmann, M. J., and Goyal, K. P., 1979. Numerical modeling studies of the Cerro Prieto reservoir, a progress report. (Presented at the Second Symposium on the Cerro Prieto Geothermal Field, Mexicali, Baja California, Mexico, October 17-19, 1979.) (LBL-9590; CP-14)

Lippmann, M. J., and Witherspoon, P. A., 1980. Summary of recent progress in understanding the Cerro Prieto geothermal field, Baja California, Mexico. (Presented at the Geothermal Conference of the Committee on Challenges of Modern Society, Paris, France, July 15, 1980.) (LBL-11100)

Lyons, D. J., and Van de Kamp, P. C., 1980. Subsurface geological and geophysical study of the Cerro Prieto geothermal field. (Presented at the Second Symposium on the Cerro Prieto Geothermal Field, Mexicali, Baja California, Mexico, October 17-19, 1979.) (LBL-10540; CP-11)

Majer, E. L., and McEvilly, T. V., 1980. Earthquake monitoring at the Cerro Prieto geothermal field. (Presented at the Second Symposium on the Cerro Prieto geothermal field, Mexicali, Baja California, Mexico, October 17-19, 1979.) (LBL-9550; CP-08)

Mangold, D. C., Tsang, C. F., Lippmann, M. J., and Witherspoon, P. A., 1979. A study of thermal effects in well-test analysis. (Presented at the 54th Annual Fall Technical Conference and Exhibition of the Society of Petroleum Engineers of AIME, Las Vegas, Nevada, September 23-26, 1979.) (LBL-9769)

McEdwards, D. G., 1979. Multiwell variable rate well test analysis. (Presented at the 54th Annual Fall Technical Conference and Exhibition of the Society of Petroleum Engineers of AIME, Las Vegas, Nevada, September 23-26, 1979.) (LBL-9460; SPE-8392)

Miller, C. W., 1979. A numerical model of transient two-phase flow in a geothermal well. (Presented at the Geothermal Resources Council, 1979 Annual Meeting, Reno, Nevada, September 24-27, 1979.) (LBL-9056)

____, 1979. Wellbore storage effects in geothermal wells. (Presented at the 54th Annual Fall Technical Conference and Exhibition of the Society of Petroleum Engineers of AIME, Las Vegas, Nevada, September 23-26, 1979.) (LBL-8844)

Miller, C. W., and Zerzan, J. M., 1979. Downhole pressure changes measured with a fluid filled capillary tube. (Presented at the Annual Meeting of the Society of Petroleum Engineers, Las Vegas, Nevada, September 23-27, 1979.) (LBL-9303)

Miller, C. W., Benson, S., O'Sullivan, M. J., and Pruess, K., 1981. Wellbore effects on the analysis of two-phase geothermal well tests. Presented at the Society of Petroleum Engineers California Regional Meeting, Bakersfield, California, March 25-27, 1981. (LBL-12220)

Narasimhan, T. N., 1979. The physical basis of groundwater hydrology. (Presented at the Fall Meeting of the American Geophysical Union, San Francisco, California, December 3-7, 1979.) (LBL-9770, abstract)

____, 1980. Subsidence due to geothermal fluid production. (Presented at the J. F. Poland Land Subsidence Symposium, Geological Society of America, Atlanta, Georgia, November 17-20, 1980.) (LBL-10967, abstract)

____, 1980. Physical aspects of the interface between the saturated and the unsaturated regimes. (Presented at the American Geophysical Union Chapman Conference on Subsurface Contributions to Stream Flow, University of New Hampshire, Durham, New Hampshire, October 5-9, 1980.) (LBL-11178)

Narasimhan, T. N., and Goyal, K. P., 1979. A preliminary simulation of land subsidence at the Wairakei geothermal field in New Zealand. (Presented at the Fifth Workshop, Geothermal Reservoir Engineering, Stanford University, December 12-14, 1979.) (LBL-10299)

Narasimhan, T. N., and Kanehiro, B. Y., 1980. Effect of earth tides on confined aquifers. (Submitted to the 1980 Annual Meeting of the Geological Society of America, Atlanta, Georgia, November 17-20, 1980.) (LBL-11060, abstract).

Nelson, P. H., and Rachiele, R., 1980. Radon as an indicator of wellbore infiltration rates in uraniferous igneous rock. Presented at the 1980 Fall Meeting of the American Geophysical Union, San Francisco, California, December 8-12, 1980 (LBL-11575, abstract)

Nichols, K. E., 1979. A 500-kW direct contact pilot plant for East Mesa (Barber-Nichols Engineering Co.). (Presented at the 1979 Annual Meeting, Salt Lake City, Utah, September 9-11, 1980.) (LBL-11107)

Noble, J. E., 1979. Stratigraphic and sedimentological analysis of the Cerro Prieto geothermal field, Baja California, Mexico. (Presented at the Second Symposium on the Cerro Prieto Geothermal Field, Mexicali, Baja California, Mexico, October 17-19, 1979.) (LBL-9592, abstract)

O'Sullivan, M. J., 1980. The DOE code comparison study: Summary of results for problem 4--Expanding two-phase system with drainage. (Presented at the Sixth Annual Workshop on Geothermal Reservoir Engineering, Stanford Geothermal Program, Stanford University, Stanford, California, December 16-18, 1980.) (LBL-12033)

O'Sullivan, M., and Pruess, K., 1980. Analysis of injection testing of geothermal reservoirs. (Presented at the Geothermal Resources Council 1980 Annual Meeting, Salt Lake City, Utah, September 9-11, 1980.) (LBL-10985)

O'Sullivan, M. J., and Pruess, K., 1980. Numerical studies of the energy sweep in five-spot geothermal production/injection systems. (Presented at the Sixth Annual Workshop on Geothermal Reservoir Engineering, Stanford Geothermal Program, Stanford University, Stanford, California, December 16-18, 1980.) (LBL-12166)

Palen, W. A., and Narasimhan, T. N., 1980. Interpretation of a hydraulic-fracture experiment, Monticello, South Carolina. (Presented at the American Geophysical Union Fall Meeting on Earthquake Prediction, Hydrological and geochemical Studies, San Francisco, California, December 8-12, 1980.) (LBL-10849)

Paulsson, B. N. P., and King, M. S., 1980. A cross-hole investigation of a rock mass subjected to heating. (Presented at Rockstore 1980, Special Session on Nuclear Waste Disposal, Stockholm, Sweden, June 23-27, 1980.) (LBL-10849).

Pitzer, K. S., 1979. Characteristics of very concentrated aqueous solutions. (Presented to the Nobel Symposium on Chemistry and Geochemistry of Solutions at High Temperature and Pressure, Bofors, Karlskoga, Sweden, September 16-21, 1979 and published by the Royal Swedish Academy of Sciences.) (LBL-9660)

Pope, W. L., Doyle, P. A., Fulton, R. L., and Silvester, L. F., 1980. The importance of the specific heat anomaly in the design of binary Rankine power plants. (Presented at the Geothermal Resources Council Annual Meeting, Salt Lake City, Utah, September 9-11, 1980.) (LBL-10974)

Pruess, K., 1980. DOE-project on geothermal reservoir engineering computer code comparison and validation--Evaluation of results for problem 6. (Presented at the Sixth Annual Workshop on Geothermal Reservoir Engineering, Stanford Geothermal Program, Stanford University, Stanford, California, December 16-18, 1980.) (LBL-12038)

Pruess, K., and Schroeder, R. C., 1979. Basic theory and equations used in the two-phase multidimensional geothermal reservoir simulator, SHAFT79. (Presented at the 1979 Annual Meeting, Geothermal Resources Council, Reno, Nevada, September 24-27, 1979.) (LBL-9464)

Pruess, K., and Schroeder, R. C., 1979. Geothermal reservoir simulations with SHAFT79. (Presented at the Fifth Geothermal Reservoir Engineering Workshop, Stanford University, Stanford, California, December 12-14, 1979.) (LBL-10066).

Pruess, K., and Truesdell, A. H., 1980. A numerical simulation of the natural evaluation of vapor-dominated hydrothermal systems. Presented at the Sixth Annual Workshop on Geothermal Reservoir Engineering, Stanford Geothermal Program, Stanford University, Stanford, California, December 16-18, 1980.) (LBL-12039)

Pruess, K., Bodvarsson, G., Schroeder, R. C., Witherspoon, P. A., Marconcini, R., Neri, G., and Ruffilli, C., 1979. Simulation of depletion of two-phase geothermal reservoirs. (Presented at the Society of Petroleum Engineers 54th Annual Technical Conference, Las Vegas, Nevada, September 23-26, 1979.) (LBL-9606)

Riveros, C. A., and Goldstein, N. E., 1979. Design and application of a megamoment electromagnetic dipole source. (Presented at the 49th Annual Meeting and Exposition, Society of Exploration Geophysics, New Orleans, Louisiana, November 4-8, 1979.) (LBL-9920)

Schroeder, R. C., Benson, S., and Goranson, C. B., 1980. High temperature geothermal reservoir engineering. (Presented at the Second Symposium on the Cerro Prieto Geothermal Field, Mexicali, Baja California, Mexico, October 17-19, 1979.) (LBL-9591)

Schwarz, W. J. (ed.), 1980. Proceedings, Workshop on Thermomechanical-Hydrochemical Modeling for a Hardrock Waste Repository, July 29-31, 1980, Berkeley, California. (Organized by Earth Sciences Divison, Lawrence Berkeley Laboratory. (LBL-11204; ONWI-164)

Silva, R. J., White, A. F., and Yee, A. W., 1980. Computer modeling of actinide sorption on geologic materials. (Submitted for presentation at the Symposium on Actinides in the Geosphere, Southwest-Southeast Regional American Chemical Society Meeting, New Orleans, Louisiana, December 10-13, 1980.) (LBL-11083, abstract)

Silva, R. J., White, A. F., and Yee, A. W., 1980. Computer modeling of nuclide adsorption on geologic materials. (Presented at the American Nuclear Society 1980 International Conference, Washington, D. C., November 17-21, 1980.) (LBL-11899)

Thorpe, R. K., 1979. Characterization of discontinuities in the Stripa granite. (Presented at the International Symposium on the Scientific Basis for Nuclear Waste Management, Boston, Massachusetts, November 27-30, 1979.) (LBL-9884).

Tleimat, B. W., Rie, H., Laird, A. D. K., and Zhao, S., 1980. Condensation film coefficients for mixtures of isobutane and isopentane. (Presented at the 15th Intersociety Energy Conversion Engineering Conference, Seattle, Washington, August 18-22, 1980.) (LBL-11025)

Tsang, C. F., and Claeson, J., 1980. Energy storage in aquifers--A survey of recent theoretical studies. (Presented at the Rockstore 80, Stockholm, Sweden, June 23-29, 1980.) (LBL-11059)

Tsang, C. F., Mangold, D. C., and Lippmann, M. J., 1979. Simulation of reinjection at Cerro Prieto using an idealized two-layer geologic model. (Presented at the Second Symposium on the Cerro Prieto Geothermal Field, Mexicali, Mexico, October 17-19, 1979.) (LBL-9589; CP-13)

Tsang, C. F., Molz, F. J., and Parr, A. D., 1980. Experimental and theoretical studies of thermal energy storage in aquifers. (Presented at the 15th Intersociety Energy Conversion Engineering Conference, Seattle, Washington, August 17-22, 1980.) (LBL-10889)

Vonder Haar, S., and Puente Cruz, I., 1979. Fault intersections and hybrid transform faults in the southern Salton Trough geothermal area, Baja California, Mexico. (Presented at the 1979 Annual Meeting, Geothermal Resources Council, Reno, Nevada, September 24-27, 1979.) (LBL-9458)

Vonder Haar, S., Wolgemuth, K., and Schatz, J., 1980. The role of newly formed clay minerals in geothermal reservoirs. (Presented at the Clay Minerals Conference, Waco, Texas, October 5-9, 1980.) (LBL-11296, abstract)

Wang, J. S. Y., and Tsang, C. F., 1979. Regional thermohydrological effects of an underground repository for nuclear wastes in hard rock. Presented at the Second International Symposium on the Scientific Basis for Nuclear Waste Management, Material Research Society, Boston, Massachusetts, November 26-30, 1979.) (LBL-11927)

____, 1980. Buoyancy flow in fractures intersecting a nuclear waste repository. (Presented at the technical session on Heat Transfer to Nuclear Waste Disposal, ASME Winter Annual Meeting, Chicago, Illinois, November 16-21, 1980.) (LBL-11112)

Weres, O., and Tsao, L., 1979. The chemistry of silica in Cerro Prieto brines. (Presented at the Second Symposium on the Cerro Prieto geothermal field, Mexicali, Baja California, Mexico, October 17-19, 1979.) (LBL-9548, abstract)

Weres, O., Tsao, L., and Iglesias, E. R., 1980. Chemistry of silica in Cerro Prieto brines. (Presented at the Second Symposium on the Cerro Prieto Geothermal Field, Mexicali, Baja California, Mexico, October 17-19, 1979.) (LBL-10166; CP-12)

Wilde, P., 1979. 1979 status of the OTEC environmental program. (Presented at the Marine Technology Society Conference, New Orleans, Louisiana, October 10-12, 1979.) (LBL-9495)

____, 1980. Status of OTEC environmental monitoring program. (Presented at the 7th Ocean Energy Conference, Washington, D. C., June 2-5, 1980.) (LBL-10887)

Wilt, M. J., and Goldstein, N. E., 1979. Resistivity monitoring at Cerro Prieto. (Presented at the Second Symposium on the Cerro Prieto Geothermal Field, Mexicali, Baja California, Mexico, October 17-19, 1979.) (LBL-9399)

Wilt, M. J., Beyer, J. H., and Goldstein, N. E., 1980. A comparison of dipole-dipole resistivity and electromagnetic induction sounding over the Panther Canyon thermal anomaly, Grass Valley, Nevada. (Presented at the 1980 Annual Meeting, Geothermal Resources Council, Salt Lake City, Utah, September 9-11, 1980.) (LBL-10987)

Wilt, M. J., Goldstein, N. E., Hoversten, M., and Morrison, H. F., 1979. Controlled-source EM experiment at Mt. Hood, Oregon. (Presented at the 1979 Annual Meeting, Geothermal Resources Council, Reno, Nevada, September 24-27, 1979.) (LBL-9399)

Witherspoon, P. A., 1980. Radioactive waste storage in mined caverns in crystalline rock--Results of field investigations at Stripa, Sweden. (Presented at the 75th Anniversary of the Illinois State Geological Survey Symposium on Perspectives in Geology, Urbana, Illinois, October 9-10, 1980.) (LBL-11651)

Witherspoon, P. A., and Cook, N. G. W., 1979. Thermomechanical experiments in granite at Stripa, Sweden. (Presented at the First Annual Office of Nuclear Waste Isolation Information Meeting, Columbus, Ohio, October 30-November 1, 1979.) (LBL-9681)

Witherspoon, P. A., Watkins, D. J., Cook, N. G. W., Hood, M., and Gale, J. E., 1979. Laboratory investigations on the hydraulic and thermomechanical properties of fractured crystalline rocks. (Presented at the First Annual Information Meeting of the Office of Nuclear Waste Isolation, Columbus, Ohio, October 30-November 1, 1979.) (LBL-9582)

Witherspoon, P. A., Wilson, C. R., Long, J. C. S., DuBois, A. O., Gale, J. E., and McPherson, M., 1979. The role of large scale permeability measurements in fractured rock and their application at Stripa. (Presented at the International Symposium on the Scientific Basis for Nuclear Waste Management, Boston, Massachusetts, November 27-30, 1979.) (LBL-9903)

APPENDIX B: EARTH SCIENCES DIVISION STAFF

PAUL A. WITHERSPOON*

Associate Director, Lawrence Berkeley Laboratory
Division Head, Earth Sciences Division

DIVISION ADMINISTRATION

Karl Olson, Deputy Division Head
Milford N. Bookman, Division Administration
Monique Adam, Division Office Administration

STAFF OF FISCAL YEAR 1980

Lennart Andersson
John Apps
Michele Arcidiacono
Lois Armetta

Lawrence Beaulaurier
Robert Bellman
Larry Benson
Eugene Binnall
Gudmundur Bodvarsson
Mary Bodvarsson
Harry Bowman
Daniel Bradley
Jeffrey Brown
Annette Bunge
Thomas Buscheck
Timothy Buscheck
Patricia Butler

Hans Carlsson
Ian Carmichael*
Coen Carmiggelt
Chalon Carnahan
Paul Chambré*
Joseph Chan
Tin Chan
Mitchell Che
Sheng-Po Chen
Cynthia Childs
Clement Chou
John Clarke*
Lewis Cohen
Marcie Commins
Mary Connell
Neville Cook*
Donald Corrigan
Alain Curneir

James Davey
Robert Davis
Edward De Zabala
Ellen Diamond
Thomas Doe
Laurie Di Fraia
Kathy Donnelly
Christine Doughty

Padraic Doyle
Allan Dubin
Andrew DuBois
Peter Duncan

Houshana Ebrahimi
Laurel Egenberger
Paul Elias
Janice Elliot
Eugene Eno
Geraldine Erickson
Daniel Estrella
James Evans

James Ferguson
Steve Flexser
George Flowers
Mauro Foglia
Conny Frisch
Jonathan Frisch
Philip Fong
Ted Fujita
Robert Fulton

Ellen Gailing
Robert Galbraith
Thomas Gamble
Anoushiravan Ghaffari
Susan Gillett
Beverly Gimeno
Orah Goldman
Norman Goldstein
Colin Goranson
Wolfgang Goubau
Keshav Goyal
Alexander Graf
Roy Greenwald
Varuttama Guvanasen

Susan Halfman
Joseph Haney
Leif Hansen
Jeri Hara
Makoto Harada
Volker Harms
Rosemary Hart

Eric Hartwig
Niamh Harty
Ramsey Haught
Kunio Higashi
Deborah Hopkins
Alex Horne*
John Howard
Michael Hood*
Richard Hsu

Eduardo Iglesias
Jeffrey Irvine
Frank Jahnke
Dennis Jamison
Alan Jassby
Abdul Rahim Jaouni
Julie Jeffrey
Peter Johnson
Anthony Jones
Barbara Jones
Keith Jones
Randall Jones

Brian Kanehiro
Allen Kearns
Jacqueline Kent
William Keyes
Tjiep Kho
Stanley Klainer
Steven Kramer
Brent Kohrt
Pavel Kurfurst

Cheng-Hsien Lai
Ki Ha Lee
Raymond Lee
Wayne Lee
Davis Leung
Peter Lichtner
Donald Lippert
Marcelo Lippmann
Nicholas Littlestone
Jane Long
Steve Lundgren

Peggy MacLean
Ernest Majer

*Faculty member, University of California

Donald Mangold
Donald McCarthy
Susan McCormick
Thomas McEvilly*
Maurice McEvoy
Ellen McKeon
Maynard Michel
Constance Miller
Coral Miller
Susan Miller
James Mitchell
Milton Moebus
David Moncada
Alison Monroe
Leuren Moret
H. Frank Morrison*
Susumu Muraoka
Larry Myer

T. N. Narasimhan
John Neil
Philip Nelson
Helen Nicholas
John Noble
Duane Norgren
Yvonne Norpchen

Maura O'Brien
John Oldson
Michael O'Sullivan
Irmgard Orzech

Walter Palen
George Parks
Bjorn Paulsson
Susan Payne
Christopher Peiper
Dale Perry
Scott Peterson
Ronald Philips
Thomas Pigford*

Kenneth Pitzer*
Cheri Plumlee
William Pope
Karsten Pruess

Richard Rachiele
Clayton Radke*
William Ralph
Pascal Rapier
Joe Ratigan
Ruthie Redic
Janet Remer
Richard Remillard
Carlos Riveros
Marc Rivers
Morris Roach
Gene Rochlin
Pamela Rogers
Donald Rondeau
Eliezer Rubin

Marie Schauer
Peter Schein
Ellory Schempp
David Schmidt
Deanna Schmidt
Ronald Schroeder
Werner Schwarz
Michael Shea
Robert Silva
Lenard Silvester
Terrance Simkin
Ray Solbau
Wilbur Somerton*
Hwaili Soo
Robin Spencer
Jonathan Stebbins
Mitchell Stark
Robert Sterrett
Andrew Stromdahl
Rebecca Sterbentz

Robert Stolzman
Beverly Strisower
Dimitri Sverjensky
Ho-Jeen Su
P. Sundaram

Lisa Teague
Jerome Thomas
Neil Thomsen
Richard Thorpe
Daniel Ting
Chin Fu Tsang
Yvonne Tsang
Leon Tsao
William Thur
Badawi Tleimat
Richard Valentine
Ashok Verma
Aylette Villemain
William Villet
Jeri Edgar-Vogt
Stephen Vonder Haar

David Watkins
Oliver Wan
Joseph Wang
Christopher Weaver
Virginia Weaver
Hans Wenk*
Oleh Weres
Jerry West
Arthur White
Richard Whiteman
Pat Wilde
Charles Wilson
Michael Wilt
Harold Wollenberg, Jr.
Lester Wong
William Wong

Andrew Yee

*Faculty member, University of California

APPENDIX C: PRINCIPAL MEETINGS OF 1980

During fiscal 1980 the Earth Sciences Division of Lawrence Berkeley (LBL) organized four major meetings and cosponsored one international symposium.

The Second Symposium on the Cerro Prieto Geothermal Field, Baja California, Mexico, was held in Mexicali, Baja California, Mexico, October 17-19, 1979. Cosponsored with the Comisión Federal de Electricidad de Mexico (CFE), this meeting was a continuation of the First Symposium on the Cerro Prieto Geothermal Field, which was held in San Diego, California, in September 1978. Over 150 scientists, engineers, and government officials from Mexico, U.S.A., and five other countries attended the symposium. Subjects covered were geology, hydrology, geochemistry, subsidence, geophysics, well drilling, reservoir engineering, and reinjection. The proceedings of the symposium will be published by CFE.

A Workshop on Numerical Modeling of Thermohydrological Flow in Fractured Rock Masses was held in Berkeley, California, February 19-20, 1980. This workshop was the result of the attention currently being given to the isolation of nuclear wastes in geological formations. The workshop provided a forum for the 60 participants from the fields of waste isolation, groundwater hydrology, geothermal energy, and petroleum engineering to discuss the discrete and continuum approaches, the generic repository studies, and the experience in modeling thermohydrologic flows in different fields. The proceedings of this workshop will be published in 1981, as LBL-11566.

The Third Invitational Well Testing Symposium was held in Berkeley, California, March 26-28, 1980. The goal of the LBL invitational well testing symposia is to encourage the interchange of ideas and technology between the fields of reservoir engineering, hydrogeology, civil engineering, and energy-related earth sciences. The initial symposium (October 1977) included papers on a wide variety of subjects relevant to geothermal well testing. For the second symposium (October 1978) the subject of injection of geothermal reservoirs was selected to limit the scope of the proceedings. The third symposium concentrated on the testing of low-permeability rocks--a problem common to waste disposal, fossil energy resource development, and underground excavation for civil or mining purposes. The symposium provided a forum for over 130 participants in which to exchange ideas and present new information on low-permeability rocks. The emphasis was on reviewing existing capabilities, identifying current limitations, and generating new ideas for research and development. The proceedings of the Third Invitational Well Testing Symposium are currently being published as LBL-10276.

A Geothermal Computer Code Workshop was held in Berkeley, California, June 17-19, 1980, in response to numerous requests from the Department of Energy, other national laboratories, and current and future users of reservoir engineering geothermal codes developed at LBL. The purpose of the workshop was to disseminate information about these codes and to describe their various applications. The workshop began with a one-day session on the basic theory of the following LBL codes: CCC, SHAFT79, ANALYZE, TRUST, and WELLF. The second day was devoted to the discussion of simple problems prepared by LBL. The third day was used to solve those problems using the LBL codes. More than 60 key computer code people participated in this workshop.

The Second Workshop on Thermomechanical-Hydrological Modeling for a Hard Rock Waste Repository was held in Berkeley, California, July 29-31, 1980. This workshop was the second in a series of DOE-sponsored rock mechanics workshops, the general objective of which is to provide a proper forum for the timely exchange of technical information vital to the National Waste Terminal Storage Program. The primary objective of this workshop was to discuss the state of the art of the codes for thermomechanical and hydrochemical modeling of repository response and to identify research and development activities needed for coupling the thermomechanical and hydrochemical models using the information developed in the previous workshop. The proceedings of this workshop were published as LBL-11204.